UNIVERSITAT POLITÈCNICA DE CATALUNYA BARCELONATECH

Constitutive model for fibre-reinforced composite materials exposed to high temperature

Rafael Pacheco Blázquez

UNIVERSITAT POLITÈCNICA DE CATALUNYA · BARCELONATECH (UPC)

Barcelona School of Nautical Studies (FNB)

DOCTORAL THESIS

Constitutive model for fibre-reinforced composite materials exposed to high temperature

---

Author:

Rafael PACHECO BLAZQUEZ

Supervisor:

Dr. Daniel DI CAPUA

Prof. Julio GARCIA ESPINOSA

A thesis submitted in fulfilment of the requirements for the degree of Doctor of Philosophy in Nautical Engineering, Marine and Naval Radioelectronics

in the

International Centre for Numerical Methods in Engineering (CIMNE)

Nautical Science and Engineering (CEN)

June 3, 2022

Declaration of Authorship

I, Rafael PACHECO BLAZQUEZ, declare that this thesis titled, "Constitutive model for fibre-reinforced composite materials exposed to high temperature" and the work presented in it are my own. I confirm that:

- This work was done wholly or mainly while in candidature for a research degree at this University.
- Where any part of this thesis has previously been submitted for a degree or any other qualification at this University or any other institution, this has been clearly stated.
- Where I have consulted the published work of others, this is always clearly attributed.
- Where I have quoted from the work of others, the source is always given. With the exception of such quotations, this thesis is entirely my own work.
- I have acknowledged all main sources of help.
- Where the thesis is based on work done by myself jointly with others, I have made clear exactly what was done by others and what I have contributed myself.

Signed: _____

Date: March 8, 2022

UNIVERSITAT POLITÈCNICA DE CATALUNYA · BARCELONATECH (UPC)

Abstract

Barcelona School of Nautical Studies (FNB)

Nautical Science and Engineering (CEN)

Doctor of Philosophy in Nautical Engineering, Marine and Naval Radioelectronics

Constitutive model for fibre-reinforced composite materials exposed to high temperature

by Rafael PACHECO BLAZQUEZ

The high strength-weight ratio of composite materials have made them one of the best materials for the design of light-weight structures. However, its special complexity has made them not suitable for the design of structures with a relative complexity or with numerous structural component and pieces. Hence, the importance in the development of adequate constitutive models which allow simulating the micro-macro scale interaction of composites, and to address the intrinsic and natural flexibility of composites that is not as relevant in traditional materials.

Meanwhile, the mechanical development of these materials is a mature research branch with more than four groundbreaking decades of life, this is not certainly met at the thermo-mechanical level which is still in an early stage and, consequently, limiting the extensive use of composites in real world and complex structures, particularly structures in which a strong and detailed fulfilment of fire criteria is necessary. E.g., this is the very situation in the large-length ship design sector, where the share in the market for ships built using composite material, tends to be very reduced and closely accompanied by tools which serve to perform structural health monitoring, in order to palliate, the amount of high uncertainty of the present thermo-mechanical response, found in the design of these structures.

The present thesis focuses on the development, formulation-wise and computational implementation, of a numerical model in order to predict the non-linear constitutive behaviour of fibre-reinforced plastic (FRP) composites exposed to thermal degradation due to high temperatures. This very model is cemented in the groundbreaking development of constitutive mechanical formulations specially tailored for composites also known as rule of mixtures – in this present context, the formulation is the so-called serial-parallel rule of mixtures – which establish a set of closure equations to obtain the suitable micro-macro scale interaction of the composite structure and, at the same time, to take into account the characterisation of the internal and state variables of the constituent phases.

Apart, the ultimate objective of this thesis, in this special context – where a structure is under thermal loads or, what is the same, exposed to fire – it is mandatory

to develop a consistent formulation and tool to perform what is referred to as a fire collapse assessment analysis. The utilisation of a more sophisticated thermal degradation or pyrolysis formulation, based on the present existing formulations, will be employed in order to obtain the internal and state variables of the thermal degradation process. Thus, the outcome of this analysis will serve as means to obtain the unknown thermal state of the structure and complete the thermo-mechanical analysis. The formulation of the thermo-mechanical problem is adapted to be used in laminated non-linear constitutive shells. The use of shells is a necessity for the right optimisation of the computational cost of analysing structures with a high number of structural reinforcements or divisions, such as the ones that appear regularly during the ship design process of large ship structures.

UNIVERSITAT POLITÈCNICA DE CATALUNYA · BARCELONATECH (UPC)

Resumen

Barcelona School of Nautical Studies (FNB)

Nautical Science and Engineering (CEN)

Doctor of Philosophy in Nautical Engineering, Marine and Naval Radioelectronics

Modelo constitutivo para materiales compuestos de fibra reforzada expuestos a altas temperaturas

by Rafael PACHECO BLAZQUEZ

Para los materiales compuestos, su relación esfuerzo-peso elevada ha hecho de ellos uno de los mejores materials para el diseño de estructuras ligeras. No obstante, su especial complejidad, hace de ellos un arduo trabajo cuando se trata del diseño de estructuras con una cierta complejidad, o, en la existencia de numerosas divisiones estructurales o piezas. Consecuentemente, el desarrollo de modelos constitutivos adecuados es de importancia, en especial aquellos que permiten la simulación de la interacción para la micro-macro escala de los compuestos, y que resuelven la flexibilidad natural e intrínseca de estos materiales avanzados, cuestión que no es tan relevante para el diseño de materials tradicionales.

Mientras tanto, el desarrollo de teorías mecánicas para estos materiales se encuentra en su madurez, con más de cuatro décadas de hallazgos en esta rama. En contraposición, en cuestiones que atañen el análisis termo-mecánico, el paradigma se encuentra relativamente verde, lo cual limita la aplicación extensiva de los compuestos en aplicaciones prácticas y estructuras complejas, de hecho, es particularmente limitante en el diseño de estructuras que requieren del cumplimiento de exigentes y detallados criterios relativos al fuego. E.g., esto mismo sucede en el diseño de embarcaciones de grandes esloras, donde la cuota de mercado de los buques construidos mediante materiales compuestos suele ser reducida, y estrechamente acompañada por herramientas de monitorización de la integridad estructural, para así poder paliar la gran incertidumbre vinculada a la respuesta termo-mecánica, fruto de las capacidades del diseño comercial actual.

La actual tesis se centra en el desarrollo, de manera teórica, y con su correspondiente implementación computacional, de un modelo numérico capaz de predecir el comportamiento no-lineal constitutivo de compuestos plásticos con fibra embebida (FRP) cuando estos son expuestos a altas temperaturas y en consecuencia a la degradación térmica. Este mismo modelo está inspirado en los desarrollos, pioneros y excepcionales, de modelos constitutivos mecánicos, las cuales están pensadas para compuestos. Estas teorías forman parte de la familia de las reglas de mezclas, en particular, la formulación escogida es la renombrada regla de mezclas serie-paralelo, la

cual establece un conjunto de ecuaciones de cierre para así obtener la adecuada interacción del material compuesto en la micro-macro escala. Esta formulación, a su misma vez, tiene en cuenta la caracterización y evolución de tanto variables internas como de estado, para las fases constituyentes, en este contexto se trataría de la fibra y la matriz.

Por otra banda, el objetivo último de esta tesis, dentro de este contexto particular, donde una estructura se somete a cargas térmicas, o en otras palabras, se expone al fuego, es de forzosa necesidad el desarrollo de una formulación consistente y una herramienta capaz de verificar lo que se puede acuñar como un análisis de colapso al fuego. El uso de una formulación más sofisticada para la degradación térmica o pirólisis, basada en formulación existente, será empleado para así obtener las variables internas y de estado de los procesos de degradación térmica. En consecuencia, los resultados de este análisis térmico sirven para obtener el desconocido estado térmico de la estructura, la distribución de temperatura a través del espesor del laminado, y complementar el análisis termo-mecánico. La formulación del problema termo-mecánico es adaptada para ser usada en láminas no lineales de materiales compuestos. Usar láminas es una necesidad para la correcta optimización del coste computacional derivado del análisis de estructuras con un alto número de refuerzos o divisiones, análisis que son frecuentemente encontrados en el proceso de diseño de embarcaciones de grandes esloras.

Dedicated to my beloved grandmother, Maria Rosa Pastor Pastor. Anima Eius Requiescat In Pace.

"Be like a rocky promontory against which the restless surf continually pounds; it stands fast while the churning sea is lulled to sleep at its feet. I hear you say, "How unlucky that this should happen to me!" Not at all! Say instead, "How lucky that I am not broken by what has happened and am not afraid of what is about to happen. The same blow might have struck anyone, but not many would have absorbed it without capitulation or complaint."

– Marcus Aurelius, Meditations. IV.49(161 to 180 AD)

trans. Hicks

Acknowledgements

This piece of work, my thesis, is a reflection of the efforts and results of the research performed during my PhD candidature. The effort and resultant work are, in its majority, to be credited to me. Nevertheless, I have to state that the authority of this work cannot solely be portrayed as mine. I feel the urge to extend my gratitude to anyone who has contributed in any way, by any means and at any level, to this thesis and to the development of my research career. I hope the following paragraphs are enough to express my endeavour to credit all the significant people that have contributed to the research or aided me in conducting it. This research has received funding from European Union's Horizon 2020 research innovation programme under grant agreement number 723360.

In the first place, I would like to acknowledge my thesis supervisor, Prof. Julio García Espinosa who lend me the opportunity to conduct and to support my research, his useful pieces of advice throughout the confection of this thesis have been of inestimable value. Analogously, to Dr Daniel Di Capua who has provided me with the guidance that I needed, be it technically or emotionally. I hold in high regard, the mentorship received by both supervisors, these lines are not enough to express how deeply indebted I am to them and their guidance.

I have to issue an acknowledgement to the research centre which took me in for the last 5 years, the International Centre of Numerical Methods in Engineering in short CIMNE, and do find my acknowledgement extended to all its researchers that have helped me in my research. Without the knowledge I obtained by collaborating with CIMNE, or the technical resources it has provided to me, I would not have been able to complete this thesis. I do want to make a special mention to the Naval Maritime Department of CIMNE and the people who integrate this department, those colleagues who welcomed me in the NT3 building and those who hold a close bond to this department, their support and friendship have been detrimental to me in the accomplishment of this thesis.

Also, I would want to acknowledge the help of any private or public institution that has helped me to progress in my research. Especially to the company Compass Ingeniería y Sistemas and to its whole team, in particular to Ovidi Casals that without his incessant help, there is no doubt, it would have been impossible to end this thesis.

At a closer and private level, I do want to thank all my friends, those before this thesis and those who I met during it, for bearing with me when times were odd and my patience was very scarce, and also for all the times of joy we shared in the forging of this thesis. Finally, I owe a sincere and huge acknowledgement to my own family, especially to my parents and sister, who have been supportive and caring of me for the last years, this thesis is as mine as yours.

Contents

List of Figures

List of Tables

List of Abbreviations

CFD	**C**omputational **F**luid **D**ynamics
CMT	**C**lassical **M**ixture **T**heory
FD	**F**inite **D**ifference
FDS	**F**ire **D**ynamics **S**imulator
FEM	**F**inite **E**lement **M**ethod
FRP	**F**ibre **R**einforced **P**lastic
FSI	**F**luid-**S**tructure **I**nteraction
FVM	**F**inite **V**olume **M**ethod
IACS	**I**nternational **A**ssociation of **C**lassification **S**ocieties
IROM	**I**nverse **R**ule **O**f **M**ixtures
LES	**L**arge **E**ddy **S**imulation
ROM	**R**ule **O**f **M**ixtures
SOLAS	**S**afety **O**f **L**ife **A**t **S**ea
SPROM	**S**erial **P**arallel **R**ule **O**f **M**ixtures
TSPROM	**T**hermal **S**erial **P**arallel **R**ule **O**f **M**ixtures

Nomenclature

Note: in the column **Units**, *the character "-" denotes multiple units are valid for a given symbol and no unit when left empty " ".*

Notation

Symbol	Description	Definition	Units
$\|a\|$	absolut operator	$\|a\| = \sqrt{a \cdot a}$	-
$\mathcal{O}()$	big O notation		-
x_1	x-axis	$x_1 = x$	m
x_2	y-axis	$x_2 = y$	m
x_3	z-axis	$x_3 = z$	m
$\delta\,()$	variational operator		-
$\nabla \cdot a$	divergence		-
:	double product		
$()\|_n$	evaluated at iteration n-th		
∇a	gradient		-
$\Delta()$	increment of a quantity		-
$\|\|a\|\|$	$\mathcal{L}_2$-norm	$\|\|a\|\| = a \cdot a$	-
$\langle a \rangle$	Macaulay bracket	$\langle a \rangle = \frac{a+\|a\|}{2}$	-
$\underline{n}$	normal		m^2
$a \otimes a$	tensor product		-
a	scalar		-
$\underline{a}$	vector		-
$\underline{\underline{a}}$	matrix		-
a	zero order tensor		-
$\underset{\bullet}{a}$	first order tensor		-
$\underset{\bullet\bullet}{a}$	second order tensor		-
$\underset{\bullet\bullet\bullet}{a}$	third order tensor		-
$\underset{\bullet\bullet\bullet\bullet}{a}$	fourth order tensor		-

General

Symbol	Description	Definition	Units
$\partial\Omega$	boundary of the problem		m^{n-1}
ρ	density		$\mathrm{kg/m}^3$
Ω	n-dimensional domain of the problem		m^n
λ	eigenvalue		
$\underline{\lambda_{\overrightarrow{v}}}$	eigenvector		
g	gravity	9.81	ms^{-2}
m	mass		kg
p	pressure		Pa
$\overrightarrow{\underset{\bullet}{e}}$	projector vector		
$\overrightarrow{\underset{\bullet\bullet\bullet\bullet}{e}}$	fourth order projector tensor		
$\overrightarrow{\underset{\bullet\bullet}{e}}$	projector matrix		
N_ξ	shape function		
e	specific energy		J/kg
e_i	specific internal energy		J/kg
e_k	specific kinetic energy		J/kg
h	specific enthalpy		J/kg
ξ	test function		
l_t	thickness length		m
v	velocity		m/s

Thermal

Symbol	Description	Definition	Units
T_∞	ambient temperature		°K
c_k	thermal conductivity coefficient		W/m°K
c_h	thermal convection coefficient		W/m^2°K
c_ε	thermal emissivity coefficient		
α	thermal expansion coefficient		°K^{-1}
c_{kc}	charred thermal density		W/m°K
c_{kv}	virgin thermal conductivity		W/m°K
ρ_c	charred density		kg/m^3
ρ_v	virgin density		kg/m^3
E_{act}	energy of activation		J/mol
$\underline{f_c}$	convection flux vector		W
$\underline{f_d}$	degradation flux vector		W
$\underline{f_r}$	radiation flux vector		W
$\underline{\underline{C_T}}$	heat capacity matrix		J/°K
$\underline{\underline{K_T}}$	heat conductivity matrix		W/°K
q	heat flux		W/m^2
Q_p	heat of decomposition	$Q_p = \frac{\partial \rho}{\partial t} h_p$	W
Q	heat source		W
T_0	initial density		kg/m^3
T_0	initial temperature		°K
J_F	jacobian of the pyrolysis fraction		s^{-1}
M_g	gas molar mass		kg/mol
κ_g	gas permeability		m^2
A_T	pre-exponential factor		s^{-1}
F	pyrolysis fraction		
N_{ro}	order of decomposition reaction		
r_F	residual of the pyrolysis fraction		s^{-1}

$\underline{r_T}$	thermal residual		W
h_p	specific enthalpy of decomposition		J/kg
c_p	specific heat capacity		J/kg°K
c_{p_c}	charred specific heat capacity		J/kg°K
c_{p_v}	charred specific heat capacity		J/kg°K
c_σ	Stefan-Boltzman constant	$5.6704 \cdot 10^{-8}$	W/m^2°K^4
$\underline{\underline{J_T}}$	tangent flux matrix	$\frac{\partial \underline{r_T}}{\partial T}$	W/°K
T	temperature		°K
R	universal gas constant	8.3145	J/°Kmol
μ_g	gas dynamic viscosity		m^2

Mechanical

Symbol	Description	Definition	Units
S_d	damaged area		m^2
S_e	effective area		m^2
S_0	intact area		m^2
x_{cl}	characteristic length		m
$\mathcal{D}$	compliance tensor		Pa^{-1}
c_{CF}	compression fraction		
c_{CR}	compression ratio		
D	constitutive tensor		Pa
D_{elast}	elastic constitutive tensor		Pa
$D_{\text{in-out}}$	in-out-of-plane constitutive tensor		Pa
D_{in}	in-plane constitutive tensor		Pa
$D_{\text{out-in}}$	out-of-in-plane constitutive tensor		Pa
D_{out}	out-of-plane constitutive tensor		Pa
D_s	shear constitutive tensor		Pa
$\hat{D}$	stress-resultant constitutive tensor		Pa
$\hat{D}_b$	stress-resultant bending constitutive tensor		
$\hat{D}_{bm}$	stress-resultant bending-membrane constitutive tensor		Pa
$\hat{D}_m$	stress-resultant membrane constitutive tensor		Pa
$\hat{D}_{mb}$	stress-resultant membrane-bending constitutive tensor		Pa
$\hat{D}_{\text{sec}}$	stress-resultant secant constitutive tensor		Pa
$\hat{D}_s$	stress-resultant shear constitutive tensor		Pa
$\hat{D}_{\text{tan}}$	stress-resultant tangent constitutive tensor		Pa
D_{tan}	tangent constitutive tensor		Pa
$\mathcal{H}_d$	hardening/softening law		
d	damage index		
β_r	damage internal variable		$Pa^{1/2}$

β_q	damage internal variable evolution law	$\mathrm{Pa}^{1/2}$
β_{q_∞}	saturated evolution law	$\mathrm{Pa}^{1/2}$
β_{r_0}	damage initial internal variable	$\mathrm{Pa}^{1/2}$
c_{pe}	pre-exponential factor	
σ_∞	damaged saturated stress	Pa
u	displacement	m
$\hat{u}$	stress-resultant displacement	-
Π_D	dissipation energy	J
Π_F	energy of fracture	J
π_F	characteristic energy of fracture	Jm^{-1}
$\mathbb{F}_\varepsilon$	strain fluency surface	$\mathrm{Pa}^{1/2}$
$\mathbb{F}_\sigma$	stress fluency surface	$\mathrm{Pa}^{1/2}$
F	total force	N
F_b	body force	$\mathrm{N/m}^3$
F_b	specific body force	N/kg
F_{ext}	external force	N
F_{int}	internal force	N
F_p	point force	N
F_t	traction or surface force	$\mathrm{N/m}^2$
Π_{HE}	Helmholtz elastic free potential energy	J
I	inertia	m^4
J_u	jacobian of mechanical system	Nm^{-1}
$\mathbb{v}_\varepsilon$	strain norm	$\mathrm{Pa}^{1/2}$
$\mathbb{v}_\sigma$	stress norm	$\mathrm{Pa}^{1/2}$
ν	Poisson's ratio	
r_u	mechanical residual	N
r_{σ_s}	serial residual	Pa
θ	rotation	
Θ	additional rotation	
Λ	rotation tensor	
c_{sf}	shear correction factor	

γ	shear strain		
τ	shear stress		Pa
ρ_g	specific weight	ρg	Nm^{-3}
K	stiffness		N/m
K_L	linear geometric stiffness		N/m
K_{NL}	non-linear geometric stiffness		N/m
ε	strain		
ε_b	bending strain		
B	strain-displacement matrix	∇u	m^{-1}
B_b	bending strain-displacement matrix		m^{-1}
B_m	membrane strain-displacement matrix		m^{-1}
B_s	shear strain-displacement matrix		m^{-1}
$\varepsilon_{\mathrm{in}}$	in-plane strain		
ε_m	membrane strain		
$\varepsilon_{\mathrm{out}}$	out-of-plane strain		
ε_{p}	parallel strain		
ε_{s}	serial strain		
ε_s	shear strain		
$\hat{\varepsilon}$	stress-resultant strain		
σ_M	bending strength		Nm
σ_N	membrane strength		N
σ_Q	shear strength		N/m
σ	stress		Pa
σ_b	bending stress		Pa
σ_{in}	in-plane stress		Pa
σ_m	membrane stress		Pa
σ_{out}	out-of-plane stress		Pa
σ_{p}	parallel stress		Pa
$\underline{\underline{S}}$	stress-resultant matrix		
σ_{s}	serial stress		Pa
σ_s	shear stress		Pa

$\hat{\sigma}$	stress-resultant stress	Pa
σ_y	effective stress	Pa
σ_y	intact stress	Pa
σ_y	yielding stress	Pa
Π_ε	total potential strain energy	J
E	Young's modulus	Pa
E	shear modulus	Pa

Species Transport

Symbol	Description	Definition	Units
a	average quantity		-
C_d	diffusion coefficient		m^2/s
Φ_ρ	density fraction		
$\hat{a}_i$	diffusion quantity		-
w	generation of mass flux	$\int_\Omega \left[\nabla \cdot q_m\right] \, d\Omega$	kg/m^3s
a_i	instantaneous quantity		-
q_m	mass flux	ρv	kg/m^2s
Φ_m	mass fraction		
Φ_Ω	volume fraction		

Thermo-mechanical

Symbol	Description	Definition	Units
P	Mouritz-Gibson generic property		-
n_{MG1}	Mouritz-Gibson coefficient 1		
n_{MG2}	Mouritz-Gibson coefficient 2		
P_r	Mouritz-Gibson relaxed property		-
P_u	Mouritz-Gibson unrelaxed property		-
T_g	glass transition temperature		°K

Chapter 1

Introduction

1.1 Background to the research

The definition of composite materials is generally accepted as heterogeneous materials composed of two or more constituent materials with different properties. Many materials fit under this definition, one of the most successful ways to classify these materials is by considering materials that contain a fibre phase and matrix phase. E.g., concrete based materials are considered granulated-reinforced materials, some like *fibre reinforced plastic* (FRP) materials are considered either long or short fibre-reinforced materials.

The current situation that the modern world faces in areas such as environment, logistics, transportation and energy, has led to an increase in the demand for the so-called composite materials. This increase is discussed thoroughly by Ashby [1] and summarised in Figure 1.1, the rise in the application of advanced materials has been impulsed by the necessity of obtaining smarter materials and designs.

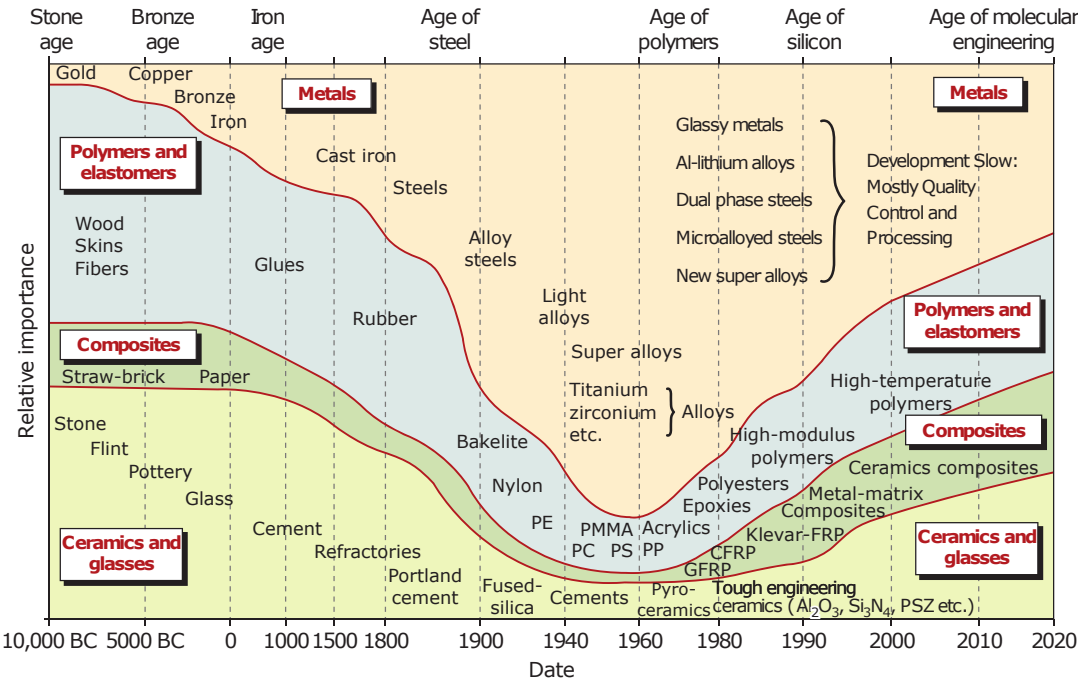

FIGURE 1.1: Historical evolution of engineering materials. Adapted from Ashby [1]

These materials tend to be tailored to meet the requirements of their applications, and they are incredibly modular in their design. One of the notorious advantages of composite materials is their lightweight density compared to common metals or even wood. Together with this reduction on the weight, they present an increase in the strength, which together with their manufacturing flexibility allows them to be optimised to endure several design loads.

The applications for composite materials have grown considerably in the aeronautical, automotive, civil and energy industries. However, in the marine industry, the introduction of such material has had an incredible impact in areas such as the small craft industry, the deployment of offshore structures and with a special interest in the latest offshore renewable applications. It has also been of importance in the military and navy industries to meet their special mission requirements. Nevertheless, the merchant and transport industry, which holds a vast share of the marine market, has been reticent about the incorporation of such materials in what is commonly described as long length ship structures.

The under-laying reasons for this reluctance have been promoted by the common misconception arising from deficiencies observed in different attempts to exploit the magnificent properties of such materials. At the current stage regarding the process of long length ship design, there is an obviously large amount of structural elements that conform to a ship structure itself. This vast amount of elements has made withdraw the use of composites in the early stages of the ship design process, in particular, due to the lack of optimal software to perform accurate simulations and at the same time presenting a cheap computational cost in the analysis of what is by definition a highly non-linear material.

Nevertheless, the use of composites would result in a reduction of the drag due to its lightweight density and thus faster or higher cargo capacity which would result in a tremendously positive effect for the environment, logistics, and transportation industries and at the same time provide an excellent corrosion resistance which is one of the crucial problems that common merchant ships are facing nowadays.

The current simulation tools in the market do not account for feasible simulation of large structures with the enormous number of degrees of freedom in addition to the extra huge degrees of freedom added by a multi-material such as a composite. However, the problem resides in the capability to predict a correct response of the structural behaviour indeed. Feasible software products tend to underestimate the strengths induced in the structure, creating two major issues, the need to apply extreme safety factors or account for high-risk designs. These two major issues are the reason the design of long-length composite ship structures become *taboo* in the shipping industry because they require costly overestimation of the material scantlings or to assume high risks by trusting the software used.

One way to reduce this uncertainty is to use extremely costly computational models, such as the ones offered by solids. In common ship structural design, solids relegate to simulate joints which manifest higher strengths than generally the rest of the structure. However, this is not practicable in the industry. On the other hand, the industry is requesting a better understanding of the failure and plasticity range for conventional and non-conventional material, which at the current stage, there is little room for formulations accountable to perform such analyses. Without a clear

understanding of what are the ultimate strengths and the capability to simulate correctly the rheological curve for a composite, the industry will not eagerly introduce the composites in their designs.

In addition to the mechanical constraints, there is an extreme difficulty in the application of fire regulations to composites, which, in comparison to conventional materials, are much more complicated to design. There is no commercial solution that can solve what is denominated as a fire collapse analysis in a feasible computational time, especially with a micro-macro scale formulation. Without a breakthrough in this line of work, there is no chance for the industry to adopt the advantages of composite materials in their commercial designs, primarily because of the derived cost induced by the correct assessment and certification, e.g., by the *International Association of Classification Societies* (IACS), of fire passive protective systems made out of composites. What is commonly understood, by all means, and in a general sense, is that a composite structure should have the same or better response than an equivalent conventional structure, and by conventional, generally steel equivalent structure.

Despite the difficulties, or expenditures, of designing long-length ship structures completely made out of composites. There are great advantages to using composites, these advantages were demonstrated in the large fires on two all-composite minehunter ships operated by the Royal Navy HMS Ledbury and HMS Cattistock. In both ships, the fire started in the engine/machinery room and in the case of HMS Cattistock, the fire burned for over four hours before being extinguished. The fires extensively damaged the compartment of both ships, with the composite hull and bulkheads being heavily charred. However, the low thermal conductivity of the composite bulkheads and decks stopped the fire from spreading by heat conduction to surrounding compartments, which is more difficult to stop in steel ships [14]. These reasons justify why composite materials are commonly used as a thermal insulator of space crafts for the re-entry process.

Consequently, the areas related to mechanical, thermal, and coupling between both models are the main objectives of the research of this dissertation. Concerning to the mechanical model, this thesis aims to use an enhanced formulation derived from the standard SPROM formulation as mentioned in Rastellini et al. [15] to obtain the composite constitutive behaviour and to integrate into it the thermal expansion due to the exposure to fire. The general mechanical approach is based on the finite element method (FEM) and, in particular, for laminate shells, the formulation is extracted from the book of Oñate [16]. The constituent materials shall be able to perform non-linear constitutive analysis and to accomplish it, the isotropic damage formulation by Simo and Ju [17] is employed. Because of the flexibility of composites, the integration of a large displacement and deformation theory in the current methodology is needed. The non-linear geometric model is based on the ideas of Felippa and Haugen [18].

Regarding the thermal model, the objective resides in delving in the work published by Henderson et al. [11, 19] and collected in Mouritz et al. [7, 20] to solve the so-called one-dimensional non-linear transient heat problem for composites. This problem is solved at the constituent level.

1.2 Research problem and hypotheses

This subsection serves as a very brief summary of the trends and technologies existent in the current paradigm. The summary is especially brief, since an extensive one is provided in chapter 2. The hypotheses are distributed in different topics, from more general to more specific, and a final italic paragraph is attached to formally introduce the question or hypothesis that needs to be researched.

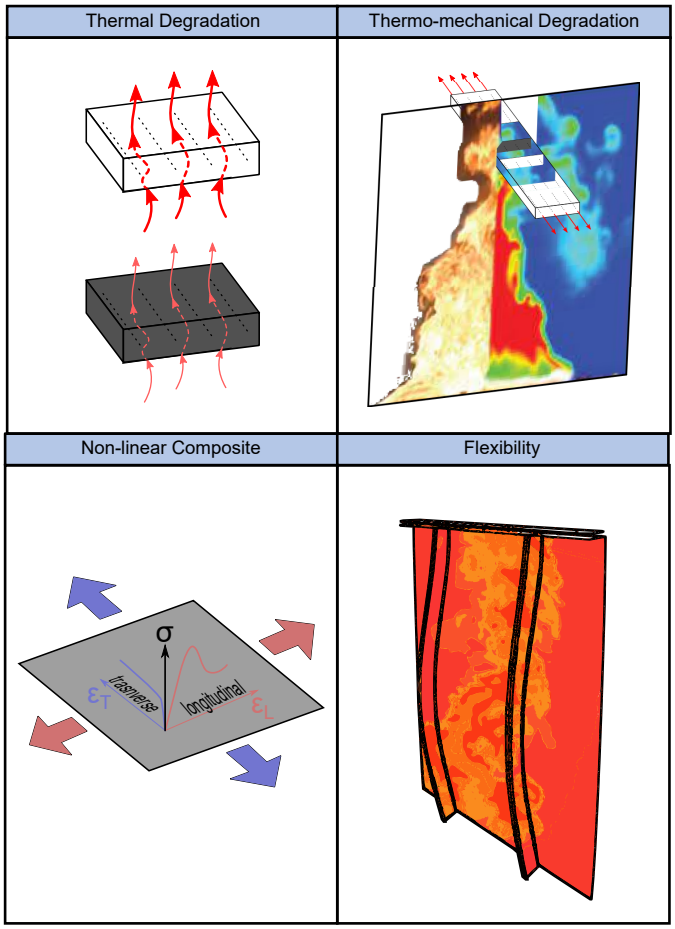

FIGURE 1.2: Compendium of the different starting topics used in the research.

Figure 1.2 serves as a quick recapitulation of the initial aspects considered at the beginning of this research. The topic of *thermo-mechanical analysis of shell structures, made out of composite, in the presence of fire* seemed to be a prestigious topic with a fair amount of research done, however, a distinction has to be made when limiting the scope to marine applications, but the current paradigm is still maturing.

When fitting the research in the scope of the marine industry, there are two types of purposes in terms of structures, either ships or offshore structures, the first was selected, specially long-length ships over 50 m. From a numerical point of view, this types of structure are rarely simulated using solids, the prominent use of shells amongst other elements is well known and one of the decisive factor in devoting the discussion done within this thesis to this type of element.

There are many aspects to consider, and many questions that are as valid as the ones formulated in this very section of the thesis. In a general sense, one of the questions to enquire oneself was *what type of approaches have been used in the industry until this moment*, this was a crucial question since the discussion offered in this thesis focuses on providing a useful and novel solution to the current problems that the industry is facing. Then minor questions started appearing, those that involve the fire and the thermal component of the problem. *What type of methods are used to characterise fire*, or, *how the thermal process is any different in composites compared to traditional materials*. Those were two of the principal questions to determine what type of fire modelling and thermal modelling was necessary for the present.

In the spectrum of mechanical/thermo-mechanical analysis, questions particularly for composites were formulated. *What is the optimal manner to simulate the constitutive behaviour of composite*, *is it possible to formulate a multi-scale approach that preserves the microstructure and at the same time is computational efficient*, *what kind of shell elements are preferred in the industry*. As the research has advanced, new questions originated, especially in certain problems that were unique in composites. *Why are composites very flexible*, *how do regulations tackle buckling of composites*, *is buckling a problem to consider when exposed to fire* or *is there a polyvalent method to assess buckling in composites*.

Special effort was put into analysing the different constitutive models existing in the industry. The idea of characterising the microstructure materials was very novel and soon questions about *how the thermal properties of fibre and resin are affected by temperature*, *what about the mechanical properties*, *if composites are simulated with damage models, does this apply to its subcomponents* or *are there any formulations that take into account the damage induced by temperature*.

Once these questions started to be round up, the more specific ones started to develop, those intrinsic to the nature of the analysis of composites structures that endure mechanical and thermal loading. Questions such as *does the temperature affect the structure* or *what about the other way around, does the deformation affect how the temperature is transported*, *is it better a monolithic approach or rather a decoupled one*, and *what sort of effects between the thermal problem and the mechanical need to be addressed*.

1.2.1 Industry

The use of fibre-reinforced plastics (FRP) or long-fibre composite (LFC) has been increasing during the past half-century [21]. This increase for such materials is well known for its excellent mechanical properties, such as resistance-weight ratio, stiffness-weight ratio, corrosion resilient, thermostability and low thermal conductivity. For this exact reason, the research on such materials has greatly increased in order to develop numerical and mathematical models that couple the micro-macro mechanical phenomena. Especially within the constitutive model fields.

However, whereas areas devoted to the constitutive modelling have been increasing, this is not met by the production of numerical failure criteria research. E.g., according to Hinton and Soden [22], there is still a difficulty in order to predict the ultimate strength of the material/structure. In the lately two past decades, the industry has started demanding more accurate solutions regarding this topic.

Moreover, very little research is performed in the numerical analysis of composite structures exposed to high-temperature [23, 24, 25]. Available thermo-mechanical solutions in commercial software products are generally focused on non-linear thermal behaviour coupled with linear laminate mechanical problems.

Therefore, the question is open to whether or not, a numerical solution can be produced to predict the inelastic response of FRP composite structures, incorporating this prediction not only to the composite, but to the constituent phases. And combine this with a non-linear thermal analysis that includes non-linear effects such as pyrolysis.

1.2.2 Mechanical Model

In their initial stage, the composite mechanical models were limited in terms of computational resources and power. Hence, the under-laying concepts introduced were those by Voigt [26] with his interpretation of the famous *rule of mixtures* (**ROM**) and later the upgrade by Reuss [27] with the introduction of the *inverse rule of mixtures* (**IROM**), the latter, able to represent better the transverse mechanical properties of the fibre-resin interaction. The different approaches agree on the assumption of the so-called *mean field methods*, which infuse *auto-consistent* approximations to simplify the distribution of the **stresses** and **strains** by assuming that the behaviour of each of the phases is solely governed by that of the average stress and average strain.

The present research areas, thermal and mechanical, need a satisfactory and cheap approach to simulate composite material structures. This is obtained by establishing an adequate relation between the micro-scale and macro-scale and also taking a multi-material approach in order to model the heterogeneous micro-structure. These prediction models focus on the concept of partial disassociation of the response of a unique **ply** or **layer** into its sub-material divisions or constituent materials (e.g., fibre and matrix). Participation and behaviour is weighted by means of the volumetric or mass fraction of each constituent material. In addition to the constitutive disassociation behaviour of phases, the lines of research, also consider the morphological distribution or what is commonly referred to as the **stack** or **laminate**.

The current trend is to obtain new technology able to determine the degradation of composite materials (plasticity, **damage** or fatigue) and to take into account the environmental factors (UV rays, humidity and **temperature**). The underlying *leitmotiv* for research fields within the finite element method (FEM) in heterogeneous materials is the design of a formulation able to correlate the experimental tests to the simulation.

During the past decades the area of study for such models has transitioned from **isotropic** constitutive composite models which have been proved to be insufficient to model what clearly is an orthotropic behaviour into purely orthotropic constitutive composite models. The last option requires a higher number of parameters to define the composite, and it has been proven to not be able to reproduce to its full extent the mechanical behaviour between experimental results and the simulation analysis [21].

Hence, there is the need to research the hypothesis of whether is it or not possible to produce a theory that can predict and correlate better the response of numerical analysis of composites

with experimental testing. This theory needs to be simple, straightforward and able to predict the failure of the composite as a whole from the failure of constituent phases, particularly for any morphology.

1.2.3 Thermal Model

The modelling of composites exposed to high temperature or fire is a complex problem involving thermal, chemical, physical and failure phenomena. Mouritz et al. [7] published a compendium on the paradigm around the analysis of composites subjected to fire.

The modelling of composites exposed to fire is derived from the conservation of energy and the resultant equation is discussed by Henderson et al. [11, 19], where the degradation of the composite is introduced by a simple rule of mixture and expresses the mass density between the solid phase and intact solid phase of the resin. Henderson et al. and many other authors choose to model the degradation evolution as an Arrhenius equation. The current research trend focuses on the one dimension simplification by Henderson et al. and the most common simplification introduced by Wickstrom Ulf et al. [28] of the problem, where two artificial and sensical boundary conditions, are imposed on the ends of the problem, forcing the direction of the flux, hence, the temperature gradient becomes monotonic.

Thermal models using the simplification introduced by Wickstrom Ulf et al. require a complex set of assumptions in order to simplify the number of constraints in the governing equation. Authors such as Henderson and Wiecek [19], Lattimer et al. [7, 29], Chippendale et al. [30] or MacDonald et al. [31] have contributed to the characterisation of different parameters for materials found in standard FRP composites.

The question then is open on whether a one-dimensional non-linear transient heat model can be proposed and if this model can be coupled simply with a thermo-mechanical model that is able to predict structural fire-collapse. This thermal model is then forced to be coherent with a micro-scale formulation, i.e., the formulation developed would have to be consistent with the constituent phases described in the thermo-mechanical model. Thus, the pyrolysis shall be evaluated at both fibre and matrix components.

1.3 Justification for the research

Fibre Reinforced Polymers are extensively used today for building the hull structure of crafts with lengths up to about 50 m. In fact, today most of the pleasure crafts and sailing yachts, passenger and car ferries, patrol and rescue crafts, and naval ships below 50 m in length are built in composites. These materials are also used in large secondary structures, but only a few complete units above 50 m length – naval vessels – have been built in composite materials.

The main reason for this limitation in the use of composites is the obligation to use 'steel equivalent' structural materials to fulfil the fire-safety requirements of the Convention for the Safety of Life at Sea (SOLAS). However, today there is no question that alternative designs with suitable risk control and the use of fire retardant resins, intumescent coatings, fire insulation and active fire-fighting systems can allow FRP structures to fulfil the strictest fire safety regulations.

In addition, despite the fact that many polymer composites are flammable, these materials have other properties that may be beneficial in the event of a fire scenario and that are not present in metals. Composites have a heat conduction rate much slower than metals. This fact is translated into a slowdown in the speed of fire spread between rooms, and therefore the composite laminate constitutes a very effective barrier against the spread of fire.

There is an incipient interest in funding the research of composite ship science, especially, motivated by the field of fire-assessment. This interest can be portrayed in the efforts of several competitive projects, such as:

1. *BESST, Breakthrough in European Ship and Shipbuilding Technologies*, is a project on the design focused on passenger ships, ferries and mega-yachts with novel advanced materials. Figure 1.3 shows a wall fire test for the effectiveness of the chosen solution.

FIGURE 1.3: Experimental testing of a wall-fire extracted from the BESST project [2].

2. *LASS, Lightweight Construction Applications at Sea and Fire Safety* [3], a project that aimed at improving the efficiency of marine transport by the development and demonstration of the technology to use lightweight materials in the ship-building industry. Figure 1.4 shows the real scale experimental tests carried out in the LASS project.

FIGURE 1.4: Experimental testing of a superstructure room extracted from the LASS project [3].

3. *FIRE-RESIST, Developing Novel Fire-Resistant High Performance Composites* [4], aims to develop the technologies to build marine applications with advanced materials. Figure 1.5 shows the testing of a built-in bulkhead in the project.

FIGURE 1.5: Experimental testing of a load-bearing bulkhead extracted from the FIRE-RESIST project [4].

4. "RAMSSES, Realisation and Demonstration of Advanced Material Solutions for Sustainable and Efficient Ships" is a project that aimed to provide novel composite solutions for long-length ships. Figure 1.6 shows a real scale demonstrable of a hull section.

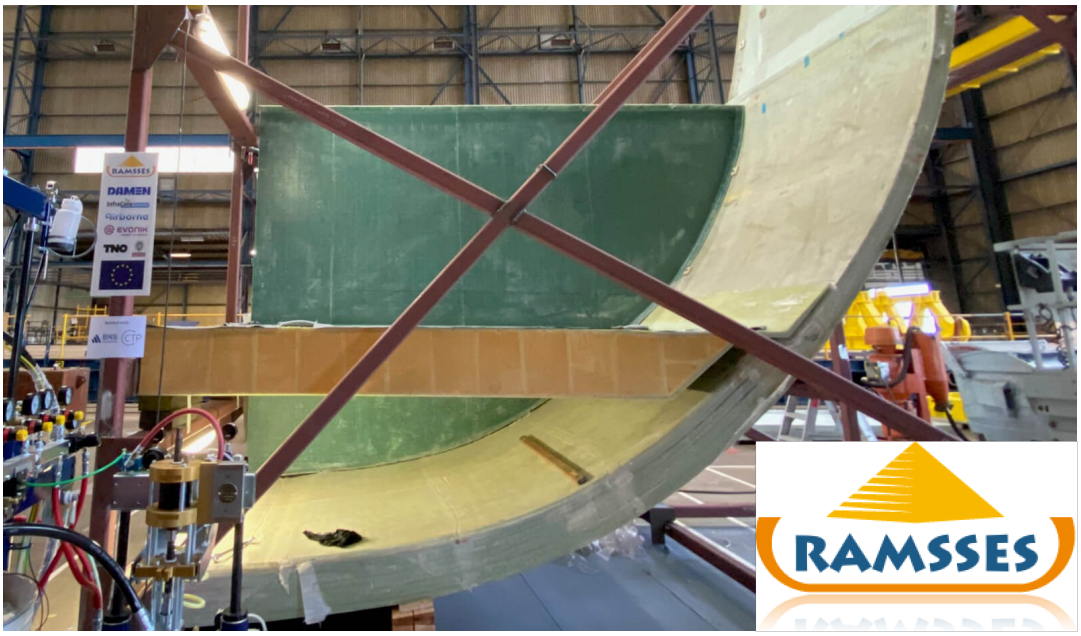

FIGURE 1.6: Composite hull demonstrable extracted from the RAMSSES project [5].

5. "FIBRESHIP, Engineering, production and lifecycle management for the complete construction of large-length FIBRE-based SHIPs", [6], a project that aimed to provide the necessary technology to build long-length ships completely made out of composite. Figure 1.7 shows the demonstrable section of a fishing boat and a fire collapse test of the bulkhead.

FIGURE 1.7: Experimental testing extracted from the FIBRESHIP project [6].

Indeed the work encompassed in this thesis emanates from the H2020 project FIBRESHIP sponsored by the EUROPEAN COMMISSION under the grant agreement 723360 "Engineering, production and life-cycle management for complete construction of large-length FIBRE-based SHIPs". More details can be found in: www.fibreship.eu/about.

> The main objective of this project, the H2020 project FIBRESHIP, has been to develop the knowledge and technology required to enable the building of the complete hull and superstructure of large-length ships in composites. This thesis describes the research performed within the scope of the H2020 project FIBRESHIP in the development and validation of a thermo-mechanical model to assess the fire performance of composite structures.

The justification on the interest of the current topic, that is, providing a thermo-mechanical model that can incorporate thermo-chemical degradation coupled with an elastic damage model, using a micro-macro scale approach in order to provide a reliable failure criterion, is found on the several attempts from a prior project which would not be able to include as many non-linearities to the thermo-mechanical model that is proposed in this thesis.

Moreover, the scientific diffusion of the ideas and theoretical framework detailed throughout this thesis is especially backup from the perspective that was necessary in order to culminate the fire-collapse assessment required in the H2020 FIBRESHIP project.

1.3.1 Selected Solution

Within the scope of the present dissertation, the mechanical model selected belongs within the *mean field methods* family and in particular, it is the so-called **Serial-Parallel Rule of Mixtures** (**SPROM**) formulation developed by Rastellini et al. [15] which fundamentally has been developed for solids and little validations have been made in the field of laminated shells and/or beams. This model will be making use of the so-called **Isotropic Damage model** published by Simo and Ju [17] and further explained by Oliver [32] to characterise the desired rheology.

The thermal model will be based on the work done mostly by Henderson et al. [11, 19] and described in Mouritz et al. [7]. The simple solution proposed by Wickstrom Ulf et al. [28] will be used to prescribe the thermal boundary conditions.

In order to take into account the flexibility of composites, this thesis proposes a non-linear geometric theory based on the approach of Felippa and Haugen [18]. By using this interesting formulation for triangles, the proposed thermo-mechanical solution is unique in the sense that can address topics such as non-linear constitutive and geometric analysis of composite shells exposed to fire.

1.4 Objectives

The previous sections have shown the interest in using FRP in the maritime industry and the clear advantages that these have shown, not only in the mechanical response, but as thermal insulators. However, composites are considered much like heterogeneous media than as homogeneous materials. The major inconvenience is that most of the approaches to simulate failure in composite materials use the homogeneous material approach rather than a micro-macro approach.

Using a homogeneous approach just only to predict mechanical failure has proven to be inaccurate, imagine when adding to the mix failure combined with a) mechanical failure and b) thermo-chemical degradation. The current paradigm is not enough robust or accurate for a commercial solution. Thus, there are only two multi-level approaches that provide a certain level of assurance, the homogenisation and the mixing theories. These theories obtain the composite behaviour from the constituent behaviour by a set of rules that describe the constituent-to-composite behaviour.

Within the scope of multi-level formulation, one that is simply coupled is the SPROM [33] that acts as both a constitutive manager and a constituent-to-composite function. However, this theory is only a mechanical theory and certain modification have to be introduced to extend its capabilities to simulate composites exposed to high temperatures. This last theory has been coined as a *thermal serial-parallel rule of mixtures* (TSPROM).

The other aspect is the thermal model, since the mechanical model is for shells, the distribution of temperature through-thickness is needed. I.e., the thermal model shall be a one-dimensional heat transient model that can introduce pyrolysis. Pyrolysis is a thermo-chemical degradation process, it is simply that composites can *burn*, more complexly does not specifically imply burn, but evaporation or degradation of the polymer matrix.

The approach that is most suitable for this task is the one introduced in [11]. However, this approach only takes into account the composite and not the constituent materials. This means that this theory shall be adapted to use the rule of mixtures to describe the composite thermal degradation and evolution from the constituent point of view.

Therefore, the main objective of this thesis is divided into three objectives. First assessing the capabilities of the Henderson et al. formulation, second assessing the capabilities of the SPROM emphasizing the mechanical failure and third the assessing of the capabilities of the thermo-mechanical model putting emphasis on the thermo-mechanical failure.

Note that this thesis's main purpose is to produce numerical solutions and the implementation of those. An enumeration of the different objectives is given below.

1.4.1 Thermal Model

1. Provide and implement a constituent formulation of the Henderson et al. equation.
2. Provide and implement a simple approach to introduce the fire as thermal boundary conditions.
3. Assess the correctness of the implementation of the thermal model.

1.4.2 Mechanical Model

4. Implement the isotropic damage formulation.
5. Implement the SPROM formulation.
6. Assess the correctness of the implementation of the mechanical formulation.
7. Address the flexibility of composites.

1.4.3 Thermo-mechanical Model

8. Provide and implement a methodology to incorporate the thermal dependence on mechanical properties.
9. Provide and implement a correction to the damage theory to be coherent with the thermal effects.
10. Provide and implement an enhanced version of the SPROM. The TSPROM.
11. Provide and implement the thermo-mechanical coupling.
12. Assess the correctness of the thermo-mechanical model.
13. Demonstrate the capabilities of the thermo-mechanical model applied to marine structures.

The ulterior motive of these implementations is non-other to contribute to the scientific community and to provide the marine industry with an efficient and optimal tool to perform numerical analysis of ship structures. All the formulation detailed in this thesis has been implemented in the Ramseries commercial software of COMPASS I.S. jointly with the International Centre of Numerical Methods in Engineering (CIMNE) to accomplish the technical requirements within the EU H2020 FIBRESHIP project.

Besides these objectives, secondary related objectives have been proposed. I.e., the diffusion of the research throughout dissemination in international congresses or paper submissions.

1.5 Outline of the thesis

The thesis structure will be based much on the structure proposed by Perry in [34] with the title 'A Structured Approach for Presenting Theses' with some minor changes.

The main objectives of this thesis were defined in the previous section, *(1)* assessing the capabilities of the Henderson et al. formulation, *(2)* assessing the capabilities of the SPROM putting emphasis in the mechanical failure and *(3)* assessing of the capabilities of the thermo-mechanical model putting emphasis in the thermo-mechanical failure.

Nevertheless, since these three main goals are broad enough by themselves, a better division of these objectives is given divided into chapters, so the reader can follow them easier. A total of 6 chapters are provided, not including the introduction itself. Three chapters are devoted to the theoretical framework that addresses the three main objectives, and a numerical result chapter is included in chapter 6 to demonstrate the assessment of certain minor objectives described in the previous three chapters. Following the guidelines of Perry, a chapter devoted only to the analysis of the literature review is provided in chapter 2. The last chapter chapter 7 is devoted to the conclusion extracted from this thesis.

In the following paragraphs, a description of the structure of each chapter has been provided. Note that each chapter detailing the main three objectives follows the pattern proposed in [34]:

1. Abstract: it starts with a brief abstract of the chapter.
2. Introduction: the introduction to the chapter.
3. Discussion of the main aspects: justification of the paradigm and chosen solution.
4. Research procedures or methodology: detailed breakdown of the different formulations used to describe the model.
5. Conclusions: summary of the main ideas and reflection of the advantages of the solution chosen.

1.5.1 Chapter 2 - Literature Review

This thesis uses an approach to concentrate all the literature research in a chapter. This chapter attempts to capture all the consulted literature and the methodology used to extract and objectively perform the research. The research cited in this chapter tries to follow a historic review of the evolution of the paradigm, all the significant and accessible contributions are enlisted with a brief definition of their contribution. The main authors that have contributed to the paradigm are as well analysed. Different infographics are attached to give the reader a better understanding of the evolution of the paradigm in question, and a very specific discussion is performed by classifying the analysed literature into several categories. The division of categories adds an interesting perspective for the reader to understand the change in trends and migration of the paradigm.

A note is issued to the reader, this chapter is solely devoted to analysing the paradigm of research through the lens of the literature revised. The author of this thesis has to state that there might be a certain bias towards the fields nearby the main topic of this thesis, *the laminated thermo-mechanical approach for marine applications*, and it may be advisable to the reader that potential literature might have been ignored based on this bias.

The second note is to inform the viewer that this chapter contains further, more information, than the actual literature review found in the core chapters (chapter 3, chapter 4 and chapter 5). The broader literature review is justified in [34] by the need to find the optimal solution to the hypotheses and the problem posed in chapter 1. Nevertheless, a much narrower description of the significant literature, is given in each respective core chapter, in particular this concise literature review is found in the sections of introduction and justification of the paradigm for each of the core chapters.

The structure of this chapter, chapter 2, starts with a brief introduction of what is the *paradigm* and what compounds it. Then it moves to the review of *parent disciplines*, in specific, in which the reader will find the introduction to the *thermal* and *mechanical* topics. Then the *immediate discipline* is introduced, by immediate [34] considers introducing those fields that intersect or neighbour the main disciplines. In this case, the *thermo-mechanical* topic is considered to be the children of both the thermal and mechanical model, and consequently, it is described in as the last.

1.5.2 Chapter 3 - Modelling fire in marine structures

The chapter starts with an introductory description of it and a justification of the chosen paradigm and methodology. Then the research methodology is broken down. This section is subdivided into three subsections, the first is to express the thermal problem from the point of view of continuum mechanics, considering the heterogeneous micro-structure as a homogeneous media in the macro-scale. The three equations of classical continuum mechanics are introduced: *mass balance*, *conservation of linear momentum* and *energy balance*.

The second subsection is devoted to breaking down the concept of the continuum to heterogeneous media. This is fulfilled by the species transport theory. Again the three equations are introduced (*mass balance*, *conservation of linear momentum* and *energy balance*), but this time they are referred to as the solid and gas phases. The third subsection serves as a nexus between the constituent and phase description and the composite as a whole, here the different simplifications are introduced to fulfil the constitutive thermal laws for composites exposed to high temperature.

The last section, conclusions, is devoted to reviewing the initial ideas and the achievement of those throughout the proposed formulation.

1.5.3 Chapter 4 - Constitutive modelling of laminate composites exposed to fire

The chapter starts with an introductory description of it and a justification of the chosen paradigm and methodology. Then the methodology is explained, and the section is subdivided into three subsections, first the constitutive modelling of shells as homogeneous media is examined. This analysis is focused on the constitutive laws at the micro-structure for fibre and matrix components. The models employed at this level are basically the *isotropic elastic mode*l and the *isotropic damage model*.

The second subsection is devoted to the constitutive modelling of composite shells, i.e., the heterogeneous media at the macrostructure level. The concept of homogenisation is explained from the different approaches available in the literature, and then a micro-macro scale approach in the field of the *classical mixing theory* is selected. The linear approach is based on the *orthotropic formulation*, and the non-linear analysis of composite shells is shaped in the form of the *serial-parallel rule of mixtures*. The third subsection focuses on the modification of the previous theories to introduce the effects of fire and thermal effects. Both at the constituent and composite levels. The most important contribution, found in this section, is the derivation of the so-called *thermal serial-parallel rule of mixtures*.

The last section, conclusions, is devoted to reviewing the initial ideas and the achievement of those throughout the proposed formulation.

1.5.4 Chapter 5 - Laminated thermo-mechanical coupling of marine structures exposed to high temperature

The chapter starts with an introductory description of it and a justification of the chosen paradigm and methodology. The methodology is subdivided into six subsections, the two first sections are devoted to the analysis of thin and thick shells, which in particular introduce the triangle and quadrilateral formulation used in the numerical section of this thesis.

The third subsection is the derivation of the weak form through the principle of virtual work to later move to the fourth subsection where the weak form is discretised, and appropriate expressions are given of the discrete quantities for triangles and quadrilaterals. Then after reaching the point of the numerical scheme used, certain considerations are taken to obtain a functional and tight formulation. One of the key problems, the inherent flexibility of composites, is treated in the next subsection. Then the sixth subsection is devoted to the summarisation of the coupling.

The last section, conclusions, is devoted to reviewing the initial ideas and the achievement of those throughout the proposed formulation.

1.5.5 Chapter 6 - Numerical Results

The chapter starts with an introductory description. Then it is subdivided into four sections, each one trying to answer the different assessment goals imposed in the

major objectives for the thermal, mechanical and thermo-mechanical models.

The first section is the thermal and serves as validation of the thermal model by incorporating a numerical benchmark. The second section is the mechanical and the numerical results provided are a tensile test, a flexural test and a demonstration of the correctness of the non-linear geometric formulation implemented to address the non-linear buckling failure. The third section is the thermo-mechanical. This section provides an analytical benchmark, an experimental calibration and a study of thermal buckling failure.

The fourth section is the marine application section. This section provides two numerical applications, one for a fluid-structure interaction of a CFD solver to obtain the thermal boundary conditions introduced in the thermal problem coupled with the thermo-mechanical tool developed. This example is focused on the analysis of the superstructure of a container ship. The second example is a study of inelastic thermal buckling of a structural section of the same container ship. This example also illustrates the potential of this tool to address the required concept of *steel equivalent* design that is required for certification.

1.5.6 Chapter 7 - Conclusions and implications

The chapter starts with an introductory description. Then it is subdivided into eight sections. Since each chapter has its own conclusions, this chapter is devoted to extractingt more general conclusions from the thesis.

The first section concludes the research questions previously mentioned. The second delves into extracting the conclusions for the research problem. The third section considers the implications for the theory, and the fourth the applications that this research has had in the scientific community. The fifth discusses the implications for policy that the research conducted in this thesis may have, and then the sixth comments the limitations present in the proposed methodology.

The seventh discusses the further research that can be done by extending the fundamental concepts explained in this thesis. Finally, the eighth section is devoted to the enumeration of original work that has been produced in the confection of this thesis.

1.6 Conclusion

This chapter laid the foundations for the thesis. It has introduced the research problem, the research questions and the hypotheses. Then the research was justified, definitions were presented, the methodology was briefly described and justified, the thesis was outlined, and the limitations were given. On these foundations, the thesis can proceed with a detailed description of the research

Chapter 2

Literature Review

This chapter is devoted to the sole analysis of the literature review of this thesis. Providing statistical data to analyse the evolution of the paradigm through time. The chapter is very extensive, thick and elaborates a discussion of the different contributions found in the research of this thesis. The reader is suggested to be guided by the pertinent introduction of each field of research and to use the infographics to obtain a more illustrative idea of the quantity of data analysed.

This section reflects the careful investigation and materialisation of it. Albeit the entirity of the research is portrayed in this section, in the core chapters dealing with the theoretical framework posed in this thesis, a reduced literature review tailored for the confection of each chapter is given.

Although it might seem redundant to add this narrow literature review at the beginning of chapter 3, chapter 4 and chapter 5, particularly when this chapter extensively covers it, it has seemed a better solution to provide the reader with a more specific literature review in the form of a prologue in each of the mentioned chapters.

2.1 Introduction

In the process to solve the intrinsic questions: (1) *What are the existent one-dimensional non-linear transient heat models for composites exposed to high-temperature?*, (2) *What are the current mechanical models to predict the failure of composites? Especially those using a micro-macro scale approach.* and (3) *How both thermal and mechanical models are coupled and which are the dependencies induced by one with the other?* The intersection of all of those questions lies in the branch of *laminated thermo-mechanical* models.

To provide a consistent methodology to analyse the best literature existent in the branch of *laminated thermo-mechanical* modelling, the set of different parent fields are needed to be identified. The branch of *laminated thermo-mechanical* modelling is the intersection of three disciplines: *composites*, *mechanical* and *thermal* modelling.

A priori, the mechanical and thermal modelling encompasses a vast and endless ramification of branches that is inexorable of being researched. Objectively, the study should be limited to those solutions that are connected to composite materials, especially those focused on FRP materials.

Nevertheless, composites are advanced materials and not all may fit in the application to marine structures, it has sense to limit the scope to especially those publications that belong to the field of *ship design*.

Objectively, the literature review has to be centred around a) *laminated thermal* and b) *laminated mechanical* models. The optimal laminated thermal model should be one that can be atomised, i.e., to solve the underlying physics at the micro-structure level. This particular case of the thermal model is found in the intersection with the field of *species transport* theory applied to thermal problems. Moreover, in the intersection of the research focused on composites and thermal modelling, especially for FRP composites, there is a branch of science that studies non-linear effects such as *pyrolysis*.

For the mechanical laminated model a similar constraint is applied, since it requires that the failure is assessed at the micro-structure level and also to link it to the composite macro-scale level, a branch of study that intersects with this would be the *mixture theory*. One last area of research that should be considered should be the *testing* field, this is necessary to contrast and validate the existent methodology with real applications.

This argumentation leads to the graphic shown in Figure 2.1. The primordial three categories are the *composites*, *mechanical* and *thermal* modelling; and in its centre there is the specific topic of investigation (*laminated thermo-mechanical* modelling). The *species transport* can be introduced in the thermal modelling, and the *pyrolysis* includes both the composites and the thermal modelling. The union of mechanical and composite modelling is found in the *SPROM* theory, which is a specific extension of the *classical mixture theory*. There are two neighbouring fields, the *ship design* and *testing*.

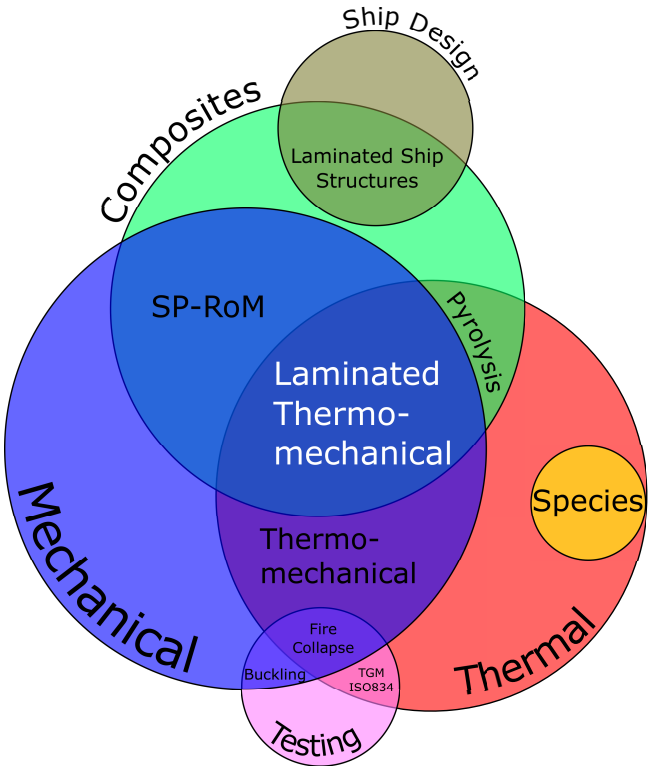

FIGURE 2.1: Venn diagram of the intersecting areas of analysis.

The research partition where *buckling* appears could also contain *damage* modelling as well, the intersection between thermal and testing contains experimental testing to obtain thermal properties, and also testing of empirical formulation to introduce the boundary conditions (fire curves). The intersection between the *thermo-mechanical* field and the testing spawns a topic that is regarded as *fire collapse*.

The topics and the schematic found in Figure 2.1 reflects the process of thought followed to initiate the research. Focusing more effort on those areas that are bigger. Indeed, the bubbles found in Figure 2.1 are non-arbitrary, the sizes correlate to the number of citations reviewed and cited in this thesis. So to be clear, the graphic, depicting the different areas of research consulted and their size, is an illustrative reflection of the result of how this chapter was weaved through time. Starting from defining the main research fields (*composites*, *mechanical* and *thermal*), to spot the intersection regions and constraining the research to scientific research of the adjacent neighbour fields (*ship design* and *testing*).

At the end of the analysis, some major, influential literature has been identified. For the laminated thermal model, the research of Henderson et al. and [20] is of crucial importance and has an impact on modern applications. In the field of laminated mechanical modelling, this thesis founds contributions of extreme importance in Oñate, Rastellini and Felippa and Haugen. The field of thermo-mechanical modelling is a mixed contribution from previous ideas imposed by the thermal and mechanical model of composites and the novel contributions from this thesis.

2.2 Thermal Model

The structure of the literature review in this subsection will follow a historic timeline in order to better interpret the evolution and specialisation of the paradigm in the research topic of *thermal modelling*. The literature review presented in this subsection has been extracted from the analysis of the available references in [7], which is the latest complete literature review of the paradigm and analysis of composite structures exposed to fire.

The major identifiable and unique subfields, which the topic of *thermal modelling* encapsulates, can be readily assessed in Figure 2.2. The diagram is presented in terms of decades and clearly identifies three major milestones: *Wood Pyrolysis Model*, *Composite Thermal Model* and *Compendium Book*.

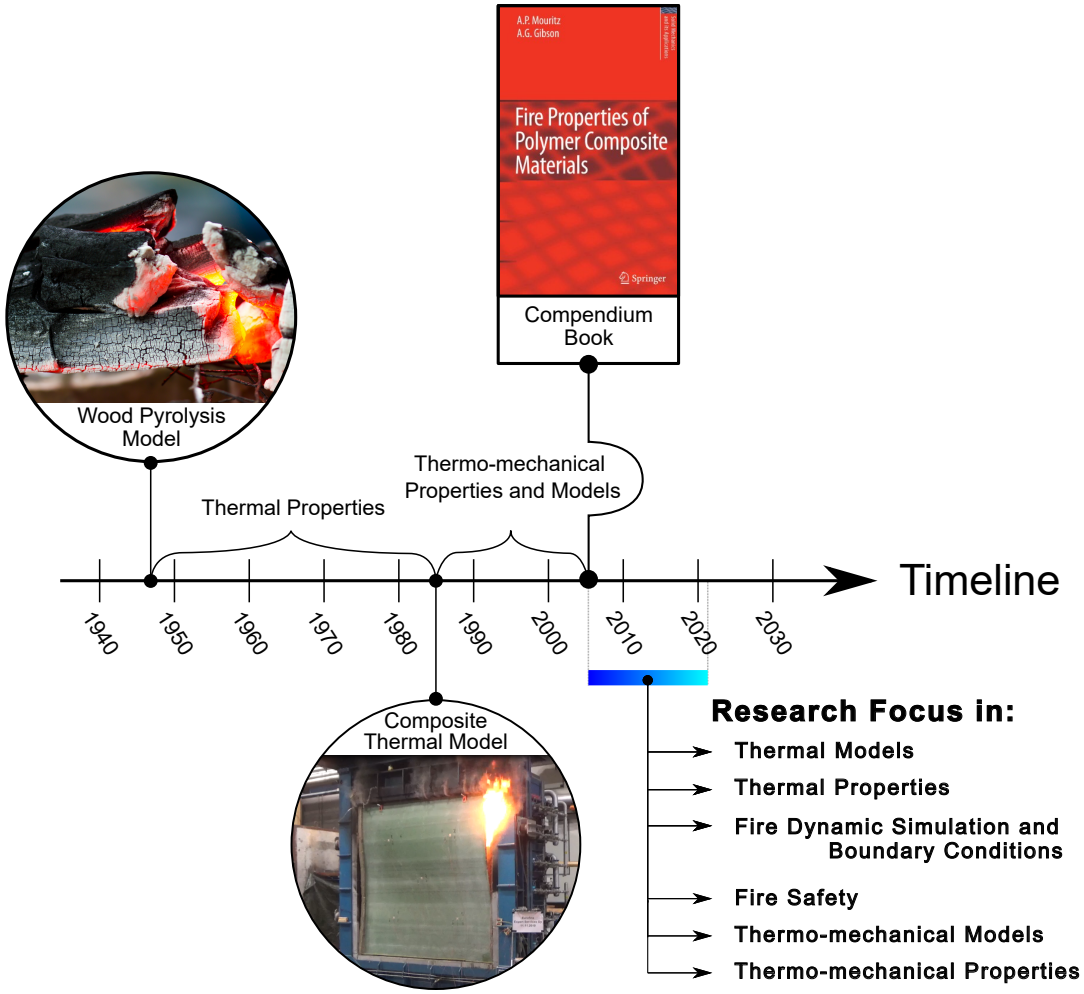

FIGURE 2.2: Road map of the research of fire and composites.

The first thermal model to be produced had the aim to reproduce the governing equations of wood when burnt. The model was a one dimensional model and the non-linear thermo-chemical degradation process called *pyrolysis* was introduced and modelled. This model is published in [35] by Bamford et al. and was enhanced in posterior decades by multiple authors [36, 37, 38]. Wood can be considered a special type of composite, not a *fibre reinforced laminate* one, however still fits the category of

composite material due to its thermal resemblances to the thermal governing equations of fibre-resin materials.

After the first milestone, the research focused also on the production of data of interest to characterise the thermal properties of different composite materials. The second milestone was the one that involved the postulation of the first one-dimensional non-linear heat transient problem for composites exposed to one-sided fire. This model is the so-called *Henderson model*, a name that originated from all the research carried out by Henderson et al., who made a significant breakthrough in the paradigm of laminate composites exposed to fire. This model can be found in [11] together with some experimental validation cases. The model is the foundation of many posterior models, and it lays down the main concepts regarding *pyrolysis* in composites.

A posteriori, many authors used this same model to produce explicit or constitutive governed thermo-mechanical models and relied on experimental data to characterise the thermo-mechanical properties needed in their formulation. Then two fruitful authors in the field, Mouritz and Gibson, published a book that would portray the principal research done regarding fire and composites with the title *Fire Properties of Polymer Composite Materials* [20]. The fact that this book covers and compresses most of the literature published until that point, has given it, the spot as the third milestone, the different topics covered in this book encompass topics such as thermal and thermo-mechanical degradation models and experimental calibrations, fire study and safety and the models used to characterise fire in terms of fire dynamics and boundary conditions for the different thermal models.

The posterior research, after this book was published, cemented mainly in finding optimal solutions to both thermo-mechanical and fire dynamic analysis of large composite structures exposed to fire and to provide better understanding of their behaviour by experimental testing.

This historiography is portrayed by Mouritz et al. in [7], which covers an extensive valuable literature that can be broken into two sets, *thermo* and *thermo-mechanical*, and because this subsection is dedicated only to the critical review of the significant research in the field of thermal modelling, the literature is a constraint to this sole scope.

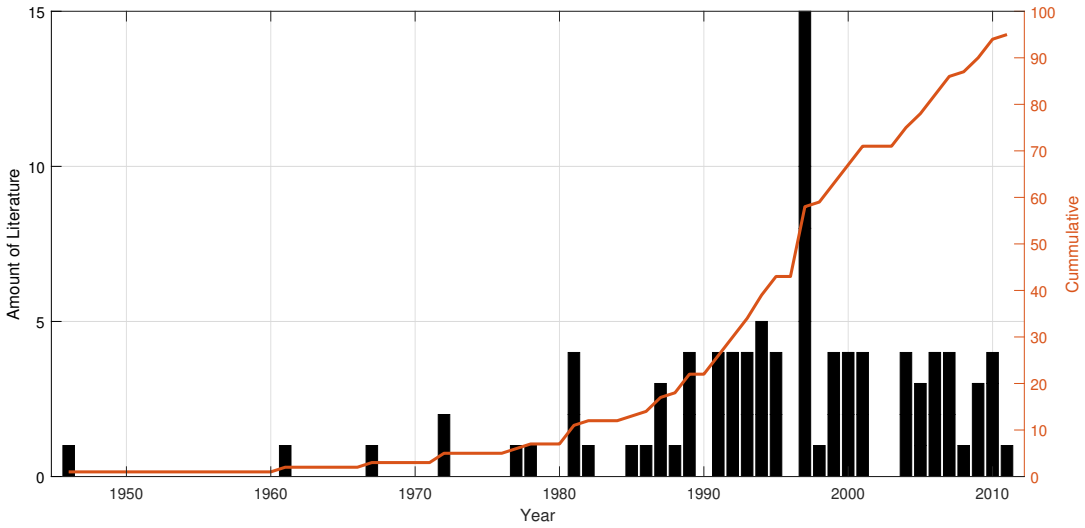

FIGURE 2.3: Bulk research contribution to the topic of thermal modelling of composites. Extracted from [7].

The available contribution to the field of research was extracted, post-processed and presented in Figure 2.3, showing an exponential bulk growth in the research produced in this field and this is intrinsically linked to the fact of the growing general interest in the topic by the scientific community.

The major contribution can be localised within the past two to three decades. This shows that only for thermal related research, almost a total of 90 research items have been produced. Note that these number is obtained according to [7], which dates back to 2009, and also understand that only the research available has been included, leaving several research publications out of the scope of this literature review.

Although [7] is a very complete overview of the paradigm, it is not sufficient for the scope of this thesis and is used as starting point to do a more careful and accurate review of the state-of-the-art contributions framed in the present. It is with the interest of updating and extending the previous literature review that the scope has been extended including the most recent research by what are considered *pivotal* and *modern* research authors found in the very same literature review from Mouritz et al., together with some other non-cited authors.

The *pivotal* authors considered are: *Mouritz*, *Feih*, *Gibson*, *Henderson*, *Sullivan*, *Dimitrienko*, *Asaro and Gu* and *Luo and Des Jardin*. Other pivotal authors such as *Lattimer*, *Lua* or *Mathys* were under the scope, but because they were commonly published together with some previous authors, they are ultimately excluded from the search since they are already reflected by the chosen authors.

Mouritz seems very proficient in the field and specifically has incorporated many types of thermo-mechanical models into the research field, especially putting emphasis on the research of thermo-mechanical constitutive laws. A vast range of his contribution focuses on the dissemination of experimental data useful in the calibration and validation of thermal and thermo-mechanical models.

Feih has contributed significantly in the same areas as Mouritz, indeed it is common to find them both as co-author of relevant articles in the field. Albeit, Mouritz has

a significant contribution in the thermal aspects of the paradigm, Feih is more notorious in the thermo-mechanical aspects of that, therefore she will be not as much represented as Mouritz in this section. A similar case is Gibson, who frequently publishes with Feih and/or Mouritz and has been focusing on the experimental characterisation of passive protective systems lately.

Individual authors that have had an important impact on the field of research are Sullivan, who was one of the earliest researchers trying to deal with many aspects of the paradigm. Specifically, Sullivan has tackled the problem of modelling the fire dynamic governing equations and also implementing thermo-porous-mechanical models that address the *porosity* of the polymer matrix [39, 40, 41, 42, 43, 44]. Although, due to its early contribution, it is imaginable that in the last decade there are no publications by this author or co-authors.

The other individual, whom there is an active track in the research field for the recent years, is Dimitrienko who has a similar profile as Sullivan but does not belong to the same nucleus or cluster of authors. Dimitrienko has interesting contributions regarding thermo-porous-mechanical models and even considering the inner radiation effect that is not generally addressed in the literature itself. The other aspects this author has covered recently are those regarding fire dynamics and very interestingly the effect of ablation of composite materials. Dimitrienko has emphasised the thermal stress terms that arise from the energy balance equation, which are not customary taken into account [45, 46].

Asaro and Gu are another cluster of authors who have been devoted to the analysis of thermal-buckling. Thus are neglected in this subsection similar to Feih. Luo and Des Jardin were important researchers found in the review from Mouritz, however, there is no significant available contributions by them after the review was published.

Consequently, a new chart that extends Figure 2.3 has been provided and can be found in Figure 2.4. If both charts are compared, the first thing that can be seen is that the amount of research produced during the last decade is around 10%, and that the tendency has considerably stagnated. Indeed, the contributions are due to different available data that was not considered in the previous review.

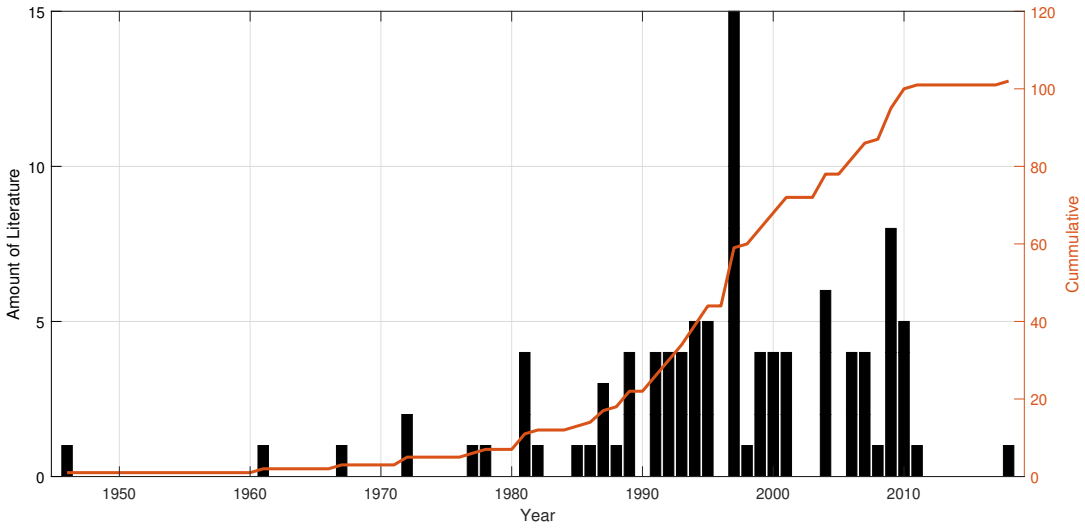

FIGURE 2.4: Bulk research contribution to the topic of thermal modelling of composites.

This tendency can be explained by the fact that the current research is not primarily focused on the development of thermal models or thecharacterisation of thermal properties for one-dimensional heat transfer problems. Indeed, using the methodology proposed, in order to update the literature review of Mouritz, is certainly biased. This can be explained by the fact that the literature review published by Mouritz prioritises the research closer to the pure thermo-mechanical analysis rather than those publications that encompass the fire dynamic analysis, which indeed has peaked during the last two decades.

The need to classify the set of publications that belong to the subfield of *thermal modelling* is crucial in the analysis of the global paradigm and its evolution. In that sense, the topic can be divided into four different sets: *Fire Dynamic Simulation (FDS) and Boundary Conditions (BC)*, *Fire Safety*, *Thermal Properties* and *Thermal Modelling per se*. Nevertheless, note that there might be certain publications that fit in one or more of the previous four sets or could belong to another specific set of their own. The publications used in the generated database are to be classified under one of these four sets by considering the set that is most predominant, in terms of percentage, in the publication. Given the methodology to categorise the publications in the aforementioned sets, a brief description of them is given in the next paragraphs.

Fire Dynamic Simulation (FDS) and Boundary Conditions (BC) is the set that collects all the research done towards the realistic simulation of fire, fire-spreading, flames, combustion, smoke, toxicity, and experimentation that is conducted with the sole purpose to obtain a better understanding of the fire scenario or thermal loading. The boundary conditions can be interpreted as a particular post-process of the fire dynamic simulation since generally are obtained as a result or at least intertwined with the latter.

Fire Safety are all those contributions that have the aim to help in the design of building composite structures resistant to thermal loads. Also, to the quantification of the risk involved in fire scenarios. These publications do not necessarily have the scope of creating or checking the regulations necessary to be enforced in the manufacturing of composite structures.

Thermal Modelling is the most extended topic and encompasses all the publications that direct their effort in the understanding of the thermal governing equations involved in re and composite. Also, publications that aim to understand the thermochemical degradation processes characteristic of composites materials exposed to high temperature or those publications that describe the issues arising from a porous media such as a polymer resin. Another key aspect taken into account in this category is the gas transfer and ow originated from the decomposition of the polymer matrix of the composite.

Thermal Properties is the research directed towards the calibration and characterisation of only the thermal properties of composites, bres or matrices. Generally, the properties can be thermal properties such as the thermal conductivity, heat capacity or thermo-chemical properties such as pyrolysis, activation energy, polymer degradation energy, reaction characterisation or any others needed to describe any variable in a thermal model (pressure, toxicity, convection surface coefcient, ignition or glass transition temperatures, etc.). This category is vastly represented by those publications that have a signicant contribution in terms of experimental testing.

Once the categories are defined, a detailed analysis of the contribution to the research is presented in Figure 2.5. The first ranked category in terms of the amount of publications is *Thermal Properties*, being especially prominent during the 90s. The second most published is the *Thermal Model* category itself, followed by the *FDS and BC* and at the bottom are publications that revolve around *Fire Safety*.

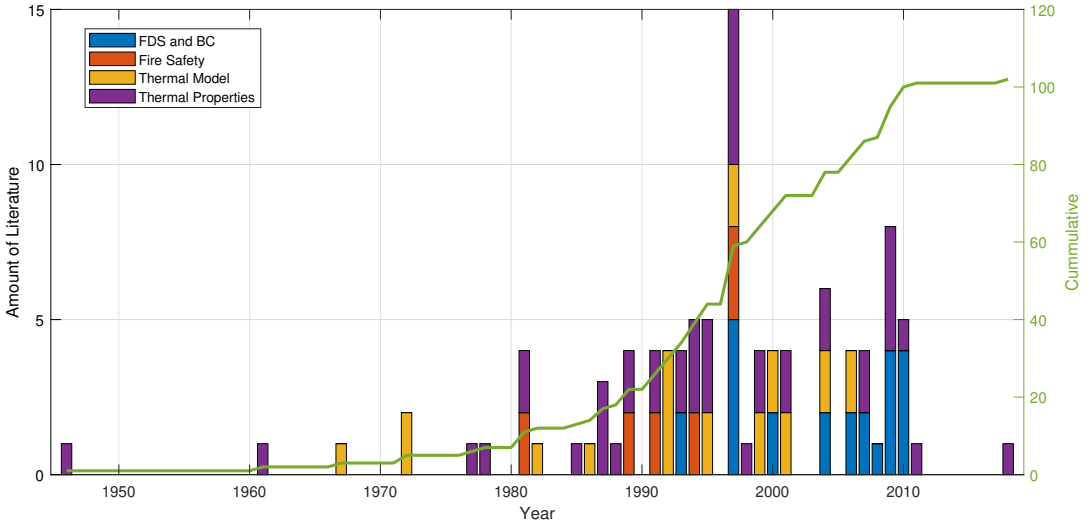

FIGURE 2.5: Research contribution to the topic of thermal modelling of composites.

The next step in the analysis of the paradigm is to delve into the analysis of the four sets of categories shown in Figure 2.5. Thus, the paradigm is indeed divided into four topics or paradigms. A carefully historic evaluation of the sources used to conform the database described previously is proportioned in the following paragraphs, note that the different underlying aspects will be pointed out during this historic review.

In addition, some publications that were found in the conformation of the work described in this thesis shall be included. Note that these publications are not reflected

in the charts provided, since they are found by other means than just updating the review from Mouritz.

2.2.1 Fire dynamic simulations and treatment of boundary conditions

The first publications devoted to the study and analysis of fires in composite structures are presented by Tewarson and Macaione in [47] and describe a series of experimental tests to characterise parameters such as heat flux, mass loss and rate of volatiles, generation of fire products, CO_2 for different composites made out of glass fibre-polyester and kevlar-phenolic constituent materials.

Then Grenier et al. in [48] attempt to characterise fire, ignition, heat release rates and smoke production, and to model the heat flux boundary conditions for marine sandwich materials. This research is further extended by one of the co-authors in [49]. Lyon et al. published [50] a detailed article describing several experimental data in terms of ignition, heat release rates, smoke, CO_2, etc. And established different analytical models and laws useful to obtain the aforementioned data, making a special effort in the modelling of the expression of heat flux.

One of the most significant contributions in terms of analytical modelling and design of fire was introduced by Lattimer and Campbell in [51], who covered a vast range of the issues arising from fire and composites. The underlying concepts explained in [51] are the starting point used in this thesis to model the boundary conditions.

The introduction of CFD methods to model fire, dates before the following publication, however, the first found in the initial literature review is attributable to Xie and DesJardin in [52] that described a 2D CFD applied to fire dynamics. This research is further enhanced in [53].

In parallel, Mouritz et al. published an extensive review on smoke toxicity in [7] and emphasis has to be made that this publication comprehends an incredible number of publications that deal with the fire dynamic simulation and boundary conditions modelling *per se*.

One of the most important publications in the CFD modelling of fire dynamics is the publication of Mcgrattan et al. in [9], which describes the theory of a fire dynamic simulation model. Albeit this is the last publication, it offers a skewed vision of the contribution of Mcgrattan et al. because it only shows the latest available reference manual that coincides with version 5, when the first version published dates of 2013. The reference manual for FDS – an open source CFD developed by Mcgrattan et al. – cites over 60 publications that are not necessarily reflected in this literature review.

In summary, it can be said that the paradigm has evolved from an empirical framework to a numerical one. Empirical data is still needed to characterise the fire for certain materials or material combinations, although as the pass of time advances, there is more information published regarding this characterisation and the efforts of the research community moves toward improving the numerical methods available today.

The other important aspect shown in the contributions is whether the characterisation of fire is performed by empirical, numerical analyses or a combination of both,

the resultant information is used to prescribe the thermal boundary conditions. This aspect needs further discussion, as the contributions provided until this point do not offer enough information.

The paradigm of thermal boundary conditions finds its origins in the experimental evaluation of fire scenarios to establish what is coined in the literature as *fire curves*. This methodology is extended to the point of standardisation and can be found, and widely used, in modern design. The most notorious curves are the ISO 834 [55], a very well-known fire curve found in civil engineering, and the Hydrocarbon and Modified Hydrocarbon fire curves, which are very standard in marine environments. Both curves establish the heat flux as a function of the time in terms of temperature.

As the modern paradigm of fire dynamic simulation has evolved to be more reliant on numerical simulations, several heat flux models have appeared in terms of temperature. Note that in engineering, temperature is one of the most natural state variables to work or describe a domain. One of these models, referred to by its author name, was proposed by Quintiere in [56]. The underlying problem that researchers dealt the most with was the fact that in a fire scenario, the temperature of the source is not the same as the heat transmitted by convection than radiation. Thus, the paradigm was centred on establishing a set of equations that described different temperatures for each source of heat and their relationship.

The research of Quintiere was upgraded by Janssens, which was especially describing the phenomenology of composite materials, in [57]. However, it was Wickstrom Ulf et al. in [28] that revolutionised the treatment of boundary conditions by the introduction of the concept of *adiabatic surface temperature*, which simplifies the problem of having to consider two different temperatures for the radiation and convection sources.

2.2.2 Fire safety

The low amount of publications is due to excluding publications that directly treat fire safety from a legal point of view rather than engineering design. In that sense, one of the first available articles by VENTRIGLIO that discusses the foundations of *passive fire protection* is [58], the article covers the research projects, the majority of which are linked to navy programs. These projects deal with the study of fire safety and risk, deepening in the study of materials, and specifically, in their hazard and resistance against fire. Another posterior paper that discusses materials for fire safety can be found in [59] by Allison et al..

An interesting article was published by Egglestone and Turley in [60], describing the risks of fire for glass reinforced plastics in ship superstructures, and Sorathia et al. published a more detailed summary of the different aspects affecting fire safety in [61]. This set is one of the smallest in comparison to the others. The paradigm concentrates rather on quantifying the risks associated with common shipbuilding materials than structural passive systems.

2.2.3 Thermal modelling

The first author to tackle the heat transfer problem was Bamford et al. in [35], in this publication the authors propose the first model for a composite. In this particular case the composite is wood and the model proposed has a certain resemblance to the modern one-dimensional non-linear heat transient models, however, it did not deal with the gas transfer nor did take into account polymeric degradation.

Further, attempts on enhancing [35] are found by Kung in [36], where a first attempt to model pyrolysis, using an Arrhenius law, was employed. This model takes into account as well the polymeric degradation, or in the particular case of wood, the generation of vapours. This model is very useful for dry wood structures. In parallel, a similar article is published in [37] by Murty Kanury. Only 5 years afterwards, Kansa et al., publishes [38], which also incorporates the model, the treatment of boundary conditions as a forced convection heat flux. Fredlund in [62] (1993) is the last publication dedicated to wood structures and fires. From this point onward, the paradigm for wood materials is encompassed inside composites.

In 1985, the first one-dimensional thermal model for composites is published by Henderson and Hagen in [63], the model is enhanced in [19] and can be considered the foundations of many of the actual models for fibre-reinforce plastic laminates. Henderson and Hagen contribution is detrimental to the development of the paradigm, which at the moment was only focused on wood structures exposed to fire.

Sullivan and Salamon reformulate the Henderson model in [40] to produce a monolithic solution that includes temperature and to lay down one of the first thermo-mechanical models. In parallel, Mcmanus and Springer presented in [64, 65] another thermo-mechanical model. These publications are included in this set since they modify the Henderson model to introduce the pressure and porosity terms, respectively.

The paradigm at this stage is focused on the new materials or advanced materials that are introduced in composite structures, starting with the glass-reinforced plastic laminates. Dimitrienko [66] introduces a thermal model that deals with the thermal stresses which often were neglected, and a third model derived from Henderson is presented in [67] by Looyeh et al. . This third model was applied to glass-reinforced plastic (GRP) materials and offshore structures. A fourth thermal model is presented by Dodds et al. in [68] and Looyeh et al. extend their previous work in [69]. The fifth thermal model derived from Henderson is found in [70] by Krysl et al..

Finally, in [20] by Mouritz and Gibson, one of the most important books is published that summarises most of the current methodology and paradigm regarding composites and fire. The modern paradigm is heavily influence by the initial model proposed by [63] and the subsequent models extend this model in order to take into account different neglected terms. Although the actual paradigm has been focused on the issues arisen from thermo-mechanical coupling, there are few contributions regarding thermal modelling that are discussed in the following paragraph.

The paradigm has been recently, effortfully, focused on real-time simulation and the concept of *apparent thermal diffusivity (ATD)* has been introduced in the research of

Miano and Gibson in [71] and [72] to try to obtain explicit solutions for the one-dimensional heat transient problem postulated by Henderson and Hagen.

2.2.4 Thermal properties

The first publication found regarding the characterisation of thermal properties for composite materials is found in [73], this publication is not solely experimental but is accompanied by an analytical description of the found experimental behaviour.

Springer and Tsai present a study of the conductivity of unidirectional materials (fibre-reinforced materials) in [74]. Conductivity characterisation is one of the main efforts inside this set. With a similar intention Han and Cosner in [75] calculated the effective thermal conductivity coefficient for FRP composites. The studies on conductivity calibration were followed up in [76] by OTT and HJ.

One of the first studies on thermo-chemical degradation for FRP was presented by HENDERSON J. B; TANT in [77]. Also, the effect of radiation and temperature distribution on composites was found interesting by Fitriah et al. in [79]. Authors such as James et al. [80] or Havis et al. [81] studied the conductivity of different FRP laminate materials. And other composite characteristics that may not be included in many thermal models, such as flammability, can be found in [82].

One important paper in the field of thermal calibration comes from Florio et al., who studied the thermo-chemical properties of composite materials exposed to fire in [83, 84]. This paper later came to be used in the validation of the so-called *Henderson thermal model*. Authors, such as Sullivan and Salamon, used instead the data found in [40] to calibrate their models.

More useful thermal calibration data was made available by Scudamore [85] who analysed specifically glass-reinforced plastic laminates or similarly by Brown et al. in [86]. Polymer resins gained popularity and were the object of analysis by authors such as Frassine and Pavan [87], who present different thermal properties for thermoplastic matrix composites or Tant et al. in [88] who analyse thermal properties for polymeric materials, Brown and Mathys [89] focused on glass-reinforced polymer plastics, extending their work from [86]. Other interesting data to understand key concepts such as size effects or flammability of certain resins, epoxy and phenolic, are provided by Ritchie et al. [90] or Hshieh and Beeson [91] respectively. The pernicious effects of pyrolysis in the failure of composites can be found in [92] by Dao and Asaro or the characterisation of the so-called glass transition temperature can be found in Mahieux and Reifsnider [93].

Other advanced material solutions have become popular in the designing of composites. E.g., the obtention of thermal properties of carbon fibre and comparison to glass fibre is presented by Kalogiannakis et al. in [94]. Asaro et al. [95] investigated the thermal properties of protective coatings in naval ship structures combined with composites, or Lattimer et al. in [29] studied the thermal response of several composites when exposed to high temperatures.

In a brief summary, the efforts of the scientific community have been driven by the

attainment of different thermal properties, being conductivity one of the most relevant. Composites present a significant lower conductivity, which is the reason for their advantages as a natural fire barrier compared to conventional materials such as steel. Thus, the need to have a reliable understanding of the thermal conductivity of certain composites found in the manufacturing of ship and marine structures.

Conductivity conforms to most of the research that has been shown during the chronological review of thermal property calibration. It is equally represented during the past years. The other important thermal properties analysed initially was the degradation or mass loss, which are directly related to the pyrolysis of composites. Or the heat capacity, which is another important variable, especially in transient phenomenology, where thermal inertia is highly affected by this parameter.

Initially, the research was driven by the calibration of thermal properties of unidirectional materials, the composite as a whole, and as the timeline approaches 1990, the efforts of the community are driven towards a better representation of the thermal properties of the polymer matrix. This is heavily influenced by the idea of characterising the composite as a whole and one of the constituent materials, the polymer matrix in this case. This technique allows extrapolating the calibration of the third unknown which is the fibre. Nevertheless, the research to obtain the thermal properties of the fibre has proven to be rather difficult due to its non-linear behaviour or its limitations when experimentally evaluated.

As the timeline advanced to 2000 and onward, it can be observed that the amount of research produced is decreased, since the paradigm is better understood and the different thermal studies of composite properties are contained in thermo-mechanical studies instead, thus being underrepresented.

2.2.5 Summary

To finish this section, a summary is shown in Figure 2.6. This figure is distributed in decades, which helps the reader to have a better understanding of the evolution of the current paradigm.

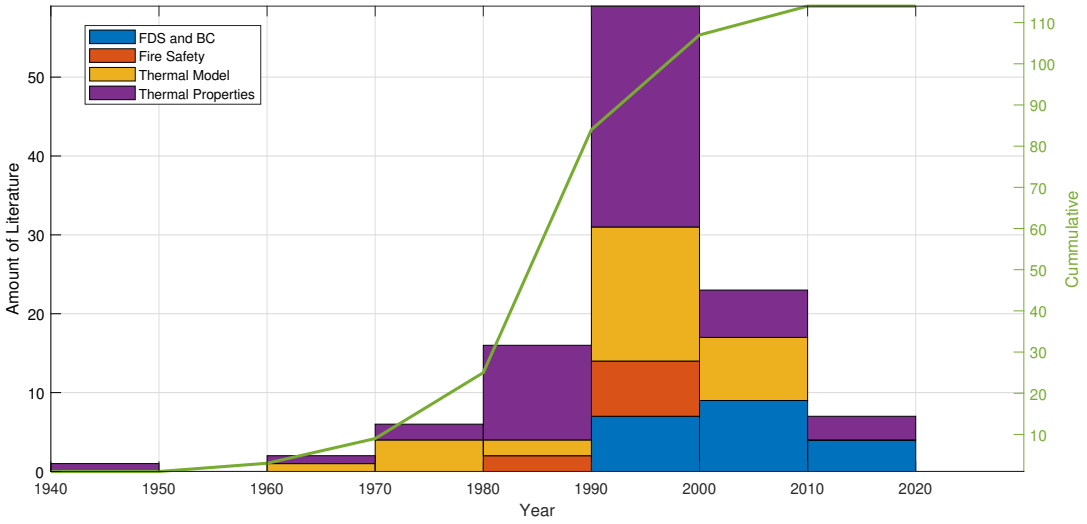

FIGURE 2.6: Research contribution to the topic of thermal modelling of composites. Timeline expressed in decades.

Observe how the set of thermal properties is the most notorious followed by the thermal model. This is explained by the fact that thermal models needed to be back up by experimental data. So it is quite common to find out, that the same authors that propose a specific thermal model, would also produce and share the finding of their experimental analysis.

It can be agreed that the decade of the 90s was the most prolic in terms of publications, and this is also the outcome of the growth in the interest of private or public investors, which had the goal to produce the technology and information necessary to use composites as new design materials. Industries such as aeronautics, automobiles or marine were one of the rst to incorporate these materials that are very ammable.

It is with this incipient problem, the fact that composites are generally inammable, that certain researchers needed to produce relevant publications on the matter of re safety. This is the reason why the re safety set can be especially found in the same peak decade.

As commented previously, the interest in reproducing fire scenarios or into modelling the thermal boundary conditions grow specially during and after the 90s. This is attributable to the need for functional boundary and fire dynamic models to solve the thermal model, otherwise it is not sensical to model fire without a purpose, that is to obtain the temperature distribution in a thermal model (in this case one-dimensional). And as the timeline would advance from 2000 to 2020, the research translates from thermal modelling to fire modelling (albeit the thermo-mechanical model is not represented here).

2.2.6 Conclusion of the thermal literature review

To close this section, the paradigm has been analysed and shown that the model proposed by Henderson and Wiecek in [19] is present in the modern paradigm. This

is the main reason to employ this so-called Henderson model in this research. The concept of adiabatic surface temperature introduced by Wickstrom Ulf et al. in [28] is recent, and it solves elegantly the issue of prescribing the boundary conditions, therefore the boundary conditions are introduced this way. In the model proposed and applications of this model, the adiabatic surface temperature can be obtained or assumed from a fire dynamic simulation, in which case the methodology used can be found from [54] by McGrattan, and in the case that a more explicit solution is taken, the use of a fire curve such as the ISO 834 [55] shall be used. If neither of those is used, a prescribed temperature from an experimental result shall be provided.

2.3 Mechanical Model

The structure of the review for the mechanical model is divided into two sections. First, a brief infographic of the whole topic is presented to analyse different trends organised in different major categories, this part of the analysis of the existing literature encompasses all the information existing regarding the mechanical model, however, bear in mind that this existent literature is centred around the topic of laminates. The second part is devoted to disseminating the major topics that have been researched during this thesis: *finite element analysis*, *damage models* and *composites*. A specic review of those elds separate is given to narrow the amount of information.

The starting point in the consultation of literature throughout this thesis was from the reference thesis of Rastellini [96]. Rastellini conducted a study specically on the topic of laminate composites and was one of the contributors to the serial-parallel rule of mixtures that have been one of the major cornerstones in the development of the thermo-mechanical model presented in this thesis. [96] provides two chapters devoted to the study of constitutive models of constituent materials, i.e., focusing on the topic of *damage models* and a brief review on the behaviour of materials when combined or *composites*.

The other relevant starting point in the research of the mechanical model is the information offered by Oñate in his book [16], where an extensive and detailed review of the current methodology involving the physics of shells and in specic for laminated shells is provided. [16] describes two fundamental nite elements, a triangle and a quadrilateral, from which most of the theoretical implementation of this research is based from.

Being these two, the major references in the study of the topic, a detailed analysis of the literature cited was reviewed, although most of the references present on [16, 96] were not picked, just those who were useful to the topics discussed in this thesis. The bulk result of this literature review can be seen in Figure 2.7. The amount of references has signicantly increased around the year 2000 and the cumulative references consulted were 150.

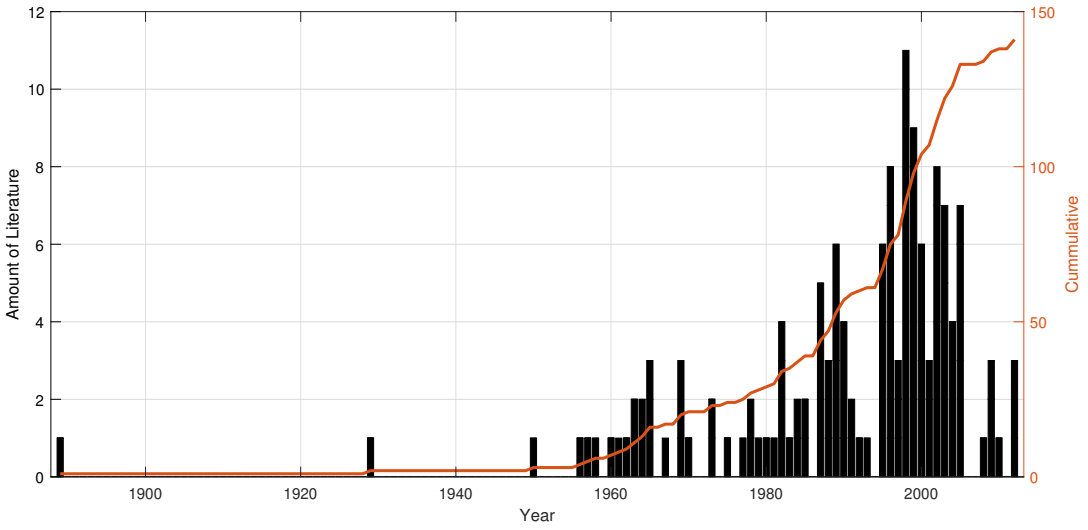

FIGURE 2.7: Bulk research contribution to the topic of mechanical modelling of composites.

Several authors who had a high impact in terms of contribution and signicance to the development of posterior research were identied. Amongst these: *Tsai, Hill, Reddy, Owen, Simo, Ju, Oller and Oñate*. Other important researchers are mentioned in the forthcoming part for each one of the three topics mentioned before.

The publications shown in Figure 2.7 were studied and classified under five categories: *linear*, *laminate linear*, *non-linear*, *laminate non-linear* and *properties*. The definition of these is given in the next paragraphs.

Linear is the category that encompasses all the nite element methodology and analysis conducted for linear materials, not differentiating between either isotropy or anisotropy. To be precise, it contains all the information that is strictly linear geometric and linear constitutive and does not try to explicitly model composite behaviour.

Laminate linear contains all the publications that address the linear behaviour of these materials, mainly, dealing with its orthotropy in a manner that is trying to reproduce composite materials. So orthotropic linear formulations are not included in this category as long as there is no derivation of these properties by imposing a composite relationship. I.e., when deriving the transverse Youngs modulus of an orthotropic composite by means of the modulus of its constituent materials. So this category implies formulation that establishes a methodology to obtain the composite behaviour utilizing the constituent behaviour or similar, however delimiting the scope to the linear range.

Non-linear is the category that extends the linear to the non-linear behaviour of the material. In this thesis, the research is driven toward damage models, so, all the non-linear constitutive models consulted are damage models. On the other hand, this category also includes non-linear geometric publications.

Laminate non-linear extends the previous non-linear category to include those publications that again add some extra component that interrelates the constituent behaviour with the composite behaviour of the heterogeneous material.

Properties are the set of publications that focus on determining the properties of either constituent or composite materials. This determination can be theoretical or experimental.

In Figure 2.8 the classication of the bulk review is presented. The evolution of the paradigm has moved from studying composites linearly to the non-linear range and observed the peak of publications is around 2000, with most of them being *laminate non-linear*. During the last decade, most of the research that has been conducted on constituent materials have been focused on the non-linear aspects of it. It is worth mentioning that since this research is focused on composites, many of the publications regarding linear or non-linear modelling of constituent materials are underrepresented in this chart. It is easily understandable that during the last decades, signicant research may have been done in areas of fracture mechanics such as plasticity which is more representative of metal constituent materials.

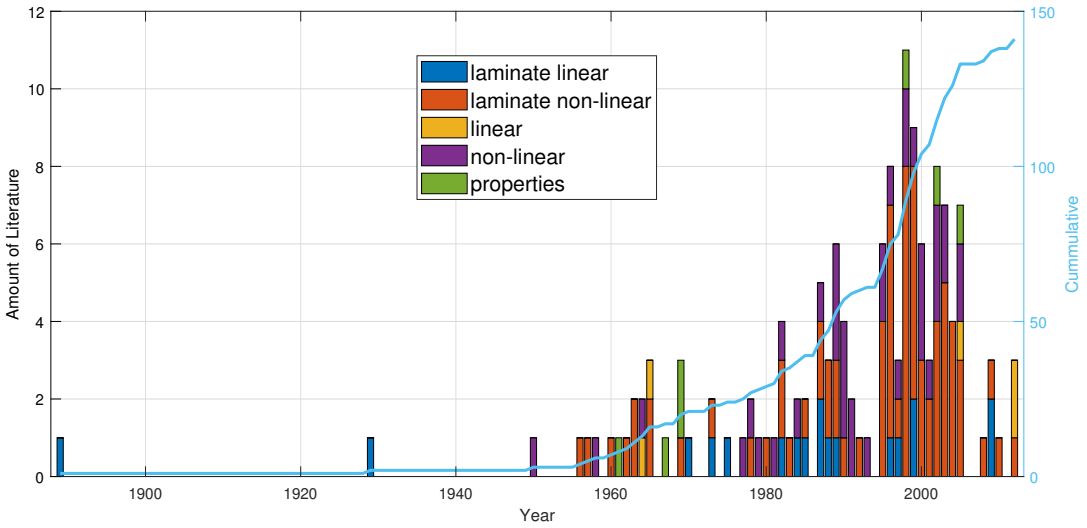

FIGURE 2.8: Bulk research contribution to the topic of mechanical modelling of composites divided by categories.

Similarly, a review of the same literature but organised in decades (see Figure 2.9) is given. The research has observed an increase during the 90s and 2000 and 2010 in the eld of *laminate non-linear*. This chart shows the historic evolution of the paradigm, starting with the study of linear laminates, some non-linear constituent models are introduced during the 50s and then the research centred on the efforts to introduce or couple the existing non-linear constituent models with existing constituent-composite rules.

From 1960 to 1970, the paradigm has focused on experimental testing of the properties of constituent and composite materials and during the period comprised from 1970to 1990, the paradigm has equally been focused to unfold different questions regarding *laminate linear*, *non-linear* and *laminate non-linear* categories. In the last decades, the paradigm has been dominated by the *laminate non-linear* category, since the research conducted until this point had fruitfully produced solutions that incorporated the non-linear range to existing linear laminate models.

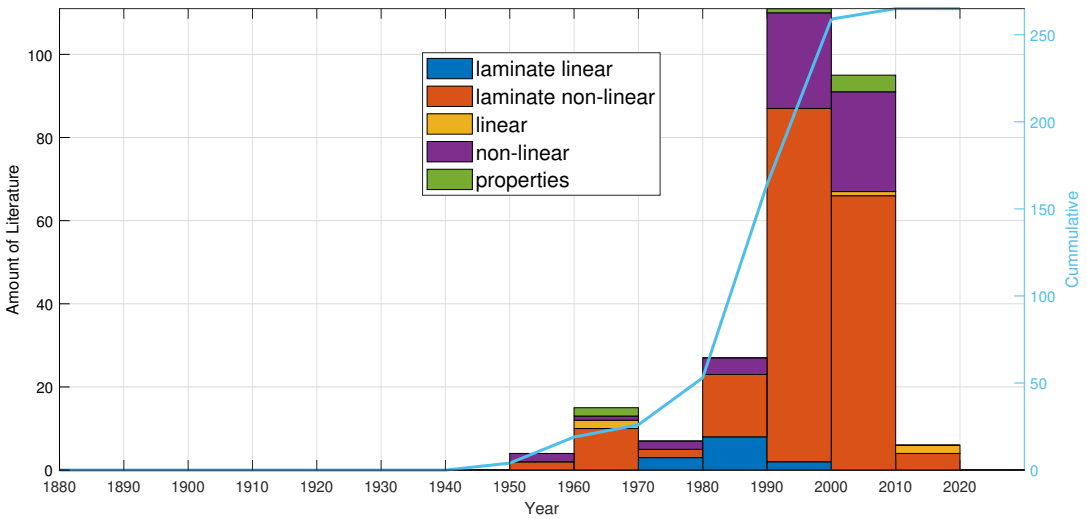

FIGURE 2.9: Bulk research contribution to the topic of mechanical modelling of composites. Timeline expressed in decades.

As commented previously, a careful examination of the literature consulted is now broken down into three main topics: *finite element analysis*, *damage models* and *composites*.

2.3.1 Finite element method

To examine which is the best methodology regarding the mechanical model employed in this thesis. A careful review of the different elements explained in [16]], specically those for linear triangles and quadrilaterals, is undertaken. The other aspects important to the formulation in composites that are exposed to re are the excessive deformation and displacements, this is commonly referred to as the non-linear geometric part of the stiffness tensor.

From [16] and some other references, bulk analysis of the paradigm surrounding nite element technology is presented. Again, note that the literature review completed under this very topic is biased towards solutions that contained or were tailored for composites. In shell terminology, dealing with layer-wise discretisation or similar issues that arise around laminated shell elements. The chart of the bulk literature reviewed can be found in Figure 2.10.

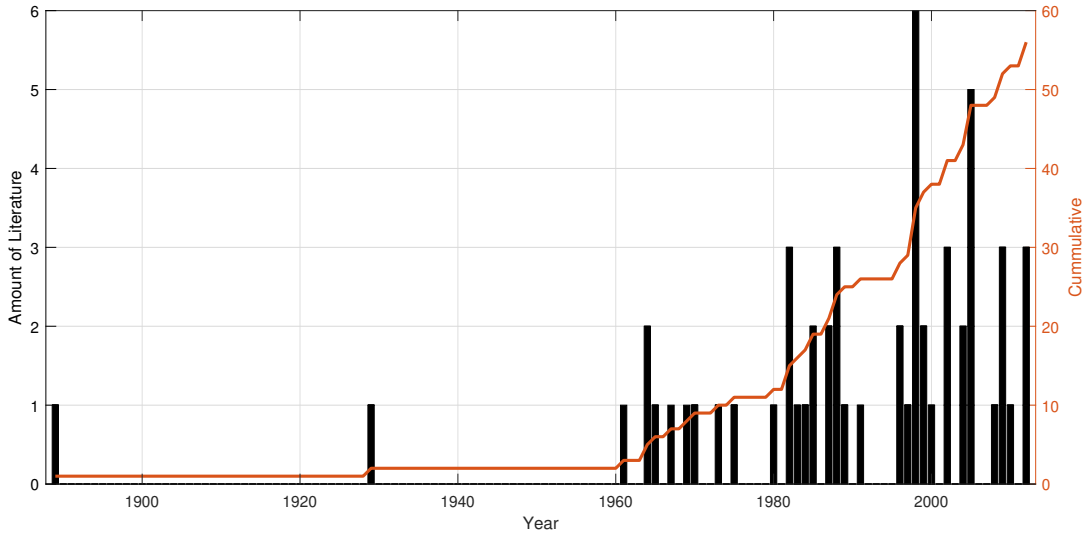

FIGURE 2.10: Bulk research contribution to the topic of mechanical modelling of composites. Contributions focused on FEM field.

There is a special increase in the contribution to the nite element method especially for composites at the beginning of the 90s and more prominent in the 2000s and onward. 56 publications were consulted and to obtain a better evolution of the paradigm, the publications were classied into six main categories as shown in Figure 2.11.

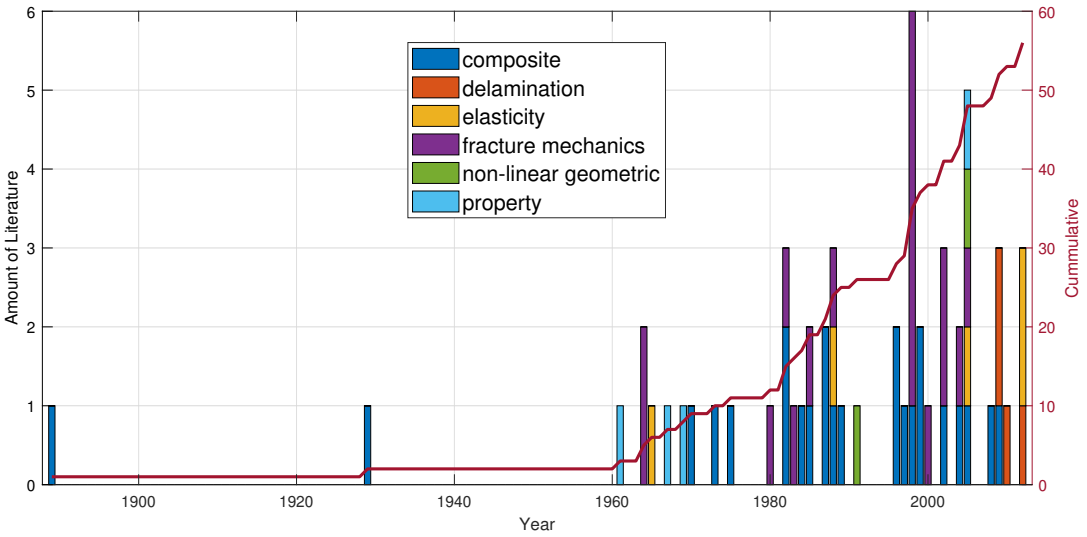

FIGURE 2.11: Bulk research contribution to the topic of mechanical modelling of composites divided by categories. Contributions focused on FEM field and divided into categories.

Observe that the categories selected were: *composite*, *delamination*, *elasticity*, *fracture mechanics*, *non-linear geometric* and *properties*. The most prominent category is the *composite* category as the publications were closely related to composite-driven research.

2.3.1.1 Composite

This category focus on all the signicant nite element method, analysis and technology that is intrinsically focused on composites and laminates. The rst publication found is by Voigt in [26] in the year 1889. Voigt can be considered one of the fathers of the composite eld since he formulated one of the earliest constituent-composite relationships for the mechanical properties in the direction of the bre or parallel direction. Another father of the eld was Reuss that published a similar paper [27] in 1929 involving the constituent-composite relationship of the transverse mechanical properties or serial direction.

The next publication relevant is the one by R.L. Foyer [97] that models laminated composites by using an orthotropic description. Jones in [98] describes the mechanics that involve composite materials and in [99] Lardeur and Batoz provides a triangular discretisation for composite plates under shear stress. Tsai and Hahn [100] are one of the first to introduce a criterion of failure for composites that has become widely uses during the past decades.

One of the most impactful publications is the article by Reddy [101] that proposes a computational model for composites discretised in a layer-wise manner. Oller et al. in [102] introduced a constitutive model that obtains the composite behaviour from the behaviour of the constituent phases. Reddy published a new book, [103], updating all his research in the field of laminate mechanics.

Other authors such as Soden et al. focus on understanding the behaviour of lamina and the interaction that those have when stacked under different load configurations for FRP composite materials [104]. Botello et al. [105] presented another triangle element that describes plate and shell theory that is suitable for layer-wise laminated materials. Car et al. in [106] extend the previous work from [102] to produce a multi-scale numerical solution for composites. The ideas of [106] are consolidated by Oller et al. in [107].

Bauchau [108] published an extensive book centred on structural analysis of composite structures for aerospace applications. Finally, one of the most remarkable publication can be found in [16] by Oñate where a complete description of low and high-order finite element solutions are found for quadrilateral and triangles, as well as, explaining the zig-zag theory to enhance the formulation to simulate the delamination between layers.

2.3.1.2 Delamination

This category is narrow because it is especially focused on the available technology to simulate delamination with shell elements, the classical formulation lacks the sufcient degrees of freedom in the layer-wise direction to introduce the effect of delamination. Moreover, because the purpose of the research conducted during this thesis does not attempt to model intra-delamination of layers, the number of literature consulted is much reduced.

Besides [16] explaining the zig-zag theory that had become very popular in 2010. Eijo et al. in [109] also present a four-node quadrilateral element that is able to reproduce laminated composites and model the delamination effect by means of the zig-zag theory. Versino et al. [110] also propose a triangular element that reproduces the behaviour of laminated composites and models delamination by means of the zig-zag theory.

2.3.1.3 Elasticity

This category introduces the major references in the eld of the elasticity equation. The publications consulted were books of importance at their respective time and explicitly focus on linear solutions to the elasticity problem and for homogeneous media. Historic evolution of the consulted bibliography starts with the book [111] by Green and Naghdi, which gives a detailed introduction to dynamic problems and how to numerically solve them. Taylor presents a book [112] that gives an excellent introduction to the finite element analysis of linear shells and Zienkiewicz et al. in [113] complement and extend these principles to solids.

2.3.1.4 Fracture mechanics

This category includes all the publications that focused on fracture mechanics (damage, plasticity, fracture, fatigue). One of the oldest publications by Hill [115], centred

in elasticity and a second publication, [114], focused on the inelastic behaviour of fibre reinforced materials.

Another significant contribution to the failure criterion of composites was the Tsai-Wu criterion that receives its name by one of its authors Tsai and Hahn [100]. Others like Dvorak and Bahei-El-Din [116] focused on the study of plasticity for fibrous composites. [117], in parallel, defines a viscous-plastic model. Hinton and Soden [22] also proposed a method of predicting failure, Faria et al. [118] defined a viscous-damage model for concrete, Puck and Schürmann [119] posed a formulation based on experimental models.

Car et al. [120] introduces an anisotropic plastic model for FRP under large deformations, Puck and Schürmann [121] expanded the research from [119] and Kaddour et al. [122] published a review of the failure theories.

2.3.1.5 Non-linear geometric

The non-linear geometric formulation is a category that includes just two publications that belong to the research of Felippa. The interest in a non-linear geometric problem is of special of importance since composites are very exible and this interlinks to the concept of large strain formulation. Although many other formulations were excluded, the main reason behind it, was the need for a non-linear geometric formulation that was very abstract and worked as a black box. Therefore, many formulations such as *total Lagrangian* or *updated Lagrangian* were directly excluded from the literature research.

First, in 1991, Militello and Felippa [123], formulated one of the first high-order triangles suited for bending that was *ANDES* formulation and capable of reproducing large deformations. Then Felippa and Haugen [18], from its previous research [124], formulated a very abstract theory regarded as co-rotational formulation, and it was suitable to reproduce large deformation phenomenology for both triangle and quadrilaterals without significant modification of pre-existing small-strain theories.

2.3.1.6 Properties

Another interesting category is the one that belongs to the study of properties and how these are affected by the environment loading. Only the research of Tsai-Wu, Halpin and Whitney was revised. During the 60s there was an interest in how to determine the properties of composites under certain loading, bending or environmental effects, by authors such as Halpin in [125], or the calibration of transverse properties of transverse isotropic laminates by Whitney from [126].

2.3.1.7 Summary

As a brief summary of the evolution of the paradigm throughout the different classied categories, Figure 2.12 shows decades, that during the 60s the paradigm centred on obtaining reliable constituent constitutive models that were able to predict fracture, some minor research in property calibration of composites and some other in the study of the elastic behaviour of composites.

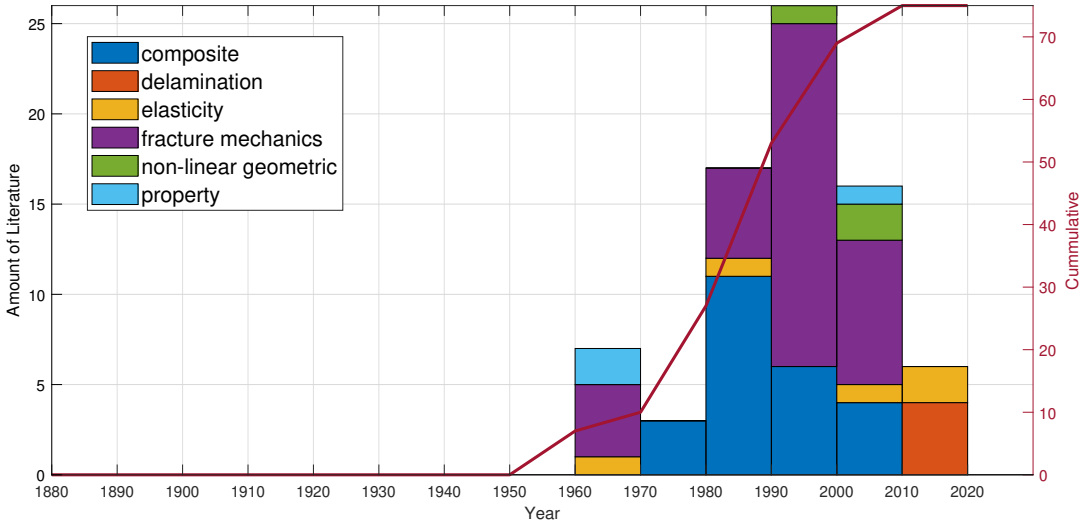

FIGURE 2.12: Research contribution to the topic of mechanical modelling of composites. Contributions focused on damage models. Timeline expressed in decades.

From the 70s until 1990, the paradigm focuses on the study of composites and producing models that reproduce their constitutive behaviour. In the 80s some early fracture models were introduced at the composite level, those were experimental driven models, tailored for specic solutions.

From the 90s and onwards, the composite category lost relevance and the apparition of non-linear constitutive models for composites gained more importance. However, these non-linear constitutive models were different to the ones found in the 70s, which focused on modelling the non-linear constitutive behaviour of the constituent materials and then homogenising them, to later obtain the non-linear constitutive behaviour of the composite. During the 90s, and 2000-2010, there are the contributions to the eld of co-rotational theory for large deformations and from 2010 onwards, the paradigm has mutated to obtain reliable solutions for shell elements that can predict delamination, which is itself a topic from fracture mechanics, but one that is rather furthermore complex for shell formulation.

2.3.2 Damage

The other subject of interest for this thesis was the damage to composites, since, FRP composites are mainly considered to experience damage as their non-linear constitutive failure mechanism. Figure 2.13 represents of the 35 publications consulted.

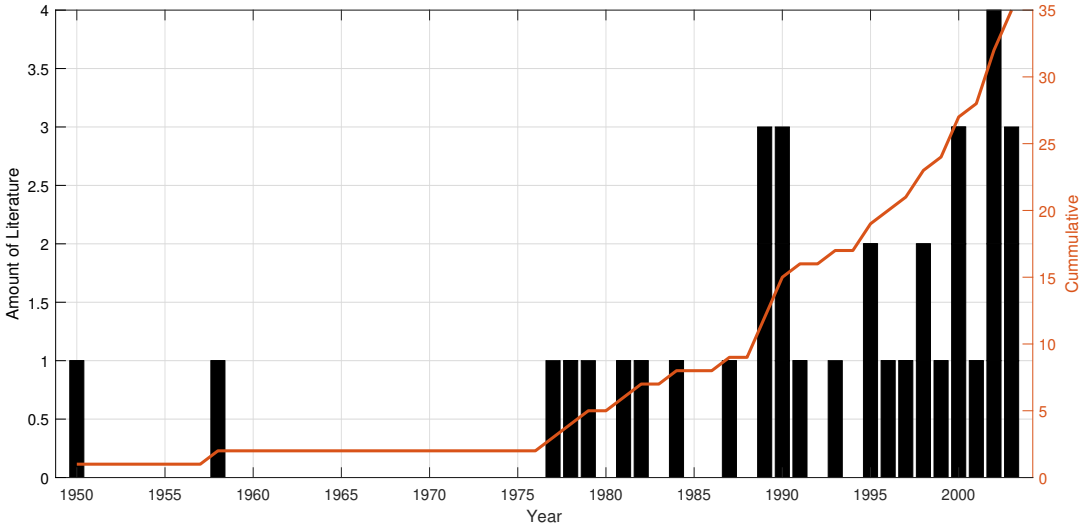

FIGURE 2.13: Bulk research contribution to the topic of damage modelling of composites.

Most of the publications after 1975, the publications reviewed addressed directly the modelling of damage for laminate materials and therefore the paradigm was divided into three categories: *isotropic*, *orthotropic* and *anisotropic*. Figure 2.14 shows this classication, the rst models to be introduced were the isotropic models. Then the orthotropic materials, which conveniently are good enough to reproduce many laminate materials. The framework then was enhanced by introducing anisotropic damage. From this point onward, the research was focused on upgrading different aspects of the consolidated and existing models.

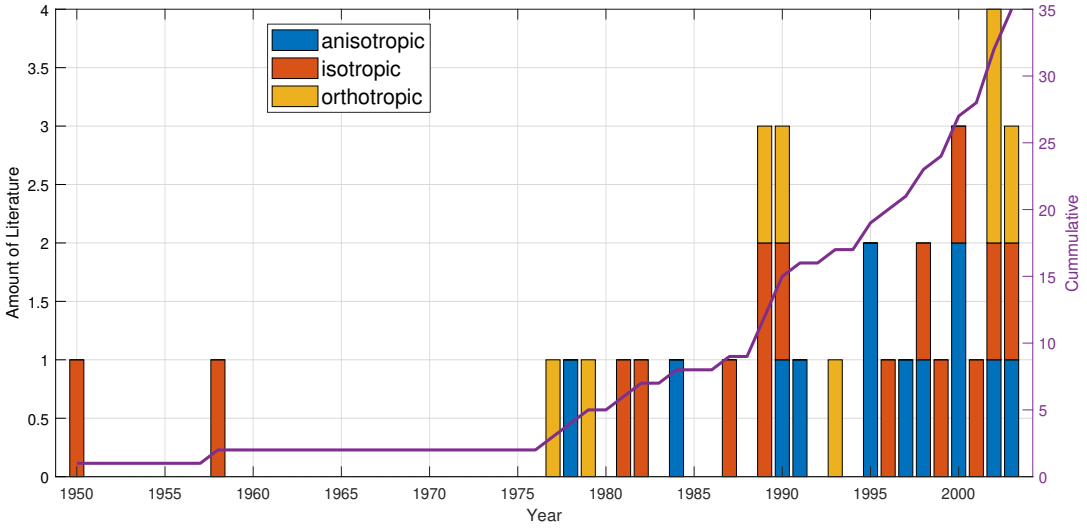

FIGURE 2.14: Bulk research contribution to the topic of damage modelling of composites divided by categories.

2.3.2.1 Isotropic

The rst efforts in modelling damage were in an isotropic manner for concrete structures. One of the rst authors to deal with non-linear constitutive models, specically for plasticity, was Hill. Kachanov used the ideas of the fluency surface to adapt this for composite materials [127]. Dvorak and Bahei-El-Din [116] studied the plastic effect of fibrous composites and then Simo and Ju [17] in 1987 posed what is considered the father of all damage models, the so-called isotropic damage model.

Ju [17] formalised the ideas of [17] in a more energetic manner of describing dissipation. Oliver [32] apply the research from Simo and Ju for concrete structures and how the cracking of those evolves. Luccioni et al. contributed to the same model in [129] and Kachanov [130] published an update on the research conducted in [127]. Krajcinovic in [131] presents a review of the current implementations related to isotropic damage models and serves as a link to those other contributions that were not referenced in this section.

2.3.2.2 Orthotropic

These models sufced in the goal of coupling nite element technology (kinematics) with orthotropic non-linear constitutive models. This coupling is interesting since a variety of FRP composites can be approximated by orthotropic non-linear theories. One of the rst authors to research the yield surface for transversely isotropic materials, i.e. metals or certain FRP laminates, was Bassani [132].

The same Hill, which previously studied the yielding of isotropic damage models in [115], extended his model to cover orthotropy behaviour [133] in order to reproduce the structural response of textured aggregates. Barlat and Lian continued the studies from [132] in an attempt to model shells rather than plates [134]. On the other hand, Hill continued in [135] his previous work from [133]. Lastly, Oller et al. [136], postulate an implicit and general theory to derive the orthotropy behaviour from the constituent phases of a composite.

2.3.2.3 Anisotropic

Albeit many composites can be considered to reproduce an orthotropic behaviour, there are many others that do not. In an attempt to obtain a theory of all, the anisotropic models were created. The rsts authors found are Shih and Lee [137] who adapted the ideas from the existing damage models and provided an anisotropic solution. In the eld of yielding surfaces, the authors Eisenberg and Yen [138] introduced a compatible yield surface for anisotropic deformation. Voyiadjis and Thiagarajan [139] with the research from [138] and [140] formulated another anisotropic damage model.

Lemaitre and Chaboche [141] investigated the damage law evolution necessary for anisotropic materials and Voyiadjis and Deliktas [142] extended their research from [139] to model anisotropic composites. Luccioni and Oller in [143] presented a directional damage model.

2.3.2.4 Summary

In Figure 2.15, the same evolution is shown in decades. This shows that the paradigm has evolved from isotropic models to orthotropic and anisotropic models. Then the paradigm has vastly concentrated to obtain reliable anisotropic models and upgrading those aspects of previously existing models.

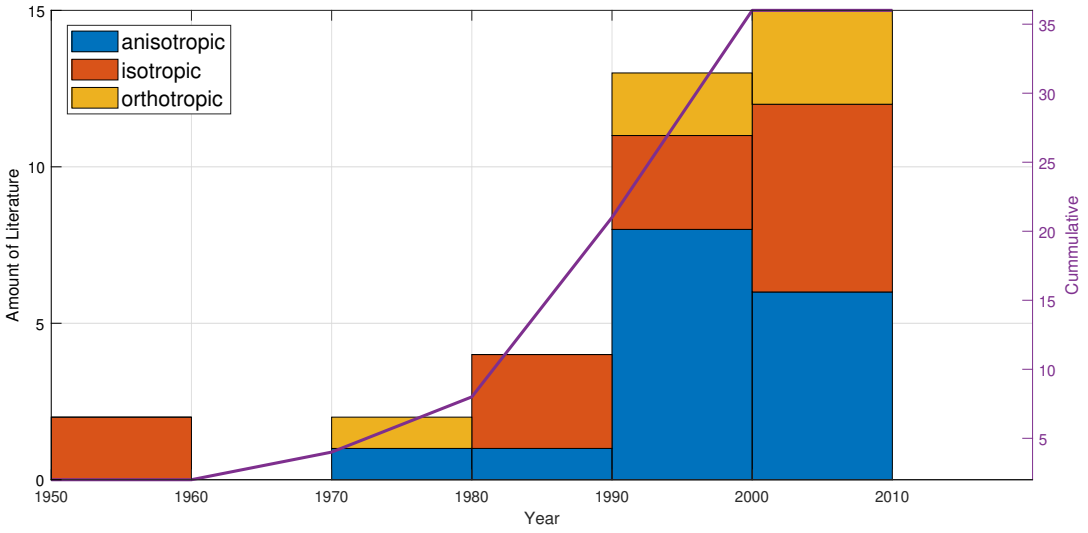

FIGURE 2.15: Research contribution to the topic of damage modelling of composites. Contributions focused on composite field. Timeline expressed in decades.

2.3.3 Composite

This subsection focuses on the modelling of the interaction and relationships between the constituent phases and their equivalent heterogeneous media. In Figure 2.16 a total of 60 publications were revised, the majority of these are published from 1995 onward.

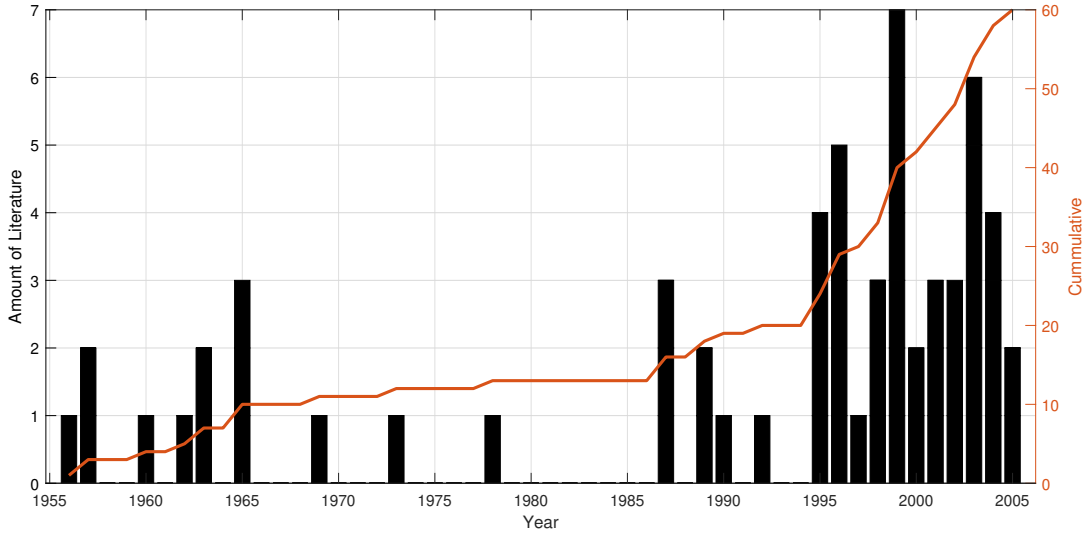

FIGURE 2.16: Bulk research contribution to the topic of constitutive modelling of composites.

If the bulk chart is then broken down into the different techniques available to model the composite behaviour from the constituent behaviour, Figure 2.17 is generated. The categories in which Figure 2.16 was classified were: *cells*, *constitutive*, *eshelby*, *macro-scale*, *micro-scale*, *mori*, *multi-scale*, *periodic* and *self-consistent*, *stochastic*.

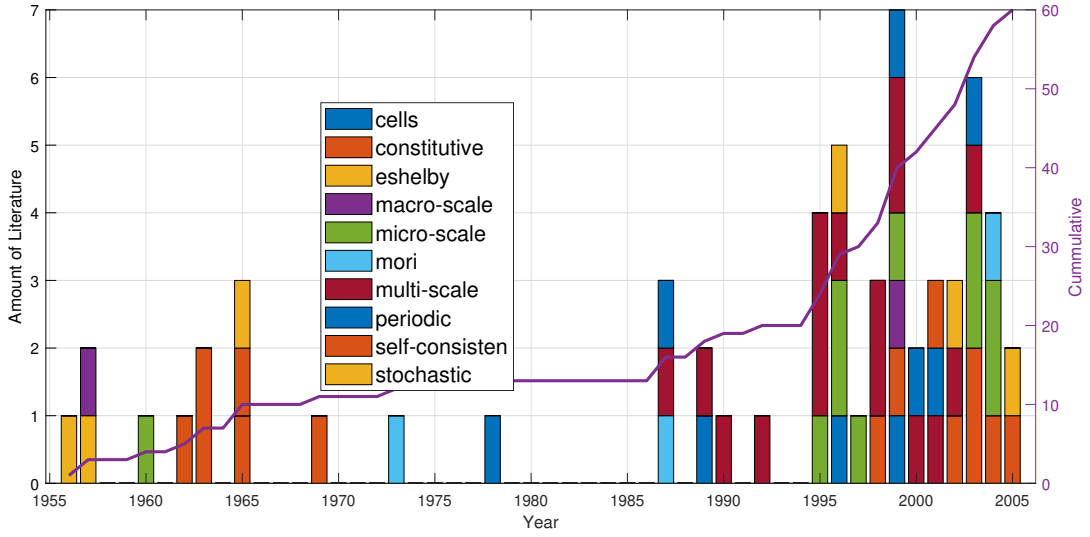

FIGURE 2.17: Bulk research contribution to the topic of constitutive modelling of composites divided by categories.

2.3.3.1 Cells

The method of cells (MOC) is a specic method to obtain the homogenised properties by subdividing the section into cells and each cell is subdivided into subcells that are either matrix or bre. The rst publications were in 1989 by Aboudi [144] that proposed a micro-mechanical method based on the ideas previously mentioned. Aboudi offered an update in the research in [145].

2.3.3.2 Constitutive

This category contains those publications that deal with obtained constitutive solutions of the heterogeneous media from the constituent materials. One of the first authors, Hashin, in [146] described a variational approach of the mechanical response of heterogeneous media based on the contributions of their constituent phases. Budiansky [147] studied the elastic modulus of heterogeneous materials from the contribution of their matrix and fibre elastic properties. One of the most interesting contributions to this thesis is the research published by Rastellini [33] who posed the underlying concepts of what later would lead to the serial-parallel rule of mixtures.

2.3.3.3 Eshelby

Eshelby models receive their name by their founding father surname. These methods use the so-called lattice defect method. A total of two publications were taken into account. Eshelby published first his method [148] in 1956 and in the following year published a paper enhanced this theory in [149].

2.3.3.4 Macro-scale

The macro-scale methods are based on modelling the heterogeneous media as a whole. There are many other publications in this area, however, with the advance in homogenisation techniques, this area has become not so used in terms of accuracy. Nevertheless, one of the models reviewed was [150] by Banks-Sills and Leiderman who focused the elasto-plastic mechanical response of composites containing aluminium sheets.

2.3.3.5 Micro-scale

Micro-scale methods are the most popular and recognisable techniques, i.e., the classical mixture theory (CMT) is a branch of it. These theories need a certain level of computational power and this is the principal reason to why from 1965 to 1995 there was no signicant contribution to the research eld until later during the 90s and 2000. In 1960, Truesdell and Toupin, published one of the most known theories, the classical field theory [151]. Later, Drugan and Willis proposed to use this theory (CMT) with the finite volume method (FVM) [152]. Alzebdeh and Ostoja-Starzewski in [153] proposed a micro-scale based on experimental and stochastic response of their

constituent phases. Oñate and E. [154] introduced the early concepts of serial and parallel rule of mixtures, which is an extension of CMT. Rastellini then formalised this theory in [15, 33, 96].

2.3.3.6 Mori

The Mori or Mori-Tanaka theory focuses on correctly assessing the constitutive behaviour of the matrix, in linear and non-linear constitutive range, to later obtain a better response under transverse loading. Mori and Tanaka [155] in 1973 introduced their method. Benveniste in [156] adapted the theory, which only focused on predicting an enhanced matrix behaviour, inside a composite theory.

2.3.3.7 Multi-scale

As more powerful computers were available, a prolic eld in the paradigm gained special attention. This is the multi-scale method, which consists of solving the problem on two or more scales. Since 1985 there has been an increase in the publications regarding this eld.

One of the firsts authors were Hollister and Kikuchi in [157], who focused on the so-called homogenisation techniques to reproduce porous heterogeneous media. Povirk [158] used an approach similar to micro-scale methods but coupled this later with a two-scale approach in order to avoid modelling the constituent-composite relationship. Similarly, Ghosh et al. [159] uses the two-scale approach with a cell method. Terada and Kikuchi in [160] uses the homogenisation technique with non-linear constitutive models. Ghosh et al. in [161] upgrades their approach from [159] by including asymptotic homogenisation.

Other relevant publications such as [162] proposed other multi-level approaches, [163] focuses on a multi-level approach to reproduce complex sectional structures, [164] introduced an analysis of damage to the composite structures based on the homogenisation method, [165] also proportioned an analysis of the damage to composite structures including viscous effects. Feyel and Chaboche in [166] proposed a multi-scale approach for non-linear viscous-plastic modelling for long-fibre reinforced composites. Zalamea et al. [167] and Car et al. [106] provided a numerical analysis by means of the homogenisation technique for composite materials. Feyel [168] continued the research in [166] to reproduce the highly non-linear response of heterogeneous materials.

2.3.3.8 Periodic

The periodic category is very linked to the category *cells*, however, publications that mainly focused on the periodicity of certain heterogeneous media are considered exclusively inside this category.. Toledano and Murakami in [169] propose a model for periodic particulate composites to reproduce the mechanical behaviour of concrete-like materials. Another similar author who used the periodic method was Michel

et al. in [170]. Graham and Baxter in [171] proposed a moving-window method to obtain the asymptotic behaviour of the heterogeneous media.

2.3.3.9 Self-consistent

Another branch is the self-consistent method. The method bases the heterogeneous behaviour of the material on derived explicit models from experimentation. Hill introduces this model in [172].

2.3.3.10 Stochastic

These models are based on determining the composite behaviour of constituent behaviour from a stochastic point of view. One of the papers consulted was the one by [153] that focuses on obtained the micro-mechanical of constituent phases by taking into account direction of the deformation and the length scale of the samples.

2.3.3.11 Summary

Figure 2.18 shows the evolution of the paradigm in decades, since there are many categories it is very difcult to establish a specic evolution of the paradigm.

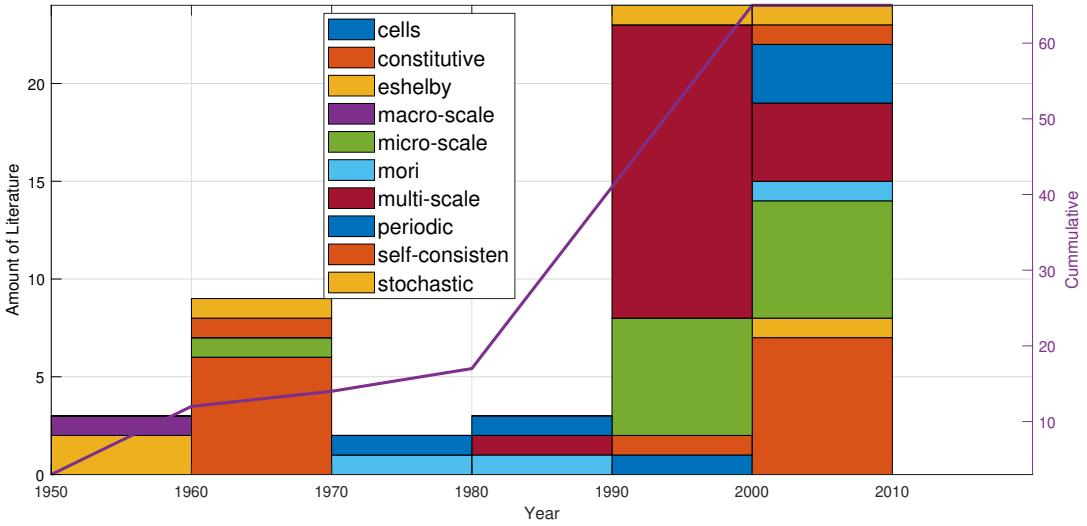

FIGURE 2.18: Research contribution to the topic of constitutive modelling of composites. Timeline expressed in decades.

One of the interesting trends that can be recognised is that there is a boom in the contributions in constitutive theories in the 60s and then the number of publications is signicant reduced since the theory is not met by the existing computational power. During the 90s and onward, the computational power meets the requirement of the algorithm postulated in the 60s and different types of models are spawned, one of the most prolic topics is the micro-scale and multi-scale methods.

2.4 Laminated thermo-mechanical model

The purpose of this section is to extend the literature review undertaken in section 2.2, recall that this literature review starts from the point of view of the literature review attributed to Mouritz et al. in [7] and that has been updated by including the most recent review (from 2009 to the present) of the authors that have considerably contributed to the field.

In section 2.2, the scope was limited to the thermal modelling of composites exposed to re. Similarly, this section will be devoted to explicit thermo-mechanical modelling publications. Nevertheless, the comparison between both bulk types of research shall be made, i.e., between the categories that t in thermal modelling and those that belong to thermo-mechanical. However, only the specic sets belonging to thermo-mechanical modelling will be discussed.

First, compare Figure 2.3 with Figure 2.19, the rst shows the literature that does not include the thermo-mechanical modelling and the second does. There is a total of 95 publications against almost 240 publications. This evidences that during the last two to three decades the contribution to the research eld has increased towards thermo-mechanical modelling, which indeed contains sometimes certain aspects of thermal modelling, rather than thermal modelling.

For the thermo-mechanical modelling, the peak is moved to 2010 in comparison to 1990 for the thermal modelling.

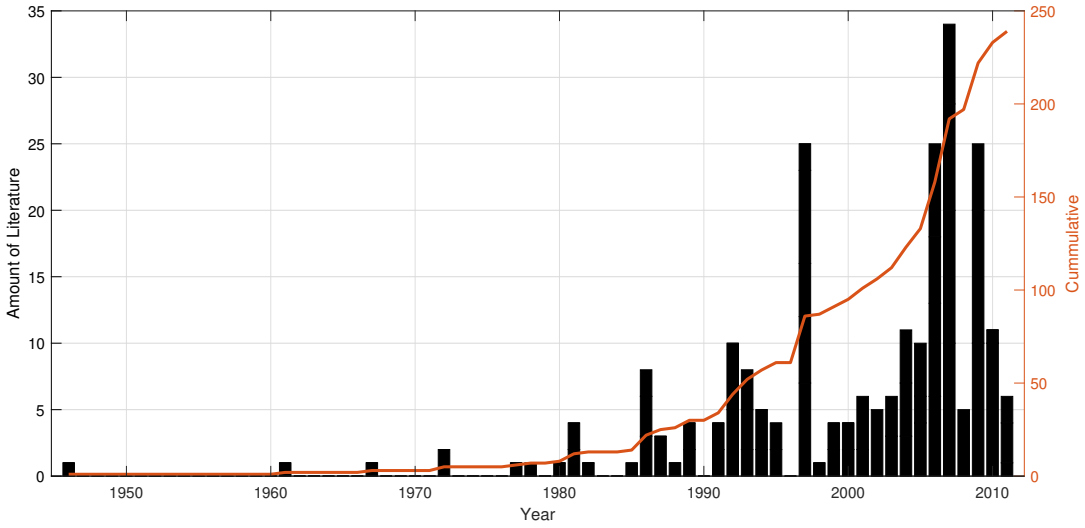

FIGURE 2.19: Bulk research contribution in the topic of thermo-mechanical modelling of composites. Extracted from [7].

Albeit this is clear proof, again the research is biased especially because it does not contain the research done during the last decade. Considering the research done during the last decade by using the same methodology in section 2.2, if Figure 2.4 is compared against Figure 2.20, the research difference is even more patent. A total of a little more than 100 publications against around 370 publications, thermal and thermo-mechanical modelling respective. This is almost a difference of 270% compared to the thermal modelling publications.

Also note that comparing Figure 2.3 and Figure 2.20, the updated information has shown that during the last decade one of the hottest topics is indeed thermo-mechanical modelling.

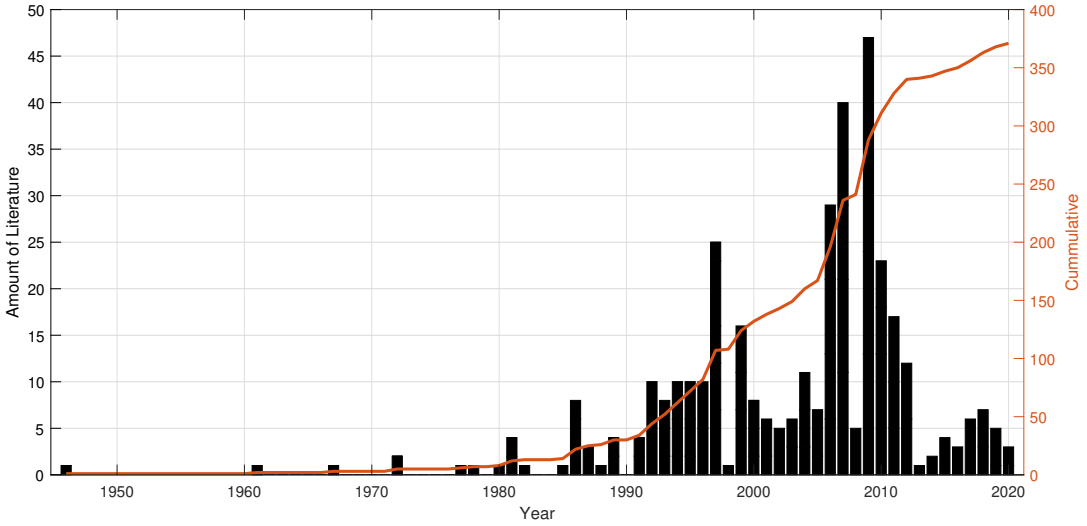

FIGURE 2.20: Bulk research contribution in the topic of thermo-mechanical modelling of composites.

Figure 2.20 shall be divided in several sets, some are the previous ones found in section 2.2 : *FDS and BC*, *Fire Safety*, *Thermal Model*, *Thermal Properties*. And the new sets that belong explicitly to thermo-mechanical modelling: *Thermo-mechanical Model* and *Thermo-mechanical Properties*. These two new sets are described in the next paragraphs.

Thermo-mechanical model is a set that covers all the thermo-mechanical models, some of them include a thermal model (generally based on the Henderson model), however, their uniqueness is in their thermo-mechanical model. This covers all the publications that focus on numerically providing unique thermo-mechanical models, excluding publications that aim to model constitutively the thermomechanical response.

Thermo-mechanical properties is a set that incorporates the research eld that has the aim to provide data to characterise thermo-mechanical properties used in the thermomechanical analysis of composite materials. Generally, this topic focuses on the evaluation of temperature-dependent properties such as the elastic modulus or yield stress, but also on how re and thermal processes affect failure mechanics (cracking, ablation, damage, delamination or buckling).

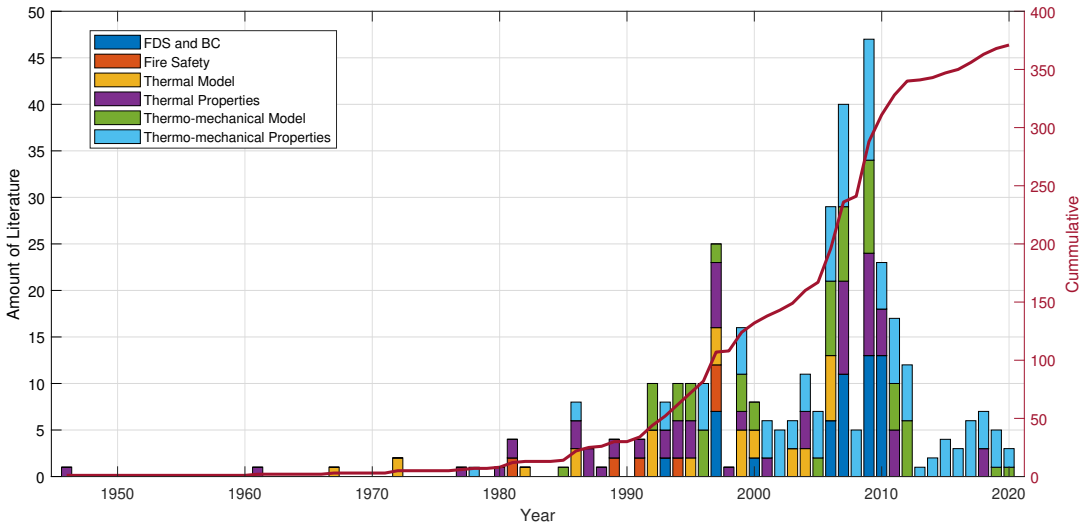

FIGURE 2.21: Bulk research contribution in the topic of thermo-mechanical modelling of composites. Classified in categories.

Hence, Figure 2.21 shows that during the last decades the thermo-mechanical properties are the most investigated set. In 2009 there is a peak led by four sets and two of them belong to thermo-mechanical modelling. The other important set present from 1990 onward is the set of thermo-mechanical models.

Before moving to the specic sets, recall that in this section, authors that were previously excluded because their content is more focused on thermo-mechanical aspects, now are included. Basically, in broad terms, the contribution of authors such as Feih in [23, 24, 25, 173, 174, 175, 176, 177]is very relevant in the determination of how the yielding surface evolves in terms of temperature and also attempts to characterise the effect of thermal-buckling. Other signicant authors such as Asaro and Gu are very relevant, especially for thermal-buckling [95, 178, 179, 180, 181, 182, 183, 184, 185].

2.4.1 Thermo-mechanical Model

The set of the thermo-mechanical models has been very prolic during the last two decades. It started to develop during the mid-90s and the earliest contribution dates from 1986. Figure 2.22 shows, that the present, the set has a total of 69 publications.

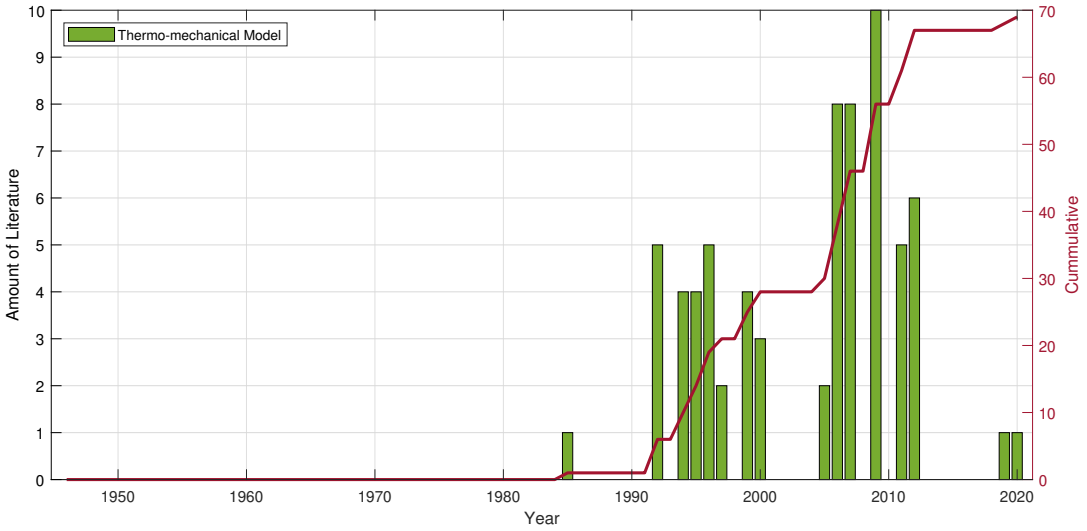

FIGURE 2.22: Research contribution in the topic of thermo-mechanical models.

One of the first thermo-mechanical models was proposed by Chang in [186]. The model focuses on the thermal analysis derived from [63] and tries to tackle the thermo-mechanical part in a very simple manner. The most complete according to the standards in the early development of the paradigm is the thermo-mechanical model published in Sullivan and Salamon by [40]. Sullivan further expands his model in [42], by incorporating the porous effects (hygrothermal model) and how those affect the mechanics of the problem. Maddocks and Mcmanus in [187] introduce a simple thermo-mechanical model in order to predict micro-cracking of composites due to loading.

Sullivan in [43] introduces the effect of thermal stress in his previous thermo-mechanical model. In [188], Sullivan, as co-author, publishes a finite discretisation of a thermo-porous-mechanical model. Park and McManus in [189] continued their research found previously in [187] and this time focuses in predicting damage to composites. Then Dimitrienko publishes a thermo-mechanical model described in [190, 191] that uses his thermal model from [66]. Sullivan and Stokes in [44] present a thermo-mechanical analysis using the rule of mixtures for phenolic composites and Dimitrienko models the transport phenomena of gas in [192] and presents an analysis of a thermo-mechanical problem subjected to radiation boundary conditions in [193]. Other thermo-mechanical analysis by the same time are presented, e.g., one focused specially on the constitutive modelling is presented by Key and Lua in [194] or the one posed by Ramroth et al. in [195], which tries to analyse thermal-buckling with a simple methodology. At this time, one of the first coupling between a fire dynamic simulator (FDS) [196] and a thermo-mechanical analysis are presented in [197] by Prasad and Baum.

Luo and DesJardin present their damage thermo-mechanical model in [198]. Lua presents a thermo-mechanical model for woven fabric composites in [199]. Luo and DesJardin [200] adapt their thermo-mechanical model [198] to enhance the gas transfer model and how this correlates with micro-cracking, by incorporating an assessment of the porosity of the composite.

Elmughrabi et al. in [201] presents another thermo-mechanical model and Luo et al. in [203] present another fluid-structure interaction (FSI) coupling of an FDS and a thermo-mechanical solver that upgrades their previous research work. Mouritz et al. [204] presents a thermo-mechanical analysis focused on naval composite materials. Kandare et al. in [205] propose a thermo-mechanical model that also takes into account intumescent coating, this is extended in [206] by Mouritz et al.. The last item found in the literature review is by [45] that presents a fully coupled model between an FDS and a thermo-mechanical model that is able to take into account ablation.

The modern paradigm of thermo-mechanical modelling of FRP composites has moved from simple thermo-mechanical models in its early stage, to incorporating the effect of porosity by, either or both, modelling the porosity for the thermal model or the mechanical model.

The next natural stage of the paradigm was the characterisation of property degradation with respect to thermo-chemical processes (temperature and pyrolysis). In the 21st century, the paradigm takes the form of solutions that incorporate a coupling between a re dynamic simulation and a thermo-mechanical model and other researchers focused on offering realistic thermo-mechanical constitutive models to take into account damage, ablation, cracking, etc.

One of the most relevant topics regarding composites was the one addressed by Ramroth et al.. Although all the previous research has its importance on the paradigm, it was the contribution of these two authors, who at the moment, 2006, seemed not of extreme importance, that nowadays maybe posing an important precedent in what is referred to as thermal-buckling. The thermo-mechanical modelling can then be identied from a few trends by some authors in the following categories:

- Thermo-mechanical models (simple, porous, hygral).

  The authors who contributed to this category are those on the initial development of the set of thermo-mechanical modelling. Notorious authors found were: *Sullivan*, *McManus* and *Dimitrienko*.

- FDS – thermo-mechanical couplings.

  These authors are located during the middle stage of the paradigm. Relevant authors found were: *Dimitrienko* and *Luo*.

- Thermo-mechanical non-linear constitutive models.

  The main contributions to this topic, found during the middle-stage and late stage of the current paradigm, are published by *Mouritz*.

- Thermo-mechanical non-linear geometrical models.

  Although there is not *per se* much contribution in this field, due to its premature stage, some authors can be identified. Initially in terms of thermo-mechanical modelling, *Asaro*,is the co-author found in a thermo-mechanical model that

aimed to analyse thermal-buckling, which is highly understudy in the current state-of-the-art. In other publications where the topic is thermo-mechanical properties, *Asaro* can be found more extensively trying to provide experimental evidence to the framework previously dened.

Another author that provides experimental evidence to model non-linear geometric phenomenology is *Feih* who appears together with *Mouritz* in this section. She has tried to introduce the non-linear geometric model directly in terms of constitutive magnitudes such as stresses.

2.4.2 Thermo-mechanical Properties

With a total number of 119 publications, the set of thermo-mechanical properties can be considered the most prolific set in terms of research publications. It presents a maximum peak in the first decade of the 21st century – particularly the peak is found in 2009 – and there has been a recent growth during the second decade of this century.

It is evident from Figure 2.23 that the topic is still a hot topic, since the slope of the cumulative curve is still very positive, and shows clear signs to keep growing.

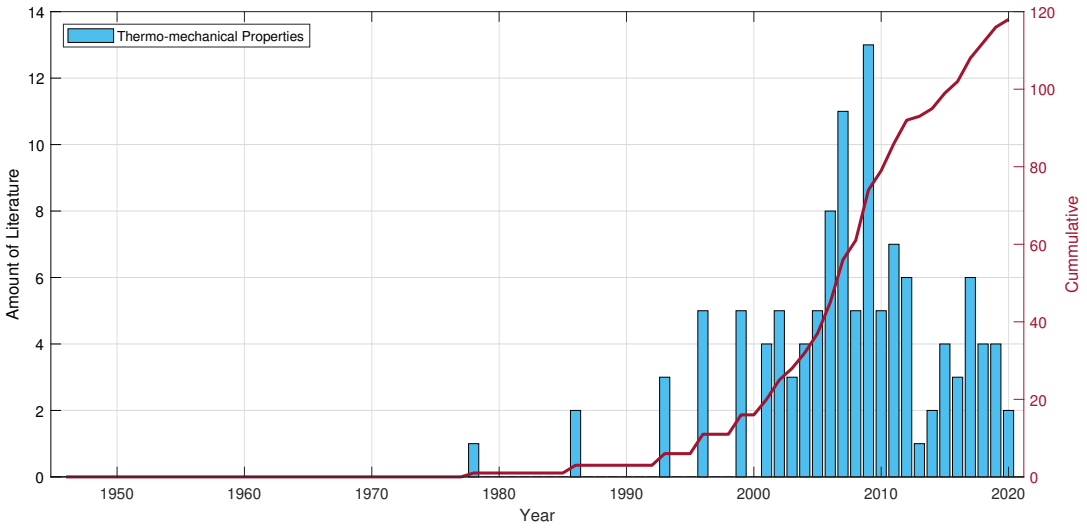

FIGURE 2.23: Research contribution in the topic of thermo-mechanical properties.

The first publication that provided experimental evidence of degradation of tensile and shear properties of composites exposed to fire is found in [207] by Pering et al. the year 1980. The second publication is found in [208] by Griffis et al. that analysed the degradation of the strength. The third by Budiansky and Fleck [209] who studied the effect of compressive failure.

Mcmanus et al. analyses the effect of thermal-fatigue in the polymeric matrix and derived in [211], Park and McManus quantify the damage. Dimitrienko investigated the thermo-structural response of FRP composites in [212]. Mahieux and Reifsnider [93] publishes an article centred in the effect of glass transition temperature on the

stiffness of composite materials. Mouritz and Mathys [213] studied the post-fire mechanical properties of composites, in [214], the study focuses on the tensile degradation, in [215], the main objective is the determination of compression degradation, and in [216], the post-fire flexural properties.

Sjögren and Asp in [217] provide more information in the effect of temperature in delamination under fatigue. Mahieux and Reifsnider provide information regarding transition temperature of thermoplastic systems. Mouritz in [219] experimentally studies the thermo-mechanical properties of materials used in aircraft. In [220] provides experimental calibrations to demonstrate the thermo-chemical degradation of mechanical properties. As co-author in the research of Gibson et al. in [14, 221], several experimental validations are given with regards thermo-mechanical properties. There is also experimental data for GRP plates in [222].

Bausano et al. studied in [223, 224] the effect of fire in composites under compression. Gu and Asaro, in [179], study the phenomenology of buckling due to the reduction of the stiffness caused by the increase of temperature. Feih et al. studies the effect in compression and tension strengths in composites exposed to fire [23]. Liu et al. in [225] studied the effect of one-dimensional buckling of a composite column. Gibson et al. in [226] presents experimental data of degradation of the thermo-mechanical properties under load in fire. Boyd et al. in [227] analyse the creep rupture of glass-vinyl-ester composites under fire loading. Others like Easby et al. [228] study the failure of phenolic and polyester pultrusions under load in fire. Feih et al. in [173] test their compression and tension models of strength against experimental data.

Gu and Asaro in [180] analyse the effect of thermo-mechanical degradation of plates due to transverse thermal gradients, or, e.g., in [182] the phenomenology of wrinkling – a non-linear geometric phenomenon – under transverse thermal gradients. In [185] conduct a similar experiment as in [182]. In [183], Gu and Asaro, provide experimental data to aid in the design of sandwich panels exposed to fire. In [184], they assess the structural stability of panels against thermal buckling. Some more recent research, from Asaro et al. in [178], focuses on the test of the structural response of FRP composites during fire.

Zhang et al. in [229], shows a validation through experimental test of their thermo-mechanical model. Summers et al. [230] provides data about the failure time of certain polymer composites exposed to fire. Burns et al. in [231] studies the compression failure of carbon-epoxy composites in fire. Feih et al. in [174] analyses the effect of fire in passive thermal barriers. In [232] studies the thermal softening and thermal recovery of compression strength for balsa wood. In [233] provides data on time-to-failure and temperature of different composite materials. In [175], they continue with the thermal recovery and treatment of recycled glass fibre.

Boyd et al. [234] provide an experimental study on a mechanistic approach of the response of composites in fire. Clifton et al. [235] provide experimental data on thermo-mechanical properties for sandwich composites. Summers et al. in [236] provide a sensitivity analysis of composite materials. Feih and Mouritz [176] analyse the tensile degradation of GRP composites. In [237] provide experimental thermo-mechanical properties of composites exposed to fire. In [238] perform experimental testing to quantify the compression failure in fire. In [239] provide a similar analysis as in [236].

Feih et al. in [25] provide skin failure experimental data for sandwich composites in fire. In [240] provide experimental data in tension failure of sandwich composites. In [241] information regarding fire resistance of basalt fibre composites. In [242] an experimental study is conducted to find the post-fire mechanical properties of sandwich structures. In [243] a similar experimental analysis is done as in [241] but for flax fibres this time. In [177] presented a determination method to obtain the strength loss during thermal recycling of waste composites. In [244] the deterioration of structural resistance when not only fire is taken into account but osmosis as well.

Ridzuan et al. in [245] experimentally assess the thermo-mechanical behaviour of purpureum/glass-epoxy hybrid composites. Grigoriou and Mouritz in [246] analysed the mechanical effect of the ply stacking pattern in the presence of fire. Anjang et al. in [247] analysed the mechanical tensile strength in terms of the ply orientation when exposed to fire. Bhat et al. [248] experimentally studied the tensile properties of plant fibre polymer composites in fire. Fitriah et al. in [78] evaluated the influence of hydro-thermal ageing and how this affects the compression strength of glass-epoxy composites. Revati et al. in [249] continued the work in [245].

Bhat et al. in [250] studied the thermo-mechanical properties of thermally recycled basalt fibre composites. Grigoriou and Mouritz in [251] tested the thermo-mechanical properties of metal laminates. Ridzuan et al. in [252] assessed the effect of moisture exposure in composites exposed to elevated temperatures and Dimitrienko et al. in [46] experimentally studied the stresses under non-uniform temperature heating.

A summary of the evolution is given in the next lines. The paradigm started with quantication of tensile and shear properties and evolved to take into account also compression since many composite solutions are non-symmetric in their axial behaviour. Testing compression proved rather difcult, since only the composite as a whole or the matrix can be tested. The modern testing involves also the quantication of bres, however, the calculus only takes into account short bre tests which are less prone to buckling. *Mouritz* has contributed especially on these areas.

After having set a testing framework and characterised the thermo-mechanical behaviour of several composite materials, the paradigm moved into the characterisation of the thermo-mechanical properties especially in post-re and after transition temperatures (glass transition temperature indeed).

In parallel, the paradigm has gained interest in topics such as thermal buckling and its methodology or the properties needed to measure the exibility that are characteristic of buckling

In the recent years, there has been an increase of publications towards the assessment of thermo-mechanical properties from thermally cured and recycled materials, and also in taking into account the hygro-thermal and osmosis effects that are very characteristic of marine environment and how this affects the thermo-mechanical response of composite structures.

Note that there is a clear common topic in research of the authors such as *Mouritz*, *Gibson*, *Feih* or *Mathys*, *Summers*, *Bhat*, *Anjang* or *Grigoriou* Grigoriou that is the characterisation of thermo-mechanical properties in terms of strengths, stiffness, elastic

modulus, yielding stresses, stack layout or bre orientation. And also, another key aspect, covered in the paradigm by authors such as *Gu* or *Asaro*, is the temperature dependent buckling.

In the lines of the previous paragraph, a topic of study that has recently emerged in the current paradigm, is the analysis of inelastic thermal buckling, which is the combination of the efforts, from past research, in merging constitutive and geometric non-linear dependencies in order to characterise the behaviour of commonly-used composite structures (generally sandwich or monolithic panels).

2.4.3 Summary

To give a more extensive view of the paradigm to the reader, a chart encompassing the publications in decades is shown in Figure 2.24. In order to avoid excessive redundancy, the scope of this subsection will be limited to just the analysis of the sets belonging to thermo-mechanical modelling (*thermo-mechanical model* and *thermo-mechanical properties*).

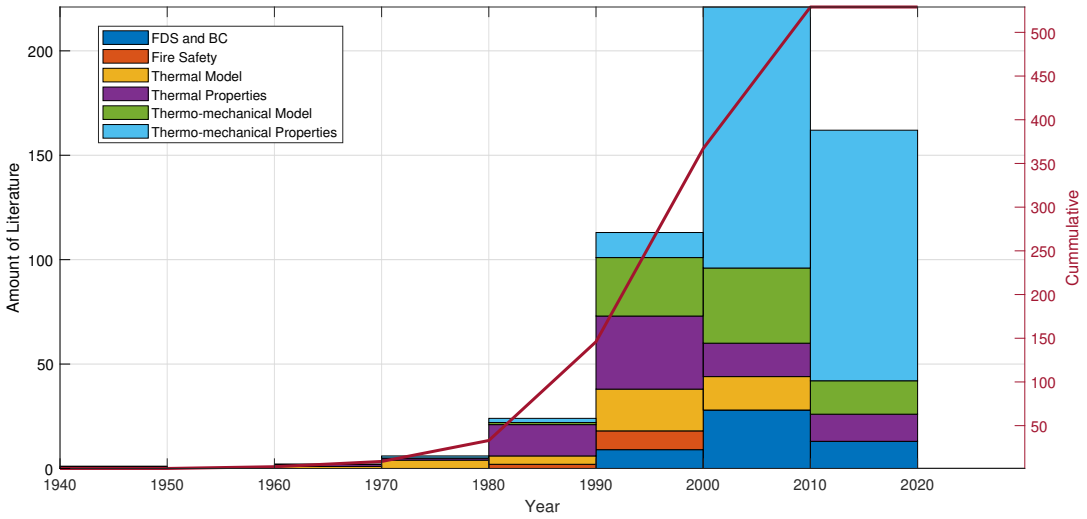

FIGURE 2.24: Bulk research contribution in the topic of thermo-mechanical modelling of composites. Timeline expressed in decades.

It is clear that, in a broader sense, the peak of the research of the paradigm was during the rst decade of this century. The set of thermo-mechanical properties is the most notorious, since it is understandable that the thermo-mechanical models are validated against experimental data.

As the paradigm on thermal modelling started to fade out from one-dimensional heat transient problems, the authors started tackling the ulterior problem that is how re affects the structural response of composite structures. This is the reason behind the fact that the set of thermo-mechanical model has a larger amount of publications compared to the set of thermal model, however it is smaller if compared with the set of thermo-mechanical properties.

2.4.4 Conclusion of the thermo-mechanical literature review

To close this subsection, the paradigm has been studied and concluded the importance of adapting the constitutive laws that model degradation of mechanical properties such as the Young's modulus or the yield stress in terms of the temperature and pyrolysis fraction [20]. Also, to use all the available thermal and thermo-mechanical data provided by the different authors in order to validate the thermo-mechanical model proposed in this thesis. And finally, it has been identified that the current paradigm demands a novel methodology to assess the large displacements that are characteristic of the intrinsic flexibility of composites, it is for this purpose that the thesis shall tackle the so-called *inelastic-thermal-buckling* phenomenology.

2.5 Conclusion

This literature review focuses the effort on solving the different questions relating to the three main topics: *thermal*, *mechanical* and *thermo-mechanical* modelling.

The thermal model has discussed the existent models that consider the composite as a heterogeneous media and focused on those that deal with the effects of pyrolysis and porosity

The thermal boundary conditions are another topic that needed special attention, some authors model the solution by simple re curves, other uses more elaborated models based on the temperature source and a third group use direct simulations using CFD analysis to obtain this latter temperature. Out of these three methods, the one where the temperature is found by means of the adiabatic surface temperature shined by its simplicity on par with its accuracy.

The mechanical models suitable for this research are triangle and quadrilateral shell lamina, and the possibility to extend the rst to include nonlinear geometric effects has been of great interest. The damage models researched have guided the solution to include the isotropic damage formulation, which indeed can be coupled with the SPROM to analyse the failure at the micro-scale level. This combination of theories produces a reliable framework with interesting precision and reduced computational cost.

The discussion on how to combine the thermal problem with pyrolysis with the mechanical problem with damage and large strains has been expanded. The combination of the different theories has led to consider also the temperature dependence of the elastic properties and the yield limit of the FRP materials. The only remnant topic that has not been addressed during the research, was how to combine all these models. The theory that plays a pivotal role here is the SPROM theory, which has been adapted to include thermal effects as well as thermo-chemical degradation.

Thanks to an objective analysis of the current literature, a novel contribution to the current paradigm has been identied, and the purpose of this thesis shall provide a novel contribution to this question.

Chapter 3

Modelling fire in marine structures

In the present chapter, the foundations are laid down, in specic, those of the study of marine structures under re load. The chapter aims to briey detail the most important topics involving re and composites and to deepen the paradigm and the proposed methodology. The chapter ends by posing the numerical model derived from the methodology that has been proposed to solve the governing equations that model the temperature evolution of composites exposed to re loads.

3.1 Introduction

Fire in structures, when undesired, is one of the major destructive reasons for the loss of human life, cargo or ultimately a potential collapse failure of the structure itself. In marine structural design, the different agents such as ship-owners, crews and IACS agree on the need of building re safe marine structures. Unfortunately, re can originate and spread in ships or offshore structures at any moment, and this is the case from time to time.

Fire safety engineering is a discipline focused on the application of scientic and engineering principles to the effects of re to minimise the loss of life and damage to property by the quantication of the risk and hazards and to adopt preventive or protective measures. Fire safety is achieved by a correct Performance-Based Fire Protection [8] and the steps that dene a successful Performance-Based Design are the identication of goals, possible re scenarios, analysis of those re scenarios and adequate criteria associated with them, effective evacuation, prediction of structural integrity and optimisation of the design in terms of reliability and durability of the protection system chosen.

Causes of re in the marine environment are attributable to several risks, such as electrical failure, equipment failure, especially those that contain inammable combustible material, residual combustible materials, those derived from the operation of the ship and also cases where structural failure or collision impact may result in the generation of re. A re represents a plausible thread when it grows in size, can to spread to other compartments and ultimately be extinguished or self-extinguished.

Once the risks are assessed, a strategy has to be adopted in order to guarantee the so-called fire-safety. Fire-safety is an area of study which contains majorly the following

categories: *physics, chemistry, fluid dynamics, material science, structural analysis, psychology and toxicology* [253].

In a broader categorical sense, re safety is intrinsically linked to re protection, which can be divide into in two categories: *Active Fire Protection* and *Passive Fire Protection*. While active requires automatic systems or human control, passive does not. Figure 3.1 illustrates the different subcategories in relation to re protection.

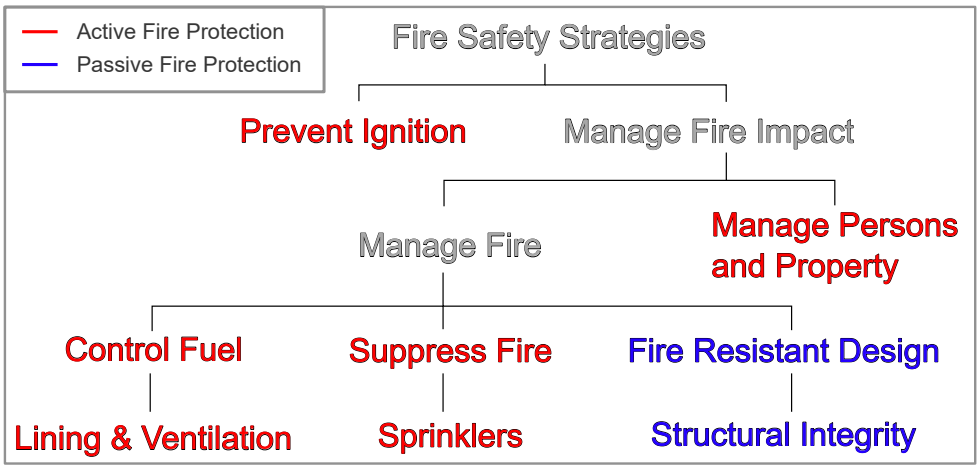

FIGURE 3.1: Strategies against fire. Adapted from [8]

This thesis aims to focus in those aspects that are characteristic of the *Passive Fire Protection*, a special distinction has to be made for its subcategories:

- Fire-Resistant Design

  Is a discipline focused on the production of materials that are highly resistant to fire, something *a priori* difficult since most of marine applications depend on polymer matrix solutions, which generally are very temperature sensitive.

  When re-resistant design is involved, the main goal of the designer is to produce a reliable design in terms of re resistance and retardancy, which are material-driven properties. The common approach is to use intumescent resins or dense insulation to avoid both the spread of re and mechanical failure.

  Current legislation and commercial applications understand that the vast range of passive re protections focuses mainly on producing an optimal re-resistant design.

- Structural Integrity

  This discipline is somehow of less importance for current requirements and focuses on the major failures or collapses a marine structure can undergo. The perception that this is somehow of less importance is related to the fact that actual requirements imposed on the fabrication of large-length ships made entirely of composite material are highly difcult to achieve as the structure to be built surpasses the limiting length of 50 meters. The reason behind this limitation is the expensiveness in experimental testing that a project of such characteristics needs to full.

  Structural integrity as a passive re protection is a type of analysis that does not solely focus on the material characterisation on board, but on the different

constraints resulting from several hypothetical re scenarios and the ability to predict the correct behaviour of the complete structure. While re-resistant design attempts to produce effective passive protection in terms of constitutive material design, structural integrity uses the previous as the starting point and incorporates the kinematic design to have an accurate prediction of the failure of the structure.

Fire is an exothermic process of oxidation of a combustible substance that releases heat and light in the form of a ame [8]. The evolution of a re can be characterised by Figure 3.2 in which the different stages are represented for a typical re load and compared against a design re curve. A real re is characterised by six stages and milestones: *ignition*, *growth*, *flashover*, *heating*, *fully developed* and *cooling*. And clearly, in comparison, the design re curve shows a more conservative re load that does not decay at any moment.

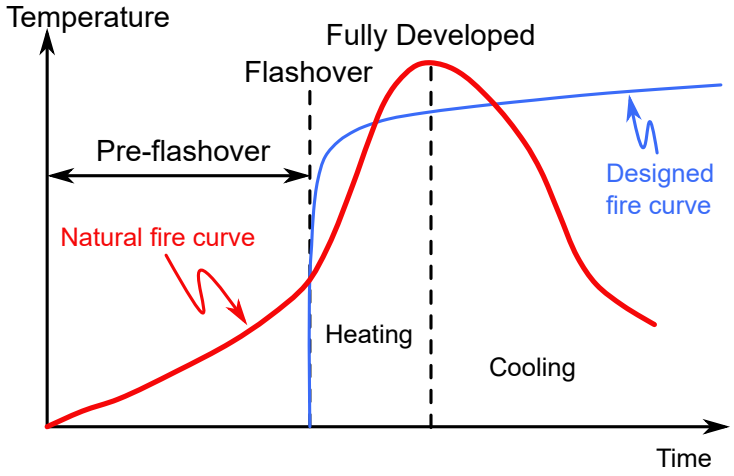

FIGURE 3.2: Characteristic stages of fire development

The question of how heat is transmitted arises when a continuous media is exposed to re. *A priori*, heat is transmitted as heat ux, however, the way a re load is introduced is by either heat ux (q) or temperature (T). From that point of view, the nature of the design re curve is generally expressed in terms of temperature and attempts to determine the re resistance of structural members.

The most iconic re curve is the *ISO 834* and the one used in most of the standards, therefore the name standard is widely used in literature to refer to this curve. Its a fairly extensive curve in terms of the range of applications and can be expressed as follows

$$T = T_\infty + 345 \log_{10}(8t + 1) \tag{3.1}$$

where T is the temperature, T_∞ is the ambient temperature. Nevertheless, for re originated in naval or marine applications, the *Hydrocarbon* re curve characterises better a real re scenario. The hydrocarbon curve differentiates concerning the standard curve on characterising a re load in the presence of burning hydrocarbon substances. This curve is expressed in the following manner.

$$T = T_\infty + 1080\left[1 - 0.325\exp\left(-0.167t\right) - 0.675\exp\left(-2.5t\right)\right] \tag{3.2}$$

Both curves defined in Equation 3.1 and Equation 3.2 can be compared in Figure 3.3, observe that the hydrocarbon curve increases rapidly its temperature than the ISO 834 curve in a shorter period of time.

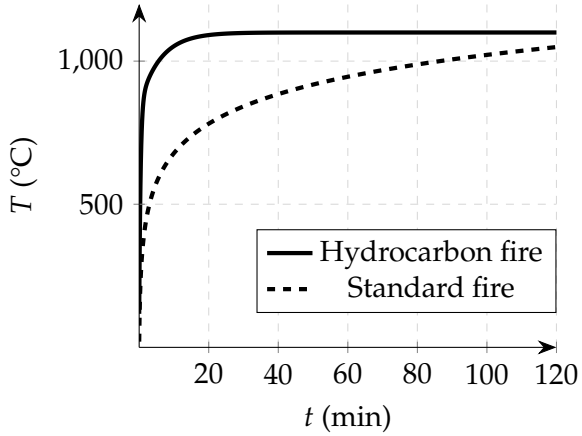

FIGURE 3.3: Hydrocarbon and ISO 834 fire curves.

When the thermal load is derived from the re in terms of heat ux, different models can be used to predict real re scenarios. One of the rst models is the re growth model from Quintiere [56] which is used to reproduce a real room-corner fire scenario. The method tries to obtain the surface temperature in the boundary by means of predicting the heat flux.

The boundary temperature can be obtained by the following relationship.

$$T_{\partial\Omega}(t) - T_\infty = \frac{1}{\sqrt{\pi c_k \rho c_p}} \int_0^{\bar{t}} \frac{\dot{q}(t)}{\sqrt{\bar{t} - t}}\, \mathrm{d}t \tag{3.3}$$

where q is the heat flux, $\partial\Omega$ is the boundary of the problem, ρ is the density, c_p is the specific heat capacity and c_k is the thermal conductivity coefficient. The term $(\bar{t})$ refers to the current instant of time and $(\partial\Omega)$ is the domain boundary. The heat flux can be defined by

$$\dot{q}(t) = \dot{q}_{\mathrm{ig}} + c_\sigma c_\varepsilon \left(T^4 - T_{\partial\Omega}^4\right) \tag{3.4}$$

where c_σ is the Stefan-Boltzman constant. The subscript in (q_{ig}) denotes the igniter flame heat flux and this means that the temperature associated with the igniter is not the same as in the radiative heat flux.

This model can be improved by the model proposed by Janssens [57], defining the different set of equations shown next

$$\dot{q}_i = \dot{q}_{cr}\left(1 + c_1^*\left(\frac{c_k \rho c_p}{c_{hig} t_{ig}}\right)^{c_2^*}\right) \tag{3.5}$$

where c_h is the thermal convection coefficient. The subscripts i, cr and ig refer to incident, critical and ignition respectively. The two coefficients (c_1^*, c_2^*) are just calibration parameters. The critical heat flux can be defined using

$$c_\varepsilon \dot{q}_{cr} = c_h\left(T_{\partial\Omega,ig} - T_\infty\right) + c_\sigma c_\varepsilon\left(T_{\partial\Omega,ig}^4 - {T_\infty}^4\right) \equiv c_{hig}\left(T_{\partial\Omega,ig} - T_\infty\right) \tag{3.6}$$

where c_ε is the thermal emissivity coefficient. Note that (c_{hig}) is the equivalent coefficient of thermal convection for the ignition heat flux. Remarkably, Janssens makes use only of the temperature of ignition of the exposed surface to predict the total flux. Another important aspect defined in [57] is that the coefficient of thermal convection is dependent on both the incident heat flux and surface temperature. E.g., [57] defines the dependency of the coefficient of thermal convection in respect to the incident heat flux as follows

$$c_h = 1.4 \cdot 10^{-4}\dot{q}_i + 2.4 \cdot 10^{-6}{\dot{q}_i}^2 \tag{3.7}$$

These methods summary up the most explicit ways to quantify the effect of re on a structural element. As explained, the purpose of these methods at the end is to either quantify the heat ux or the temperature on the surface from the re source. When a more detailed solution is needed, the requirements to full that are only met by the use of *Computational Fluid Dynamics (CFD)* in order to estimate the temperature generated in the exposed surface by a re source. One of the most popular solutions is the use of *Large Eddy Simulations (LES)* by using the *Finite Volume Method (FVM)*, e.g., [196] describes the implementations of an LES model to calculate the burning rate of combustion using hexahedra elements that contain a mixture of different material or phases such as air, fuel and combustion subproducts. This implementation, the so-called *Fire Dynamics Simulation (FDS)* solver, takes into account also the pyrolysis effect present on composite materials, and also it is an open-source software that can be coupled to any existing solution. FDS solvers can then be used to obtain a detailed solution for the prediction of through-thickness temperature in *FRP composites*.

3.2 Justification for the paradigm and methodology

When modelling composites exposed to high temperatures, the most organic manner to deal with the thermal problem is generally in terms of the temperature. The model proposed in this thesis adopts a similar approach as described in [11], that is, a one-dimensional non-linear heat transfer partial differential equation that is only exposed to re on one side. The thermal analysis of composites is rather complex since the heat transfer is heavily inuenced by a multitude of temperature-dependent processes.

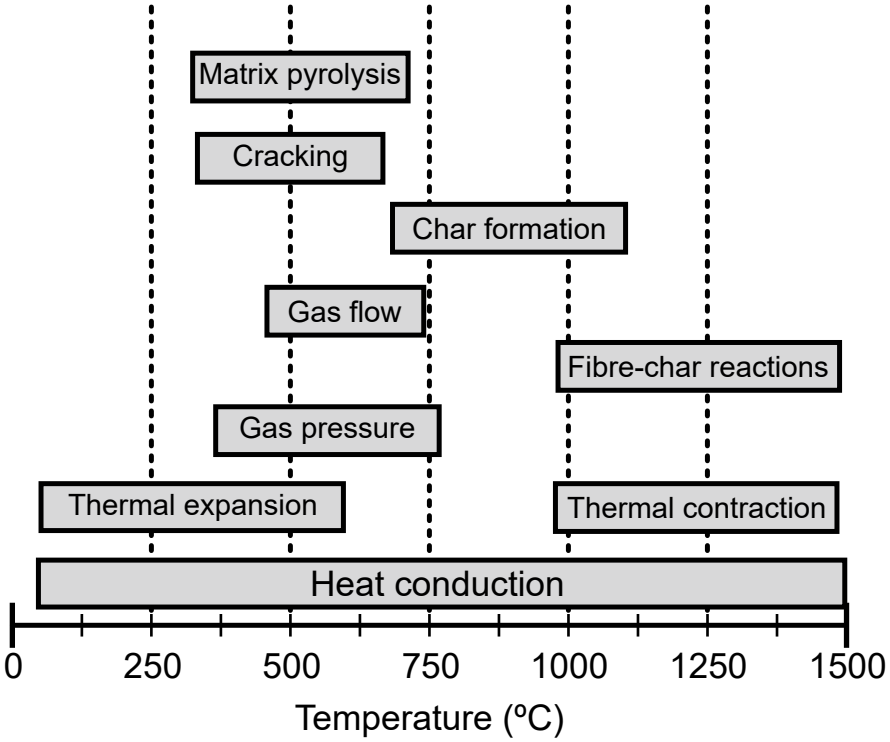

FIGURE 3.4: Thermal processes that are temperature-dependent in fibreglass laminates. Adapted from [7]

In naval applications, one of the most common types of laminates is the ones that employ breglass as their reinforce material. Figure 3.4 shows the different sort of temperature-dependent processes that a laminate of such characteristics can undergo in the presence of re. Albeit, not all the processes are considered in the model proposed by Henderson et al., it is very useful to understand the complexity and how this problem is heavily non-linear.

The current paradigm has adopted a solution in line with the model proposed by Henderson et al. This has its justication in the idea that ships and marine structures are largely characterised by beam and shell members. The concern regarding the degree of accuracy that a three-dimensional approach could add to the solution, is with ease dismissed when it comes to the computational cost if all the temperature-dependent processes are taken into account. However, if some are neglected, the advantage of the three-dimensional approach is not so clear. Therefore, the paradigm regarding composite structures exposed to high temperature is centred on the research pioneered by Henderson et al.

The paradigm can be analysed through the lens of the most important one-dimensional non-linear transfer models existent in the literature. The main aspects covered in the current paradigm are:

- *Virgin* and *char* states of the constituent materials.

  Pyrolysis plays a major role in the degradation of mechanical and thermal properties of the polymer matrix. In certain cases this thermo-chemical process may be considered in certain organic bres.

  This degradation process is crucial in composite laminates and it is one of the basic characteristics that differentiate them from metals. Therefore, all the reference thermal models do take into account this aspect. *Pyrolysis* then can be broken down into two sub-aspects: *Heat transfer through virgin and char material* and *Pyrolysis of matrix and also fibre constituent materials*. The first considers how the thermal properties depend on the pyrolysis fraction and the second on rather pyrolysis is considered *per se* only on the resin or resin and fibre.

- Gas transfer model.

  One of the key aspects of composites exposed to one-sided re is the generation of gas and how this is transferred. This aspect is also non-negligible and thus is covered in all the existent models. In the current paradigm, there are two methods to deal with this issue.

  The most common and oldest, especially if the governing equations are considered just one-dimensional, is to assume that the re is one-sided and that on the other side (*cold* side) the gas cannot escape. This is forcing the gas to escape in one direction and is the key to obtaining a rather simple gas modelling.

  The second approach is to introduce the gas pressure as another unknown and to solve the problem utilizing a Darcy or Flicks law and coupling this with a Darcy problem.

- Pressure-dependence.

  Generally, the pressure effect derived from the internal stresses is neglected. Albeit certain models use a monolithic approach [39] to take into account the pressure from the internal stress and its effects on the thermal transient problem, generally this effect is neglected. Instead, the gas pressure due to pore formation is usually addressed in various models [30, 39, 65, 190].

- Delamination, cracking and voids

  In the present paradigm, little research has been conducted on the delamination effect in the thermal model, especially because it should meet the same requirement in the mechanical model and to meet this second requirement is non-trivial. If delamination is considered at the mechanical level, then the next question that arises is the level of importance of this phenomenon in order to consider a two ways of coupling. In a practical sense, when delamination has occurred the structure is bound to rapidly rupture, therefore the interest in predicting the effect that delamination has on the heat transfer model is negligible when considering load-bearing structures.

  If the question revolves around the idea that delamination can be understood not only as a mechanical process but rather as a thermo-mechanical process, then as long as the effect of temperature and gas pressure is translated into the

mechanical model, the problem should be resolved by using standards cohesive techniques.

A similar discussion can be done on the effect of cracking in the sense of how cracking affects the accuracy of the heat transient model. E.g., for load-bearing structures, a two-way coupling is negligible due to its incipient mechanical failure. If it is the other way, as long as a suitable cohesive technique is employed, the question should be resolved.

Regarding voids, intrinsically addressing the porosity phenomenon, is very clear that porosity is always present in any load-bearing member and it does not correlate with structure imminent failure as with the other two fracture mechanisms. Virgin structures, those not being exposed to re yet, have a certain low level of porosity which affects their thermal properties rather than mechanical properties, it is generally when the porosity has evolved and covers an extensive zone that other failure mechanisms such as cracking, delamination, damage, plasticity or ablation may generate.

Thus these three aspects are not taken into account in the oldest models, however, Chippendale et al. in [30] proposed a way to model the evolution of porosity present in a porous media such as a laminate composite. This latter is interesting because porosity has a signicant impact on the thermal properties and enhances the prediction of heat transfer.

- Reaction between char and fibre.

  Another key aspect is the chemical reaction in the interaction between the charred resin and virgin bre and how this affects the heat transfer. This question is quite unexplored and at least non-considered in the current methodology.

- Ablation.

  The detachment of material is hardly taken into account at any level since for marine applications, ablation is rare to be found in re passive protection designs of structural members. Nevertheless, [65] and [30] do take into account this in their models. However, this question would be more of interest if the research was considering the ablation of the insulation material that in practice does not contribute to the structural stiffness of a load-bearing member.

	[11]	[39]	[65]	[254]	[190]	[30]
Heat conduction through virgin and char material	✓	✓	✓	✓	✓	✓
Pyrolysis of matrix and organic fibre	✓	✓	✓	✓	✓	×
Gas transfer model	✓	✓	✓	✓	✓	✓
Pressure-dependence	×	✓	✓	×	✓	✓
Delamination, cracking and voids	×	×	×	×	×	✓
Reaction between char and fibre	×	×	×	×	×	×
Ablation	×	×	✓	×	×	✓

TABLE 3.1. Summary table of the main temperature-dependent process taken into account in the current paradigm. Adapted from [7].

Table 3.1 describes the major differences between the models found in the literature. The category regarding thermal expansion is taken out from [7], since this section is

devoted purely to the thermal model and the addition of the research performed by Chippendale et al. are added, as is one of the most recent contributions regarding the introduction of porosity. This would conclude the justication to use the Henderson et al. model as a foundation for the research from this thesis. All the similar models in the actual paradigm derive from this rstborn model.

The other key aspect is regarding the treatment of the boundary conditions. The current paradigm divides into two main branches, treatment of the boundary conditions in the form of heat ux or in terms of a characteristic temperature. By characteristic, recall that the different sources of heat may be described concerning a different source temperature.

The most natural way to impose the boundary conditions is as heat ux, although in reality or experimental testing this proves to be rather difcult to meet (natural and forced heat convection). Hence, most of the methods introduce their boundary conditions as a heat ux, since it is naturally a heat ux boundary condition, however, they attempt to describe the evolution of this non-linear convection or radiation heat ux boundary condition in terms of the temperature.

If a heat ux of any sort is considered, the problem is *per se* solved. If temperature is considered, the research by Quintiere and Janssens is very useful and can be found across many of the current solutions. However, in this research, the solution based on the concept of adiabatic surface temperature by Wickstrom Ulf et al. in [28] is preferred.

The adoption of the methodology presented by Wickstrom Ulf et al. comes from the high impact this has on current standards such as the ISO 834 [255] or similar. Especially, regulations such as [256], require experimental testing of load-bearing structural elements such as decks or bulkheads according to a re curve characterised by the ISO 834.

3.3 Methodology

The research procedures described in the thermal model are ordered as follows:

1. Continuum mechanics.

   This subsection introduces the principal concepts to derive the one-dimensional non-linear heat transient model for a continuum media.

2. Species transport.

   The species transport theory expresses the same procedures detailed in the continuum mechanics subsection, however, in a phase or species manner. So each constituent phase has to full its own set of balance equations.

3. Composites exposed to fire.

   This subsection covers mostly the derivation of the thermal model. It describes what are composites, in specic *fibre reinforced plastic (FRP) composites* and the concept of *laminates*.

   Then it uses the species transport theory to explain the physics underneath composites when exposed to high temperature the species present in the continuum media will be the solid phase and the gas phase. I.e., the composite is indeed a porous continuum media.

   The last part of this subsection details the different aspects regarding constitutive properties of the thermal model, gas transfer and boundary conditions. And presents the temporal and spatial discretisation of the governing problem.

3.3.1 Continuum mechanics

The concepts introduced regarding continuum mechanics are very similar to those explained in any book. For example, the principle of balance of mass, linear momentum and energy are described in this subsection.

The interest in these three balance equations is principally focused on the obtention of the non-linear heat transfer equation for composites. Thus, the mass balance is introduced to later be expanded by the species theory, and the conservation of linear momentum is postulated to be used in the energy balance. And the energy balance is the governing partial differential equation that is of interest to be solved in order to obtain the through-thickness temperature distribution.

The basic principles of continuum mechanics are detailed in much different literature. In this thesis, the underlying concepts are extracted from [257].

3.3.1.1 Mass balance

The principle of mass balance is established by the following relationship

$$\int_{\Omega} \left[\frac{\partial \rho}{\partial t} + \underset{\bullet}{v} \cdot \nabla \rho + \rho \nabla \cdot \underset{\bullet}{v} \right] \mathrm{d}\Omega = w \tag{3.8}$$

where v is the velocity, Ω is the n-dimensional domain of the problem, σ is the stress and w is the generation of mass flux.

The generation of mass flux (w) may be considered zero only if the there is conservation of mass and negative if the mass flows through the boundary of the domain.

3.3.1.2 Conservation of linear momentum

From the point of view of the thermal model, the conservation of linear momentum can be postulated as

$$\int_{\Omega} \left[\frac{\partial \left(\rho \underset{\bullet}{v} \right)}{\partial t} + \nabla \cdot \left(\rho \underset{\bullet}{v} \right) \right] \mathrm{d}\Omega = \int_{\Omega} \left[\nabla \cdot \left(\underset{\bullet\bullet}{\sigma} \right) + \rho f_b \right] \mathrm{d}\Omega \tag{3.9}$$

The interest in the conservation of linear momentum or at least its balance is in its expression, which generally is employed in the simplication of the energy balance.

3.3.1.3 Energy balance

$$\begin{aligned} \int_{\Omega} \left[\frac{\partial \left(\rho \left(e_i + \frac{1}{2} \| \underset{\bullet}{v} \| \right) \right)}{\partial t} + \nabla \cdot \left(\rho \underset{\bullet}{v} \left(e_i + \frac{1}{2} \| \underset{\bullet}{v} \| \right) \right) \right] \mathrm{d}\Omega \\ = \int_{\Omega} \left[-\nabla \cdot \underset{\bullet}{q} + \nabla \cdot \left(\underset{\bullet\bullet}{\sigma} \cdot \underset{\bullet}{v} \right) + \rho \underset{\bullet}{v} \cdot f_b \right] \mathrm{d}\Omega + Q \end{aligned} \tag{3.10}$$

where e_i is the specific internal energy, Q is the heat source. Since conservation of linear momentum is enforced, Equation 3.10 can be simplified using Equation 3.9.

$$\int_{\Omega} \left[\frac{\partial \left(\rho e_i \right)}{\partial t} + \nabla \cdot \left(\rho \underset{\bullet}{v} e_i \right) \right] \mathrm{d}\Omega = \int_{\Omega} \left[-\nabla \cdot \underset{\bullet}{q} + \underset{\bullet\bullet}{\sigma} : \nabla \underset{\bullet}{v} \right] \mathrm{d}\Omega + Q \tag{3.11}$$

Specic internal energy is a thermodynamic state variable that is rarely used in applied engineering. The use of specic enthalpy is more common, the latter can be introduced using the relationship between the specic enthalpy and the specic internal energy, Equation 3.11 can be re-written in its enthalpy form

$$e_i = h - \frac{p}{\rho} \tag{3.12}$$

where h is the specific enthalpy, p is the pressure. Substituting Equation 3.12 into Equation 3.11 and using Equation 3.8 the energy balance equation yields

$$\begin{aligned}\int_\Omega \left[\rho\frac{\partial h}{\partial t} + \rho\underset{\bullet}{v}\cdot\nabla h + h\cancelto{0}{\left[\frac{\partial \rho}{\partial t} + \nabla\cdot(\rho\underset{\bullet}{v})\right]}\right] \mathrm{d}\Omega \\ = \int_\Omega \left[-\nabla\cdot\underset{\bullet}{q} + \underset{\bullet\bullet}{\sigma} : \nabla\underset{\bullet}{v}\right] \mathrm{d}\Omega + Q\end{aligned} \tag{3.13}$$

Although formulating energy balance concerning specic enthalpy is feasible and less rare than specic internal energy, engineers widely prefer the choice of temperature to express the conservation of energy. Thus, the specic enthalpy is related to the temperature by

$$\begin{cases} \mathrm{d}h = c_p\,\mathrm{d}T + \frac{1}{\rho}(1-\alpha T)\,\mathrm{d}p \\ \alpha T = 1, \quad \text{(ideal gas)} \end{cases} \tag{3.14}$$

where α is the thermal expansion coefficient. If the heat flux within the material is considered to be conductive and be described by the Fourier's Law

$$\underset{\bullet}{q} = -c_k\nabla T \tag{3.15}$$

Therefore Equation 3.13 can be re-written in terms of temperature by means of the relationship described in Equation 3.14 and Equation 3.15.

$$\begin{aligned}\int_\Omega \left[\rho c_p\frac{\partial T}{\partial t} + (1-\alpha T)\frac{\partial p}{\partial t} + \rho c_p\underset{\bullet}{v}\cdot\nabla T + (1-\alpha T)\,\underset{\bullet}{v}\cdot\nabla p\right] \mathrm{d}\Omega \\ = \int_\Omega \left[\nabla\cdot(c_k\nabla T) + \underset{\bullet\bullet}{\sigma} : \nabla\underset{\bullet}{v}\right] \mathrm{d}\Omega + Q\end{aligned} \tag{3.16}$$

Assuming that the gas is ideal, incompressible and its viscosity is negligible. Equation 3.16 becomes

$$\int_\Omega \left[\rho c_p\frac{\partial T}{\partial t} + \rho c_p\underset{\bullet}{v}\cdot\nabla T\right] \mathrm{d}\Omega = \int_\Omega \left[\nabla\cdot(c_k\nabla T)\right] \mathrm{d}\Omega + Q \tag{3.17}$$

3.3.2 Species transport

The concept of species is very useful to model heterogeneous media.Figure 3.5 represents a medium that at the macroscopic level can be perceived as a continuum media, however, at the microscopic level, two different species can be observed.

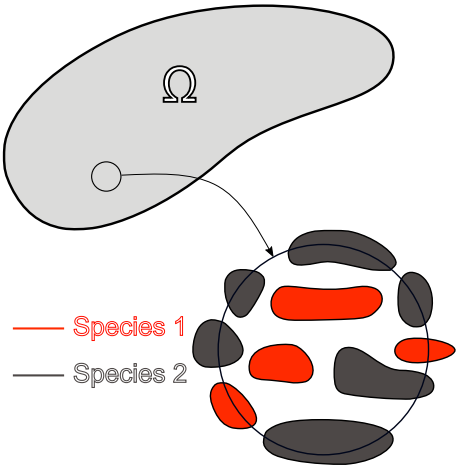

FIGURE 3.5: Biphasic species domain

The species transport theory aims to achieve macroscopic equilibrium of the continuum mechanics equations described before while not violating them at the microscopic level. Instantaneous quantities are the resultant of the interaction of macroscopic (average) and microscopic (diffusion) quantities. Note that quantities of interest are the same as dened before but expressed by the subscript $_i$, when the subscript $_i$ may be present under a certain quantity, it shall indicate that the quantity is characterised by the properties of species $_i$. Also, the domain is composed of n number of species.

The foundations from species transport theory can be understood as a convection-diffusion equation applied to the mass and partitioned in different phases. Useful literature can be found [258] tthat treats the problem from a gas transfer perspective, or [259], that uses a biphasic approach and considers the solid phase as a hollow skeleton.

Generally, the velocity of the media is chosen as the quantity of interest. The velocity of a species at microscopic level is dened as

$$\underset{\bullet}{v}_i = \underset{\bullet}{v} + \hat{\underset{\bullet}{v}}_i \tag{3.18}$$

where v_i, vi and $\hat{v}_i$ are the instant, average and diffusion velocity of the species i respectively. The average velocity can be found by means of the mass-averaged participation.

$$\underset{\bullet}{v} = \frac{\sum_i^n m_i \underset{\bullet}{v}_i}{\sum_i^n m_i} \equiv \sum_i^n \Phi_{mi} \underset{\bullet}{v}_i \tag{3.19}$$

where m is the mass, Φ_m is the mass fraction. The following relationships are established.

$$\begin{cases} \Phi_{mi} = \frac{m_i}{\sum_i^n m_i} \\ \Phi_{\Omega i} = \frac{\Omega_i}{\sum_i^n \Omega_i} \\ \Phi_{\rho i} = \dfrac{m_i/\Omega_i}{\sum_i^n m_i / \sum_i^n \Omega_i} = \frac{\rho_i}{m/\Omega} \end{cases} \tag{3.20}$$

where Φ_Ω is the volume fraction, Φ_ρ is the density fraction. Note that the domain of the species (Ω_i) is equivalent to its occupied volume. Therefore, the mass fraction can be related to the density fraction and the volume fraction. The latter can also be referred to as *porosity*.

$$\Phi_{mi} = \Phi_{\rho_i} \cdot \Phi_{\Omega i} \tag{3.21}$$

The net diffusion is considered in the macroscopic scale to be negligible. At the microscopic level, the diffusion can be modelled by a diffusion law, either Flicks law for gasses or Darcys law in the case of uids.

$$\sum_i^n \Phi_{mi} \hat{\underset{\bullet}{v}}_i = 0 \tag{3.22}$$

$$\Phi_{mi} \hat{\underset{\bullet}{v}}_i = -C_{di} \nabla \Phi_{mi} \tag{3.23}$$

where C_d is the diffusion coefficient.

3.3.2.1 Mass balance

The mass balance defined in Equation 3.8 is described in Equation 3.24 for each species $_i$. Note that the summation over all the species retrieves its original form.

$$\begin{aligned} \int_\Omega \left[\frac{\partial \left(\Phi_{mi} \rho \right)}{\partial t} + \nabla \cdot \left(\rho \Phi_{mi} \underset{\bullet}{v}_i \right) \right] \mathrm{d}\Omega &= \int_\Omega \left[\nabla \cdot \underset{\bullet}{q}_{m_i} \right] \mathrm{d}\Omega \\ &= - \int_{\partial\Omega} \left[\underline{n} \cdot \underset{\bullet}{q}_{m_i} \right] \mathrm{d}\Omega = -w_i \end{aligned} \tag{3.24}$$

where q_m is the mass flux, $\underline{n}$ is the normal. The negative sign convention in the rate of generation of mass flux term indicates that a positive generation rate defines an outward flux of mass rate in the domain, and negative an inward flux of mass rate.

The generation of mass flux, either in microscopic and macroscopic level, might be positive (source), negative (sink) or null (zero) in the domain (Ω) and its boundaries ($\partial\Omega$). However, it makes sense that inside the domain – excluding the boundaries –

the generation rate has to be null in the macroscopic level. I.e., all the species have to equilibrate their generation rate of mass flux.

$$\sum_{i}^{n} w_i = 0 \tag{3.25}$$

3.3.2.2 Conservation of linear momentum

The procedure for deriving the linear momentum expressed using the species transport theory is similar to the continuity derivation. Since the expression without species transport was previously derived and used in the simplication of the energy balance, the energy balance expressed in terms of species transport will be derived similarly to Equation 3.13 that cancels certain terms assuming conservation of the linear momentum.

3.3.2.3 Energy balance

The balance of energy expressed in species can be described as follows. Note that, similarly to the continuity equation, the macroscopic energy balance would be the resultant from the summation overall species.

$$\begin{aligned} &\int_{\Omega} \left[\frac{\partial \left(\rho \Phi_{mi} h_i\right)}{\partial t} + \nabla \cdot \left(\rho \Phi_{mi} \underset{\bullet}{v}_i h_i \right) \right] \mathrm{d}\Omega \\ &= \int_{\Omega} \left[\nabla \cdot \left(\Phi_{mi} c_k \nabla T \right) + \underset{\bullet\bullet}{\sigma}_i : \nabla \left(\Phi_{mi} \underset{\bullet}{v}_i \right) \right] \mathrm{d}\Omega + Q_i \end{aligned} \tag{3.26}$$

Expanding Equation 3.26

$$\begin{aligned} &\int_{\Omega} \left[h_i \frac{\partial \left(\rho \Phi_{mi}\right)}{\partial t} + \rho \Phi_{mi} \frac{\partial h_i}{\partial t} + \rho \Phi_{mi} \underset{\bullet}{v}_i \nabla h_i + h_i \nabla \cdot \left(\rho \Phi_{mi} \underset{\bullet}{v}_i \right) \right] \mathrm{d}\Omega \\ &= \int_{\Omega} \left[\nabla \cdot \left(\Phi_{mi} c_k \nabla T \right) + \underset{\bullet\bullet}{\sigma}_i : \nabla \left(\Phi_{mi} \underset{\bullet}{v}_i \right) \right] \mathrm{d}\Omega + Q_i \end{aligned} \tag{3.27}$$

Since enthalpy is specific for each species, the relationship in Equation 3.12 can be introduced to describe the energy balance concerning two state variables (temperature and pressure) that are equal at microscopic and macroscopic levels.

$$\begin{aligned} &\int_{\Omega} \left[h_i \frac{\partial \left(\rho \Phi_{mi}\right)}{\partial t} + \rho \Phi_{mi} \left(c_{p_i} \frac{\partial T}{\partial t} + \frac{1}{\rho} (1 - \alpha T) \frac{\partial p}{\partial t} \right) + \rho \Phi_{mi} \underset{\bullet}{v}_i \nabla h_i \right] \mathrm{d}\Omega \\ &= \int_{\Omega} \left[\nabla \cdot \left(\Phi_{mi} c_{k_i} \nabla T \right) + \underset{\bullet\bullet}{\sigma}_i : \nabla \left(\Phi_{mi} \underset{\bullet}{v}_i \right) - h_i \nabla \cdot \left(\rho \Phi_{mi} \underset{\bullet}{v}_i \right) \right] \mathrm{d}\Omega + Q_i \end{aligned} \tag{3.28}$$

Note that Equation 3.28 can be further expanded using Equation 3.12. The energy balance of a media, described in Equation 3.17, can be obtained by adding the contribution of each species.

$$\sum_{i}^{n}\int_{\Omega}\left[h_i\frac{\partial\left(\rho\Phi_{mi}\right)}{\partial t}+\rho\Phi_{mi}\left(c_{p_i}\frac{\partial T}{\partial t}+\frac{1}{\rho}(1-\alpha T)\frac{\partial p}{\partial t}\right)+\rho\Phi_{mi}\underset{\bullet}{v}_i\nabla h_i\right]\mathrm{d}\Omega$$
$$=\sum_{i}^{n}\int_{\Omega}\left[\nabla\cdot(\Phi_{mi}c_{ki}\nabla T)+\underset{\bullet\bullet}{\sigma}_i:\nabla\left(\Phi_{mi}\underset{\bullet}{v}_i\right)-h_i\nabla\cdot\left(\rho\Phi_{mi}\underset{\bullet}{v}_i\right)\right]\mathrm{d}\Omega+Q_i \tag{3.29}$$

3.3.3 Composites exposed to fire

Composites are materials that are composed of two or more constituent materials. Generally, the composites studied in this thesis are those that fit inside the categories of *laminate* and *fibre reinforced plastic (FRP)* composites. The *lamina*, layer or ply, is the unit that composes a *laminate* when stacked in normal direction to the *lamina* as shown in Figure 3.6.

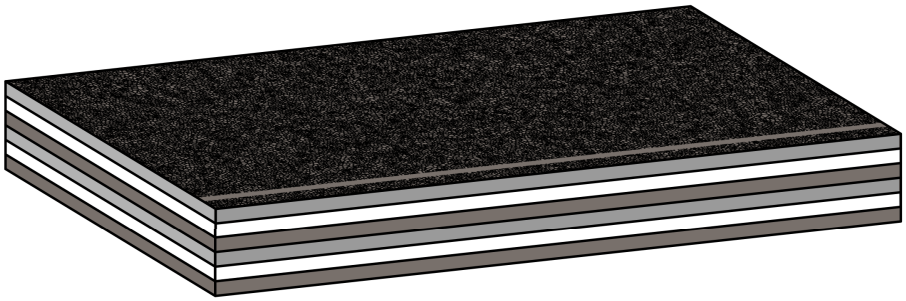

FIGURE 3.6: Composite media made of lamina stacking.

The special case of *FRP composite laminate* is described in Figure 3.7, formally, as long as one *lamina* in the stacking of the *FRP laminate* is an *FRP lamina*, the whole material can be considered as an *FRP composite laminate*. An *FRP lamina* is a layer of a polymer (resin) that is reinforced with fibres aligned in certain orientation.

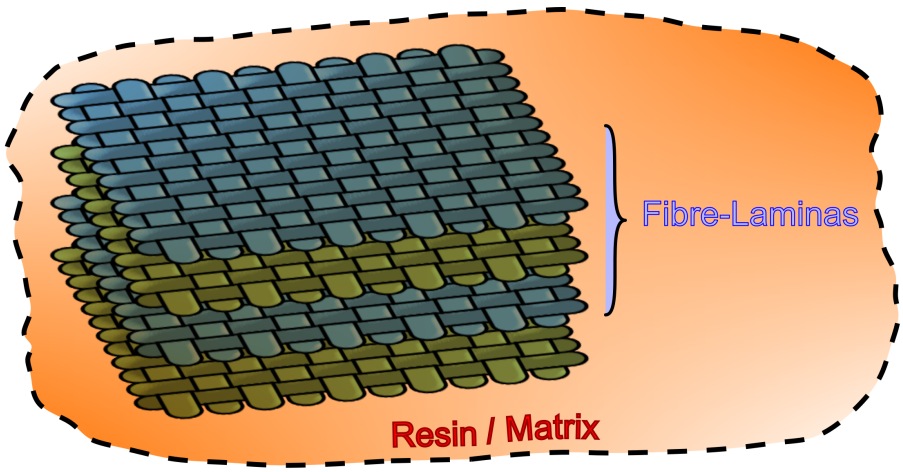

FIGURE 3.7: Composite media made of FRP lamina stacking.

Laminates are materials that present a very characteristic orthotropic behaviour. If Equation 3.29 is to be considered for a material such as a *laminate*, a few simplifications can be made regarding the continuum domain. Figure 3.8 shows a *laminate*-like structure that is exposed to high temperatures, *laminate*-like structures transport heat in three main directions (orthotropy) and thus for a *lamina*, the heat transfer from the exposed or hot surface to the unexposed or cold surface can be essentially assumed as a one-dimensional heat transfer problem.

This figure also shows the different types of thermal loads and illustrates the concept of *pyrolysis*, which is intrinsically related to the charring of a polymeric resin after being exposed to excessive temperatures [7]. The gas flow generally follows a path from a cold zone to a hotter zone.

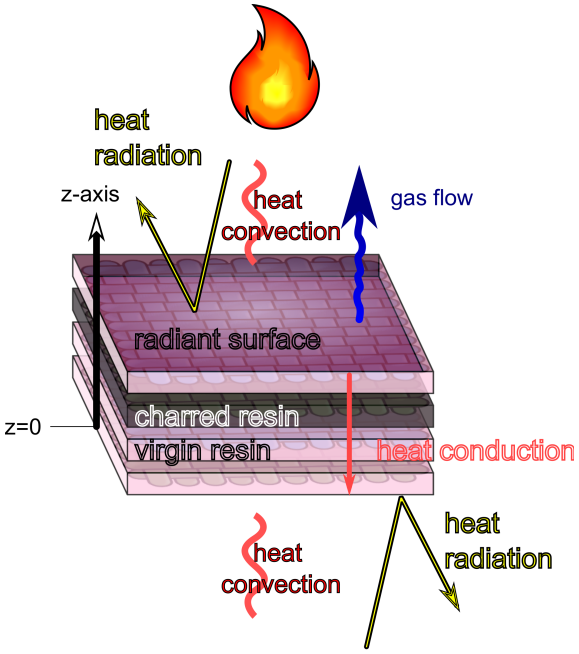

FIGURE 3.8: One-dimensional heat transfer problem.

Considering that Equation 3.28 is one-dimensional and expressed differentially, it can be re-written and divided into the following terms:

$$\underbrace{\rho\Phi_{mi}c_{p_i}\frac{\partial T}{\partial t}}_{\text{thermal transient heat}} = -\underbrace{\Phi_{mi}(1-\alpha T)\frac{\partial p}{\partial t}}_{\text{volumetric transient heat}} - \underbrace{h_i\frac{\partial\left(\rho\Phi_{mi}\right)}{\partial t}}_{\text{mass transient heat}} + \underbrace{\nabla Q_i}_{\text{specific internal heat source}}$$

$$+\underbrace{\nabla\cdot\left(\Phi_{mi}c_{ki}\nabla T\right)}_{\text{conductive heat}} + \underbrace{\underset{\bullet\bullet}{\sigma}_i : \nabla\left(\Phi_{mi}\underset{\bullet}{v}_i\right)}_{\text{adiabatic heat}} - \underbrace{\left(\rho\Phi_{mi}\underset{\bullet}{v}_i\right)\nabla h_i}_{\text{species heat transfer}} - \underbrace{h_i\nabla\cdot\left(\rho\Phi_{mi}\underset{\bullet}{v}_i\right)}_{\text{convective mass flux heat}} \tag{3.30}$$

3.3.3.1 Solid phase

Considering the solid phase, composed of fibre and matrix, Equation 3.30 yields

$$\underbrace{\rho\Phi_{ms}c_{p_s}\frac{\partial T}{\partial t}}_{\text{thermal transient heat}} = -\underbrace{\Phi_{ms}(1-\alpha T)\frac{\partial p}{\partial t}}_{\text{volumetric transient heat}} - \underbrace{h_s\frac{\partial\left(\rho\Phi_{ms}\right)}{\partial t}}_{\text{mass transient heat}} + \underbrace{\nabla Q_s}_{\text{specific internal heat source}}$$

$$+\underbrace{\nabla\cdot\left(\Phi_{ms}c_{k_s}\nabla T\right)}_{\text{conductive heat}} + \underbrace{\underset{\bullet\bullet}{\sigma}_s : \nabla\left(\Phi_{ms}\underset{\bullet}{v}_s\right)}_{\text{adiabatic heat}} - \underbrace{\left(\rho\Phi_{ms}\underset{\bullet}{v}_s\right)\nabla h_s}_{\text{solid heat transfer}} - \underbrace{h_s\nabla\cdot\left(\rho\Phi_{ms}\underset{\bullet}{v}_s\right)}_{\text{convective mass flux heat}} \tag{3.31}$$

Each term in Equation 3.31 can be analysed based upon certain physical assumptions.

- Thermal transient heat

  It is more than reasonable that a solid material has thermal inertia associated, which is described by the solid specic heat capacity. Thus, this term cannot be neglected.

- Volumetric transient heat

  A solid that experiments a change in its volume will necessarily change its temperature. This is very common when exerting a certain external work into a thermo-dynamical system. Nevertheless, volumetric transient heat refers to the rate of heat associated to a material due to changes in pressure and that it is linearly dependent on the rate of change of the pressure. If the rate of change of the pressure can be assumed negligible – which is very sensical for thermo-mechanical applications in the field of solid mechanics– the heat generated due to the changes of the internal pressure is also negligible.

  This is similar to assume that the expansion of the solid has no significant contribution to the thermal problem.

- Mass transient heat

  As any thermal problem, the rate of change of density is important since from a thermo-dynamic point of view, a material has an enthalpy associated to the quantity of mass it has. Thus, it is obvious that the rate of change of the mass in a continuum media generates a heat flux proportional to the specific enthalpy of the so-called media.

- Specific internal heat source

  This term it is more general and it is not constraint to be a specific quantity. This term incorporates all the different source models that a thermo-dynamic system can have, and they do not even need to be specific (per unit of mass) or volumetric (per unit of volume). E.g., in polymeric materials the ignition or degradation due to thermal loading of the polymeric resin generates a heat associated to its decomposition and this degradation heat source needs to be modelled, commonly by establishing a rate of degradation associated to an enthalpy of degradation (see Equation 3.32).

$$Q_p = -\frac{\partial \rho}{\partial t} h_p \tag{3.32}$$

where Q_p is the heat of decomposition, h_p is the specific enthalpy of decomposition.

- Conductive heat

  Conduction is the thermal transfer of energy that is characteristic only between solids. Thus, conduction is taken into account in *FRP laminate* consisting of *FRP lamina*s.

- Adiabatic heat

  The adiabatic heat is the term that incorporates the constitutive model into the energy balance. The stress tensor generally can be divided into a hydrostatic and a deviatoric term. If, again, the stress effects due to thermal loading are negligible to those from mechanical loading, both terms can be negligible in the solid phase.

  The adiabatic heat conceptually is similar to the volumetric transient heat in the sense that in the solid phase, the contraction or expansion (due to self-temperature or due to external mechanical loading), has no impact on the distribution of the temperature across the thickness of an *FRP laminate*.

- Solid heat transfer and convective mass flux heat

  Both terms are negligible, since both involve the mass flux inside a solid media. Solids in certain times can be considered to loss mass by means of mass flux, however composites are characteristic for degrading by pyrolysis which not necessarily implies the loss of mass by mass flux. If species transport is considered, the mass fraction participation can be used to address the loss of mass in order to not violate the continuity equation (Equation 3.24). Therefore, mass flux of the solid phase is equal to zero because no mass is being transported inside the domain, the only mass loss is the one in the boundaries with the gas phase.

$$\dot{q}_{m_s} = \rho_s \dot{\underline{v}}_s = 0 \Rightarrow \int_\Omega \left[\rho \Phi_{ms} \dot{\underline{v}}_s \right] \, \mathrm{d}\Omega = 0 \tag{3.33}$$

  Equation 3.33 intrinsically imposes a constraint in the continuity equation (Equation 3.24) for the solid phase.

$$\int_\Omega \left[\frac{\partial \left(\Phi_{ms} \rho \right)}{\partial t} \right] \, \mathrm{d}\Omega = -\int_\Omega \left[\nabla \cdot \dot{q}_{m_s} \right] \, \mathrm{d}\Omega = -\int_{\partial\Omega} \left[\underline{n} \cdot \dot{q}_{m_s} \right] \, \mathrm{d}\Omega = -w_s \tag{3.34}$$

  Note that generation of mass flux in the boundary (w) is negative since the solid mass is decreased.

The energy balance for the solid species then can be re-formulated.

$$\underbrace{\rho\Phi_{m_s}c_{p_s}\frac{\partial T}{\partial t}}_{\text{thermal transient heat}} = -\underbrace{h_s\frac{\partial\left(\rho\Phi_{m_s}\right)}{\partial t}}_{\text{mass transient heat}} - \underbrace{\frac{\partial\rho_s}{\partial t}h_p}_{\text{polymer's degradation rate}} + \underbrace{\nabla\cdot\left(\Phi_{m_s}c_{k_s}\nabla T\right)}_{\text{conductive heat}} \tag{3.35}$$

3.3.3.2 Gas phase

The other phase in the composite media is the gas, which is the result from the mixture of reaction gases and moisture vapours generated from the ignition of the composite (generally associated to the resin).

$$\underbrace{\rho\Phi_{m_g}c_{p_g}\frac{\partial T}{\partial t}}_{\text{thermal transient heat}} = -\underbrace{\Phi_{m_g}(1-\alpha T)\frac{\partial p}{\partial t}}_{\text{volumetric transient heat}} - \underbrace{h_g\frac{\partial\left(\rho\Phi_{m_g}\right)}{\partial t}}_{\text{mass transient heat}} + \underbrace{\nabla Q_g}_{\text{specific internal heat source}}$$

$$+\underbrace{\nabla\cdot\left(\Phi_{m_g}c_{k_g}\nabla T\right)}_{\text{conductive heat}} + \underbrace{\underset{\bullet\bullet}{\sigma}_g : \nabla\left(\Phi_{m_g}\underset{\bullet}{v}_g\right)}_{\text{adiabatic heat}} - \underbrace{\left(\rho\Phi_{m_g}\underset{\bullet}{v}_g\right)\nabla h_g}_{\text{gas heat transfer}} - \underbrace{h_g\nabla\cdot\left(\rho\Phi_{m_g}\underset{\bullet}{v}_g\right)}_{\text{convective mass flux heat}} \tag{3.36}$$

Again, the terms in Equation 3.36 are analysed.

- Thermal transient heat

  The gas has impact on the transient evolution of the temperature due to its thermal inertial, and thus this term is not negligible. The main difficulty is to quantify the gas specific heat capacity, since experimentally the heat capacity of the gas generated inside a composite is not the same as the one associated to the pure gas itself.

- Volumetric transient heat

  In engineering applications and specifically, for composites exposed to high temperatures, the assumption that the compressibility factor of the gases resulting from the polymer degradation is close to unity is very sensical. I.e., the gas phase is assumed to behave like an ideal gas and the volumetric transient heat is negligible then.

$$\Phi_{m_g}\left(1-\cancel{\alpha T}^{1}\right)\frac{\partial p}{\partial t} \tag{3.37}$$

- Mass transient heat

  Physically the generation of gas is positive, this implies that conceptually a media composed of solid and gas phases in equilibrium at a certain time cannot eliminate the gas phase since the process from gas to solid is irreversible. Therefore, the gas mass transient can only be zero if the gas is assumed to escape or greater than zero if assumed to accumulate.

Laminated composites exposed to fire in one of its surfaces tend to generate uniformly a gas decomposition front. Thus, it would be very strange to have gas formation close to the unexposed surface if those layers close to the exposed have not generated gas yet. I.e., a decomposition front at a certain time associated to a certain temperature is form on those layers close to the fire and with the pass of the time, if the heat source has not decreased, the front will advanced through the thickness to ultimately the last layer furthest from the exposed surface or, which is equivalent, the unexposed surface.

Therefore, it is quite understandable to assume that the gas has no impediment to escape and consequently to assume that there is no accumulation of gas.

$$\int_{\Omega} \left[\cancelto{0}{\frac{\partial \left(\Phi_{m_g} \rho \right)}{\partial t}} + \nabla \cdot \left(\rho \Phi_{m_g} \overset{\bullet}{v}_g \right) \right] \mathrm{d}\Omega = -w_g \tag{3.38}$$

This neglects the mass transient heat and according to the equilibrium of the generation rate of mass flux (Equation 3.25), the following relationship is also true.

$$\begin{gathered} \int_{\partial\Omega} \left[\underline{n}_s \cdot \overset{\bullet}{q}_{m_s} \right] \mathrm{d}\Omega = \int_{\partial\Omega} \left[\underline{n}_g \cdot \overset{\bullet}{q}_{m_g} \right] \mathrm{d}\Omega \\ \underline{n}_s = -\underline{n}_g \Rightarrow w_s = -w_g \end{gathered} \tag{3.39}$$

- Specific internal heat source

  The gas has no enthalpy of degradation associated, nevertheless any other sort of special heat source associated to the gas could be added. In the particular case of FRP composite materials, this term is negligible.

- Conductive heat

  Conduction is the thermal transfer of energy that is characteristic only between solids. Thus, conduction would not be taken into account for gasses.

- Adiabatic heat

  Gas is associated with the porosity, since gas is generate inside pores. Adiabatic heat generally can be neglected, however it is worth to comment that despite the deviatoric term certainly is negligible, which is related to the gas viscosity, the hydrostatic term could have a certain impact on the pore generation.

  If a decomposition front is assumed in the one-dimensional heat transfer problem, it is very realistic that the gradient of the hydrostatic pressure found on the pores should be negligible if the gas can freely escape. Otherwise, it would invalidate certain hypothesis that ultimately relate to the treatment of the gas phase as an ideal gas. If the gas is not considered ideal, this term cannot be neglected. As for the hypothesis established until this point, the term can be neglected.

- Gas heat transfer and convective mass flux heat

  It is fair to assume that mass flux heat will exist on the gas, since it is able to escape. Both terms are considered. Note that Equation 3.38 and Equation 3.39 can be used to simplify the convective mass flux heat.

$$h_g \nabla \cdot \left(\rho \Phi_{m_g} \overset{\bullet}{v}_g \right) = h_g w_s \tag{3.40}$$

Thus, Equation 3.36 yields

$$\underbrace{\rho \Phi_{m_g} c_{p_g} \frac{\partial T}{\partial t}}_{\text{thermal transient heat}} = - \underbrace{\left(\rho \Phi_{m_g} \overset{\bullet}{v}_g \right) \nabla h_g}_{\text{gas heat transfer}} - \underbrace{h_g w_s}_{\text{convective mass flux heat}} \tag{3.41}$$

3.3.3.3 Composite

The simplified energy balance of the composite media is the combination of both solid and gas species, Equation 3.35 and Equation 3.41 respectively.

$$\begin{aligned} \int_\Omega \left[\rho \Phi_{m_s} c_{p_s} \frac{\partial T}{\partial t} + \rho \Phi_{m_g} c_{p_g} \frac{\partial T}{\partial t} \right] \mathrm{d}\Omega = \int_\Omega \left[-h_s \frac{\partial \left(\rho \Phi_{m_s} \right)}{\partial t} - \frac{\partial \rho_s}{\partial t} h_p \right] \mathrm{d}\Omega \\ + \int_\Omega \left[\nabla \cdot \left(\Phi_{m_s} c_{k_s} \nabla T \right) - \left(\rho \Phi_{m_g} \overset{\bullet}{v}_g \right) \nabla h_g - h_g w_s \right] \mathrm{d}\Omega \end{aligned} \tag{3.42}$$

The transient heat terms containing the specific heat capacity of each solid and gas in Equation 3.42 can be added together in integral form to obtain the equivalent composite specific heat capacity.

$$\int_\Omega \left[\rho \Phi_{m_s} c_{p_s} \frac{\partial T}{\partial t} + \rho \Phi_{m_g} c_{p_g} \frac{\partial T}{\partial t} \right] \mathrm{d}\Omega = \int_\Omega \left[\rho c_p \frac{\partial T}{\partial t} \right] \mathrm{d}\Omega \tag{3.43}$$

Similarly, the continuity equation has to be fulfilled as stated in Equation 3.24. This leads to the following relationship.

$$\int_\Omega \left[\frac{\partial \left(\Phi_{m_s} \rho \right)}{\partial t} + \cancelto{0}{\frac{\partial \left(\Phi_{m_g} \rho \right)}{\partial t}} \right] \mathrm{d}\Omega = \int_\Omega \left[\frac{\partial \rho}{\partial t} \right] \mathrm{d}\Omega \tag{3.44}$$

Recall Equation 3.34 and Equation 3.39. Substituting Equation 3.44 into Equation 3.42.

$$\begin{aligned} \int_\Omega \left[\rho c_p \frac{\partial T}{\partial t} \right] \mathrm{d}\Omega = \int_\Omega \left[\nabla \cdot \left(\Phi_{m_s} c_{k_s} \nabla T \right) - \left(\rho \Phi_{m_g} \overset{\bullet}{v}_g \right) \nabla h_g \right] \mathrm{d}\Omega \\ - \int_\Omega \left[\frac{\partial \rho}{\partial t} \left(h_p + h_s - h_g \right) \right] \mathrm{d}\Omega \end{aligned} \tag{3.45}$$

3.3.3.4 Porosity

Porosity is always present in composites, it is unreal and unfeasible to manufacture a composite that has not a single pore in its structure. Moreover, composites exposed to re are bound to develop pores since it is the self-decomposition of the matrix that in its process of conversion to several subproducts, generally referred to as the gas phase, requires increasing the volumetric fraction of the gas, which in this case are the pores in the microscopic structure. Figure 3.9 illustrates how the gas flows throughout the pores. Pores when big enough start connecting and generate a *sponge*-like structure, this allows the gas to escape to the atmosphere.

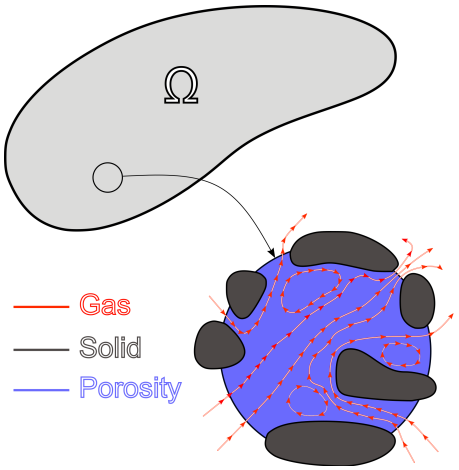

FIGURE 3.9: Composite media divided in gas and solid phases.

Porosity affects the balance of energy for composites because the velocity of escapement of the gas is affected from it. This can be reflected in the gas transfer term in Equation 3.41. There are different ways to model the gas transfer term.

1. **Basic gas transfer model**

   In the case of the one-dimensional heat transient equation, the hypothesis of the generated decomposition front was discussed to be realistic for a wide range of applications. Furthermore, the fact of assuming that there is a front of decomposition implies that the gradient of internal pressure in the *sponge*-like structure has to be negligible compared to the atmospheric.

   If the through-thickness mass flux (q_m) is analysed in a *laminate* media, it is safe to assume that the gas will flow from the cold end to the hot end. Assume that the distribution through-thickness of the temperature is similar to the one shown in Figure 3.10, it can be seen that the gradient of mass flux is reasonably positive in z-axis since it flows upwards. If the hypothesis of no mass flux escapes through the unexposed surface is assumed, the mass flux can be calculated as follows

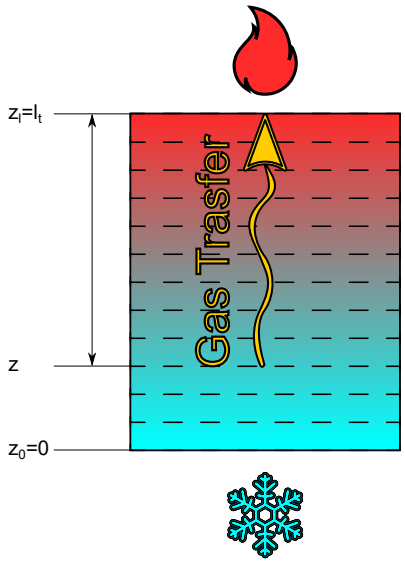

FIGURE 3.10: Gas transfer hypothesis in one-dimensional heat transient problem.

$$\cancel{\dot{q}_{m_g}(z=l_t,t)}^{0} - \dot{q}_{m_g}(z,t) = \int_z^{l_t} \nabla \cdot \dot{q}_m \, \mathrm{d}z = \int_z^{l_t} w \, \mathrm{d}z \equiv -\int_z^{l_t} \frac{\partial \rho}{\partial t} \, \mathrm{d}z$$
$$\Downarrow \tag{3.46}$$
$$\left(\rho \Phi_{m_g} \dot{v}_g\right) = \dot{q}_{m_g}(z,t) = \int_z^{l_t} \frac{\partial \rho}{\partial t} \, \mathrm{d}z$$

where l_t is the thickness length. The assumption of no mass flux of the cold end in 1D is valid for a vast range of real applications. Nevertheless, some clarifications or delimitation has to be discussed.

The basic gas transfer model finds its limitation when the gradient of temperature relatively tends to 0, i.e., both sides – exposed and unexposed surfaces – of the structure present similar temperatures. In that case, it is very difficult to hypothesise on whether the gas transfer moves in one direction or the other, even if not both.

Although the previous consideration seems logical, *a priori*, describes an unrealistic phenomenon. Not indeed because a negligible gradient of temperature cannot occur, but in the sense of even considering the gas transfer heat important any longer.

Two possibilities may arise when considering unrealistic the basic gas transfer assumption, on both possibilities consider a relatively low temperature gradient between the exposed and unexposed surfaces. First, consider that both ends have a relatively low temperature. Consequently, the temperature through-thickness should range in between the temperature of the surfaces and in practice the degradation or decomposition, which originates the gas transfer phenomena, shall not occur. In that sense, for low gradient and low surface temperatures, the contribution of the gas transfer heat is negligible and thus it would not invalidate the basic gas transfer assumption.

Second, consider that both ends have a high temperature. This is theoretically true, but in practice itis unfeasible. This scenario has a non-negligible

gas transfer heat, however, from a structural point of view, the integrity of the structure would have to collapse and the correct prediction of the gas transfer heat not might even be valid due to the excessive through-thickness deformation.

When the temperature on both sides has stagnated to relatively mild temperatures (close to glass temperature), a better approximation of the gas transfer model may be desired.

The other reason to be addressed, which considers a signicant gradient of temperature, happens when different thermal decomposition properties are present in the composite stacking. I.e., situations where the advancing decomposition front may not necessarily start close to the exposed surface and that might lead to unexpected directions of the gas transfer than the usual prescribed from the cold to the hot end.

2. **Enhanced gas transfer model**

   An enhanced approximation to the gas transfer model might be needed in certain cases, specially in nth-dimensional heat transfer problem when $n > 1$. In this regard, a better approximation to the through-thickness mass flux (q_m) is required. The simplest solution is to couple the heat transient problem with a Darcy problem by means of defining the velocity using a Darcy/Flick's law.

$$\overset{\bullet}{v}_g = -\frac{\kappa_g}{\mu_g}\nabla p \tag{3.47}$$

   where κ_g is the gas permeability, μ_g is the gas dynamic viscosity. Considering that the gas behaves like an ideal gas, the following relationship can be considered.

$$\rho_g = \frac{M_g}{RT}p \tag{3.48}$$

   where R is the universal gas constant, M_g is the gas molar mass. The differential of the density is

$$\frac{\mathrm{d}\rho_g}{\mathrm{d}t} = \frac{M_g}{RT}\frac{\mathrm{d}p}{\mathrm{d}t} - \frac{M_g p}{RT^2}\frac{\mathrm{d}T}{\mathrm{d}t} \tag{3.49}$$

   The expansion, in differential manner, of the gas mass balance in Equation 3.38 in terms of the porosity or volume fraction defined in Equation 3.21 poses the Darcy problem. Note that this time there is no assumption of *no gas accumulation* and hence the transient of the density is not null.

$$\frac{\partial\left(\Phi_{\Omega_g}\rho_g\right)}{\partial t} + \nabla\cdot\left(\rho_g\Phi_{\Omega_g}\overset{\bullet}{v}_g\right) = -w_g \tag{3.50}$$

   Substituting Equation 3.47, Equation 3.48 and Equation 3.49 into Equation 3.50 yields

$$\frac{\Phi_{\Omega_g}M_g}{RT}\frac{\partial p}{\partial t} - \frac{\Phi_{\Omega_g}M_g p}{RT^2}\frac{\partial T}{\partial t} - \nabla\cdot\left(\frac{\rho_g\Phi_{\Omega_g}\kappa_g}{\mu_g}\nabla p\right) = \frac{\partial\rho}{\partial t} \tag{3.51}$$

   Note that also the generation of mass flux (w) has been substituted in the same manner as in Equation 3.45 and this same equation can be substituted now to pose the Darcy-heat coupled problem in 1D.

$$\left(\rho\Phi_{m_g}\overset{\bullet}{v}_g\right)\nabla h_g \equiv -\frac{\rho_g\Phi_{\Omega_g}\kappa_g c_p}{\mu_g}\nabla p\cdot\nabla T \tag{3.52}$$

This approach can be extended with the research of Chippendale et al., who proposes an interesting methodology in order to address the evolution of porosity by means of the permeability, and makes use of the hypothesis in [31, 260, 261] regarding how to model of the permeability via the Kozeny-Blake equation.

3.3.3.5 Pyrolysis

Pyrolysis is a thermal-chemical process involving the absorption of heat via the decomposition of the polymer matrix, organic fibres and organic core materials (sandwich materials). FRP composites experimenting pyrolysis decompose, generally it involves only the polymer matrix, into different subproducts such as gas, vapours, tar (liquid phase) and char (solid phase). The pyrolysis of a cell inside a composite media can be depicted in Figure 3.11, which includes the effect of porosity if needed. Variation of the porous volume is considered to be negligible under the effects of pyrolysis.

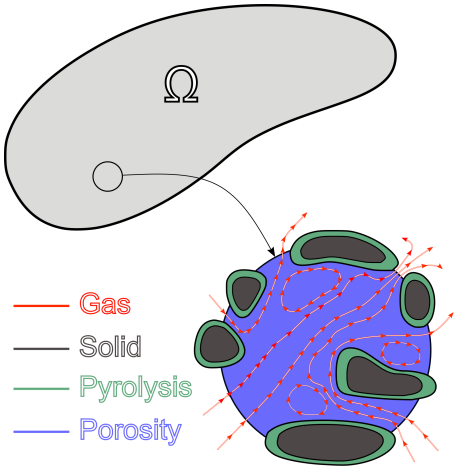

FIGURE 3.11: Composite media divided in solid and gas phases with pyrolysis.

According to Henderson and Wiecek in [11, 19, 63], pyrolysis in composites can be described as a *linear interpolation* or *mixture equation* between the virgin and char/degraded densities.

$$F = \frac{\rho_s - \rho_c}{\rho_v - \rho_c} \Longleftrightarrow \rho = F\rho_v + (1-F)\rho_c \tag{3.53}$$

where F is the pyrolysis fraction, ρ_c is the charred density and ρ_v is the virgin density. The density fraction can then be related by means of Equation 3.20 to Equation 3.53.

$$\Phi_{\rho_i} = \frac{\rho_i}{F\rho_v + (1-F)\rho_c} \tag{3.54}$$

Equation 3.54 links the evolution of pyrolysis in the solid phase with the conservation of mass, linear momentum and energy by means of the density fraction that compounds the mass fraction.

The pyrolysis model defines the pyrolysis fraction (F) as an internal variable which controls the degradation process. The evolution of this variable can be defined by using nth-order Arrhenius law.

$$\frac{\mathrm{d}F}{\mathrm{d}t} = -A_T \left(\frac{\rho_s - \rho_c}{\rho_v - \rho_c}\right)^{N_{\mathrm{ro}}} \exp\left(-\frac{E_{\mathrm{act}}}{RT}\right) = -A_T F^{N_{\mathrm{ro}}} \exp\left(-\frac{E_{\mathrm{act}}}{RT}\right) \tag{3.55}$$

where E_{act} is the energy of activation, N_{ro} is the order of decomposition reaction and A_T is the pre-exponential factor. Note that temperature in Equation 3.55 is defined in Kelvin (°K) and recalling that the rate of change of solid phase is equivalent to the one of the composite as defined in Equation 3.44, the relationship between the rate of pyrolysis fraction and the density itself is defined.

$$\frac{\partial \rho}{\partial t} = (\rho_v - \rho_c)\frac{\partial F}{\partial t} \tag{3.56}$$

3.3.3.6 Enthalpy

The final terms to be characterised in the energy balance equation, Equation 3.45, are those related to the enthalpy. The enthalpy of decomposition of the polymer matrix (h_p) can be quantified based on the experimental testing. However, both solid and gas enthalpies (h_s, h_g), can be obtained by assuming that both specific enthalpies are a function depending only on the temperature.

$$\begin{aligned} h_s &= \int_{T_0}^{T} c_{p_s}\,\mathrm{d}T \\ h_g &= \int_{T_0}^{T} c_{p_g}\,\mathrm{d}T \end{aligned} \tag{3.57}$$

where T_0 is the initial temperature.

3.3.3.7 Laminate one-dimensional heat transfer - Henderson

Using the different assumptions exposed previously, the Equation 3.45 with the *basic gas transfer model*, can be re-written as Henderson and Wiecek explain in [19].

$$\int_{\Omega}\left[\rho c_p \frac{\partial T}{\partial t}\right]\,\mathrm{d}\Omega = \int_{\Omega}\left[\nabla\cdot(\Phi_{ms}c_{ks}\nabla T) - \dot{q}_{g}^{m}\nabla h_g\right]\,\mathrm{d}\Omega - \int_{\Omega}\left[\frac{\partial\rho}{\partial t}\left(h_p + h_s - h_g\right)\right]\,\mathrm{d}\Omega \tag{3.58}$$

The governing equations of the one-dimensional heat transfer problem for *FRP laminate* materials are posed. The boundaries of such problem have been labelled as hot and cold ends, which for a real problem of analysis seemed the more feasible.

Thus, in the delimitation of the problem (boundary and initial conditions), the initial point of departure would be – redundantly – to define the initial conditions that *a priori* are easier to be established. The two state variables to be initially defined would be the density (ρ) and the temperature (T), since the heat transfer equation and the gas transfer model depend on them.

$$\rho(t=0) = T_0 \tag{3.59}$$

where T_0 is the initial density.

$$T(t=0) = T_0 \tag{3.60}$$

Generally, the initial temperature, although not obligatory, can be interchangeable with the ambient temperature for most real application analysis.

$$T_0 = T_\infty \tag{3.61}$$

Again, recall that it is a likely possibility but not an obligation.

The other constraints needed to be determined are the boundary conditions. These are fairly more complex, the reason of this complexity resides in the concept of fire, specially from the point of view of temperature. The first assumption to be made to simplify the boundary conditions is to list the different ways heat can be transmitted from a temperature source. Since the boundary conditions are in technically introduced in the boundary, there are three ways the heat can propagate.

- Conduction

  The conduction is a way to transmit heat between solids. If marine structures are to be taken into account, it is very strange that a structural member made of a composite material is adhered to another solid member in the boundary and if so, if the area of contact is relatively enough, the heat by conduction can be neglected.

- Convection

  Convection involves the exchange of heat between a fluid and a solid or *vice versa*. Indeed, it is very feasible that in the present of fire in a marine structure, e.g., a fire originated in the engine room of a ship, one of the major heat sources through the boundary of a structural member is going to be due to convection

of the hot air and the exposed surface. Then convection would be present in the problem, not only for the hot end, but also for the cold end.

$$\dot{q} = c_h(T_{\partial\Omega} - T_\infty) \tag{3.62}$$

The subscript ($\partial\Omega$) indicates that the quantity is of the material nodes located in the boundary, i.e., in this case the temperature ($T_{\partial\Omega}$) is of those material nodes located in the boundary.

- Radiation

  Thermal radiation is a form of heat transmission created by the thermal motion of the material particles. Thermal radiation is one of the most important sources of heat when

$$\dot{q} = c_\sigma c_\varepsilon(T_{\partial\Omega}^4 - T_\infty{}^4) \tag{3.63}$$

  Note that the temperature is in kelvin. In addition, the radiation is considered in the boundary however, the model does not consider self radiation as a body heat flux.

Because both radiation and convection are taken into account in the boundary, there is no explicit solution by analytical methods. Convection and conduction can be catalogued as linear boundary conditions and can be solved by means of methods that deal with Neumann or Robin boundary conditions. Nevertheless, radiation are pure non-linear boundary conditions and thus no analytical solution can be derived.

Even though non-linear boundary conditions can be solved by means of numerical methods, it is still unclear on how to model the temperature on those boundaries. It is a well-known fact that the temperature on the boundaries for Equation 3.62 and Equation 3.63, convection and radiation respectively, are not equal. Conceptually, if a fire is originated, it will generate radiation at a different gradient of temperature than the convection derived from the fire itself that will present another gradient. I.e., although the convection and radiation heat can be quantified, there is uncertainty on the quantification of either the boundary temperature or the source since both do not match experimentally due to different factors such heat losses, apparent heat sources, non-linear dependency on the convection or radiation heat functions.

In order to simplify the amount of unknowns arisen in the non-linear boundary conditions, Wickstrom Ulf et al. in [28] proposed the concept of adiabatic temperature where it is assumed that both source temperature are equal and that the temperature in the boundary is the same.

$$\begin{aligned}\dot{q} &= -\int_\Omega \left[\nabla \cdot (c_k \nabla T)\right] \, \mathrm{d}\Omega = -\int_{\partial\Omega} \left[\underline{n} \cdot (c_k \nabla T)\right] \, \mathrm{d}\Omega \\ &= \int_{\partial\Omega} \left[c_h(T_{\partial\Omega} - T_\infty) + c_\sigma c_\varepsilon(T_{\partial\Omega}^4 - T_\infty{}^4)\right] \, \mathrm{d}\Omega\end{aligned} \tag{3.64}$$

The ambient temperature (T_∞) would be different on the hot and cold ends. This can be interpreted as the ambient temperature is a function of the location and thus the boundary can be split into two sets, cold boundary and hot boundary ($\partial\Omega_h, \partial\Omega_c$).

In addition, observe that for Equation 3.64 establishes by the Fourier law that the hot boundary ($\partial\Omega_h$) is prescribed as an in-flux boundary condition and that the cold boundary ($\partial\Omega_c$) is prescribed as out-flux boundary condition and thus the normal, whether the boundary is cold or hot, is multiplied by -1 or 1 respectively.

Once the considered boundary conditions are defined, the problem is definitely posed. To solve this problem numerically, the partial differential equation in integral (Equation 3.58 form is transformed into its weak form equivalent.

$$\begin{aligned}\int_\Omega \left[\xi \rho c_p \frac{\partial T}{\partial t}\right] \mathrm{d}\Omega - \int_\Omega \left[\nabla\xi \cdot (c_k \nabla T)\right] \mathrm{d}\Omega + \int_\Omega \left[\xi c_{p_g} \dot{q}_g^{m} \nabla T\right] \mathrm{d}\Omega \\ + \int_{\partial\Omega} \left[\xi \left(c_h (T_{\partial\Omega} - T_\infty) + c_\sigma c_\varepsilon (T_{\partial\Omega}^4 - {T_\infty}^4)\right)\right] \mathrm{d}\Omega \\ + \int_\Omega \left[\xi \left(\rho_v - \rho_c\right) \frac{\partial F}{\partial t} \left(h_p + h_s - h_g\right)\right] \mathrm{d}\Omega = 0\end{aligned} \tag{3.65}$$

where ξ is the test function. It is important to note that the thermal conductivity coefficient of the composite media is the summation of the solid and gas phase, the latter was assumed negligible, and the solid phase can incorporate the pyrolysis effect by the pyrolysis fraction contained in the mass fraction.

$$c_k = \sum_{i=s,g} \Phi_{mi} \cdot c_{ki} \tag{3.66}$$

3.3.3.8 Spatial Discretisation

The discretisation method employed to numerically obtain the system of equations of the discrete domain arisen from Equation 3.65 is the so-called *Finite Element Method* or in short *FEM*.

First, consider that any function field can be expressed in their discrete form by means of a set of material nodes and this may take the form of a vector or a matrix or its equivalent tensor representation by Einstein notation. For example, for a given vector field (a) defined inside the domain for a given time:

$$\dot{\underline{a}}(\Omega, t) \equiv \underline{a} \equiv a_i \equiv \begin{bmatrix} a_1 \\ a_2 \\ \vdots \\ a_n \end{bmatrix} \tag{3.67}$$

And for matrix field (b) defined inside the domain for a given time:

$$\ddot{\underline{\underline{b}}}(\Omega, t) \equiv \underline{\underline{b}} \equiv b_{i,j} \equiv \begin{bmatrix} b_{11} & b_{12} & \dots & b_{1n} \\ b_{21} & b_{22} & \dots & b_{2n} \\ \vdots & \vdots & \ddots & \vdots \\ b_{n1} & b_{n2} & \dots & b_{nn} \end{bmatrix} \tag{3.68}$$

The heat transient problem will be considered a temperature-driven problem, and therefore, the unknown to be found will be the temperature. Suppose that the temperature field in the domain can be approximated by a finite vector of material nodes and suitable shape functions.

$$T(\Omega, t) = \underline{N_\xi}^T(\Omega)\underline{T}(t) \tag{3.69}$$

where N_ξ is the shape function. Note that the domain (Ω) in one-dimensional space is equivalent to the through-thickness dimension (z).

The Galerkin method is employed to approximate the test function in Equation 3.65. The Galerkin method proposes that the same interpolation functions or *shape functions* will be used in the approximation of both the unknown variable and the test function.

$$\xi(\Omega, t) = \underline{N_\xi}(\Omega) \tag{3.70}$$

The discrete domain can be as well discretised.

$$\int_\Omega [] \, \mathrm{d}\Omega \equiv \sum_{\mathrm{e}}^{n_\mathrm{e}} \int_{\Omega_{(e)}} [] \, \mathrm{d}\Omega_{(e)} \tag{3.71}$$

The subscript e here denotes the element index and n_e number of elements. The discrete weak form can be then defined as follows.

$$\begin{aligned}
\sum_{\mathrm{e}}^{n_\mathrm{e}} \int_{\Omega_{(e)}} \left[\underline{N_\xi} \underline{N_\xi}^T \rho c_p \frac{\partial \underline{T}}{\partial t} \right] \mathrm{d}\Omega_{(e)} - \sum_{\mathrm{e}}^{n_\mathrm{e}} \int_{\Omega_{(e)}} \left[\nabla \underline{N_\xi} \cdot \left(c_k \nabla \underline{N_\xi}^T \underline{T} \right) \right] \mathrm{d}\Omega_{(e)} \\
+ \sum_{\mathrm{e}}^{n_\mathrm{e}} \int_{\Omega_{(e)}} \left[\underline{N_\xi} c_{p_g} \underline{q_{m_g}} \nabla \underline{N_\xi}^T \underline{T} \right] \mathrm{d}\Omega_{(e)} \\
+ \sum_{\mathrm{e}}^{n_\mathrm{e}} \int_{\partial\Omega_{(e)}} \left[\underline{N_\xi} \left(c_h (\underline{N_\xi}^T \underline{T_{\partial\Omega}} - \underline{N_\xi}^T \underline{T_\infty}) + c_\sigma c_\varepsilon (\underline{N_\xi}^T \underline{T_{\partial\Omega}}^4 - \underline{N_\xi}^T \underline{T_\infty}^4) \right) \right] \mathrm{d}\Omega_{(e)} \\
+ \sum_{\mathrm{e}}^{n_\mathrm{e}} \int_{\Omega_{(e)}} \left[\underline{N_\xi} \left(\rho_v - \rho_c \right) \frac{\partial F}{\partial t} \left(h_p + h_s - h_g \right) \right] \mathrm{d}\Omega_{(e)} = 0
\end{aligned} \tag{3.72}$$

Equation 3.72 can be re-formulated as the following system of equations.

$$\underline{\underline{C_T}} \frac{\partial \underline{T}}{\partial t} - \underline{\underline{K_T}} \underline{T} + \left(\underline{f_d} + \underline{f_c} + \underline{f_r} \right) = 0 \tag{3.73}$$

where $\underline{f_d}$ is the degradation flux vector, $\underline{f_c}$ is the convection flux vector, $\underline{f_r}$ is the radiation flux vector, $\underline{\underline{C_T}}$ is the heat capacity matrix and $\underline{\underline{K_T}}$ is the heat conductivity matrix.

A brief list of equations describing the system matrices and vectors is provided:

- Heat capacity matrix

$$\underline{\underline{C_T}} = \sum_{\mathrm{e}}^{n_\mathrm{e}} \int_{\Omega_{(e)}} \left[\underline{N_\xi} \underline{N_\xi}^T \rho c_p \right] \, \mathrm{d}\Omega_{(e)} \tag{3.74}$$

- Heat conductivity matrix

$$\underline{\underline{K_T}} = -\sum_{\mathrm{e}}^{n_\mathrm{e}} \int_{\Omega_{(e)}} \left[\nabla \underline{N_\xi} \cdot \left(c_k \nabla \underline{N_\xi}^T \right) \right] \, \mathrm{d}\Omega_{(e)} \tag{3.75}$$

- Degradation flux vector

$$\begin{aligned} \underline{f_d} = \sum_{\mathrm{e}}^{n_\mathrm{e}} \int_{\Omega_{(e)}} \left[\underline{N_\xi} \left(\rho_v - \rho_c \right) \frac{\partial F}{\partial t} \left(h_p + h_s - h_g \right) \right] \, \mathrm{d}\Omega_{(e)} \\ + \sum_{\mathrm{e}}^{n_\mathrm{e}} \int_{\Omega_{(e)}} \left[\underline{N_\xi} c_{p_g} \underline{q_{m_g}} \nabla \underline{N_\xi}^T \underline{T} \right] \, \mathrm{d}\Omega_{(e)} \end{aligned} \tag{3.76}$$

- Convection flux vector

$$\underline{f_c} = \sum_{\mathrm{e}}^{n_\mathrm{e}} \int_{\partial\Omega_{(e)}} \left[\underline{N_\xi} c_h (\underline{N_\xi}^T \underline{T_{\partial\Omega}} - \underline{N_\xi}^T \underline{T_\infty}) \right] \, \mathrm{d}\Omega_{(e)} \tag{3.77}$$

- Radiation flux vector

$$\underline{f_r} = \sum_{\mathrm{e}}^{n_\mathrm{e}} \int_{\partial\Omega_{(e)}} \left[\underline{N_\xi} c_\sigma c_\varepsilon (\underline{N_\xi}^T \underline{T_{\partial\Omega}}^4 - \underline{N_\xi}^T \underline{T_\infty}^4) \right] \, \mathrm{d}\Omega_{(e)} \tag{3.78}$$

3.3.3.9 Time discretisation

The thermal capacity matrix in Equation 3.73 is multiplied by the rate of temperature. A proper time discretisation is needed, for instance, a finite difference scheme such as the *Backward Euler method*. If the time domain is discretised in uniformly distributed increments of time (Δt) and the time at a given moment is defined with the subscript (t_n). The rate of temperature can be reformulated in finite difference form, such as

$$\frac{\mathrm{d}T}{\mathrm{d}t}(\Omega(t_{n+1}), t_{n+1}) \approx \frac{\underline{\underline{T_{n+1}}} - \underline{\underline{T_n}}}{\Delta t}, \qquad \Delta t = t_{n+1} - t_n \tag{3.79}$$

The *Backward-Euler* scheme presents a local truncation error of $\mathcal{O}\left(\Delta t^2\right)$ and the error at a specific time t is $\mathcal{O}\left(\Delta t\right)$. It is also stable for the given partial differential equation.

3.3.3.10 Iterative non-linear solution

Since the posed problem is highly non-linear, an iterative scheme is proposed in order to solve the system of equations in Equation 3.73. The approach used is a residual form of the fluxes at time (t_n)

$$\underline{r_T}\big|_{n+1} \equiv \underline{r_T}\left(\underline{T_{n+1}}, \underline{F_{n+1}}\right) = \underline{\underline{C_T}}\Big|_{n+1} \frac{\underline{T_{n+1}} - \underline{T_n}}{\Delta t} - \underline{\underline{K_T}}\Big|_{n+1} \underline{T_{n+1}} + \left(\underline{f_d} + \underline{f_c} + \underline{f_r}\right)\Big|_{n+1} \tag{3.80}$$

which has to be minimised by using the classical approach of first order Taylor series expansion of the residual

$$\underline{r_T}\big|_{n+1,k+1} = \underline{r_T}\big|_{n+1,k} + \frac{\partial \underline{r_T}\left(\underline{T}, \underline{F}\right)}{\partial T}\Big|_{n+1,k} \left(\underline{T_{n+1,k+1}} - \underline{T_{n+1,k}}\right) \qquad \lim_{k+1\to\infty} \underline{r_T}\big|_{n+1,k+1} = 0 \tag{3.81}$$

and solution of the derived system of equations

$$\underline{\underline{J_T}}\Big|_{n+1,k} \underline{\Delta T}|_{n+1,k} = -\underline{r_T}\big|_{n+1,k} \tag{3.82}$$

where $\underline{r_T}$ is the thermal residual, $\underline{\underline{J_T}}$ is the tangent flux matrix. The tangent flux matrix is equivalent to the derivative of the residual in respect to the temperature.

Finally, the thermal transient problem is solved iteratively using Equation 3.82, the unknown would be the increment of temperature that is used to obtain the current temperature ($\underline{T_{n+1,k+1}}$) and the internal variable of the problem is the converged pyrolysis factor ($\underline{F}|_{n+1,k}$).

3.3.3.11 One-dimensional discrete thermal problem

The global process used to solve the thermal model is detailed in algorithm 1.

Algorithm 1: Thermal Solver

$T_0 = T(t=0)$

$F = F(t=0)$

for $n = 0$ **to** n_{end} **do**

  $m = 0; \quad T_{n+1,0} = T_n$

  while $\left.\dfrac{\underline{r_T}}{\underline{f_d} + \underline{f_c} + \underline{f_r}}\right|_{n+1,m+1} <$ *tolerance* **do**

    obtain the residual $\left(\underline{r_T}\big|_{n+1,m+1}\right)$ and jacobian $\left(\underline{\underline{J_T}}\big|_{n+1,m}\right)$

    solve $\Delta T|_{n+1,m}$ in Equation 3.82

    update $F_{n+1,m} = F_n$

    go to: algorithm 2

    $m = m + 1$

  end

  $T_{n+1} = T_{n+1,m} \quad , \quad F_{n+1} = F_{n+1,m} \quad , \quad n = n + 1$

end

From algorithm 1 the definition of the tangent flux matrix in Equation 3.82 is needed.

$$\underline{\underline{J_T}} = \frac{\underline{\underline{C_T}}\big|_{n+1,k}}{\Delta t} + \left.\frac{\partial \underline{\underline{C_T}}}{\partial \underline{T}}\right|_{n+1,k} \frac{\underline{\underline{T_{n+1,k}}} - \underline{\underline{T_n}}}{\Delta t} - \underline{\underline{K_T}}\big|_{n+1,k} - \left.\frac{\partial \underline{\underline{K_T}}}{\partial \underline{T}}\right|_{n+1,k} \underline{T_{n+1,k}} + \left.\left(\frac{\partial \underline{\underline{f_d}}}{\partial \underline{T}} + \frac{\partial \underline{\underline{f_c}}}{\partial \underline{T}} + \frac{\partial \underline{\underline{f_r}}}{\partial \underline{T}}\right)\right|_{n+1,k} \tag{3.83}$$

The different terms in Equation 3.83 that conform the tangent flux matrix can be obtained as follows.

- Differential of the heat capacity matrix with respect to the temperature

$$\left.\frac{\partial \underline{\underline{C_T}}}{\partial T}\right|_{n+1,k} \frac{\underline{\underline{T_{n+1,k}}} - \underline{\underline{T_n}}}{\Delta t} = \sum_{\mathrm{e}}^{n_{\mathrm{e}}} \int_{\Omega_{(e)}} \left[\underline{\underline{N_\xi}} \left(\frac{\partial \rho}{\partial T} c_p + \frac{\partial c_p}{\partial T} \rho\right)\Big|_{n+1,k} \underline{\underline{N_\xi}}^T \frac{\underline{T_{n+1,k}} - \underline{T_n}}{\Delta t}\right] \mathrm{d}\Omega_{(e)} \tag{3.84}$$

- Differential of the heat conductivity matrix with respect to the temperature

$$\left.\frac{\partial \underline{\underline{K_T}}}{\partial T}\right|_{n+1,k} \underline{T_{n+1,k}} = \sum_{\mathrm{e}}^{n_\mathrm{e}} \int_{\Omega_{(e)}} \left[\nabla \underline{N_\xi} \cdot \left(\left.\frac{\partial c_k}{\partial T}\right|_{n+1,k} \nabla \underline{N_\xi}^T \right) T_{n+1,k} \right] \mathrm{d}\Omega_{(e)} \quad (3.85)$$

- Differential of the degradation flux vector with respect to the temperature

$$\left.\frac{\partial \underline{\underline{f_d}}}{\partial \underline{T}}\right|_{n+1,k} = \sum_{\mathrm{e}}^{n_\mathrm{e}} \int_{\Omega_{(e)}} \left[\left.\frac{\partial \underline{\underline{f_{d_1}}}}{\partial \underline{T}}\right|_{n+1,k} + \left.\frac{\partial \underline{\underline{f_{d_2}}}}{\partial \underline{T}}\right|_{n+1,k} \right] \mathrm{d}\Omega_{(e)} \quad , \quad (3.86)$$

such that

$$\begin{cases} \left.\dfrac{\partial \underline{\underline{f_{d_1}}}}{\partial \underline{T}}\right|_{n+1,k} = \sum_{\mathrm{e}}^{n_\mathrm{e}} \int_{\Omega_{(e)}} \left[\underline{N_\xi} c_1^* \underline{N_\xi}^T \right] \mathrm{d}\Omega_{(e)} \\ \left.\dfrac{\partial \underline{\underline{f_{d_2}}}}{\partial \underline{T}}\right|_{n+1,k} = \sum_{\mathrm{e}}^{n_\mathrm{e}} \int_{\Omega_{(e)}} \left[\underline{N_\xi} c_2^* \nabla \underline{N_\xi}^T \underline{T} \right] \mathrm{d}\Omega_{(e)} + \sum_{\mathrm{e}}^{n_\mathrm{e}} \int_{\Omega_{(e)}} \left[\underline{N_\xi} c_{p_g} \underline{q_{m_g}} \nabla \underline{N_\xi} \right] \mathrm{d}\Omega_{(e)} \\ c_1^* = (\rho_v - \rho_c) \left(\frac{\partial^2 F}{\partial t \partial T} \left(h_p + h_s - h_g \right) + \dfrac{\partial F}{\partial t} \left(\dfrac{\partial h_s}{\partial T} - \dfrac{\partial h_g}{\partial T} \right) \right) \Big|_{n+1,k} \\ c_2^* = \left(c_{p_g} \dfrac{\partial \underline{\underline{q_{m_g}}}}{\partial T} + \underline{q_{m_g}} \dfrac{\partial c_{p_g}}{\partial T} \right) \Big|_{n+1,k} \end{cases}$$

- Differential of the convection flux vector with respect to the temperature

$$\left.\frac{\partial \underline{\underline{f_c}}}{\partial \underline{T}}\right|_{n+1,k} = \sum_{\mathrm{e}}^{n_\mathrm{e}} \int_{\partial\Omega_{(e)}} \left[\underline{N_\xi} c_h \underline{N_\xi}^T \right] \mathrm{d}\Omega_{(e)} \quad (3.87)$$

- Differential of the radiation flux vector with respect to the temperature

$$\left.\frac{\partial \underline{\underline{f_r}}}{\partial \underline{T}}\right|_{n+1,k} = \sum_{\mathrm{e}}^{n_\mathrm{e}} \int_{\partial\Omega_{(e)}} \left[\underline{N_\xi} \left(4 c_\sigma c_\varepsilon T_{\partial\Omega}{}^3 \right) \underline{N_\xi}^T \right] \mathrm{d}\Omega_{(e)} \quad (3.88)$$

The previous expressions use the definition of the differential of the density with respect to the temperature, this can be formulated with respect to the pyrolysis fraction by using the relationship in Equation 3.53 and expressed it in a discrete manner.

$$\left.\frac{\partial \rho}{\partial T}\right|_{n+1,k} = (\rho_v - \rho_c) \left.\frac{\partial F}{\partial T}\right|_{n+1,k} \quad (3.89)$$

With Equation 3.91, the numerical problem is defined. The numerical one-dimensional heat transient problem is expressed in terms of the state variable (temperature, T) that depends on its internal variable (pyrolysis fraction, F). The next step if fundamentally to describe the scheme used to evaluate and update the internal variable in order to be able to solve the numerical problem.

3.3.3.12 Internal variables

For real applications where fire has not been generated or the composite structure has not undergone degradation, the internal variable or pyrolysis fraction (F) can be considered initially to be one. Otherwise, it can be assumed to be an initial value between [0,1].

$$F(\Omega, t=0) = F_0 \quad , \quad \begin{cases} \text{Generally:} & F_0 = 1 \\ \text{Otherwise:} & F_0 \in [0,1] \end{cases} \tag{3.90}$$

Equation 3.55 is a non-linear scalar differential equation. Similarly to the heat transient equation, the constitutive relationships in the pyrolysis process, can be discretised in time by using a backward-Euler scheme and by defining an iterative scheme based on Taylor expansion series, a Newton-Rapshon method is employed to minimise the problem.

$$\frac{\mathrm{d}F}{\mathrm{d}t} = \frac{F_{n+1} - F_n}{\Delta t} \tag{3.91}$$

Introducing the backward-Euler time scheme for the pyrolysis fraction into the differential equation in Equation 3.55 yields

$$\frac{F_{n+1} - F_n}{\Delta t} = -A_T \left(F_{n+1}\right)^{N_{\mathrm{ro}}} \exp\left(-\frac{E_{\mathrm{act}}}{R T_{n+1}}\right) \tag{3.92}$$

The Equation 3.92 is expressed in residual form as

$$r_F = \frac{F_{n+1} - F_n}{\Delta t} + A_T \left(F_{n+1}\right)^{N_{\mathrm{ro}}} \exp\left(-\frac{E_{\mathrm{act}}}{R T_{n+1}}\right) \tag{3.93}$$

The Taylor expansion of the residual in Equation 3.93 is

$$\begin{gathered} r_F|_{n+1,k+1} = r_F|_{n+1,k} + \left.\frac{\partial r_F\left(F\right)}{\partial F}\right|_{n+1,k} \left(F_{n+1,k+1} - F_{n+1,k}\right) \\ \lim_{k+1 \to \infty} r_F|_{n+1,k+1} = 0 \end{gathered} \tag{3.94}$$

And the Jacobian of the pyrolysis residual can be used to minimise the problem iteratively.

$$J_F|_{n+1,k}\, \Delta F|_{n+1,k} = -\, r_F|_{n+1,k} \tag{3.95}$$

where r_F is the residual of the pyrolysis fraction, J_F is the jacobian of the pyrolysis fraction.

Algorithm 2: Update of internal variable

initialization $\rightarrow T_{n+1,m+1}$; $k = 0$; $F_{n+1,m,0} = F_n$

while $\left.\dfrac{r_F}{\dfrac{\mathrm{d}F}{\mathrm{d}t}}\right|_{n+1,m,k} <$ *tolerance* **do**

obtain the residual $\left(r_F|_{n+1,m+1}\right)$ and jacobian $\left(J_F|_{n+1,m}\right)$

solve $\Delta F|_{n+1,m}$ in Equation 3.95

update $F_{n+1,m,k+1} = F_{n+1,m,k} + \Delta F|_{n+1,m,k}$; $k = k+1$

end

$F_{n+1,m} = F_{n+1,m,k}$

Once the internal variable can be obtained in a discrete time manner, it is necessary to define as well its evolution with respect to the temperature, as required in Equation 3.89, since temperature depends on the time scheme as well.

Rewriting Equation 3.92 in order to update the pyrolysis fraction for the new step of time

$$F_{n+1,m} = F_n - \Delta t A_T \left(F_{n+1,m}\right)^{N_{\mathrm{ro}}} \exp\left(-\frac{E_{\mathrm{act}}}{RT_{n+1,m}}\right) \tag{3.96}$$

Note that the subscript k in Equation 3.89 has been exchanged for the subscript m in order to avoid confusions with the iterative scheme of the pyrolysis residual that has been detailed previously. The subscript m is denoting that the expression is iterative only in the thermal scheme and that the pyrolysis fraction (F) is already the converged value in the pyrolysis scheme. I.e., the pyrolysis fraction has a two level iterative scheme, one for the temperature (m) and another, inside the latter, for the time (k). Thus, the temperature in Equation 3.92 and Equation 3.93 can be regarded as the temperature from the first level iterative scheme (m) or $T_{n+1,m}$, this shows that the pyrolysis scheme depends both on the time iteration (k) and temperature iteration (m).

Then differentiating Equation 3.96 with respect to the temperature yields

$$\begin{aligned}\left.\frac{\partial F}{\partial T}\right|_{n+1,m} = &-\Delta t A_T N_{\mathrm{ro}} \left(F_{n+1,m}\right)^{N_{\mathrm{ro}}-1} \exp\left(-\frac{E_{\mathrm{act}}}{RT_{n+1,m}}\right) \left.\frac{\partial F}{\partial T}\right|_{n+1,m} \\ &-\Delta t A_T \left(F_{n+1,m}\right)^{N_{\mathrm{ro}}} \exp\left(-\frac{E_{\mathrm{act}}}{RT_{n+1,m}}\right)\left(\frac{E_{\mathrm{act}}}{RT^2_{n+1,m}}\right)\end{aligned} \tag{3.97}$$

The last term needed to characterise for the pyrolysis fraction is the cross partial

derivative with respect to time and temperature. This is achieved by deriving Equation 3.55 with respect to the temperature.

$$\begin{aligned}\left.\frac{\partial^2 F}{\partial t \partial T}\right|_{n+1,m} = &-N_{\text{ro}} A_T \left(F_{n+1,m}\right)^{N_{\text{ro}}-1} \exp\left(-\frac{E_{\text{act}}}{RT_{n+1,m}}\right) \left.\frac{\partial F}{\partial T}\right|_{n+1,m} \\ &-A_T \left(F_{n+1,m}\right)^{N_{\text{ro}}} \exp\left(-\frac{E_{\text{act}}}{RT_{n+1,m}}\right)\left(\frac{E_{\text{act}}}{RT^2_{n+1,m}}\right)\end{aligned} \tag{3.98}$$

Note that Equation 3.98 is direct related to Equation 3.97 by the time step.

3.3.3.13 Characteristic constitutive laws

The theoretical formulation is fundamentally posed, and the one-dimensional heat problem for laminated composites can be solved by the procedures explained prior to this point. Nevertheless, an enumeration of useful literature in the characterisation of certain thermal properties for composites is provided, together with a more generalist numerical description of the different constitutive laws involved in the one-dimensional discrete thermal problem.

1. Thermal conductivity

   Considering that the thermal conductivity of the whole composite varies from a virgin state to a degraded state, authors such as Henderson et al., Lattimer et al. have modelled the behaviour of the thermal conductivity by using a linear expression for both virgin and charred states.

$$\begin{aligned} c_k(T) &= F c_{kv}(T) + (1-F) c_{kc}(T) \\ c_{kv}(T) &:= c_{kv0} + c_{kv1} T \\ c_{kc}(T) &:= c_{kc0} + c_{kc1} T \end{aligned} \tag{3.99}$$

   where c_{kv} is the virgin thermal conductivity, c_{kc} is the charred thermal density. The variation of the thermal conductivity coefficient with respect to the temperature is

$$\begin{aligned}\left.\frac{\partial c_k}{\partial T}\right|_{n+1,m} = &\left.\frac{\partial c_{kc}}{\partial T}\right|_{n+1,m} + \left.\frac{\partial F}{\partial T}\right|_{n+1,m} (c_{kv} - c_{kc}) \\ &+F_{n+1,m}\left(\left.\frac{\partial c_{kv}}{\partial T}\right|_{n+1,m} - \left.\frac{\partial c_{kc}}{\partial T}\right|_{n+1,m}\right) \\ &\left.\frac{\partial c_{kv}}{\partial T}\right|_{n+1,m} := c_{kv1} \\ &\left.\frac{\partial c_{kc}}{\partial T}\right|_{n+1,m} := c_{kc1}\end{aligned} \tag{3.100}$$

2. Specific heat capacity

   The specific heat capacity of the whole composite is also considered varying from the virgin state to the degraded state, authors such as Henderson and Wiecek define the variation of the virgin and charred specific heat capacity as a linear function depending on the temperature.

$$\begin{aligned} c_p(T) &= F c_{p_v}(T) + (1-F) c_{p_c}(T) \\ c_{p_v}(T) &:= c_{p_{v0}} + c_{p_{v1}} T \\ c_{p_c}(T) &:= c_{p_{c0}} + c_{p_{c1}} T \end{aligned} \tag{3.101}$$

   where c_{p_c} is the charred specific heat capacity, c_{p_v} is the charred specific heat capacity. The specific heat capacity of the gas phase is modelled by a parabolic function in terms of the temperature.

$$c_{p_{vg}}(T) := c_{p_{vg_0}} + c_{p_{vg_1}} T + c_{p_{vg_2}} T^2 \tag{3.102}$$

   Hence the derivatives with respect to the temperature of the different specific heat coefficients above are

$$\begin{aligned} \left.\frac{\partial c_p}{\partial T}\right|_{n+1,m} &= \left.\frac{\partial c_{p_c}}{\partial T}\right|_{n+1,m} + \left.\frac{\partial F}{\partial T}\right|_{n+1,m} (c_{p_v} - c_{p_c}) \\ &\quad + F_{n+1,m} \left(\left.\frac{\partial c_{p_v}}{\partial T}\right|_{n+1,m} - \left.\frac{\partial c_{p_c}}{\partial T}\right|_{n+1,m} \right) \\ \left.\frac{\partial c_{p_v}}{\partial T}\right|_{n+1,m} &:= c_{p_{v1}} \\ \left.\frac{\partial c_{p_c}}{\partial T}\right|_{n+1,m} &:= c_{p_{c1}} \\ \left.\frac{\partial c_{p_{vg}}}{\partial T}\right|_{n+1,m} &:= c_{p_{vg_1}} + 2 c_{p_{vg_2}} T_{n+1,m} \end{aligned} \tag{3.103}$$

Analogously, the enthalpies described in Equation 3.57 are to be derived with respect to temperature in order to be introduced in the discrete problem. By using the Leibniz integral rule, the derivatives take the form of

$$\frac{\partial h}{\partial T} = \int_{T_0}^{T} \frac{\partial c_p}{\partial T} \, \mathrm{d}T = \frac{\partial c_{p_c}}{\partial T} + \frac{\partial F}{\partial T} (c_{p_v} - c_{p_c}) + F \left(\frac{\partial c_{p_v}}{\partial T} - \frac{\partial c_{p_c}}{\partial T} \right) \tag{3.104}$$

and the gas transfer model, the basic, yields

$$\left.\frac{\partial q_m}{\partial T}\right|_{n+1,m} = \int_z^{l_t} (\rho_v - \rho_c) \left.\frac{\partial^2 F}{\partial t \partial T}\right|_{n+1,m} \mathrm{d}z \tag{3.105}$$

3.4 Conclusions

This chapter has described the balance of energy from a continuum mechanics point of view and how, using the species transport theory, the problem can be divided or fractioned in different phases.

Then the problem is postulated, a composite media that is exposed to a one-side fire. The composite can be conceptualised as a stack of layers and each layer is best described as the mixture of one or more constituent materials. The materials can experiment different temperature-dependent processes, the most notable is *pyrolysis*. The model proposed accounts for both pyrolysis of the matrix and fibre. The other major aspect that is solved is the gas transfer model, which in this particular case is featured by the *basic gas transfer model*.

A fair discussion is given regarding the different terms – pyrolysis and gas transfer included – that form the one-dimensional non-linear heat transfer problem (Equation 3.29). A brief summary of the assumptions is given for both the solid phase and gas phase.

The composite is assumed to be a saturated porous media, therefore the solid phase assumes that there is no thermal expansion of either matrix or fibre and that only the polymer matrix has an associated enthalpy of decomposition. The solid phase in this particular model assumes that, inside the solid domain, the solid material cannot be transported.

When considering the gas phase, the model treats the gas as an ideal gas and assumes that it does not accumulate, this is of important implication, as in the *basic gas transfer model*, the unexposed side of the composite media assumes that not only the gas is not accumulated, but it finds forbidden its escapement throughout this side. I.e., the one-dimensional direction of the flow of gas is prescribed from cold to hot ends.

Concluded the discussion on the heat flux terms involved in the governing equation, a brief introduction to porosity is given and an advanced treatment of this phenomenon is described in the *enhanced gas transfer model*. The chapter proceeds with the definition of *pyrolysis*, which is a characteristic thermal-chemical degradation process present in composites, and how the evolution of these processes is expressed by an Arrhenius law of nth-order.

The penultimate part of the chapter devotes to the treatment of initial and boundary conditions. The discussion on the type of boundary conditions is settled by opting to consider both radiation and convection boundary conditions, and the introduction of the *adiabatic surface temperature* is detrimental in the simplification of both the radiation and convection source temperature.

Finally, the chapter presents the spatial and temporal discrimination of the governing equations and different schemes and algorithms are presented to understand the procedures regarding the state variables and the internal variables, temperature and pyrolysis fraction respectively. The numerical solution is then complimented with some characteristic or experimental constitutive laws in order to quantify the rest of parameters involved in the numerical energy balance model for composites.

3.4.1 Goals

The goals imposed in chapter 1 are fulfilled. The goal number 1, *Provide and implement a constituent formulation of the Henderson et al. equation*, is fulfilled as the vast majority of the chapters in the conclusions explain different assumptions needed to obtain the thermal model and its discretisation.

The goal number 2, *Provide and implement a simple approach to introduce the fire as thermal boundary conditions*, is accomplished as well and is reflected in the paragraph of the conclusions that summaries the penultimate part of the chapter and talks about the concept of adiabatic surface temperature.

Chapter 4

Constitutive modelling of laminate composites exposed to fire

In the present chapter, the constitutive behaviour of composites is discussed. The chapter is structured with a brief introduction to the subject, the justication for the methodology selected, and the explanation of the methodology per se. The methodology of this chapter discusses the behaviour at both the microstructure and the macrostructure levels and then introduces the effects that re has on both. There is an accurate discussion of linear and non-linear solutions, and the chapter ends with the Thermal Serial-Parallel Rule of Mixtures which is one of the cornerstones of the thermomechanical formulation explained in this thesis.

4.1 Introduction

The constitutive model of the thermo-mechanical theory presented in this thesis is fragmented into three parts: *constituent phases*, *composite behaviour* and *effects of fire*. The first part, constituent phases, is centred on the modelling of the homogeneous constituent materials, which when joined, comprise the composite or heterogeneous material. The second part, composite behaviour, is devoted to the amalgamation of the constituent materials and how this recreates the composite behaviour. The third part is the effects originated at these two different levels by the action of fire. In this manner, the analysis of composites becomes very compartmented and tight for the reader to follow the different aspects of the laminated mechanical model.

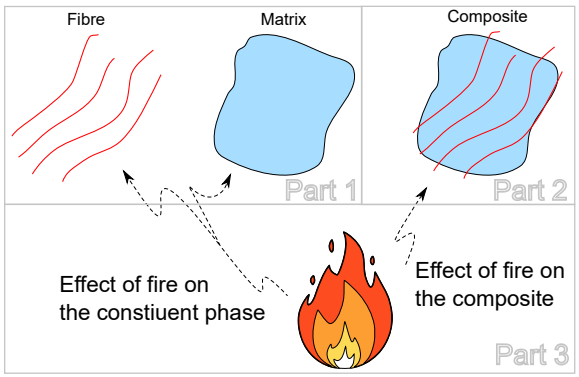

FIGURE 4.1: Illustration of the subdivision of parts of these chapters.

As shown in Figure 4.1, the first part is formulated from references such as the book [16] of Oñate that details the principles of solid mechanics applied to shell elements – triangle and quadrilaterals – and also extends these concepts for composite laminates that would be the second part. The other reference of importance is the thesis [96] of Rastellini, who explains very well the different solutions to the current paradigm of simulations of composite materials. The third part is the novel contribution of the thermo-mechanical analysis developed in this thesis.

4.1.1 Part 1 - Constitutive models for homogeneous media

At the microstructure level, the heterogeneous media is diverse and presents a clear outline of the different materials that comprise the composite. The study of the constitutive laws that these individual and unique materials is one of the topics devoted in this thesis.

Provided that the constituent materials are identified and separable, fibre and matrix, the study of thin and thick shells is of high interest. These two types of shells are best explained with the theories of *Kirchhoff-Love* and *Reissner-Mindlin*, in this particular application, the common triangle (DKT) and quadrilateral (QLLL) are discussed. Although it is not explicitly mentioned, the limitations of the quadrilateral regarding problems such as shear locking are corrected (shear correction factor). The triangle employs the *Kirchhoff-Love* theory and the quadrilateral *Reissner-Mindlin* theory.

The section is structured by the introduction to the linear modelling of the two elements using isotropic constitutive models, the stress-resultant notation found in [16] is enforced throughout this chapter and subsequent chapter. Then the so-called *isotropic damage* model is discussed. This model represents the core of the non-linear constitutive behaviour used in this thesis. Composites present behaviour that suits very well the fluency rules established by this theory. So by inference, the constituent materials will obey this sort of rule.

4.1.2 Part 2 - The equivalent heterogeneous media

Once the particular laws of each material at the micro-structure level are defined, the laws that mix both together are derived, i.e., the composite behaviour. A careful review of the existent methods used to obtain the constitutive behaviour of the composite is given. Then the concept of orthotropy is introduced and with it the most common ways to obtain elastic orthotropy.

The section ends with the introduction of the non-linear constitutive behaviour of the composite. The key aspects introduced here are the Serial-Parallel Rule of Mixtures [15], and the possibility of using this formulation in conjunction with the non-linear constitutive model for fibre and matrix.

4.1.3 Part 3 Modelling the effect of fire

The effects of fire, or more rigorously, the effects of temperature and pyrolysis, affect both the constituent materials of the composite and the composite as a whole. The effects considered are one-way, i.e., the resultant effect of the constitutive analysis is assumed to not impact or exert any change in the temperature or fire dynamics of the problem.

4.1.3.1 At the constituent level

The effects that are considered at the constituent level are for example the thermal expansion of the different phases since each constituent material does not necessarily have the same thermal expansion coefficient. Other non-linear effects taken into account in the mechanical response are the loss of mechanical properties due to temperature, and especially for composites, the pyrolysis, or the mechanical damage induced by the temperature itself. In the framework of advanced materials such as composites, these effects are detrimental, since most of them generate irreversible damage to the structure.

4.1.3.2 At the composite level

At this level, the effects induced in the structure are due to the bounding of the different phases. This is what is commonly known as the constituent-to-composite relationship. It is not simple to find the adequate relationship when describing the loss of mechanical properties of the composite as a whole as certain assumptions need to be made when describing this effective mechanical loss.

Other effects are related to the very hypothesis of Voigt or Reuss. I.e., the transverse stress considered in the serial hypothesis is only applicable to the mechanical stress, therefore when considering the composite as a whole, the thermal stresses need to be subtracted to correctly fulfil the composite response.

4.2 Justification for the paradigm and methodology

The anisotropic behaviour of composites makes their mechanical response very complex physic to be predicted. Extracting this behaviour from the constituent phases found in heterogeneous micro-structure is one of the easiest and most reliable methods. The constitutive models for homogeneous materials are best described from the Kirchhoff-Love theory [262] for the linear triangle element and the Reissner-Mindlin theory [263] for the linear quadrilateral element. Both elements are extracted from the derivation granted in [16].

One of the goals of this thesis is to provide a shell mechanical model that can account for non-linear constitutive degradation. In the case of composites, it has already been discussed, that the phenomenology is best described by damage models. The non-linear constitutive model is based on the ideas of Simo and Ju [17] which later were generalised in [32, 106, 107]. This model will be regarded as the *isotropic damage model*.

At the constituent level, the model is isotropic, as its name refers. This requires that the constituent-to-composite model fulfils the two major hypotheses (serial [27] and parallel [26]). The theory used to accomplish this is the *serial-parallel rule of mixtures* (SPROM) [15]. One of the main advantages of this theory is that it allows any non-linear elastic model to be incorporated for each constituent phase, and the theory itself obtains the serial and parallel behaviour of the composite.

This advantage is crucial because, combining the isotropic damage model and also being able to obtain the transverse orthotropic behaviour of the composite, it enables the analysis of non-linear constitutive composites by just using isotropic homogeneous models. This advantage translates in a significant reduction in the amount of data required, since no orthotropic parametrisation is needed. The other advantage relies on the nature of the SPROM formulation, which can be understood as some type of algorithm that works as an external layer to the standard finite element algorithm at the constitutive level, and this is extremely useful since it works like a black box.

Once the laminated mechanical model is formulated, the effects of fire are taken into account. First, the mechanical model is adapted to include thermo-chemical effects, this is the so-called thermo-mechanical model of the constituent phases. The effects of fire on the constituent phases are examined, carefully modifying the damage model of [32] by including the procedure detailed in [264] by Cervera Ruiz et al. in which the concept of *thermal induced* mechanical damage is introduced.

Another important thermal effect found at the constituent level is the thermal degradation of mechanical properties – elastic and inelastic properties – due to temperature and pyrolysis. This mechanical degradation is modelled with the function defined by Mouritz and Gibson [20]. This function is defined for the composite level. However, the latter is originally applied at the composite level. Therefore, an approach is proposed to establish a composite-to-constituent relationship, this relationship is a novel contribution that aims to solve the problem of not having enough information to characterise the loss of mechanical properties of both constituent phases.

Finally, at the composite level, the laminated thermo-mechanical model shall extend the ideas of the SPROM by Rastellini [33] into the *thermal serial-parallel rule of mixtures* (TSPROM). The TSPROM contributes on extending the theory to take into account the thermal expansion and is applied to laminated shells in this particular case.

4.3 Methodology

An important early distinction has to be made for the derivation of constitutive related concepts. Composites, and typically the standard finite element methodology, employ the concept of a local and global systems of references. It is customary to derive the kinematics and constitutive laws from a local perspective. Therefore, the nomenclature between local kinematics and global kinematics is different and is denoted in the notation found in the following equation.

$$\begin{aligned} {}^{l}\_ &\rightarrow \text{LOCAL} \\ {}^{g}\_ &\rightarrow \text{GLOBAL} \end{aligned} \tag{4.1}$$

The relationship between these two systems of reference is obtained by the rotation matrix (Λ) that is represented in Figure 4.2, in this illustration the local and global nomenclature are represented as well.

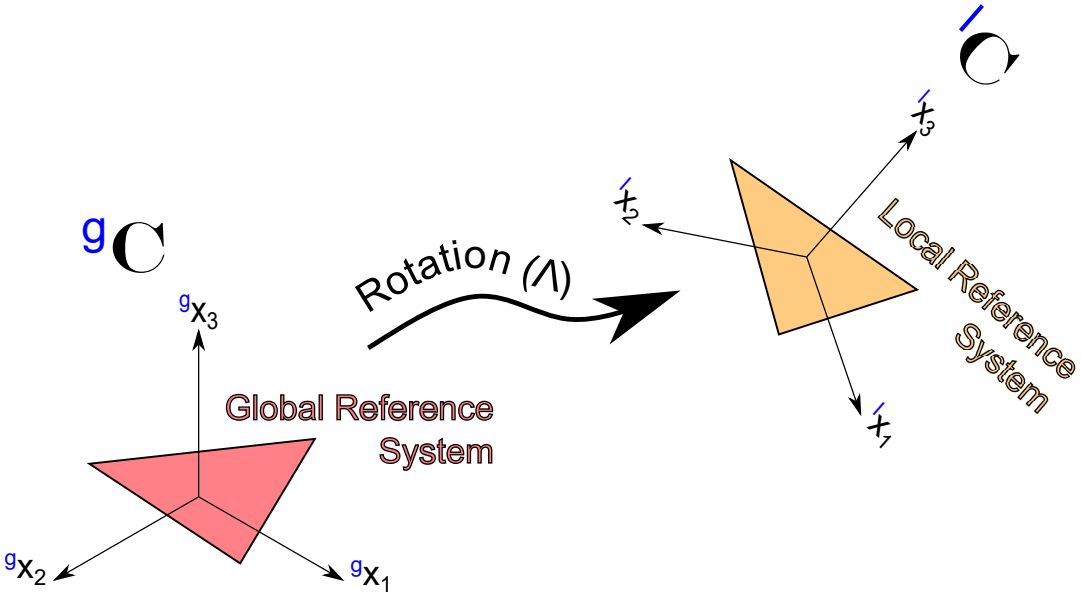

FIGURE 4.2: Transformation between a global and a local system of reference.

In the next sections, the constitutive models applied to single materials such as fibre or matrix are derived, then, the models for composite materials and finally the effects that fire has on independent materials and composite materials.

4.3.1 Constitutive modelling of shells

This section is devoted only to the study of the constituent materials, those that when combined comprise the composite material (see Figure 4.3). In particular, to the study of the relationship that exists between the stress and strain fields, i.e., the so-called constitutive relationship.

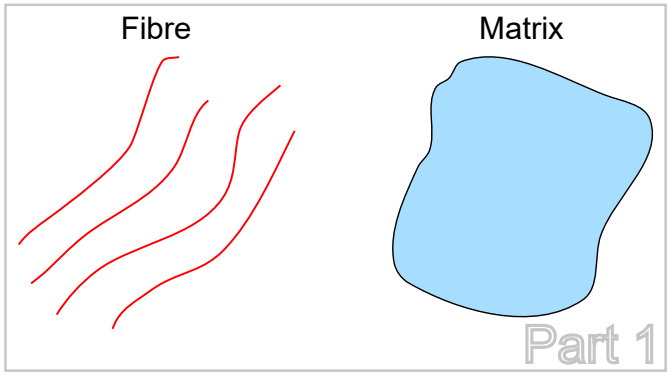

FIGURE 4.3: Illustration of part 1, focused on the modelling of the constituent materials.

There are two types of study within the field of constitutive modelling, those models that are considered linear, generally the simplest and oldest ones, and the more complex models that take into account non-linear effects. This research has concentrated in describing the linear relationship, an isotropic one, between stresses and strains for triangle and quadrilateral elements and the non-linear mechanical effects are introduced by applying a general theory that extends isotropic elasticity to isotropic inelasticity. The last is the so-called *isotropic damage model*.

4.3.1.1 Linear constitutive elasticity - The isotropic elastic model

The linear constitutive models shown below describe elements that do not depend on the strain or displacement fields of the problem. The DKT is an element that is good at predicting strain but not stress, while the QLLL can adequately predict the latter. This is the reason behind introducing both elements, since international regulations rely, majorly, on quadrilateral formulations than triangle ones. Nevertheless, there are interesting formulations available nowadays that complement the limitations of the triangle elements, for example, the formulation found in [124] by Felippa.

Both elements fulfil the so-called plane stress theory. The assumption is that the stress is negligible in the direction of the normal axis.

$$\sigma_{33} = 0 \tag{4.2}$$

It is important to note that the 3-node triangular shell employs the Kirchhoff-Love thin shell theory [16, 262] and the 4-node quadrilateral shell uses the Reissner-Mindlin thick shell theory [16, 263]. However, the assumption that the stress (σ_{33}) is negligible is shared amongst both theories. The stress tensor is defined in Voigt notation and can be expressed in local or global systems of reference. In the case of stress, the relationship between shear stresses in engineering notation and standard stress tensor notation is equal, this is not the same for the strains.

$$\tau_{ij} = \sigma_{ij}, \quad i \neq j \quad \Rightarrow \begin{bmatrix} \sigma_{11} \\ \sigma_{22} \\ \sigma_{33} \\ \tau_{21} \\ \tau_{31} \\ \tau_{32} \end{bmatrix} \tag{4.3}$$

where τ is the shear stress. In order to formalise the constitutive model, an expression has to be taken for the relationship between the stresses and strain. Each numerical layer that is found in the thickness of a shell has stress (σ) for a given deformation (ε) in local or global reference systems. Therefore, the constitutive tensor (D) needs to be characterised to obtain a pertinent stress quantity. For instance, an isotropic model can be used.

$$^{l}\underline{\sigma_{\text{in}}} = \underline{\underline{D_{\text{in}}}}\, ^{l}\underline{\varepsilon_{\text{in}}} \tag{4.4}$$

where σ_{in} is the in-plane stress, D_{in} is the in-plane constitutive tensor and ε_{in} is the in-plane strain. Note that the generalised constitutive tensor (D) has been exchanged for the in-plane constitutive tensor (D_{in}) to denote that the first refers to the integrated constitutive tensor of the shell element and the second describes the constitutive tensor at the layer/ply level. The in-plane stress and strain are ($[\sigma_1, \sigma_2, \tau_{21}]^T$) and ($[\varepsilon_1, \varepsilon_2, \gamma_{21}]^T$) respectively.

In the following paragraphs the stress-resultant notation shall be used to maintain coherence with the section on kinematics, where Oñate in [16] describes a method to express the strain by decoupling the membrane, bending and shear effects. To reduce the unnecessary repetition of text, the stress is therefore considered as stress-resultant ($\hat{\sigma}$) and depends on the stress-resultant strain ($\hat{\varepsilon}$). This stress-resultant stress is referred always to the mid-plane of the shell element.

4.3.1.1.1 3-node triangular shell element

First note that the constitutive model in the 3-node triangle element takes into account only in-plane effects, therefore the generalised stress is the same as the in-plane stress.

$$\underline{\sigma} \equiv \underline{\sigma_{\text{in}}} \tag{4.5}$$

The generalised stress vector ($\hat{\sigma}$) at the middle plane is found by the following relationship

$$^{l}\underline{\hat{\sigma}} = {}^{l}\begin{bmatrix} \underline{\sigma_m} \\ \underline{\sigma_b} \end{bmatrix} = \int_{\frac{-l_t}{2}}^{\frac{l_t}{2}} \begin{bmatrix} ^{l}\underline{\sigma} \\ x_3\, ^{l}\underline{\sigma} \end{bmatrix} \mathrm{d}x_3 = \sum_i \begin{bmatrix} \left((x_3)_{i+1} - (x_3)_i\right) ^{l}\underline{\sigma_i} \\ \frac{1}{2}\left((x_3)^2_{i+1} - (x_3)^2_i\right) ^{l}\underline{\sigma_i} \end{bmatrix} \tag{4.6}$$

where $\hat{\sigma}$ is the stress-resultant stress, x_3 is the z-axis. The σ_m and σ_b are the membrane ($[\sigma_{Nx_1}, \sigma_{Nx_2}, \sigma_{Nx_3}]^T$) and bending ($[\sigma_{Mx_1}, \sigma_{Mx_2}, \sigma_{Mx_3}]^T$) strengths, respectively. The

summation, over the iterator i, represents the discrete integral over all the layers that divide the thickness.

Equation 4.3 can be expressed in terms of the stress-resultant components and holds true when combined with Equation 4.6, the stress-resultant constitutive tensor is then obtained.

$$ {}^{l}\underline{\hat{\sigma}} = {}^{l}\begin{bmatrix} \underline{\sigma_m} \\ \underline{\sigma_b} \end{bmatrix} = \int_{\frac{-l_t}{2}}^{\frac{l_t}{2}} \begin{bmatrix} \underline{\underline{D_{\text{in}}}} & x_3\underline{\underline{D_{\text{in}}}} \\ x_3\underline{\underline{D_{\text{in}}}} & x_3^2\underline{\underline{D_{\text{in}}}} \end{bmatrix} \mathrm{d}x_3 \cdot {}^{l}\begin{bmatrix} \underline{\varepsilon_m} \\ \underline{\varepsilon_b} \end{bmatrix} \tag{4.7} $$

where σ_m is the membrane stress, σ_b is the bending stress, ε_m is the membrane strain and ε_b is the bending strain. The stress-resultant constitutive tensor can be arranged as follows

$$ {}^{l}\underline{\hat{\sigma}} = \underline{\underline{\hat{D}}}\,{}^{l}\underline{\hat{\varepsilon}}, \quad \underline{\underline{\hat{D}}} = \begin{bmatrix} \underline{\underline{\hat{D}_m}} & \underline{\underline{\hat{D}_{mb}}} \\ \underline{\underline{\hat{D}_{bm}}} & \underline{\underline{\hat{D}_b}} \end{bmatrix} \tag{4.8} $$

where $\hat{\varepsilon}$ is the stress-resultant strain, $\hat{D}$ is the stress-resultant constitutive tensor, $\hat{D}_m$ is the stress-resultant membrane constitutive tensor, $\hat{D}_{mb}$ is the stress-resultant membrane-bending constitutive tensor, $\hat{D}_{bm}$ is the stress-resultant bending-membrane constitutive tensor and $\hat{D}_b$ is the stress-resultant bending constitutive tensor. The stress-resultant constitutive ($\hat{D}$) tensor is symmetric, thus the membrane-bending and bending-membrane constitutive tensors are identical.

The terms that compose the stress-resultant constitutive tensor are defined below.

$$ \underline{\underline{\hat{D}_m}} = \int_{\frac{-l_t}{2}}^{\frac{l_t}{2}} \left[\underline{\underline{D_{\text{in}}}}\right] \mathrm{d}x_3 = \sum_i \left((x_3)_{i+1} - (x_3)_i\right) \underline{\underline{D_{\text{in}}}}_i \tag{4.9} $$

$$ \underline{\underline{\hat{D}_{mb}}} = \underline{\underline{\hat{D}_{bm}}} = \int_{\frac{-l_t}{2}}^{\frac{l_t}{2}} \left[x_3\underline{\underline{D_{\text{in}}}}\right] \mathrm{d}x_3 = \sum_i \frac{1}{2}\left((x_3)_{i+1}^2 - (x_3)_i^2\right) \underline{\underline{D_{\text{in}}}}_i \tag{4.10} $$

$$ \underline{\underline{\hat{D}_b}} = \int_{\frac{-l_t}{2}}^{\frac{l_t}{2}} \left[x_3^2\underline{\underline{D_{\text{in}}}}\right] \mathrm{d}x_3 = \sum_i \frac{1}{3}\left((x_3)_{i+1}^3 - (x_3)_i^3\right) \underline{\underline{D_{\text{in}}}}_i \tag{4.11} $$

For a symmetric shell, a shell that is symmetric in the thickness-wise direction, the membrane-bending and bending-membrane constitutive tensors are zero. This is a special case for an isotropic shell.

4.3.1.1.2 4-node quadrilateral shell element

When shear effects are taken into account the constitutive model for an isotropic material, Equation 4.4, has to be modified in order to include the out-of-plane terms as well.

$$ {}^{l}\underline{\sigma} = \begin{bmatrix} {}^{l}\underline{\sigma}_{\text{in}} \\ {}^{l}\underline{\sigma}_{\text{out}} \end{bmatrix} = \begin{bmatrix} \underline{\underline{D}}_{\text{in}} & \underline{\underline{D}}_{\text{in-out}} \\ \underline{\underline{D}}_{\text{out-in}} & \underline{\underline{D}}_{\text{out}} \end{bmatrix} \begin{bmatrix} {}^{l}\underline{\varepsilon}_{\text{in}} \\ {}^{l}\underline{\varepsilon}_{\text{out}} \end{bmatrix} \tag{4.12} $$

where σ_{out} is the out-of-plane stress, $D_{\text{in-out}}$ is the in-out-of-plane constitutive tensor, $D_{\text{out-in}}$ is the out-of-in-plane constitutive tensor, D_{out} is the out-of-plane constitutive tensor and ε_{out} is the out-of-plane strain. The out-of-plane stress and strain are $([\tau_{32}, \tau_{32}]^T)$ and $([\gamma_{31}, \gamma_{32}]^T)$ respectively.

Similar to the triangle, the constitutive model is expressed in stress-resultant notation and the main difference is that the Reissner-Mindlin theory introduces the shear effect by taking into account the out-of-plane or transverse stress.

$$ {}^{l}\underline{\hat{\sigma}} = {}^{l}\begin{bmatrix} \underline{\sigma_m} \\ \underline{\sigma_b} \\ \underline{\sigma_s} \end{bmatrix} = \int_{\frac{-l_t}{2}}^{\frac{l_t}{2}} \begin{bmatrix} {}^{l}\underline{\sigma} \\ x_3\,{}^{l}\underline{\sigma} \\ x_3^2\,{}^{l}\underline{\sigma} \end{bmatrix} \mathrm{d}x_3 = \sum_i \begin{bmatrix} \left((x_3)_{i+1} - (x_3)_i\right) {}^{l}\underline{\sigma}_i \\ \frac{1}{2}\left((x_3)_{i+1}^2 - (x_3)_i^2\right) {}^{l}\underline{\sigma}_i \\ \frac{1}{3}\left((x_3)_{i+1}^3 - (x_3)_i^3\right) {}^{l}\underline{\sigma}_i \end{bmatrix} \tag{4.13} $$

where σ_s is the shear strength $([\sigma_{Q_{x_1}}, \sigma_{Q_{x_2}}]^T)$. And the stress-resultant constitutive relationship is

$$ {}^{l}\underline{\hat{\sigma}} = \underline{\underline{\hat{D}}}\,{}^{l}\hat{\varepsilon}, \quad \underline{\underline{\hat{D}}} = \begin{bmatrix} \underline{\underline{\hat{D}}}_m & \underline{\underline{\hat{D}}}_{mb} & 0 \\ \underline{\underline{\hat{D}}}_{bm} & \underline{\underline{\hat{D}}}_b & 0 \\ 0 & 0 & \underline{\underline{\hat{D}}}_s \end{bmatrix} \tag{4.14} $$

where $\hat{D}_s$ is the stress-resultant shear constitutive tensor. The classical assumption is to consider membrane-shear and bending-shear effects negligible because the in-out and out-in effects are decoupled ($D_{\text{in-out}}, D_{\text{out-in}}$).

The stress-resultant shear constitutive tensor is formulated in the following manner

$$ \underline{\underline{\hat{D}}}_s = \int_{\frac{-l_t}{2}}^{\frac{l_t}{2}} \begin{bmatrix} c_{\text{sf11}}\,\underline{\underline{D_s}}_{11} & c_{\text{sf12}}\,\underline{\underline{D_s}}_{12} \\ c_{\text{sf21}}\,\underline{\underline{D_s}}_{21} & c_{\text{sf22}}\,\underline{\underline{D_s}}_{22} \end{bmatrix} \mathrm{d}x_3 \tag{4.15} $$

where c_{sf} is the shear correction factor, D_s is the shear constitutive tensor. For an isotropic material, considering that the shear is decoupled in each direction, the off-diagonal terms of the shear constitutive tensor vanish and the shear correction factor is the same ($c_{\text{sf11}} = c_{\text{sf22}} = 5/6$).

The expressions that define both the in-plane and the out-of-plane isotropic constitutive tensors are

$$ \underline{\underline{D}}_{\text{in}} = \frac{E}{1-\nu^2} \begin{bmatrix} 1 & \nu & 0 \\ \nu & 1 & 0 \\ 0 & 0 & \frac{1-\nu}{2} \end{bmatrix} \tag{4.16} $$

where E is the shear modulus, ν is the Poisson's ratio.

$$\underline{\underline{D_{\text{out}}}} \equiv \underline{\underline{D_s}} = G \begin{bmatrix} 1 & 0 \\ 0 & 1 \end{bmatrix} \tag{4.17}$$

4.3.1.2 Non-linear constitutive elasticity – The isotropic damage model

One of the recurrent topics for the research community is the loss of mechanical properties of certain materials when non-linear events such as defects or cracks are present in the crystalline structure. In particular, the first attempt to characterise the failure of structures comes by the hand of Kachanov in 1958 who published a paper [127] where, throughout several experimental tests, micro-cracks of the specimens were quantified. The quantification of micro-cracking and the measure of the loss of stiffness, permitted the formulation of a global and macro model by means of an internal variable that characterised the density of the micro-defects in the structure. This internal variable was stored along with its evolution and inelastic deformation.

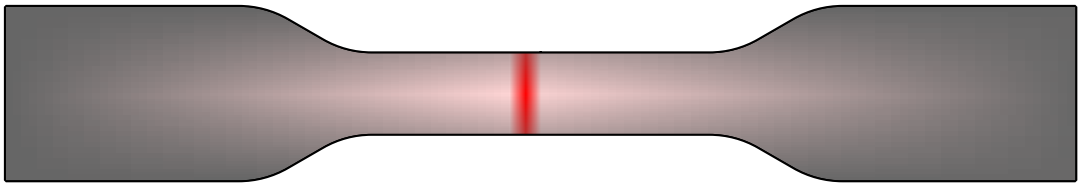

FIGURE 4.4: Loss of properties signalled in red when over-stretched.

This theory lacks a detailed and local prediction of the crack formation and founds its physical principles in irreversible thermodynamic processes originating when the micro-structure is over-stretched beyond its yield strain. The amount of testing needed when using the Kachanov model is enormous, it requires different types of testing: tensile, compression, an inelastic threshold in compression and tension for yielding and ultimate failure. However, these parameters are associated with a macro-structure of a specific material.

The model allowed to characterise the rupture of a structure as a whole in a manner that is explicit and analytical. However, this was found limiting, since non-global events such as crack propagation or induced anisotropy were not considered. Krajcinovic and Fonseka [265] pointed out, indeed, that modelling reality is a task far more complex. One of the most discussed approaches is to characterise the cracks both globally or locally. The evolution of cracks and how they are generated locally are a subject of special interest, since as Krajcinovic and Fonseka [265] previously commented, there are local interactions that compromise the rupture of a structure beyond their global characterisation.

The prompt collapse of a structure is the result of how an existing crack in a feeble local area grows into a patch of damaged elements that have undergone substantial degradation. Figure 4.4 exemplifies this problema, in which a patch of elements in red has connected and created a global cracking. It is then understandable that locally, the appearance of cracks – in certain local zones – may induce the origination of micro-cracking in its neighbourhood (see Figure 4.5).

Authors such as Luccioni et al. have proposed solutions that introduce a meso or micro-modelling of hyperparameters that are intrinsically related to this local cracking.

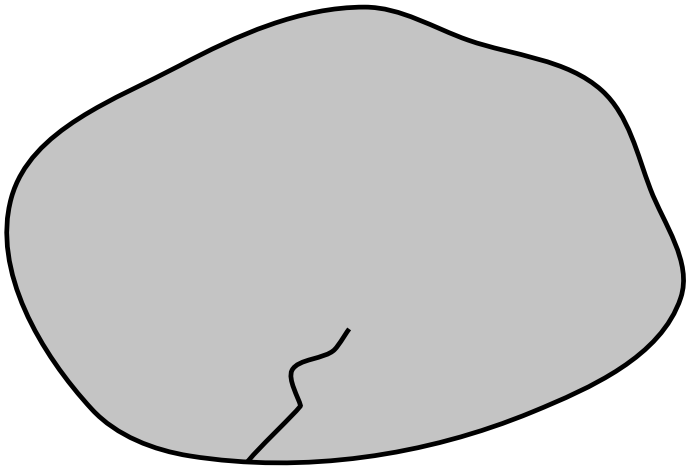

FIGURE 4.5: Global crack development.

When considering that the micro-cracks are scattered randomly in all directions, the evolution of damage can be assumed to be isotropic. One of the most known and classical damage models is the so-called *isotropic damage model*, which is attributed to Simo and Ju [17]. This damage model is extremely intuitive and simple, since using the isotropic simplification leads to a damage model with only a scalar damage variable. A similar theory is proposed by Oliver [32], this paper analyses one of the limitations of this theory and this is the fact that this model is only suitable for materials that once a crack is originated, the distribution of cracks remains isotropic.

Several authors have worked in providing models that take into account, and more important predict, oriented distributions of micro-cracks. In these models, the variable of damage is no longer a unique scalar variable. These models – either orthotropic or anisotropic – can be found in [131, 141, 143].

The idea of damage is closely linked to the effective sectional area left after the crack or flaw starts to grow. This effective area is the result of subtracting the damaged sectional area (crack size) from the intact or original sectional area. A sketch of the sectional area can be found in Figure 4.6. The discussed *isotropic damage* model in this thesis is derived from the research of Simo and Ju in [17]. The model proposed by the latter establishes a degradation of the mechanical properties which has a monotonic evolution of the damage history, i.e., no healing or recovery of the mechanical response of the structure is considered. The specific formulation for the damage model in this thesis is the one proposed by Chaves [266], which is based on the Simo and Ju model.

The rheological model used to describe the deformation of a solid under stress is best described by considering an initial mechanical structure that is enduring uni-axial loading. Observe Figure 4.6, the initial or intact sectional area (S_0) of the structure - the section perpendicular to the application of the uni-axial loading – shall decrease as the cracks or flaws developed, this is referred to as damaged sectional area (S_d), due to the increase of the magnitude of the stress over the elastic limit or yielding

stress (σ_y). The resultant sectional area is the effective one (S_e).

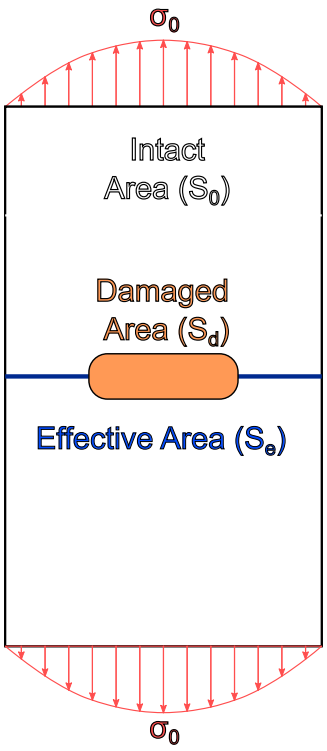

FIGURE 4.6: Effective area and uni-axial rheological damage model.

Hence, the hypothesis is that for infinitesimal strain theory, in the absence of any damage, the original sectional area shall remain unperturbed. Once the damage occurs – irreversible damage to be precise – the effective sectional area shall decrease due to the generation of internal flaws in the sectional area. These flaws, cracks or holes, represent a quantity of the damage found in the structure, a proportional one, and can be best described as the ratio between the damaged and undamaged sectional area.

The uni-axial rheological model can be extended to a three-dimensional rheological by using tensor algebra and defining the damage in the so-called HaighWestergaard stress space. This stress space identifies three spatial axes that represent the three principal stresses of a body subject to three-dimensional loading.

The main fundamentals of the isotropic damage model are detailed in the paragraphs below. A compacted thread of the discussion is provided in these lines, in an attempt to assure the correct advancement throughout the subject of discussion in the forthcoming steps. The discussion starts with stating a basic principle, this is the equilibrium of the internal stresses, then the stress is disseminated by finding an appropriated constitutive model that correlates the stress and the strains. The constitutive law and its damage evolution are then examined to link this evolution to a unique damage variable, after the introduction of this damage parameter, the evolution is studied from an elastic energetic point of view. After this energetic approach is taken, the evolution of the damage variable is characterised by a series of constitutive parameters. The isotropic damage model ends with the introduction of the so-called *tangent constitutive tensor*.

4.3.1.2.1 Force equilibrium

Consider a differential of volume under uni-axial loading (Figure 4.7). If force equilibrium is enforced, this differential must satisfy

$$S_0\sigma_0 = S_e\sigma_e \tag{4.18}$$

where S_0 is the intact area, S_e is the effective area.

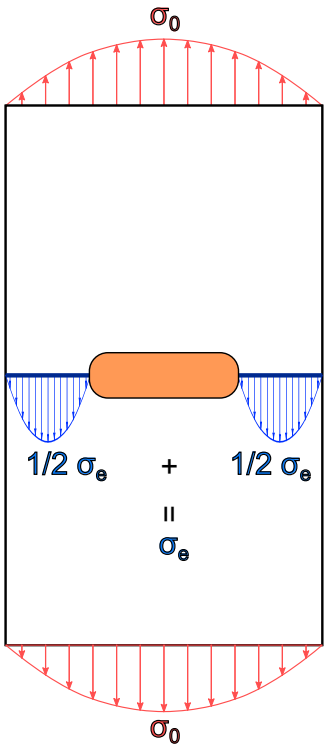

FIGURE 4.7: Differential volume under uni-axial loading.

Equation 4.19 can be rearranged to introduce the concept of damage.

$$\sigma_0 = \frac{S_e}{S_0}\sigma_e = \left(1 - \frac{S_0 - S_e}{S_0}\right)\sigma_e = \left(1 - \frac{S_d}{S_0}\right)\sigma_e \tag{4.19}$$

where S_d is the damaged area. Therefore the amount of damage a section has suffered is defined by the ratio between the damaged area and the intact or initial area.

$$d = \frac{S_d}{S_0} \Rightarrow \sigma_0 = (1-d)\sigma_e \quad , \quad 0 \leq d \leq 1 \tag{4.20}$$

where d is the damage index. When this index is zero, the section is intact and when it becomes one the section is completely damaged.

4.3.1.2.2 Constitutive equation

The constitutive relationship established in Equation 4.14 can be applied to the effective tension and, by combining with Equation 4.20, the so-called secant constitutive tensor can be formulated for the initial or intact stress. Both effective and intact stresses shall be expressed using the stress-resultant notation as per usual.

$$ {}^{l}\hat{\underline{\sigma}}_{e} = \hat{\underline{\underline{D}}}^{l}\hat{\underline{\varepsilon}} \Rightarrow {}^{l}\hat{\underline{\sigma}}_{0} = (1-d)\hat{\underline{\underline{D}}}^{l}\hat{\underline{\varepsilon}} = \hat{\underline{\underline{D}}}_{\text{sec}}{}^{l}\hat{\underline{\varepsilon}} \tag{4.21} $$

where $\hat{D}_{\text{sec}}$ is the stress-resultant secant constitutive tensor. The secant allows representing the loading and unloading either in the elastic or inelastic range. Figure 4.8 to illustrate the concept of the secant, note that this chart replaces the constitutive tensor (D) by Young's modulus (E), nevertheless the analogy to the three-dimensional space remains.

In the intact or initial region of the stress-strain curve, the damaged sectional area has not originated and the rate of variation of this with respect to time is as well zero.

$$ \begin{aligned} S_d = 0 \Rightarrow \quad & d = 0 \\ \frac{\mathrm{d}S_d}{\mathrm{d}t} = 0 \Rightarrow \quad & \frac{\mathrm{d}d}{\mathrm{d}t} = 0 \end{aligned} \tag{4.22} $$

This is especially valid for the elastic limit prior to damage initialisation and for this specific case the secant constitutive tensor recovers its original form which is the elastic constitutive tensor.

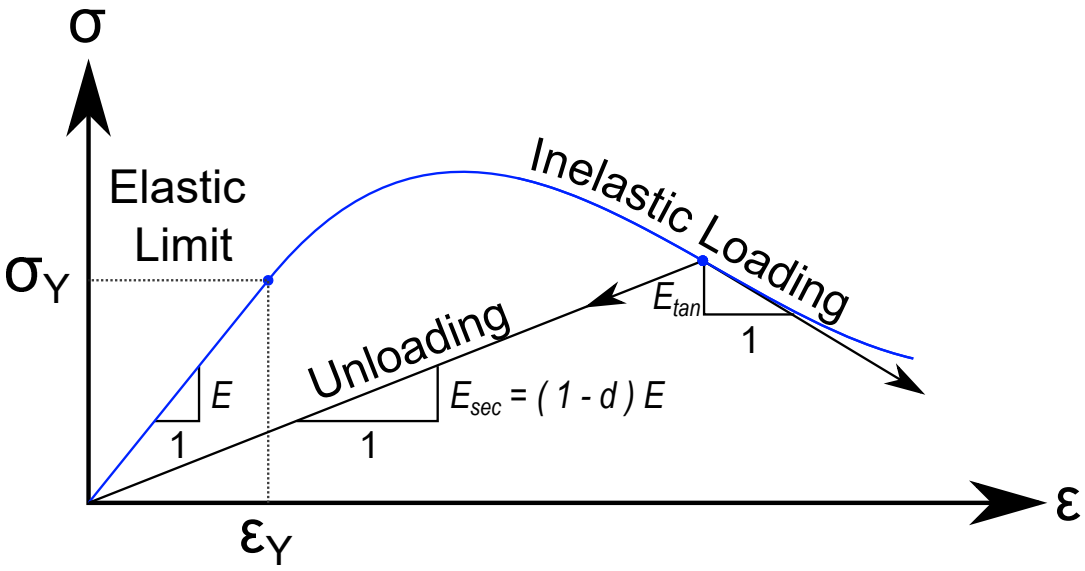

FIGURE 4.8: Stress-strain relationship for the isotropic damage model.

When damage is generated, the stress-strain curve no longer unloads or loads using the elastic slope, but the secant as shown in Figure 4.8.

$$\begin{aligned} S_d \neq 0 \Rightarrow \quad & d \neq 0 \\ \frac{\mathrm{d}S_d}{\mathrm{d}t} = 0 \Rightarrow \quad & \frac{\mathrm{d}d}{\mathrm{d}t} = 0 \end{aligned} \tag{4.23}$$

The secant loading holds as long as the stress or strain does not surpass a certain threshold. These respective thresholds can be derived from the so-called Helmholtz free energy potential.

4.3.1.2.3 Energy Norms

As commented previously, the thresholds used to determine whether the process of damage has evolved or not, are determined by the so-called energy norms in the stress or strain spaces. Assume a thermodynamic process where dissipation is non-zero

$$\frac{\mathrm{d}d}{\mathrm{d}t} > 0 \tag{4.24}$$

The thresholds that define the fluency surface are found by

$$\begin{cases} \mathbb{v}_\sigma = \|\sigma\| = \sqrt{\underset{\sim}{\sigma} : \underset{\sim\sim}{D_{\text{elast}}}^{-1} : \underset{\sim}{\sigma}} \\ \mathbb{v}_\varepsilon = \|\varepsilon\| = \sqrt{\underset{\sim}{\varepsilon} : \underset{\sim\sim}{D_{\text{elast}}} : \underset{\sim}{\varepsilon}} \end{cases} \tag{4.25}$$

where $\mathbb{v}_\sigma$ is the stress norm, D_{elast} is the elastic constitutive tensor and $\mathbb{v}_\varepsilon$ is the strain norm. Note that the elastic constitutive tensor is the one when no damage ($d = 0$) has originated.

A relationship between both norms can be found in terms of the damage index.

$$\mathbb{v}_\sigma = (1 - d)\mathbb{v}_\varepsilon \tag{4.26}$$

These norms are used to define the fluency surfaces in Figure 4.9. Each norm is defined by what can be termed an internal variable.

$$\begin{cases} \mathbb{F}_\varepsilon(\mathbb{v}_\varepsilon, \beta_r) = 0 \\ \mathbb{F}_\sigma(\mathbb{v}_\sigma, \beta_q) = 0 \end{cases} \tag{4.27}$$

where $\mathbb{F}_\varepsilon$ is the strain fluency surface, β_r is the damage internal variable, $\mathbb{F}_\sigma$ is the stress fluency surface and β_q is the damage internal variable evolution law. The damage internal variable evolution law is also referred to as the hardening/softening variable, which depends on the internal variable.

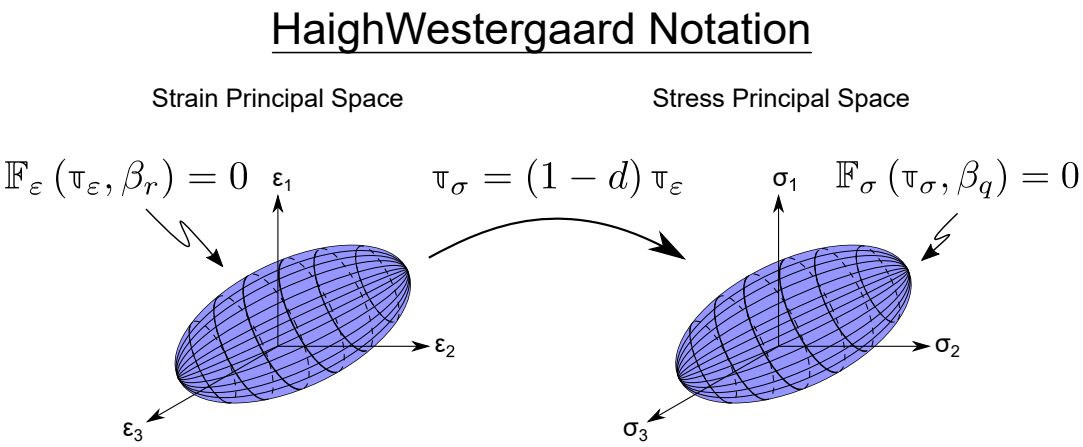

FIGURE 4.9: Fluency surface from the isotropic damage model.

The criterion to define thus if damage has been originated would be

$$\mathbb{F}_\varepsilon(\mathbb{r}_\varepsilon, \beta_r) = \mathbb{r}_\varepsilon - \beta_r < 0 \tag{4.28}$$

for the strain norm and

$$\mathbb{F}_\sigma(\mathbb{r}_\sigma, \beta_q) = \mathbb{r}_\sigma - \beta_q\,(\beta_r) < 0 \tag{4.29}$$

for the stress norm.

4.3.1.2.4 Internal variables and evolution laws

Equation 4.28 in combination with Equation 4.29 defines the expression of the hardening/softening variable.

$$\beta_q\,(\beta_r) = (1-d)\beta_r \tag{4.30}$$

The evolution of the hardening or softening can be either positive or negative, nevertheless, the hardening or softening variable (β_q) is a positive quantity. Previously, the damage index (d) was analysed and the consideration that the damage index has monotonic positive evolution implies the same for the internal variable (β_r).

Implying that $\beta_r \in [\beta_{r_0}, \infty)$ and similarly the range for the evolution law variable would be $\beta_q \in [0, \infty)$. Observe the lower bound of the damage internal variable, which is not null, i.e., the damage internal variable initially has a value that is equivalent to the virgin or undamaged threshold, and it is intrinsically linked to the idea of fracture energy.

However, one question to solve is how this internal variable evolves concerning time or pseudo-time (loading and unloading).

$$\beta_r(t) = \max\left(\beta_{r_0}, \max_{\hat{t}\in[t_0,t]} \mathbb{T}_\varepsilon(\hat{t})\right) \tag{4.31}$$

where β_{r_0} is the damage initial internal variable. Therefore, the damage internal variable at a given time or pseudo-time associated with a load increment is the resultant of the maximum value between the damage initial internal variable and the maximum value of the threshold history. The damage initial internal variable is defined by the ratio of the elastic limit and Young's modulus.

$$\beta_{r_0} = \frac{\sigma_y}{\sqrt{E}} \tag{4.32}$$

where σ_y is the intact stress. Taking Equation 4.30 and rearranging, the damage can be then defined in terms of the internal variable and the evolution law variable.

$$d = 1 - \frac{\beta_q\left(\beta_r\right)}{\beta_r} \tag{4.33}$$

And the variation of damage concerning the internal variable is defined by

$$\frac{\mathrm{d}d}{\mathrm{d}t} = \frac{\beta_q - \dfrac{\partial \beta_q}{\partial \beta_r}}{{\beta_r}^2} \frac{\mathrm{d}\beta_r}{\mathrm{d}t} \tag{4.34}$$

where

$$\mathcal{H}_d = \frac{\partial \beta_q}{\partial \beta_r} \tag{4.35}$$

where $\mathcal{H}_d$ is the hardening/softening law. Hence Equation 4.33 imposes an initial value for the evolution law variable.

$$0 \leq d \leq 1 \quad , \quad \beta_{r_0} \leq \beta_r \leq \infty \quad , \quad \beta_q \in \left[\beta_{r_0}, \beta_{q_\infty}\right] \tag{4.36}$$

where β_{q_∞} is the saturated evolution law. The saturated evolution law value has to be positive.

In the standard formulation, the evolution law variable (β_q) is continuous, and generally, the model is postulated in the following manner.

$$\beta_q = \begin{cases} \beta_{r_0} & , \beta_r \leq \beta_{r_0} \\ \int_{\beta_{r_0}}^{\beta_r} \mathcal{H}_d \, \mathrm{d}\beta_r & , \beta_r \geq \beta_{r_0} \end{cases} \tag{4.37}$$

The most common models used are the linear and exponential models. These models can be sub-classified by the hardening/softening law.

$$\begin{array}{lcl} \text{Damage with hardening} & \Rightarrow & \mathcal{H}_d > 0 \\ \text{Perfect damage} & \Rightarrow & \mathcal{H}_d = 0 \\ \text{Damage with softening} & \Rightarrow & \mathcal{H}_d < 0 \end{array} \tag{4.38}$$

4.3.1.2.5 Linear hardening/softening

The linear hardening/softening is one of the most used models, it is simpler since it involves only one parameter that controls the type of hardening/softening law it follows.

$$\beta_q = \begin{cases} \beta_{r_0} & \beta_r \leq \beta_{r_0} \\ \beta_{r_0} + \mathcal{H}_d \left(\beta_r - \beta_{r_0}\right) & \beta_r > \beta_{r_0} \end{cases} \tag{4.39}$$

The values of hardening/softening law ($\mathcal{H}_d$) range from $(-\infty, \infty)$.

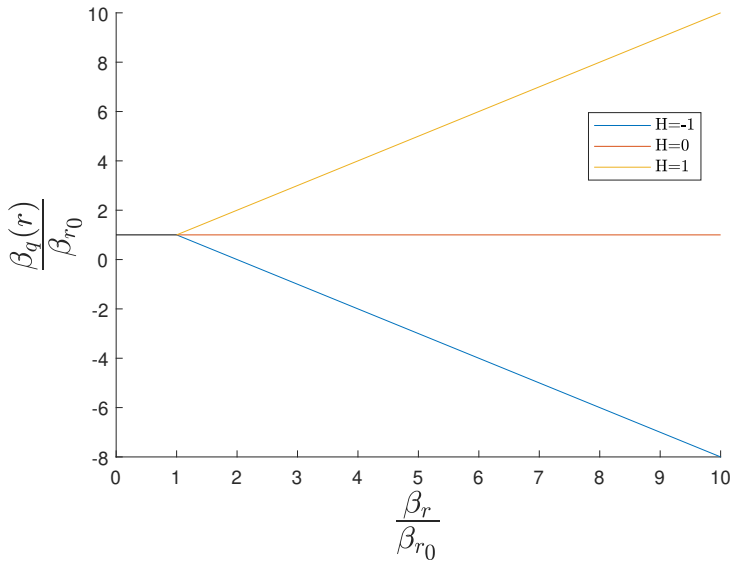

FIGURE 4.10: Evolution law: linear.

This model presents certain problems since it is not a smooth function, the derivative is not continuous when $\beta_{q_\infty} = 0$ and softening is considered (see Figure 4.10).

$$\beta_q = 0 \Rightarrow \beta_r = \frac{\left(\mathcal{H}_d - 1\right)\beta_{r_0}}{\mathcal{H}_d} \tag{4.40}$$

This is the upper limit for the damage internal variable in the linear model, and it can be used to quickly assess if the damage is completed ($d = 1$). Note again that this is only for softening, nevertheless softening is the most common behaviour of materials in the non-linear range.

4.3.1.2.6 Exponential hardening/softening

The exponential hardening/softening model is the most natural and presents a smooth continuous curve.

$$\begin{aligned} \beta_q &= \begin{cases} \beta_{r_0} \\ \beta_{q_\infty} - (\beta_{q_\infty} - \beta_{r_0}) \exp\left(c_{\text{pe}}\left(1 - \frac{\beta_r}{\beta_{r_0}}\right)\right) \end{cases} \\ \mathcal{H}_d &= \frac{(\beta_{q_\infty} - \beta_{r_0})}{\beta_{r_0}} \exp\left(c_{\text{pe}}\left(1 - \frac{\beta_r}{\beta_{r_0}}\right)\right) \end{aligned} \tag{4.41}$$

Provided the saturated evolution law (β_{q_∞}) cannot be negative, the saturated damage law value has to be positive, thus $\beta_{q_\infty} \in [0, \infty)$. This is shown in Figure 4.11, note that the evolution curve for $\beta_{q_\infty} = 1$ retrieves the perfect damage model.

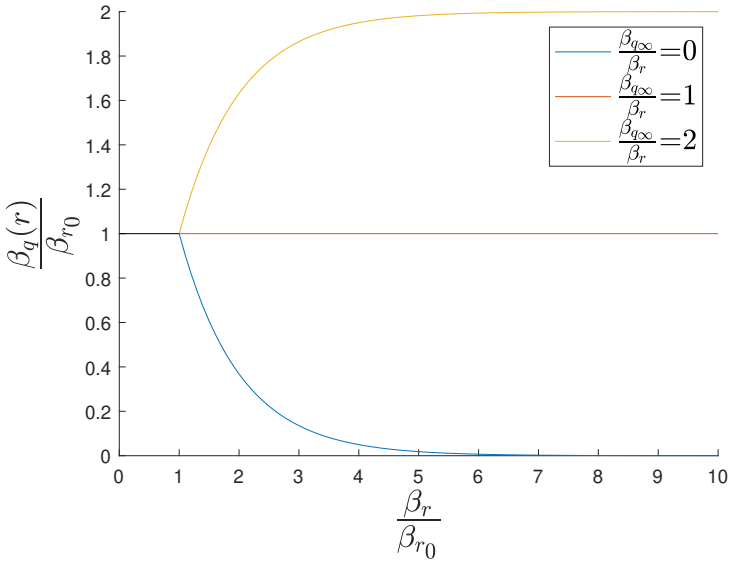

FIGURE 4.11: Evolution law: exponential.

4.3.1.2.7 Norms

There are three classical norms: *symmetric*, *tension-only* and *non-symmetric*. These three norms define the uni-axial behaviour of the constitutive material in the three dimensions.

The *symmetric* norm, as the name indicates, considers that tension and compression response is exactly the same. The norm is exactly the same defined in Equation 4.25.

$$\begin{cases} \mathbb{T}_{\sigma I} = \sqrt{\underset{\sim}{\sigma} : \underset{\sim\sim}{D_{\text{elast}}}^{-1} : \underset{\sim}{\sigma}} = (1-d)\sqrt{\underset{\sim}{\sigma_e} : \underset{\sim}{\varepsilon}} \\ \mathbb{T}_{\varepsilon I} = \sqrt{\underset{\sim}{\varepsilon} : \underset{\sim\sim}{D_{\text{elast}}} : \underset{\sim}{\varepsilon}} = \sqrt{\underset{\sim}{\sigma_e} : \underset{\sim}{\varepsilon}} = \frac{1}{1-d}\mathbb{T}_{\sigma I} \end{cases} \tag{4.42}$$

In Equation 4.42, it can be appreciated that the norm is symmetric.

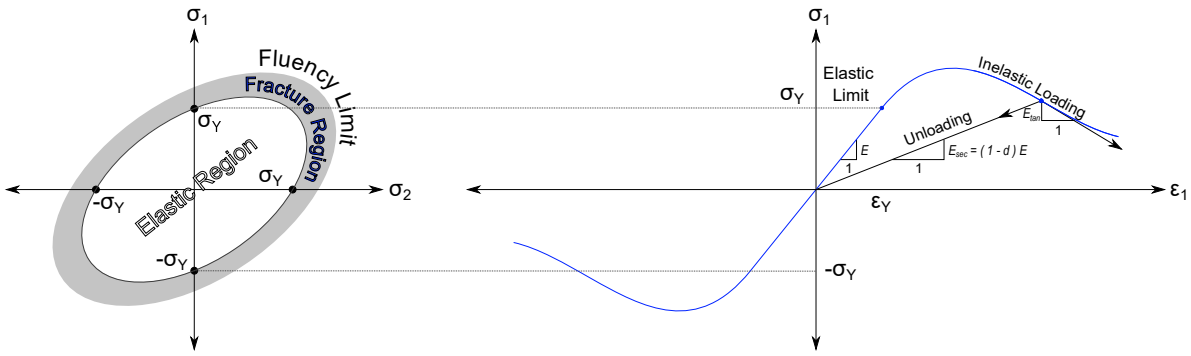

FIGURE 4.12: Norm I: symmetric damage.

In the case of the tension-only norm,

$$\langle \underset{\sim}{\sigma} \rangle = \frac{\underset{\sim}{\sigma} + |\underset{\sim}{\sigma}|}{2} \tag{4.43}$$

where $\langle \sigma \rangle$ is the Macaulay bracket for the stress tensor. This stress tensor can be represented in terms of its principal stresses by eigendecomposition.

$$\begin{aligned} \underset{\sim}{\sigma} &= \sum_{i=1}^{3} \lambda_i \underline{\lambda_{\vec{v}}}_i \otimes \underline{\lambda_{\vec{v}}}_i \\ \langle \underset{\sim}{\sigma} \rangle &= \sum_{i=1}^{3} \langle \lambda_i \rangle \, \underline{\lambda_{\vec{v}}}_i \otimes \underline{\lambda_{\vec{v}}}_i \end{aligned} \tag{4.44}$$

where λ is the eigenvalue, $\underline{\lambda_{\vec{v}}}$ is the eigenvector. The eigenvalues and eigenvectors are the correspondents to the stress tensor (σ).

The major difference in the norm compared to Equation 4.42 is the introduction of the tension-only term in the norms.

$$\begin{cases} \mathbb{v}_{\sigma II} = \sqrt{\langle \underset{\sim}{\sigma} \rangle : \underset{\sim\sim}{D_{\text{elast}}}^{-1} : \underset{\sim}{\sigma}} = (1-d)\sqrt{\left\langle \underset{\sim}{\sigma_e} \right\rangle : \underset{\sim}{\varepsilon}} \\ \mathbb{v}_{\varepsilon II} = \sqrt{\left\langle \underset{\sim}{\sigma_e} \right\rangle : \underset{\sim}{\varepsilon}} = \frac{1}{1-d} \mathbb{v}_{\sigma II} \end{cases} \tag{4.45}$$

In Figure 4.13, the fluency surface can be observed, showing that the elastic zone is found for three quadrants and only there is damage in the case of tension. This can be seen in the stress-strain chart where for negative stresses, the constitutive model retrieves the linear model.

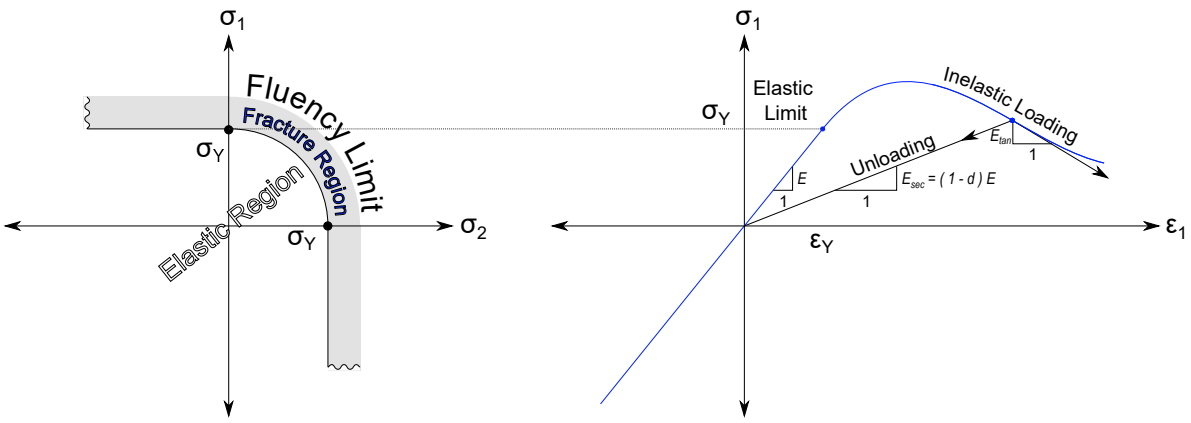

FIGURE 4.13: Norm II: tension-only damage.

The last model is an intermediate between the *only-tension* and *symmetric*. The *non-symmetric* defines that the fluency criterion for compression is different from tension, to simplify the model, it assumes that the difference is defined by a compression-tension ratio.

$$c_{CR} = \frac{\sigma_{y_{\text{compression}}}}{\sigma_{y_{\text{traction}}}} \tag{4.46}$$

where c_{CR} is the compression ratio. The fluency surface, shown in Figure 4.14, is considered to be linearly interpolated from the traction region to the compression region by the ratio defined in Equation 4.46. In order to achieve this, a fraction between traction and compression has to be defined.

$$c_{CF} = \frac{\sum_{i=1}^{3} \langle \lambda_i \rangle}{\sum_{i=1}^{3} |\lambda_i|} \tag{4.47}$$

where c_{CF} is the compression fraction. The compression fraction is defined by the ratio of the eigenvalue of the stress for only-tension and its absolute value. The norms can then be formulated.

$$\begin{cases} \mathbb{T}_{\sigma III} = \left(c_{CF} + \frac{1-c_{CF}}{c_{CR}} \right) \sqrt{\underset{\sim}{\sigma} : \underset{\sim\sim}{D_{\text{elast}}}^{-1} : \underset{\sim}{\sigma}} \\ \mathbb{T}_{\varepsilon III} = \frac{1}{1-d} \mathbb{T}_{\sigma III} \end{cases} \tag{4.48}$$

This norm is very useful for example for materials such as concrete where $c_{CR} = 10$.

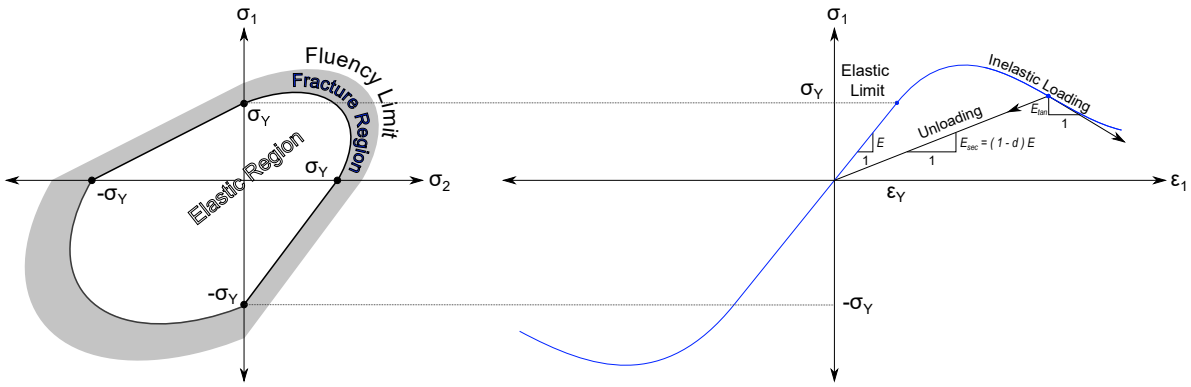

FIGURE 4.14: Norm III: non-symmetric damage.

4.3.1.2.8 Fracture Energy

One of the most difficult problems is to properly select the rate of change of the evolution law, or what is the same, i.e., how to select the optimal hardening/softening law. In [267], the concept of energy of fracture is used to infer a relationship between the hardening/softening law and the total potential strain energy. The rate of dissipation is written in terms of the Helmholtz elastic free potential energy given by

$$\frac{\mathrm{d}\Pi_D}{\mathrm{d}t} = \Pi_{HE}\frac{\mathrm{d}d}{\mathrm{d}t} = \Pi_{HE}\frac{\partial d}{\partial \beta_r}\frac{\mathrm{d}\beta_r}{\mathrm{d}t} \tag{4.49}$$

where Π_D is the dissipation energy, Π_{HE} is the Helmholtz elastic free potential energy. The total specific dissipation energy is then

$$\Pi_F = \int_0^{t(\beta_q=0)} \frac{\mathrm{d}\Pi_D}{\mathrm{d}t} = \int_0^{t(\beta_q=0)} \Pi_{HE}\frac{\partial d}{\partial \beta_r}\frac{\mathrm{d}\beta_r}{\mathrm{d}t}\,\mathrm{d}t = \int_{\beta_{r_0}}^{\beta_r(\beta_q=0)} \Pi_{HE}\frac{\partial d}{\partial \beta_r}\,\mathrm{d}\beta_r \geq 0 \tag{4.50}$$

where Π_F is the energy of fracture. The Helmholtz elastic free potential energy can be substituted for the following relationship

$$\beta_r{}^2 = 2\left(c_{CF} + \frac{1-c_{CF}}{c_{CR}}\right)\Pi_{HE} = \begin{cases} 2\Pi_{HE} & \text{tension} \\ 2{c_{CR}}^{-2}\Pi_{HE} & \text{compression} \end{cases} \tag{4.51}$$

The physical significance is that the energy associated with the Helmholtz elastic free potential, must be equal to the energy under the curve of elastic range. The introduction of the third norm is useful because it can retrieve all the previous norms, by the selection of the compression ratio (c_{CR}).

For the sake of simplicity, the derivation shall be done with the compression ratio and if tension is considered, the compression ratio must be considered one. The simplest and most used model would be the exponential softening model. Equation 4.50 yields

$$\Pi_F = \int_0^{t(\beta_q=0)} \frac{\mathrm{d}\Pi_D}{\mathrm{d}t} =$$
$$\int_{\beta_{r_0}}^{\beta_r(\beta_q=0)} \frac{1}{2}{\beta_r}^2 \frac{\beta_{q_\infty}\beta_{r_0} - \left(\beta_{r_0} + c_{\mathrm{pe}}\beta_r\right)\left(\beta_{q_\infty} - \beta_{r_0}\right)\exp\left(c_{\mathrm{pe}}\left(1 - \frac{\beta_r}{\beta_{r_0}}\right)\right)}{\beta_{r_0}{\beta_r}^2}\,\mathrm{d}\beta_r \quad (4.52)$$
$$= \left[\frac{\beta_{q_\infty}\beta_r}{2} + \left(\frac{\beta_r}{2} + \frac{\beta_{r_0}}{c_{\mathrm{pe}}}\right)\left(\beta_{q_\infty} - \beta_{r_0}\right)\exp\left(c_{\mathrm{pe}}\left(1 - \frac{\beta_r}{\beta_{r_0}}\right)\right)\right]_{\beta_{r_0}}^{\beta_r(\beta_q=0)} \geq 0$$

From Equation 4.52, it can rapidly be seen that if $\beta_{q_\infty} = 0$, the result of the integral is infinity. Assuming that the saturated value of the evolution law variable is zero, an interesting compatibility equation can be formulated.

$$c_{\mathrm{pe}} = \left(\frac{\Pi_F}{\left(c_{CR}\beta_{r_0}\right)^2} - \frac{1}{2}\right)^{-1} \geq 0 \quad (4.53)$$

where c_{pe} is the pre-exponential factor. Note that in the case of traction, the compatibility equation considers $c_{CR} = 1$. So this establishes a lower limit for the energy of fracture. However, this energy of fracture cannot be considered, numerically, the same for elements of different size. Therefore, the fracture energy is defined as averaged length fracture energy.

$$\Pi_F = \frac{\pi_F}{x_{cl}} \quad (4.54)$$

where x_{cl} is the characteristic length, π_F is the characteristic energy of fracture. The characteristic length can be the length of linear elements, the square root of the area of shells and the cubic root of the volume of solids.

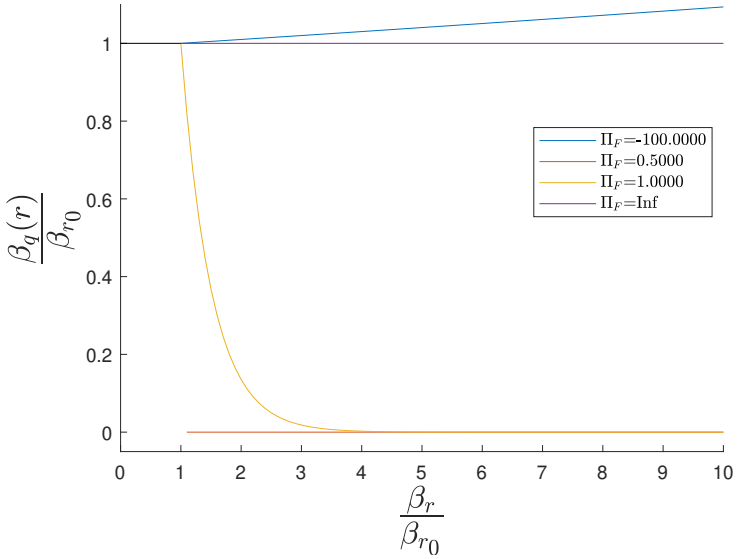

FIGURE 4.15: Energy of fracture for exponential softening.

Figure 4.15 shows the behaviour of the evolution law variable against the internal variable for different values of fracture energy. Note that both axes are normalised concerning the initial damage internal variable (β_{r_0}) and the figure shows that for values below 0.5, the evolution law is inconsistent, which is in accordance with Equation 4.53. When the energy is infinite, the model retrieves the perfect damage.

Considering the linear evolution, the energy of fracture can be derived again from Equation 4.50. It is important to note that considering linear softening, the value of the internal variable for when the evolution law intersects the axis of abscissas is

$$\beta_r(\beta_q = 0) = \frac{\mathcal{H}_d - 1}{\mathcal{H}_d}\beta_{r_0} \tag{4.55}$$

$$\begin{aligned} \Pi_F = \int_0^{t(\beta_q=0)} \frac{\mathrm{d}\Pi_D}{\mathrm{d}t} &= \int_{\beta_{r_0}}^{\beta_r(\beta_q=0)} \frac{1}{2}{\beta_r}^2 - \frac{\beta_{r_0}\left(\mathcal{H}_d - 1\right)}{{\beta_r}^2}\,\mathrm{d}\beta_r \\ &= \left[-\frac{\beta_r\beta_{r_0}\left(\mathcal{H}_d - 1\right)}{2}\right]_{\beta_{r_0}}^{\beta_r(\beta_q=0)} \geq 0 \end{aligned} \tag{4.56}$$

Equation 4.56 is useful to define a lower limit to the slope.

$$\mathcal{H}_d = \left(1 - \frac{2\Pi_F}{\left(c_{CR}\beta_{r_0}\right)^2}\right)^{-1} \geq 0 \tag{4.57}$$

Again the compression ratio is included and depends on the state, traction or compression. The different slopes obtained can be observed in Figure 4.16. Since it is softening, the optimal slopes are negative, thus the values below 0.5 for the normalised energy of fracture over the initial internal variable (β_{r_0}), return hardening. To obtain softening, the value should be greater than 0.5, and when it tends to infinity, the model retrieves the perfect damage model.

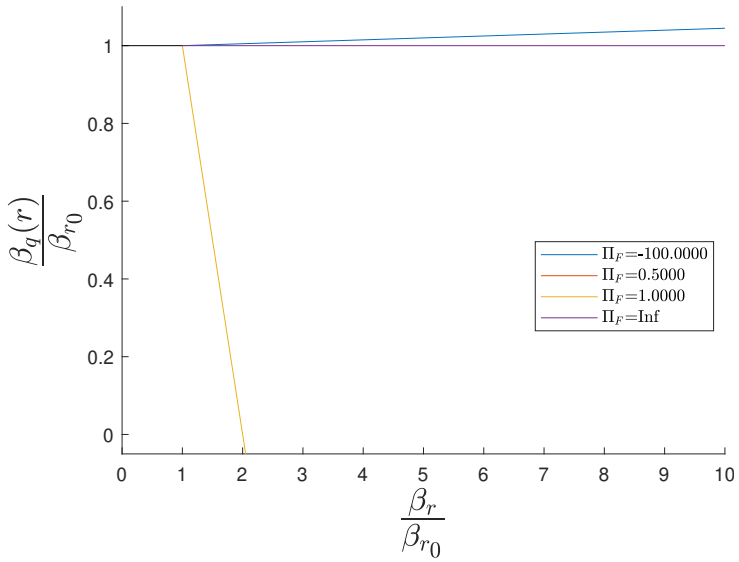

FIGURE 4.16: Energy of fracture for linear softening.

4.3.1.2.9 Tangent Constitutive Tensor

The last concept that needs to be derived is the rate of change of the stress in time or what is the same, the so-called *tangent* constitutive tensor found in Figure 4.8. The rate of change of the stress was defined when the evolution of damage was considered to be zero.

$$\begin{aligned} S_d \neq 0 \Rightarrow \quad & d \neq 0 \\ \frac{\mathrm{d}S_d}{\mathrm{d}t} \neq 0 \Rightarrow \quad & \frac{\mathrm{d}d}{\mathrm{d}t} \neq 0 \end{aligned} \tag{4.58}$$

Now considering that the evolution of damage is not zero

$$\frac{\mathrm{d}\underset{\bullet\bullet}{\sigma}}{\mathrm{d}t} = (1-d)\underset{\bullet\bullet\bullet\bullet}{D}_{\text{elast}} : \frac{\mathrm{d}\underset{\bullet\bullet}{\varepsilon}}{\mathrm{d}t} - \underset{\bullet\bullet}{\sigma}_e \otimes \frac{\mathrm{d}d}{\mathrm{d}t} \tag{4.59}$$

The variation of time of the damage can be found by the variation of the damage index with respect to the internal variable or what is equivalent to the strain norm.

$$\begin{aligned} \frac{\mathrm{d}\mathbb{r}_\varepsilon}{\mathrm{d}t} &= \frac{\mathrm{d}\beta_r}{\mathrm{d}t} \\ \frac{\mathrm{d}d}{\mathrm{d}t} = \frac{\partial d}{\partial \beta_r}\frac{\partial \beta_r}{\partial t} &= \frac{\partial d}{\partial \beta_r}\frac{\partial \mathbb{r}_\varepsilon}{\partial t} \\ \frac{\partial \mathbb{r}_\varepsilon}{\partial t} \equiv \frac{\mathrm{d}\mathbb{r}_\varepsilon}{\mathrm{d}t} &= \frac{\partial d}{\partial \mathbb{r}_\varepsilon}\frac{1}{\mathbb{r}_\varepsilon}\underset{\bullet\bullet}{\sigma}_e : \frac{\mathrm{d}\underset{\bullet\bullet}{\varepsilon}}{\mathrm{d}t} \end{aligned} \tag{4.60}$$

By combining Equation 4.59 and Equation 4.57, the tangent constitutive tensor can be defined.

$$\frac{\mathrm{d}\underset{\bullet\bullet}{\sigma}}{\mathrm{d}t} = \left[(1-d)\underset{\bullet\bullet\bullet\bullet}{D}_{\text{elast}} - \frac{\partial d}{\partial \mathbb{r}_\varepsilon}\frac{1}{\mathbb{r}_\varepsilon}\underset{\bullet\bullet}{\sigma}_e \otimes \underset{\bullet\bullet}{\sigma}_e\right] : \frac{\mathrm{d}\underset{\bullet\bullet}{\varepsilon}}{\mathrm{d}t} = \underset{\bullet\bullet\bullet\bullet}{D}_{\text{tan}} : \frac{\mathrm{d}\underset{\bullet\bullet}{\varepsilon}}{\mathrm{d}t} \tag{4.61}$$

where D_{tan} is the tangent constitutive tensor. Note that the tangent tensor can be either represented as the standard nomenclature (D_{tan}) or using the stress-resultant nomenclature introduced previously ($\hat{D}_{\text{tan}}$).

4.3.2 Constitutive modelling of composite shells

The constitutive theory introduced until this point describes the relationship between stresses and strains at the constituent or phase level. Nonetheless, when materials are joined or bounded, similar to Figure 4.17, the constitutive relationship of the resultant is not only not guaranteed, but generally not expected to be the same as the behaviour of its constituent materials. For instance, albeit the behaviour of the constituent materials can be considered isotropic, once combined to generate the composite material, the material presents an anisotropic behaviour, at its best orthotropic. Therefore, the shell theory found in this section is focused solely on the study of shell theory that reproduces composite behaviour.

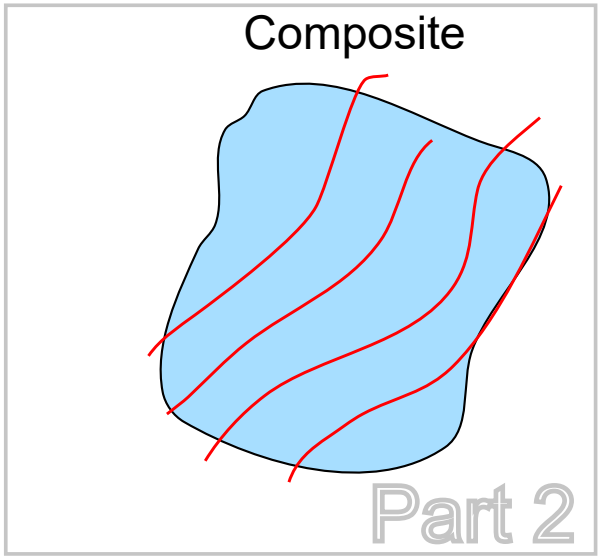

FIGURE 4.17: Illustration of part 2, the concept of a composite material.

Laminated shell theory is the theory that connects the kinematics and constitutive laws of composite structures when discretised in elements. For the sake of simplicity, only first-order theories of laminated shells are considered, other high-order techniques can be found in [101, 103]. One of the first theories is the classical laminated plate theory (CLPT) postulated by Reddy [103], this theory is based on the *Kirchhoff-Love* theory [262], and is generally suitable for composites with thin thicknesses and especially where transverse shear deformation is not significant [268].

If either important transverse shear deformation (sandwiches) or thick composite structures are considered, the formulation by excellence is the *Reissner-Mindlin* theory [263]. One of the main issues derived from the Reissner-Mindlin theory is the shear-locking phenomenon, where thin-wall structures experiment with singular behaviour as the thickness of the structure is reduced. Lardeur and Batoz [99] introduced the reduced shear correction factor to amend this problem.

The models previously introduced can be derived for isotropic materials and therefore coupled with the damage models detailed in subsection 4.1.1. However, this would only account for finite element solutions of homogeneous materials, since,

for heterogeneous materials, especially composites, the mechanical response is no longer isotropic.

The constitutive modelling of composite shells is generally addressed and characterised by orthotropic models. Especially, for laminated shells, the transverse orthotropic model. One of the first publications to introduce the orthotropic constitutive matrix was Kings in [269]. Interestingly, the orthotropic solutions in [269] can be easily coupled with the damage models that are orthotropic in subsection 4.1.1. This allows the prediction of the failure of composite structures by the finite element method. Nevertheless, these orthotropic theories are not generally the best method to predict failure since many non-linear issues developed during the damage process are not well approximated. One of these problems is the underestimation of the transverse mechanical properties

4.3.2.1 The concept of homogenisation

In this subsection, the different methods used to obtain the structural and mechanical response of the composite as a whole from the behaviour of its constituent phases are briefly explained. These methods match the classification and enumeration of the chapter devoted to the literature review of the mechanical model. The different techniques used to obtain the response of the composite from its constituent are classified in three scales:

1. Micro-scale

   The micro-scale is at the level of the constituent phases, fibre, matrix, pores, filling, etc. This scale is very detailed and high in terms of computational cost, it can analyse issues such as delamination or even unbinding between the solid phases such as the fibre and resin. This scale allows keeping track of the non-linear constitutive phenomena of every single phase by using the models derived from the analysis of homogeneous continuum media.

2. Meso-scale

   These methods deal with an intermediate scale where the constituent phases are denoted by packets or groups of homogeneous media inside the heterogeneous structure. I.e., groups of fibre or lamina. These methods are highly dependent on the heterogeneous structure, since the elements that pack certain regions of the meso-scale are defined by the length of these same groups.

3. Macro-scale

   The macro-scale methods are the least costly in terms of computational power and less detailed in principle. These methods study the complete structure or structural elements. One of the advantages of these methods is the simplicity of the discretisation of the whole domain, since the computational models at this scale are generally simpler to be defined. However, this comes with the cost of neglecting certain characteristics of the micro-scale structure.

   In order to palliate this problem, the theory of *homogenisation* has gained its reputation. This theory tries to infer certain characteristics or traits of the micro-structure into the macro-scale domain. This homogenisation techniques

offer an interesting solution since a more detailed solution can be obtained at the cost of less calculation time.

Although the classification is very clear and distinct, sometimes the line between certain methods is not simply traced. In addition, some other multi-level methods have gained popularity in the recent decades. These multi-scale methods are similar to the concept of homogenisation, indeed *homogenisation* can be considered as some sort of two-level or micro-macro-scale method.

4.3.2.1.1 Obtention of the composite constitutive model

The interest of the research is to obtain the composite behaviour from the behaviour of the constituent phases. From the discrete mechanical problem, there are two terms, the left-hand side (l.h.s.) matrix and the right-hand side (r.h.s.) vector of the discrete system of equations. The constitutive tensor or matrix is shared on both sides of the equilibrium of linear momentum, and it is sensical to obtain the composite constitutive matrix from the constituent constitutive matrix of each phase. In order to obtain this composite constitutive model, several formulations are offered at different scales. The three areas of research that are contemplated in this section are: *macro-scale*, *micro-scale* and *multi-scale*.

At the macro-scale level, one of the simplest formulations is found by the combination of an orthotropic shell theory [269] and the simplest way to obtain the composite behaviour from a biphasic material is to use the hypothesis of Voigt [26] and Reuss [27]. The first explains details, based on experimentation, which is the relationship between the parallel Young's modulus of the composite and the constituent phases. The second stipulates how to obtain, again based on empirical tests, the constituent to composite relationship in the transverse or serial orientation for both the Young's and Shear modulus. This formulation can easily be brought to the non-linear constitutive analysis if combined with one of the orthotropic damage theories mentioned previously. Within these non-linear constitutive theories, the study of two relevant theories is given below:

1. **Hill fluency**

   In 1964 Hill [115] proposed a fluency surface that was similar to the modern plasticity surfaces – the yielding is produced by deviatoric loading instead of hydrostatic – that was suitable for orthotropic materials. Dvorak and Bahei-El-Din [116] remarked that the model proposed by [115] had several problems, one of the most important was the definition of a yielding surface for the whole laminate, i.e., the yielding was associated with the complete stack of plies. This introduces non-realistic solutions, since only when the composite is monolithic – the same material for all the layers in the stack – the yielding surface is correct. The classical arrangement, for a sandwich or non-monolithic stacks, was to associate an equivalent yielding surface as a weighted solution of the different layers that compounded the stack, this is done in order to obtain a failure of the whole stack instead. Nonetheless, this leads to unfeasible results [150], and the Tsai and Wu criteria are more encouraged if failure of the whole section of a laminate is contemplated. Other orthotropic-based inelastic macro-scale models using the same principles as Hill's model are found in [142].

2. **Vanishing fibre diameter**

   In 1982 Dvorak and Bahei-El-Din [116] an interesting model is proposed. This model is very well suited for reinforced composites, especially for reinforced concrete. The so-called vanishing fibre diameter model obtains its name from the fact that the constitutive model of the composite material is obtained by the contribution of the fibre and matrix phases. Albeit, the composite behaviour comes from both fibre and matrix, the diameter of the fibre vanishes in those directions not aligned with the fibre orientation.

   Therefore, this model is realistic when satisfying the Voigt hypothesis. But underestimates the real transverse rigidity since it is not fulfilling the Reuss hypothesis. Another classic problem arising from this model is the incorrect prediction of yielding in the transverse direction, however this can be mitigated if coupled correctly with some other anisotropic damage model. This model has been subsequently enhanced in [139].

Theories formulated within the micro-scale are one of the most used ones. These are theories that properly introduce the iso-strain and iso-stress hypotheses of Voigt [26] and Reuss [27] respectively at the micro-scale level. Two main branches, the *mean field* and *cells* methods, are the most prolific theories within the micro-scale approach. These theories are well detailed in the enumeration below.

1. **Mean field**

   This theory receives its name from the assumption that the mean of the strain and stress fields for the matrix and fibre phases are representative of the behaviour. By assuming this behaviour, the iso-strain and iso-stress hypothesis can be then used to formulate the relationship between the constituent phases and the composite as a whole.

   The constituent-to-composite relationship is then defined by a set of functions that depend on the morphology of the fibre phase, e.g., the fibre phase in concrete is modelled as granulated particles whereas as long fibres in marine FRP composites; the spatial orientation and the volumetric fraction.

   One of these amalgamation functions is the one that receives the name of the *rule of mixtures*. It employs the ideas of Voigt and Reuss to estimate Young's modulus and Shear's modulus. These functions receive the name of the *rule of mixtures* (ROM) in the direction parallel to the fibre phase [26] and the *inverse rule of mixtures* (IROM) in the direction serial/transverse to the fibre phase [27].

   Note that these functions describe behaviour in the range of elastic behaviour. Authors such as Taylor [112] enhanced these functions to the non-linear range.

   The consolidation of these formulations is introduced in Truesdell and Toupin by [151] who formalise the *classical mixing theory* (CMT) based on the concepts from the *ROM* and *IROM*. The main difference is that this theory defines these relationships, at the Gauss level, by enforcing the iso-strain or parallel and iso-stress or serial hypothesis. By enforcing the relationships in this manner, the possibility of using non-linear constitutive models at the phase level is enabled. However, this theory is not as sophisticated as imagined. The need to produce particular constitutive models does not allow combining different existing models.

In [154], an enhanced version of the theory proposed by Truesdell and Toupin is proposed. This theory, named *serial-parallel rule of mixtures* (SPROM), is indeed formalised by Rastellini et al. in their posterior contributions [15, 33]. The advantages of this theory with respect to the CMT by Truesdell and Toupin are important because this new formulation is able to work as a black box by combining any pre-existing constitutive theory for each constituent phase. Moreover, the theory achieves a natural orthotropic behaviour at the composite level by simply imposing the serial hypothesis for each constituent phase, even when the structure has gone beyond the linear constitutive analysis.

There are other models such as the ones proposed by Eshelby in [148] in 1956 which derives a model in which the matrix phase has inclusions or defects in the embedded into it. These models are very useful for the amalgamation of composite materials such as concrete. Eshelby further expands this theory in [149] and the most popular method is found in the work of Mori and Tanaka [155] in 1973.

Models such as the self-consistent method consider that the reinforcement is embedded in the matrix and this is embedded in the composite. However, the effective properties are considered from the composite, which requires obtaining them from experimental data [172]. This model is significantly developed by authors such as Hashin [146] or Budiansky [147].

2. **Cells**

   The *method of cells* (MOC) was first introduced by Aboudi [144] in 1989. This method considers that a discretisation of the micro-structure can be made in subcells, assigning each subcell a constituent material, the proportion is determined by the volumetric fraction of each constituent material. Then it establishes a certain amalgamation of functions and continuity in terms of stress to achieve the solid mechanical equilibrium of the cell.

   This method has been extended by the same creator, such as in [145] to formalise a general method of cells (GMOC) to enable the prediction of more complex micro-structures.

The other approaches are based at the multi-scale level and generally are grouped inside the category of *homogenisation*. This approach is a micro-macro model and sometimes involves more than two scales. Generally, homogenisation is obtained from the assumption that the heterogeneous media can be perceived as a periodic micro-structure that is repeated in the macro-scale domain.

One of the approaches inside homogenisation is the asymptotic technique found in [157, 164, 169] which models the micro-macro interaction by means of introducing an asymptotic expansion in the displacement and tension fields and that is integrated into using the variational form to later derive the discrete system.

Other techniques such as the ones described in [162, 165] are regarded as the unitary cell techniques and these obtain the macroscopic properties of the composite by resolving, at the micro-scale, the heterogeneous micro-structures. These methods allow for solving very complex micro-structures, however, they are limited to linear analysis since when large deformation or non-linear constitutive phenomena appear, the micro-structure may change significantly from its material or initial description.

This has been substantially upgraded using the same ideas as in direct numerical simulations (DNS), however, the computational cost has been increased. These techniques, the micro-macro direct methods, obtain the tension-strain state variables at the macro-scale level from the micro-scale level where the complex micro-structure is solved by applying the corresponding constitutive laws.

At the macro-scale level, the methods can be coupled easily with the finite element method [166, 167, 170], the Voronoi cell approach described in [159, 161] or solving the variational form approximately by using the Fourier expansion series [163]. The micro-scale can be solved with a similar methodology, however, the micro to the macro of the state variables (strain and stresses) are generally obtained by some of the homogenisation techniques explained above.

The major problem of these direct methods is the computational cost that is intrinsic to them. An interesting approach to model this micro-macro homogenisation, resembling the approach used in data science such as machine learning or reduced order modelling, comes from the ideas of Terada and Kikuchi in which the micro-macro interaction is obtained from a statistical or data-driven model [160, 188].

Composites are materials that are a compound of different layers that conform in a stack. Each layer can contain one or more *constituent* materials. Composites are very non-linear constitutive materials and need careful and extensive material calibrations in order to obtain all the parameters that define the constitutive model.

One of the most remarkable features of composites is their orthotropic behaviour. This is reflected in Figure 4.18 and Figure 4.19. These figures show that the in-plane and out-of-plane tension distribution is determined through different tests.

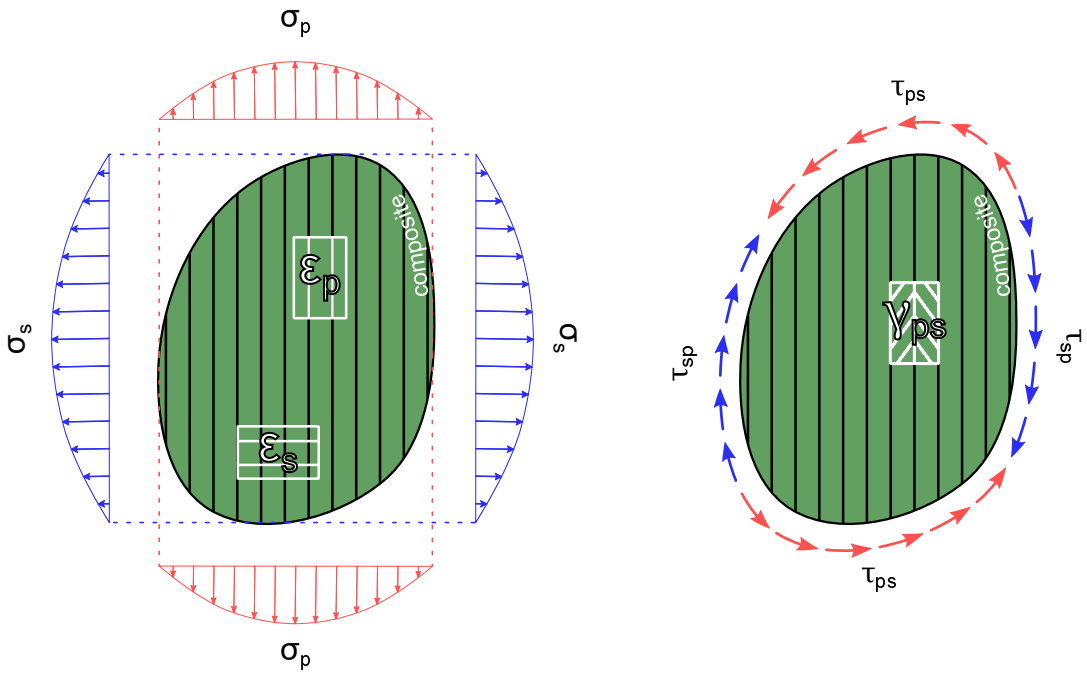

FIGURE 4.18: In-plane tension distribution for an orthotropic material.

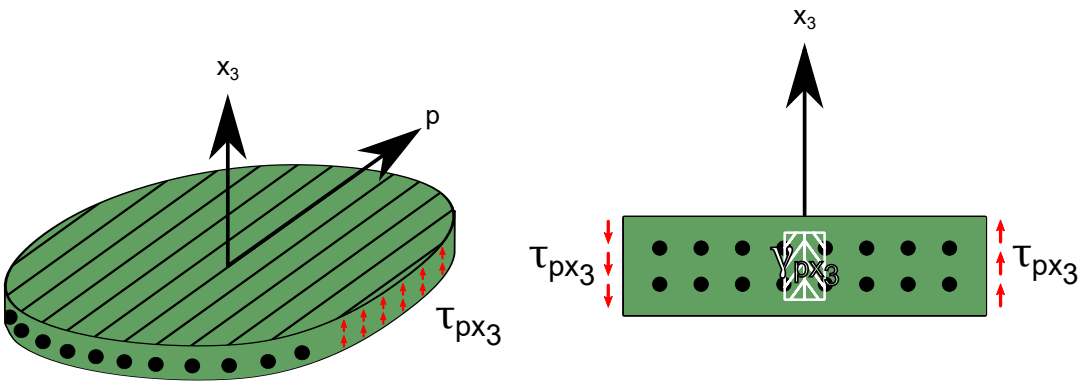

FIGURE 4.19: Out-of-plane tension distribution for an orthotropic material.

The classical model – the lineal model – to express the constitutive tensor is the so-called orthotropic shell model. However, this model is in direct conflict with the isotropic damage model from Simo and Ju, since the latter is derived from isotropic materials. Some solutions extend the isotropic damage model to orthotropic models [271, 272].

The behaviour of the composite as a whole can be generally reproduced by the orthotropic theory for shells if experimental testing is given for a certain material. However, if the number of layers or some constituent materials is added, removed or modified, the resultant behaviour may be similar but not the same. The need to establish a formulation that reproduced the behaviour of composites not as a whole but from the perspective of the constituent materials is preferable.

The mechanical properties of the composite or a layer of the composite – a layer can be considered as a composite as well if it is comprised from more than one constituent material – can be infused from the mechanical properties of the constituent materials. This correlation between the micro-scale and macro-scale is generally inferred by using the classical mixture theory (CMT). The first authors to theorise this mixing theory are Voigt [26] and Reuss [27], both introducing the relationship or stress behaviour in the different principal local axes.

4.3.2.2 Linear constitutive elasticity of composites

Once the concept of homogenisation has been extensively discussed, the constitutive laws that characterise composites can be introduced. The simplest formulation existent is the one that focuses on the study of the linear elastic response of composite. Do please not be misled by the term *linear*, since composites are by definition non-linear, that is, the relationship between the stresses and strains cannot be catalogued as linear.

In further detail, exploring one of the best linear theories of composites, which is the orthotropic constitutive model, rapidly adverts that composites behaviour is oriented-based, and more importantly, its range of application, the linear one, may not be the same for one direction compared to others. Within this scope, the linearity of composites is studied through the lens of the general orthotropic theory and with

special emphasis, since the ulterior motive is the study of marine FRP composites, the transverse isotropic models.

Continuing the linear study of transverse isotropy, the constitutive law of the transverse isotropic composite is formulated by the introduction of the classical mixing theory (CMT). This theory poses the relationship between constituent materials and the composite itself.

4.3.2.2.1 The orthotropic constitutive model

The orthotropy of a material defines that the properties can be characterised through three-principal axes. Composites are orthotropic dominated materials. These relationships were shown in Figure 4.18 and Figure 4.19, the compliance matrix can be postulated as

$$\underline{\varepsilon} = \begin{bmatrix} \varepsilon_{11} \\ \varepsilon_{22} \\ \varepsilon_{33} \\ \gamma_{21} \\ \gamma_{31} \\ \gamma_{32} \end{bmatrix} = \underline{\underline{D}}^{-1}\underline{\sigma} = \underline{\underline{\mathcal{D}}} \cdot \underline{\sigma} = \begin{bmatrix} \mathcal{D}_{11} & \mathcal{D}_{12} & \mathcal{D}_{13} & 0 & 0 & 0 \\ \mathcal{D}_{21} & \mathcal{D}_{22} & \mathcal{D}_{23} & 0 & 0 & 0 \\ \mathcal{D}_{31} & \mathcal{D}_{32} & \mathcal{D}_{33} & 0 & 0 & 0 \\ 0 & 0 & 0 & \mathcal{D}_{44} & 0 & 0 \\ 0 & 0 & 0 & 0 & \mathcal{D}_{55} & 0 \\ 0 & 0 & 0 & 0 & 0 & \mathcal{D}_{66} \end{bmatrix} \begin{bmatrix} \sigma_{11} \\ \sigma_{22} \\ \sigma_{33} \\ \tau_{21} \\ \tau_{31} \\ \tau_{32} \end{bmatrix} \tag{4.62}$$

where D is the constitutive tensor, $\mathcal{D}$ is the compliance tensor. The components of the compliance tensor are found by using the different modulus that defined the relationship between stress and strains in the three-principal or orthotropic axes.

$$\begin{array}{lll} \mathcal{D}_{11} = \frac{1}{E_1}, & \mathcal{D}_{12} = \frac{-\nu_{21}}{E_2}, & \mathcal{D}_{13} = \frac{-\nu_{31}}{E_3}, \\ \mathcal{D}_{21} = \frac{-\nu_{12}}{E_1}, & \mathcal{D}_{22} = \frac{1}{E_2}, & \mathcal{D}_{23} = \frac{-\nu_{32}}{E_3}, \\ \mathcal{D}_{31} = \frac{-\nu_{13}}{E_1}, & \mathcal{D}_{32} = \frac{-\nu_{23}}{E_2}, & \mathcal{D}_{33} = \frac{1}{E_3}, \\ \mathcal{D}_{44} = \frac{1}{G_{12}}, & \mathcal{D}_{55} = \frac{1}{G_{13}}, & \mathcal{D}_{66} = \frac{1}{G_{23}} \end{array} \tag{4.63}$$

The compliance matrix due is symmetric since both strain and stresses are.

$$E_i \nu_{ji} = E_j \nu_{ij}, \quad \forall i, j = 1, 2, 3 \text{ and } i \neq j \tag{4.64}$$

This formulates the following constitutive matrix

$$\underline{\underline{D}} = \begin{bmatrix} \frac{1-\nu_{23}\nu_{32}}{E_2E_3\hat{c}} & \frac{\nu_{21}+\nu_{23}\nu_{31}}{E_2E_3\hat{c}} & \frac{\nu_{31}+\nu_{21}\nu_{32}}{E_2E_3\hat{c}} & 0 & 0 & 0 \\ \frac{\nu_{21}+\nu_{23}\nu_{31}}{E_1E_3\hat{c}} & \frac{1-\nu_{13}\nu_{31}}{E_1E_3\hat{c}} & \frac{\nu_{32}+\nu_{12}\nu_{31}}{E_1E_3\hat{c}} & 0 & 0 & 0 \\ \frac{\nu_{31}+\nu_{21}\nu_{32}}{E_2E_3\hat{c}} & \frac{\nu_{32}+\nu_{12}\nu_{31}}{E_1E_3\hat{c}} & \frac{1-\nu_{12}\nu_{21}}{E_1E_2\hat{c}} & 0 & 0 & 0 \\ 0 & 0 & 0 & G_{12} & 0 & 0 \\ 0 & 0 & 0 & 0 & G_{23} & 0 \\ 0 & 0 & 0 & 0 & 0 & G_{13} \end{bmatrix} \tag{4.65}$$

$$\hat{c} = \frac{1-\nu_{12}\nu_{21}-\nu_{13}\nu_{31}-\nu_{23}\nu_{32}-2-\nu_{21}\nu_{13}\nu_{32}}{E_1E_2E_3}$$

Furthermore, if transversely isotropy is considered, then

$$E_2 = E_3, \quad \nu_{12} = \nu_{13}, \quad G_{12} = G_{13} \quad \text{and} \quad G_{23} = \frac{E_2}{2\,(1+\nu_{23})} \tag{4.66}$$

4.3.2.2.2 Transverse orthotropy in shells

Shells consider the plane stress hypothesis, neglecting the stress in the normal direction of the shell. For composite shells, the assumptions of transverse isotropy are used. Equation 4.65 can be modified using Equation 4.66 in order to obtain the expression of the constitutive tensor for transverse isotropic shells.

$$D = \begin{bmatrix} \frac{E_1}{1-\nu_{12}\nu_{21}} & \frac{\nu_{12}E_1}{1-\nu_{12}\nu_{21}} & 0 & 0 & 0 \\ \frac{\nu_{12}E_2}{1-\nu_{12}\nu_{21}} & \frac{E_2}{1-\nu_{12}\nu_{21}} & 0 & 0 & 0 \\ 0 & 0 & G_{12} & 0 & 0 \\ 0 & 0 & 0 & G_{23} & 0 \\ 0 & 0 & 0 & 0 & G_{12} \end{bmatrix} \tag{4.67}$$

This can be broken down to follow the stress-resultant notation used in Equation 4.15, for composite shells the previous assumption to neglect the off-diagonal (c_{sf12}, c_{sf21}) shear correction factors is not necessarily true. Generally, for composite shells, the consideration that shear is not coupled is feasible, however, the shear coefficients do not necessarily need to be the same.

The in-plane and out-of-plane constitutive tensors are then

$$\underline{\underline{D_{in}}} = \begin{bmatrix} \frac{E_1}{1-\nu_{12}\nu_{21}} & \frac{\nu_{12}E_1}{1-\nu_{12}\nu_{21}} & 0 \\ \frac{\nu_{12}E_2}{1-\nu_{12}\nu_{21}} & \frac{E_2}{1-\nu_{12}\nu_{21}} & 0 \\ 0 & 0 & G_{12} \end{bmatrix} \tag{4.68}$$

$$\underline{\underline{D_{out}}} = \begin{bmatrix} c_{sf11}G_{23} & 0 \\ 0 & c_{sf22}G_{12} \end{bmatrix} \tag{4.69}$$

4.3.2.2.3 The classical mixing theory

The Classical Mixing Theory (CMT) is one of the most used models to obtain the constituent-to-composite relationships. It is a generalised theory based on the Rule of Mixtures (ROM) and Inverse Rule of Mixtures (IROM) and is extensively applicable to the area of fibre reinforced plastic materials.

Voigt or iso-strain hypothesis:

Voigt in [26] introduces the concept of parallel behaviour. This behaviour describes that the resultant properties in the direction aligned to fibre are found by a linear interpolation or rule of mixture by the participation (volumetric or mass) of each constituent material.

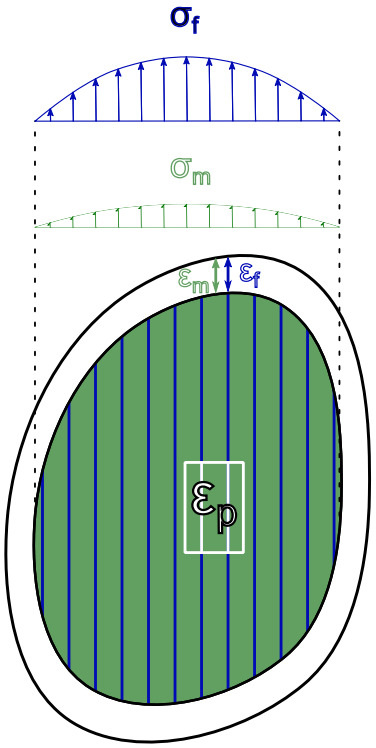

FIGURE 4.20: Parallel or iso-strain hypothesis.

A ply of an FRP composite under a certain uni-axial stress shares the same strain in the matrix and fibre constituent materials (see Figure 4.20).

$$\underset{\bullet\bullet}{\varepsilon_m} = \underset{\bullet\bullet}{\varepsilon_f} \equiv \underset{\bullet\bullet}{\varepsilon_{\mathrm{p}}} \tag{4.70}$$

where ε is the strain, ε_{p} is the parallel strain. Consider the parallel strain tensor as the first component of the in plane strain (ε_{11}). From Figure 4.20, it can be considered that the stress is the composition of the stress generated in the fibre and matrix by participation.

$$\underset{\bullet\bullet}{\sigma} = \Phi_{\Omega m}\underset{\bullet\bullet}{\sigma_m} + \Phi_{\Omega f}\underset{\bullet\bullet}{\sigma_f} = \left(\Phi_{\Omega m}\underset{\bullet\bullet\bullet\bullet}{D_m} + \Phi_{\Omega f}\underset{\bullet\bullet\bullet\bullet}{D_f}\right)_{\text{parallel}} : \underset{\bullet\bullet}{\varepsilon_{\text{p}}} \tag{4.71}$$

The component of the constitutive tensor (D) in the serial direction can be considered as the parallel Young's modulus (E_1). Thus, the serial constitutive tensor can be formulated in elastic regime as

$$E_1 = \left(\Phi_{\Omega m}E_m + \Phi_{\Omega f}E_f\right) \tag{4.72}$$

Reuss or iso-stress hypothesis

Reuss in [27] realised that in the transverse directions, transverse directions to the orientation of the alignment of the fibre or i.e. serial direction, the constitutive tensor was not consistent with the rule of mixture hypothesis.

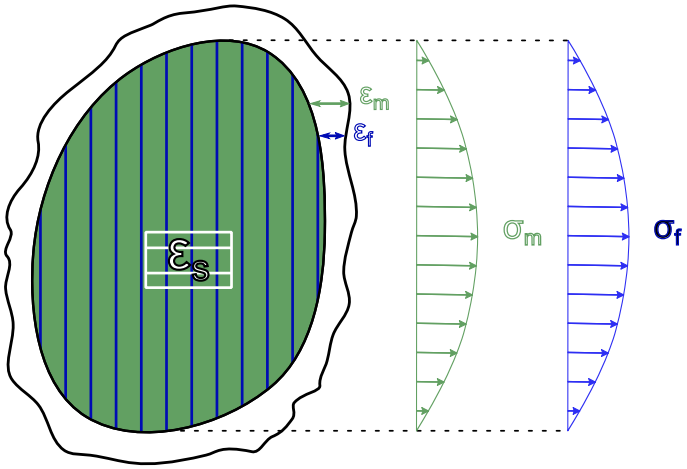

FIGURE 4.21: Serial or iso-stress hypothesis.

The experimental data was very consistent that the serial behaviour was characterised by the fact that what is shared amongst constituent materials is the stress.

$$\underset{\bullet\bullet}{\sigma_m} = \underset{\bullet\bullet}{\sigma_f} \equiv \underset{\bullet\bullet}{\sigma_{\text{s}}} \tag{4.73}$$

where σ_{s} is the serial stress. Therefore, the constitutive tensor can be derived as

$$\begin{aligned} \underset{\bullet\bullet}{\varepsilon} = \Phi_{\Omega m}\underset{\bullet\bullet}{\varepsilon_m} + \Phi_{\Omega f}\underset{\bullet\bullet}{\varepsilon_f} &= \left(\frac{\Phi_{\Omega m}}{\underset{\bullet\bullet\bullet\bullet}{D_m}} + \frac{\Phi_{\Omega f}}{\underset{\bullet\bullet\bullet\bullet}{D_f}}\right)_{\text{serial}} : \underset{\bullet\bullet}{\sigma_{\text{s}}} \\ \left(\underset{\bullet\bullet\bullet\bullet}{D^{-1}}\right)_{\text{serial}} = \left(\frac{\underset{\bullet\bullet}{\varepsilon}}{\underset{\bullet\bullet}{\sigma}}\right)_{\text{serial}} &= \left(\frac{\Phi_{\Omega m}}{\underset{\bullet\bullet\bullet\bullet}{D_m}} + \frac{\Phi_{\Omega f}}{\underset{\bullet\bullet\bullet\bullet}{D_f}}\right)_{\text{serial}} \end{aligned} \tag{4.74}$$

Again for the in-plane stress that is serial the young modulus can be defined as

$$E_2 = \left(\frac{\Phi_{\Omega m}}{E_m} + \frac{\Phi_{\Omega f}}{E_f} \right)^{-1} \tag{4.75}$$

Similarly the in-plane shear modulus is obtained by using an iso-stress hypothesis.

$$G_{12} = \left(\frac{\Phi_{\Omega m}}{G_m} + \frac{\Phi_{\Omega f}}{G_f} \right)^{-1} \tag{4.76}$$

And since the matrix and fibre constituent materials can be considered isotropic, their respective shear modulus becomes

$$G_i = \frac{E_i}{2\,(1+\nu_i)}, \quad \forall i \in m, f \tag{4.77}$$

Note that the subscript i represents the i-th constituent material, generally fibre or matrix.

4.3.2.3 Non-linear constitutive elasticity of composites

The linear study of composites is of high interest, however the current state-of-the-art research, as demanded by the composite industry, is in the hot-pursue of reliable non-linear formulations. The failure of composites is a topic of high value in many areas of design such automotive, aeronautic, civil or, in this particular case, marine.

In the following paragraphs, the introduction to failure mechanics is done by the hand of two non-linear methods. The first is the so-called Tsai and Wu failure criteria, a well known criteria, that is used to characterise the failure of composite laminates. The second theory is the serial-parallel rule of mixtures (SPROM), which has been one of the pivotal theories in the study of this thesis and one that has incredible synergy with the aforementioned formulations.

4.3.2.3.1 Failure criteria of composites

In the scope of failure from the point of view of an element itself, different aspects are worth mentioning. The failure of a certain element can be given by the damage models introduced in subsection 4.1.1, however there are some other interesting developments in the field of shells that will be commented on the following paragraphs.

One important problem is the incapability of shells to model delamination. Delamination, represented in Figure 4.22, is a fracture mechanism where the adherence between two layers of a laminate is lost, effectively detaching partially or completely the two laminae in contact.

While solid elements are able to model delamination since they have enough degrees of freedom in the direction of the thickness, however, shells lack this characteristic

because of how the integration through the thickness of the shell cannot split the Gauss points to capture this delamination phenomenon, at least by the standard FEM.

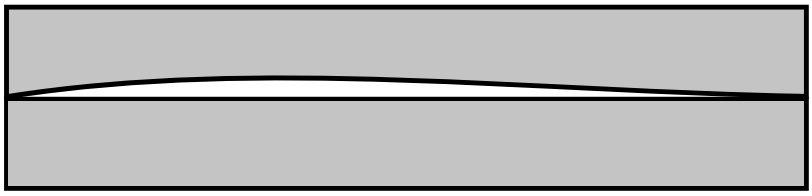

FIGURE 4.22: Illustration of the failure by delamination.

One of the most used theories to include the effect of delamination in shells is the *zig-zag* theory, which includes some extra degrees of freedom in the section integral of the shell element. Doing so can impose certain conditions to accurately integrate the stresses, since delamination modifies the through-thickness stress distribution.

The zig-zag theory can be found, with application to the linear triangle and linear quadrilateral, in [16]. [16] derives its formulation from the work of Tessler et al. [273] where the concept of zig-zag kinematics is introduced to be applied to laminated plates. The zig-zag theory can be conceptualised as some weight function used to introduce delamination and to modify the stress distribution from this induced delamination.

In the case of triangle elements, Eijo et al. in [109], propose a linear quadrilateral that is coupled with the zig-zag theory in order to include delamination. Versino et al. [110] includes the zig-zag theory into the classical discrete Kirchhoff triangle.

The other relevant topic in the study of failure for composite is the one introduced by Tsai and Wu. The criterion receives the same name as their authors and this same criterion is classified as a macro-scale failure, which means that it is not possible to retrieve a priori the layer of failure in the stack of a laminate composite and neither which phase – fibre or matrix – is the one that failed.

A detailed explanation of this criterion is found in either [16, 108] and [96] has an introductory explanation in the chapter devoted to the mechanics of composites. The concept of the Tsai and Wu criterion was first published in [270] in 1971 and it introduces a polynomial of third order that attempts to describe a surface of failure or also regarded in the literature as yielding.

This surface is tailored for orthotropic composites and is defined by

$$\hat{c}_i\sigma_i + \hat{c}_{ij}\sigma_i\sigma_j + \hat{c}_{ijk}\sigma_i\sigma_j\sigma_k - 1 = 0 \tag{4.78}$$

where the parameters $i, j, k = 1, 2, 3, 4, 5, 6$ and the coefficients, $\hat{c}$, are the Tsai and Wu coefficients, which are relative to the strengths in the principal directions of the stress tensor.

These coefficients are determined from experimental analysis to the associated yield

and ultimate strengths at different loading directions. Although to obtain experimentally all the coefficients is in practice impossible and thus the criterion is simplified to a second-order polynomial.

$$\begin{aligned} \hat{c}_1\sigma_1 + \hat{c}_2\sigma_2 + \hat{c}_3\sigma_3 + 2\hat{c}_{12}\sigma_1\sigma_2 + 2\hat{c}_{13}\sigma_1\sigma_3 + 2\hat{c}_{23}\sigma_2\sigma_3 \\ +\hat{c}_{11}\sigma_1^2 + \hat{c}_{22}\sigma_2^2 + \hat{c}_{33}\sigma_3^2 + \hat{c}_{44}\sigma_4^2 + \hat{c}_{55}\sigma_5^2 + \hat{c}_{66}\sigma_6^2 + -1 = 0 \end{aligned} \tag{4.79}$$

However, this method is less precise than a direct calculation, an intermediate method will be explained in the following section, where the isotropic damage model is combined with a composite theory. The correctness of this method can be used to predict damage [274] or even delamination [275].

4.3.2.3.2 The Serial-Parallel Rule of Mixtures

The so-called Serial-Parallel rule of mixtures or in short SPROM is a theory that solves iteratively the hypothesis from Voigt and Reuss. The theory was derived from Rastellini et al. in [15] and the importance of the theory resides in the treatment of the constitutive materials.

This formulation achieves the orthotropy and fulfils the iso-strain and iso-stress hypothesis. The most intuitive and conceptual explanation for the theory is that it acts as a constitutive manager for a given bi-phasic material – a material that is composed of two constituent materials or phases – and it combines the isotropic behaviour of these constituent materials in order to obtain the orthotropic equivalent material.

The fact that at the constituent level there is the existence of an isotropic behaviour makes the theory very suitable to be combined with the isotropic damage theory and consequently reduces the vast number of hyperparameters needed to be introduced for the classical orthotropic model. This implies that the model can describe non-linear orthotropic constitutive behaviour.

The strongest aspect of the SPROM theory is explained when considering how this theory affects pre-existing constitutive models. The theory is implemented in a very organic manner, and it ends acts as a black box theory inside the constitutive model in an exterior and abstract layer. This renders the theory a powerful tool to be combined with pre-existing constitutive models and extend them to obtain the so-called orthotropic behaviour, which is very characteristic of FRP laminates.

Before delving into the details of the theory, a remark on the notation is presented. In this section, the common use of the i-th subscript is employed to generally refer to a constituent material and the constituent materials defined in this section are two, matrix and fibre, defined by the subscript m and f.

In the explanation given for the iso-strain and iso-stress hypothesis, the concepts of parallel and serial were used to address these respective hypotheses, and they were denoted by the subscript p and s. On the other hand, the quantities referred to as the constituent materials are denoted by m and f (see Figure 4.23a), and the quantities referred to as the combination of both, i.e., the composite, are denoted by c (see Figure 4.23b).

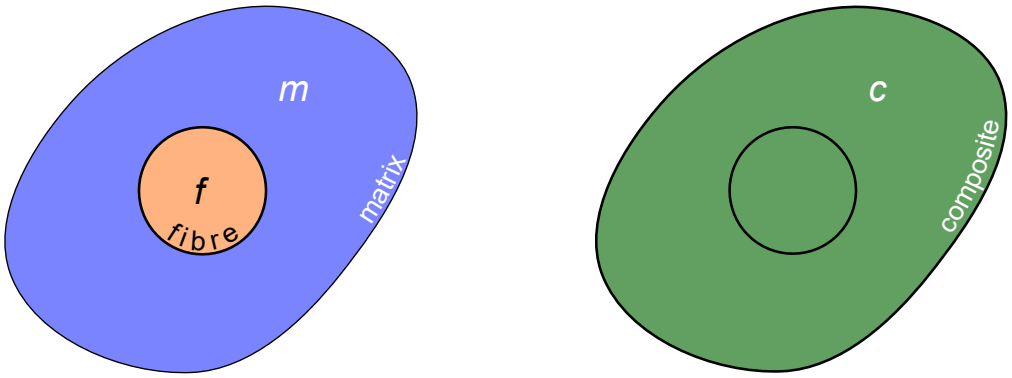

(A) heterogeneous media composed of fibre and matrix.

(B) homogenised media or composite equivalent.

FIGURE 4.23: Analogous description of the same media but with a different perspective.

The strain field is a continuous field, in particular, if taken the averaged strain of a cell or a differential of volume, one can consider the specific cell – numerically equivalent to Gauss interpolation point – to be uniform at the heterogeneous level as well as for its constituent phases (see Figure 4.24).

$$\varepsilon = \frac{\int_\Omega \varepsilon \, \mathrm{d}\Omega}{\int_\Omega \mathrm{d}\Omega} \quad , \quad \varepsilon_c = \frac{\int_{\Omega_c} \varepsilon_c \, \mathrm{d}\Omega}{\int_{\Omega_c} \mathrm{d}\Omega} \quad , \quad \varepsilon_f = \frac{\int_{\Omega_f} \varepsilon_f \, \mathrm{d}\Omega}{\int_{\Omega_f} \mathrm{d}\Omega} \quad , \quad \varepsilon_m = \frac{\int_{\Omega_m} \varepsilon_m \, \mathrm{d}\Omega}{\int_{\Omega_m} \mathrm{d}\Omega} \tag{4.80}$$

Note that the strain here is implying that on average the strains of the composite and phases can be considered proportional.

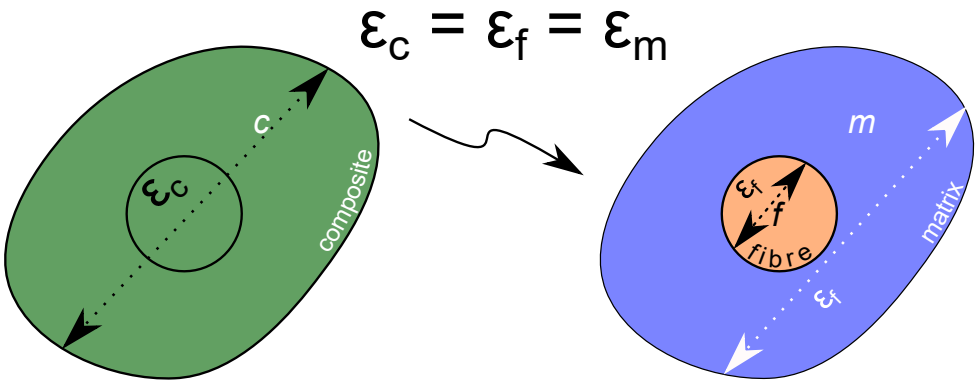

FIGURE 4.24: Average strains of the heterogeneous media and its constituent phases.

At the differential level, the composite quantities are obtained from those of the constituent materials by the rule of mixtures.

$$\varepsilon_c = \Phi_{\Omega f} \varepsilon_f + \Phi_{\Omega m} \varepsilon_m \tag{4.81}$$

Figure 4.25 illustrates the relationship defined in Equation 4.81. It shows that the total strain is the summation of the respective constituent strains multiplied by their volumetric fraction.

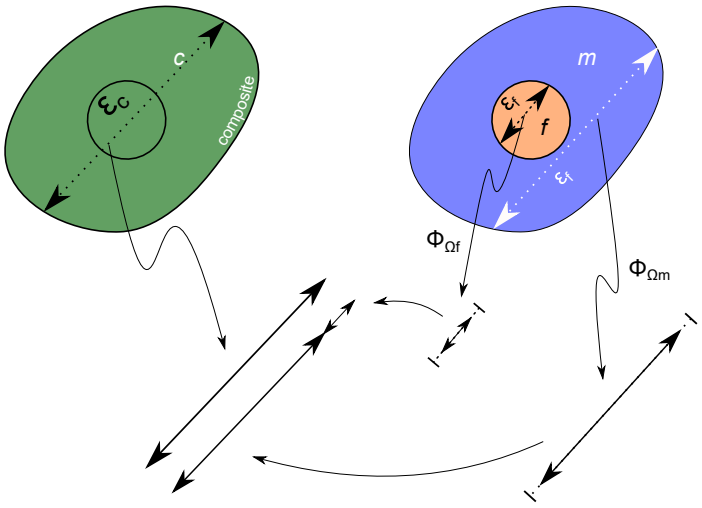

FIGURE 4.25: Graphic representation of the rule of mixtures.

The media under a certain load might generate a failure mode. Within fracture mechanics, the crack propagation can be defined by means of an internal variable model (isotropic damage model). The composite as a whole has generally a set of internal variables at the equivalent homogenised level, whoever at the micro-mechanics level the composite internal variables are infused from the internal variables of the constituent phases. Therefore, the stress of each phase includes the inelastic effects and keeps track of their own constituent internal variables.

$$\sigma_i \left(\varepsilon_i, \beta_{r_i} \right), \quad \forall i \in m, f \tag{4.82}$$

The damage evolution then is obtained for each constituent material and the inelastic stress of the heterogeneous media is infused by the composite model from the constitutive model of the constituent materials as shown in Figure 4.26.

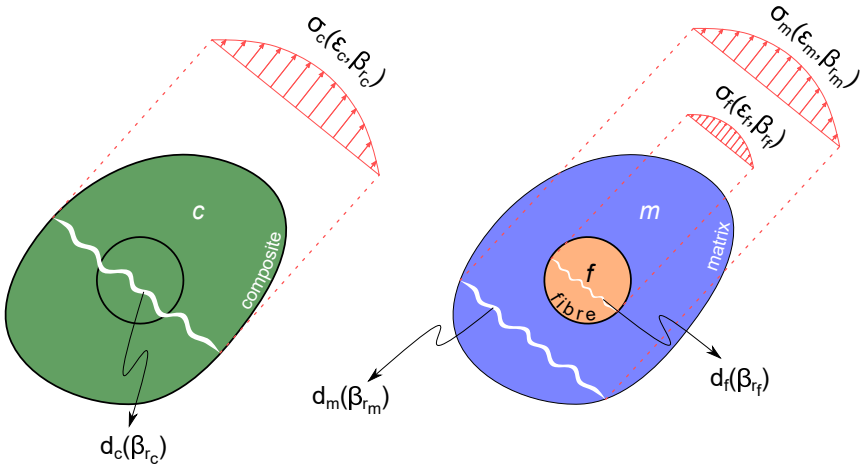

FIGURE 4.26: Graphic representation of the internal variables for the fracture mechanics of composites.

4.3.2.3.3 Projections

The SPROM introduces the concept of projections, these projections are classified in two, serial and parallel according to the behaviour expected (iso-stress or iso-strain respectively). Each layer of a composite stack has its local axes and the first axis (x_1) is aligned to the fibre orientation. Based on this previous convention, the stress and stress components can be assigned one of these two categories. Generally, the strain in the fibre direction is considered parallel (ε_{11}) and the rest of the components can be considered serial ($\sigma_{22}, \sigma_{33}, \tau_{21}, \tau_{31}, \tau_{32}$).

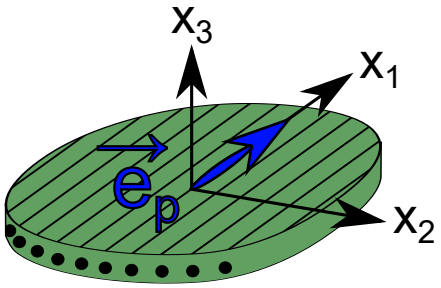

FIGURE 4.27: Representation of the local axes of reference in each ply, the parallel projector is aligned in the fibre direction.

$$\overrightarrow{\underset{\bullet\bullet}{e}}_p = \overrightarrow{\underset{\bullet}{e}}_p \otimes \overrightarrow{\underset{\bullet}{e}}_p \tag{4.83}$$

where $\overrightarrow{\underset{\bullet}{e}}$ is the projector vector, $\overrightarrow{\underset{\bullet\bullet}{e}}$ is the projector matrix. Note that the denomination of vector and matrix are exchangeable with first and second-order tensor. These projections are defined to retrieve the certain components classified as serial and parallel, indeed this is the parallel projector vector since it is defined by the p denominator. To retrieve this behaviour for the second order tensors (strain and stress), a fourth order tensor can be defined

$$\overrightarrow{\underset{\bullet\bullet\bullet\bullet}{e}}_p = \overrightarrow{\underset{\bullet\bullet}{e}}_p \otimes \overrightarrow{\underset{\bullet\bullet}{e}}_p \tag{4.84}$$

where $\overrightarrow{\underset{\bullet\bullet\bullet\bullet}{e}}$ is the fourth order projector tensor. I.e., if considering the parallel behaviour of the strain tensor

$$\underset{\bullet\bullet}{\varepsilon} : \overrightarrow{\underset{\bullet\bullet\bullet\bullet}{e}}_p \equiv \overrightarrow{\underset{\bullet\bullet\bullet\bullet}{e}}_p : \underset{\bullet\bullet}{\varepsilon} = \underset{\bullet\bullet}{\varepsilon}_{pp} = \varepsilon_{11} \tag{4.85}$$

or for any given projection direction/behaviour

$$\begin{cases} \underset{\bullet\bullet}{\varepsilon} : \overrightarrow{\underset{\bullet\bullet\bullet\bullet}{e}}_i \equiv \overrightarrow{\underset{\bullet\bullet\bullet\bullet}{e}}_i : \underset{\bullet\bullet}{\varepsilon} = \underset{\bullet\bullet}{\varepsilon}_i \\ \underset{\bullet\bullet}{\sigma} : \overrightarrow{\underset{\bullet\bullet\bullet\bullet}{e}}_i \equiv \overrightarrow{\underset{\bullet\bullet\bullet\bullet}{e}}_i : \underset{\bullet\bullet}{\sigma} = \underset{\bullet\bullet}{\sigma}_i \end{cases} \quad \forall i \in p, s \tag{4.86}$$

The fact that we can divide the strain and stress into their respective parallel and serial projections is useful to later impose the closure equations. However, this projection can be re-formulated to be included at the constitutive level.

Basically.there are two types of projectors, the parallel and the serial projectors, which are described by the 4-th order tensors

$$\overrightarrow{\underset{\bullet\bullet\bullet\bullet}{e}}_p \quad , \quad \overrightarrow{\underset{\bullet\bullet\bullet\bullet}{e}}_s = \underset{\bullet\bullet\bullet\bullet}{1} - \overrightarrow{\underset{\bullet\bullet\bullet\bullet}{e}}_p \tag{4.87}$$

Where $\overrightarrow{\underset{\bullet\bullet\bullet\bullet}{e}}_p$ and $\overrightarrow{\underset{\bullet\bullet\bullet\bullet}{e}}_s$ are the parallel and serial projectors respectively. The notation $\underset{\bullet\bullet\bullet\bullet}{1}$ describes the unity fourth tensor. The following relationships are defined by using Equation 4.87 together with Equation 4.86.

$$\begin{aligned} \underset{\bullet\bullet}{\varepsilon} = \underset{\bullet\bullet}{\varepsilon}_p + \underset{\bullet\bullet}{\varepsilon}_s = \underset{\bullet\bullet}{\varepsilon} : \overrightarrow{\underset{\bullet\bullet\bullet\bullet}{e}}_p + \underset{\bullet\bullet}{\varepsilon} : \overrightarrow{\underset{\bullet\bullet\bullet\bullet}{e}}_s = \underset{\bullet\bullet}{\varepsilon} \cancel{\left(\overrightarrow{\underset{\bullet\bullet\bullet\bullet}{e}}_p + \overrightarrow{\underset{\bullet\bullet\bullet\bullet}{e}}_s \right)} \underset{\bullet\bullet\bullet\bullet}{1} \\ \underset{\bullet\bullet}{\sigma} = \underset{\bullet\bullet}{\sigma}_p + \underset{\bullet\bullet}{\sigma}_s = \underset{\bullet\bullet}{\sigma} : \overrightarrow{\underset{\bullet\bullet\bullet\bullet}{e}}_p + \underset{\bullet\bullet}{\sigma} : \overrightarrow{\underset{\bullet\bullet\bullet\bullet}{e}}_s = \underset{\bullet\bullet}{\sigma} \cancel{\left(\overrightarrow{\underset{\bullet\bullet\bullet\bullet}{e}}_p + \overrightarrow{\underset{\bullet\bullet\bullet\bullet}{e}}_s \right)} \underset{\bullet\bullet\bullet\bullet}{1} \end{aligned} \tag{4.88}$$

4.3.2.3.4 Closure equations

The projections are defined in terms of the *homogenised* equivalent of the heterogeneous media (composite). Nevertheless, these same projections can be applied to the constituent material level. First, the hypothesis of Voigt and Reuss [26, 27] are described with the notation of parallel and serial behaviour respectively. According to Voigt, composites exhibit an iso-strain behaviour in the parallel direction (aligned in the direction of fibres).

$$\varepsilon_p = \varepsilon_{p,f} = \varepsilon_{p,m} \tag{4.89}$$

and Reuss posed that the stress of the constituent phases is identical in the serial directions.

$$\sigma_s = \sigma_{s,f} = \sigma_{s,m} \tag{4.90}$$

Equation 4.89 is fulfilled directly since the strain or displacements are not unknown. The formulation is strain-driven or displacement-driven and this fulfils directly the hypothesis, at least in the parallel direction.

On the other hand, Equation 4.90 is not fulfilled by definition, since stress is an unknown. The strategy is then to minimise the stress as per usual in the global solver system and also minimise the serial closure equation. Consequently, there is the global minimisation of the residual of forces in terms of the increment of the displacement and the local minimisation of the residual of stresses in the serial direction at the Gauss point level.

$$\underline{\Delta u} = -\underline{\underline{\left(\frac{\partial r_u}{\partial u}\right)^{-1}}}\ \underline{r_u\left(u\right)} \qquad \text{(GLOBAL)}$$
$$\underline{r_{\sigma_s}} \equiv \underline{\Delta\sigma_s} = \underline{\sigma_{s,m}} - \underline{\sigma_{s,f}} \quad , \quad \underline{\Delta\varepsilon_{s,m}} = -\underline{\underline{\left(\frac{\partial r_{\sigma_s}}{\partial \varepsilon_{s,m}}\right)^{-1}}}\ \underline{r_{\sigma_s}\left(\varepsilon_{s,m}\right)} \qquad \text{(LOCAL)} \tag{4.91}$$

where r_u is the mechanical residual, r_{σ_s} is the serial residual and u is the displacement. Global minimisation has been addressed at the continuum level. The local strategy is described in the following paragraphs.

4.3.2.3.5 Constitutive tensor

The local equilibrium is defined in terms of the stress, the strain and the constitutive tensor. Figure 4.28 shows the tangent constitutive tensor which is useful in incremental and iterative mechanical problems, therefore, when referring to constitutive tensor (D), the term extends directly to the tangent constitutive tensor (D_{tan}) in order to avoid excessive subscripts.

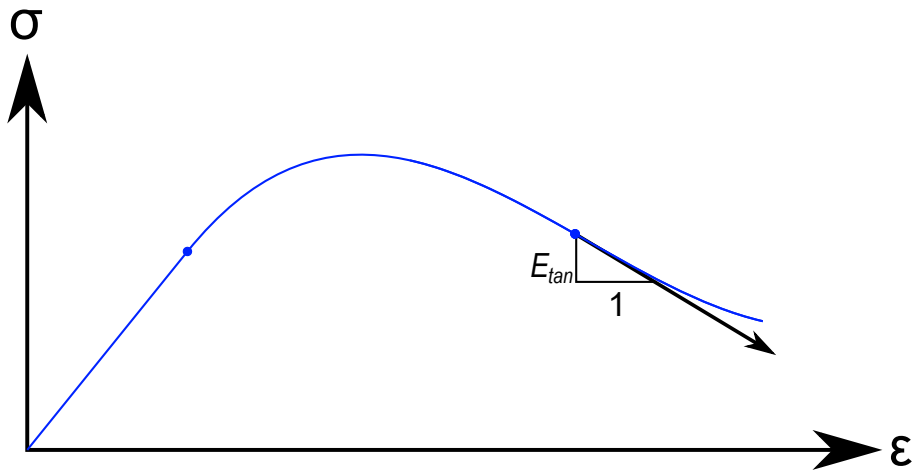

FIGURE 4.28: one-dimensional equivalence of the tangent constitutive tensor.

When the local equilibrium is formulated in terms of the parallel and the serial behaviour, the tangent constitutive tensor can be broken down into the combination of these states.

$$\begin{bmatrix} \underset{\bullet\bullet}{\sigma_p} \\ \underset{\bullet\bullet}{\sigma_s} \end{bmatrix} = \begin{bmatrix} \underset{\bullet\bullet\bullet\bullet}{\overrightarrow{e}_p} \\ \underset{\bullet\bullet\bullet\bullet}{\overrightarrow{e}_s} \end{bmatrix} : \underset{\bullet\bullet}{\sigma} = \begin{bmatrix} \underset{\bullet\bullet\bullet\bullet}{\overrightarrow{e}_p} \\ \underset{\bullet\bullet\bullet\bullet}{\overrightarrow{e}_s} \end{bmatrix} : \underset{\bullet\bullet\bullet\bullet}{D} : \underset{\bullet\bullet}{\varepsilon} = \begin{bmatrix} \underset{\bullet\bullet\bullet\bullet}{\overrightarrow{e}_p} \\ \underset{\bullet\bullet\bullet\bullet}{\overrightarrow{e}_s} \end{bmatrix} : \underset{\bullet\bullet\bullet\bullet}{D} : \begin{bmatrix} \underset{\bullet\bullet}{\varepsilon_p} & \underset{\bullet\bullet}{\varepsilon_s} \end{bmatrix} \begin{bmatrix} 1 \\ 1 \end{bmatrix} =$$
$$\begin{bmatrix} \underset{\bullet\bullet\bullet\bullet}{\overrightarrow{e}_p} \\ \underset{\bullet\bullet\bullet\bullet}{\overrightarrow{e}_s} \end{bmatrix} : \underset{\bullet\bullet\bullet\bullet}{D} : \begin{bmatrix} \underset{\bullet\bullet\bullet\bullet}{\overrightarrow{e}_p} & \underset{\bullet\bullet\bullet\bullet}{\overrightarrow{e}_s} \end{bmatrix} \begin{bmatrix} \underset{\bullet\bullet}{\varepsilon} \\ \underset{\bullet\bullet}{\varepsilon} \end{bmatrix} = \begin{bmatrix} \underset{\bullet\bullet\bullet\bullet}{D_{pp}} & \underset{\bullet\bullet\bullet\bullet}{D_{ps}} \\ \underset{\bullet\bullet\bullet\bullet}{D_{sp}} & \underset{\bullet\bullet\bullet\bullet}{D_{ss}} \end{bmatrix} : \begin{bmatrix} \underset{\bullet\bullet}{\varepsilon} \\ \underset{\bullet\bullet}{\varepsilon} \end{bmatrix} \tag{4.92}$$

The components of the tangent constitutive tensor in their respective serial or parallel behaviours are defined as

$$\underset{\bullet\bullet\bullet\bullet}{D} = \begin{bmatrix} 1 & 1 \end{bmatrix} \begin{bmatrix} \underset{\bullet\bullet\bullet\bullet}{D_{pp}} & \underset{\bullet\bullet\bullet\bullet}{D_{ps}} \\ \underset{\bullet\bullet\bullet\bullet}{D_{sp}} & \underset{\bullet\bullet\bullet\bullet}{D_{ss}} \end{bmatrix} \begin{bmatrix} 1 \\ 1 \end{bmatrix} \equiv \begin{bmatrix} 1 & 1 \end{bmatrix} \begin{bmatrix} \dfrac{\partial \sigma_p}{\partial \underset{\bullet\bullet}{\varepsilon_p}} & \dfrac{\partial \sigma_p}{\partial \underset{\bullet\bullet}{\varepsilon_s}} \\ \dfrac{\partial \sigma_s}{\partial \underset{\bullet\bullet}{\varepsilon_p}} & \dfrac{\partial \sigma_s}{\partial \underset{\bullet\bullet}{\varepsilon_s}} \end{bmatrix} \begin{bmatrix} 1 \\ 1 \end{bmatrix} = \underset{\bullet\bullet\bullet\bullet}{D_{pp}} + \underset{\bullet\bullet\bullet\bullet}{D_{ps}} + \underset{\bullet\bullet\bullet\bullet}{D_{sp}} + \underset{\bullet\bullet\bullet\bullet}{D_{ss}} \tag{4.93}$$

where

$$\underset{\bullet\bullet\bullet\bullet}{D_{pp}} = \underset{\bullet\bullet\bullet\bullet_p}{\overrightarrow{e}} : \underset{\bullet\bullet\bullet\bullet}{D} : \underset{\bullet\bullet\bullet\bullet_p}{\overrightarrow{e}} \tag{4.94}$$

$$\underset{\bullet\bullet\bullet\bullet}{D_{ps}} = \underset{\bullet\bullet\bullet\bullet_p}{\overrightarrow{e}} : \underset{\bullet\bullet\bullet\bullet}{D} : \underset{\bullet\bullet\bullet\bullet_s}{\overrightarrow{e}} \tag{4.95}$$

$$\underset{\bullet\bullet\bullet\bullet}{D_{sp}} = \underset{\bullet\bullet\bullet\bullet_s}{\overrightarrow{e}} : \underset{\bullet\bullet\bullet\bullet}{D} : \underset{\bullet\bullet\bullet\bullet_p}{\overrightarrow{e}} \tag{4.96}$$

$$\underset{\bullet\bullet\bullet\bullet}{D_{ss}} = \underset{\bullet\bullet\bullet\bullet_s}{\overrightarrow{e}} : \underset{\bullet\bullet\bullet\bullet}{D} : \underset{\bullet\bullet\bullet\bullet_s}{\overrightarrow{e}} \tag{4.97}$$

4.3.2.3.6 Local problem

At the local level, the problem to be minimised was

$$\underline{r_{\sigma_s}} = \underline{\Delta \sigma_s} \left(\underline{\varepsilon_{s,m}} \right) = \underline{\sigma_{s,m}} \left(\underline{\varepsilon_{s,m}} \right) - \underline{\sigma_{s,f}} \left(\underline{\varepsilon_{s,f}} \right) \tag{4.98}$$

where the serial deformation of the fibre can be expressed in terms of the matrix one by using the rule of mixture relationship.

$$\underline{\varepsilon_{s,f}} \left(\underline{\varepsilon_{s,m}} \right) = \frac{1}{\Phi_{\Omega f}} \underline{\varepsilon_s} - \frac{\Phi_{\Omega m}}{\Phi_{\Omega f}} \underline{\varepsilon_{s,m}} \tag{4.99}$$

The derivative of the serial residual can be then expanded.

$$\frac{\partial \underline{r_{\sigma_s}}}{\partial \underline{\varepsilon_{s,m}}} = \frac{\partial \left(\underline{\sigma_{s,m}} - \underline{\sigma_{s,f}} \right)}{\partial \underline{\varepsilon_{s,m}}} = \frac{\partial \underline{\sigma_{s,m}}}{\partial \underline{\varepsilon_{s,m}}} - \frac{\partial \underline{\sigma_{s,m}}}{\partial \underline{\varepsilon_{s,f}}} \cdot \frac{\partial \underline{\varepsilon_{s,f}}}{\partial \underline{\varepsilon_{s,m}}} = \underline{\underline{D_{ss,m}}} + \frac{\Phi_{\Omega m}}{\Phi_{\Omega f}} \underline{\underline{D_{ss,f}}} \tag{4.100}$$

If Equation 4.100 is then evaluated iteratively at iteration k-th, the serial matrix deformation or unknown yields

$$\underline{\varepsilon_{s,m}}\Big|_{k+1} = \underline{\varepsilon_{s,m}}\Big|_{k} - \left(\frac{\partial \underline{r_{\sigma_s}}}{\partial \underline{\varepsilon_{s,m}}}\right)^{-1}\Bigg|_{k} \cdot \underline{\Delta\sigma_s}\Big|_{k} \tag{4.101}$$

4.3.2.3.7 Initial approximation of the unknown

The local algorithm is solved iteratively, the goal is to pose the differential relationships to latter equate the differential form of the quantities to their respective increment. The parallel approximation on the constituent materials is strictly imposed.

$$\underset{\bullet\bullet}{\mathrm{d}\varepsilon_p} = \underset{\bullet\bullet}{\mathrm{d}\varepsilon_{p,f}} = \underset{\bullet\bullet}{\mathrm{d}\varepsilon_{p,m}} \tag{4.102}$$

Employing the relationships in Equation 4.98 and Equation 4.93 the serial deformation yields

$$\begin{cases} \underset{\bullet\bullet\bullet\bullet}{D_{ss,f}} : \underset{\bullet\bullet}{\mathrm{d}\varepsilon_{s,f}} = \underset{\bullet\bullet\bullet\bullet}{D_{ss,m}} : \underset{\bullet\bullet}{\mathrm{d}\varepsilon_{s,m}} - \left(\underset{\bullet\bullet\bullet\bullet}{D_{sp,f}} - \underset{\bullet\bullet\bullet\bullet}{D_{sp,m}}\right) : \underset{\bullet\bullet}{\mathrm{d}\varepsilon_p} \\ \underset{\bullet\bullet\bullet\bullet}{D_{ss,f}} : \underset{\bullet\bullet}{\mathrm{d}\varepsilon_s} = \Phi_{\Omega f}\underset{\bullet\bullet\bullet\bullet}{D_{ss,f}} : \underset{\bullet\bullet}{\mathrm{d}\varepsilon_{s,f}} + \Phi_{\Omega m}\underset{\bullet\bullet\bullet\bullet}{D_{ss,f}} : \underset{\bullet\bullet}{\mathrm{d}\varepsilon_{s,m}} \end{cases} \tag{4.103}$$

Substituting and rearranging the terms in Equation 4.103

$$\begin{gathered} \underset{\bullet\bullet\bullet\bullet}{D_{ss,f}} : \underset{\bullet\bullet}{\mathrm{d}\varepsilon_s} = \Phi_{\Omega f}\left(\underset{\bullet\bullet\bullet\bullet}{D_{ss,m}} : \underset{\bullet\bullet}{\mathrm{d}\varepsilon_{s,m}} - \left(\underset{\bullet\bullet\bullet\bullet}{D_{sp,f}} - \underset{\bullet\bullet}{D_{sp,m}}\right) : \underset{\bullet\bullet}{\mathrm{d}\varepsilon_p}\right) \\ +\Phi_{\Omega m}\underset{\bullet\bullet\bullet\bullet}{D_{ss,f}} : \underset{\bullet\bullet}{\mathrm{d}\varepsilon_{s,m}} \\ \Downarrow \\ \underset{\bullet\bullet}{\mathrm{d}\varepsilon_{s,m}} = \hat{c} : \left(\underset{\bullet\bullet\bullet\bullet}{D_{ss,f}} : \underset{\bullet\bullet}{\mathrm{d}\varepsilon_s} + \Phi_{\Omega f}\left(\underset{\bullet\bullet\bullet\bullet}{D_{sp,f}} - \underset{\bullet\bullet\bullet\bullet}{D_{sp,m}}\right) : \underset{\bullet\bullet}{\mathrm{d}\varepsilon_p}\right) \\ \hat{c} = \left(\Phi_{\Omega f}\underset{\bullet\bullet\bullet\bullet}{D_{ss,m}} + \Phi_{\Omega m}\underset{\bullet\bullet\bullet\bullet}{D_{ss,f}}\right)^{-1} \end{gathered} \tag{4.104}$$

The same arrangement can be made for the fibre

$$\begin{gathered} \underset{\bullet\bullet}{\mathrm{d}\varepsilon_{s,f}} = \hat{c} : \left(\underset{\bullet\bullet\bullet\bullet}{D_{ss,m}} : \underset{\bullet\bullet}{\mathrm{d}\varepsilon_s} + \Phi_{\Omega m}\left(\underset{\bullet\bullet\bullet\bullet}{D_{sp,m}} - \underset{\bullet\bullet\bullet\bullet}{D_{sp,f}}\right) : \underset{\bullet\bullet}{\mathrm{d}\varepsilon_p}\right) \\ \hat{c} = \left(\Phi_{\Omega f}\underset{\bullet\bullet\bullet\bullet}{D_{ss,m}} + \Phi_{\Omega m}\underset{\bullet\bullet\bullet\bullet}{D_{ss,f}}\right)^{-1} \end{gathered} \tag{4.105}$$

Equation 4.104 and Equation 4.105 allow calculating the serial increment for the strain of the matrix and fibre phases in terms of the serial and parallel strains of the composite.

$$
\begin{aligned}
\mathrm{d}\underset{\bullet\bullet}{\varepsilon}_s \approx \Delta\underset{\bullet\bullet}{\varepsilon}_s = \underset{\bullet\bullet}{\varepsilon}_s(t+\Delta t) - \underset{\bullet\bullet}{\varepsilon}_s(t) = \underset{\bullet\bullet}{\varepsilon}_s\Big|_{k+1} - \underset{\bullet\bullet}{\varepsilon}_s\Big|_{k} \\
\mathrm{d}\underset{\bullet\bullet}{\varepsilon}_p \approx \Delta\underset{\bullet\bullet}{\varepsilon}_p = \underset{\bullet\bullet}{\varepsilon}_p(t+\Delta t) - \underset{\bullet\bullet}{\varepsilon}_p(t) = \underset{\bullet\bullet}{\varepsilon}_p\Big|_{k+1} - \underset{\bullet\bullet}{\varepsilon}_p\Big|_{k} \\
\Delta\underset{\bullet\bullet}{\varepsilon}_{s,m} = \hat{c} : \left(\underset{\bullet\bullet\bullet\bullet}{D}_{ss,f} : \Delta\underset{\bullet\bullet}{\varepsilon}_s + \Phi_{\Omega f} \left(\underset{\bullet\bullet\bullet\bullet}{D}_{sp,f} - \underset{\bullet\bullet\bullet\bullet}{D}_{sp,m} \right) : \Delta\underset{\bullet\bullet}{\varepsilon}_p \right) \\
\Delta\underset{\bullet\bullet}{\varepsilon}_{s,f} = \hat{c} : \left(\underset{\bullet\bullet\bullet\bullet}{D}_{ss,m} : \Delta\underset{\bullet\bullet}{\varepsilon}_s + \Phi_{\Omega m} \left(\underset{\bullet\bullet\bullet\bullet}{D}_{sp,m} - \underset{\bullet\bullet\bullet\bullet}{D}_{sp,f} \right) : \Delta\underset{\bullet\bullet}{\varepsilon}_p \right) \\
\hat{c} = \left(\Phi_{\Omega f} \underset{\bullet\bullet\bullet\bullet}{D}_{ss,m} + \Phi_{\Omega m} \underset{\bullet\bullet\bullet\bullet}{D}_{ss,f} \right)^{-1}
\end{aligned}
\tag{4.106}
$$

This implies that the initial approximation of the increment of the serial matrix deformation is found at the iteration $k = 0$. Note that for the initial iteration, the constitutive quantities are evaluated from the previous converged step of the global algorithm. I.e., the constitutive tensor adopts the form of the converged solution of the previous global increment.

$$
D_i|_{k=0} = D_i\left(\varepsilon_i(t), \beta_{r_i}(t)\right) \quad , \quad \forall i \in m, f \tag{4.107}
$$

Note that the description of the constitutive tensor encompasses the non-linear range by including the internal variables (β_r) of each constituent material (fibre and matrix). Both the strain and the internal variables are the converged quantities from the previous global step.

4.3.2.3.8 Evaluation of the residual

The fact that the differential form – note that differential indistinctly can be exchanged by the incremental form – of the serial deformation of the fibre and matrix phases were obtained in Equation 4.106 allowing the problem to be formulated in a constituent manner, thus the differential form of the stresses can be derived.

$$
\begin{aligned}
\mathrm{d}\underset{\bullet\bullet}{\sigma}_p = \Phi_{\Omega f} \left(\underset{\bullet\bullet\bullet\bullet}{D}_{pp,f} : \mathrm{d}\underset{\bullet\bullet}{\varepsilon}_p + \underset{\bullet\bullet\bullet\bullet}{D}_{ps,f} : \hat{c} : \left(\underset{\bullet\bullet\bullet\bullet}{D}_{ss,m} : \mathrm{d}\underset{\bullet\bullet}{\varepsilon}_s + \Phi_{\Omega m} \left(\underset{\bullet\bullet\bullet\bullet}{D}_{sp,m} - \underset{\bullet\bullet\bullet\bullet}{D}_{sp,f} \right) : \mathrm{d}\underset{\bullet\bullet}{\varepsilon}_p \right) \right) \\
+ \Phi_{\Omega m} \left(\underset{\bullet\bullet\bullet\bullet}{D}_{pp,m} : \mathrm{d}\underset{\bullet\bullet}{\varepsilon}_p + \underset{\bullet\bullet\bullet\bullet}{D}_{ps,m} : \hat{c} : \left(\underset{\bullet\bullet\bullet\bullet}{D}_{ss,f} : \mathrm{d}\underset{\bullet\bullet}{\varepsilon}_s + \Phi_{\Omega f} \left(\underset{\bullet\bullet\bullet\bullet}{D}_{sp,m} - \underset{\bullet\bullet\bullet\bullet}{D}_{sp,m} \right) : \mathrm{d}\underset{\bullet\bullet}{\varepsilon}_p \right) \right) \\
\hat{c} = \left(\Phi_{\Omega f} \underset{\bullet\bullet\bullet\bullet}{D}_{ss,m} + \Phi_{\Omega m} \underset{\bullet\bullet\bullet\bullet}{D}_{ss,f} \right)^{-1}
\end{aligned}
\tag{4.108}
$$

Factorising the terms by the increment of the serial and parallel strains as customary

$$\begin{aligned} \mathrm{d}\underset{\bullet\bullet}{\sigma_p} = & \left[\left(\Phi_{\Omega f} \underset{\bullet\bullet\bullet\bullet}{D_{pp,f}} + \Phi_{\Omega m} \underset{\bullet\bullet\bullet\bullet}{D_{pp,m}} \right) \right. \\ & \left. + \Phi_{\Omega m}\Phi_{\Omega f} \left(\Phi_{\Omega f} \underset{\bullet\bullet\bullet\bullet}{D_{ps,f}} - \Phi_{\Omega f} \underset{\bullet\bullet\bullet\bullet}{D_{ps,m}} \right) : \hat{c} : \left(\Phi_{\Omega f} \underset{\bullet\bullet\bullet\bullet}{D_{sp,m}} - \Phi_{\Omega f} \underset{\bullet\bullet\bullet\bullet}{D_{sp,f}} \right) \right] : \mathrm{d}\underset{\bullet\bullet}{\varepsilon_p} \\ & + \left(\Phi_{\Omega f} \underset{\bullet\bullet\bullet\bullet}{D_{ps,f}} : \hat{c} : \underset{\bullet\bullet\bullet\bullet}{D_{ss,m}} + \Phi_{\Omega,m} \underset{\bullet\bullet\bullet\bullet}{D_{ps,m}} : \hat{c} : \underset{\bullet\bullet\bullet\bullet}{D_{ss,f}} \right) : \mathrm{d}\underset{\bullet\bullet}{\varepsilon_s} \end{aligned} \tag{4.109}$$

$$\hat{c} = \left(\Phi_{\Omega f} \underset{\bullet\bullet\bullet\bullet}{D_{ss,m}} + \Phi_{\Omega m} \underset{\bullet\bullet\bullet\bullet}{D_{ss,f}} \right)^{-1}$$

The same can be formulated for the differential of serial stress in terms of the differential of the serial and parallel strains. Recall that the serial stress is the same for the constituent materials and the composite material $\sigma_s = \sigma_{s,m} = \sigma_{s,f}$.

$$\begin{aligned} \mathrm{d}\underset{\bullet\bullet}{\sigma_s} = & \left(\Phi_{\Omega m} \underset{\bullet\bullet\bullet\bullet}{D_{ss,m}} : \hat{c} : \underset{\bullet\bullet\bullet\bullet}{D_{sp,m}} + \Phi_{\Omega f} \underset{\bullet\bullet\bullet\bullet}{D_{ss,m}} : \hat{c} : \underset{\bullet\bullet\bullet\bullet}{D_{sp,f}} \right) : \mathrm{d}\underset{\bullet\bullet}{\varepsilon_p} \\ & + \frac{1}{2} \left(\underset{\bullet\bullet\bullet\bullet}{D_{ss,m}} : \hat{c} : \underset{\bullet\bullet\bullet\bullet}{D_{ss,f}} + \underset{\bullet\bullet\bullet\bullet}{D_{ss,f}} : \hat{c} : \underset{\bullet\bullet\bullet\bullet}{D_{ss,m}} \right) : \mathrm{d}\underset{\bullet\bullet}{\varepsilon_s} \end{aligned} \tag{4.110}$$

$$\hat{c} = \left(\Phi_{\Omega f} \underset{\bullet\bullet\bullet\bullet}{D_{ss,m}} + \Phi_{\Omega m} \underset{\bullet\bullet\bullet\bullet}{D_{ss,f}} \right)^{-1}$$

Therefore the incremental residual can be minimised using the expression in Equation 4.110.

4.3.2.3.9 Convergence criteria

The convergence criterion is only imposed in the serial stress part of the stress tensor. The main difficulty is to normalise the residual in terms of the absolute magnitude of the tensions. A two-level convergence criteria are imposed. The magnitude of the reference tensions used depends on:

1. The minimum between the serial stress of the fibre and matrix in the previous and converged step.

$$\sigma_{\mathrm{ref}_1} = \min \left(\left| \sigma_{s,m}(t) \right|, \left| \sigma_{s,f}(t) \right| \right) \tag{4.111}$$

   Of course this is singular when both tensions are zero.

2. The minimum of the linearised stresses at the previous step.

$$\sigma_{\mathrm{ref}_2} = \min \left(\left| D_{s,m}(t) : \varepsilon_{s,m}(t) \right|, \left| D_{s,f}(t) : \varepsilon_{s,f}(t) \right| \right) \tag{4.112}$$

   The constitutive tensor does not necessarily need to be the linear one.

The two sets of tolerance criteria used is very self-explanatory. In Equation 4.111, the minimum of the stress of the previous step is used and if the problem has not yet been initialised this would yield a singular result since the magnitude of those stresses would be zero.

The criterion in Equation 3.98 is then used when the problem is not initialised, if the step is considered not great enough to trigger the non-linear elastic behaviour of the material, the reference tension should be the linear one from the previous step.

If the non-linear constitutive tensor is used instead in Equation 3.98, when the problem has already been initialised, otherwise the non-linear will coincide with the linear constitutive tensor, and it should retrieve again the same stress calculated in Equation 4.111. Therefore, the following constraints are prescribed in terms of convergence tolerance.

$$\begin{aligned} \sigma_{\text{ref}_1} > 0 &\Rightarrow \sigma_{\text{ref}} = \sigma_{\text{ref}_1} \\ \sigma_{\text{ref}_1} = 0 &\Rightarrow \sigma_{\text{ref}} = \sigma_{\text{ref}_2} \end{aligned} \tag{4.113}$$

where σ_{ref} is the general absolute stress reference. Then the increment of stress can be considered to have solved the local algorithm approximately when

$$|\Delta\sigma_s| \leq \text{tolerance} \cdot \sigma_{\text{ref}} \tag{4.114}$$

In the literature, i.e. [15], a standard tolerance criterion is in the order of 10^{-4}.

4.3.2.3.10 Serial-parallel tangent constitutive tensor

The local algorithm is well-posed in terms of the stresses and strains. At the constituent level, the stresses and strains can be obtained and the equations that allow the problem to be minimised with respect to the serial strain of the matrix phase were derived. At the composite level, the equations are as well-posed and principally expressed with respect to the differential or incremental form of the serial and parallel behaviour of both strain and stresses.

However, the constitutive tensor, albeit at the local level can be obtained for each one of the constituent materials, at the composite level this was not defined. In Equation 4.93, the composite existent relationships were defined, these are

1. The total constitutive tensor for the composite material is the result of the sum of the parallel-parallel, parallel-serial, serial-parallel, and serial-serial constitutive tensors.
2. The respective parallel and serial behaviours of the constitutive tensor are found by the projections of the composite tensor.

It is obvious that although the projection tensor is a priori given if the total constitutive tensor (tangent one) is to be found, the parallel and serial descriptions of it cannot involve this same unknown.

In this sense, Equation 4.93 provides another description of this projected behaviour. This expression holds at the constituent and composite material level, and conveniently uses the differential expressions derived previously ($\mathrm{d}\sigma_p$, $\mathrm{d}\sigma_s$, $\mathrm{d}\varepsilon_p$, $\mathrm{d}\varepsilon_s$). The projected tangent constituent tensors then become

$$\begin{aligned}\frac{\mathrm{d}\sigma_p}{\mathrm{d}\varepsilon_p} \equiv \underset{\bullet\bullet\bullet\bullet}{D_{pp}} = &\left(\Phi_{\Omega f}\underset{\bullet\bullet\bullet\bullet}{D_{pp,f}} + \Phi_{\Omega m}\underset{\bullet\bullet\bullet\bullet}{D_{pp,m}}\right) \\ &+\Phi_{\Omega f}\Phi_{\Omega m}\left(\underset{\bullet\bullet\bullet\bullet}{D_{ps,f}} - \underset{\bullet\bullet\bullet\bullet}{D_{ps,m}}\right) : \hat{c} : \left(\underset{\bullet\bullet\bullet\bullet}{D_{sp,m}} - \underset{\bullet\bullet\bullet\bullet}{D_{sp,f}}\right)\end{aligned} \tag{4.115}$$

$$\frac{\mathrm{d}\sigma_p}{\mathrm{d}\varepsilon_s} \equiv \underset{\bullet\bullet\bullet\bullet}{D_{ps}} = \Phi_{\Omega f}\underset{\bullet\bullet\bullet\bullet}{D_{ps,f}} : \hat{c} : \underset{\bullet\bullet\bullet\bullet}{D_{ss,m}} + \Phi_{\Omega m}\underset{\bullet\bullet\bullet\bullet}{D_{ps,m}} : \hat{c} : \underset{\bullet\bullet\bullet\bullet}{D_{ss,f}} \tag{4.116}$$

$$\frac{\mathrm{d}\sigma_s}{\mathrm{d}\varepsilon_p} \equiv \underset{\bullet\bullet\bullet\bullet}{D_{sp}} = \Phi_{\Omega m}\underset{\bullet\bullet\bullet\bullet}{D_{ss,f}} : \hat{c} : \underset{\bullet\bullet\bullet\bullet}{D_{sp,m}} + \Phi_{\Omega f}\underset{\bullet\bullet\bullet\bullet}{D_{ss,m}} : \hat{c} : \underset{\bullet\bullet\bullet\bullet}{D_{sp,f}} \tag{4.117}$$

$$\frac{\mathrm{d}\sigma_s}{\mathrm{d}\varepsilon_s} \equiv \underset{\bullet\bullet\bullet\bullet}{D_{ss}} = \frac{1}{2}\left(\underset{\bullet\bullet\bullet\bullet}{D_{ss,m}} : \hat{c} : \underset{\bullet\bullet\bullet\bullet}{D_{ss,f}} + \underset{\bullet\bullet\bullet\bullet}{D_{ss,f}} : \hat{c} : \underset{\bullet\bullet\bullet\bullet}{D_{ss,m}}\right) \tag{4.118}$$

$$\hat{c} = \left(\Phi_{\Omega f}\underset{\bullet\bullet\bullet\bullet}{D_{ss,m}} + \Phi_{\Omega m}\underset{\bullet\bullet\bullet\bullet}{D_{ss,f}}\right)^{-1} \tag{4.119}$$

The total tangent constitutive tensor of the composite material can be found using the expressions found in Equation 4.115, Equation 4.116, Equation 4.117 and Equation 4.118. This is useful for the global problem since the tangent stiffness can then be found.

Moreover, these expressions can be further simplified if the constitutive tensors of the constituent materials are symmetric (D_m, D_f). In the case of this symmetry, the following relationships apply

$$\underset{\bullet\bullet\bullet\bullet}{D_{sp,i}} = \underset{\bullet\bullet\bullet\bullet}{D_{ps,i}}^T \quad \forall i \in m, f, c \tag{4.120}$$

Note that the subscript "m" denotes matrix, "f" fibre and "c" composite.

4.3.2.3.11 Local algorithm

Once the different aspects involving the SPROM theory are posed, the description of the algorithm is given in algorithm 3.

Algorithm 3: SPROM Solver

1) Approximation of the unknown (Equation 4.106)
2) Evaluation of the residue (Equation 4.90)
3) Condition: Stress Equilibrium (Equation 4.106)
   $\longrightarrow$ No: **go to:** 4)

   $\longrightarrow$ Yes: **go to:** 5)

4) Correction of the unknown. (Equation 4.114)
   go to: 2)

5) Update of state and internal variables. (Equation 4.121)
6) Update of the composite stress state. (Equation 4.122)

Once the algorithm has reached convergence, the state of flow of the program moves to update the state and internal variables and to compute the composite stress.

The first update to be done is the one that belongs to the constituent level. The state variable would be the stress that is needed to compose the composite stress. The strain and damage internal variable can be perceived as internal variables – one for the damage model and the second for the SPROM theory – since what is really needed to be stored is the history of the serial strain of the matrix phase. Recall that the serial deformation of matrix phase was the unknown that was used to minimise the stress residual for the serial projection.

$$\begin{gathered}\varepsilon_{s,i}(t+\Delta t) = \varepsilon_{s,i}|_k \quad , \quad \beta_{r_{s,i}}(t+\Delta t) = \beta_{r_{s,i}}\Big|_k \quad , \quad d_{s,i}(t+\Delta t) = d_{s,i}|_k \\ \sigma_{s,i}(t+\Delta t) = \sigma_{s,i}|_k \, \forall i \in m, f\end{gathered} \tag{4.121}$$

This would represent the "5)" step in algorithm 3 and the "6)" step is the retrieve of the stress state at the composite level.

$$\sigma_s(t+\Delta t) = \Phi_{\Omega m}\sigma_{s,m}(t+\Delta t) + \Phi_{\Omega f}\sigma_{s,f}(t+\Delta t) \tag{4.122}$$

4.3.3 Modelling the effect of fire

The thermo-mechanical analysis takes into account the effects of the temperature on the mechanical response of the structures. The following assumptions are considered:

1. Thermal → Mechanical

   The thermal model is used to obtain the through-thickness temperature, it solves the one-dimensional transient model posed by Henderson et al., and this is introduced as a state variable to the thermo-mechanical model.

   A priori, one of the most sensical effects that have temperature over a solid is the so-called dilation or thermal expansion. Metals present a higher thermal expansion coefficient than composites, and thus, the dilation is higher.

   The expansion of the material point is considered in either the linear or non-linear regime of a material. However, it is interesting to note that for non-linear processes such as damage – inelastic behaviour – the theory proposed in the mechanical chapter, the so-called *isotropic damage model* by Simo and Ju, does consider that the thermal dissipation was null.

   Chaves in [266] introduces the Classius-Planck-Duhem inequality. This certainly was skipped in the mechanical chapter in order to avoid overloading the reader with non-mechanical information. The inequality is best described as

$$\Pi_D = \sigma : \varepsilon - \hat{c}\left(\frac{\mathrm{d}T}{\mathrm{d}t}\right) - \Pi_{HE} \geq 0 \tag{4.123}$$

   Equation 4.123 shows that there is a term that depends on the rate of temperature. The general approach for constitutive damage models in mechanical applications, where the temperature of a system does not change, is to assume that the rate is zero.

   On a thermo-mechanical model, this assumption is no longer true. This raises a special warning that needs to be discussed to properly address this problem.

   This term that appears in the dissipation inequality is related to the rate of change in temperature. The best way to illustrate this term is to use the analogy of a rubber band that is stretched. This rubber band, when stretched, especially when stretched largely and rapidly, raises the temperature of the zone that has stretched the most.

   Therefore, excessive stretch can generate a change in the temperature field in the material domain. Subsequently, this temperature change can lead into heat loss by releasing it to the surrounding. This means that heat originated from deformation, particularly deformations that are significant over the yielding band, can be lost or dissipated. Being this term, an effective thermo-mechanical mechanism of dissipating energy.

   Consider then two scenarios that would render this term negligible. The first would be that the rate of change of temperature would be significantly smaller. Imagine the term could be modelled as

$$\hat{c}\left(\frac{\mathrm{d}T}{\mathrm{d}t}\right) = \hat{c}_1 \frac{\mathrm{d}T}{\mathrm{d}t} \tag{4.124}$$

Depending on the value of the coefficient that multiplies the rate of temperature, the thermodynamic process can be considered almost isothermal. In these scenarios, this is a factual argument to consider the term negligible. However, this is uncertain unless it can be measured for the material and structure thermal term from experimentation.

Nevertheless, this discussion renders it unnecessary when considering the next argument. Considering a thermo-mechanical analysis, which is solved in the standard step-wise manner, if the increment of time is significantly higher than the increment of temperature, the dissipation due to the rate of change of temperature can be negligible ($\Delta T << \Delta t$). So this argument can be used as the main hypothesis. There is an extra layer to add to this argument, however it will be unveiled after all the different casuistic are revealed.

2. Mechanical $\rightarrow$ Thermal

   It seems feasible that in nature, if the ideal physics are postulated, not only the effect of a state variable such as temperature can have an impact on another such as the displacement.

   It may be arguable that the self-deformation of a structure introduces changes in the thermal constitutive laws. This can be perceived as simply that the convection boundary conditions of the thermal model may change or that significant deformations may lead to a change of the nominal cross-section, thus modifying heat transfer mechanisms such as the conduction.

   The argument then revolves around the idea if this is generally a good idea to take into account or not. In engineering, thermo-mechanical problems, are generally solved with a one-way coupling and thus this second order effect is not generally taken into account. Composites are flexible and this may indeed introduce certain modification on how the convection is perceived in the structure, when the structure undergoes large deformation, however, this flexibility is not so significant that it could argued that large displacements and large deformations are effectively changing the thermal characteristics of the structured in question.

Therefore, from the beginning the thermo-mechanical problem is postulated in the following manner:

$$\begin{bmatrix} \hat{c}_{11} & \hat{c}_{12} \\ \hat{c}_{21} & \hat{c}_{22} \end{bmatrix} \begin{bmatrix} T \\ u \end{bmatrix} = \begin{bmatrix} \hat{c}_T \\ \hat{c}_u \end{bmatrix} \tag{4.125}$$

As usual, the notation $\hat{c}$ is used to describe some arbitrary coefficient. Equation 4.125 represents the coupling of a system of equations that depend on two state variables – temperature (T) and displacement (u) – and the system to solve is the standard system with the left-hand side (l.h.s.) matrix and the right-hand side (r.h.s.) vector. The state variables can be represented as absolute or in an incremental manner, and then the r.h.s. becomes the residuals as usual.

What has been assumed is that the system is one-way coupled, being the temperature decoupled from the displacement.

$$\begin{bmatrix} \hat{c}_{11} & 0 \\ \hat{c}_{21} & \hat{c}_{22} \end{bmatrix} \begin{bmatrix} T \\ u \end{bmatrix} = \begin{bmatrix} \hat{c}_T \\ \hat{c}_u \end{bmatrix} \tag{4.126}$$

4.3.3.1 Effects on each constituent phase

If the decoupled system in Equation 4.126 is analysed from the point of view of the constituent materials, the meaning of the off-diagonal term has to represent the effects from fire that have a repercussion on every single phase (see Figure 4.29).

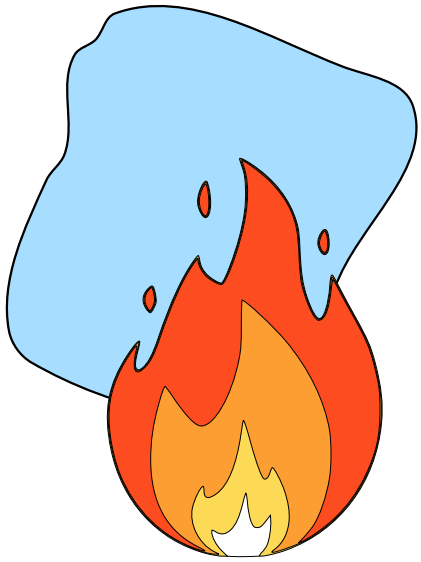

FIGURE 4.29: Illustration of part 3, the effect of fire on homogeneous materials.

The interest now relies on the determination of what is the physical meaning of $\hat{c}_{21}$. From the assumptions, there are two effects to take into account, thermal expansion and thermal dissipation. The following paragraphs contain a description of the thermal expansion and how this is introduced in the constitutive model, and then the thermal dissipation effects are taken into account. The proposed constitutive models deal with two conditions, one is the loss of mechanical response of the constituent materials and the other is a thorough discussion on the subject of *thermal-induced* mechanical damage.

4.3.3.1.1 Thermal expansion

The off-diagonal coefficient, $\hat{c}_{21}$, represents these two effects, the thermal expansion usually can be introduced in any mechanical model by means of defining the total strain in function of the mechanical strain and thermal strain.

$$\varepsilon_{\text{total}} = \varepsilon_{\text{mechanical}} + \varepsilon_{\text{thermal}} \tag{4.127}$$

So the mechanical strain is simply the subtraction between the total and the thermal strains.

$$\varepsilon_{\text{mechanical}} \equiv \varepsilon = \varepsilon_{\text{total}} - \varepsilon_T \tag{4.128}$$

where ε_T is equivalent to the thermal strain.

From Equation 4.126, the problem in the mechanical part is solved step-wise, i.e., the incremental of displacement is obtained. This displacement is the total displacement indeed. And the total strain can be calculated by the derivation of this with respect to the position field.

The other unknown, to find the mechanical strain, would be the thermal strain.

$$\varepsilon_T = \alpha \Delta T \quad , \quad \Delta T\left(\Omega, t\right) = T\left(\Omega, t\right) - T\left(\Omega, t = 0\right) = T - T_0 \tag{4.129}$$

Once the mechanical strain has been obtained, the model in chapter 4, would be used to solve the displacements of the system. Note that the displacements are referred to as *total* and to avoid any confusion, what is done, at the mechanical level, is to subtract the thermal expansion in order to obtain the effective mechanical strain used in the evaluation of the constitutive model.

Considering that the strain is the mechanical or effective, some warnings are raised regarding one of the previous assumptions. Remember that previously, it was mentioned that having an increment of time bigger than the increment of temperature would satisfactorily avoid the thermal losses in the dissipation laws used to derive the isotropic damage model.

This assumption is true, however, that would not account for the real reason behind neglecting the dissipation generated from a thermal process. The argument is somehow simpler, consider that a fully developed fire has a temperature (hot end prescribed boundary), that is around 1000°C, an internal change in the temperature in the order of 1, 10 or even 100 would not account even in a 10% of the total change of the temperature.

This means that the effect of the thermal expansion is much more important than the elastic losses due to internal thermal processes at a material point. Because of this, the non-linear mechanical model, the isotropic damage model, is not modified. At least, regarding the consideration of effects due to the thermal dissipation term in the Classius-Planck-Duhem inequality.

4.3.3.1.2 Loss of mechanical properties

The off-diagonal term, the one that couples the thermal problem with the mechanical one, in Equation 4.126 should contain all the linear dependencies with respect to the temperature.

Until this point, the FEM solution proposed was subjected to the discussion, analysing the generalities of what has to be considered and what can be neglected. However,

there are some important considerations to be made regarding the mechanical properties of the constituent phases because empirical observations have already confirmed that temperature plays a key role in the degradation of effective mechanical properties.

This effect is very natural in metals, e.g., steel reduces significantly its effective structural stiffness when heated. One of the advantages of metals like steel is that the effective loss of structural stiffness is produced at temperatures that surpass easily the 600°C. The other advantage is that, although heating produces some changes in the micro-structure, the properties of steel can be recovered when cooled if no substantial changes have been produced in the crystalline structure of the material.

Composites are a different topic because they burn, or more academically, they undergo thermo-chemical degradation processes that fit under the pyrolysis effect. These effects were detailed in the chapter devoted to the thermal model, and it was concluded that when the composite is deprived of the heat source that is causing the thermo-chemical degradation of the polymeric matrix, the induced damage is due to pyrolysis is irreversible.

Structurally, composites that have pyrolysed, do not recover their virgin structural stiffness and this is one of the main flaws in post-fire design. Composite structures focus on avoiding pyrolysis at all costs, since the generation of it is irreversible.

Many efforts have been directed to the understanding of how composite materials lose their effective mechanical properties. In this thesis, and widely accepted in the scientific community, the main two mechanical quantities of interest are Young's modulus (E) and yielding stress (σ_y).

One of the most realistic and extended methods to quantify the loss of properties in composites was introduced by Mouritz and Gibson, and it is collected in the book [20]. This model includes both temperature and pyrolysis fraction, and it proves to be interesting in modelling metals when no pyrolysis effect is considered.

$$P\left(T,F\right)=\left(\frac{P_r+P_u}{2}-\frac{P_r-P_u}{2}\tanh\left(n_{\text{MG1}}\left(T-T_g\right)\right)\right)F^{n_{\text{MG2}}} \tag{4.130}$$

where P is the Mouritz-Gibson generic property, T_g is the glass transition temperature, n_{MG1} is the Mouritz-Gibson coefficient 1, n_{MG2} is the Mouritz-Gibson coefficient 2, P_r is the Mouritz-Gibson relaxed property and P_u is the Mouritz-Gibson unrelaxed property.

The generic property described in Equation 4.130 could be any of the desired mechanical properties. The two quantities generally described by Equation 4.130 are Young's modulus and yield stress [276].

The evolution law in Equation 4.130 introduces the concept of the glass transition temperature, this is a temperature where the material transitions from a solid state to a viscous/glass state. This is a point is of extreme interest since the loss of properties is abrupt in arriving at this temperature.

Figure 4.30 shows how the different parameters, in Equation 4.130, affect the evolution of the mechanical property. Note how detrimental is the glass temperature and how abruptly the loss becomes after the material reaches the glass temperature.

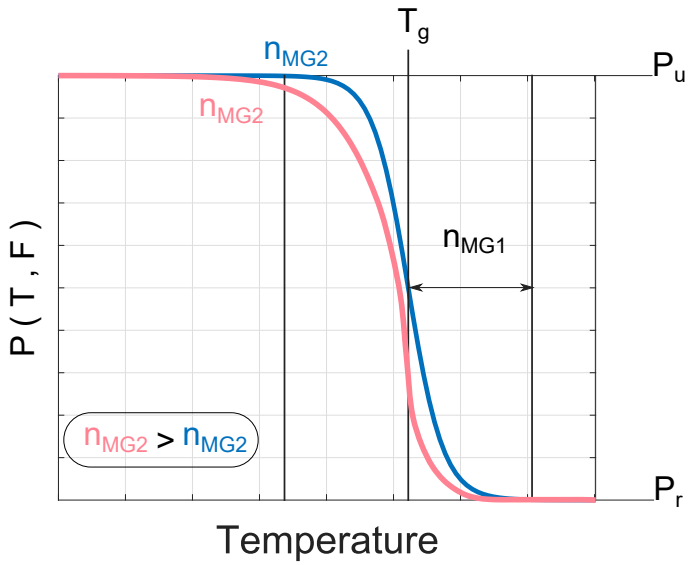

FIGURE 4.30: Mouritz-Gibson degradation function illustrated.

The pyrolysis fraction (F) in Figure 4.30 was assumed to be one, if pyrolysis is generated in the structure, the intact properties cannot be recovered. This is of importance because even if the temperature is not close to the glass temperature, the structure can rapidly fail if the pyrolysis index is close to zero. Recall that in Equation 4.130, the degradation function was implemented at the constituent level. I.e., there is an evolution law for the matrix and one for the fibre. Matrix and fibre have different evolution laws.

4.3.3.1.3 Damaged induced by temperature

The discussion about the importance of neglecting the thermal dissipation in the Classius-Planck-Duhem has been settled, the sensical was to assume that the thermal dissipation is of less importance to the overall dissipation in comparison to the induced thermal strains. However, the correction introduced for the loss of elastic properties introduces several conflicts with the current mechanical formulation. The isotropic damage model has to be extended to include the temperature as a state variable.

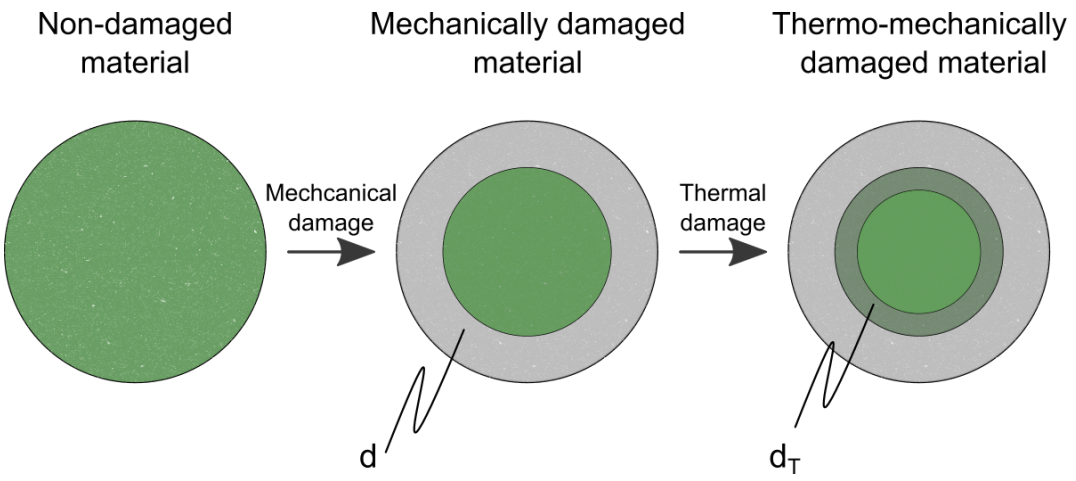

FIGURE 4.31: Explanation of the origination of thermo-mechanical damage due to temperature.

A detailed explanation of the changes needed to be introduced in the damage model can be found in the thesis of Di Capua [277]. A summary of the process described in Figure 4.31 is given in the following paragraphs.

The constitutive equations described in Equation 4.20 can be formulated such as

$$\underset{\sim\sim}{\sigma_i} = (1 - d_i)\, \underset{\sim\sim\sim\sim}{D_i} : \left(\underset{\sim\sim}{\varepsilon_{\text{total},i}} - \underset{\sim\sim}{\varepsilon_{T,i}}\right) \quad \forall i \in m, f \tag{4.131}$$

Equation 4.131 is very meaningful as it is describing the secant constitutive tensor that is the compound of the elastic tensor and the damage index. The previous subsection, Equation 4.130, introduced a thermo-chemical degradation for Young's modulus and the yielding stress.

$$\underset{\sim\sim\sim\sim}{D_i}\left(E_i\left(T, F_i\right), \nu\right) \quad \forall i \in m, f \tag{4.132}$$

$$d_i\left(\sigma_{y_i}\left(T, F_i\right)\right) \quad \forall i \in m, f \tag{4.133}$$

This set of equations established that both the damage and the elastic constitutive tensor have a dependency on the temperature and the pyrolysis. This is because Young's modulus and the yield stress depend on the thermal model. The Poisson ratio is considered to not be affected by the thermo-chemical processes in the media.

This dependence introduces some potential conflicts when considering the energy norms. Take for example the most complete norm, the non-symmetrical norm, in Equation 4.48 by including the potential effects of temperature and pyrolysis.

$$\mathbb{T}_{\sigma III} = \left(c_{CF} + \frac{1 - c_{CF}}{c_{CR}}\right) \sqrt{\underset{\sim\sim}{\sigma}(T, F) : \left(\underset{\sim\sim\sim\sim}{D_{\text{elast}}}\right)^{-1} : \underset{\sim\sim}{\sigma}(T, F)} \tag{4.134}$$

When Equation 4.134 is expressed like this, it becomes difficult to analyse. In the work of Cervera et al. [278], a normalised equivalent can be introduced by normalising it with respect to the internal variable.

$$\beta_r = \frac{\sigma_y(T,F)}{\sqrt{E(T,F)}} \tag{4.135}$$

And therefore Equation 4.134 yields

$$\mathbb{r}_{\sigma III} = \left(c_{CF} + \frac{1-c_{CF}}{c_{CR}}\right)\sqrt{E(T,F)}\sqrt{\frac{\underset{\sim}{\sigma}(T,F)}{\sigma_y(T,F)} : \left(\underset{\sim\sim}{D}_{\text{elast}}\right)^{-1} : \frac{\underset{\sim}{\sigma}(T,F)}{\sigma_y(T,F)}} \tag{4.136}$$

This equation is simpler to analyse. Start by the scenario where Young's modulus degrades, the material has already generated a certain level of damage. The norm before this thermal degradation had a certain damage threshold. The question is what would happen to this norm if only Young's modulus was degraded?

$$E(T,F,t+\Delta t) < E(T,F,t) \longrightarrow \mathbb{r}_{\sigma III}(t+\Delta t) < \mathbb{r}_{\sigma III}(t) \tag{4.137}$$

Analysing the term where Young's modulus is involved, the normalised Equation 4.139 can be used to discuss the reduction of the threshold and this is incompatible with its historic evolution which can not be reduced. A threshold that can reduce is clearly a sign of healing, which is a reversible process and non-present on standard marine composites.

Consequently, the norm has to be evaluated with the virgin Young's modulus. This leaves the last question open to what happens with the decrease of the yielding stress by assuming that Young's modulus is constant.

$$\sigma_y(T,F,t+\Delta t) < \sigma_y(T,F,t) \longrightarrow \mathbb{r}_{\sigma III}(t+\Delta t) > \mathbb{r}_{\sigma III}(t) \tag{4.138}$$

In that scenario, when the yield stress decreases, the norm increases. I.e., the effective damage increases. It is sensical, given a structure that is enduring a given load, e.g. in the elastic regime, if the elastic limit is reduced due to the increase of temperature. If the elastic limit decreases below the given load, damage should occur.

The other aspect to be commented on is the fact that also the stress depends on the temperature because the stress depends on Young's modulus. Depending on which of the two – Young's modulus or yield stress – decreases quicker, the damage may be increased or remain equal.

The norm is then formulated taking into account the discussion made previously and normalised.

$$\mathbb{T}_{\sigma III} = \left(c_{CF} + \frac{1 - c_{CF}}{c_{CR}} \right) \sqrt{E_0} \sqrt{\frac{\underset{\sim}{\sigma}(T,F)}{\sigma_y(T,F)} : \left(\underset{\sim\sim}{D}_{\text{elast}} \right)^{-1} : \frac{\underset{\sim}{\sigma}(T,F)}{\sigma_y(T,F)}} \tag{4.139}$$

Note that despite it has not specifically addressed, the constitutive tensor is the virgin elastic one. There is only one last constraint that is needed to be modified from the standard isotropic damage model. This arises from the *fracture energy*, it is very uncertain or at least difficult to characterise the evolution of the energy of fracture with respect to the temperature.

The same approach from [277] is employed. The basic idea behind this approach is to maintain a constant slope or pre-exponential factor. This is exemplified by the expressions found in Equation 4.53 and Equation 4.57. The problem is that if not constrained, the slope can become negative or singular. Therefore, in both exponential and linear cases, the following constraint is imposed

$$\frac{\Pi_F}{\beta_{r_0}^2} = \frac{\Pi_F E(T,F)}{\left(\sigma_y(T,F)\right)^2} \tag{4.140}$$

where the initial internal variable for damage (β_{r_0}) is a constant value set at the beginning of the analysis. Therefore, the r.h.s. becomes constant as well. In this way, the temperature and pyrolysis dependence is erased for any given pair of values of the elastic modulus and elastic limit.

4.3.3.2 Effects on the composite

If the effects of fire on the constituent materials are already studied, the only side-effects of temperature and degradation are at the composite level (see Figure 4.32). One effect, potentially fictitious, originates from the real limitation of the model, the impossibility to determine the loss of mechanical properties of each constituent material, fibre and matrix, separately. Therefore, a solution to this problem needs to be addressed.

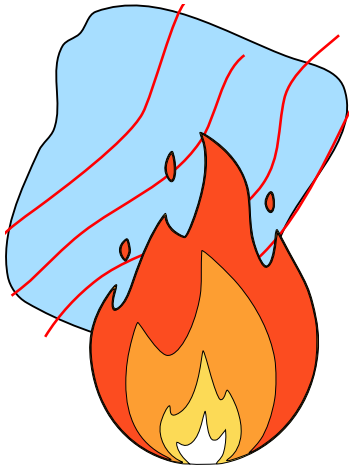

FIGURE 4.32: Illustration of part 3, the effect of fire on heterogeneous materials.

The other effect, which is a real one, is the adaptation of the current SPROM in order to take into account the effect of thermal expansion of the constituent phases. This adaptation is an original contribution and a detrimental part of the theory presented in this thesis, the name assigned to this theory is *thermal serial-parallel rule of mixtures* or in short TSPROM.

4.3.3.2.1 Loss of the mechanical properties of the whole composite

Equation 4.130 is one of the best models from the current paradigm to analyse the degradation of composites, however, it is inconvenient because it is employed at the composite level.

This is in direct conflict with the formulation proposed in this thesis, a formulation that analyses the thermo-mechanical problem with a micro-macro scale approach. Since both phases, fibre and matrix, present different laws of evolution under degradation, the composite should be formed by the composition of both.

This is not a linear combination and with the current techniques, it would require an extensive experimental campaign to characterise the fibre, the matrix and the composite. This campaign should be centred around calibrating the materials for different volumetric participation, fibre orientation, layer configurations or direction and magnitude of the strength at which the specimen is loaded. This is without mentioning the difficulties of calibrating the fibre properties experimentally, e.g., fibres present non-symmetric mechanical response to axial loading.

The standard procedure is to characterise this loss of elastic performance by experimenting with the composite. This renders the solution with much fewer unknown variables, however it is incompatible with the micro-scale formulation proposed.

In order to provide a theory that contemplates the micro-scale degradation, the following shall be assumed: in the absence of experimental data on each constituent material and with only the composite data gathered, the following constituent-to-composite relationships shall be fulfilled

$$\frac{P_{rc}}{P_{rc}} = \frac{P_{rm}}{P_{rm}} = \frac{P_{rf}}{P_{rf}} \tag{4.141}$$

$$n_{\mathrm{MG1}c} = n_{\mathrm{MG1}m} = n_{\mathrm{MG1}f} \tag{4.142}$$

$$n_{\mathrm{MG2}c} = n_{\mathrm{MG2}m} = n_{\mathrm{MG2}f} \tag{4.143}$$

The set of three equations constrain the evolution of both fibre and matrix in a manner that the evolution of matrix, fibre and composite shall be the same. I.e., these assumptions are an attempt to enforce the composite evolution onto the evolution of the constituent phases.

Nevertheless, note that in the case the experimental data of the constituent materials is given, the evolution shall not fulfil these relationships.

4.3.3.2.2 The thermal serial-parallel rule of mixtures

Although the mechanical strain was corrected in Equation 4.128, the SPROM algorithm needs to be reformulated using the same approach. The procedure will follow the same steps as the mechanical model, particularly the definition given in paragraph 4.3.2.3.5 and onward. Since the procedures are chronologically similar to those explained in the mechanical chapter, it will be briefly discussed in order to avoid redundancy.

The differential calculus, equivalent to the incremental form with the applied numerical scheme, is derived for stress.

$$\underset{\bullet\bullet}{\mathrm{d}\sigma_i} = \underset{\bullet\bullet\bullet\bullet}{D_{\tan i}} : \left(\underset{\bullet\bullet}{\mathrm{d}\varepsilon_{\text{total},i}} - \underset{\bullet\bullet}{\mathrm{d}\varepsilon_{T,i}} \right) \quad \forall i \in m, f \tag{4.144}$$

Now the serial and parallel differential of stresses can be postulated like previously in Equation 4.93.

$$\begin{bmatrix} \underset{\bullet\bullet}{\mathrm{d}\sigma_{p,i}} \\ \underset{\bullet\bullet}{\mathrm{d}\sigma_{s,i}} \end{bmatrix} = \begin{bmatrix} \underset{\bullet\bullet\bullet\bullet}{D_{pp,i}} & \underset{\bullet\bullet\bullet\bullet}{D_{ps,i}} \\ \underset{\bullet\bullet\bullet\bullet}{D_{sp,i}} & \underset{\bullet\bullet\bullet\bullet}{D_{ss,i}} \end{bmatrix} : \begin{bmatrix} \underset{\bullet\bullet}{\mathrm{d}\varepsilon_{\text{total},p,i}} - \underset{\bullet\bullet}{\mathrm{d}\varepsilon_{T,p,i}} \\ \underset{\bullet\bullet}{\mathrm{d}\varepsilon_{\text{total},s,i}} - \underset{\bullet\bullet}{\mathrm{d}\varepsilon_{T,s,i}} \end{bmatrix} \quad \forall i \in m, f \tag{4.145}$$

Note these are the constituent constitutive relationships for the i-th phase. The following procedures are exactly the same as defined in the mechanical chapter. There are going to be skipped to avoid extra text.

4.3.3.2.3 Initial approximation of the unknown

Similarly to the mechanical chapter, in the serial direction, the stresses have to be equal. This means, $\Delta\sigma_{s,m} = \Delta\sigma_{s,m}$, which is the iso-stress hypothesis.

By combining the iso-stress hypothesis with Equation 4.144 and Equation 4.145, the differential/incremental of the serial strain for the matrix can be used. This new expression diverges from Equation 4.106 by including the thermal expansion effects of both constituent phases.

$$\begin{aligned}
\underset{\sim\sim}{\mathrm{d}\varepsilon}_s \approx \underset{\sim\sim}{\Delta\varepsilon}_s &= \underset{\sim\sim}{\varepsilon}_s(t+\Delta t) - \underset{\sim\sim}{\varepsilon}_s(t) = \underset{\sim\sim}{\varepsilon}_s\Big|_{k+1} - \underset{\sim\sim}{\varepsilon}_s\Big|_k \\
\underset{\sim\sim}{\mathrm{d}\varepsilon}_p \approx \underset{\sim\sim}{\Delta\varepsilon}_p &= \underset{\sim\sim}{\varepsilon}_p(t+\Delta t) - \underset{\sim\sim}{\varepsilon}_p(t) = \underset{\sim\sim}{\varepsilon}_p\Big|_{k+1} - \underset{\sim\sim}{\varepsilon}_p\Big|_k
\end{aligned}$$

$$\begin{aligned}
\underset{\sim\sim}{\Delta\varepsilon}_{s,m} &= \underset{\sim\sim\sim\sim}{\hat{c}} : \left(\underset{\sim\sim\sim\sim}{D}_{ss,f} : \underset{\sim\sim}{\Delta\varepsilon}_s + \Phi_{\Omega f} \left(\underset{\sim\sim\sim\sim}{D}_{sp,f} - \underset{\sim\sim\sim\sim}{D}_{sp,m} \right) : \underset{\sim\sim}{\Delta\varepsilon}_p + \Phi_{\Omega f} \underset{\sim\sim}{\Delta\sigma}_{T,m} - \Phi_{\Omega m} \underset{\sim\sim}{\Delta\sigma}_{T,f} \right) \\
\underset{\sim\sim}{\Delta\varepsilon}_{s,f} &= \underset{\sim\sim\sim\sim}{\hat{c}} : \left(\underset{\sim\sim\sim\sim}{D}_{ss,m} : \underset{\sim\sim}{\Delta\varepsilon}_s + \Phi_{\Omega m} \left(\underset{\sim\sim\sim\sim}{D}_{sp,m} - \underset{\sim\sim\sim\sim}{D}_{sp,f} \right) : \Delta\varepsilon_p + \Phi_{\Omega m} \underset{\sim\sim}{\Delta\sigma}_{T,f} - \Phi_{\Omega f} \underset{\sim\sim}{\Delta\sigma}_{T,m} \right)
\end{aligned}$$

$$\underset{\sim\sim\sim\sim}{\hat{c}} = \left(\Phi_{\Omega f} \underset{\sim\sim\sim\sim}{D}_{ss,m} + \Phi_{\Omega m} \underset{\sim\sim\sim\sim}{D}_{ss,f} \right)^{-1}$$

$$\underset{\sim\sim}{\Delta\sigma}_{T,m} = \underset{\sim\sim\sim\sim}{D}_{sp,m} : \underset{\sim\sim}{\Delta\varepsilon}_{T,p,m} + \underset{\sim\sim\sim\sim}{D}_{ss,m} : \underset{\sim\sim}{\Delta\varepsilon}_{T,s,m}$$

$$\underset{\sim\sim}{\Delta\sigma}_{T,f} = \underset{\sim\sim\sim\sim}{D}_{sp,f} : \underset{\sim\sim}{\Delta\varepsilon}_{T,p,f} + \underset{\sim\sim\sim\sim}{D}_{ss,f} : \underset{\sim\sim}{\Delta\varepsilon}_{T,s,f} \tag{4.146}$$

This is the last change introduced into the standard SPROM theory from Rastellini et al. [15]. With the inclusion of the terms $\Delta\sigma_{T,m}, \Delta\sigma_{T,f}$, the SPROM is modified to incorporate the thermal expansion.

The formulation hereby is coined as the *thermal serial-parallel rules of mixtures* (TSPROM). The algorithm 3 maintains its structure, however in the first step, Equation 4.106 is replaced by Equation 4.146 instead. The other significant change is to use the proper definition of the mechanical strain defined in Equation 4.128.

4.4 Conclusions

This chapter has described the elastic equation from a continuum mechanics point of view. It was divided in three parts and the different goals set during the literature research of the mechanical model were met. First, the micro-scale approach where the mechanics of the *constituent* phases were introduced. The second part was devoted to the micro-macro scale interaction or *homogenisation* technique. And the third and last part described the effects that fire has on the previous two parts.

A detailed introduction to damage mechanics was given for the constitutive models of the constituent materials. The model chosen was the *isotropic damage model*, this model was described for both linear and exponential hardening/softening laws and with the capability of using symmetric, tension-only or non-symmetric norms. In all, this only fulfils the goal at the micro-structure level.

At the composite level, a suitable constituent-to-composite model has been derived. It starts with a linear model represented by orthotropic theory and later the *classical mixing theory* was introduced. However, the chosen solution for the model is the *serial-parallel rule of mixtures*, which can be simplified to the *classical mixing theory* again by assuming an iso-strain hypothesis in all directions. The chapter concludes with algorithm of the serial-parallel rule of mixtures.

By combining the non-linear constitutive model for the constituent materials with the constituent-to-composite model, the goal of providing a suitable non-linear constitutive model for composites is achieved.

The effects of fire started with a brief discussion regarding the unnecessary inclusion of the rate of change of temperature in the Classius-Planck-Duhem inequality. The argument provided is based on the fact that the thermal dissipation is significantly lower than the induced thermal strains.

Then, the degradation of mechanical properties with respect to temperature and pyrolysis was addressed in two parts. First, at the constituent level, the Mouritz and Gibson formulation was introduced and discussed. Then the concerns regarding how feasible it is to model the degradation of fibre and matrix separately were discussed.

The key point is that in reality it is much more costly to quantify the degradation of both fibre and matrix, plus the composite. It is more logical to obtain the degradation of the composite. Several problems arise due to this simplification and these are dicussed.

In order to overcome this issue, there is an elaborated discussion on how to infer the mechanical degradation of the composite to the constituent phases. The proposed method was developed in the absence of experimental data for the fibre and matrix phases. The main objective of this thesis revolves around the idea of proposing a suitable micro-macro approach and solve the problem from the constituent perspective, therefore the method proposed seems the most sensical.

The choice in employing the isotropic damage model introduces certain limitations that have been analysed. In particular, the proposed solution is based on a similar solution for concrete structures. The choice to modify the norms by normalisation

has been proven to be the best solution after a detailed discussion on how the norm would evolve based on different fire scenarios.

The other important problem discussed was the consistency with respect to the energy of the fracture. From chapter 4, some limitations were introduced for the softening of composite materials. These limitations try to avoid unrealistic softening. Since the internal variable depends on both Young's modulus and the yield stress, which in turn depend on the temperature and pyrolysis, a constraint is imposed on the mechanical formulation in order to avoid any strange behaviour.

The penultimate part of this section deals with the changes necessary to modify the SPROM algorithm to introduce the effects of thermal expansion. This thesis enhances the current formulation of the SPROM to include the thermal effects, and thus, is renamed to TSPROM. The TSPROM is a formulation especially developed to predict the composite behaviour under high-temperature, while taking into account inelastic effects and thermo-chemo-mechanical degradation.

Finally, the need to provide an algorithm for this chapter has been met by the attachment of the non-linear thermo-mechanical coupling found in algorithm 4. This algorithm meets with all the necessities to analyse a non-linear thermo-mechanical problem for composites.

4.4.1 Goals

The goals imposed in chapter 1 are fulfilled. The goal number 4, *Implement the isotropic damage formulation*, is fulfilled by the isotropic damage model proposed in combination with the constituent-to-composite formulation used, defined as the SPROM formulation. The goal number 5, *Implement the SPROM formulation*, is a very specific implementation since to provide a damage model for the composite the SPROM formulation is needed.

Therefore, the thermo-mechanical modification to the problem is also fulfilled by satisfying goal number 8, *Provide and implement a methodology to incorporate the thermal dependence on mechanical properties*, goal number 9, *Provide and implement a correction to the damage theory to be coherent with the thermal effects* and goal number 10, *Provide and implement an enhanced version of the SPROM. The TSPROM*.

Chapter 5

Laminated thermo-mechanical coupling of marine structures exposed to high temperature

5.1 Introduction

The strain-displacement transformation tensor has different representations depending on the type of element used in the discretisation of the problem. In this thesis, for shells, two elements based on the known *Discrete Kirchhoff Triangle (DKT)* and *Linear Shear Quadrilateral (QLLL)* are derived according to the theory described by Oñate in [16] that introduces a decoupled version of these elements in order to take into account membrane, bending and, if allowed, shear effects. These two elements are described in their matrix representation in the following subsection, recall that these elements are linear or in other words, they do comply with linear elasticity.

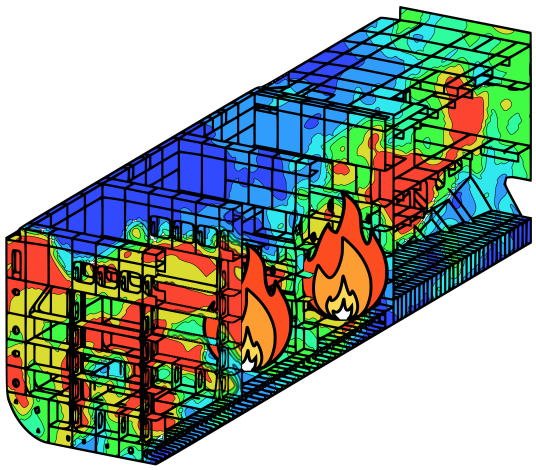

FIGURE 5.1: Representation of a thermo-mechanical analysis on a ship structure.

5.2 Justification for the paradigm and methodology

The choice of the type of elements found in this chapter is indirectly conditioned by the chapter 4. This chapter is devoted to the coupling of the thermo-mechanical model for laminates and the thermal model. However, there are still missing some minor holes in the formulation presented until this point, this missing information is the related to the kinematics of the elements selected (triangle and quadrilateral).

In the maritime industry, the use of quadrilateral is more extended because this type of element predicts better the stress distribution. However, triangles are far easier to be used in terms of meshing and certain formulations such as the *drilling rotations* formulation [124] by Felippa can be used to enhance this element and to obtain a better prediction for the stress field.

In the assembling of the system of equations, the role of the TSPROM is very interesting. The TSPROM by nature mimics the behaviour of a black box. This means that it does not modify substantially the assembling process of the finite element method. There is a more obscure justification, on purpose neglected previously, for the selection of this algorithm over other non-linear laminated constitutive models, and this finds its answer in the concept of flexibility of composites.

Most composites are very flexible when used in the design of structures. Marine applications are not an exception, and thus a theory that can incorporate large deformations is highly encouraged. Previously, a discussion on the justification on which type of element – quadrilateral or triangle – was better to be implemented, stated that the quadrilateral element was better provided that most of the International Association of Classification Societies (IACS) recommend performing these calculations using quadrilaterals and this is a major reason on why to implement a laminate quadrilateral shell.

However, there is an excellent justification for implementing a triangle formulation as well. It was discussed that Felippa provided a framework to enhance the stress prediction of the classical constant strain triangle described in [16]. Felippa and Haugen also provide the theory to extend the linear geometric formulation into non-linear geometric. This is the so-called co-rotational theory, and it is useful because it provides a method to enhance the standard triangle used in his previous work [124] to account for large deformations and displacements.

The justification of implementing the triangle is partially back up by this reason, nevertheless, there is another crucial reason and that is that the co-rotational formulation combines very well with the SPROM. Since both theories do not clash, the co-rotational models the non-linear geometric kinematics from the local-to-global transformation matrix and the SPROM obtains the non-linear composite constitutive model by applying the SPROM algorithm to the constituent constitutive matrices. This second argument is the most important in choosing the co-rotational theory to model large deformations that are very characteristic of composite materials.

5.3 Methodology

Before delving into the specific formulations of both elements, the displacement and strain tensor are presented for a three-dimensional shell element. Note that depending on the element, quadrilateral or triangle, some of the components of the tensor fields may be neglected.

The displacement of a three-dimensional solid can be expressed from a reference axis defined by (x_1, x_2, x_3). Therefore the displacement field should be a three-dimensional vector and the strain, which is the gradient of the displacement, a 3×3 matrix.

$$\underline{u} = \begin{bmatrix} u_1 \\ u_2 \\ u_3 \end{bmatrix}, \quad \underline{\underline{\varepsilon}} = \begin{bmatrix} \varepsilon_{11} & \varepsilon_{12} & \varepsilon_{13} \\ \varepsilon_{21} & \varepsilon_{22} & \varepsilon_{23} \\ \varepsilon_{31} & \varepsilon_{32} & \varepsilon_{33} \end{bmatrix} \equiv \begin{bmatrix} \varepsilon_1 & \varepsilon_{12} & \varepsilon_{13} \\ \varepsilon_{21} & \varepsilon_2 & \varepsilon_{23} \\ \varepsilon_{31} & \varepsilon_{32} & \varepsilon_3 \end{bmatrix} \tag{5.1}$$

Note how the diagonal strains are equivalent using the single or double subscript.

The strain can be further re-formulated in the so-called Voigt space notation, assuming that the strain is a symmetric tensor.

$$\underline{\varepsilon} = \begin{bmatrix} \varepsilon_{11} \\ \varepsilon_{21} \\ \varepsilon_{22} \\ \varepsilon_{31} \\ \varepsilon_{32} \\ \varepsilon_{33} \end{bmatrix} \tag{5.2}$$

And it is customary to use the so-called engineering notation where the shear strains are modified by the following relationship

$$\gamma_{ij} = 2\varepsilon_{ij}, \quad i \neq j \quad \Rightarrow \begin{bmatrix} \varepsilon_{11} \\ \varepsilon_{22} \\ \varepsilon_{33} \\ \gamma_{21} \\ \gamma_{31} \\ \gamma_{32} \end{bmatrix} \tag{5.3}$$

where γ is the shear strain. Moreover, this strain vector is the mechanical strain and this means that it contains the subtracted effects of thermal expansion, as mentioned in Equation 4.128. Therefore, assume that all the derivations in the following sections are concerning the mechanical strain and not the total strain.

5.3.1 Analysis of thin composite shell structures - triangles

The theory employed to describe the kinematics of thin shell structures is the so-called Kirchhoff-Love theory. The kinematics of the triangular shell element is the

result of the combination of a plate element based on the classical DKT element [262] and a membrane element based on the optimal triangle element with drilling rotations presented in [124]. The total number of degrees of freedom per node is six, three translations and three rotations.

The shell element in question is discretised thickness-wise, having a set of local axes systems (${}^{l}x_1, {}^{l}x_2, {}^{l}x_3$) being ${}^{l}x_3$ the local normal axis of the shell. The shell is discretised in a total of n-th number of layers (n_{layers}). A schematic of this shell element can be found in Figure 5.2

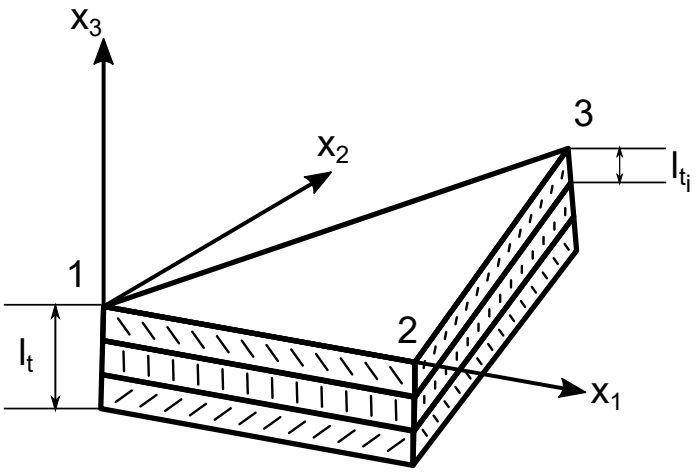

FIGURE 5.2: Local and global axes of the 3-node triangular shell element.

In this theory, several assumptions regarding the kinematics and stress distributions, are made:

1. There is no membrane displacement in the mid-plane.

$$u_1 = u_2 = 0 \quad , \quad x_3 = 0 \tag{5.4}$$

   The denomination 1 or 2 is equivalent to the directions x_1 and x_2 respectively. Therefore, the mid-plane can only displace in the out-of-plane direction.

2. There is no deformation in the out-of-plane direction, so the thickness cannot vary.

3. The normal stress is considered negligible.

$$\sigma_3 = 0 \quad , \quad x_3 \in [-\frac{l_t}{2}, \frac{l_t}{2}] \tag{5.5}$$

4. The in-plane deformation is considered linear and normal to the mid-plane, this is the so-called *normal orthogonality* condition.

5.3.1.1 Displacements

After describing the basic assumptions, the displacement field of the formulated problem is described as

$$\begin{cases} u_1(x_1, x_2, x_3) = -x_3\theta_1(x_1, x_2) & ,\forall x_1, \forall x_2, \forall x_3 \in \Omega \\ u_2(x_1, x_2, x_3) = -x_3\theta_2(x_1, x_2) & ,\forall x_1, \forall x_2, \forall x_3 \in \Omega \\ u_3(x_1, x_2, x_3) = u_3(x_1, x_2) & ,\forall x_1, \forall x_2, \forall x_3 \in \Omega \end{cases} \tag{5.6}$$

where θ is the rotation, x_1 is the x-axis and x_2 is the y-axis.

The rotations are directly defined in this theory as a linear slope due to the previous assumptions, and thus the following expressions are valid.

$$\begin{aligned} \theta_1 &= \frac{\partial u_3}{\partial x_1} \\ \theta_2 &= \frac{\partial u_3}{\partial x_2} \end{aligned} \tag{5.7}$$

The displacement field at any local point is there expressed as

$$\underline{u} = \begin{bmatrix} u_3 \\ \theta_1 \\ \theta_2 \end{bmatrix} \tag{5.8}$$

5.3.1.2 Deformation

Once the displacements are defined, the strains can be derived using the proper definitions from 3D elasticity. Note the relationship between the expression in Equation 5.18 and Equation 5.19.

$$\begin{aligned} \varepsilon_1 = \frac{\partial u_1}{\partial x_1} = -x_3\frac{\partial^2 u_3}{\partial x_1^2} \qquad & \varepsilon_{12} = \frac{\partial u_1}{\partial x_2} + \frac{\partial u_2}{\partial x_1} = 2\frac{\partial^2 u_3}{\partial x_1 \partial x_2} \\ \varepsilon_2 = \frac{\partial u_1}{\partial x_2} = -x_3\frac{\partial^2 u_3}{\partial x_2^2} \qquad & \varepsilon_{13} = \frac{\partial u_1}{\partial x_3} + \frac{\partial u_3}{\partial x_1} = 0 \\ \varepsilon_3 = 0 \qquad & \varepsilon_{23} = \frac{\partial u_2}{\partial x_3} + \frac{\partial u_3}{\partial x_2} = 0 \end{aligned} \tag{5.9}$$

The strain vector is rearranged with the non-zero components and, similarly to the constitutive model, the quantities are expressed using the stress-resultant notation defined by Oñate in [16]. The advantage of using this notation relies on the idea that the in-plane and bending strains are decoupled.

$$ {}^{l}\underline{\varepsilon} = {}^{l}\begin{bmatrix} \varepsilon_{11} \\ \varepsilon_{22} \\ \gamma_{21} \end{bmatrix} = \begin{bmatrix} 1 & 0 & 0 & -{}^{l}x_3 & 0 & 0 \\ 0 & 1 & 0 & 0 & -{}^{l}x_3 & 0 \\ 0 & 0 & 1 & 0 & 0 & -{}^{l}x_3 \end{bmatrix} {}^{l}\begin{bmatrix} \underline{\varepsilon_m} \\ \underline{\varepsilon_b} \end{bmatrix} = \underline{\underline{S}} \cdot {}^{l}\hat{\varepsilon} \tag{5.10} $$

where $\underline{\underline{S}}$ is the stress-resultant matrix. Note that the stress-resultant transformation matrix is defined for the Kirchhoff-Love theory, i.e., this matrix may be slightly different depending on the theory considered. Nevertheless, the matrix serves as some sort of transformation between the stress-resultant strain and the generalised strain.

The stress-resultant strain is the one that contains the membrane and bending strains and these two, for a shell formulation, are expressed in the following manner

$$ {}^{l}\varepsilon_m = {}^{l}\begin{bmatrix} \dfrac{\partial u_{1,0}}{\partial x_1} \\ \dfrac{\partial u_{2,0}}{\partial x_2} \\ \dfrac{\partial u_{1,0}}{\partial x_2} + \dfrac{\partial u_{2,0}}{\partial x_1} \end{bmatrix} \tag{5.11} $$

$$ {}^{l}\varepsilon_b = {}^{l}\begin{bmatrix} \dfrac{\partial \theta_1}{\partial x_1} \\ \dfrac{\partial \theta_2}{\partial x_2} \\ \dfrac{\partial \theta_1}{\partial x_2} + \dfrac{\partial \theta_2}{\partial x_1} \end{bmatrix} \tag{5.12} $$

The translational displacements are defined with respect to the middle plane of the shell. The zero-ish subscript denotes the initial displacements found in the middle-plane, where previously, they were neglected. By the strain-displacement nomenclature, if membrane effects are taken into account, the following relationship holds true

$$ \hat{u}_i = u_{i,0} \quad , \qquad i = 1, 2 \tag{5.13} $$

and the displacement field vector, in strain-displacement notation, can be reformulated as

$$ \underline{\hat{u}} = \begin{bmatrix} u_{1,0} \\ u_{2,0} \\ \underline{u} \end{bmatrix} = \begin{bmatrix} u_{1,0} \\ u_{2,0} \\ u_3 \\ \theta_1 \\ \theta_2 \end{bmatrix} \tag{5.14} $$

5.3.1.3 Stress-strain relationship

The relationships betweem the stress and strain were defined in the previous chapter. The generalised stress is composed of the following components.

$$\underline{\sigma} = \begin{bmatrix} \sigma_1 \\ \sigma_2 \\ \tau_{12} \end{bmatrix} = \underline{\underline{S}}^T \cdot \begin{bmatrix} \sigma_m \\ \sigma_b \end{bmatrix} \tag{5.15}$$

Equation 4.8 presents the stress resultant relationship, however, the constitutive tensor was expressed directly in stress resultant nomenclature, and the expression is equivalent to the following definition.

$$\underline{\underline{\hat{D}}} = \int_{-\frac{l_t}{2}}^{\frac{l_t}{2}} \underline{\underline{S}}^T \cdot \underline{\underline{D}} \cdot \underline{\underline{S}} \, \mathrm{d}x_3 \tag{5.16}$$

5.3.1.4 Strengths

In the stress resultant notation, the strengths, were already derived. With the introduction of the stress resultant transformation matrix ($\underline{\underline{S}}$), these strengths are equivalent to

$$\hat{\sigma} = \begin{bmatrix} \sigma_{Nx_1} \\ \sigma_{Nx_2} \\ \sigma_{Nx_1x_2} \\ \sigma_{Mx_1} \\ \sigma_{Mx_2} \\ \sigma_{Mx_1x_2} \end{bmatrix} = \int_{-\frac{l_t}{2}}^{\frac{l_t}{2}} \underline{\underline{S}}^T \cdot \underline{\sigma} \, \mathrm{d}x_3 = \int_{-\frac{l_t}{2}}^{\frac{l_t}{2}} \underline{\underline{S}}^T \cdot \underline{\underline{D}} \cdot \underline{\underline{S}} \, \mathrm{d}x_3 = \underline{\underline{\hat{D}}} \cdot \hat{\underline{\varepsilon}} \tag{5.17}$$

5.3.2 Analysis of thick composite shell structures - quadrilaterals

This quadrilateral shell element is as well discretised thickness-wise and presents a set of local axes systems (${}^l x_1, {}^l x_2, {}^l x_3$) being ${}^l x_3$ the local normal axis of the shell. A detailed picture of this shell element can be found in Figure 5.3.

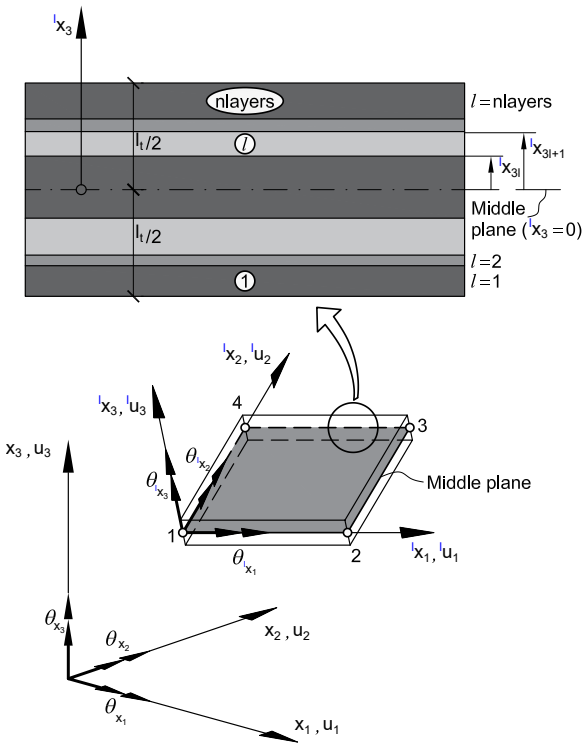

FIGURE 5.3: Local and global axes of the 4-node quadrilateral shell element.

The theory assumes the same key points found in subsection 5.3.1, however, the fourth assumption is modified for:

4. The in-plane deformation is considered linear but not normal to the mid-plane, this is the so-called *not necessarily normal orthogonality* condition.

To maintain a certain structure and to ease the lecture to the reader. The derivation of the formulation of this quadrilateral element follows the same steps described in the triangle derivation.

5.3.2.1 Displacements

The basic assumptions were described for the quadrilateral and the displacement field of the formulated problem describes

$$\begin{cases} u_1(x_1,x_2,x_3) = -x_3\theta_1(x_1,x_2) & ,\forall x_1,\forall x_2,\forall x_3 \in \Omega \\ u_2(x_1,x_2,x_3) = -x_3\theta_2(x_1,x_2) & ,\forall x_1,\forall x_2,\forall x_3 \in \Omega \\ u_3(x_1,x_2,x_3) = u_3(x_1,x_2) & ,\forall x_1,\forall x_2,\forall x_3 \in \Omega \end{cases} \tag{5.18}$$

Again, the rotations are directly defined in this theory as a linear slope due to the previous assumptions, but in this case the slope is not normal.

$$\begin{aligned} \theta_1 &= \frac{\partial u_3}{\partial x_1} + \Theta_1 \\ \theta_2 &= \frac{\partial u_3}{\partial x_2} + \Theta_2 \end{aligned} \tag{5.19}$$

where Θ is the additional rotation. This induces an extra additional degree of freedom both for the x_1 axis and the x_2 axis. The displacement field at any local point can be expressed as

$$\underline{u} = \begin{bmatrix} u_3 \\ \theta_1 \\ \theta_2 \end{bmatrix} \tag{5.20}$$

And similarly to the triangle, when membrane effects are taken into account, the strain-resultant notation of the displacement is analogous to Equation 5.14.

5.3.2.2 Deformation

Using [16], the kinematics are derived for the thick shell theory. The first difference in the model is that thick shells/plates undergo shearing, thus this effect needs to be taken into account.

$${}^{l}\varepsilon = {}^{l}\begin{bmatrix} \varepsilon_{11} \\ \varepsilon_{22} \\ \varepsilon_{33} \\ \gamma_{21} \\ \gamma_{31} \\ \gamma_{32} \end{bmatrix} = \begin{bmatrix} 1 & 0 & 0 & -{}^{l}x_3 & 0 & 0 & 0 & 0 \\ 0 & 1 & 0 & 0 & -{}^{l}x_3 & 0 & 0 & 0 \\ 0 & 0 & 0 & 0 & 0 & 0 & 0 & 0 \\ 0 & 0 & 1 & 0 & 0 & -{}^{l}x_3 & 0 & 0 \\ 0 & 0 & 0 & 0 & 0 & 0 & 1 & 0 \\ 0 & 0 & 0 & 0 & 0 & 0 & 0 & 1 \end{bmatrix} {}^{l}\begin{bmatrix} \varepsilon_m \\ \varepsilon_b \\ \varepsilon_s \end{bmatrix} = \underline{\underline{S}} \cdot {}^{l}\hat{\varepsilon} \tag{5.21}$$

Note that the stress-resultant transformation tensor ($\underline{\underline{S}}$) has another matrix description for the 4-node quadrilateral shell element. It is implicit that this shell fulfils the plane stress hypothesis where the strain in the axis-normal direction (ε_{33}) does not generate work ($\sigma_{33} = 0$) and therefore can be neglected.

The other significant term that appears in the stress-resultant strain ($\hat{\varepsilon}$) corresponds to the added shear effect. The formal definition for these terms is as follows

$${}^{l}\varepsilon_s = {}^{l}\begin{bmatrix} \dfrac{\partial u_3}{\partial x_1} - \theta_1 \\ \dfrac{\partial u_3}{\partial x_2} - \theta_2 \end{bmatrix} \tag{5.22}$$

where ε_s is the shear strain. Similarly to Equation 5.9, if applied in combination with the kinematics described in the displacement section, the shear strain, indeed, yields the additional rotation (Θ_i) for each component.

5.3.2.3 Stress-strain relationship

The relationships between the stress and strain were defined in the previous chapter. The generalised stress is composed of the following components.

$$\underline{\sigma} = \begin{bmatrix} \sigma_1 \\ \sigma_2 \\ \tau_{12} \\ \tau_{13} \\ \tau_{23} \end{bmatrix} = \underline{\underline{S}}^T \cdot \begin{bmatrix} \sigma_m \\ \sigma_b \\ \sigma_s \end{bmatrix} \tag{5.23}$$

Equation 4.14 presents the stress resultant relationship for the thick shell theory. The constitutive tensor expressed in stress resultant notation is defined exactly as for the triangle, however, note that the representation of both constitutive matrix and strain stress transformation matrix is different.

$$\underline{\underline{\hat{D}}} = \int_{-\frac{l_t}{2}}^{\frac{l_t}{2}} \underline{\underline{S}}^T \cdot \underline{\underline{D}} \cdot \underline{\underline{S}} \, \mathrm{d}x_3 \tag{5.24}$$

5.3.2.4 Strengths

Similarly to the triangle, the quadrilateral strengths are defined, there are a total of

$$\hat{\sigma} = \begin{bmatrix} \sigma_{Nx_1} \\ \sigma_{Nx_2} \\ \sigma_{Nx_1x_2} \\ \sigma_{Mx_1} \\ \sigma_{Mx_2} \\ \sigma_{Mx_1x_2} \\ \sigma_{Qx_1} \\ \sigma_{Qx_2} \end{bmatrix} = \int_{-\frac{l_t}{2}}^{\frac{l_t}{2}} \underline{\underline{S}}^T \cdot \underline{\sigma} \, \mathrm{d}x_3 = \int_{-\frac{l_t}{2}}^{\frac{l_t}{2}} \underline{\underline{S}}^T \cdot \underline{\underline{D}} \cdot \underline{\underline{S}} \, \mathrm{d}x_3 = \underline{\underline{\hat{D}}} \cdot \hat{\underline{\varepsilon}} \tag{5.25}$$

where σ_Q is the shear strength. In particular, the shear strengths present in the quadrilateral are aligned in the directions x_1 and x_2.

5.3.3 Principle of virtual work

To obtain the partial differential equation in what is called the weak form, there are two standard methods to proceed, one is using the variational method and the second is the principle of the virtual works. The latter is described here for the three-dimensional equation of elasticity (PDE).

$$\int_\Omega \left[\delta \left(\underline{\varepsilon} \right)^T \cdot \underline{\sigma} \right] \, \mathrm{d}\Omega = \int_{\partial\Omega} \left[\delta \left(\underline{u} \right)^T \cdot \underline{F_t} \right] \, \mathrm{d}\Omega + \sum_i \delta \left(\underline{u} \right)^T \cdot \underline{F_p} \tag{5.26}$$

where $\delta(\,)$ is the variational operator, F_t is the traction or surface force and F_p is the point force. The quantities on which the variational operator is applied, are mainly the strains, $\delta(\varepsilon)$, and the displacements, $\delta(u)$. Indeed, the virtual strains are intrinsically linked to the virtual displacements, and this will be exchanged later in the discretisation. Note that the objective of the principle of virtual work is to analyse the variation of this virtual work in terms of the variation of virtual displacements.

One of the advantages of expressing the solution in terms of the stress resultant notation is that the l.h.s. yields the following equivalence.

$$\int_{\Omega} \left[\delta\left(\underline{\varepsilon}\right)^T \cdot \underline{\sigma} \right] \, \mathrm{d}\Omega \equiv \int_{\Omega_2} \left[\delta\left(\hat{\underline{\varepsilon}}\right)^T \cdot \hat{\underline{\sigma}} \right] \, \mathrm{d}\Omega \tag{5.27}$$

Interestingly, the PDE has become a two-dimensional equation instead, observe that the domain in the integral is denoted in two dimensions by the subscript (Ω_2) in contrast to the three-dimensional integral denoted by (Ω). Do please not confuse this nomenclature with the boundary integral ($\partial\Omega$).

5.3.4 Finite Element Method

The finite element method is a well-known procedure to discretise weak or variational forms of partial differential equations. The method can be further studied in [279] and this section will follow a very similar structure that can be found in [16].

The fundaments of the constitutive model (elastic, inelastic, composite homogenisation) and kinematics of composite shells have been derived. The unknown of the structural problem is the displacement field, which is a continuous field in the variational formulation found in Equation 5.26. The variational quantities introduced here can be substituted by an arbitrary function, the so-called *test function*. Indeed, this function is not completely arbitrary, since it has to comply with certain conditions ($\mathcal{L}^2$-space functions).

Consequently, assume that in Equation 5.26, the variational terms can be substituted by a test function (ξ). In particular, the variational of the strain can be perceived as the variational of the displacement, since the strains are the derivative of the displacement with respect to the spatial coordinate system.

$$\int_{\Omega} \left[\frac{\partial \underline{\xi}}{\partial x}^T \cdot \underline{\sigma} \right] \, \mathrm{d}\Omega = \int_{\partial\Omega} \left[\delta\left(\underline{\xi}\right)^T \cdot \underline{F_t} \right] \, \mathrm{d}\Omega + \sum_i \delta\left(\underline{\xi}\right)^T \cdot \underline{F_p} \tag{5.28}$$

Equation 5.28 is *per se* the weak form of the problem, which can be achieved by either the PVW or the variational formulation of the conservation of linear momentum.

5.3.4.1 Discretisation

The general procedure to produce the discrete solution is to leave the displacement as the unknown variable and approximate it by a discrete solution (point-wise).

$$\underline{u} = \sum_{i=1}^{n} \begin{bmatrix} N_{\xi_i} u_{3i} \\ N_{\xi_i} \theta_{1i} \\ N_{\xi_i} \theta_{2i} \end{bmatrix} = \begin{bmatrix} \underline{N_{\xi 1}} & \dots & \underline{N_{\xi n}} \end{bmatrix} \begin{bmatrix} \underline{u_1}_{(e)} \\ \dots \\ \underline{u_n}_{(e)} \end{bmatrix} = \underline{N_\xi} \cdot \underline{u}_{(e)} \tag{5.29}$$

Note the notation $\underline{u}_{(e)}$, refers to the displacement vector of each of the nodes inside an element. This comes from approximating the continuous field of the displacement by a discretised spatial mesh, this mesh is composed of nodes and each element contains a certain number of these nodes. Note that the same procedure is applicable if the notation used is the stress-resultant notation, the only difference is in the number of vector components.

In Equation 5.26, describing the weak form of the problem, the variational is applied to the strain and this is related to the displacement in the following manner.

$$\underset{\bullet\bullet}{\varepsilon} = \nabla \underset{\bullet}{u} \rightarrow \underline{\varepsilon} = \nabla \underline{N_\xi} \cdot \underline{u}_{(e)} = \underline{\underline{B}} \cdot \underline{u}_{(e)} \tag{5.30}$$

where B is the strain-displacement matrix. Note that on the left of the arrow, the description is given in tensor nomenclature, and on the right in vector/matrix description. The strain is expressed as a vector because it uses the Voigt notation.

In addition, the definition of the test function (ξ) in Equation 5.28 is still unknown. The definition of the strain is found employing of the shape functions of the discrete displacement. A very simple methodology that yields discrete solutions is the so-called *Galerkin* method [280].

$$\underline{\xi} = \underline{N_\xi} \tag{5.31}$$

I.e., the method employs the same description for the test functions (ξ) as the interpolation functions of the grid, the shape functions (N_ξ).

5.3.4.1.1 Kirchhoff-Love theory

The particular DKT element, a triangular element with linear shape functions, is composed of three nodes. The strain within this element expressed locally, yields

$$^{l}\underline{\hat{\varepsilon}} = \underline{\underline{B}}_i \cdot {}^{l}\underline{\hat{u}}_i = \begin{bmatrix} \underline{\underline{B}}_1 & \underline{\underline{B}}_2 & \underline{\underline{B}}_3 \end{bmatrix} \begin{bmatrix} {}^{l}\underline{\hat{u}}_{1(e)} \\ {}^{l}\underline{\hat{u}}_{2(e)} \\ {}^{l}\underline{\hat{u}}_{3(e)} \end{bmatrix} \quad , \quad \underline{\underline{B}}_i = \begin{bmatrix} \underline{\underline{B_m}}_i \\ \underline{\underline{B_b}}_i \end{bmatrix} \tag{5.32}$$

where B_m is the membrane strain-displacement matrix, B_b is the bending strain-displacement matrix. Note the Einstein notation is used to describe the scalar product between the strain-displacement matrix and the displacement vector at the nodal level, i.e., $a_i \cdot b_i \equiv \sum_i a_i \cdot b_i$.

Recall that the definition in stress-resultant form contains the membrane terms as well, the membrane and bending strain-displacement matrix at a given *gauss point*

are expressed in the following manner

$$\underline{\underline{B_m}}_i = \begin{bmatrix} \frac{\partial N_{\xi i}}{\partial x_1} & 0 & 0 & 0 & 0 \\ 0 & \frac{\partial N_{\xi i}}{\partial x_2} & 0 & 0 & 0 \\ \frac{\partial N_{\xi i}}{\partial x_1} & \frac{\partial N_{\xi i}}{\partial x_2} & 0 & 0 & 0 \end{bmatrix} \tag{5.33}$$

$$\underline{\underline{B_b}}_i = \begin{bmatrix} 0 & 0 & 0 & \frac{\partial N_{\xi i}}{\partial x_1} & 0 \\ 0 & 0 & 0 & 0 & \frac{\partial N_{\xi i}}{\partial x_2} \\ 0 & 0 & 0 & \frac{\partial N_{\xi i}}{\partial x_1} & \frac{\partial N_{\xi i}}{\partial x_2} \end{bmatrix} \tag{5.34}$$

5.3.4.1.2 Reissner-Mindlin theory

For the quadrilateral, the 4-node CLLL element with linear shape functions, the discretisation would be

$${}^{l}\underline{\hat{\varepsilon}} = \underline{B}_i \cdot {}^{l}\underline{\hat{u}}_i = \begin{bmatrix} \underline{\underline{B}}_1 & \underline{\underline{B}}_2 & \underline{\underline{B}}_3 & \underline{\underline{B}}_4 \end{bmatrix} \begin{bmatrix} {}^{l}\underline{\hat{u}}_{1(e)} \\ {}^{l}\underline{\hat{u}}_{2(e)} \\ {}^{l}\underline{\hat{u}}_{3(e)} \\ {}^{l}\underline{\hat{u}}_{4(e)} \end{bmatrix} \quad , \quad \underline{\underline{B}}_i = \begin{bmatrix} \underline{\underline{B_m}}_i \\ \underline{\underline{B_b}}_i \\ \underline{\underline{B_s}}_i \end{bmatrix} \tag{5.35}$$

where B_s is the shear strain-displacement matrix. In this particular case, the strain-displacement matrices are redefined as follows

$$\underline{\underline{B_m}}_i = \begin{bmatrix} \frac{\partial N_{\xi i}}{\partial x_1} & 0 & 0 & 0 & 0 \\ 0 & \frac{\partial N_{\xi i}}{\partial x_2} & 0 & 0 & 0 \\ \frac{\partial N_{\xi i}}{\partial x_1} & \frac{\partial N_{\xi i}}{\partial x_2} & 0 & 0 & 0 \end{bmatrix} \tag{5.36}$$

$$\underline{\underline{B_b}}_i = \begin{bmatrix} 0 & 0 & 0 & \frac{\partial N_{\xi i}}{\partial x_1} & 0 \\ 0 & 0 & 0 & 0 & \frac{\partial N_{\xi i}}{\partial x_2} \\ 0 & 0 & 0 & \frac{\partial N_{\xi i}}{\partial x_1} & \frac{\partial N_{\xi i}}{\partial x_2} \\ 0 & 0 & 0 & & 0 \\ 0 & 0 & 0 & & 0 \end{bmatrix} \tag{5.37}$$

$$\underline{\underline{B_s}}_i = \begin{bmatrix} 0 & 0 & \dfrac{\partial N_{\xi i}}{\partial x_1} & -N_{\xi i} & 0 \\ 0 & 0 & \dfrac{\partial N_{\xi i}}{\partial x_2} & 0 & -N_{\xi i} \end{bmatrix} \tag{5.38}$$

5.3.4.2 Discrete system

Once the unknown has been discretised and the *Garlerkin* method is used to define the test function, the discrete system of equations, element-wise, can be described. Equation 5.28, for each element, yields:

$$\underline{\underline{K}}_{(e)} \cdot \underline{u}_{(e)} = \underline{F_t}_{(e)} + \underline{F_p}_{(e)} \tag{5.39}$$

where K is the stiffness. Note the element description underneath each discrete quantity. Indeed, the r.h.s can be just written as one vector of forces, since both point and traction forces of the element are derived from the Neumann boundary conditions. Other forces could be considered such as the body forces (F_b) and again added as just one generic force vector.

$$\underline{\underline{K}}_{(e)} \cdot \underline{u}_{(e)} = \underline{F_{\text{ext}}}_{(e)} \tag{5.40}$$

where F_{ext} is the external force. The numerical definition of each of the terms that contributes to the system of equations at the element level is given below.

$$\underline{\underline{K}}_{(e)} = \int_{\Omega_{(e)}} \left[\underline{\underline{B}}^T \cdot \underline{\underline{\hat{D}}} \cdot \underline{\underline{B}} \right] \mathrm{d}\Omega_{(e)} \quad \rightarrow \quad \underline{\underline{K}}_{ij\,(e)} = \int_{\Omega_{(e)}} \left[\underline{\underline{B}}_i^T \cdot \underline{\underline{\hat{D}}} \cdot \underline{\underline{B}}_j \right] \mathrm{d}\Omega_{(e)} \tag{5.41}$$

$$\begin{aligned} \underline{F_{\text{ext}}}_{(e)} &= \int_{\partial\Omega_{(e)}} \left[\underline{N_\xi} \cdot \underline{F_t} \right] \mathrm{d}\Omega_{(e)} + \underline{N_\xi} \cdot \underline{F_p} \\ &\downarrow \\ \underline{F_{\text{ext}}}_{i\,(e)} &= \int_{\partial\Omega_{(e)}} \left[\underline{N_\xi}_i \cdot \underline{F_t}_i \right] \mathrm{d}\Omega_{(e)} + \underline{N_\xi}_i \cdot \underline{F_p}_i \end{aligned} \tag{5.42}$$

As already discussed, the traction and point forces are (F_t) and (F_p) respectively. When the element notation appears beneath these two forces, it refers to the element vector (integrated over the element) and when it does not, it refers to the very traction or point forces at the node. Therefore, in the external force vector of the element ($\underline{F_{\text{ext}}}_{(e)}$), the contribution of the traction and point loads, discrete at each node, are obtained once more by the multiplication of the continuous distribution of loads and the shape function (N_ξ).

5.3.4.3 Assembling of the discrete solution

The element system of equations is completely defined at this point, and only the assembling of the different elements is left in order to obtain the global and total response of the structure domain.

Equation 5.40 represents only the integral over an element domain. To obtain the solution over the whole domain, referred to as Equation 5.28, the following discrete system has to be assembled

$$\begin{aligned} \underline{\underline{K}} \cdot \underline{u} &= \underline{F_{\text{ext}}} \\ \underline{\underline{K}} &= \sum_{\text{e}}^{n_{\text{e}}} {}^{g}\underline{\underline{K}}_{(e)} \\ \underline{F_{\text{ext}}} &= \sum_{\text{e}}^{n_{\text{e}}} {}^{g}\underline{F_{\text{ext}}}_{(e)} \end{aligned} \tag{5.43}$$

The summation over all the elements (n_{e}) yields the final system found in Equation 5.43. The conceptual procedure is exemplified in Figure 5.4

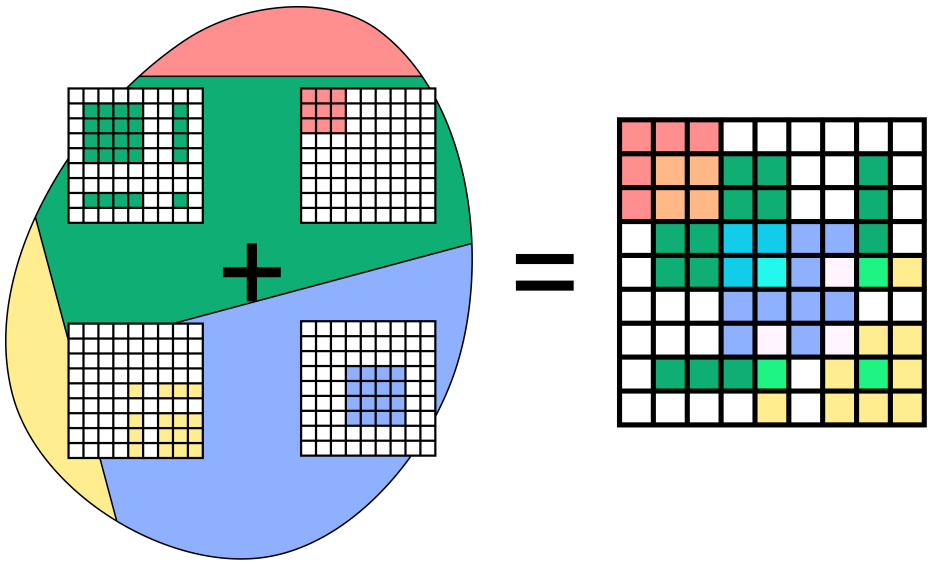

FIGURE 5.4: Illustration of the assembling process characteristic of the finite element method.

The assembled quantities, expressed in Equation 5.43, were expressed directly in the global coordinate system, whereas the definition for the elemental quantities was expressed in the local coordinate system. In order to pass from one system to another, the following relationships are given

$${}^{g}\underline{\underline{K}}_{(e)} = \underline{\underline{\Lambda}}^{T} \cdot {}^{l}\underline{\underline{K}} \cdot \underline{\underline{\Lambda}} \equiv \underline{\underline{\Lambda}}^{T} \cdot \underline{\underline{K}}_{(e)} \cdot \underline{\underline{\Lambda}} \tag{5.44}$$

$${}^{g}\underline{F_{\text{ext}}}_{(e)} = \underline{\underline{\Lambda}} \cdot {}^{l}\underline{F_{\text{ext}}} \equiv \underline{\underline{\Lambda}} \cdot \underline{F_{\text{ext}}}_{(e)} \tag{5.45}$$

5.3.4.4 Numerical scheme

The numerical scheme of the thermo-mechanical solver is detailed in this section. Starting by introducing the difference between the thermo-mechanical *solver* and *coupling*, the first refers to the mechanical model that introduces the non-linear dependencies with the temperature and the second refers to the combination of the thermal solver and the thermo-mechanical solver.

To visualise this difference, the thermo-mechanical solver is the one dealing with the thermal and mechanical loads, and, also taking into account the mechanical loss of the thermo-chemical effects. This is illustrated in Figure 5.5 where the solver first has a configuration with loads, and then a thermal profile of temperatures through-thickness is introduced. The problem is solved iteratively until the optimal displacement is for the given thermal and mechanical loads and thermo-chemical degradation.

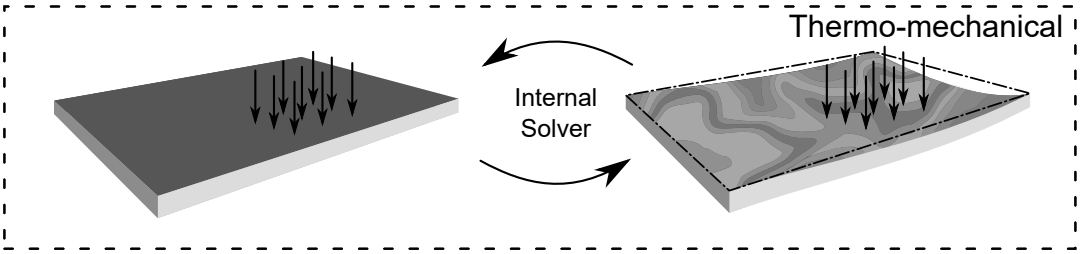

FIGURE 5.5: Illustration of the thermo-mechanical solver.

The procedure is similar to the one explained in the thermal scheme. From Equation 5.43, the residual of the assembled system is obtained.

$$\underline{r_u} = \underline{\underline{K}} \cdot \underline{u} - \underline{F_{\text{ext}}} \tag{5.46}$$

In this case, a fractional load step is introduced.

$$\underline{r_u}\big|_{n+1} \equiv \underline{r_u}\left(\underline{u}|_{n+1}\right) = \underline{\underline{K}}\big|_{n+1}\, \underline{u}|_{n+1} - \underline{F_{\text{ext}}}\big|_{n+1} \tag{5.47}$$

The fractional stepping scheme is very useful when leading with non-linear problems (mechanically and thermally). The external force at each fractional step can be described as some final load (F_{ext_∞}) multiplied by a fractional coefficient (c).

$$\underline{F_{\text{ext}}}\big|_{n+1} = c|_{n+1}\, \underline{F_{\text{ext}_\infty}} \tag{5.48}$$

As customary, using Taylor expansion around the iteration (k) yields

$$\underline{r_u}\big|_{n+1,k+1} = \underline{r_u}\big|_{n+1,k} + \left.\frac{\partial \underline{r_u}\,(\underline{u})}{\partial u}\right|_{n+1,k} \left(\underline{u_{n+1,k+1}} - \underline{u_{n+1,k}}\right)$$
$$\lim_{k+1\to\infty} \underline{r_u}\big|_{n+1,k+1} = 0 \tag{5.49}$$

The incremental solution of the unknown form, Equation 5.49, is posed.

$$\underline{\underline{J_u}}\Big|_{n+1,k} \underline{\Delta u}|_{n+1,k} = \underline{r_u}\big|_{n+1,k} \tag{5.50}$$

where J_u is the jacobian of mechanical system. Some important comments need to be discussed regarding the Jacobian of the system.

1. **Time scheme**

   The scheme proposed in this thesis is a non-time dependent scheme, i.e., it does not include the effects of inertia and damping. Nevertheless, if inertia and damping were introduced, with a suitable time scheme, they would be included both in the Jacobian and residual.

   A fractional or incremental scheme is used here, for obvious reasons such as to later be coupled with the thermal analysis depending on time. This is very convenient here, since it adds a similar structure that would be used if for example time-dependent forces would be introduced. This could be modelled by having a non-monotonic increasing fractional coefficient, but a time-dependent one. However, the effects of inertia and damping are still neglected with this approach.

2. **The true nature of the Jacobian**

   Time-related assumptions were given, however, the Jacobian still needs some more clarifications. If equation Equation 5.46 is examined, the Jacobian term is the derivative of this equation with respect to the unknown displacement. Therefore, this derivative can take a general form such as

   $$\frac{\partial \underline{\underline{r_u}}}{\partial u} \equiv \underline{\underline{J_u}} = \underline{\underline{\frac{\partial K}{\partial u}}} u + \underline{\underline{K}} - \underline{\underline{\frac{\partial F_{\text{ext}}}{\partial u}}} \tag{5.51}$$

   This reveals that there are a few dependencies that need to be clarified. Starting with the external forces, if those depend on the deformation or point of application, the Jacobian matrix needs to add this behaviour. This for example happens with hydrostatic loads or non-following loads. The theory described within the scope of this thesis is not applied to scenarios where this type of load are present, and thus it can be neglected.

   The standard dependency found for linear elasticity is that the Jacobian matrix is equal to the stiffness, which is the main reason behind the term tangent stiffness associated with the derivative of the residuals. This term is not neglected, as it is always necessary.

   This leaves the last term which is the combination of the derivative of the stiffness for the displacement and the displacement itself. This term appears when

the stiffness has a dependency on the displacement. Recalling the expression found in Equation 5.41, the stiffness depends on either the strain-displacement matrix (B) or the constitutive matrix (D).

5.3.5 Flexible composite structures

The term flexibility is used in structural analysis to refer to large displacement analysis. Marine structures, such as ships, are a type of structure that often presents a natural large displacement distribution along the length of the vessel. Moreover, composites are materials that are advantageous in many aspects, but one disadvantage can be rapidly noticed when considering two similar structures, one made out of composites and another of traditional materials. For an identical mechanical load, the composite vessel will present higher displacements, given it has a lower Young's modulus (more flexible). It is the combination of composites and marine structure design, in which large displacements need to be taken into account.

The problems that arise when considering such a formulation have not yet been fully addressed, the discussion was left at the point where the Jacobian matrix was disseminated, and it was assumed that the external forces did not present a dependence with respect to the displacements.

$$\frac{\partial \underline{\underline{r_u}}}{\partial u} \equiv \underline{\underline{J_u}} = \underline{\underline{\frac{\partial K}{\partial u}}} u + \underline{\underline{K}} \tag{5.52}$$

The only two necessary terms were the stiffness itself and the derivative of the stiffness. If the governing problem is assumed to be linear geometric and constitutive, the Jacobian would be just the stiffness matrix. The chapter 4 covers a wide range of non-linear models that depend on the strain and indirectly on the displacement. It seems then necessary to include this term inside the Jacobian of the system, only if the non-linear constitutive analysis is desired. In that case scenario, the derivative of the system can be calculated as

$$\begin{aligned} \underline{\underline{\frac{\partial K}{\partial u}}} &= \int_\Omega \left[\underline{\underline{B}}^T \cdot \frac{\partial \sigma\left(\epsilon\left(u\right)\right)}{\partial u} \right] \mathrm{d}\Omega \\ &= \int_\Omega \left[\underline{\underline{B}}^T \cdot \underline{\underline{\frac{\partial \sigma}{\partial \epsilon}}} \frac{\partial \epsilon}{\partial u} \right] \mathrm{d}\Omega = \int_\Omega \left[\underline{\underline{B}}^T \cdot \underline{\underline{D_{\tan}}} \cdot \underline{\underline{B}} \right] \mathrm{d}\Omega \end{aligned} \tag{5.53}$$

So in non-linear constitutive problems, the tangent stiffness, besides needing the stiffness itself, needs the tangent constitutive tensor. Although this may seem complex enough, the small-displacement simplifications in the strain-displacement matrix are certainly helpful. The other major inconvenience, after addressing the non-linear constitutive effect, is the non-linear geometric effect or the dependency of the strain-displacement matrix with the displacement. A priory, the strain-displacement matrix, as the name suggests, depends on the displacement. One of the solutions, to solve Equation 5.53, is to change the residual definition in Equation 5.54 as follows

$$\frac{\partial \underline{r_u}}{\partial u} \equiv \underline{\underline{J_u}} = \underline{\underline{\frac{\partial F_{\text{int}}}{\partial u}}} - \underline{\underline{\frac{\partial F_{\text{ext}}}{\partial u}}} \tag{5.54}$$

where F_{int} is the internal force. The first term of the Jacobian of the system is minimised with respect to the internal forces instead of the stiffness. This approach is the most standard way to solve a FEM problem, only taking care of the non-linear constitutive effect by obtaining the tangent constitutive tensor. Then, as commented previously, if large displacements are considered, this very definition of the tangent constitutive tensor changes and needs to be adapted to the previous formulation explained in chapter 4.

When the non-linear kinematics (geometry) are taken into account inside the non-linear constitutive model, things become fuzzier. Theories such as the total Lagrangian theory use this approach, however, in the case of composites, using such theory makes it very costly to generate these new non-linear geometric definitions of the constitutive model, and the applications are unique and narrow. It does not make the resultant derived formulation compatible with other approaches. Consider that it would even require modifying TSPROM by using the total Lagrangian theory, which would add more effort to the whole derivation. Consequently, the non-linear geometrical model has to be a solution that allows for uncoupling both the constitutive and kinematic laws, which would present a great synergy between the large-displacement theory and the composite constitutive (TSPROM) theory. Albeit the desired solution is not the total Lagrangian, a brief explanation of the most common methods used to deal with non-linear geometric problems is given below.

Typical solutions to adapt the finite element method to incorporate non-linear geometric analysis (large deformations) are found in [281] or [282]. The total Lagrangian formulation, [281], introduces some extra dependencies in the constitutive tensor to include the large deformation effects. The theory uses an intermediate system of reference to capture the large rotations introduced in the element, this intermediate system is then embedded into the kinematics and constitutive laws. Suitable formulations for shells, expressly developed for laminate shells, are found in the work of Oliver and Onate [281].

The updated Lagrangian formulation is very similar to the total Lagrangian, both produce the same result, however, the latter does not include an intermediate system of references and instead updates the material description of the domain every certain steps. Indeed, this update is the pseudo-intermediate reference system. For shells, the work of Jiang et al. [282] is an interesting example of the application of this methodology. An important limitation of this technique is the requirement to update the material mesh, since, as the problem size increases, the method becomes very computationally costly.

Nevertheless, both methodologies are difficult in combination with the damage model, in particular when the inelastic behaviour of the composite structure is obtained from the inelastic behaviour of the constituent phases. This is because these two technologies introduce certain changes in the core of the constitutive matrix. To separate the non-linear geometric and constitutive effects, into different terms for the finite element discretisation, the research of Felippa and Haugen introduced in [123] the so-called assumed natural deviatoric strain (ANDES) and the formalisation of

the co-rotational theory in [18].

The co-rotational theory is a tight and compartmented theory that allows the current linear geometric theory of shells to a non-linear geometric range. The most interesting part of it is that it uses an intermediate configuration similarly to the total Lagrangian formulation, however, this non-linear geometric effects are not introduced in the constitutive tensor and rather are introduced in the local to global transformation matrices.

5.3.5.1 Co-rotational formulation

For composite structures, the capability to simulate a non-linear geometric analysis using a definition that is similar to the one in a linear geometric formulation is certainly of interest. However, recall that the TSPROM is very efficient because its scope is just at the constitutive level (constitutive tensor). Therefore, a question arises whether it is possible to use a similar approach for the non-linear kinematics without invading the scope of the TSPROM and maintaining the same structure as for linear geometric analysis. A theory of this kind, signifies almost no major change in the FEM structure of any standard code. Also, provided that the SPROM in [283] demonstrated to be able to assess correctly buckling, it would be a major upgrade to provide an approach that separates the constitutive and geometric non-linearities.

The previous formulation has delved into the linear kinematics, however, a more robust solution including non-linear kinematics can be derived using the co-rotational theory by Felippa and Haugen [18]. The importance of the manner, in which the co-rotational theory addresses the problem of non-linear kinematics or better referred as non-linear geometry, is found in the fact that this theory extends standard linear geometric models by introducing the non-linear dependency in the transformation between local and global axes of reference.

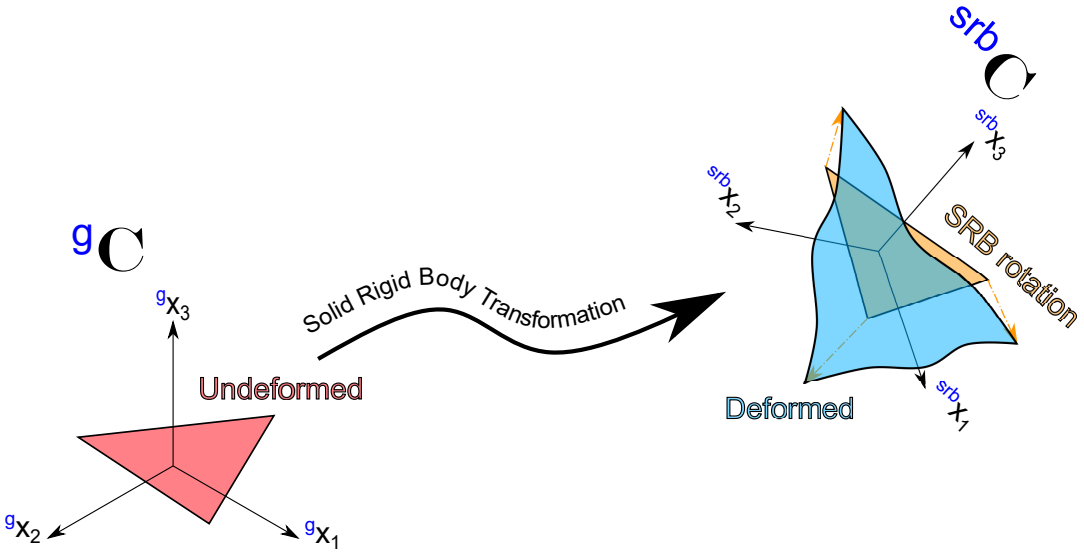

FIGURE 5.6: Co-rotational formulation schematic.

Figure 5.6 illustrates how the co-rotational theory works. It uses a set of two reference axes, resembling the underlying physics of the *total Lagrangian* approach, the first reference system (${}^{g}\mathcal{C}$) is the material or Lagrangian reference axis, and the formulation then defines a set of solid rigid body transformations that link the material reference system to the solid rigid body rotated reference system or in short SRB reference system (${}^{SRB}\mathcal{C}$). Then the element in question, expressed in the SRB reference system, is deformed.

The qualitative advantage when using the co-rotational formulation is that the stiffness or the constitutive tensors remain the same and the non-linear geometric is directly translated to the set of axes used in the transformation between global and local reference systems. The displacements are reformulated and expressed in either local or global reference systems by introducing the transformation tensor that transforms a quantity expressed in the global reference system to the local reference system and viceversa.

$$ {}^{g}\underline{u} = \underline{\underline{\Lambda}}^{T}\,{}^{l}\underline{u} \Longleftrightarrow {}^{l}\underline{u} = \underline{\underline{\Lambda}}\,{}^{g}\underline{u} \tag{5.55} $$

where Λ is the rotation tensor. Furthermore, according to the co-rotational formulation, the non-linear geometric dependency is introduced in this rotation tensor ($\Lambda(u)$).

$$ \begin{cases} \underline{r_u}({}^{g}u) = {}^{g}\underline{F_{\text{int}}} - {}^{g}\underline{F_{\text{ext}}} = \underline{\underline{\Lambda}}({}^{g}u)^{T}\,{}^{l}\underline{F_{\text{int}}} - \underline{\underline{\Lambda}}({}^{g}u)^{T}\,{}^{l}\underline{F_{\text{ext}}} \\ \dfrac{\partial \underline{r_u}\,({}^{g}u)}{\partial {}^{g}u} = \dfrac{\partial \underline{\underline{\Lambda}}({}^{g}u)^{T}}{\partial {}^{g}u}\,{}^{l}\underline{F_{\text{int}}} + \underline{\underline{\Lambda}}({}^{g}u)^{T}\dfrac{\partial\,{}^{l}\underline{F_{\text{int}}}}{\partial {}^{g}u} \end{cases} \tag{5.56} $$

Note that in this derivation, instead of considering the l.h.s. as the product of the stiffness by the displacement, the internal force term is used. Also, the external force has no dependence with respect to the displacement. Thus, expanding the derivative of the internal force concerning the displacement leads to

$$ \underline{\underline{\Lambda}}({}^{g}u)^{T}\frac{\partial\,{}^{l}F_{\text{int}}}{\partial {}^{g}u} = \underline{\underline{\Lambda}}({}^{g}u)^{T}\frac{\partial\left({}^{l}K\,{}^{l}u\right)}{\partial {}^{g}u} = \underline{\underline{\Lambda}}({}^{g}u)^{T}\,{}^{l}\underline{\underline{K\Lambda}}({}^{g}u)\,{}^{g}\underline{u} \tag{5.57} $$

Since one of the purposes of this formulation is for the stiffness matrix, at least what is referred to as *material* stiffness, to not contain any dependence with respect to displacements, Equation 5.57 directly yields the classical stiffness expression. This can be rearranged with the following nomenclature

$$ \underline{\underline{\Lambda}}({}^{g}u)^{T}\frac{\partial\,{}^{l}F_{\text{int}}}{\partial {}^{g}u} = \underline{\underline{\Lambda}}^{T}\cdot{}^{l}\underline{\underline{K}}_{M}\cdot\underline{\underline{\Lambda}}\cdot{}^{g}\underline{u} = {}^{g}\underline{\underline{K}}_{M}\cdot{}^{g}\underline{u} \tag{5.58} $$

where K_M denotes the material stiffness. However, the question arises on what is the transformation matrix (rotation matrix) exactly. An intricate derivation of this formulation can be found in [284] by Almeida and Awruch. The rotation matrix

contains a set of three transformations useful to describe the large rotation of the solid rigid body movement.

$$\underline{\underline{\Lambda}}({}^{g}u)^{T} \equiv \underline{\underline{\Lambda}}^{T} = \underline{\underline{\Lambda}}_{1}^{T} \cdot \underline{\underline{\Lambda}}_{2}^{T} \cdot \underline{\underline{\Lambda}}_{3}^{T} \tag{5.59}$$

These three transformations are the ones that define the non-linear geometric, sometimes referred just as *geometric* [284], stiffness. The other term in Equation 5.56 if expanded yields

$$\frac{\partial \underline{\underline{\Lambda}}({}^{g}u)^{T}}{\partial {}^{g}u} {}^{l}\underline{F}_{\text{int}} = \left(\frac{\partial \underline{\underline{\Lambda}}_{1}^{T}}{\partial {}^{g}u} \cdot \underline{\underline{\Lambda}}_{2}^{T} \cdot \underline{\underline{\Lambda}}_{3}^{T} + \underline{\underline{\Lambda}}_{1}^{T} \cdot \frac{\partial \underline{\underline{\Lambda}}_{2}^{T}}{\partial {}^{g}u} \cdot \underline{\underline{\Lambda}}_{3}^{T} + \underline{\underline{\Lambda}}_{1}^{T} \cdot \underline{\underline{\Lambda}}_{2}^{T} \cdot \frac{\partial \underline{\underline{\Lambda}}_{3}^{T}}{\partial {}^{g}u} \right) {}^{l}\underline{F}_{\text{int}} \tag{5.60}$$

If the internal force is substituted by the stiffness and displacement, the r.h.s. becomes

$$\begin{aligned} \left(\frac{\partial \underline{\underline{\Lambda}}_{1}^{T}}{\partial {}^{g}u} \cdot \underline{\underline{\Lambda}}_{2}^{T} \cdot \underline{\underline{\Lambda}}_{3}^{T} + \underline{\underline{\Lambda}}_{1}^{T} \cdot \frac{\partial \underline{\underline{\Lambda}}_{2}^{T}}{\partial {}^{g}u} \cdot \underline{\underline{\Lambda}}_{3}^{T} + \underline{\underline{\Lambda}}_{1}^{T} \cdot \underline{\underline{\Lambda}}_{2}^{T} \cdot \frac{\partial \underline{\underline{\Lambda}}_{3}^{T}}{\partial {}^{g}u} \right) {}^{l}\underline{\underline{K}}_{M} \cdot {}^{l}\underline{u} \\ = \left({}^{g}\underline{\underline{K}}_{GR} + {}^{g}\underline{\underline{K}}_{GP} + {}^{g}\underline{\underline{K}}_{GM} \right) {}^{g}\underline{u} \end{aligned} \tag{5.61}$$

or

$${}^{g}\underline{\underline{K}}_{NG} = {}^{g}\underline{\underline{K}}_{GR} + {}^{g}\underline{\underline{K}}_{GP} + {}^{g}\underline{\underline{K}}_{GM} \tag{5.62}$$

where K_{NG} is the non-linear geometric stiffness and K_{GR}, K_{GP}, K_{GM} are the rotational geometric, equilibrium projection and moment-correction stiffnesses. The same notation can be found in [284] with further detail.

The final form of the residual derivative is

$$\frac{\partial \underline{r}_{u}({}^{g}u)}{\partial {}^{g}u} = \left({}^{g}\underline{\underline{K}}_{M} + {}^{g}\underline{\underline{K}}_{NG} \right) \cdot {}^{g}\underline{u} \tag{5.63}$$

5.3.5.2 Non-linear geometric buckling

One of the most interesting aspects of deriving the non-linear geometric formulation does not only reside in the possibility to understand better the natural large-displacement behaviour of composites, but also, assesses the occurrence of buckling.

Buckling is a phenomenon which denominates sudden failure due to non-linear geometric behaviour. This mechanical failure is determined by the degree of eccentricity a structural member endures. In Figure 5.7, an illustration of a single beam under compression is shown which generates a buckling mode when a certain force P is applied to it. In general circumstances, the compressive load would not generate significant deflection and the bending moment experienced by the beam would be negligible. However, in practice, the load may not be applied directly to the neutral

axis and this would be the cause of a certain eccentricity. The phenomenon of buckling is best describe as the collapse, like shown in this figure, once the beam is no longer able to endure the load, it ceases to stop on deforming.

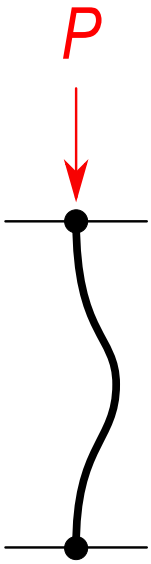

FIGURE 5.7: A buckling schematic.

This non-stopping behaviour (endless deformation) is the reason that buckling is regarded as a failure. In more complex structures, the buckling of a single member does not condition the buckling of the rest of the structure. E.g., Figure 5.8 shows neatly that one structural pillar has undergone buckling, meaning that the effective stress in for the beam is close to the failure load which characterises it, however at a certain point, the load has been redistributed to the adjacent pillars that now endure the vast majority of the load. By this redistribution and relaxation of the loads, in complex structures, a new regime, the *post-buckling*, appears.

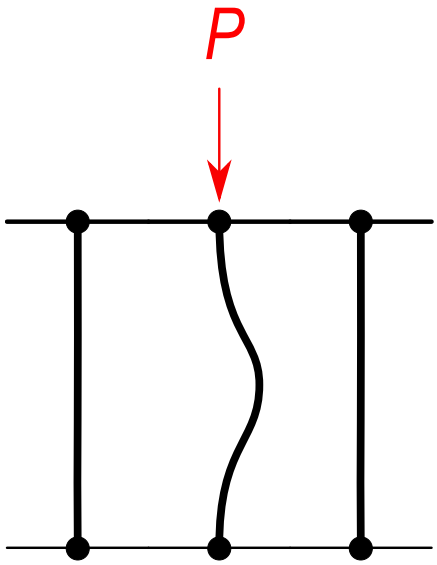

FIGURE 5.8: Post-buckling of a complex structure.

Post-buckling is appealing since it does not imply the total collapse of the structure,

that would be buckling, and it is a behaviour that classical buckling analysis such as the linear buckling method by perturbations is not able to capture. Normally post-buckling is accompanied by inelastic effects, i.e., imagine that on the zone of maximum deflection a hinge-like mechanism is formed, the more it deflects, the more the hinge plasticises. This is regarded as *inelastic buckling* or, in the lack of total collapse, *inelastic post-buckling*.

Although the difference between *buckling* and *post-buckling* has been introduced as if *post-buckling* is the result of almost achieving the *buckling* state. That would be a very intuitive explanation, however, some minor details need to be considered. In reality, *post-buckling* refers to a situation immediately or nearby the *buckling* phenomenon. Using maths to correctly phrase it, *post-buckling* is the outcome of undergoing *buckling* and not collapsing. This last definition adjusts better with the discussion offered previously. Therefore, there are structures such as the *Euler-beam* that once undergoing buckling, collapse and some such in Figure 5.9, a case of *snap-through* buckling, that after buckling, deform in such a way that finds an equilibrium position.

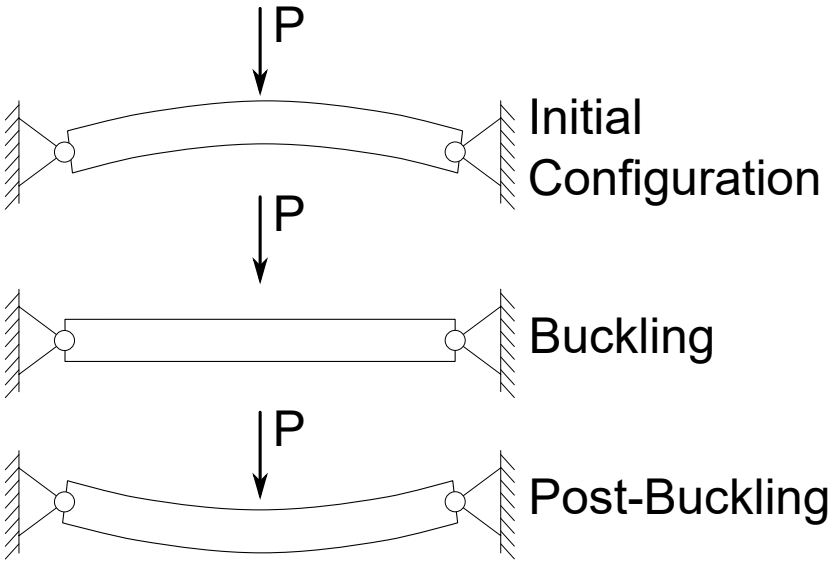

FIGURE 5.9: Buckling: snap-through mechanism.

Observe how the meaning of buckling is more intricate than it may seem, a priory. In a general sense, buckling can be recognised mathematically as a configuration that is unstable, specifically, when the stiffness matrix has become singular. Then the problem evolution after that singularity is reached is called post-buckling analysis, and the evolution before to that singularity is regarded as general buckling. Figure 5.9 shows very well this type of problems, at top of the image, there is a structure that is approximating buckling (snap-through buckling), the second row belongs to the point when the singularity is achieved and then the third schematic represents the evolution after buckling is reached. In the snap-through buckling, the process is able to avoid failure by reaching a geometric configuration that is stable.

So it has been clearly stated that buckling is a collapsing phenomenon that occurs especially when a structure or part of it is very eccentric. It has been discussed that for composites, due to their low elastic properties, these structures are prone to present large deflections. Then the question is whether incorporation or even the study of buckling is of importance when fire is present in the analysis.

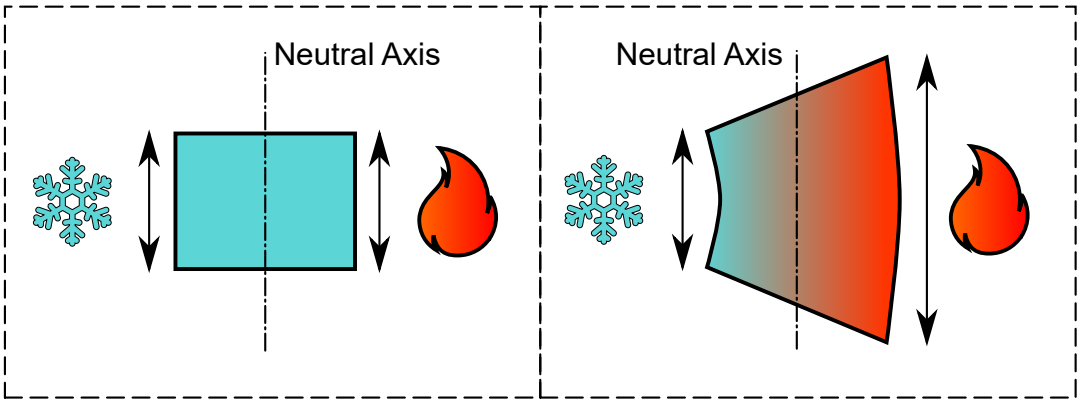

FIGURE 5.10: Buckling in the presence of temperature gradients.

Figure 5.10 gives a very intuitive example of one of the major issues of fire, the *temperature gradients*, these gradients originated from the exposure of the structure to fire, and they are of importance. The thermal dilation or thermal expansion of materials is generally of high importance, since the rate of expansion due to temperature, generally, is higher than due to elastic deformation.

So when a structure is exposed to fire, and a gradient of temperature can be found from the *hot* end to the *cold* end, large deformations are originated at least in the hot side of the structure. Any structure that has a face in traction, while the other face is consequently in contraction, can be conceptualised as a structure under bending effects. These bending effects can also be transformed to a parallel (axial) load with a certain eccentricity. It is this analogy that best explains the importance of being at least able to address buckling when a thermo-mechanical analysis is desired. The latter failure is sometimes coined *thermal buckling*, and it can be extended to the respective *post-buckling* and *inelastic* categories as well.

The formulation of non-linear geometric buckling arises from the singularity of the eigenvalue problem described in Equation 5.64. This considers, in Equation 5.63, the possibility that the equation is equal to zero discarding the trivial solution.

$$\frac{\partial r_u}{\partial u} = \left({}^{g}\underline{\underline{K}}_{M} + {}^{g}\underline{\underline{K}}_{NG} \right) {}^{g}\underline{u} = 0 \Rightarrow |K_L - \lambda K_{NL}| = 0 \tag{5.64}$$

where K_L is the linear geometric stiffness, K_{NL} is the non-linear geometric stiffness. The subscripts *linear* and *non-linear* are interchangeable with *material* and *non-linear geometric*, respectively.

Therefore, Equation 5.64 is posing the buckling problem, with the non-linear geometric approach, if the conditions are suitable, the system becomes ill-posed. Otherwise, if the r.h.s. of the arrow is examined, the problem is posed as an eigendecomposition problem, one to find the suitable eigenvector that makes the system unstable, this is the typical method for linear buckling based on bifurcation methodology. Nevertheless, both expressions are interrelated, proving that the *co-rotational theory* is, at least theoretically, able to assess buckling by producing a non-linear geometric stiffness that is of equal magnitude, but opposite sign, as the material stiffness.

5.3.6 Non-linear thermo-mechanical coupling

The thermo-mechanical algorithm proposed for laminate composite materials exposed to high temperatures is presented as a decoupled thermo-mechanical problem, where the thermal problem is solved first and updated in the thermo-mechanical problem that attempts to find mechanical equilibrium.

The thermo-mechanical algorithm updates the mechanical properties that depend on either the temperature or the pyrolysis and solves the TSPROM algorithm. Then the system is assembled to be iteratively solved.

The stages of the analysis are two, observe Figure 5.11. In an initial phase where the mechanical loads or pre-stress are introduced, the solver seeks the convergence of the structure to obtain its initial configuration. The models used here can be any of the non-linear constitutive or geometric theories.

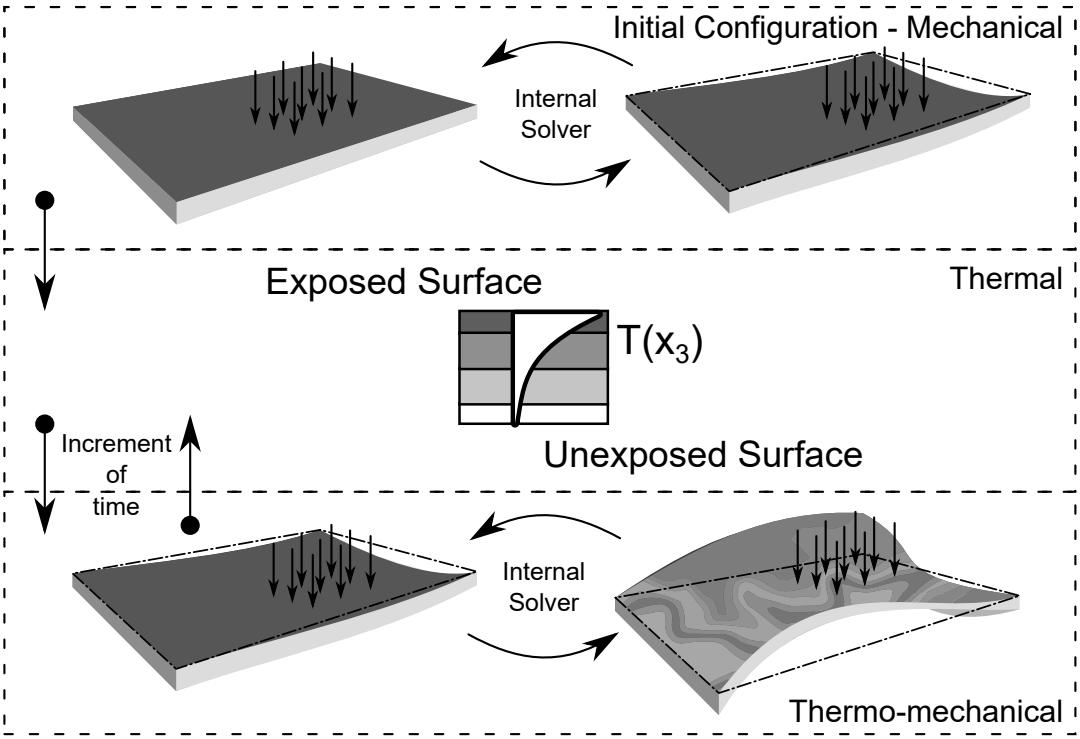

FIGURE 5.11: Flow diagram of the derived coupling.

Once the model has converged, the analysis advances to the second stage where the thermal solver acts as the master, it has sense since it is the uncoupled part of the problem, and the thermo-mechanical solver awaits for the thermal to obtain the converged temperature and pyrolysis fraction through the thickness of the different fire zones or elements.

Once the thermal problem is solved for a given increment of time, the thermo-chemical properties are updated in the thermo-mechanical analysis to correctly assess the current mechanical state induced by temperature. The thermal expansion is then introduced in the mechanical system and the thermo-mechanical iterates in an attempt to find the equilibrium. Once the equilibrium is satisfied, the analysis advances one step in time to repeat the same process.

This algorithm can be found in algorithm 4.

Algorithm 4: Non-linear thermo-mechanical coupling

INITIALISE THE PROBLEM

$T_0 = T(t=0)$
$F_0 = F_(t=0)$
$u_0 = u(t=0)$

for $n = 0$ **to** n_{end} **do**

THERMAL PROBLEM

$m = 0; \quad T_{n+1,0} = T_n$
while $\left.\dfrac{\underline{r_T}}{\underline{f_d} + \underline{f_c} + \underline{f_r}}\right|_{n+1,m+1} < tolerance$ **do**

obtain the residual $\left(\underline{r_T}|_{n+1,m+1}\right)$ and jacobian $\left(\underline{\underline{J_T}}\Big|_{n+1,m}\right)$

solve $\Delta T|_{n+1,m}$ in Equation 3.82

update $F_{n+1,m} = F_n$

go to: algorithm 2

$m = m + 1$

$T_{n+1} = T_{n+1,m} \quad , \quad F_{n+1} = F_{n+1,m}$

THERMO-MECHANICAL PROBLEM

$m = 0; \quad u_{n+1,0} = u_n$
while $\left.\dfrac{r_u}{F}\right|_{n+1,m+1} < tolerance$ **do**

Update thermal-dependent properties (T_{n+1}, F_{n+1})
Obtain the mechanical strain in *Equation* 4.128
go to: algorithm 3

obtain the residual $\left(r_u|_{n+1,m+1}\right)$ and jacobian $\left(J_u|_{n+1,m}\right)$

solve $\Delta u|_{n+1,m}$ in Equation 5.50 ; $\quad m = m + 1$

$u_{n+1} = u_{n+1,m}; \quad n = n + 1$

Note that for F the same letter is designated to represent either the force vector and F is the pyrolysis fraction. In the section on the thermo-mechanical problem, note

that inside the thermal-dependent properties line, the variable in question is the pyrolysis fraction.

5.3.6.1 Fire Dynamic Simulator

An important feature to take into account is the compatibility of this framework with the so-called CFD code, Fire Dynamics Simulator (FDS), this software helps to predict realistically the boundary conditions of the thermal solver by obtaining the adiabatic surface temperature of the *hot* and *cold* ends, e.g., in Figure 5.12 a building is thermally analysed under a fire scenario. It also grants the possibility to analyse other effects such as the smoke for toxicity analysis. The software, which capabilities are described in [54], is open source and funded by the *National Institute of Standards and Technology* (NIST) and actively used in research and developed by specialised centres such as the *VTT Technical Research Centro of Finland* (VTT). The application of this software to the marine industry is well extended, this is supported by the research found in [285, 286, 287, 288, 289].

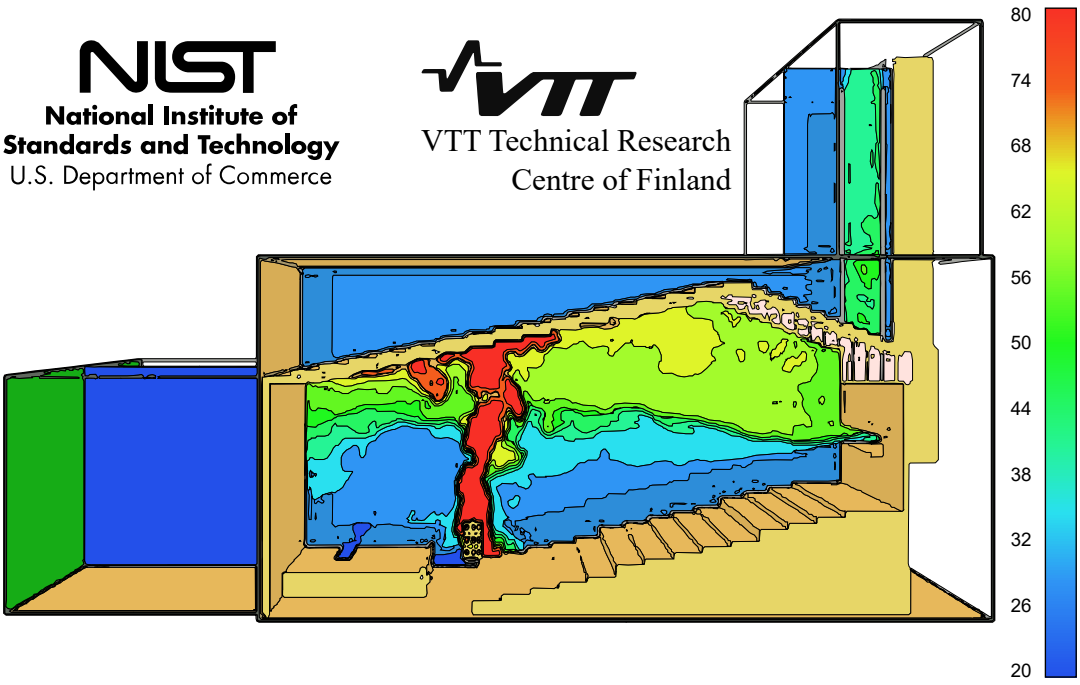

FIGURE 5.12: Snapshot of the temperature distribution inside a building with a fire source obtained from the FDS software product [9]. Adapted from [10].

The FDS is a large eddy simulation (LES) code for modelling incompressible thermally driven flows with low Mach number. The governing equations for the flow, consisting of conservation equations of mass, momentum and energy as well as the ideal gas law, are solved with a finite difference method using an explicit predictor-corrector scheme. FDS is both temporally and spatially second-order accurate. To simulate enclosure fires, FDS can be used to model, e.g., combustion, radiation, thermal degradation of solids and mechanical ventilation. [196].

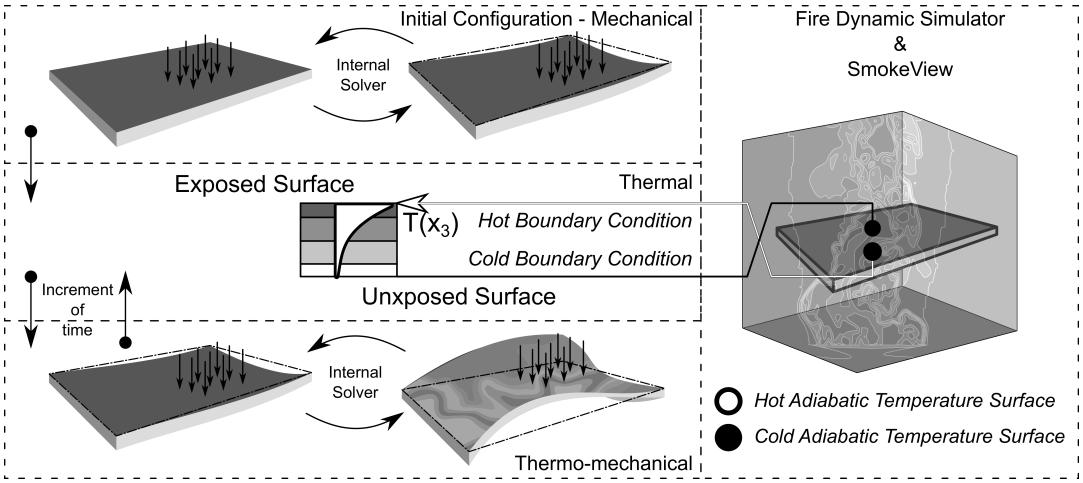

FIGURE 5.13: Flow diagram of the fire dynamic simulator and the thermo-mechanical structural solver.

The coupling is best described in the flow diagram found in Figure 5.13. The software is used to introduce the temperature, as an adiabatic surface type, of the surrounding of the structure under analysis. This is a one-way coupling, similar to the thermal solver, where the deflection of the structure is considered to not affect the fire dynamics, and therefore, the fire dynamic simulation can be simulated a priory and then post-processed to obtain the boundary conditions introduced in the thermo-mechanical analysis.

5.4 Conclusions

This chapter is brief and provides a link to the two previous chapters (chapter 3, chapter 4). The chapter 4 already examinates the type of thermo-mechanical coupling to introduce the different effects that the thermal problem has in the thermo-mechanical analysis. In this case, the coupling can be described as a decoupled thermo-mechanical problem, a one-way coupling from the thermal to the thermo-mechanical model.

The chapter has given two formulations, one for triangles and a second for quadrilaterals, that can describe the kinematics and constitutive laws of composites. The procedure used to derive the system is similar to the one used in [16], starting from the Principle of Virtual Work and then applying the finite element method to obtain the discretisation. A fair amount of discussion is given on the issues derived in the non-linear constitutive thermo-mechanical model proposed, and then the concepts relative to flexibility are introduced.

The non-linear geometric problem is analysed from the frameworks of [281] and [282], however the most successful theory is the one provided in [18]. The problem of buckling is explained and an interesting examination of thermal-induced buckling is given. With this approach, the thermo-mechanical coupling is now able to take into account, non-linear thermal analysis (pyrolysis) and non-linear thermo-mechanical analysis, the non-linear constitutive thermo-mechanical effects such as temperature-dependent properties, thermal-induced damage, and the non-linear geometric thermo-mechanical effects by using the co-rotational theory. This is unique and novel, since the co-rotational theory allows performing non-linear geometric buckling analysis, without significant modification of the FEM algorithm and without modifying the constitutive thermo-mechanical laws already derived.

At the end of this chapter, the thermo-mechanical coupling is expressed in its numerical form with a summarised algorithm. This algorithm summarises all the theoretical derivations examined during the previous chapters (chapter 3, chapter 4).

5.4.1 Goals

The goals imposed in chapter 1 are fulfilled. Goal number 7, *Address the flexibility of composites*, fulfilled since the theory proposed, solves elegantly the flexibility of composites. And goal number 11, *Provide and implement the thermo-mechanical coupling*, is as well completed in this chapter since at the end of it, the coupling is completely described.

Both goals are represented in the conclusion and are structured in this order.

Chapter 6

Verification, validation and demonstration of the computational model

6.1 Introduction

This chapter is structured according to the necessities and goals that were posed in the objectives. The different verification, validation and demonstration cases are organised in the following sections.

1. Validation of the thermal model

   The thermal model was validated for linear analysis, i.e., linear homogeneity in the micro-structure and no pyrolysis, but it seemed unnecessary to exemplify the correctness of the code for a trivial solution such as the one-dimensional heat transient problem. Nevertheless, in the thermo-mechanical analysis some analytical analysis is presented based upon the linear analysis of thermal modelling.

   Due to its more complex solution and in order to achieve goal 3 *Assess the correctness of the implementation of the thermal model*, a numerical analysis is provided in order to reproduce the experimental data found in [11].

2. Validation of the mechanical model

   To assess the correct implementation of the SPROM, the FIBRESHIP project proposed different mechanical tests, an axial, a flexural and a shear. The aim was to compare the different materials and to provide experimental data used to calibrate the mechanical models. This thesis shows the results of the axial and flexural analysis. Further details on similar results applied to solid elements can be found in [12].

   These two tests, axial and flexural, allow accomplishing the goal 6, *Assess the correctness of the implementation of the mechanical formulation*.

   Also, to address the large deflection problems characteristic of composites and to accomplish the goal 7, *Address the flexibility of composites*, a non-linear geometric buckling analysis is performed to corroborate that the co-rotational theory predicts non-linear geometric buckling.

3. Validation of the thermo-mechanical model

   Once validated in both models, the new changes introduced in the numerical validations are the thermo-chemical dependence of mechanical properties and the thermo-mechanical coupling itself. To fulfil goal 11, *Provide and implement the thermo-mechanical coupling*, an analytical benchmark is simulated to validate the thermo-mechanical model.

   The analytical benchmark is rather simple and is more a proof of verification than validation *per se*. An analysis is performed against the thermo-mechanical response of a bulkhead test specimen under fire and mechanical loading to validate the implementation.

   This experimental test is the result of the FIBRESHIP project. Another experimental test comparison is provided from the LASS campaign [2].

   Regarding the flexibility of composites exposed to fire, and to introduce important concepts on the topic of inelastic thermal buckling. Three examples are provided, two analytical and one experimental.

4. Demonstration in marine applications

   Once the knowledge and validation have been built up, in order to accomplish goal 12, *Assess the correctness of the thermo-mechanical model*, two study cases are proposed.

   First, a fluid-structure interaction (FSI) problem in which a CFD tool, the *fire dynamics simulator* (FDS), is used to obtain the adiabatic surface temperature and this is input as a boundary condition in the thermo-mechanical problem. The domain of study is one of the decks of a container ship.

   Another marine application analysis is performed, aiming to demonstrate the capabilities of the present thermo-mechanical analysis. The analysis uses both non-linear geometric and non-linear constitutive modules in order to simulate the risk of inelastic thermal buckling and the evolution of load-bearing structural divisions. The domain in question is the engine room and cargo hold of the same container ship.

   The definition of different variables should coincide with the definition given in the nomenclature, however, it might happen that for each particular example the reader might encounter certain variables that have different meanings. These variables shall only apply to each particular analysis, and therefore their scope withstands inside it. To avoid excessive confusion, the examples shall try to adapt as much as possible the nomenclature, which has been consistent in all previous chapters.

This page was left blank intentionally.

6.2 Validation of the thermal model

For this section, the numerical validation is tested against the Henderson benchmark, a benchmark that involves non-linear thermal transfer and degradation for composite materials.

6.2.1 Non-linear thermal problem - Henderson benchmark

The experimental data presented in Henderson et al. in [11] will be used to validate the non-linear transient thermal model described in chapter 3. In the experimental tests, a composite material consisting of $\Phi_{\Omega m} = 39.5\%$ of phenolic resin and $\Phi_{\Omega f} = 60.5\%$ of glass and talc filler was studied. The test samples were of the cylindrical shape of 1cm diameter by 3cm height. The tests consisted of exposing one side of these samples to a radiant heat flux of 279.7kW/m^2. The temperature evolution of the samples was monitored using four thermocouples at depths of 0.1, 0.5, 1.0 and 2.9cm from the heated side. The instrumentation, sensors and experimental procedure is described in [63].

This experimental test has been simulated with the numerical model developed in this thesis. The cylindrical samples have been modelled with 30 finite elements of 1D. The material properties and boundary conditions that have been used in the simulations are the same as those reported in [11]. A table with the most important properties is given in Table 6.1.

Property	Value
Virgin density (kg/m^3)	1810
Final char density (kg/m^3)	1440
Virgin thermal conductivity (W/m°C)	$0.804 + 2.76 \cdot 10^{-4} T$
Final thermal conductivity (W/m°C)	$0.955 + 8.42 \cdot 10^{-4} T$
Virgin specific heat (kJ/kg°C)	$1.089 + 1.09 \cdot 10^{-3} T$
Final specific heat (kJ/kg°C)	$0.870 + 1.02 \cdot 10^{-3} T$
Gas specific heat (kJ/kg°C)	9.63
Activation energy (kJ/kg°C)	$2.6 \cdot 10^5$
Pre-exponential factor (s^{-1})	$8.16 \cdot 10^{18}$
Order of reaction	6.30
Heat of decomposition (kJ/kg)	234
Surface emissivity	0.9
Temperature of glass transition (°C)	400

TABLE 6.1. Calibrated material properties extracted from [11].

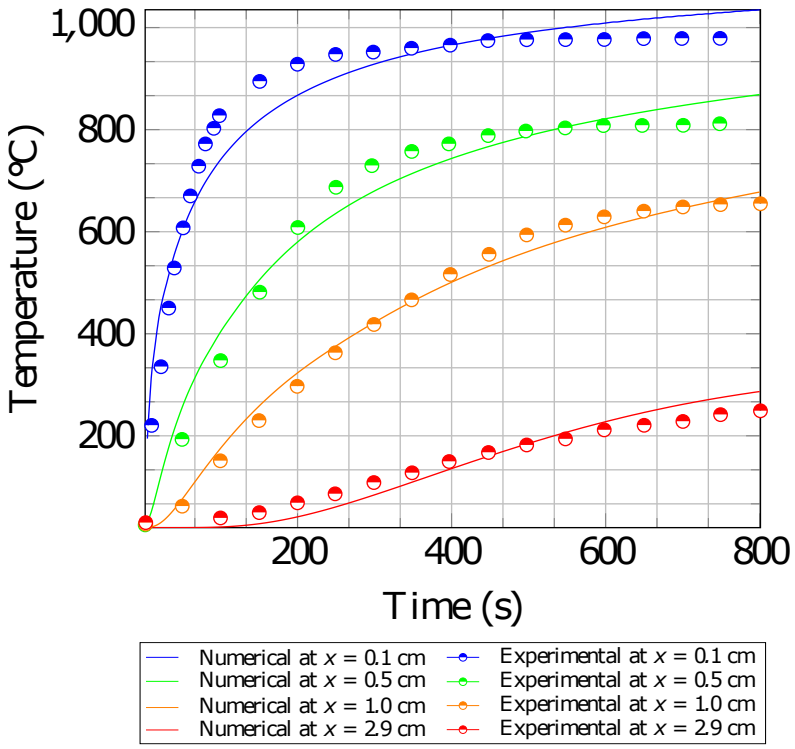

FIGURE 6.1: Evolution of the temperature ($T(x_3, t)$) of the experimental and numerical results at different thickness positions.

As seen in Figure 6.1, the numerical simulation by the thermal model is in correspondence with the experimental data carried out by Henderson et al.. This serves as a validation benchmark for the one-dimensional non-linear transient thermal model. Observe in Figure 6.2 the evolution of the temperature distribution through-thickness and time. Each of the snapshots represents the instant temperature distribution through-thickness at a given time. The heat is being transported from the hot end to the cold end.

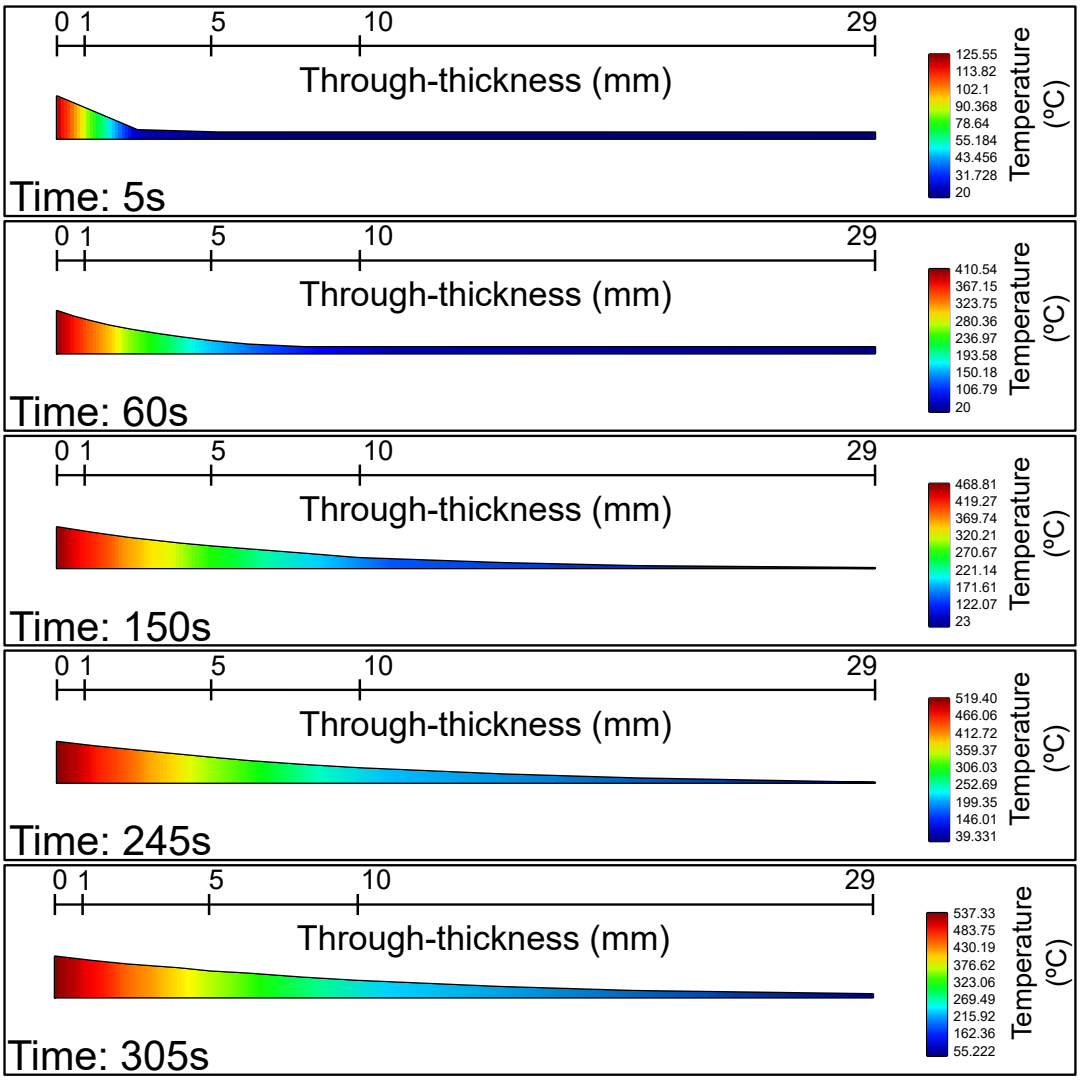

FIGURE 6.2: Temperature evolution.

Similarly, the pyrolysis evolution can be assessed with the pyrolysis fraction. Observe in Figure 6.3 the evolution of the thermal degradation parameter through-thickness and time. The material starts pyrolysis in the hot end and then the front of degradation starts advancing from the hot end to the cold end as is supposed to do in reality. This is in agreement with the temperature map shown in Figure 6.2, in which temperatures over 400°C are over the glass temperature of the resin and thus the pyrolysis process starts.

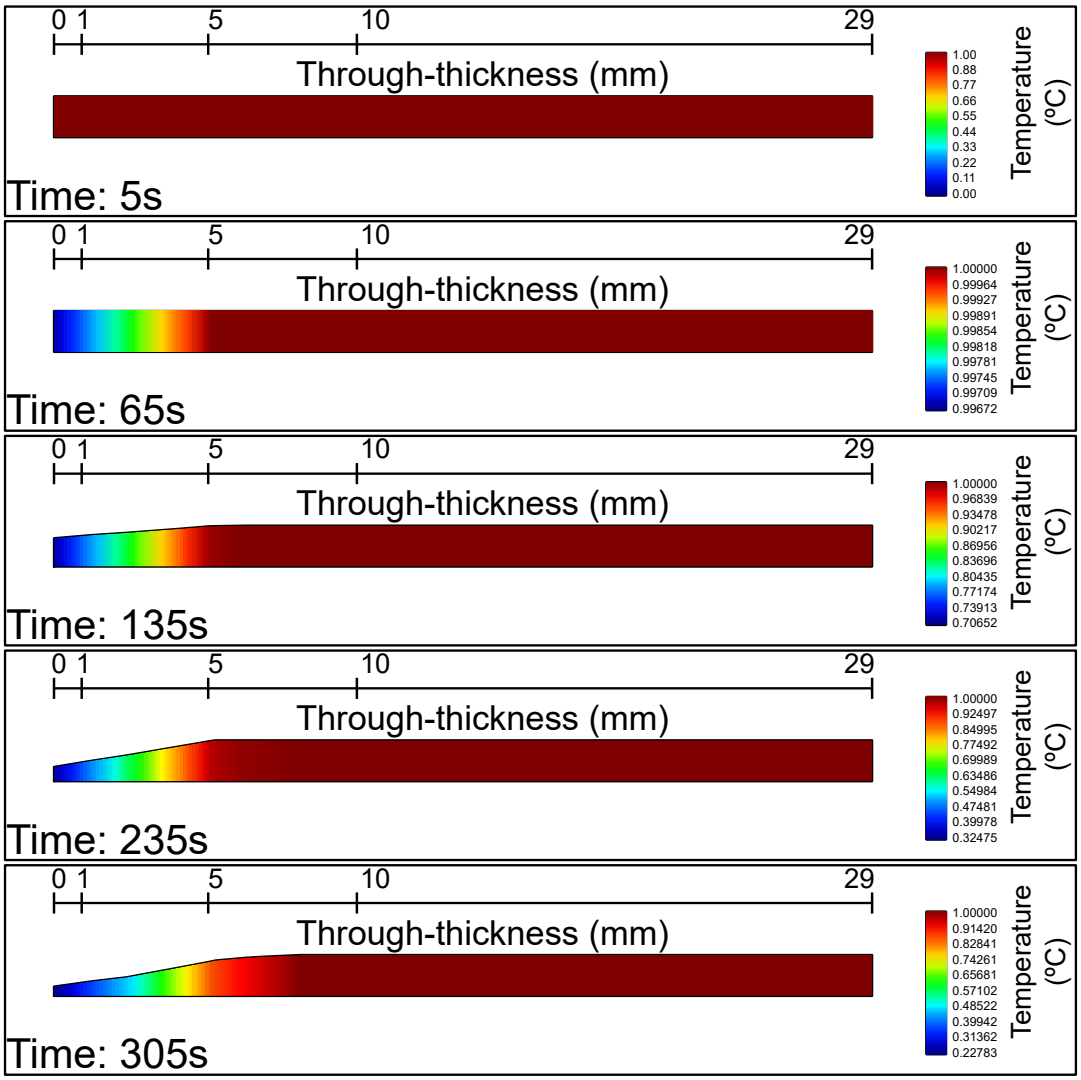

FIGURE 6.3: Thermal degradation index evolution. 1 means intact and 0 is completely degraded

The pyrolysis is indeed related to the fraction mass. The benchmark and the numerical results, see Figure 6.4, present similar, not exactly, evolution. In the benchmark original paper [11] a few comments are issued regarding inaccuracies in the material calibrations and testing that may lead to these minor differences.

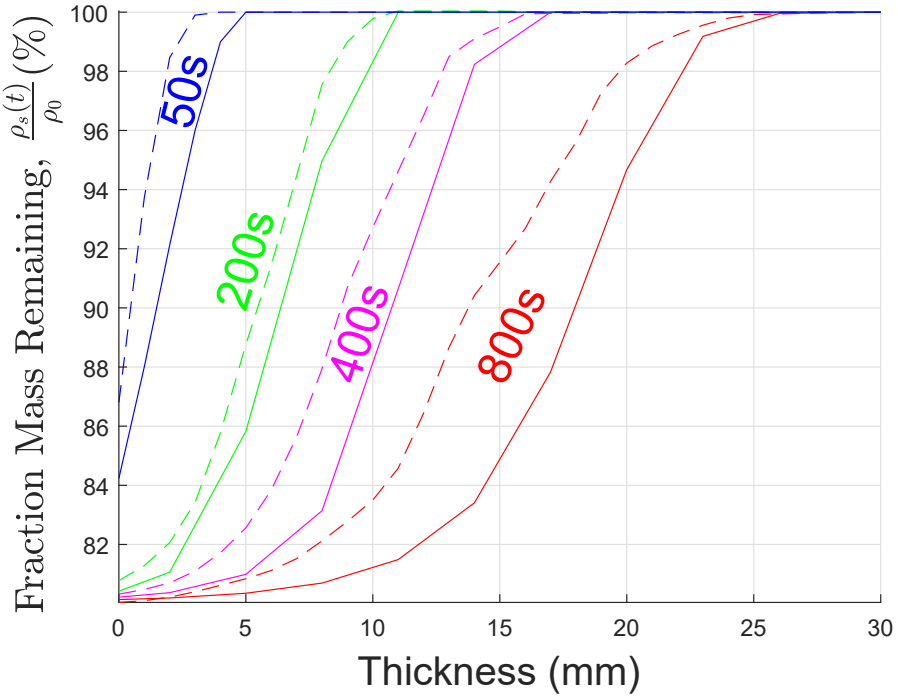

FIGURE 6.4: Evolution of the fraction mass remaining of the experimental and numerical results at different thickness positions.

6.2.2 Conclusion of the numerical implementation

The experimental results provided by Henderson et al. in [11] were reproduced by the thermal model developed with the methodology derived in this thesis. This proves the capability of the numerical implementation to predict non-linear thermal behaviour, such in:

- Pyrolysis

  The thermo-chemical degradation of the polymer matrix is shown in Figure 6.3. The numerical tool can assess the amount of degraded fraction left in the thickness of a shell.

  Moreover, this pyrolysis fraction is contemplated for the matrix in this example, but it can be retrieved also for fibre is needed.

- Composites

  The model proposed uses a layer-wise approach, so it allows using non-homogeneous materials. This difference in the materials found in the thickness stack, makes the solution non-linear due to having different thermal properties in the stack. This can easily be seen in Figure 6.1, where the numerical output matches precisely the non-linear evolution and distribution of the experimental results.

In conclusion, this section has served to accomplish the proposed goal number 3, '*Assess the correctness of the implementation of the thermal model*'.

This page was left blank intentionally.

6.3 Validation of the mechanical model

The validation results presented here will address the problems of inelastic and buckling behaviours. Two inelastic tests based on the test campaign developed, in the FIBRESHIP project, are detailed, and then validation of the non-linear geometric module is proven against the theoretical buckling of an Euler beam.

6.3.1 FIBRESHIP Campaign

During the FIBRESHIP campaign, among the several testing, two calibrations of the mechanical properties were carried out. These two calibrations, which are shown below, belong to the category of tensile and flexural tests, courtesy of the University of Limerick. In both tests, the same material is employed and the calibration shown is useful to show a practical procedure based on the SPROM theory and to demonstrate that this theory is capable of simulating the non-linear constitutive range.

6.3.1.1 Tensile test

This numerical validation shows the accuracy that the SPROM has in reproducing non-linear composite failure. The validation is divided into five parts and it focuses on the so-called LEO system composite. This material is the composition of fibreglass with a vinylester resin, and more relevant information about it is given in Appendix A. The other material simulated is a fibreglass and epoxy solution named SR1125, further detail can be found in [12].

1. Domain

   The domain for the longitudinal (0°with respect to the fibres) and transverse (90°) axial loading computational model is described.

2. Experimental data

   Here the most relevant information for the specimen data is given. The experimental data provided is the one that belongs to the composite, made out of the Saertex's LEO system [290], since this was the finalist material from the initial poll of material to be used in the FIBRESHIP project.

3. Specimen results

   The test results are shown for both the LEO system and SR1125, the latter is shown to demonstrate how well the SPROM can predict the transverse stiffness.

4. Linear correction

   From here onward, the analysis is focused on the LEO system, the FRP that offered better performance. This part delves into some deficiencies that have been detected from the results provided by the University of Limerick, which carried out the experimental campaign. In short, the tests used two sets of instrumentation to measure force-displacement and stress-strain curves. The

first curve is usually measured with grips and the second with an extensometer, which indeed should be more precise. However, axial testing at 0° requires that the extensometer is dismounted before damaging the specimen since the rupture in that axial direction is very abrupt and may damage the instrumentation. After a dedicated analysis, it was found that one of the two curves was deriving the displacement/strain field from the other. Thus, certain corrections had to be derived in order to predict well the longitudinal curves.

5. Non-linear assessment

   Once the problem has been solved, an accurate solution is provided for the two axial tests for the LEO system composite.

6.3.1.1.1 Domain

A sketch of the model indicating the sample sizes and boundary conditions is presented in Figure 6.5. Note that only a fourth of the specimen is modelled by the FEM method, to reduce the computational cost by application of appropriate boundary conditions in the longitudinal and transverse centre lines of the sample.

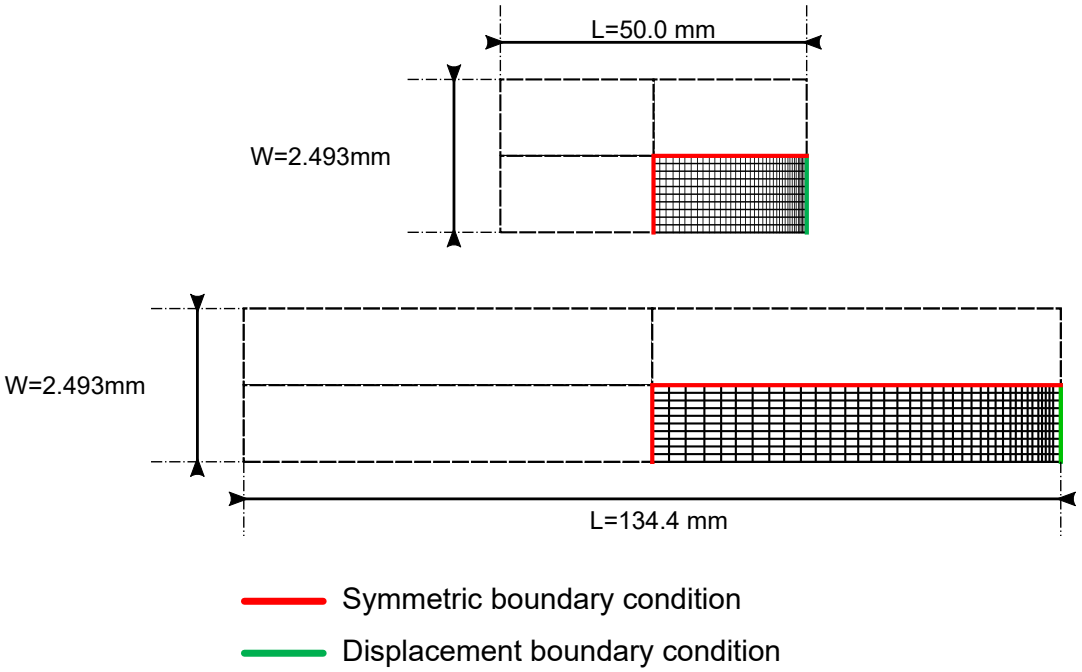

FIGURE 6.5: Chart describing axial testing at 0°of a specimen.

Displacement boundary conditions are further applied to the free edges of the specimen (green boundaries in Figure 6.5), these should be the same as the maximum value of the displacement found in the force-displacement curve. In the case of the longitudinal samples, the length of the simulated specimen was considered to be the distance between grips. By contrast, the transversely oriented specimens were modelled assuming the effective length to be the distance between extensometers.

6.3.1.1.2 Experimental data

The effective data found from the experimental tests are described in Table 6.2 for the longitudinal tests and Table 6.3 for transverse tests. The meaningful information to simulate the SR1125 can be found in [12]. It can be seen that the problemat regarding the different elastic modulus readings by the two instrumentation is patent in Table 6.2, in this table, there are two readings of E1 and E2 that are inconsistent with 30% respect to the theoretical value that a composite made out of fibreglass and vinylester should have. The other important problem comes from the definition of the testing, this testing used a UD laminate, however when consulting the datasheet found in Appendix A, the fibreglass used in the LEO system material is not purely UD.

Following the specifications of the data sheet, each layer nominally contains 90% of unidirectional (UD) fibres and 10% of transverse fibres and stitching. Nevertheless, these percentages are in terms of pure areal weight. This means that a correction factor may be necessary to calibrate a more appropriate ratio of unidirectional and transverse fibre distribution. Note also that the reinforcement fibres in the transverse direction (90°) have a lower density (200 and 60 TEX) than those in the longitudinal direction (2400 TEX). This must be also considered in order to assess a precise equivalent thickness for the 0°and 90°fractions of the monolithic stack.

The best option to calibrate the effective volumetric fraction, thickness-wise, i.e., the percentage of fibres in the 0°and the percentage in 90°, is by trying to find the correct proportion for the given volumetric fraction ($\Phi_\Omega = 55\%$). Using the curves in Figure 6.11 and Figure 6.12, the correct proportion is the one that best fits the elastic slope on both curves. Throughout an iterative process, it has been found to be a proportion of 83% and 17% of longitudinal (0ž) and transverse (90ž) fibres respectively.

Sample ID		LEO UD - T1	LEO UD - T2	LEO UD - T3	LEO UD - T4	LEO UD - T5	Average	CV
Length (grips)	(mm)	134	134	134	135	135	134.4	0.40%
Length	(mm)	294	294	294	295	295	294	0.20%
Width	(mm)	24.74	24.79	24.82	24.81	24.82	24.8	0.13%
Thickness	(mm)	3.19	3.213	3.237	3.1	3.183	3.2	1.63%
Failure Load	(kN)	62.9	60.5	53.4	54.3	54.2	57.1	7.6%
Failure Stress	(MPa)	818.5	765.5	677.2	681.9	674.8	732.6	9.0%
Stroke (@ failure)	(mm)	5.4	5.3	4.2	4.5	4.7	4.8	10.70%
Strain (@ failure)	(%)	4.0	3.9	3.1	3.3	3.5	3.6	10.80%
Young's modulus, E1	(GPa)	37.9	36.8	35.6	33.6	33.8	35.5	5.30%
Young's modulus, E2	(GPa)	26.3	25.3	25.2	26.9	25.8	25.9	2.80%

TABLE 6.2. Properties of the LEO system experiment when the axial test is at 0°.

Sample ID		LEO 90°- T1	LEO 90°- T2	LEO 90°- T3	LEO 90°- T4	LEO 90°- T5	Average	CV
Length (grips)	(mm)	128	128	128	128	128	128	0.00%
Length	(mm)	288	288	288	288	288	288	0.00%
Width	(mm)	25.27	25.14	25.15	25.15	24.95	24.93	3.02%
Thickness	(mm)	3.573	3.393	3.303	3.277	3.397	3.4	3.43%
Failure Load	(kN)	4.7	5	4.8	4.5	5	4.8	4.4%
Failure Stress	(MPa)	51.9	61.1	57.3	54	58.8	56.6	6.5%
Stroke (@ failure)	(mm)	0.3	0.7	0.6	0.5	0.7	0.6	29.90%
Strain (@ failure)	(%)	0.6	1.3	1.3	0.9	1.3	1.1	29.60%
Young's modulus, E1	(GPa)	11.6	12.3	12.2	12.4	12.1	12.1	2.60%

TABLE 6.3. Properties of the LEO system experiment when the axial test is at 90°.

6.3.1.1.3 Specimen results

The results are presented as shown in Figure 6.6, this data is defined as follows

- Solid line in colour: the experimental data of the specimen
- Solid line in black: the numerical model with a constitutive type such as orthotropic homogeneous equivalent.
- Crossed points in black: the numerical model with a constitutive type such as ROM.
- Circled points in black: the numerical model with a constitutive type such as SPROM.

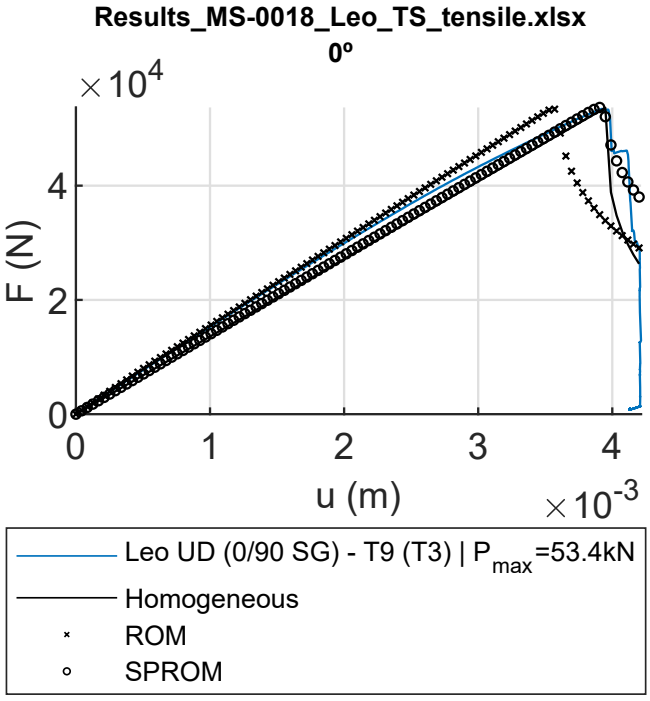

FIGURE 6.6: Example of a diagram force-displacement obtained from the axial testing at 0°of a specimen.

From Figure 6.6 it can be observed that the homogeneous solution (the easiest and quickest model) produces an accurate prediction of the longitudinal stiffness. The SPROM is also able to predict very well this non-linear behaviour and breaks abruptly when arriving at the ultimate strength. The other formulation is the ROM, which assumes iso-strain in all directions, it shows that even in this case, the ROM is worse at predicting the longitudinal response than the SPROM or the homogeneous equivalent model.

In Figure 6.7 the longitudinal analysis of all five specimens is given and compared against the experimental data. Generally, the homogenised formulation is much better in the prediction of the longitudinal strength. This is an apparent result, because as commented before, it will be seen later that indeed these curves are not scaled correctly in the horizontal axis. The ROM performs significantly worse than the SPROM and the SPROM more or less can to predict the rupture, however it tends to fail a bit earlier than it should.

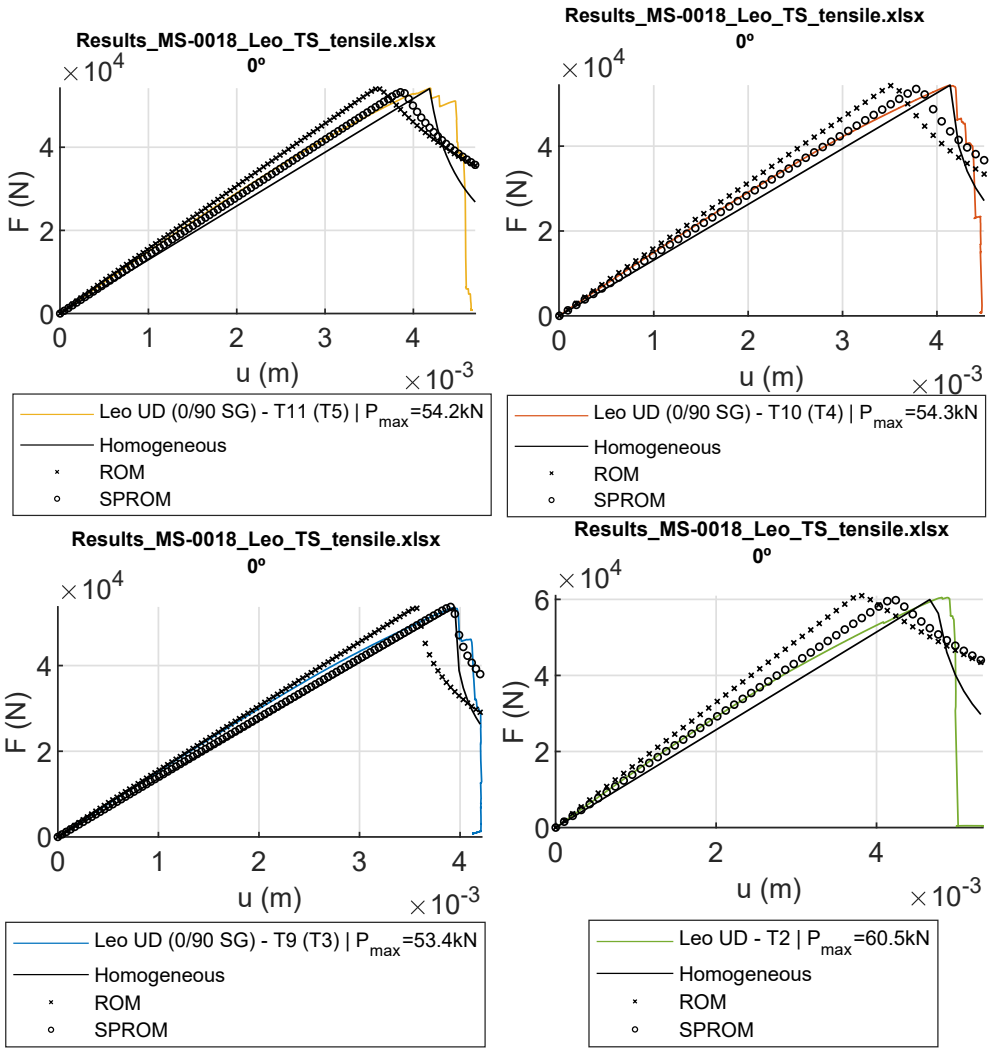

FIGURE 6.7: Leo system composite material. Axial testing at 0°

If the transverse stiffness is analysed in Figure 6.8, it is found that the SPROM can predict better the transverse stiffness, while the homogeneous method underestimates the stiffness. The ROM here since uses an iso-strain hypothesis instead of the

iso-stress hypothesis returns unreasonable predictions.

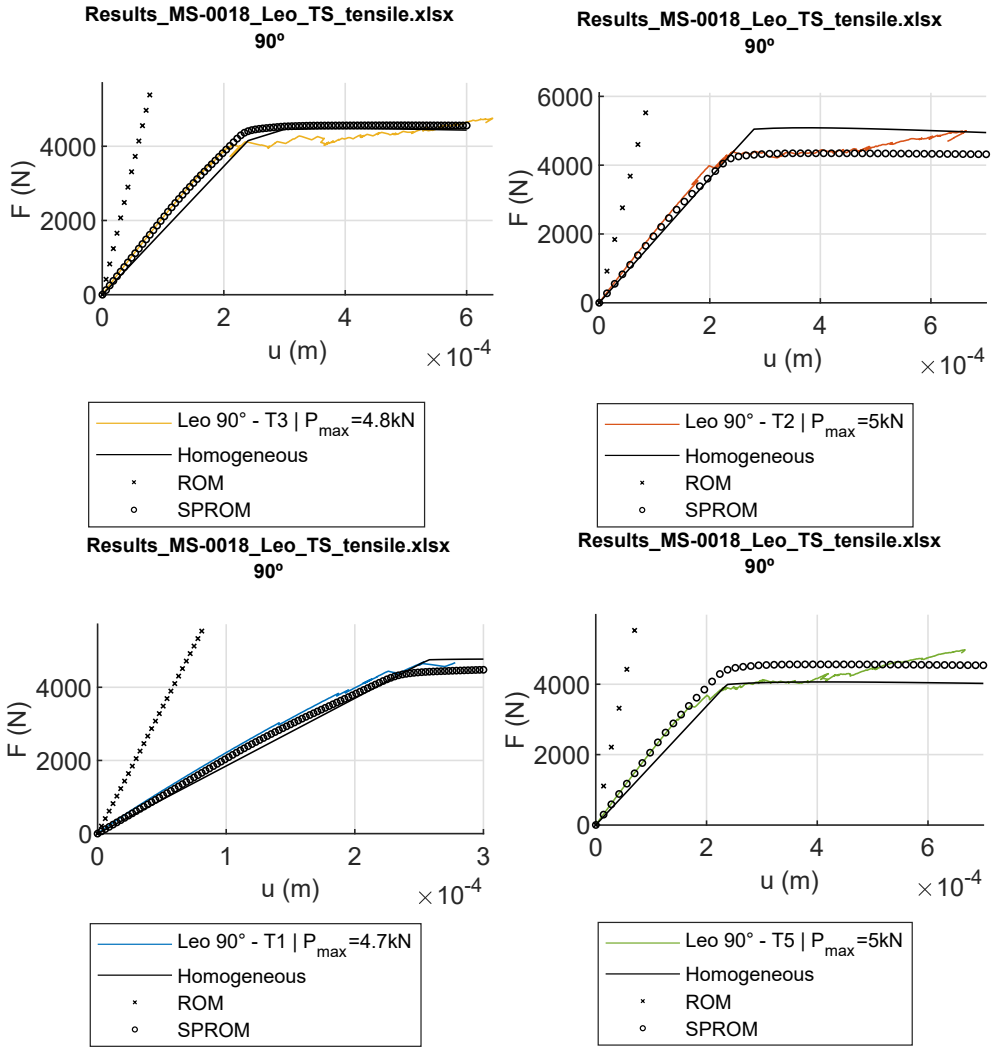

FIGURE 6.8: Leo system composite material. Axial testing at 90°

It seemed obvious that it would take longer to find the correct calibration, however when the SR1125, a simple fibreglass-epoxy composite was simulated, a major flaw in the data was rapidly noticed. Observe Figure 6.9, the ROM and the SPROM correctly address the stiffness at the very beginning, but this is nothing more than a visual effect, the truth is that thanks to checking the stiffness of this material, which did not qualify as a finalist material, some major problem was found. The stiffness of a material can be inferred from Young's modulus by using a simple rod theory, because this experimental test is a pure axial test. When doing so, the stiffness found was aligned with the curves of the ROM and SPROM and not the experimental data. This proved that something was not correct in the provided charts.

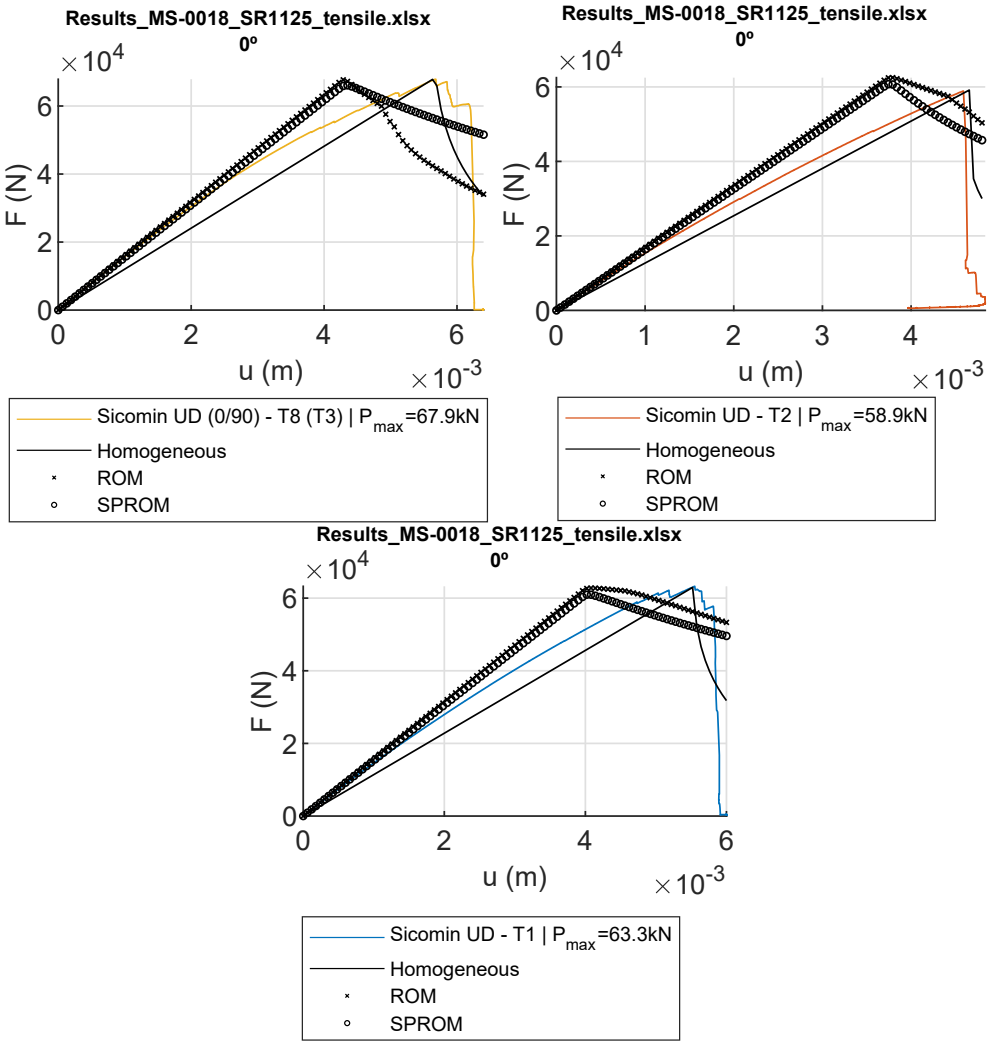

FIGURE 6.9: SR1125 system composite material. Axial testing at 0°

Whereas the longitudinal charts seemed to be incorrect, once the flaw was spotted and the numerical analysis was re-run, with the standard values for fibreglass and epoxy, the transverse prediction was extremely outstanding for the SR1125 material (see Figure 6.10). Notice how neither the ROM and homogeneous theory are able to obtain the curve, the closest that can be obtained with the homogeneous equivalent material is when using a perfect damage curve and this is still very poor.

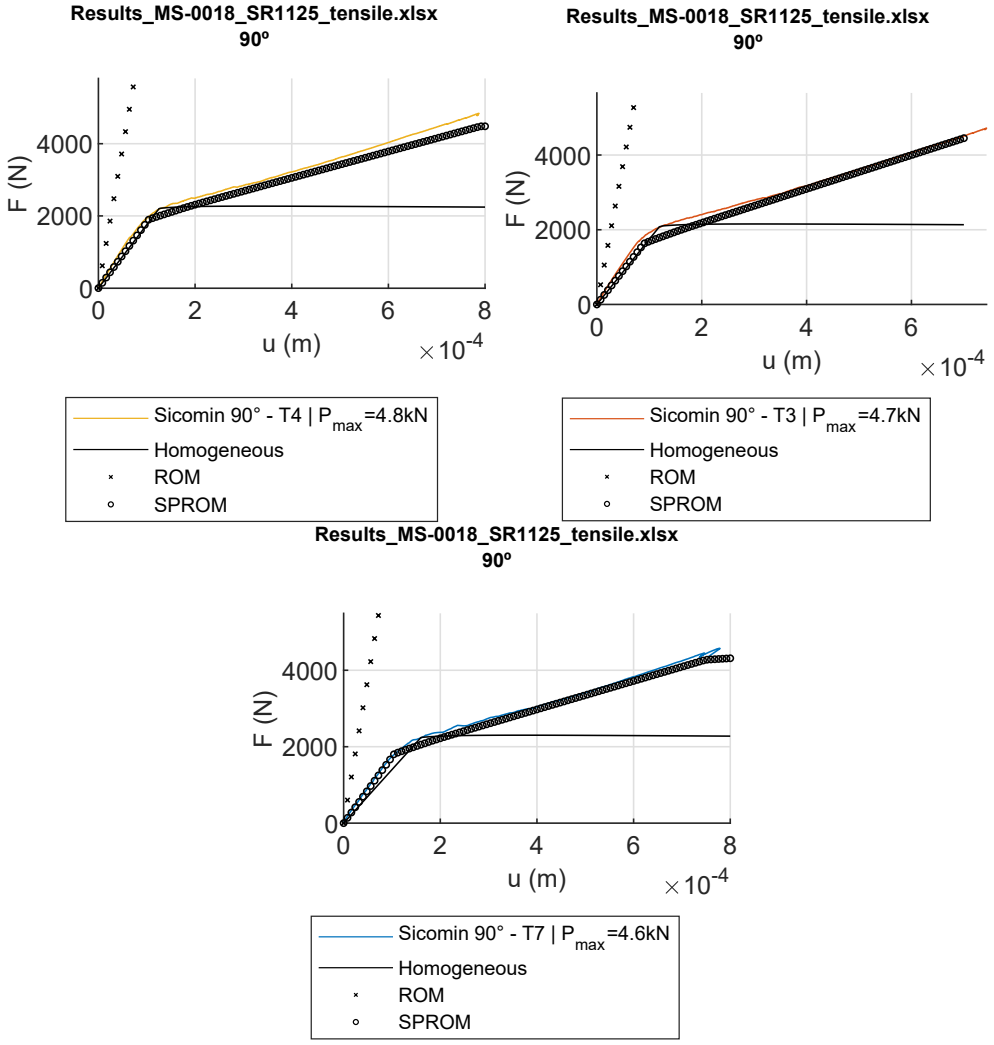

FIGURE 6.10: SR1125 system composite material. Axial testing at 90°

6.3.1.1.4 Linear correction

Once the problem was spotted, a thorough analysis of the problem was performed. The LEO system composite remains the case of interest since it is the one which is going to be used in building the demonstrable as well as design material in structural members. The longitudinal test was analysed to find which should be the equivalent stiffness for the theoretical Young's modulus found in the extensometer. In practice, if both instrumentations are good enough, they should predict correctly the same stiffness. Although in reality, it is true that composites suffer from length-scale problems and this can introduce uncertainties, however this uncertainty is of -30% which is not feasible even if large-scale effects are taking place in the readings. The rod theory established that for a rectangular bar, the following relationship holds true

$$\frac{K}{E} = \frac{l_t l_w}{l_L} \tag{6.1}$$

where l_w is the width and l_L is the length of the specimen. Considering the elastic modulus of the grips and the elastic modulus of the extensometer, the resultant difference is shown in Figure 6.11.

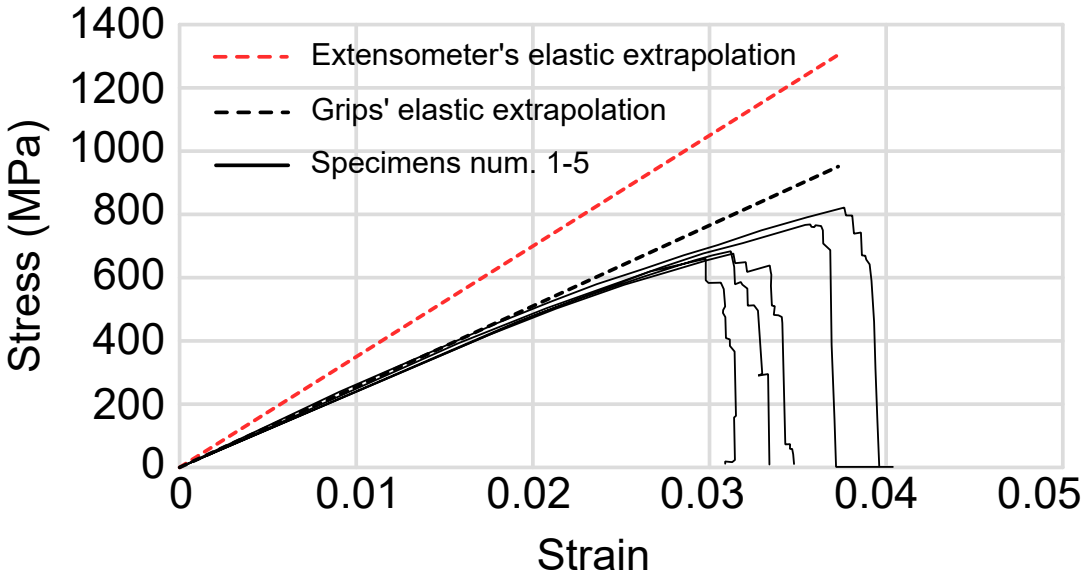

FIGURE 6.11: Comparison of elastic modulus for 0° including the experimental data and the two instrument readings.

The provided curves do not match the young modulus that is given. Hence, the scale of the displacement needs to be modified by the following relationship.

$$\frac{K_{\text{ext}}}{K_{\text{grips}}} = \frac{E_{\text{ext}}}{E_{\text{grips}}} = \frac{35.5}{25.9} = 1.37 \tag{6.2}$$

Therefore, assuming that both instruments should read the same force.

$$K_{\text{grips}} \cdot u_{\text{grips}} = F = K_{\text{ext}} \cdot u_{\text{ext}} \tag{6.3}$$

The following relationship is defined

$$u_{\text{ext}} = \frac{u_{\text{grips}}}{1.37} \tag{6.4}$$

The next question is whether in the transverse test, an axial test where the same methodology can be applied, the given Young's modulus is correct or not. *A priori*, the transverse stiffness was very well captured before, however, it shall be checked to reduce any uncertainty.

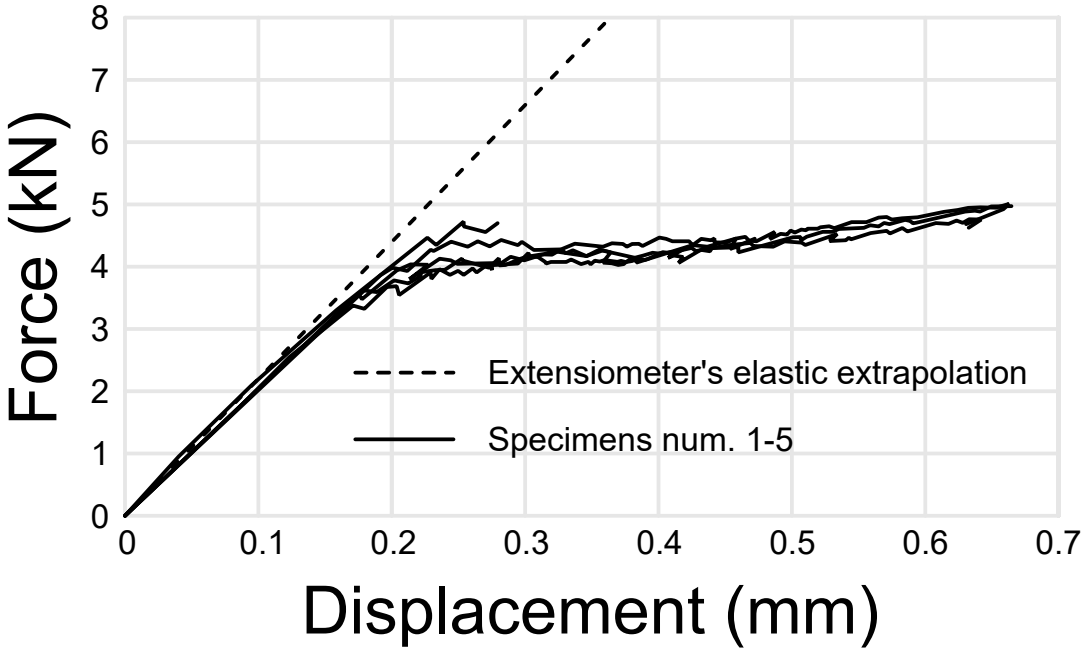

FIGURE 6.12: Comparison of elastic modulus for 90° including the experimental data and the extensometer reading.

Figure 6.12 shows the correctness in Young's modulus measured in the transverse direction. The curves match the theoretical measured elastic modulus.

6.3.1.1.5 Non-linear assessment

Property	Symbol	Units	Matrix	Fibre
Young modulus	E	(GPa)	3.35	72
Poison coefficient	ν	-	0.26	0.21
Specific weight	ρ_g	(N/m3)	10791	24900
Yield stress	σ_y	(MPa)	20	1800
Fracture energy	Π_F	(N/m)	1.2E+04	8.0E+05
Saturation stress	σ_∞	(MPa)	0	0
Traction/Compression ratio	c_{CR}	-	1	1
Damage law			Exponential	Exponential
Damage norm			Symmetric	Symmetric

TABLE 6.4. Mechanical properties calibrated for the LEO system material.

By using the standard rule of mixtures and a first estimate of the fibre volume fraction inferred from the information provided by the manufacturer, together with the stacking sequence information of the tested samples, a first estimation of the fibres and matrix elastic properties are obtained. This data is used as an input for the material properties in the numerical model used in RamSeries to reproduce the tensile test experiments. The force-displacement curves obtained with RamSeries are further refined iteratively by adjusting the material properties until a satisfactory prediction

of both, longitudinal and transverse tensile curves are obtained. The fine-tuning of the predicted tensile curves is done by adjusting both, the elastic properties and the damage model parameters necessary to capture the non-linear part of the experimental curves. The final set of properties that best match the experimental results is summarised in Table 6.4.

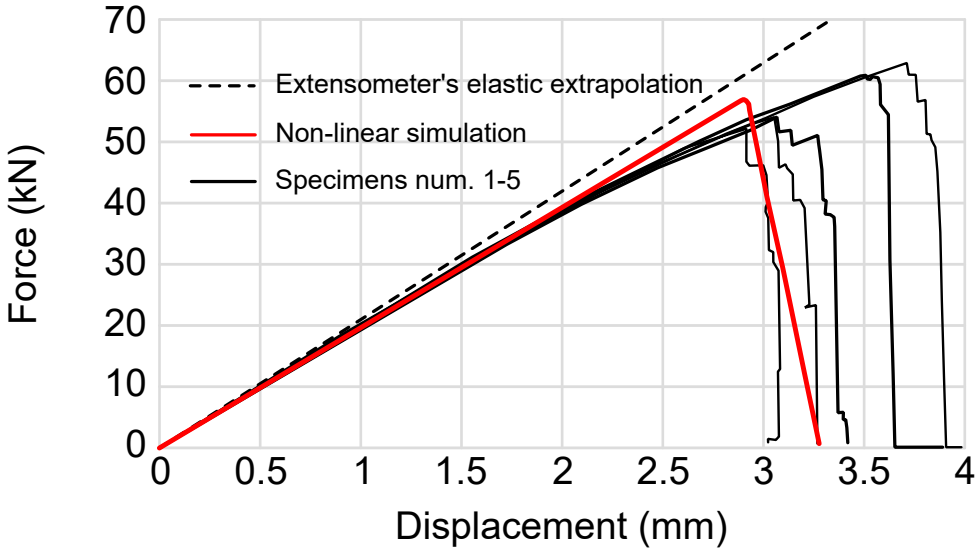

FIGURE 6.13: Numerical non-linear prediction for 0° compared against the experimental data.

In Figure 6.13 the force-displacement curve obtained in the simulations of the tensile test along the longitudinal direction is presented together with the re-scaled Force-Displacement curves of the experiments. The numerical results exhibit a perfect match of the elastic part of the curves (i.e. up to a displacement of about 0.5 mm). The gradual loss of stiffness due to the damage to the matrix is also well captured up to a displacement of about 2.25 mm. From this point on, in advanced stages of damage, the numerical curve is slightly higher than the experimental one.

Nevertheless, the failure load is about 56.9 kN, which is in perfect accordance with the 57.1 kN average failure load observed in the experiments (see Table 7). The stroke at failure is also in quite good agreement with the experiments. Although its actual value of about 2.91 mm is significantly smaller than the average experimental stroke at failure, it coincides well with the 2.93 mm exhibited by the earlier breaking specimen.

Note that this can be explained by the fact that the numerical simulation completely loses convergence when a single finite element gets completely damaged. When this occurs, a sudden drop in the curve appears, giving complete failure of the sample itself. In the experiments, the phenomena are slightly different since the sample breaks also abruptly but exhibits a series of discontinuous steps during the breaking process of the specimen. Hence, the numerical stroke at failure should be best compared to the occurrence of the first breaking step in the experimental samples. Note also that trying to reproduce numerically the abrupt failure of the longitudinal experimental samples is a challenging problem since a very small-time increment should be used to be able to capture the rapid change in the slope of the force-displacement curve during the ultimate damage stage. The use of such small-time

increments is very expensive in terms of computing time for this type of simulation since the advanced material model being used is already computationally expensive on its own.

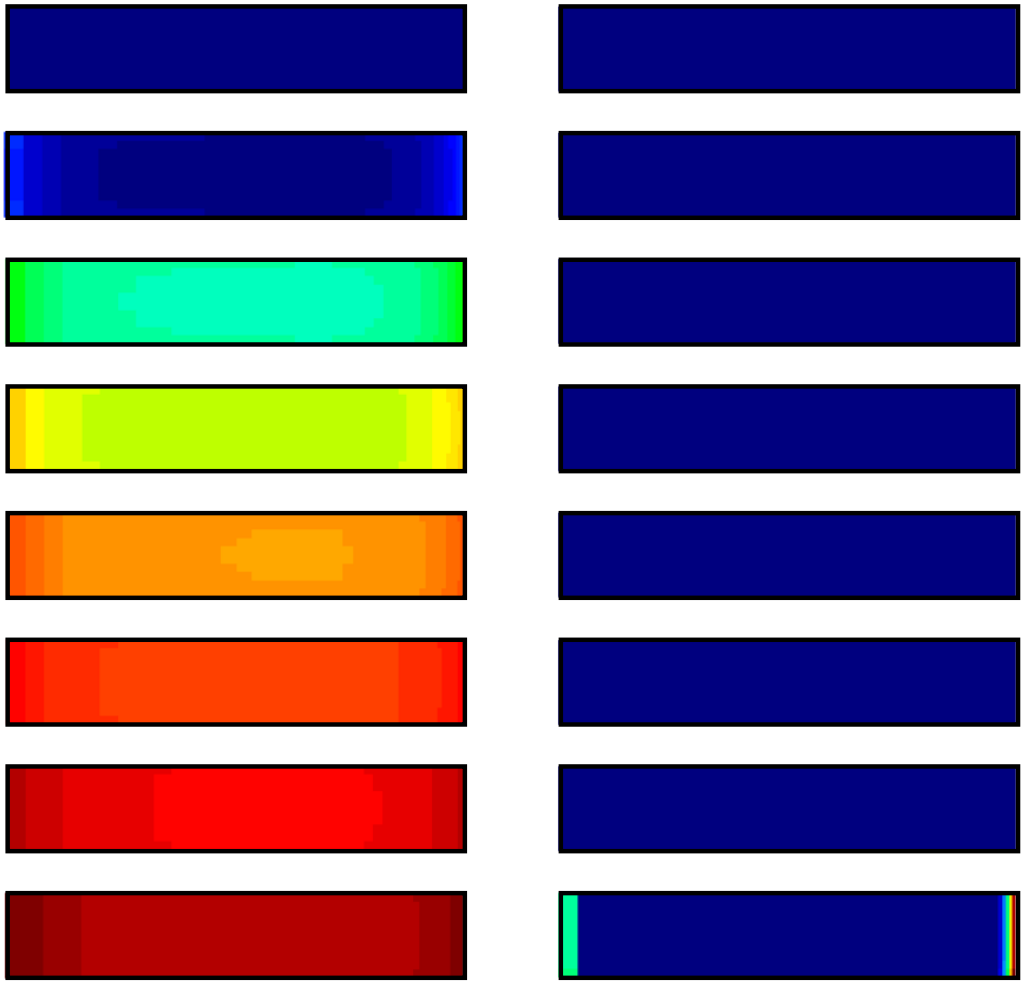

FIGURE 6.14: Damage evolution of matrix (left) and fibre (right) for the 0°test. The index of damage goes from 0 to 1 which is equivalent to the colour map from blue to red.

In Figure 6.14 the damage to the matrix and fibre are examined at different stages of the force-displacement curve. As it can be observed, the damage in the matrix starts to develop very soon and increases continuously during the numerical experiment. This explains the non-linear behaviour and the gradual loss of stiffness in the intermediate part of the force-displacement curve. By contrast, the fibres remain undamaged during almost the entire simulation. Only at the very end of the simulation, damage occurs in the fibre phase at the centre of the specimen and close to the grips (i.e. where the displacement boundary conditions are applied). When damage appears in the fibre phase, the first layer of elements in the centre of the specimen gets completely damaged since the matrix there was already fully damaged. Hence, the last snapshot in Figure 6.14 represents the instant when the abrupt rupture because a bundle of fibres go suddenly from almost no damage to a critical failure mechanism, as clearly exemplifies by the picture in Figure 6.15.

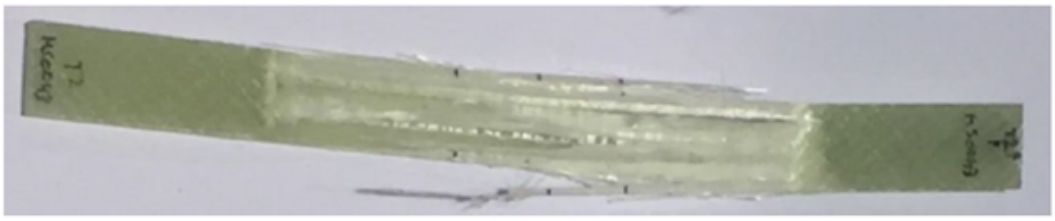

FIGURE 6.15: Failure of a specimen for 0° testing, abrupt fibre fracture happens in the centre and grips.

In Figure 6.16 the force-displacement curve obtained in the simulations of the tensile test along the transverse direction is presented together with the corresponding experimental curves. As with the previous case, the linear range is perfectly captured. The non-linear range is smoothly captured in the intermediate region of the curve, where the behaviour of the material is governed by the degradation of the matrix.

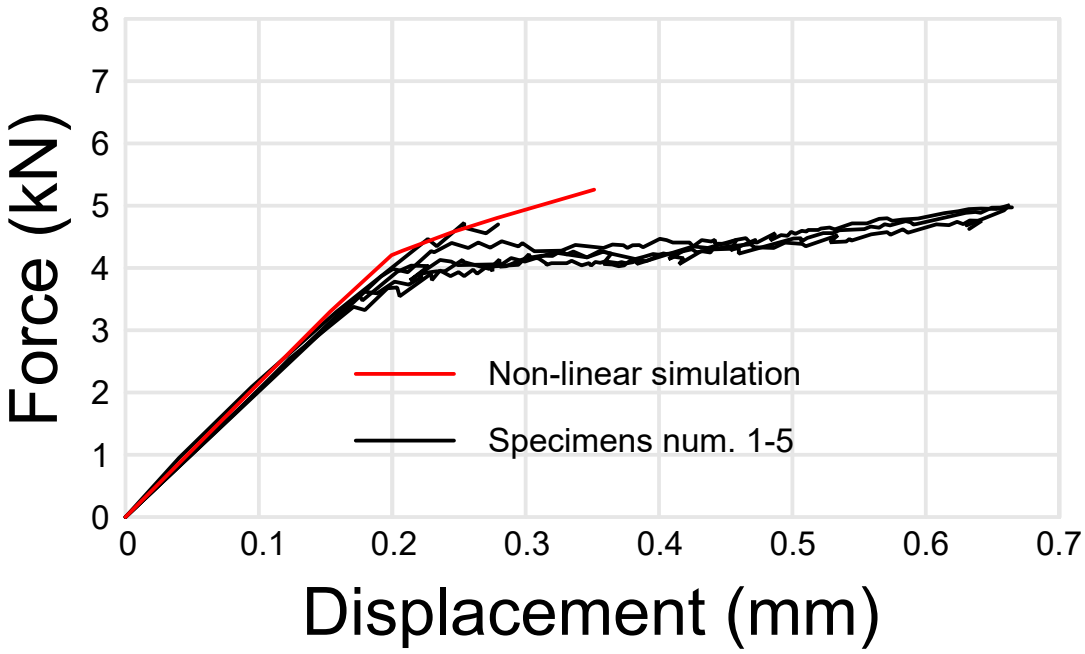

FIGURE 6.16: Numerical non-linear prediction for 90° compared against the experimental data.

The failure mechanism seems to be different for some specimens, visco-elastic failure or brittle fracture, as shown in Figure 6.17.

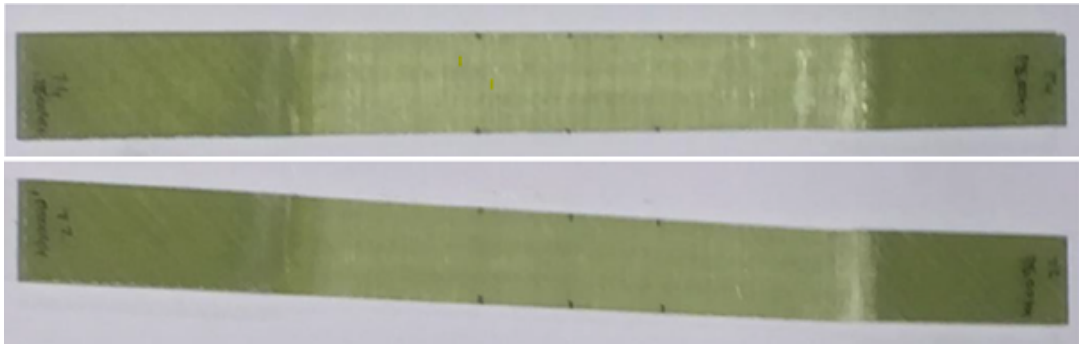

FIGURE 6.17: Failure of a specimen for transverse testing, mild and inconsistent damage found.

The numerical prediction, Figure 6.18, does not really give much information, aside from the fact that it matches well the curve of one of the specimens.

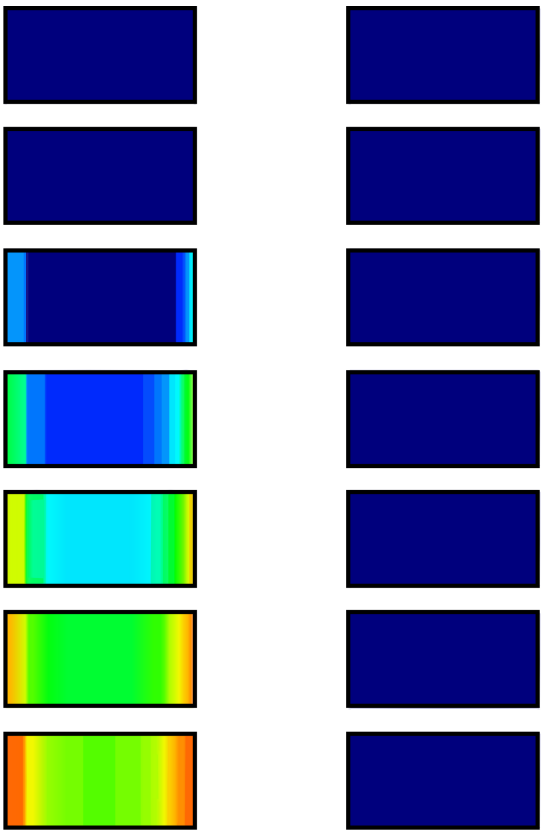

FIGURE 6.18: Damage evolution of matrix (left) and fibre (right) for the 90°test. The index of damage goes from 0 to 1 which is equivalent to the colour map from blue to red.

6.3.1.2 ISO 14125 - flexural test

The materials used in this example are the same as in subsubsection 6.3.1.1. This means that there is no need to calibrate the material again.

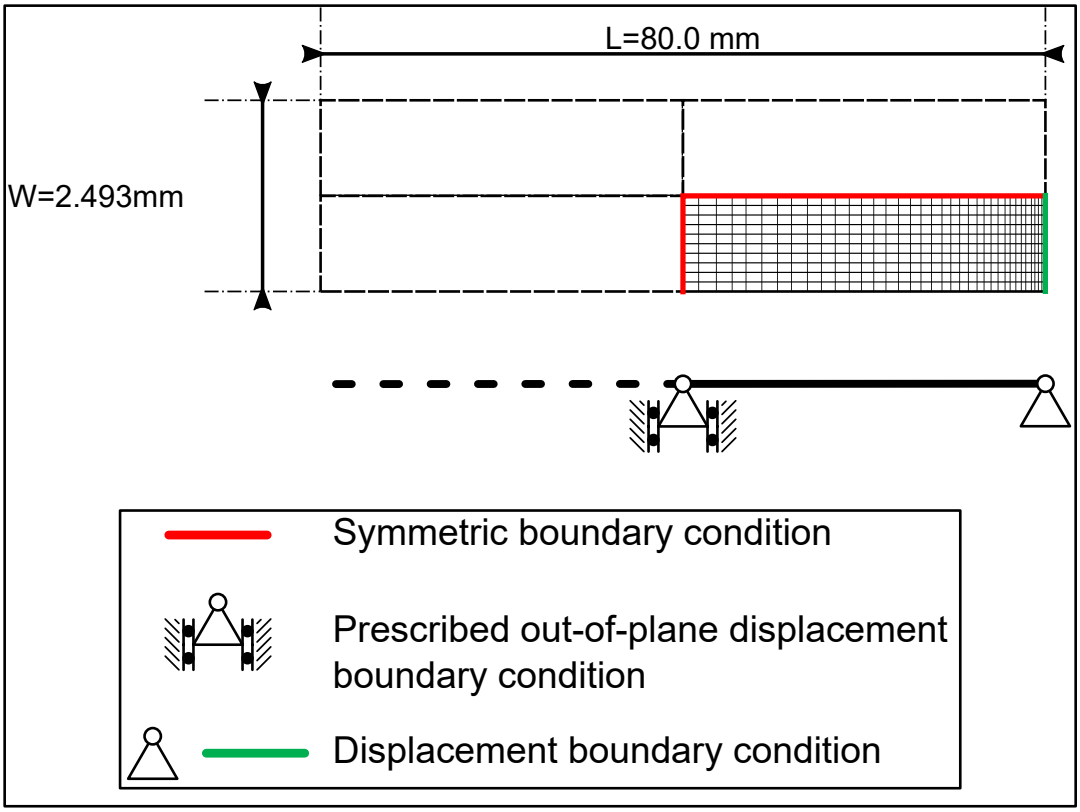

FIGURE 6.19: Computational domain of the flexural test, both longitudinal (0°) and transverse (90°)

The total length of the flexural specimens is L = 200 mm. Nevertheless, the effective span is 80 mm. As in the previous section, only a fourth of the sample is modelled because of the symmetry in the configuration of the experiments. To this aim, appropriate symmetry boundary conditions in the in-plane directions are applied along the longitudinal and transverse centre lines of the sample. In the out-of-plane direction, a simply supported constraint is applied at the free edge of the simulated sample, while a prescribed displacement resembling the deflection of the specimen is applied at the transverse centreline of the specimen.

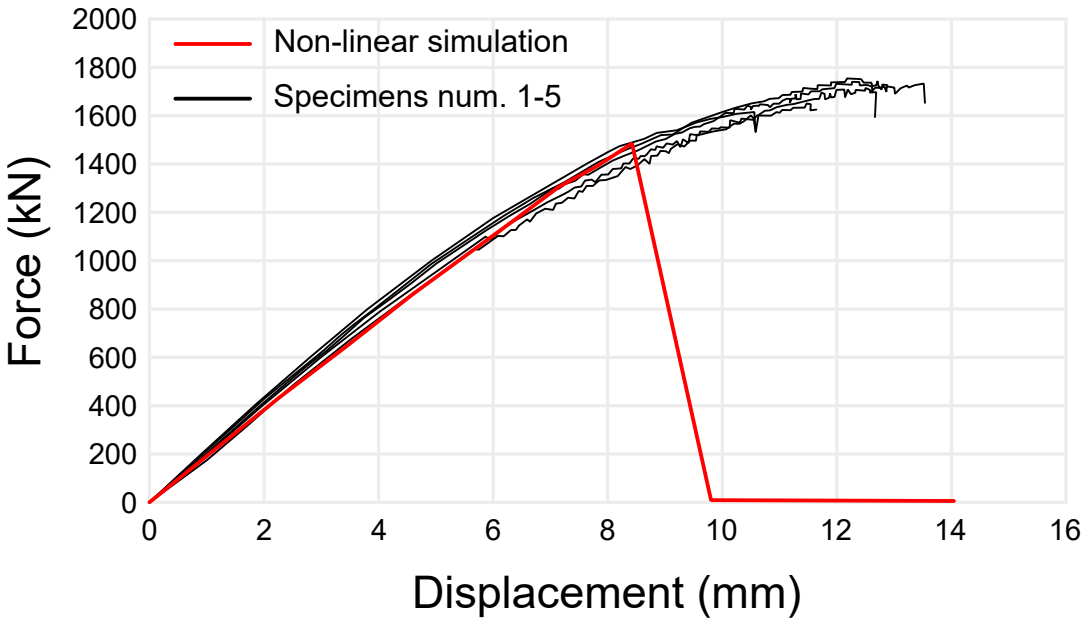

FIGURE 6.20: Numerical non-linear prediction for 0°compared against the experimental data of the flexural test.

The experimental curves corresponding to the longitudinal flexural tests are presented in Figure 6.20 together with the response simulated in RamSeries. As it can be observed, the longitudinal flexural response can be perfectly reproduced in the linear rane and up to around 75% of the averaged non-linear range of the curves. Although it has a premature break-point, the non-linear phenomenon is well captured as shown by the decreasing stiffness given by the slope of the force-deflection curve which is reduced from an initial value of about 194 kN/mm to a final value of 144 kN/mm just before the abrupt failure.

FIGURE 6.21: Failure of a specimen for the longitudinal flexural testing, damage localised in the centre.

Damage localisation is also in accordance with the observations made in the experimental samples. As can be observed in Figure 6.21, the damage is localised in the centre of the specimen.

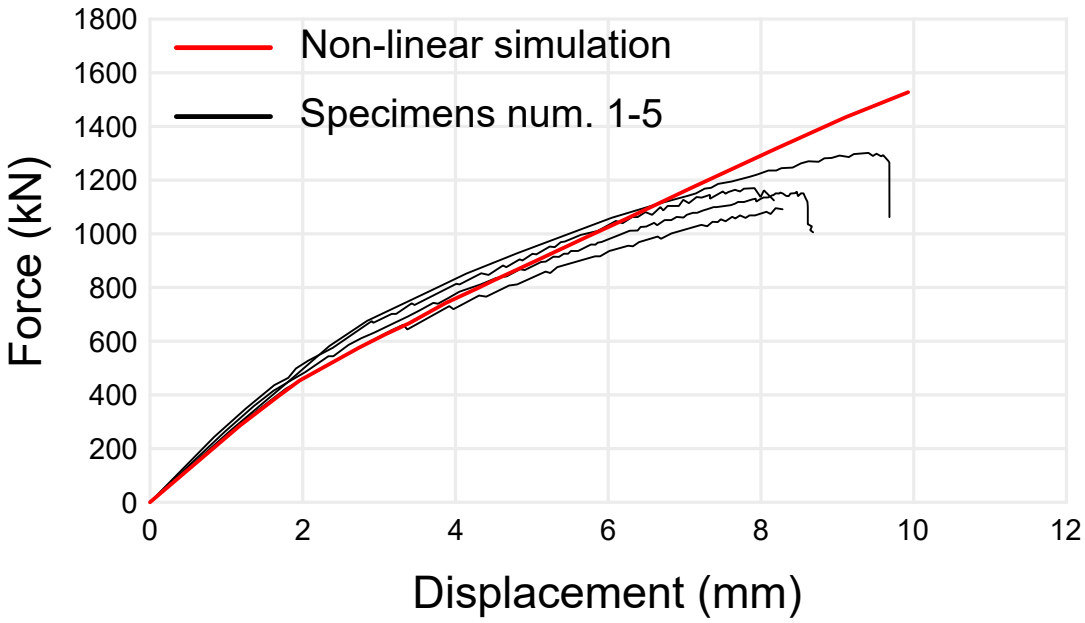

FIGURE 6.22: Numerical non-linear prediction for 90°compared against the experimental data of the flexural test.

The transverse, in Figure 6.22, approximation however is not as great as the longitudinal, since it is able to capture the non-linear phenomenon but breaks on a greater value than expected. The same pattern of damage is obtained as it is supposed from a flexural test (Figure 6.23).

FIGURE 6.23: Failure of a specimen for the transverse flexural testing, damage localised in the centre.

6.3.2 Sandwich buckling

A mechanical model is proposed to serve as a validation of the non-linear geometric formulation found in [18]. This problem is not considered pure buckling, the details shall be explained in the following paragraphs.

The laminate used is a 3 layer sandwich laminate. The first layer is a fibreglass-epoxy UD laminate, the second would be a standard PVC H80 core from Divinycell. The third would be identical to the first layer. Each layer belongs to a third of the total thickness of 0.05 m and the volumetric fraction of the laminate is 60%.

The mechanical buckling model is defined as a 1×1 (m^2) square, where the bottom edge is simply supported, and the upper edge is a simply supported in the out-of-plane direction. The vertical (longitudinal) direction is movable and has a prescribed displacement of -0.1 m. This means that the plate is compressed along the vertical axis.

The computational model is generated by a mesh of 20×20 elements in the in-plane directions and for the thermal problem, a one-dimensional mesh of 30 elements in the thickness direction is considered.

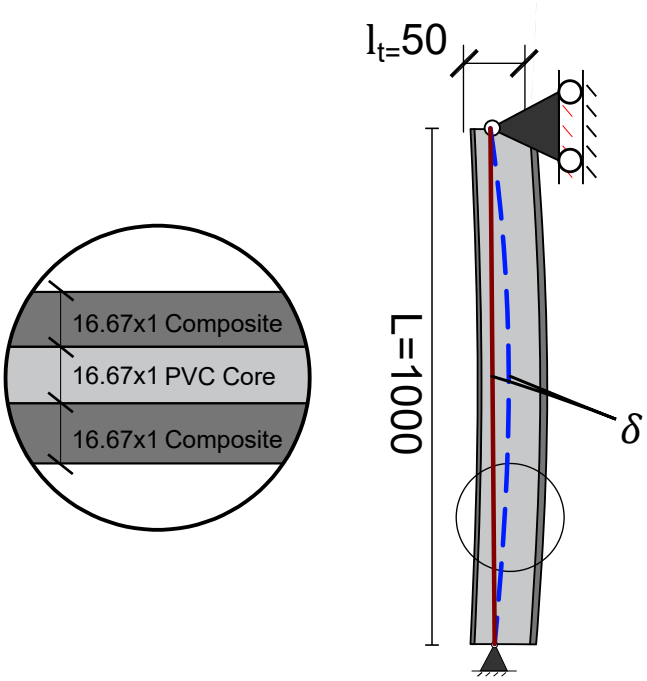

FIGURE 6.24: Sketch of the sandwich panel under axial compression and with a small initial deflection.

This numerical problem uses a non-linear geometric shell model, thus, with the described boundary conditions the problem would be ill-conditioned unless some perturbation is introduced to propitiate the first mode of deflection. In order to achieve the perturbation and trigger the buckling phenomena, an initial deflection is introduced (arc shape). This initial deflection is 0.01 m.

The mechanical problem described is limited in the sense that the effective length of

the critical buckling load is non-constant. The critical buckling load is defined by the relationship

$$P_{cr} = \frac{\pi^2 \bar{D}}{(L)^2} \tag{6.5}$$

Since the effective length L decreases due to the movable boundary condition, the critical load tends to increase instead of stagnating. This is an important limitation compared to a pure buckling scenario. The other issue is that since the model presents an initial maximum deflection of 0.01 m in $L/2$, the effective length needs to be corrected by calculating the arc-length of the deflected curve. This curve is defined by the end nodes and the deflected node in the mid-span of the length.

The effective inertial elastic modulus ($\bar{D}$) in a laminate composite is defined by the following equation

$$\bar{D} = \int_A E(z) z^2 dA = \int_{-\frac{t}{2}}^{\frac{t}{2}} E(z) z^2 b \cdot dz \tag{6.6}$$

The critical load – for a fibreglass of 72 GPa, epoxy of 3.5 GPa and PVCH80 of 100 MPa – is 4.41 MN. This is in accordance with the numerical simulation.

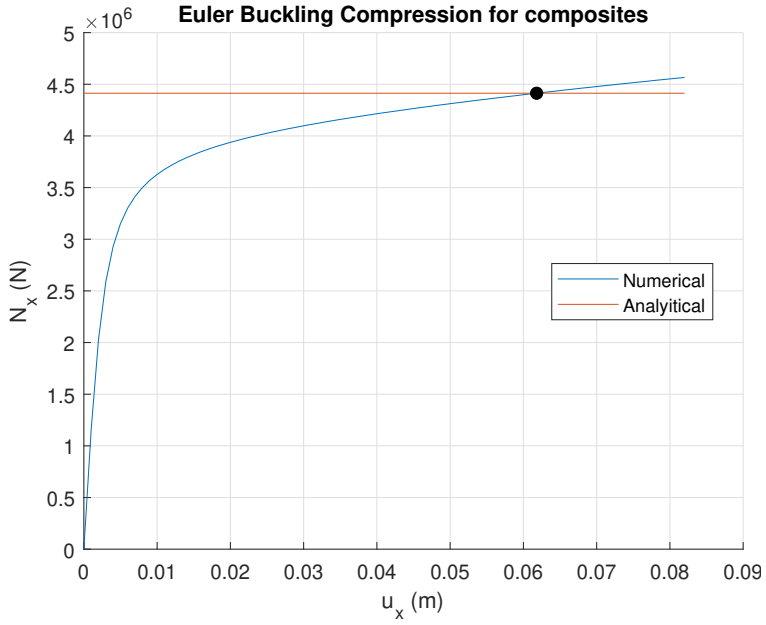

FIGURE 6.25: Critical load evolution with respect to the prescribed movable axial boundary condition.

In Figure 6.25 the axial force tends to the critical load, however, due to the prescription of the movable boundary conditions shown in Figure 6.26, this is not achieved since the problem is not a pure buckling problem as explained before. This behaviour is well known in the simulation of post-buckling [291].

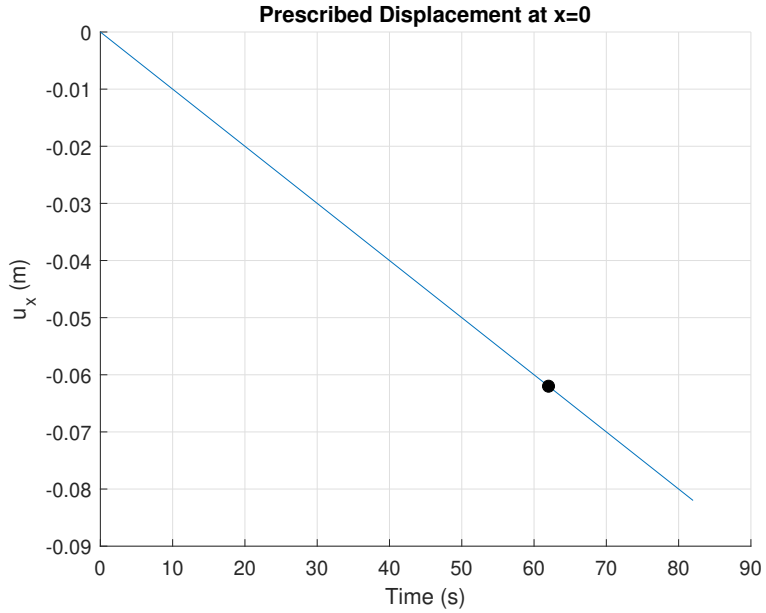

FIGURE 6.26: Movable boundary condition and its evolution respect a pseudo-time (incremental non-linear static analysis).

In the pure buckling phenomenon, the flexural tangent stiffness tends to zero as the introduced load approaches the nominal critical load. In Figure 6.27 the analytical evolution for pure buckling can be compared to the numerical solution, showing that in the numerical solution, the problem is governed by post-buckling phenomenon. The analytical solution, with respect to the maximum deflection, can be obtained from the derivation in [292]. This difference, entering into post-buckling due to the prescribed displacement situation, shows that the non-linear geometric module is functional and that it can even reproduce post-buckling behaviour.

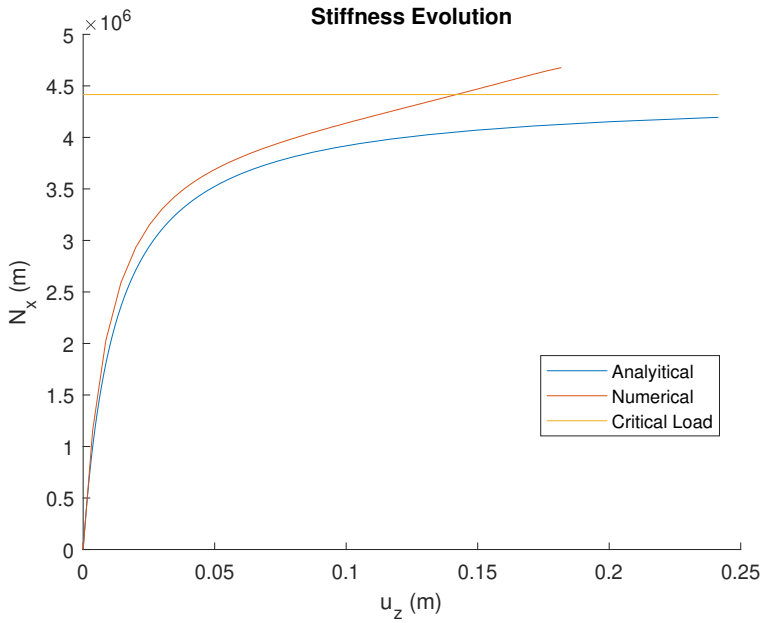

FIGURE 6.27: Flexural stiffness evolution.

6.3.3 Conclusion of the numerical implementation

In this section, devoted to the validation of the proposed mechanical approach, has shown the capability to analyse the failure of composites from the perspective of damage and buckling. These two failure mechanisms exemplify the non-linear constitutive approach, proposed by means of the SPROM and the isotropic damage theory at the constituent level, and the non-linear geometric approach by using the co-rotational theory.

The examples given have shown interesting feats for the numerical tool developed:

- Damage

  In the axial testing, the experimental results of the LEO-system material were compared against three numerical approaches: *homogeneous*, *ROM* and *SPROM*. The most notorious comparison is the one given by the *homogeneous* theory, which is one of the standard methods to predict failure in composites nowadays.

  It has been shown that once the material properties were calibrated, the SPROM obtained a perfect prediction of the linear longitudinal and transverse elastic stiffness and a good agreement on the inelastic stiffness of both longitudinal and transverse testing. The homogeneous equivalent composite model showed a poorer prediction of the inelastic transverse stiffness as discussed in Figure 6.10.

  The damage evolution, especially for the longitudinal computational model, was very similar as shown in Figure 6.15, the damage is uniform in the matrix until it breaks abruptly. When it breaks abruptly, it is shown in Figure 6.14, that the zone of rupture is in the grips and the centreline of the specimen and this is replicated in the numerical result.

  The flexural response has also been modelled for longitudinal and transverse testing. The model has clearly shown to match well the non-linear constitutive behaviour in both longitudinal and transverse directions, although the numerical transverse curve of force-deflection does not break as quick as supposed for the experimental test.

- Buckling

  One of the hypotheses posed at the beginning of the research was whether the co-rotational theory would be able to predict failure due to buckling or not. Buckling or non-linear geometric governed effects are very characteristic in the analysis of composites due to their higher flexibility. Therefore, there was a need to properly check if the formulation proposed is suitable for composites.

  A very simple verification example is proposed based on the Euler-buckling problem of a beam. The computational model is modelled with a shell and an initial deflection is introduced to trigger the non-linear buckling phenomenon. However, this case is not a pure-buckling problem because one of the ends is movable.

Nevertheless, the behaviour obtained for the numerical assessment is very close to the analytical, with the problem that the analysis enters into a post-buckling stage and goes beyond the critical load. Before entering into post-buckling, the curves of both, the analytical solution and the one provided by the numerical example, match very close.

In conclusion, this section has served to accomplish the proposed goals '*Assess the correctness of the implementation of the mechanical formulation*' and '*Address the flexibility of composites*', which are number 6 and 7 respectively.

This page was left blank intentionally.

6.4 Validation of the thermo-mechanical model

The examples presented an attempt to exemplify and verify the correctness of the different implemented aspects in the thermo-mechanical tool. The section starts with a simple benchmark case based on an analytical solution and shows how the numerical tool is able to correlate the deflections when considering different temperature profiles through the thickness. It also shows the possibility of adding the effect of temperature on mechanical properties.

The next example is used to explain the concept of thermal buckling and the different effects this has on composite structures. The example builds up the necessary knowledge to introduce the concept of inelastic thermal buckling. However, this only shows the capabilities for beams or, i.e., one-dimensional mechanical structures. There is another example presented that shows thermal buckling in two dimensions, basically applied to plates. This last example also serves as proof of the capability of the TSPROM to predict the buckling of composites.

The next examples rely on experimental data. In order to demonstrate that this tool can predict thermal buckling, an experimental benchmark is used to compare against the numerical solution. Besides this experiment, three more experimental tests are provided, with far more complexity, these three are derived from the tests required by regulations such as the FTP – necessary to certify the fire safety of a ship being designed – and not only show the capabilities of the tool but also how good it complements the design process of the passive fire protection, which again, is required by regulations.

Within the three experimental tests from the FTP code, two of them are for bulkheads and one also introduces a bulkhead with beam reinforcements. The last is also very interesting in showing that the shell theory implemented can be used to simulate beam structures in the presence of fire.

6.4.1 Thermo-mechanical analysis of a shell

A simple verification case is demonstrated based on the thermo-mechanical solution of the Euler-Bernouilli beam theory. Two examples are shown: *simply supported shell with a loose edge* and *clamped shell on both edges*.

6.4.1.1 Domain

The computational example is a square of 1m×1m with a thickness of 1 m as well. The computational model is divided by a regular quadrilateral mesh of 8×8 elements. To solve the one-dimensional transient problem, the thickness is discretised in 30 linear elements.

6.4.1.2 Thermal model

Property	Value
Virgin density (kg/m^3)	1
Final char density (kg/m^3)	0
Virgin thermal conductivity (W/m°C)	1
Final thermal conductivity (W/m°C)	0
Virgin specific heat capacity (kJ/kg°C)	1
Final specific heat (kJ/kg°C)	0
Gas specific heat capacity (kJ/kg°C)	0
Activation energy (kJ/kg°C)	0
Pre-exponential factor (s^{-1})	0
Order of reaction	0
Heat of decomposition (kJ/kg)	0
Surface emissivity	0.9

TABLE 6.5. Thermal properties of the analytical solution.

The model proposed is a linear one-dimensional through-thickness heat transient problem. The parameters are considered unitary. I.e., the conductivity, the specific heat, the coefficient of thermal expansion, etc. (see Table 6.5). A linear thermal gradient is imposed by using a homogeneous material, note that the same profile or expression is assumed in all cases. These expressions are defined as

$$\begin{aligned} \Delta T &= \bar{T} + x_3 \hat{T} \\ \bar{T} &= \frac{\Delta T_2 + \Delta T_1}{2} \\ \hat{T} &= \frac{\Delta T_2 - \Delta T_1}{l_t} \end{aligned} \tag{6.7}$$

where ΔT_1 and ΔT_2 are the respective increments of temperature on both ends. The boundary conditions introduced in the thermal model will be considered stationary, which means that given enough time, the thermal model will tend to have a

linear distribution from the hot end to the cold end. The boundaries are considered as a heat flux where the convection coefficient is assumed to be very high, e.g., $1 \cdot 10^6$ $Wm^{-2}°C^{-1}$, therefore the temperature at both ends is almost immediately prescribed. Then the cold end temperature (ΔT_1) is exposed to the ambient temperature of 0 °C and the hot end (ΔT_2) will be specified in each example by the mean temperature ($\bar{T}$) and the gradient temperature over the thickness ($\hat{T}$) values.

6.4.1.3 Mechanical model

Dimensions	Value
Length (m)	1
Width (m)	1
Thickness (m)	1
Property	**Value**
Thermal expansion coefficient ($°C^{-1}$)	1
Poisson ratio	0
Virgin Young's Modulus (Pa)	1
Char Young's Modulus (Pa)	0.5
Virgin Young's Modulus (Pa)	1
Char Young's Modulus (Pa)	0.5
Mouritz-Gibson coefficient 1	1
Mouritz-Gibson coefficient 2	1
Temperature of glass transition (°C)	0.5

TABLE 6.6. Thermo-mechanical properties of the analytical solution.

The mechanical properties are considered unitary. I.e., Young's modulus, the thickness, the width, the length, etc. (see Table 6.6). The constitutive model of the Euler-Bernouilli beam is defined as

$$\sigma_1 = E\left(\varepsilon_1 - \alpha \Delta T\right) \tag{6.8}$$

The following relationship is defined to be later used

$$\int_{-\frac{l_w}{2}}^{\frac{l_w}{2}} \int_{-\frac{l_t}{2}}^{\frac{l_t}{2}} x_3 S \, \mathrm{d}x_3 \, \mathrm{d}x_2 = 0 \tag{6.9}$$

l_w is the width of the beam and S represents the area. The axial strength of a beam problem can be found by

$$\sigma_m(x_1) = \int_{-\frac{l_w}{2}}^{\frac{l_w}{2}} \int_{-\frac{l_t}{2}}^{\frac{l_t}{2}} \sigma_1 S \, \mathrm{d}x_3 \, \mathrm{d}x_2 = \int_{-\frac{l_w}{2}}^{\frac{l_w}{2}} \int_{-\frac{l_t}{2}}^{\frac{l_t}{2}} ES\left(\varepsilon_1 - \alpha \Delta T\right) \, \mathrm{d}x_3 \, \mathrm{d}x_2 = ES\left(u_{0,1} x_3 - \alpha \bar{T}\right) \tag{6.10}$$

where $u_{0,1}$ is the through-thickness displacement in the middle plane. Some minor simplifications were skipped, these simplifications come from the definition of the strain in the Euler-Bernouilli formulation. The bending can also be derived

$$\sigma_b(x_1) = \int_{-\frac{l_w}{2}}^{\frac{l_w}{2}} \int_{-\frac{l_t}{2}}^{\frac{l_t}{2}} \sigma_1 S x_3 \, \mathrm{d}x_3 \, \mathrm{d}x_2 = \int_{-\frac{l_w}{2}}^{\frac{l_w}{2}} \int_{-\frac{l_t}{2}}^{\frac{l_t}{2}} ES x_3 \left(\varepsilon_1 - \alpha \Delta T\right) \, \mathrm{d}x_3 \, \mathrm{d}x_2 = -EI3S \left(u_3 x_3^2 + \alpha \hat{T}\right) \tag{6.11}$$

where I is the inertia.

6.4.1.4 Simply supported shell with a loose end

Given the hexahedral domain defined as $\Omega = \forall x_1, x_2, x_3 \in [0,1] \cup [0,1] \cup [0,1]$. The in-plane directions are considered to be x_1 and x_2 and the out-of-plane direction or through-thickness of the shell is x_3. The boundary conditions on both ends are:

$$\begin{cases} u_1(x_1, x_2, x_3) = u_2(x_1, x_2, x_3) = u_3(x_1, x_2, x_3) = 0 & , \quad x_1 = 0, \forall x_2, x_3 \in \Omega \\ u_2(x_1, x_2, x_3) = u_3(x_1, x_2, x_3) = 0 & , \quad x_1 = L, \forall x_2, x_3 \in \Omega \\ \sigma_m = 0 & , \quad \forall x_1, x_2, x_3 \in \Omega \end{cases} \tag{6.12}$$

where L is the length, which in this case is 1 m. From the axial and bending equilibrium, the following analytical solutions are obtained

$$\begin{cases} u_{0,1}(x_1) = \alpha \bar{T} x_1 & , \quad \forall x_1 \in [0, L] \\ u_3(x_1) = \frac{1}{2} \alpha \hat{T} (L - x_1) x_1 & , \quad \forall x_1 \in [0, L] \end{cases} \tag{6.13}$$

6.4.1.4.1 Isothermal ($\hat{T} = 0, \bar{T} = 1$)

All the thermal and mechanical variables are one. Hence, using the isothermal constraints in Equation 6.13, the longitudinal displacement becomes $u_{0,1}(x_1) = x_1$ matching the numerical solution in Figure 6.28.

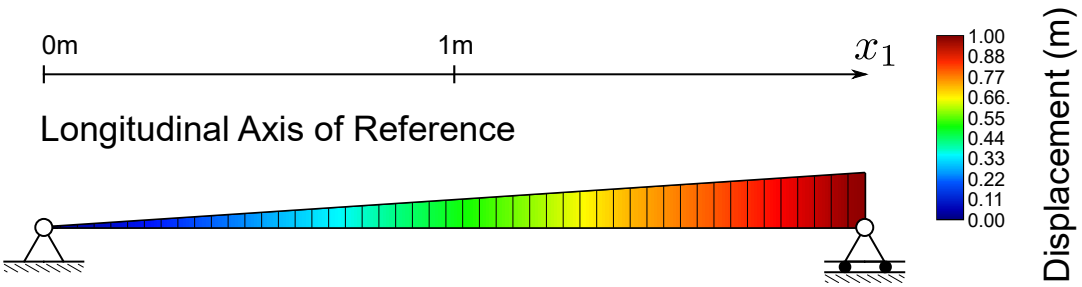

FIGURE 6.28: Uniform displacement distribution as result of increasing the mean temperature in 1°C.

Indeed, this structure is an isostatic mechanism and no internal reactions are built in the structure since it dilates in the longitudinal direction x. The plot is in correspondence with the analytical solution, thus proving the correctness of the thermo-mechanical implementation.

6.4.1.4.2 Linear gradient ($\hat{T} = 1, \bar{T} = 0.5$)

All the thermal and mechanical variables are one. Hence, using the linear-gradient constraints in Equation 6.13, the longitudinal displacement becomes $u_{0,1}(x_1) = \frac{1}{2}x_1$ and the deflection $u_3(x_1) = \frac{1}{2}x_1(1 - x_1)$, both are in agreement with the numerical solution in Figure 6.29.

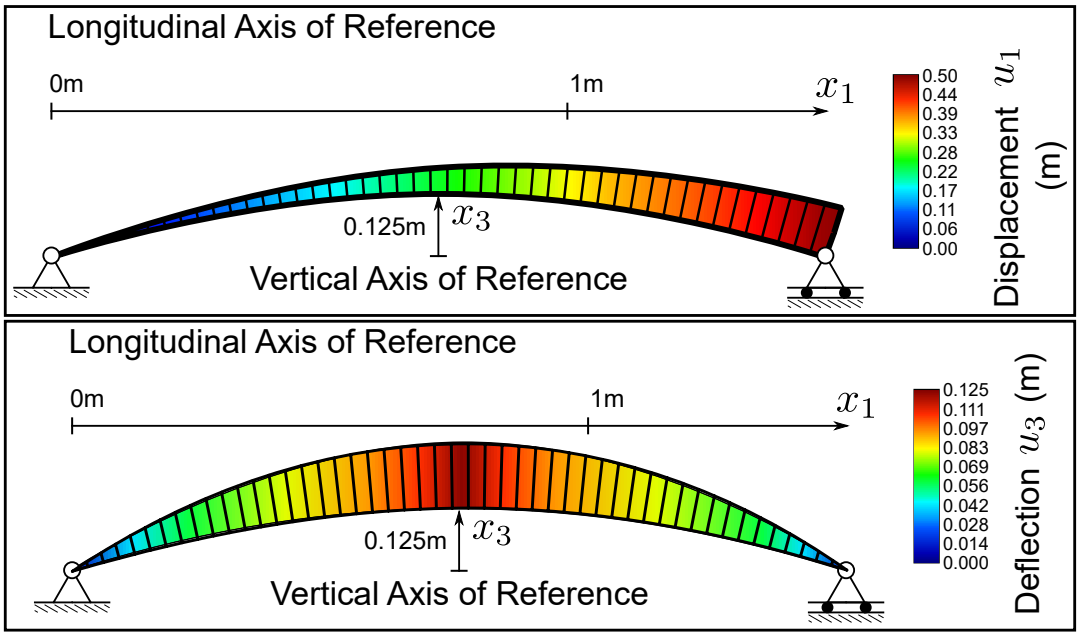

FIGURE 6.29: Parabolic bending due to imposing a linear gradient of temperature.

This is still a mechanism since it is not constrained, however it bends due to the gradient of temperature from the hot end to the cold end.

6.4.1.5 Clamped shell on both ends

The domain remains the same, this time the boundary conditions are:

$$\begin{cases} u_1(x_1, x_2, x_3) = u_2(x_1, x_2, x_3) = u_3(x_1, x_2, x_3) = 0 & , \quad x_1 = 0, \forall x_2, x_3 \in \Omega \\ u_1(x_1, x_2, x_3) = u_2(x_1, x_2, x_3) = u_3(x_1, x_2, x_3) = 0 & , \quad x_1 = L, \forall x_2, x_3 \in \Omega \\ \sigma_m = 0 & , \quad \forall x_1, x_2, x_3 \in \Omega \end{cases} \tag{6.14}$$

$$\begin{cases} u_{0,1}(x_1) = \alpha \bar{T} x_1 & , \quad \forall x_1 \in [0, L] \\ u_3(x_1) = \frac{1}{2}\alpha \hat{T}(L - x_1)x_1 & , \quad \forall x_1 \in [0, L] \end{cases} \tag{6.15}$$

6.4.1.5.1 Linear gradient ($\hat{T} = 1, \bar{T} = 0$)

All the thermal and mechanical variables are one, except Young's modulus, which now is temperature-dependent. Therefore, using the linear-gradient constraints in Equation 6.13, the longitudinal displacement becomes $u_{0,1}(x_1) = \frac{1}{2}x_1$ and the deflection $u_3(x_1) = \frac{1}{2}x_1(1 - x_1)$, both are in agreement with the numerical solution in Figure 6.30.

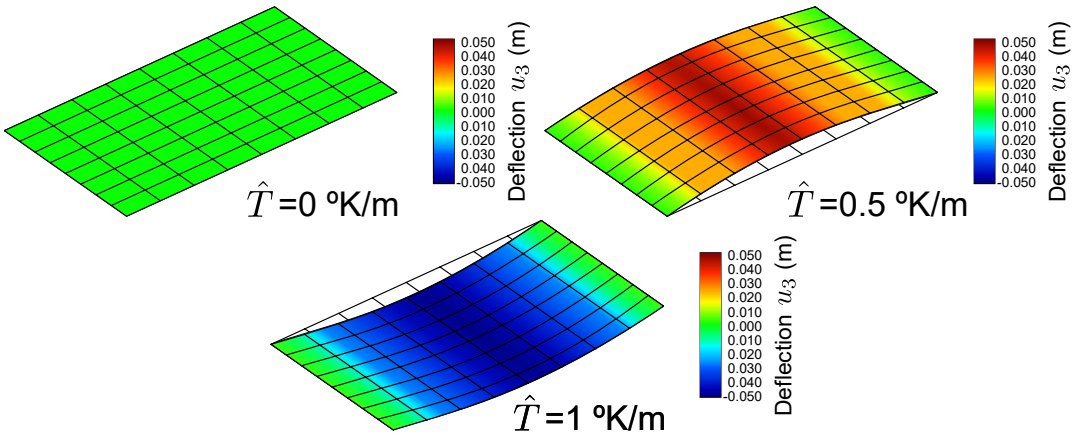

FIGURE 6.30: A clamped shell enduring a linear gradient load.

Since both ends are clamped it is a hyper-static mechanism. Therefore, internal stress is generated creating a reaction and introducing the possibility for the model to vary with respect to the temperature. If it was not a hyper-static mechanism, in the equation of the Euler-Bernoulli beam, the mechanical and thermal strain would always cancel each other out since Young's modulus is outside the parenthesis and never affects the result of the calculus. That is why thermal dependency is tested with a hyper-static mechanism.

In Figure 6.30, observe that the shell first inflates in the positive z-direction, but as in the upper layers Young's modulus becomes less stiff than in the lower layers due to the increase of the temperature, it inverts the through-thickness bending configuration.

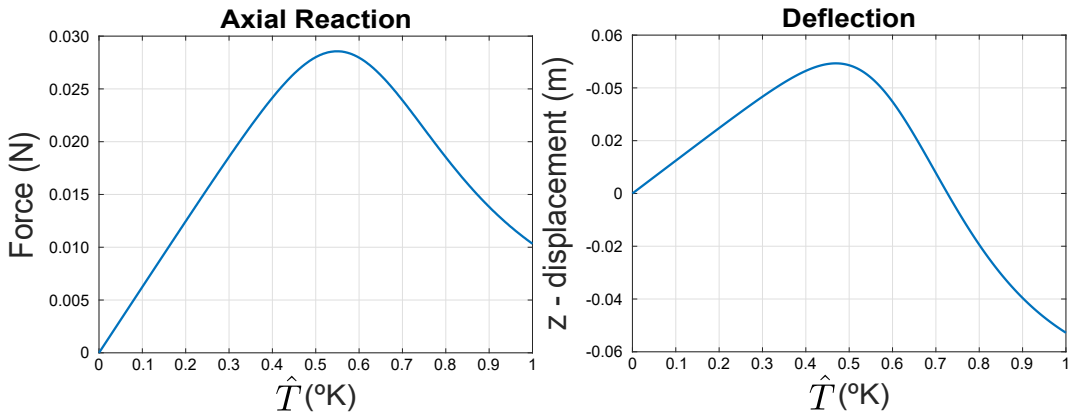

FIGURE 6.31: Load and deflection evolution for a linear-gradient thermal load with mechanical loss due to temperature.

The dependency of Young's modulus with respect to temperature follows the equation provided by Mouritz-Gibson. The analytic solution is a complex equation to obtain, however, the evolution of Young's modulus can be understood from the results in Figure 6.31 where the force increases until a certain point and the material becomes less rigid. The magnitude of the reaction force starts decreasing, since the transmitted internal forces are reduced when the stiffness of the material diminished. In the deflection, the traction-compression interaction from the loss of mechanical properties can be observed due to the temperature.

6.4.2 One dimensional buckling collapse of a laminated shell exposed to fire

The laminate used is a 3 layer sandwich laminate. The first layer is a fibreglass-epoxy UD laminate, the second would be a standard PVC H80 core from Divinycell [293]. The third would be identical to the first layer. Each layer belongs to a third of the total thickness of 0.05 m and the volumetric fraction of the laminate is 60%. The material properties are the same as defined in subsection 6.3.2, nevertheless, it will be specified in each of the different cases considered.

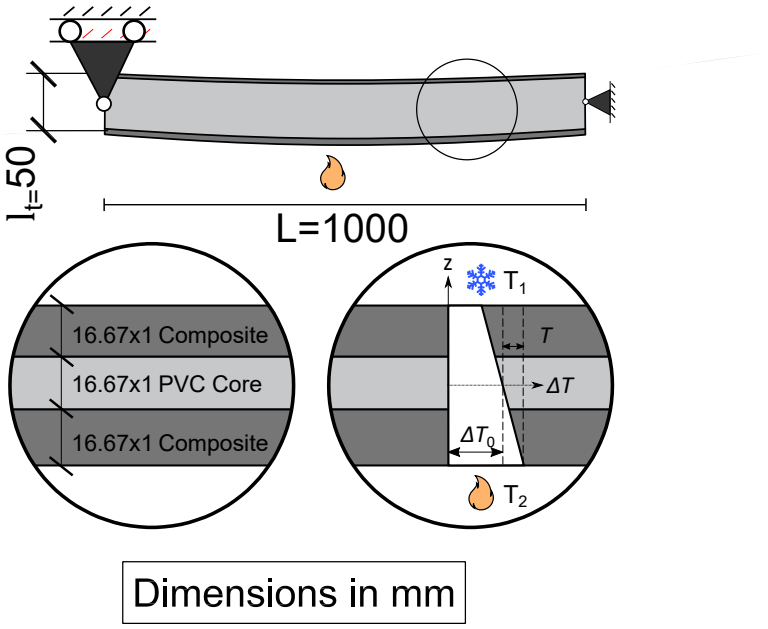

FIGURE 6.32: Sketch of the buckling of a sandwich due to thermal loading.

The thermal buckling model is defined by two simply supported and articulated ends (see Figure 6.32). This model has a constant effective length and therefore can reproduce the pure buckling phenomenon that was the main problem compared to subsection 6.3.2. Similar to the mechanical buckling problem, the computational model is generated by a mesh of 20×20 elements in the in-plane directions and for the thermal problem a one-dimensional mesh of 30 elements in the thickness direction is considered.

6.4.2.1 Thermal model

Figure 6.32 shows a sandwich, since this is a numerical validation and in order to obtain a simple analytical solution to compare them, the thermal properties of the core will be identical to the monolithic fibreglass-epoxy stack. With this, the analytical distribution of the temperature through-thickness can be obtained. Indeed, the solution should approximately be a linear gradient of temperature from the hot to the cold end whilst the rest of the minor differences will be due to the transient effects.

The evolution of the increment of temperature is defined by

$$\Delta T(x_1, x_3) = T(x_1, x_3, t) - T(x_1, x_3, 0) \tag{6.16}$$

The intention is to obtain a stationary linear solution. The incremental is then

$$\Delta T(x_1, x_3) = \Delta T + z\delta T \tag{6.17}$$

where

$$\Delta T_0 = \frac{\Delta T_H(t) + \Delta T_C(t)}{2} \tag{6.18}$$

is the mean temperature and

$$\delta T = \frac{\Delta T_H(t) - \Delta T_C(t)}{l_t} \tag{6.19}$$

is the gradient temperature. The gradient temperature (δT) is chosen to be 1 °C in order to have a small deflection to compare with the linear geometric solution. The evolution of temperature at hot (T_H) and cold (T_C) ends is described in Figure 6.33. The temperature evolution is saturated around time 5000 s and both thermal boundary conditions are introduced as Neumann boundary conditions

$$q = \pm h_{\text{conv}}(T - T_\infty) \cdot \underline{n} \tag{6.20}$$

where the surrounding temperature (T_∞) corresponds to the hot and cold end temperature. The hot end has a positive sign since it is considered an in-flux heat, and the cold end is considered negative since it is an out-flux heat. The value for the convection coefficient (h_{conv}) is defined 10^6 ($\text{W°C}^{-1}\text{m}^{-2}$), which physically can be understood as both surfaces – exposed and unexposed – have a really quick transmission between the surrounding temperature and the one on the surface. This can be seen in Figure 6.33, as both numerical and analytical solutions match perfectly.

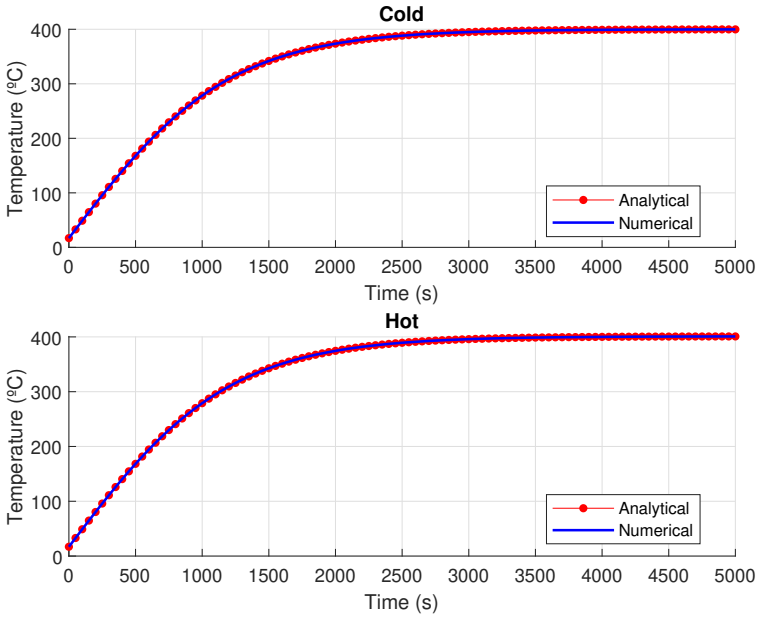

FIGURE 6.33: Temperature on both ends due to the thermal boundary conditions.

The stationary solution at time 5000 s can be observed in Figure 6.34. It shows a good agreement on the assumption of the linear distribution of the temperature through-thickness.

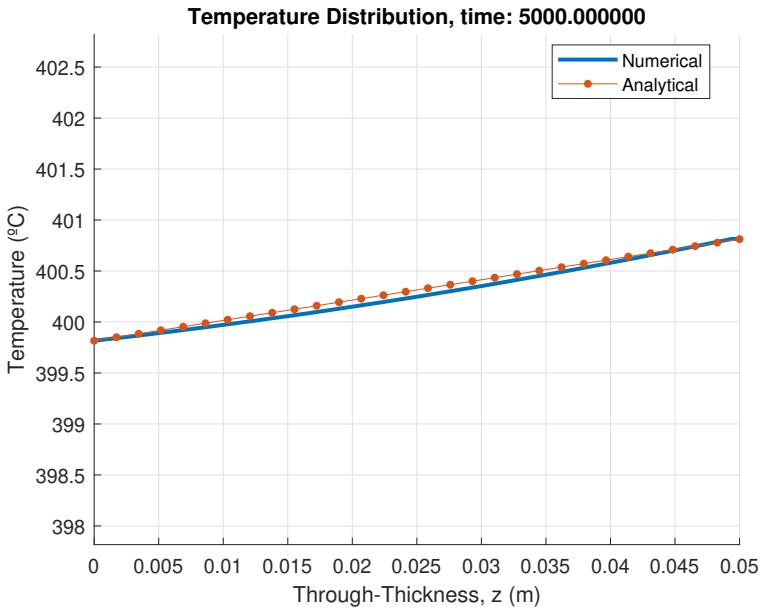

FIGURE 6.34: Stationary temperature distribution through-thickness. It approximates a linear solution.

The analytical temperature through-thickness can be found from

$$\begin{cases} T(x_3,t) = \frac{\Delta T_H(t)-\Delta T_C(t)}{l_t}x_3 + \Delta T_C(t) + \sum_{n=1}^{\infty} \hat{c}_n \exp\left(\left(\frac{n\pi\bar{\alpha}}{l_t}\right)^2 t\right) \sin\left(\frac{n\pi\bar{\alpha}}{l_t}x_3\right) \\ \hat{c}_n = \frac{2}{l_t}\int_0^{l_t} \sin\left(\frac{n\pi\bar{\alpha}}{l_t}x_3\right) T_t(x_3,t)\,\mathrm{d}x_3 \\ T_t = T(x_3,0) - \frac{T_H(0)-T_C(0)}{l_t}x_3 + T_H(0) \end{cases} \tag{6.21}$$

where $\bar{\alpha}$ is the thermal inertia.

The analytical evolution of the mean temperature and gradient temperature terms can be observed in Figure 6.35. The gradient temperature term shows the difference between the hot and cold temperatures, indeed the gradient temperature term would be the ratio between that difference over the thickness.

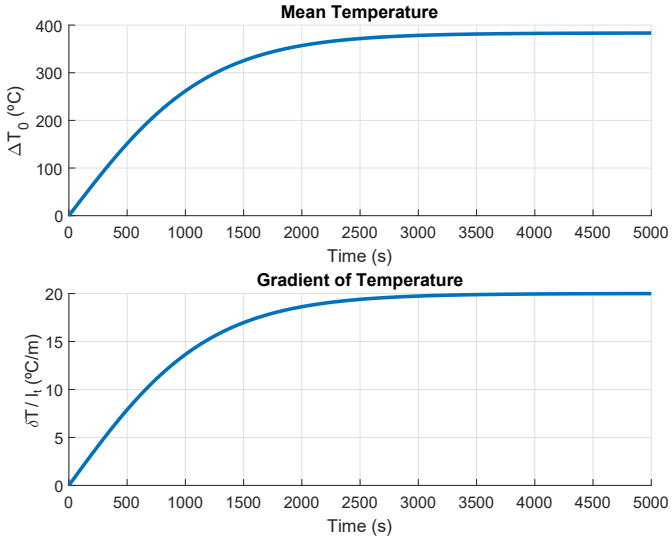

FIGURE 6.35: Temperature of the split terms that describe the stationary linear gradient of temperature through-thickness.

The mean temperature is chosen to be higher than the critical mean temperature to prove that the thermo-mechanical model stagnates to a critical load, even though the temperature is over the critical. The critical temperature will be derived from the mechanical model.

6.4.2.2 Mechanical model

The thermal expansion effect exerts a deformation expressed by the constitutive relationship

$$\sigma_{x_1}(x_1, x_3) = E\left(\varepsilon(x_1, x_3) - \alpha\Delta T(x_1, x_3)\right) \tag{6.22}$$

Note that x_1 is the longitudinal axis of the beam model and x_3 is the through-thickness direction. Then, the integration of the sectional strengths for the axial force and bending moment becomes

$$\sigma_m(x_1) = \int_S \sigma_{x_1}(x_1, S)\,\mathrm{d}S = l_w \int_{-\frac{l_t}{2}}^{\frac{l_t}{2}} E(x_3)\left(\varepsilon(x_1, x_3) - \alpha\Delta T(x_1, x_3)\right)\,\mathrm{d}z \tag{6.23}$$

$$\sigma_b(x_1) = \int_S \sigma(x_1, S)x_3\,\mathrm{d}S = l_w \int_{-\frac{l_t}{2}}^{\frac{l_t}{2}} E(x_3)x_3\left(\varepsilon(x_1, x_3) - \alpha\Delta T(x_1, x_3)\right)\,\mathrm{d}z \tag{6.24}$$

where S is the surface and l_w is the width. Thus, Equation 6.23 can be rearranged with the introduction of these two split terms such that

$$\sigma_m(x_1) = l_w \int_{-\frac{l_t}{2}}^{\frac{l_t}{2}} E(x_3)\left(-\frac{\partial^2 u_{x_3}}{\partial x_1^2}x_3 + \frac{\partial u_0}{\partial x_1} - \alpha\Delta T - \alpha x_3\Delta\delta T\right)\,\mathrm{d}x_3 \tag{6.25}$$

The buckling problem can be posed such as

$$\sigma_b(x_1) + P_{cr} \cdot u_{x_3} = 0 \Rightarrow \frac{\partial u_{x_3}}{\partial x_1} + \frac{P_{cr}}{\bar{D}} u_{x_3} = 0$$
$$\sigma_m \equiv P_{cr} = \frac{\pi^2 \bar{D}}{l_L^2} \tag{6.26}$$
$$\bar{D} = \int_{-\frac{l_t}{2}}^{\frac{l_t}{2}} E(x_3) {x_3}^2 l_w \, \mathrm{d}x_3$$

In the case of a sandwich section, the odd power terms of x_3 will become zero. Using Equation 6.26 and Equation 6.28, the critical mean temperature can be found.

$$\Delta T_0 = \frac{\pi^2 \bar{D}}{\alpha l_w \bar{E} (l_L)^2}$$
$$\bar{E} = \int_{-\frac{l_t}{2}}^{\frac{l_t}{2}} E(x_3) l_w \, \mathrm{d}x_3 \tag{6.27}$$

In this case, the critical mean temperature is found at 296.695 (°C), nevertheless a greater temperature of 400 (°C) is chosen to demonstrate the correctness of the implemented methodology and, also, to compare using linear and non-linear geometric approximations.

$$\sigma_b(x_1) = l_w \int_{-\frac{l_t}{2}}^{\frac{l_t}{2}} E(x_3) \left(-\frac{\partial^2 u_{x_3}}{\partial x_1^2} {x_3}^2 + \frac{\partial u_0}{\partial x_1} x_3 - \alpha x_3 \Delta T - \alpha {x_3}^2 \Delta \delta T \right) \mathrm{d}x_3 \tag{6.28}$$

Again, for a sandwich section, the odd power terms of x_3 will become zero. The linear deflection can be derived by applying the boundary conditions of a simply supported and articulated beam and the deflection can be expressed as

$$u_3(x_1) = -\alpha \delta T \left(x_1^2 - l_L x_1 \right) \tag{6.29}$$

And the maximum deflection is obtained at

$$u_3 \left(\frac{l_L}{2} \right) \equiv u_z = \frac{-\alpha \delta T {l_L}^2}{8} \tag{6.30}$$

The analytical maximum deflection due to the thermal loading is compared in Figure 6.36 against the linear geometric numerical solution at $l_L/2$. It shows an excellent agreement between both curves, demonstrating the correctness of the model.

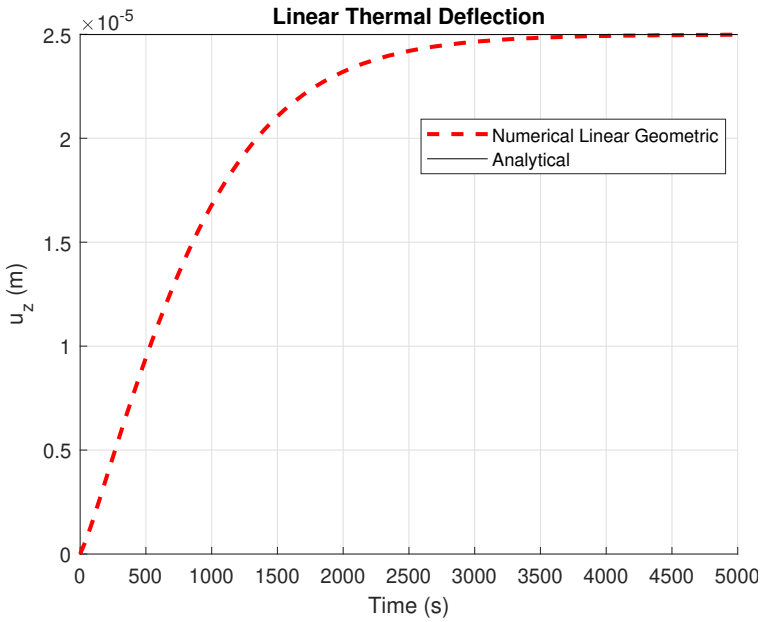

FIGURE 6.36: Linear deflection. It converges to the stationary analytical solution.

While the linear geometric agrees with the analytical maximum deflection, the non-linear geometric gives a larger deflection for the stationary regime (Figure 6.37).

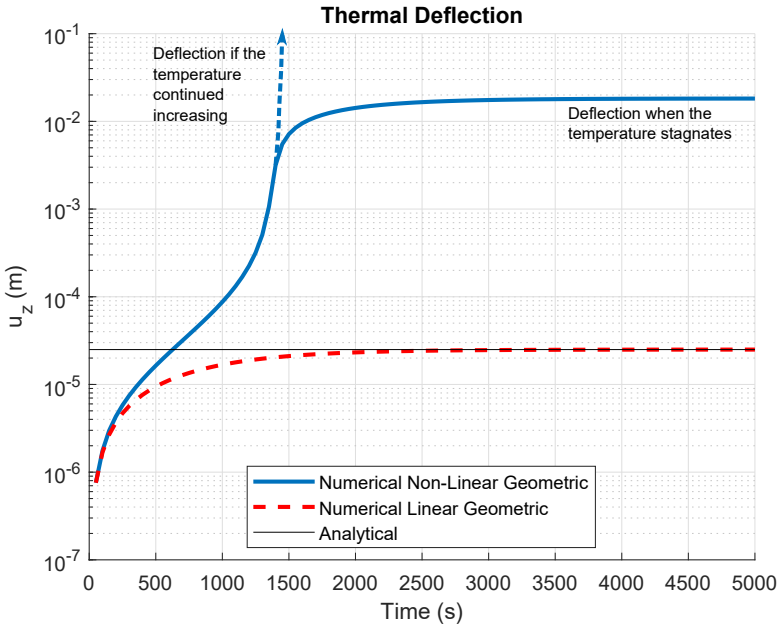

FIGURE 6.37: Linear and non-linear geometric deflection.

Based on the fact that the boundary conditions introduced in this example tend to a saturated final temperature value, the deflection observed numerically for the non-linear geometric analysis also tends to stagnate. In Figure 6.37, observe that there is a point where the non-linear geometric simulation is bifurcated into the saturated solution of this example and the case when the temperature keeps increasing.

The case of pure thermal buckling would be the one where the temperature keeps increasing, and this matches very well the analytical solution presented in the mechanical buckling case (see Figure 6.27). As the temperature increases, so does the deflection, which tends rapidly to infinity.

Albeit the deflection stagnates, and thus it does not tend to infinity, which would be the real solution to a buckling problem, the internal force obtained from Equation 6.28 matches perfectly the phenomenon of pure buckling. Figure 6.38 demonstrates the correctness of the non-linear geometric analysis. Whereas the linear converges to the axial force characteristic for a mean temperature of 400 (°C), it is the non-linear model that reproduces the buckling phenomena and stalls to the magnitude of the critical load closely to time 1500 s. This is in concordance with the value of critical mean temperature at 1500s (see Figure 6.35).

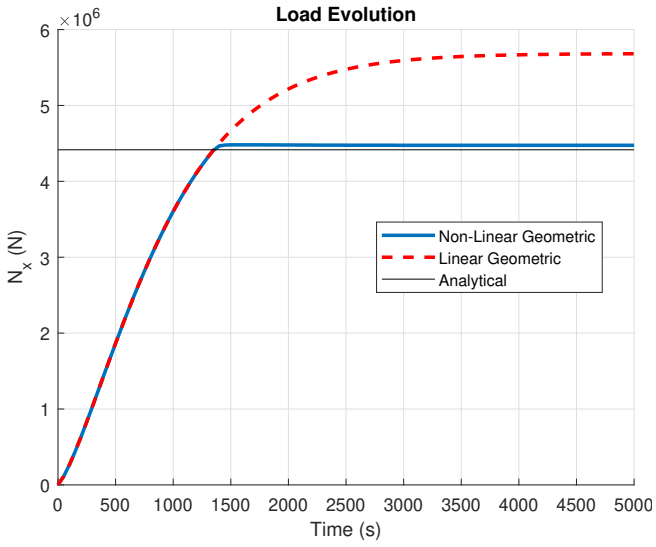

FIGURE 6.38: Load evolution. The linear converges to the predicted axial load due to thermal loading, and the non-linear reaches the critical load and stagnates.

Note that in the graphics presented in this section, the quantities N_x and u_z are equivalent to σ_m and u_{x_1} respectively.

6.4.2.3 Thermal Buckling with Degradation

The degradation effect is the reduction of the mechanical properties due to the effect of temperature rather than pyrolysis. The same heat transient model presented above is used to analyse this scenario.

The critical mean temperature is the same since Equation 6.27 contains both the equivalent Young's modulus ($\bar{E}$) and the inertial Young's modulus ($\bar{D}$) and those terms cancel any degradation in the constituent materials. In this manner, the variation on Young's modulus is described in Table 6.7 where the ratio between the degraded and virgin Young's modulus is 2 and the parameters that control the evolution itself are identical for all materials. The evolution of the laminate fibreglass-epoxy layer is shown in Figure 6.39 and the PVCH80 core in Figure 6.40.

Material	P_u	P_r	n_{MG1}	n_{MG2}	T_g
Fibreglass	72000000000	36000000000	3.800201e-02	6	261
Epoxy	3500000000	1750000000	3.800201e-02	6	261
PVCH80	100000000	50000000	3.800201e-02	6	261

TABLE 6.7. Mouritz-Gibson formula for Young's modulus variation.

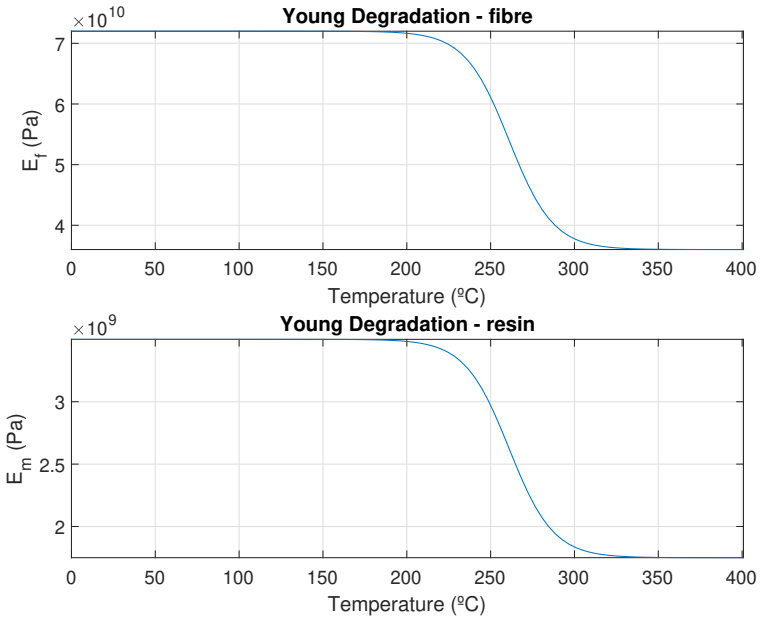

FIGURE 6.39: Layer corresponding to fibreglass-epoxy laminate.

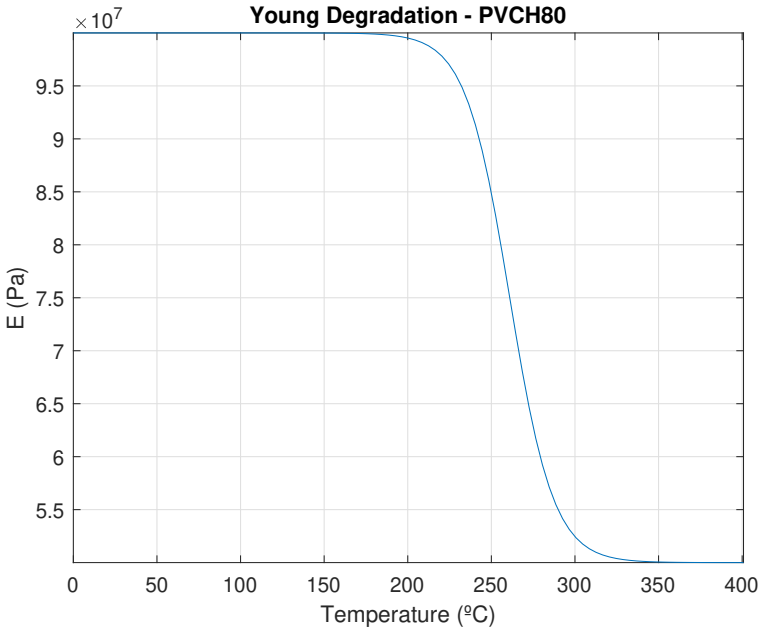

FIGURE 6.40: Layer corresponding to PVCH80 core.

Figure 6.41 shows the effect on degradation to the critical load. All the materials present the same evolution where their mechanical properties, namely the elastic

modulus, are reduced to half of their virgin value when the temperature reaches 300 (°C) or higher. Note that for the stationary solution, the temperature through-thickness is close to 400 (°C) as shown in Figure 6.34. This is a known phenomenon, leading to a critical load of half of the virgin critical load, and it can be better appreciated in Figure 6.42. Here the ratio between the degraded over the virgin critical load is equal to 0.5.

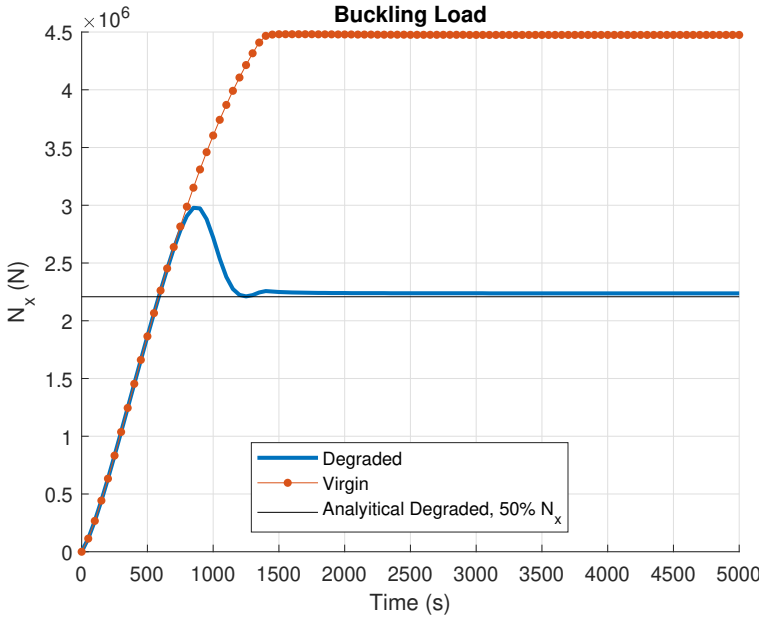

FIGURE 6.41: Buckling load evolution, with and without, degradation of Young's modulus due to temperature.

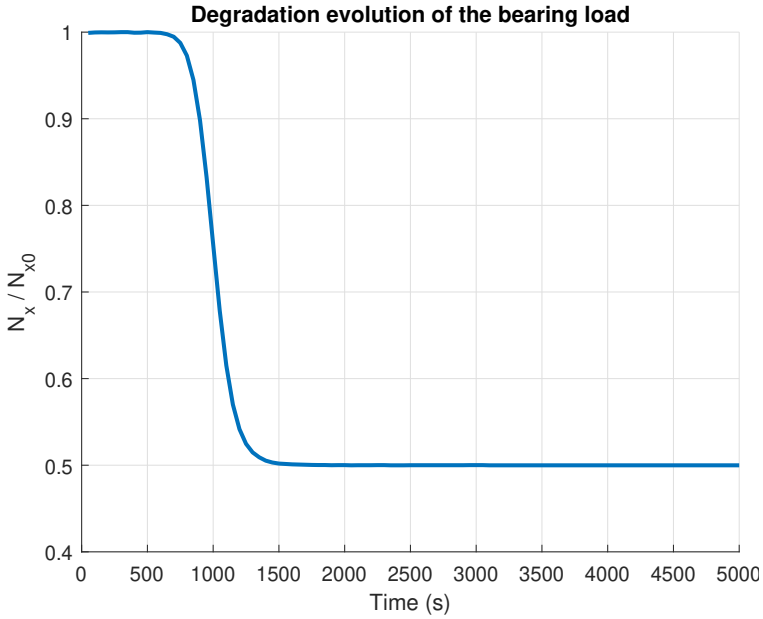

FIGURE 6.42: Load bearing ratio evolution between degraded and virgin curves.

Interestingly, the deflection obtained from the degraded model is similar to the virgin model. Note that both deflections are simulated with non-linear geometric approximations, thus the elevated deflection is observed at time 5000 s. Moreover, the main difference can be found in the range of time between 1000 and 1500 s.

This difference and oscillation are due to the abrupt transition in the mechanical properties, the layers exposed to a greater temperature become more flexible and the compression-traction distribution of stresses through the thickness changes until all the layers have surpassed the glass transition temperature. Note that it is during the range of time that the temperature on both surfaces, unexposed and exposed, reach the glass.

This can be seen in Figure 6.33 where the temperature of the surfaces is in the range of 261 (°C) and also in Equation 6.27 that shows the mean temperature. This is supposed to be close to the temperature in the mid-plane of the thickness.

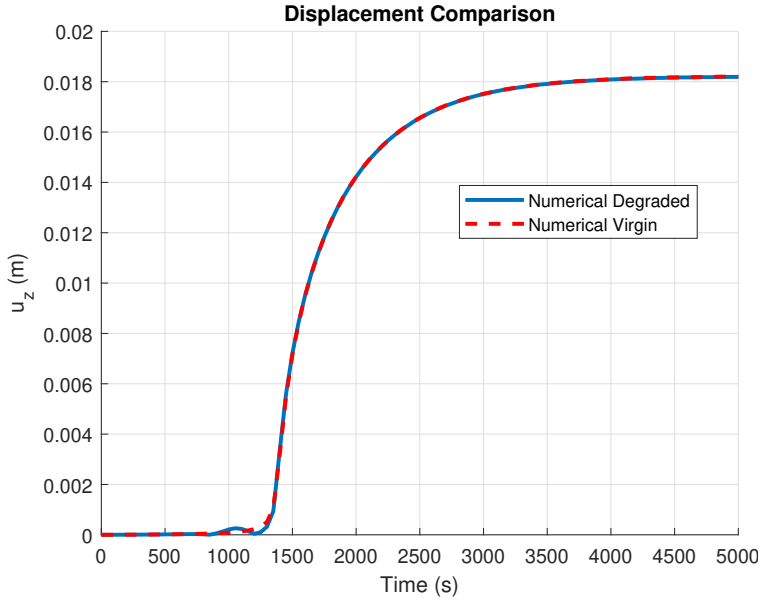

FIGURE 6.43: Deflection evolution for the virgin and degraded sandwiches.

The stiffness evolution portrayed by the evolution of the load against the deflection is shown in Figure 6.44. It can be seen that the critical load and stiffness of the structure have become half of its virgin value.

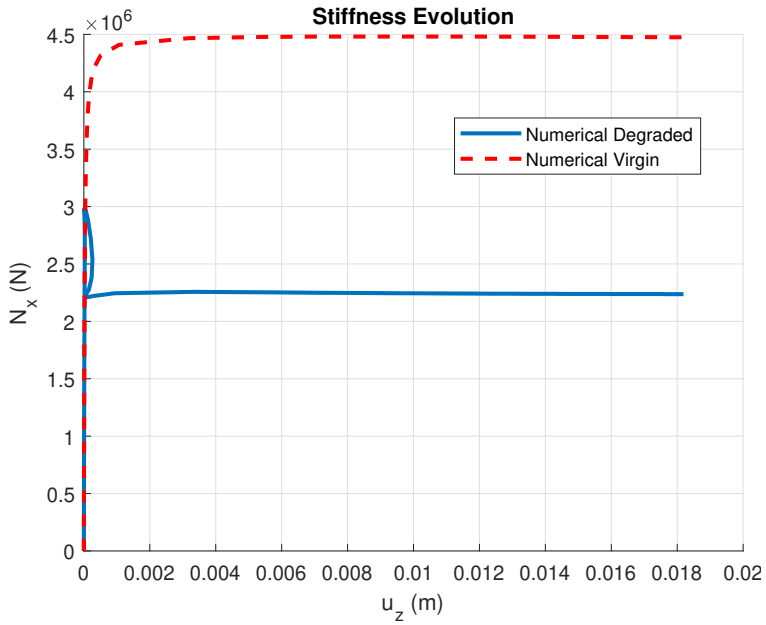

FIGURE 6.44: Flexural stiffness evolution for the virgin and degraded sandwiches.

6.4.2.4 Thermal Buckling with Damage

The damage used is the isotropic damage model with a mild linear hardening. All the materials are characterised with exactly the same damage properties, and thus the first constituent material to damage will be the fibre that presents the highest Young's modulus. In this example, only the fibre will present damage.

Material	σ_y	$\mathcal{H}_d$	c_{CR}	$\mathbb{T}_\sigma$
Fibreglass	$5 \cdot 10^7$	-0.5	1	Symmetric
Epoxy	$5 \cdot 10^7$	-0.5	1	Symmetric
PVCH80	$5 \cdot 10^7$	-0.5	1	Symmetric

TABLE 6.8. Properties of the isotropic damage model.

In Table 6.8, it can be seen that the properties for all the materials are the same. In this case, Young's modulus does not depend on the temperature. The properties were considered homogeneous, although it could be any other value. The objective of this example is to see how the buckling load changes with the damage generated in the structure. I.e., to assess the inelastic buckling phenomenon.

In Figure 6.45 the evolution of damage is presented. The threshold of damage sustained in the structure is around a 45%.

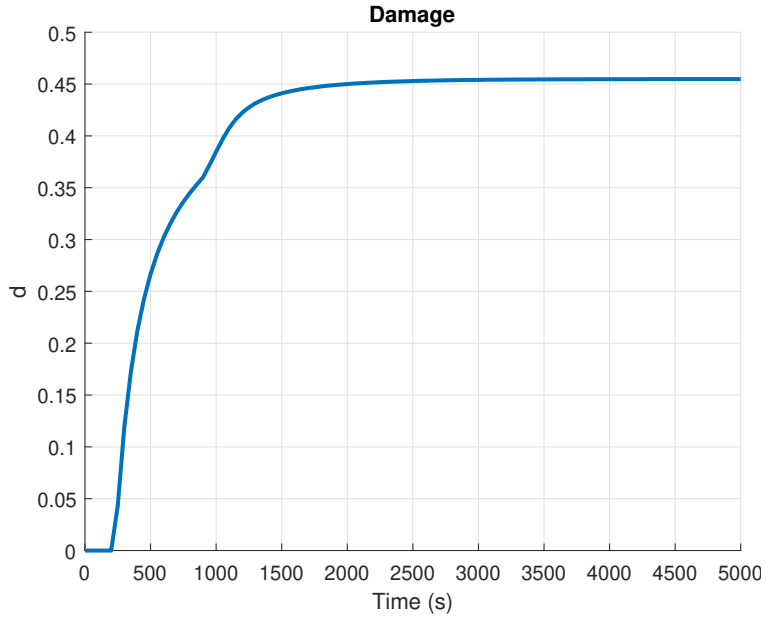

FIGURE 6.45: Damage generation at x=$L/2$.

Figure 6.46 shows the axial load evolution for the virgin model and the damaged model. It also plots the maximum damage solution.

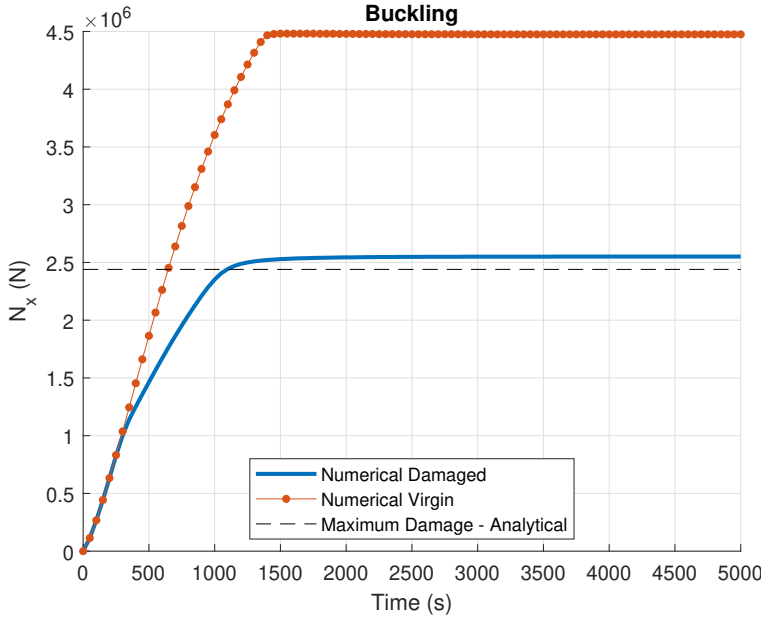

FIGURE 6.46: Load Evolution between the damaged and virgin models.

The maximum damage load is calculated using the constitutive secant tensor by the following manner

$$N_{\text{damaged, max}} = (1 - d_{max})N_{\text{virgin}} \tag{6.31}$$

The loss of rigidity due to the increment of the damage, as Figure 6.45 shows, leads to a major deflection than the virgin deflection since the constitutive secant tensor tends to decrease as the damage evolves. This effect can be observed in Figure 6.47.

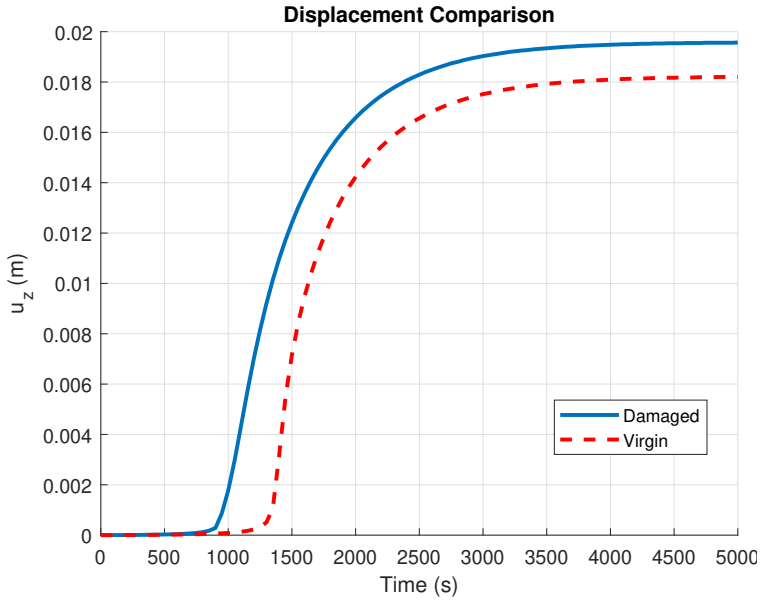

FIGURE 6.47: Displacement comparison at x=$L/2$ between the damaged and virgin models.

The comparison of the flexural stiffness between the virgin and damage model is shown in Figure 6.48. It can be seen that while the virgin is able to arrive to the critical buckling load, and thus it would fail due to buckling, the damaged model saturates to an axial load that is below the buckling load and which corresponds to an inelastic buckling load.

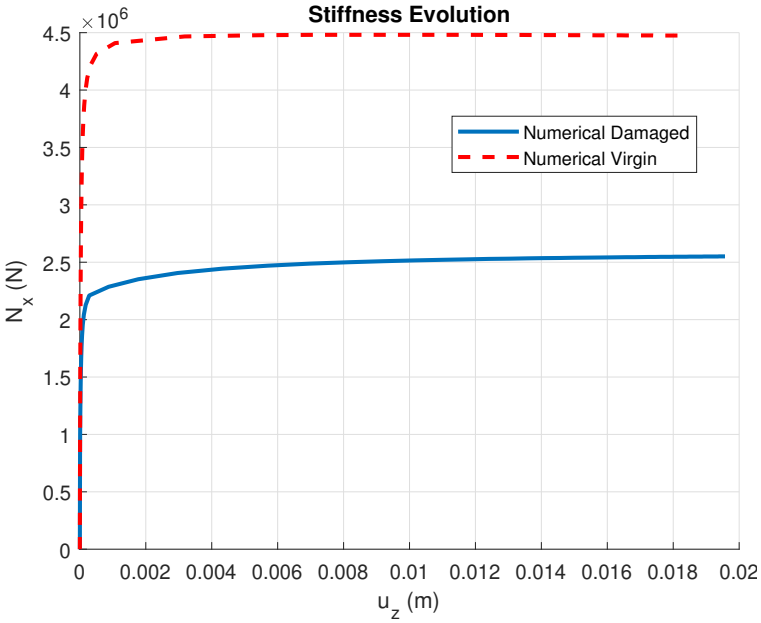

FIGURE 6.48: Flexural stiffness evolution for the damaged and virgin models.

The latter demonstrates that the failure mechanism in this case scenario would be governed by damage and the structure would collapse once the damage factor reaches to one, e.g., when all the layers of the composite have surpassed the yield stress. If the damage does not arrive to unity, then the structure will enter into post-buckling, but this buckling is of less magnitude since the effective elastic properties that are considered would be the secant properties.

Notwithstanding that this is numerically possible, in reality, the buckling load is lesser than the fluency load, so it is quite an unlikely that the structure reaches the full damage scenario, however, special emphasis has to be given to the degradation of the yielding stress, which in certain cases is many times lesser than the degradation that Young's modulus suffers [294]. Therefore, when considering post-thermal-buckling, where composites are present, the pyrolysis effect may lead to a yielding rather than buckling failure. So under these circumstances the structure might either completely yield or yield and buckling.

6.4.2.5 Thermal Buckling with Damage and Degradation

From the two previous examples, it has been demonstrated:

1. Temperature reduces Young's modulus and reduces the critical load that a structure with such properties can withstand.
2. Thermal strain may induce yielding in the structure, however the structure is more prone to buckle than yielding generally speaking. As a rule of thumb, consider that a structure will rather fail from buckling than completely damaging a section.

   However, inelastic buckling was shown in the previous example where the thermal strain may induce some damage in the structure and thus the critical load is reduced in proportion to that damage.

   A very rare case can happen when the yielding stress is significantly reduced due to temperature, in that case it may happen that if the reduction of the yielding properties is higher than the one of the elastic properties, the structure can be induced to damage failure by the temperature.

In practice there is a more limiting scenario, the pyrolysis of composites may lead to premature failure with the combination of buckling and damage. This is due to the nature of pyrolysis, which is more restrictive than temperature. Therefore, in this example, the temperature will be taken into account for Young's modulus (Table 6.7) and the yielding stress (Table 6.9) by maintaining the same evolution found in (Table 6.8). The pyrolysis properties can be found in Table 6.10, again they are assumed to be equal for all materials.

Material	σ_{y_u}	σ_{y_r}
Fibreglass	$5 \cdot 10^7$	$3.75 \cdot 10^7$
Epoxy	$5 \cdot 10^7$	$3.75 \cdot 10^7$
PVCH80	$5 \cdot 10^7$	$3.75 \cdot 10^7$

TABLE 6.9. Properties of the isotropic damage model.

Material	A_T	E_{act}	N_{ro}
Fibreglass	$1 \cdot 10^{20}$	$2 \cdot 10^5$	6
Epoxy	$1 \cdot 10^{20}$	$2 \cdot 10^5$	6
PVCH80	$1 \cdot 10^{20}$	$2 \cdot 10^5$	6

TABLE 6.10. Pyrolysis evolution properties.

Table 6.8 assumes the same evolution for the yielding stress and a reduction of 25%. For the boundary conditions established in the thermal model, the resultant evolution of the pyrolysis can be found in Figure 6.49.

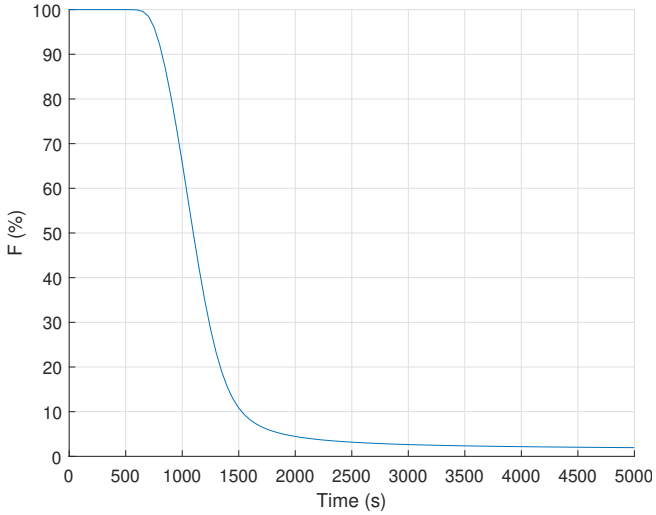

FIGURE 6.49: Evolution of the pyrolysis fraction.

It clearly shows that between 1500 - 2000 seconds, the pyrolysis fraction has almost reduced to 0%. This leads to an inelastic buckling where the damage is close to 1 and thus the structure has lost most of its stiffness. This is shown in Figure 6.50, where the curve of buckling is similar to the damage without temperature degradation case.

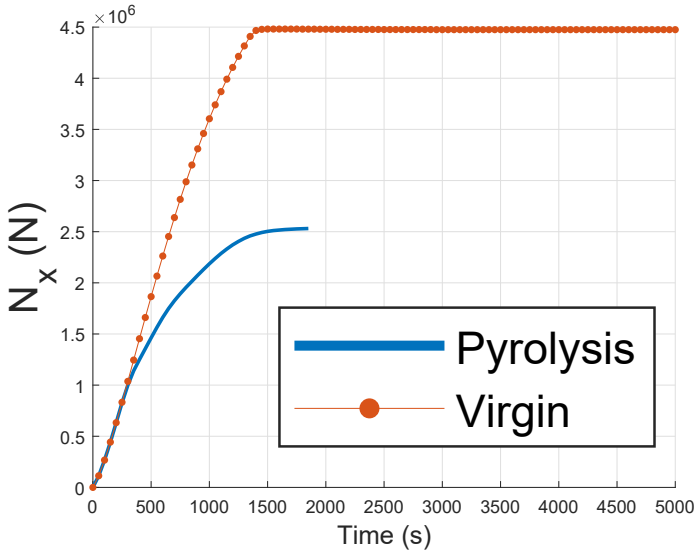

FIGURE 6.50: Load Evolution between the pyrolysed and virgin models.

However, since now the elastic limit depends on the temperature and pyrolysis, as soon as the pyrolysis fraction reaches 0%, the elastic limit is significantly reduced and generates damage close to 1. Although the damage is almost complete, the mechanism of failure is still buckling, since Young's modulus is 50% and a 75% yield stress. Therefore, the buckling load suddenly becomes close to 0 and the numerical model is unable to capture this unless the time is discretised in smaller steps. The final outcome is a failure due to thermal inelastic buckling.

6.4.3 Two-dimensional orthotropic thermal buckling of laminated composites

In subsection 6.4.2 the capabilities of the proposed methodology were shown. The effect of temperature degradation, inelastic buckling and pyrolysis degradation were illustrated for a one-dimensional sandwich case where only the mechanical properties were different and the thermal, damage and pyrolysis were assumed the same. However, this proves the correctness of the buckling module (co-rotational theory) in one direction and not in two directions, as it happens in laminate plates. In this example, the TSPROM in combination with the co-rotational theory will be shown to work excellently to predict the thermal buckling of orthotropic shells.

Laminate-plate buckling is a well-known problem studied in [295, 296, 297, 298]. This benchmark case shows the buckling phenomenon of orthotropic shells. The dimensions of this example can be found in Figure 6.51. The material is a symmetric monolithic composite stack of ten layers of uni-directional glass fibre and vinylester with a fibre volumetric fraction of 60%. The thermal properties of the fibre and matrix are considered the same as the composite. The mechanical properties are the standard values found in this thesis for fibre and resin (72 and 3.5 GPa). The mesh generated in this example is the same as in subsection 6.4.2, but it is simply supported on all edges.

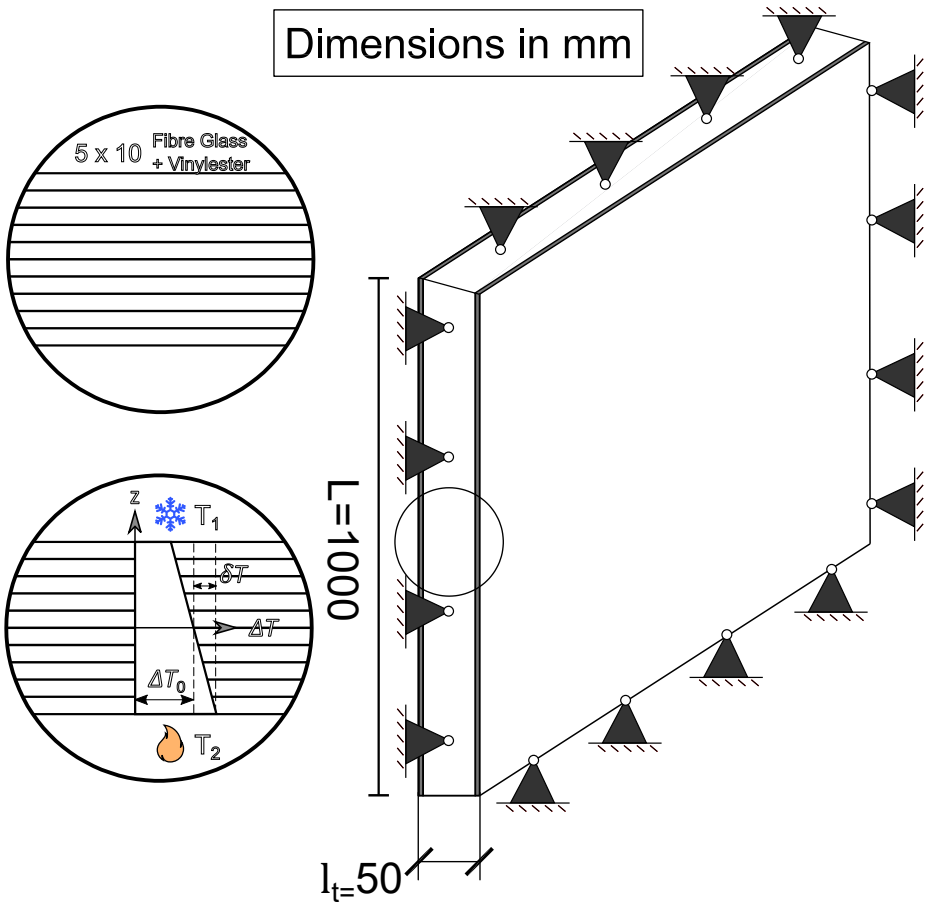

FIGURE 6.51: Description of the two-dimensional buckling problem.

The critical buckling temperature for different fibre orientations is compared against the analytical orthotropic solution. Fibre angle orientation is defined as follows, a 0° fibre orientation is aligned to the horizontal axis and 90° to the vertical axis. The height of the plate is 1000 mm and the widths is variable, considering a total of 3 different width over height aspect ratios $(0.75, 1, 2)$. The minimum critical buckling temperature is found (the ambient and initial temperatures are considered 0 °C) for these different aspect ratios.

Similarly to [298], the orthotropic definition of the critical buckling increment of temperature can be derived from plate theory for simply supported plates. Using the definition of the elastic constitutive matrix (D_{elast}), and defining the plate flexural rigidity matrix (D) and the thermal buckling coefficient (η), the critical buckling increment of temperature yields

$$D = \int_{l_t} D_{\text{elast}} \cdot \begin{bmatrix} -x_3 & 0 & 0 \\ 0 & -x_3 & 0 \\ 0 & 0 & -4x_3 \end{bmatrix} \cdot x_3 \mathrm{d}x_3 \tag{6.32}$$

$$\eta = \int_{l_t} D_{\text{elast}} \cdot \alpha \, \mathrm{d}x_3 \tag{6.33}$$

$$\Delta T_{\text{cr}} = \frac{D_{11}\bar{a}^4 + \bar{a}^2\bar{b}^2(D_{12} + D_{21} + 2D_{33}) + D_{22}\bar{b}^4}{\eta_1\bar{a}^2 + \eta_2\bar{b}^2} \tag{6.34}$$

where $\bar{a} = \frac{\pi n}{W}$ and $\bar{b} = \frac{\pi m}{L}$, W is the width of the plate, L is the length of the plate, n and m are the horizontal and vertical modes (the most critical ones are when $n = m = 1$).

The computational domain is discretised by a mesh of 20×20 elements in the in-plane directions, and a total of 30 layers in the thickness direction. These 30 layers coincide with the amount of one-dimensional thermal elements for the thermal analysis.

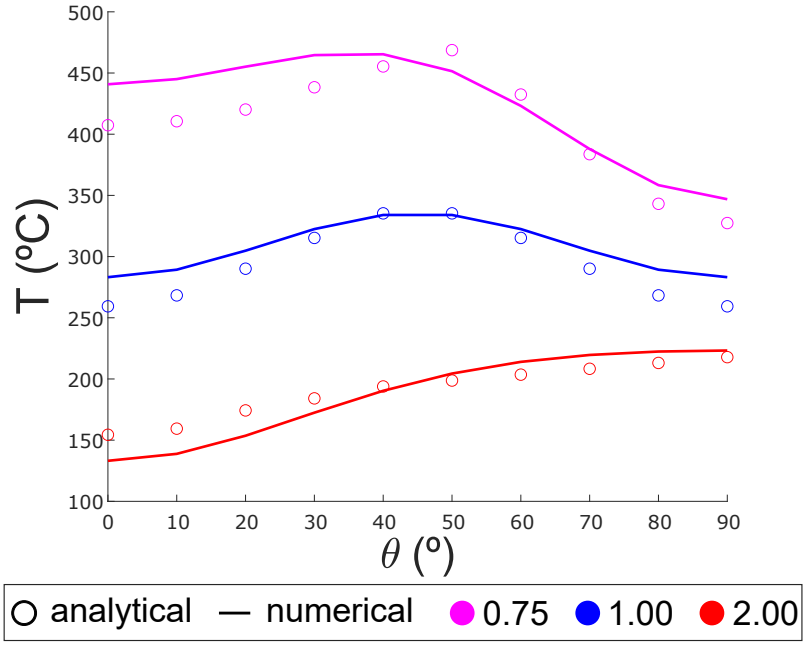

FIGURE 6.52: Critical temperature at different angles and aspect ratios (width/length).

Figure 6.52 shows the numerical results for the critical buckling mean temperature, for different angles and aspect ratios, against the analytical orthotropic result obtained from Equation 6.34. It shows a very good agreement for aspect ratios of 0.75, 1 and 2. Note that in this example, the constitutive model is considered without pyrolysis and elastic as well, in contraposition to the subsection 6.4.2 example.

The TSPROM theory demonstrates to correctly predicts the two-dimensional thermal buckling of the plate, guaranteeing the correct prediction of buckling in laminate structures and also the possibility of adding thermal degradation (pyrolysis) and inelastic buckling as shown in the subsection 6.4.2 example.

6.4.4 Thermal-damage - Feih experimental benchmark

In order to check that the thermo-mechanical model can predict real experimental data, it is compared against the experimental data found in [23] by Feih et al., in particular the experimental data provided for the compression test. The test calibrates experimentally the thermal decomposition, softening and failure of the FRP laminate when heated by one side and under uniaxial compressive load and finally the time-to-failure of the structure is registered for different heat flux loads. The thermal properties are set up as described in [23], the calibration is based on TGA, DMTA and DSC analyses.

The standard manner to prescribe the boundary conditions is to prescribe a numerical constant heat flux, in this work, the concept of adiabatic temperature is employed instead [28]. The adiabatic temperature is calculated based on the hot surface temperature Equation 3.64 assuming a prescribed constant heat flux at each time step for free convection. The thermal properties for the conductivity and the specific heat coefficient can be found in Figure 6.53 and Figure 6.54

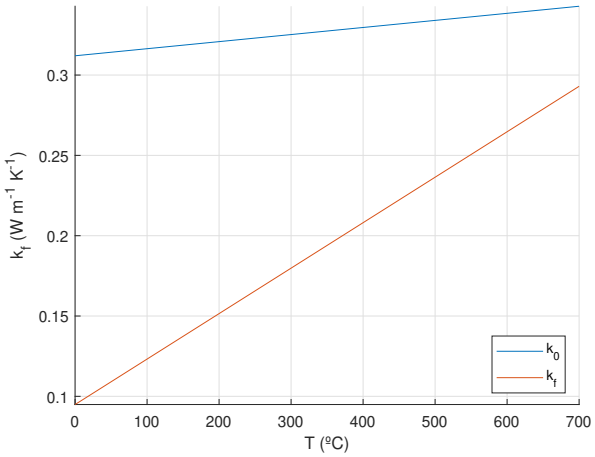

FIGURE 6.53: Evolution of the virgin and degraded conductivity with respect to the temperature.

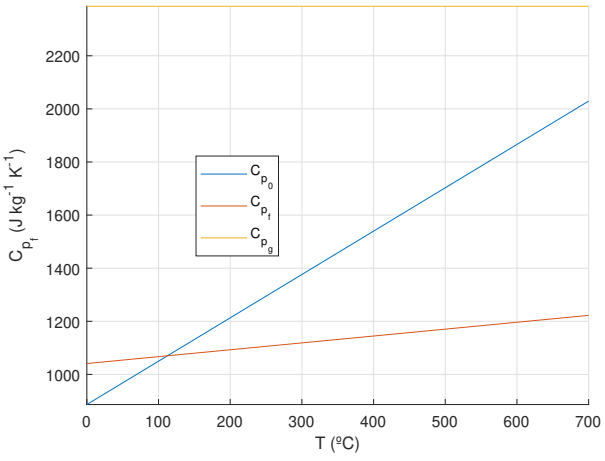

FIGURE 6.54: Evolution with a temperature of the virgin and degraded specific heat coefficient of the solid phase and also the gas specific heat coefficient.

The pyrolysis is obtained from [23] and Figure 6.55 it shows the TGA used to calibrate the Arrhenius coefficients.

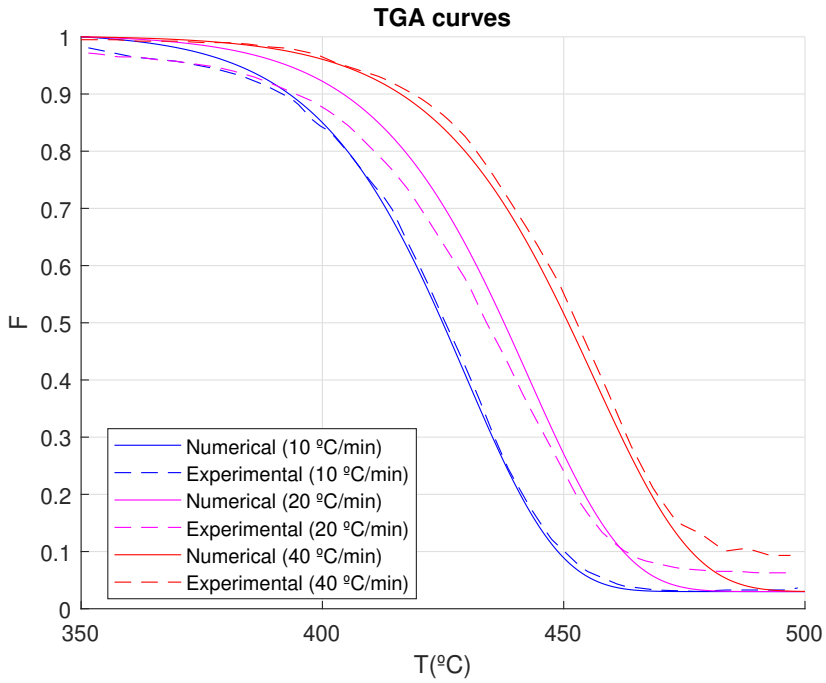

FIGURE 6.55: Comparison of numerical and experimental remaining mass evolution with respect to the time for different heat flux loads.

The Young's modulus and the yield stress are assumed to vary with the temperature. In Figure 6.56 the evolution of both is shown for the composite.

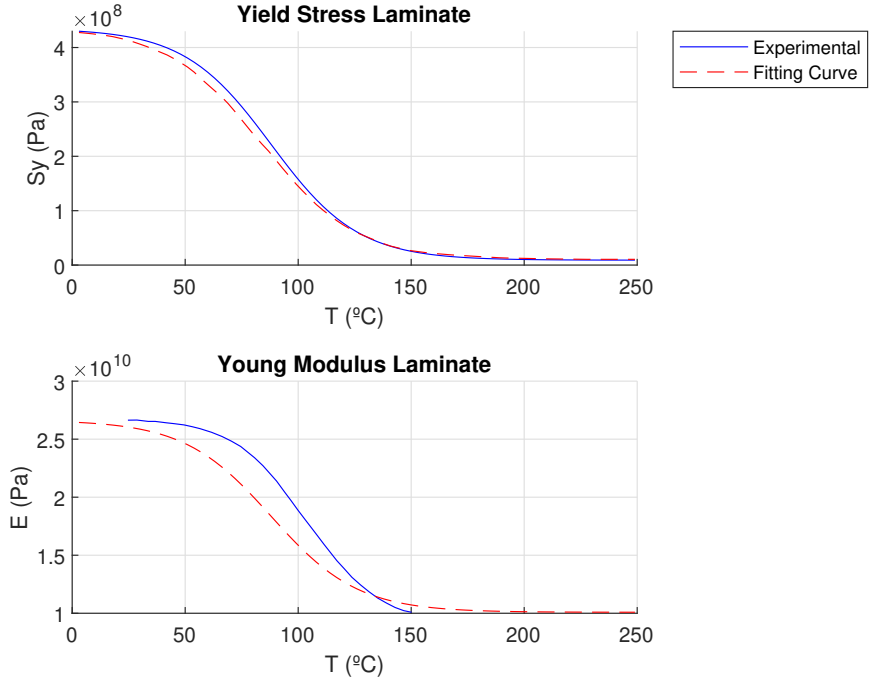

FIGURE 6.56: Temperature dependence of Young's modulus and the yield stress of the laminate composite.

However, this is at the composite level, then Equation 4.130 is used to infer the properties from the composite level to the constituent level. I.e., the resulting evolution of the yield property is found in Figure 6.57.

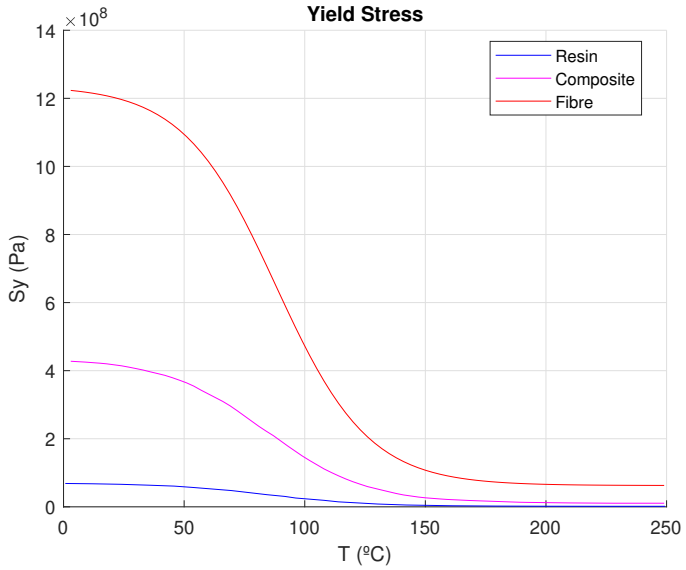

FIGURE 6.57: Temperature evolution of the yield stress of the constituent materials, inferred from the composite properties.

The thermal model is then compared against the experimental tests of a specimen exposed to high temperatures, this experiment aims to generate a temperature profile through the thickness of the specimen by applying a constant heat flux. The specimen is subjected to heat flux of magnitude $10, 25, 50$ and 75 kWm^2. The remaining mass fraction can be observed in Figure 6.58, where the numerical and experimental models show a good agreement for the three lowest heat fluxes.

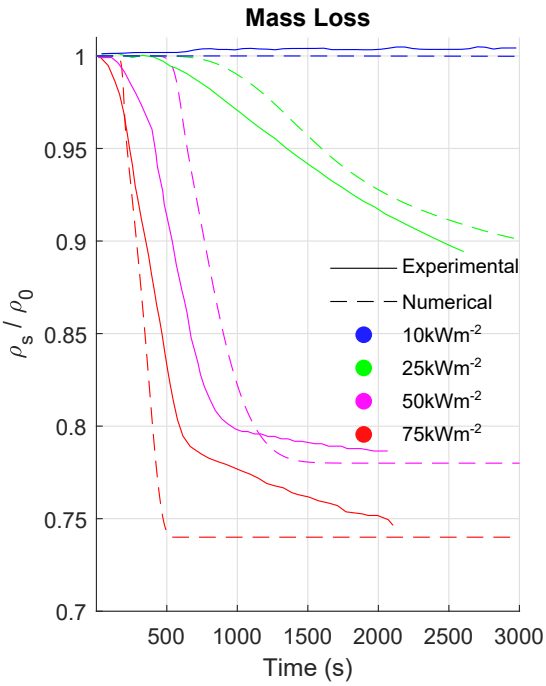

FIGURE 6.58: Comparison of numerical and experimental remaining mass evolution with respect to the time for different heat flux loads.

The flux of 75 kWm^2 has proven to be more difficult to reproduce because, for the calibrations given in [23], the specimen should follow a more harsh curve, however in reality the specimen ignites, and thus it becomes more difficult to reproduce.

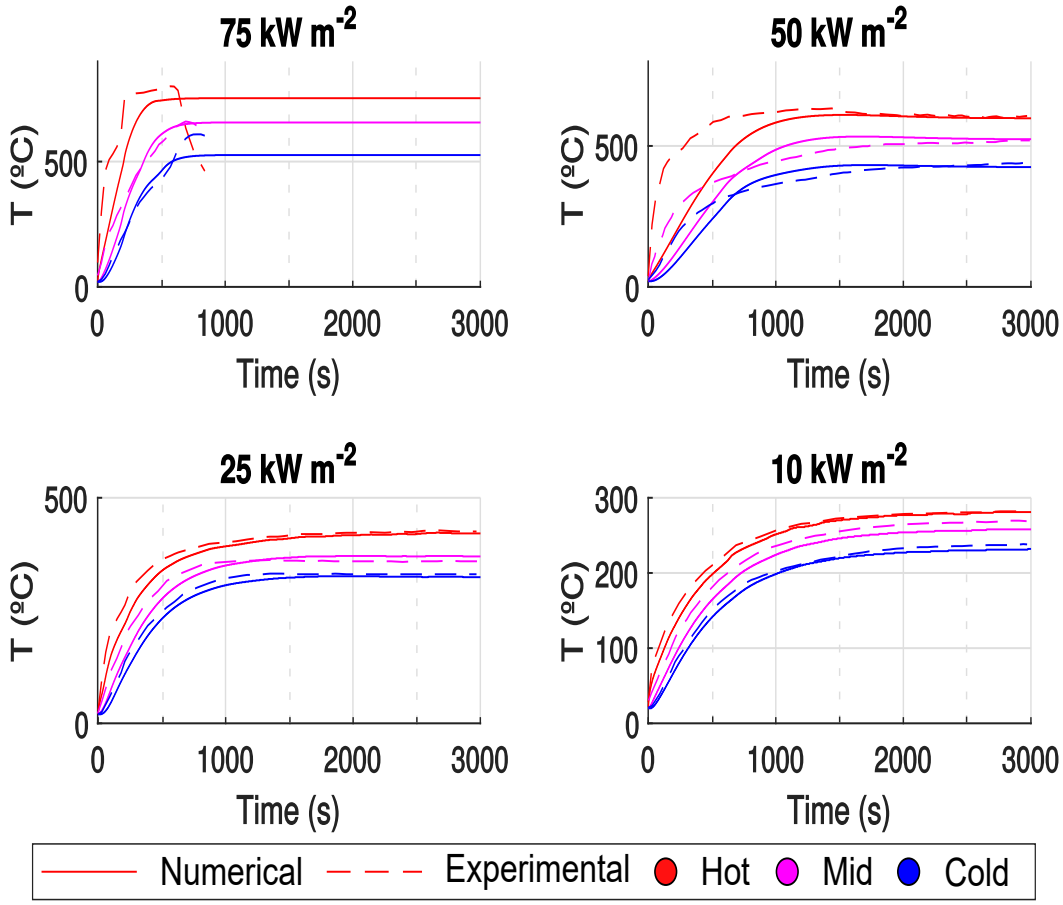

FIGURE 6.59: Experimental and numerical thermocouple readings at different positions through-thickness (Cold = 0 mm, Mid = 4.5 mm and Hot = 9 mm) and different heat fluxes.

Figure 6.59 shows the evolution of the experimental data measured by the thermocouples located at the cold, mild and hot layers at 0, 4.5 and 9mm respectively. The evolution of the temperature in respect to time is almost identical for heat flux loads of 10 and 25 kW/m^2. The main discrepancies are again for higher heat fluxes, e.g., the 50 kW/m^2 case shows a good steady solution however the transient presents a steeper evolution in the experimental test. This difference is mentioned in the original paper [23] and it is attributed to the escape of the gas through the thermocouples and even the numerical solutions provided by Feih et al. do not match the experimental ones.

The special case of 75 kW/m^2 is also reproduced, even though the hot end ignites. In the numerical simulation, it has been considered what would happen if the temperature remains the maximum instead of decaying in order to maintain the heat flux constant. The numerical results, which Feih et al. provide for this case, match perfectly at the beginning and then diverge significantly. The results provided in this thesis match for a wider range of time especially for the cold and mid-curves, however, the hot slope is lower compared to the experimental data.

The thermo-mechanical model is validated against the compression test results. These tests evaluate the compression endurance of the specimens, which are prone to buckling rather than yielding when exposed to high temperatures. The main objective is

to infer a relationship between yield failure and temperature. Feih et al. employ Equation 4.130 to establish a relationship between the yielding stress and the temperature, then loads the specimens for different values below the buckling load at ambient temperature. According to Feih et al., the specimens are constrained in such a manner that avoids global buckling, therefore the specimens shall only fail by yielding as the temperature rises and the yielding stress is reduced.

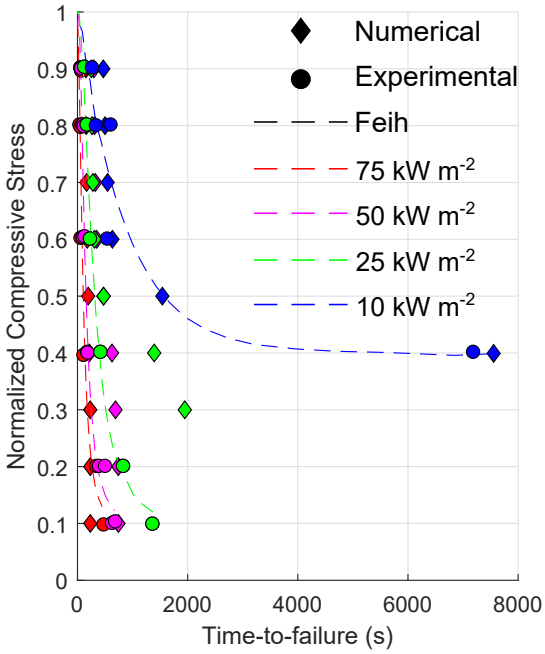

FIGURE 6.60: Thermo-mechanical failure of the compression specimens for a combination of different thermal and mechanical loads.

The compression failure of the specimens is then summarised and detailed in Figure 6.60. The experimental and the numerical results, provided by the analysis of flexible laminates exposed to fire, match the heat flux of 10 kW/m^2 and present a close agreement for 50 and 75 kW/m^2. On the other hand, the case of 25 kW/m^2 shows an initial good agreement but as the load is decreased, lower or equal to 30% of the buckling critical load, the numerical and experimental solutions diverge. One of the reasons for this mismatch may be due to the neglect of Young's modulus degradation, since the degradation of this property leads to a lower flexural rigidity (EI), the latter is linearly related to the buckling load. Since the thermo-mechanical analysis presented in this example focuses on linear geometric kinematics, this final remark cannot be checked.

6.4.5 FTP - Code

One of the objectives of FIBRESHIP is to build and test actual stiff components and structures that have to fulfil the strict IMO/SOLAS fire safety requirements. To address this question, large-scale fire-resistance tests of chosen components will be carried out according to the IMO FTP Code Part 11 [256, Part 11]. These tests consider simultaneous thermal and mechanical loading, and their purpose is to demonstrate that relevant fire safety objectives and functional requirements are met. The fire resistance tests will comply with the requirements of classification societies for their use in large-length ships. These tests will include the evaluation of the performance of the advanced intumescent coatings selected in previous phases of the project.

These tests will serve as a validation of the numerical tools developed using the methodology derived in this thesis. The specimens under study are those, found in the FTP code, which analyse the fire collapse of bulkheads under fire and mechanical loads, i.e., load-bearing bulkheads. In particular, *non-reinforced* and *reinforced* bulkheads are similar to the illustration found in Figure 6.61.

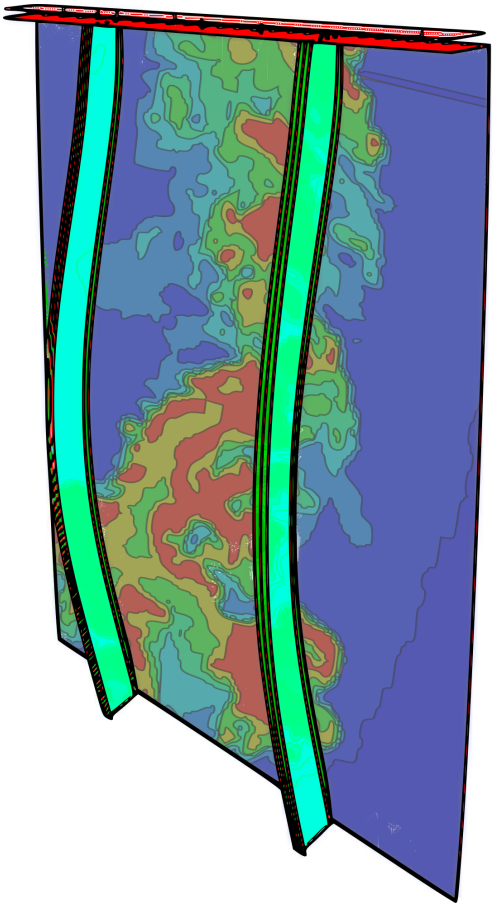

FIGURE 6.61: An illustration of a load-bearing reinforced bulkhead deformed due to a mechanical load on top and a thermal load induced by the exposed surface.

6.4.5.1 FIBRESHIP Campaign

The experimental test consists of the analysis of a load-bearing FRP bulkhead designed following the standards of the International Code for Application of Fire Test Procedures (2010 FTP Code) [256, Part 11]. This test has been carried out within the scope of the H2020 FIBRESHIP project in the vertical furnace of Eurofins Expert Services. The test was aimed the demonstration of the performance of the bulkhead at 60 minutes load bearing fire-resistant division. In order to study the performance of the bulkhead beyond those 60 minutes, the test was extended until 5100 s, where it had to be finished due to safety reasons. At that instant, the panel deformation created a significant gap from the frame, allowing the flames to start escaping.

An FRP division was manufactured with the dimensions and characteristics shown in Figure 6.63. A total of 5 sensors – represented as groups of three squared pattern markers in Figure 6.63 – are placed at (25%,25%), (75%,25%), (50%,50%), (25%,75%) and (75%,75%) where each coordinate is relative to the width (2.9m) and height (2.98m) of the panel. Each of these groups of sensors are composed of 3 through-thickness thermocouples placed on the unexposed surface, in the middle of the PVC core and behind the monolithic laminate bounded to the insulation (see Figure 6.63).

FIGURE 6.62: Experimental setup for the bulkhead test. Picture by courtesy of Eurofins Expert Services.

The experiment was performed as established by the standards ([55], [255]), which determined the heat flux based on a design temperature curve. The calibrated heat flux is correct as the furnace temperature matches perfectly the ISO 834 curve . The standard emissivity value of 0.9 is used for both unexposed and exposed surfaces,

the standard convection coefficient for the unexposed surface is 9 ($W/m^2°K$) and for the exposed it should be 25 ($W/m^2°K$), however the sensitivity tests have shown that its real value is more in the order of 15 ($W/m^2°K$). The temperature, at which the unexposed surface is considered to be the ambient, is 17(°C).

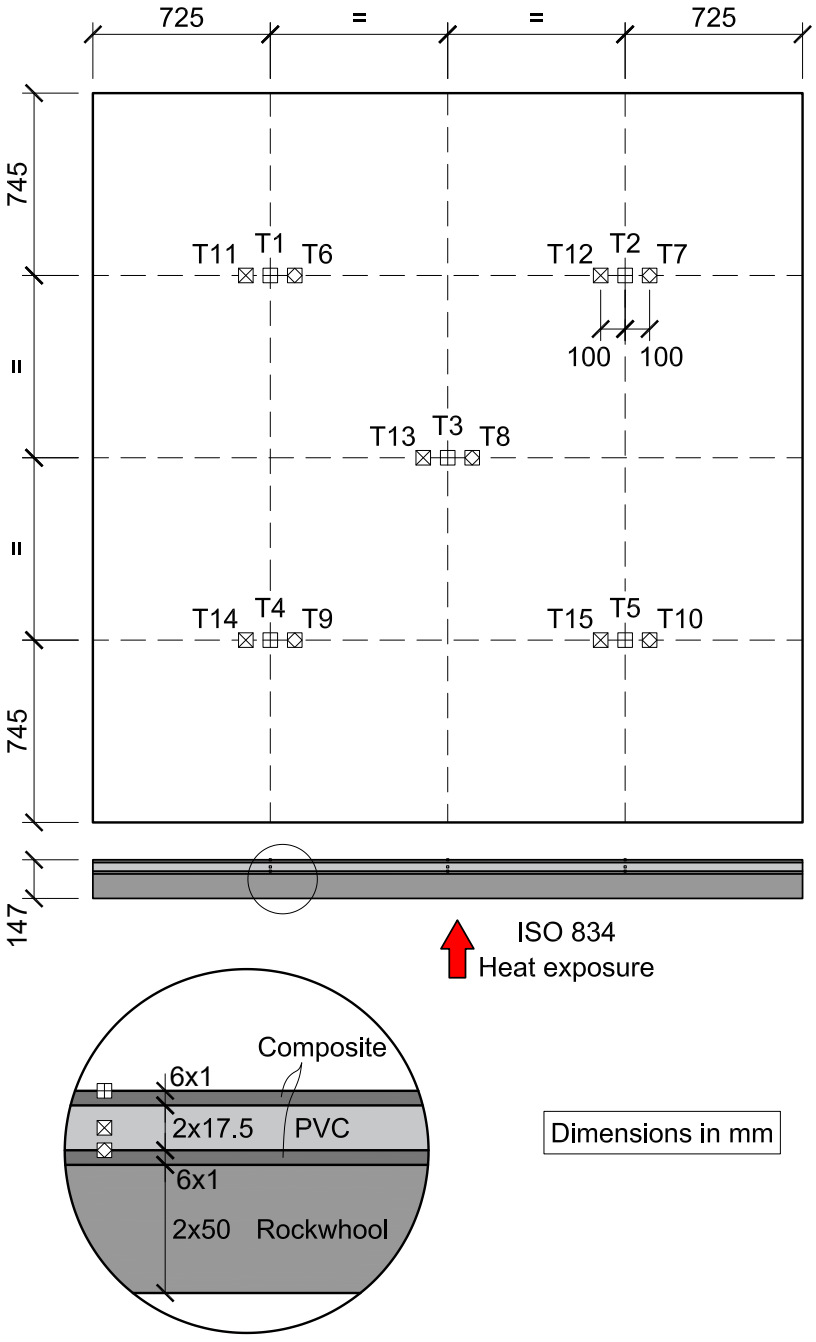

FIGURE 6.63: Schematic of the test panel.

The International Maritime Organisation (IMO) in their Fire Test Procedures guidelines [256, Part 11] establish the mechanical load conditions used in the test. The load condition is a compression load of 7.0 kN/m placed on the top edge. The mechanical deflection in the centre of the panel was measured by an actuated cable sensor and later compared to the numerical results.

The composite laminate is composed of the following stack, where the layup is shown in Figure 6.63:

Layer 1: 1×0.375mm layers of unidirectional glass/vinylester (LEO Injection Resin 8500 from BÜFA; this resin is part of the Saertex LEO® fire retardant composite system) and the fibre orientation of the stack is [0 90 ,0 ,90 ,0 ,45 ,-45 ,90 ,0 ,90 ,0 ,45 ,-45 ,90 ,0 ,90] degrees [290].

Layer 2: 2×17.5mm layers of PVC which works as the core of the sandwich (PVC-H80 from Diab Group; this is the core part of the Divinycell H® materials) [293].

Layer 3: 16×0.375mm layers of unidirectional glass/vinylester (LEO Injection Resin 8500 from BÜFA; this resin is part of the Saertex LEO® fire retardant composite system) and the fibre orientation of the stack is [90 ,0 ,90 ,-45 ,45 ,0 ,90 ,0 ,90 ,-45 ,45 ,0 ,90 ,0 ,90 ,0] degrees [290].

Layer 4: 2×50mm layers of mineral wool, which works as an insulation of the composite laminate material (SeaRox® SL 620 from Rockwool) [299].

The thermal properties of each layer material are presented in Table 6.11

Material	c_k (W/m°K)	c_p (J/m^2°K)	c_{p_g} (J/m^2°K)	ρ_s (kg/m^3)	Q_p (J/kg)
glass/vinylester	0.5135	858.55	1000 - 1200	1780	$2{\cdot}10^5$
PVC	0.02-0.06	1170	1200	80	0
Rockwool	0.03-0.8	1000-750	0	60	0

TABLE 6.11. Calibrated thermal properties of the layer materials.

The decomposition energy of the PVC is neglected, since the temperature measured in the core of the bulkhead throughout the test was lower than the degradation temperature threshold. The pyrolysis model of the laminate used to build the bulkhead was calibrated against the experimental thermo-gravimetric test, which has also been carried out within the context of the FIBRESHIP project. Figure 6.64a shows the agreement of the mass fraction evolution of the model in the thermo-gravimetric test of the laminate after the calibration. On the other hand, the pyrolysis of the core material of the laminate is taken from the thermo-gravimetric analysis presented in [300] and Figure 6.64b compares the experimental data from the literature to the selected pyrolysis model for the PVC.

Material	A_T (s^{-1})	E_{act} (J/mol)	N_{ro} (J/m^2°K)
glass/vinylester	$6 \cdot 10^{20}$	$2.8{\cdot}10^5$	6
PVC	1202604.28	90000	2

TABLE 6.12. Calibrated pyrolysis properties of layer materials.

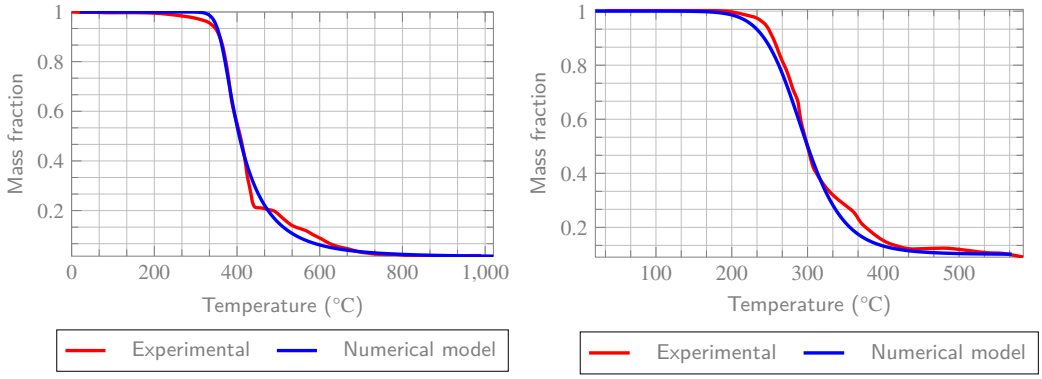

(A) Leo System®. (B) PVC-H80 [300].

FIGURE 6.64: Evolution of the experimental and modelled mass fraction $\left(\frac{\partial \rho_s(T)}{\partial t}\right)$.

The values of the parameters for the Arrhenius law (Equation 3.56, Equation 3.55) of the calibrated pyrolysis model in Figure 6.64a and Figure 6.64b are given in Table 6.12. The insulation can be considered pyrolysis free. This means that the degradation factor will remain equal to one and the evolution zero.

The mechanical properties of the components in the Leo System® material are taken from the experimental data presented in [12]. The PVC is calibrated against the data provided in [293] and any missing information is completed by standard low density PVC values.

Material	E (Pa)	ν	σ_y (MPa)	Π_F (N/m)	c_{CR}	Φ_Ω
Matrix	$3.35 \cdot 10^9$	0.26	20	$1.2 \cdot 10^4$	1	0.40
Fibre	$72.4 \cdot 10^9$	0.21	1800	$8.0 \cdot 10^5$	1	0.60
PVC	$49 \cdot 10^6$	0.4				
Rockwool	2466060.9905	$1.17647 \cdot 10^{-6}$				

TABLE 6.13. Calibrated mechanical properties of constituent materials based on subsubsection 6.3.1.1 and can be found in [12, 13].

The characterisation of the evolution of Young modulus in respect to the temperature is obtained from a dynamic mechanical thermal analysis (DMTA) of the Leo System® material and for PVC, the storage modulus, is obtained from the research by Earl and Shenoi in [301].

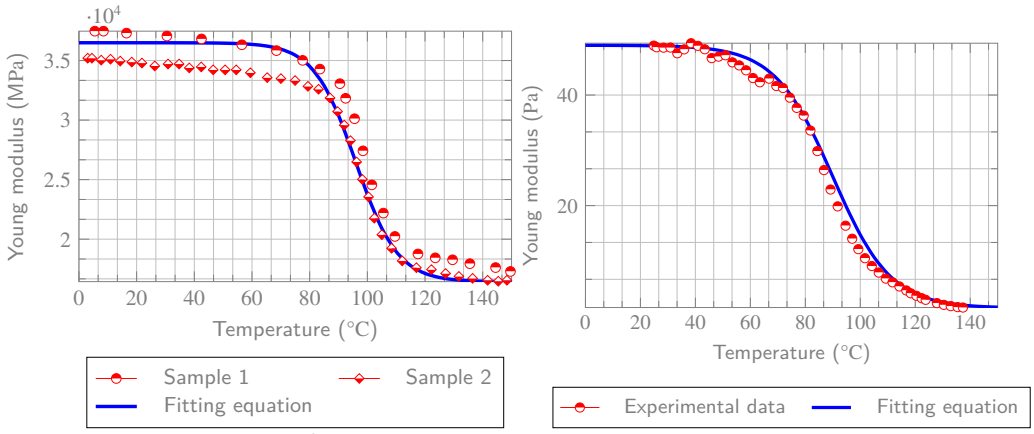

(A) Leo System®. (B) PVC-H80. (Adapted from [301]).

FIGURE 6.65: Experimental and numerical evolution of the storage modulus with respect to the temperature.

Material	E_u (MPa)	E_r (MPa)	n_{MG1}	n_{MG2}	T_g (°K)	α (°K^{-1})
Matrix	3350	1507.5	0.0691	6	96	$36{\cdot}10^{-6}$
Fibre	72400	32580	0.0691	6	96	$36{\cdot}10^{-6}$
PVC	49	1.47	0.0475	6	90	$40{\cdot}10^{-6}$
Rockwool						$60{\cdot}10^{-6}$

TABLE 6.14. Calibrated thermo-mechanical properties of the constituent materials.

Note that in Table 6.14, the insulation only takes into account the thermal expansion coefficient which is considered isotropic. The fitting equation in Figure 6.65 represents the evolution of the Young modulus described in Equation 4.130 and with the assumptions in Equation 4.141, Equation 4.142 and Equation 4.143. The glass transition temperature or the thermal expansion coefficient are assumed to be identical for both matrix and fibre since the experimental data is referring to the composite material. Therefore, for simplicity, the properties of the composite are ingrained into its constituent materials.

6.4.5.2 Results of the fire-resistant test on the bulkhead

This section presents the results of the fire-resistant test on the bulkhead and compares them with those of the computational model. Figure 6.67 compares the time evolution of the temperatures obtained from the experimental test and the numerical model. The thermal numerical model consists of a discretisation of the thickness of the composite, with a total of 112 1D finite elements. The glass/vinyl-ester layers are discretised with 16 uniform spaced elements each. The PVC core is discretised with 20 uniform spaced elements and the insulation with a total of 60 uniform spaced elements. Further information about the boundary conditions and discretisation is shown in Figure 6.66.

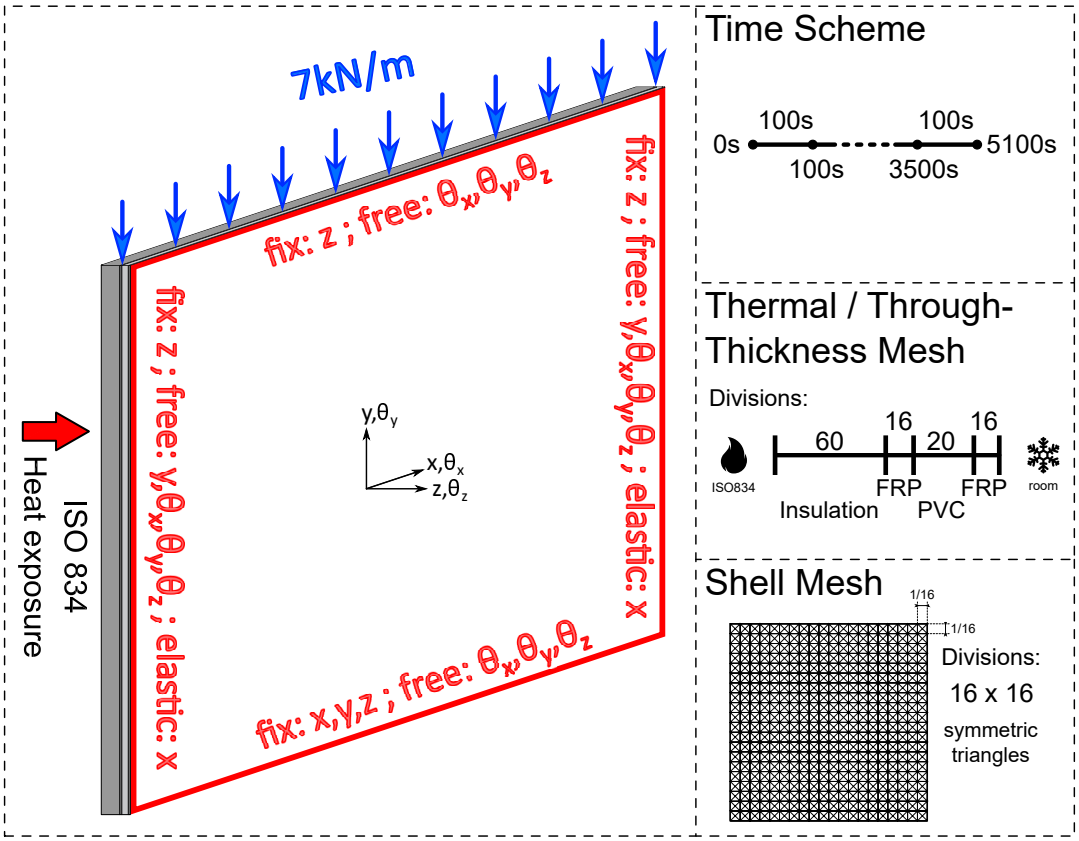

FIGURE 6.66: Boundary conditions, and time and spatial discretisation. Note that the dimensions and divisions are not proportional.

The temperature of the furnace is prescribed on the exposed surface using the ISO 834 curve and the ambient temperature prescribed in the unexposed surface is considered to be initially 17 °C and by the end of the experimental test it is 25 °C. Note that these two temperatures do not refer to the temperature in the exposed/unexposed surfaces themselves, but rather to temperatures nearby these surfaces. Hence, the flux can be calculated as established in Equation 3.77 and Equation 3.78 and the convection coefficient and emissivity of both surfaces were described in the setup of the experiment in Figure 6.4.5.1.

The thermo-mechanical model consists of a total of 256 equally distributed linear geometric quadrilateral elements with a non-linear constitutive model. From Figure 6.63 the horizontal axis is defined as x, the vertical axis as y and the out-of-plane axis as z. The lower horizontal edge fixes the translation degrees of freedom in x, y, z, the upper horizontal edge fixes the translation degree of freedom z and has a load applied of 7 kN/m as described in Figure 6.4.5.1.

Both left and right vertical edges, fix the translation degree of freedom in z and have a dynamic variable elastic constraint. These two elastic constraints are symmetric and are controlled by the horizontal dilatation of the edges. There are two stages, first the translation degree of freedom in x is given a certain rigidity to simulate the friction between the panel and the frame and later the translation degree of freedom in x is fixed completely. The plausible phenomenon that is addressed in this example is that the panel is able to slide in the test frame, meaning there is a little space

left, and it is occupied as the bulkhead starts dilating due to the increase of temperature. Gradually, the first stage blocks the movement in x and in the second stage, considering there is no extra space, the boundary condition becomes fully fixed.

Both thermal and thermo-mechanical analysis are solved incrementally with a total simulation time of 5100 s in intervals of 100 s.

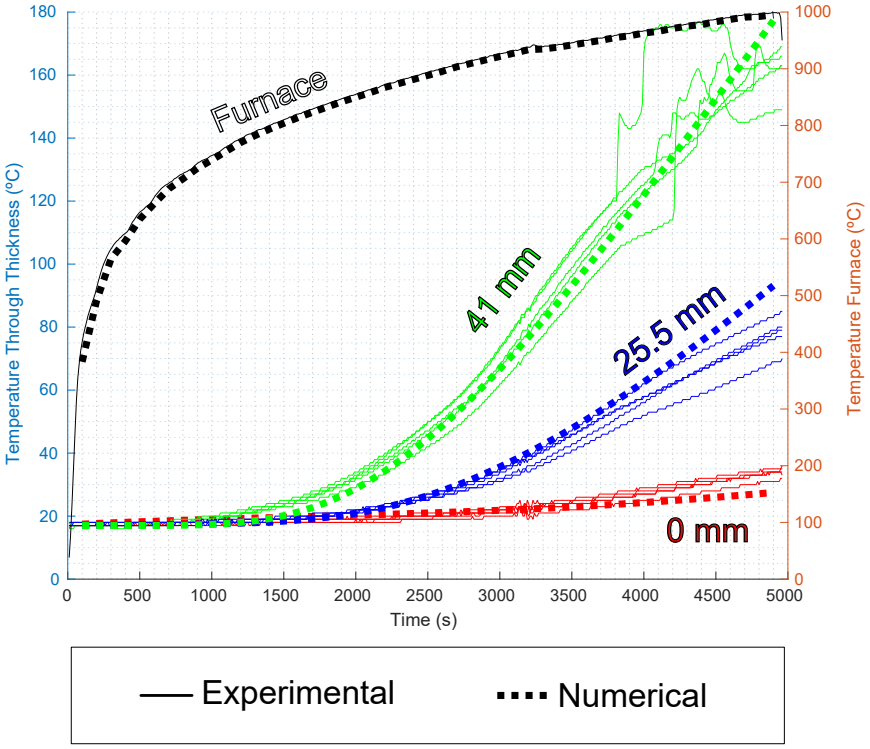

FIGURE 6.67: Evolution of the temperature ($T(x,t)$) at different positions of thickness. The temperature through thickness represents the sets in red, blue and green and the temperature furnace the orange set. Thermocouples T1, T2, T3, T4 and T5 in red were placed at $x = 0.0$ mm, thermocouples T11, T12, T13, T14 and T15 in blue were placed at $x = 25.5$ mm and thermocouples T6, T7, T8, T9 and T10 in green were placed at $x = 41.0$ mm. All measures are with respect to the unexposed surface.

Note that both the experimental and computational data closely match. There is a minor fluctuation of the temperature (green) at the interface between the glass/vinylester layer and the core, which is closest to the fire exposed surface. This fluctuation is produced close to the time the upper right corner of the panel starts to bulge outwards producing a gap between the specimen and the test frame. The two thermocouples, which have registered these fluctuations, coincide exactly with those that are situated in the upper right and upper left of the panel.

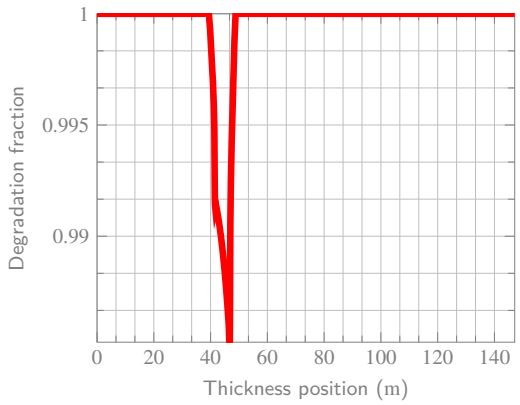

(A) Sectional degradation fraction (F) at time 5100s.

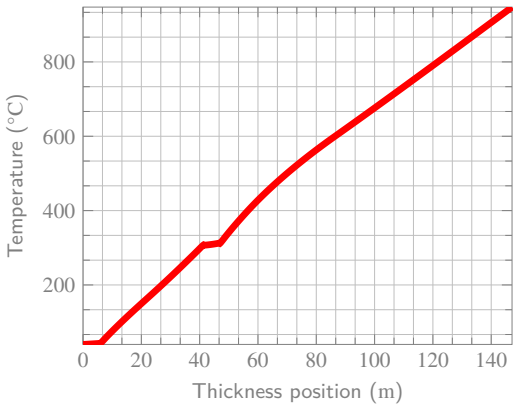

(B) Sectional temperature (T) at time 5100s.

FIGURE 6.68: The final computed profile of the degradation and temperature through thickness of the section in the mid-point of the panel.

The profile of the degradation fraction at 5100s, computed by the pyrolysis model at the mid-point of the panel, is presented in Figure 6.68a. Notice that the degradation can be considered zero, since the minimum degradation fraction is 0.985. This implies that the fire-resistant performance of the panel is excellent.

The corresponding profile of temperature can be found in Figure 6.68b, which agrees with the fact that the composite is well insulated. The 4 layers of the composite described previously can be observed by checking the slope variation. Within those 4 regions, only two regions show a temperature over the range of 200 °C.

The degradation shown is in accordance to what was presented in Figure 6.64a. Notice that the mass fraction presents a substantial change for temperatures higher than $300 - 400$ °C and this is the primary reason why the LEO System® closest to the exposed surface does not present a significant degradation. Similarly, Figure 6.64b shows that the mass fraction of the PVC starts degrading for temperatures above 200 °C and the PVC region almost reaches this temperature in the union with the Leo System® layer closest to the exposed surface.

The deflection in the middle of the panel is measured with a cable actuated sensor. The thermo-mechanical evolution of the deflection can be found in Figure 6.69.

FIGURE 6.69: Evolution of the experimental test until collapse. Photographies by courtesy of Eurofins Expert Services.

In Figure 6.70, the deflection at the mid-point of the unexposed surface is registered experimentally and compared to the numerical simulation, finding a good global agreement between computed and measured data. However, relevant differences are found in some phases of the test, likely due to the complexity of the problem and the uncertainties in some material properties. This is discussed below.

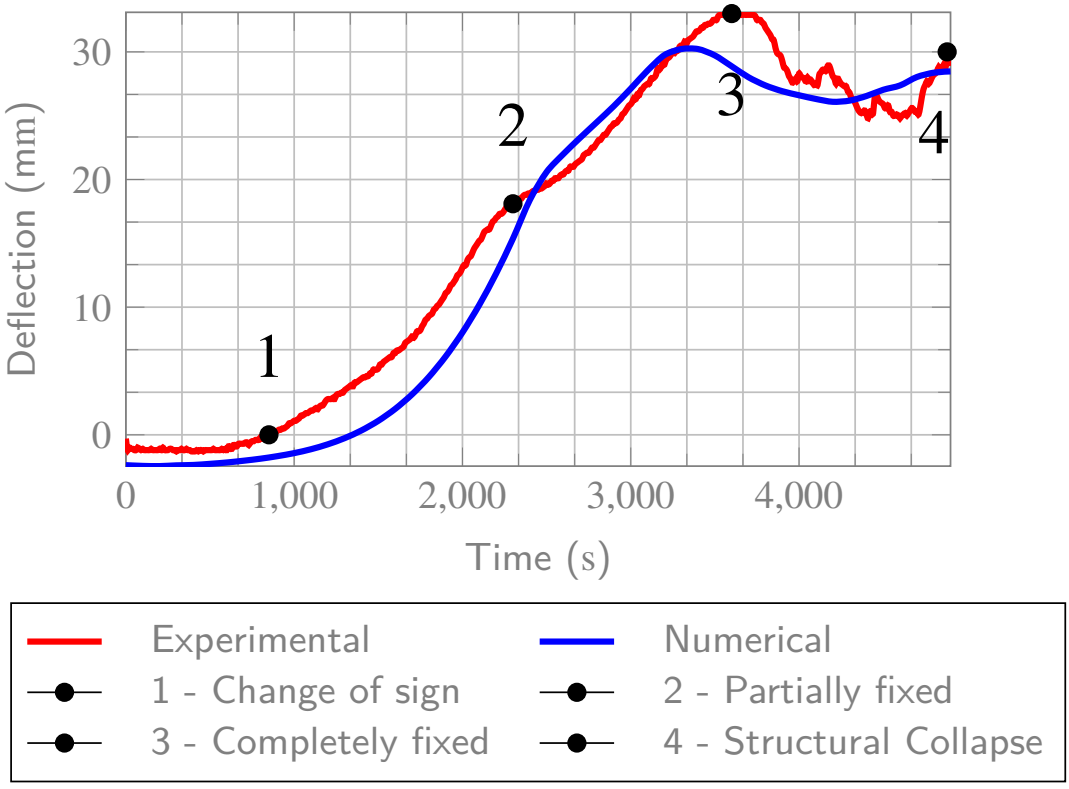

FIGURE 6.70: Deflection evolution in mm.

Throughout the experiment, we can identify four phases, defined by the points 1, 2, 3 and 4 in Figure 6.70. The panel starts deflecting negatively due to the compression load that the panel endures according to [256]. Note from Figure 6.63, the section is non-isotropic and hence the load, theoretically placed in the middle of the thickness, does not coincide with the neutral axis of the section. This generates two points in the upper and lower edges that bend the structure. Moreover, since the elastic modulus of the section is lower in the insulation than in the glass/vinyl-ester layer, the composite initially experiments a higher compression on the exposed surface (insulation). Thus, the exposed surface is relatively compressed and the unexposed is relatively tensed. The numerical simulation does not fit exactly the early deflection, however, it captures the phenomenology, starting with a negative deflection and once the temperature is high enough, it bends the opposite direction (point 1).

The panel is inserted into the test frame, meaning it is not fixed in any other direction other than the out-of-plane direction. This combined with the increase of temperature make the panel proportionally dilate. This occurs around the time step of point 2, in Figure 6.70, when the specimen edges have started to partially contact the frame and become fixed to it. In order to model this phenomenon, two boundary conditions – namely two dynamic elastic constraints – were introduced on both vertical edges (right and left) which add an extra fixation on the horizontal direction opposite to the dilatation of the panel. As shown from point 2 onward, these dynamic elastic constraints are able to reproduce the friction condition between the bulkhead and the test frame.

Once the simulation arrives to point 3, the panel becomes fixed as it experiments an elevated temperature and there is no extra space left to dilate. The dynamic boundary conditions from the third point onward fix the in-plane horizontal translation.

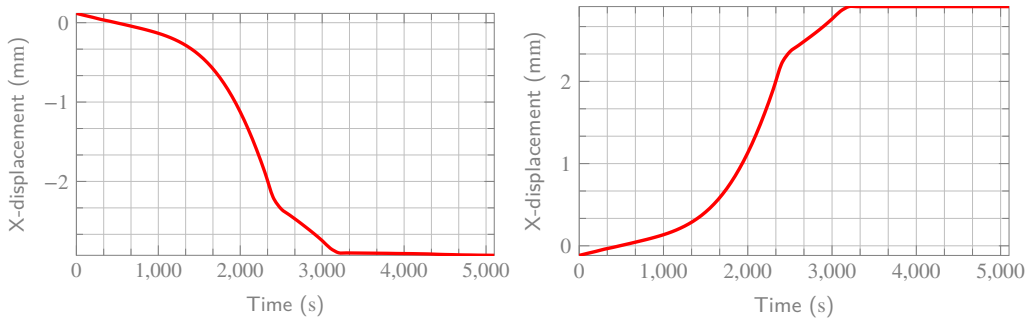

(A) Left mid-point.

(B) Right mid-point.

FIGURE 6.71: Horizontal displacement in terms of time. Note the dynamic boundary condition stages.

The numerical model is able to reproduce the behaviour of the third stage to a certain extent, note that the uncertainties and limitations of the experimental test play a fundamental role in this stage. The panel approaching point 4 starts to present a non-symmetrical behaviour, and finally the panel collapses when the upper right corner bulges from the test frame. At the fourth point, the structure collapses due to the augment of effective mechanical load, since the upper right corner is no longer enduring any load.

The collapse could be reproduced, since the non-symmetric behaviour is very complex to be incorporated in this example. It is not even likely to happen in a real bulkhead fire collapse scenario. However, the bulging can be explained through the deflection of a sectional cut passing through the mid-point of the panel (Figure 6.72a) and the maximum damage index (Figure 6.72b).

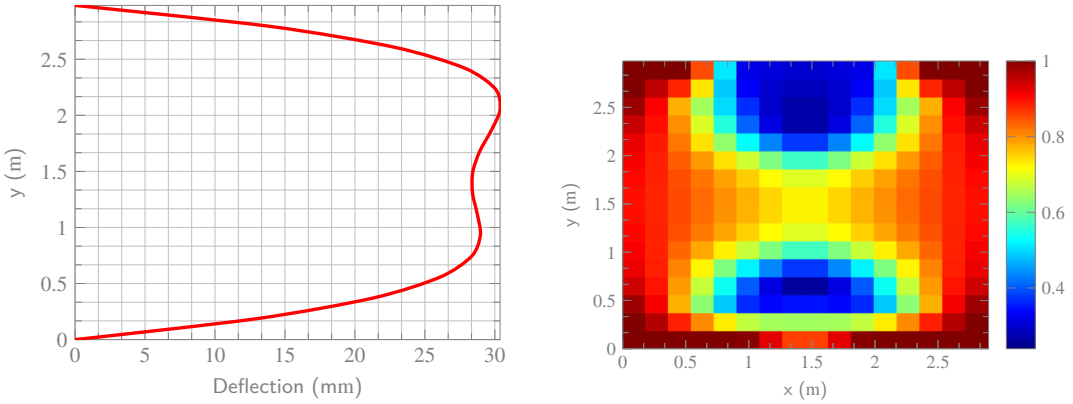

(A) Symmetric vertical section. (B) Damage index (d).

FIGURE 6.72: Final snapshot of the panel at time 5100 s before the experimental test collapses. The damage localisation can be observed

In Figure 6.72 it can be seen that the deflection of the panel presents two protuberances. This is equivalent to the two blue regions found in Figure 6.72b, observe that the lower end of the section cut presents a milder stepper rotation than the upper end, this explains why the bulging occurs on the top rather than on the bottom. The bulging is considered to occur due to uncertainties that cannot be controlled, however, the methodology used in this thermo-mechanical analysis shows that the occurrence of this phenomenon is feasible since the degradation has a double triangle shape which localises the damage in all four corners, however, – numerically speaking – it is still able to mantain the perfect contact between the frame and the specimen.

The experimental test has some certain limitations when it comes to maintaining a perfect contact between the bulkhead and the test frame. Once the upper right corner bulges, the fire security protocol, establishes to cease the testing. However, it is quite interesting to extend the simulation beyond the scope of 5100 seconds and see that the bulging phenomenon can be addressed in the model. Not the phenomenon *per se*, but the prelude to it. Short after the experimental model collapses, the numerical model shows a good agreement with this bulging behaviour since around all four corners a negative deflection starts to form and this very change of the deflection explains the sudden bulge of one of the corners.

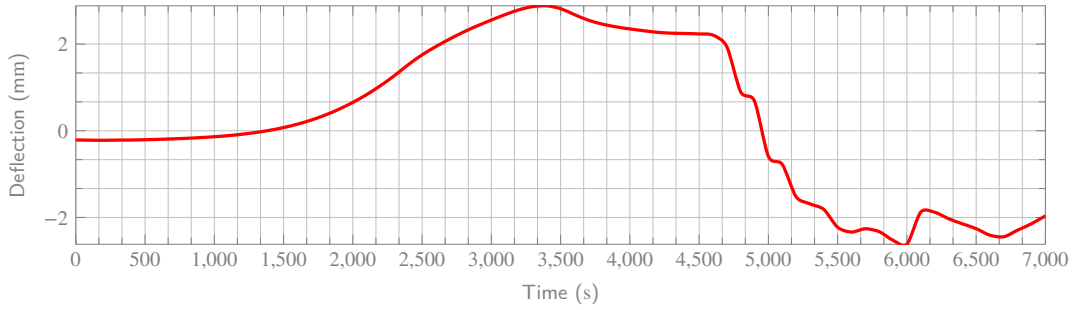

FIGURE 6.73: Deflection close to the upper right corner.

Figure 6.73 shows the evolution of the deflection in the closest node to the corner and does not belong to any of the edges. This node is inside the domain and has no boundary condition applied of any kind. Notice how just close to time 5000s it bulges outwards of the test frame. The rest of the analysis contemplates a scenario that has not been capable to test in the experiment, however the numerical model assesses the bulging of the node closest to the right upper corner and maintains it for the rest of the extended simulation time. So this clearly shows that the bulging phenomenon – which is the sole reason for the collapse, since the effective section of the bulkhead is reduced considerably – is the product of the inability to perfectly retain the edges fixed to the test frame and that the thermo-mechanical model allows to the extension of the empirical testing to the hypothetical real scenario.

6.4.5.3 BESST Campaign

The results in subsubsection 6.4.5.1 show a good match between the numerical and experimental data. The purpose of this example was to prove that the theory exposed in this thesis is able to predict the results of the experimental test. This can significantly reduce the cost derived from the construction of composite ships.

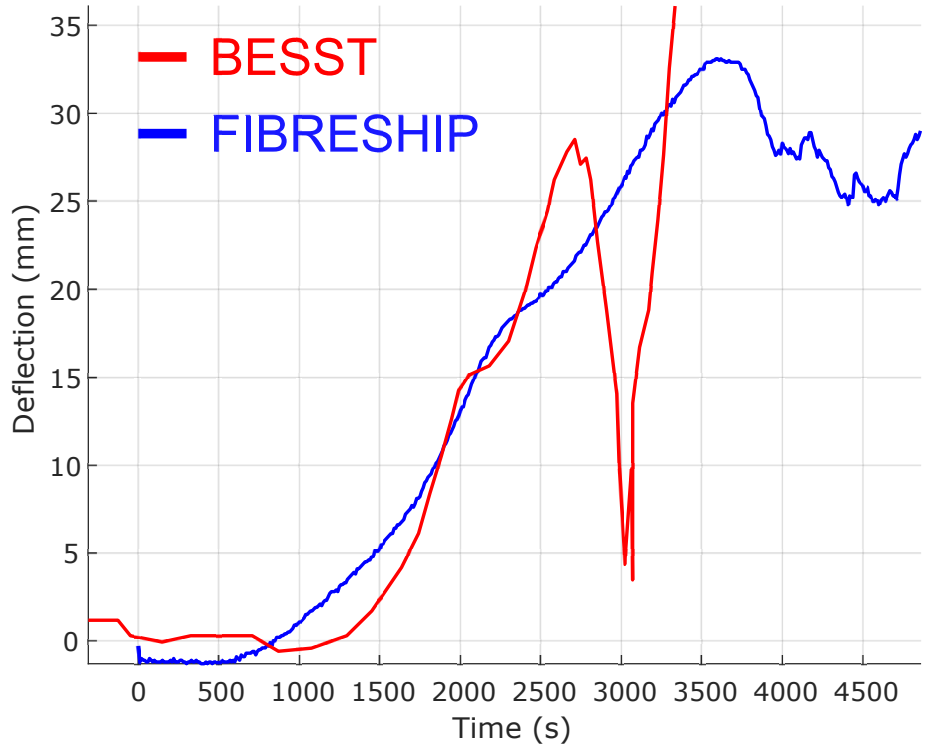

FIGURE 6.74: Deflection shown for the same test in BESST and FIBRESHIP.

However, the problem derived from the bulging of the top-right corner complicates the analysis, therefore, it is not the most typical result. A comparison between similar bulkheads for the same test conditions is found in Figure 6.74. The results shown are very similar for both projects for the first 30 minutes of testing, although, the material configuration used on both projects is different in terms of composite and insulation. This difference explains the different responses of both cases in the early stages of the test (0 to 2300s).

The other difference comes from the bulging, it can be seen in the BESST case that there is a sudden drop due to a collapse. However, in the FIBRESHIP case, the bulging phenomenon leads to a less abrupt failure, as pointed out in subsubsection 6.4.5.1.

Since the FRP code [256, Part 11] is a standard code, other significant experimental results can be obtained. From the BESST campaign, a report by Evegren et al. was issued [2]. In this report, the same analysis can be found for a slightly different bulkhead in terms of cross-section stacking. This report will be used to validate

the numerical tool against the experimental data for a bulkhead with and without reinforcement. The bulkhead without reinforcement matches the same criteria as the one designed in the FIBRESHIP campaign.

6.4.5.3.1 Non-reinforced bulkhead

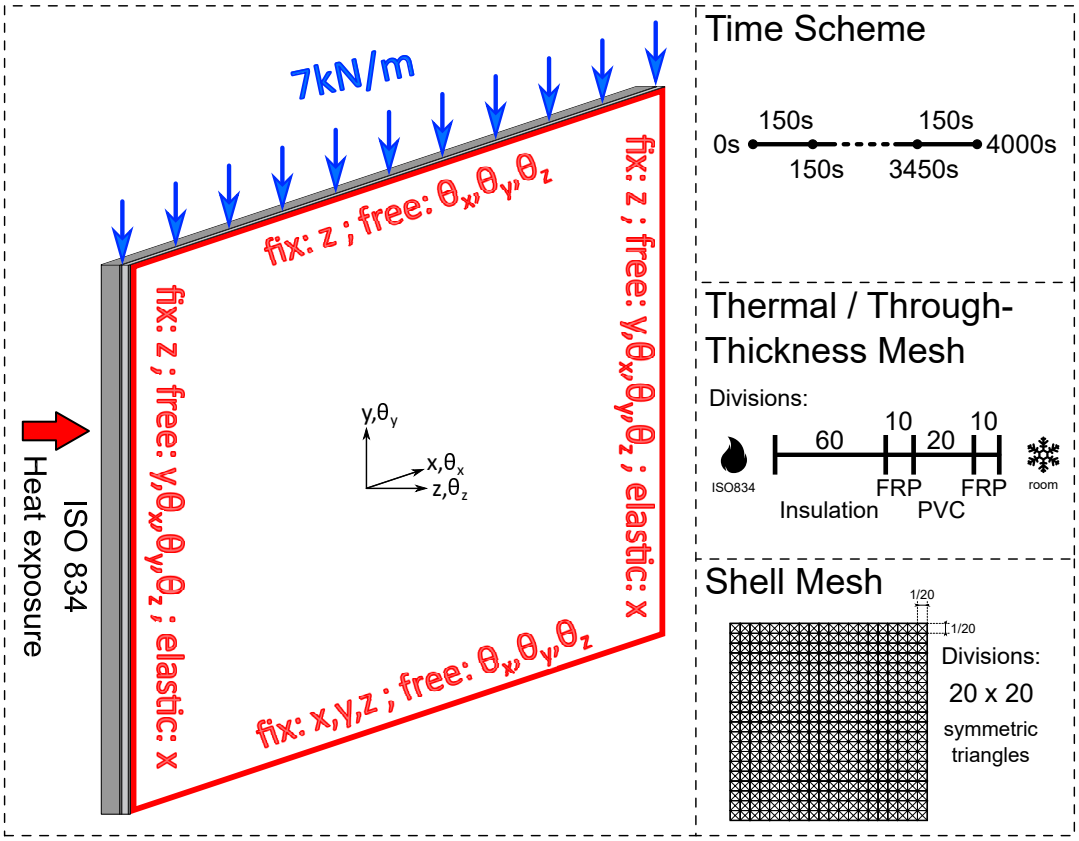

FIGURE 6.75: Description of the computational domain that represents the bulkhead test defined in the FTP code part 11.

The analysis is the same explained in subsubsection 6.4.5.1, the same specimen described in Figure 6.63 and the sensors are exactly the same, however the thickness of the core is slightly higher (see Figure 6.76). A description of the computational model is provided in Figure 6.75, note this was the same computational model used in subsubsection 6.4.5.1 but with a different layup.

The layup follows the same structure, however the monolithic composite used in the sandwich is a fibreglass reinforced polyester laminate. The layup description and direction are described in [2] :

Layer 1: 1×1.3mm layers of unidirectional glass/polyester, and the fibre orientation of the stack is [0] degrees [2].

Layer 2: 1×50mm layers of PVC which works as the core of the sandwich (PVC-H80 from Diab Group; this core is part of the Divinycell H® materials) [293].

Layer 1: 1×1.3mm layers of unidirectional glass/polyester, and the fibre orientation of the stack is [0] degrees [2].

Layer 4: 4×25mm layers of FireMaster Marine Plus Blanket®, which works as insulation of the composite laminate material [2].

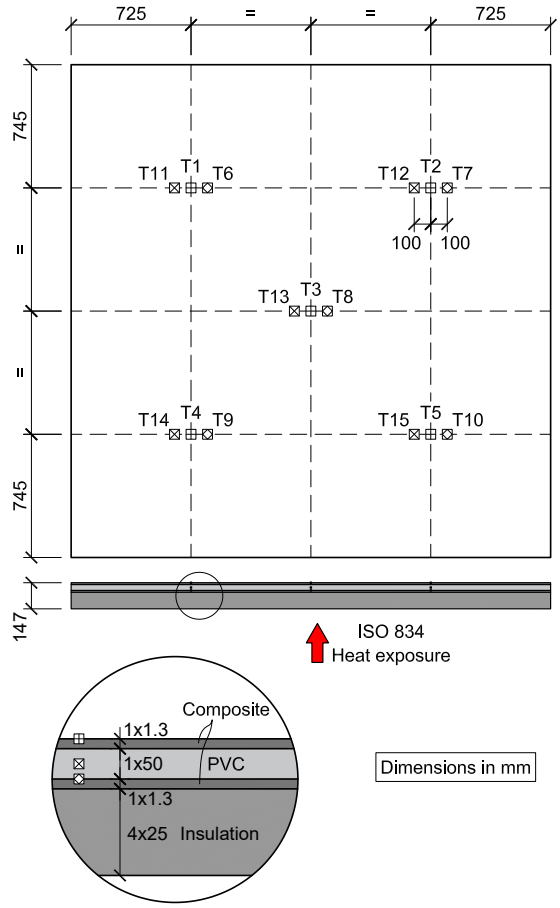

FIGURE 6.76: Description of the dimensions, materials and conditions of the specimen that represents the bulkhead test defined in the FTP code part 11.

The thermal response for the new load-bearing division is calibrated starting from the similar values of the FIBRESHIP case. The core and the fibreglass assigned similar properties initially. The values chosen for the insulation are as well similar to an insulation made of rockwool, and the polyester resin is chosen to present the same properties as a vinylester. After some iterations, the converged results are shown in the following tables. The thermal properties are similar, although the temperature, in this case, was transmitted quicker since the laminate layer and the insulation are different. The PVC was also modified, in its conduction and specific heat coefficients, to obtain a better thermal response. The resultant selection of thermal properties can be found in Table 6.18.

Material	c_k (W/m°K)	c_p (J/m^2°K)	c_{p_g} (J/m^2°K)	ρ_s (kg/m^3)	Q_p (J/kg)
Glass/polyester	0.5135	500	1000 - 1200	1780	$2{\cdot}10^5$
PVC	0.08	600	1200	80	0
Insulation	0.03-0.8	700-900	0	100	0

TABLE 6.15. Calibrated thermal properties of the layer materials.

The original data from the BESST project did not provide thermal degradation experimental data, the pyrolysis was selected to be the same as in the FIBRESHIP analysis.

Material	A_T (s^{-1})	E_{act} (J/mol)	N_{ro} ($J/m^2°K$)
Glass/vinylester	$6 \cdot 10^{20}$	$2.8 \cdot 10^5$	6
PVC	1202604.28	90000	2

TABLE 6.16. Calibrated pyrolysis properties of layer materials.

The resultant temperature evolution can be found in Figure 6.77

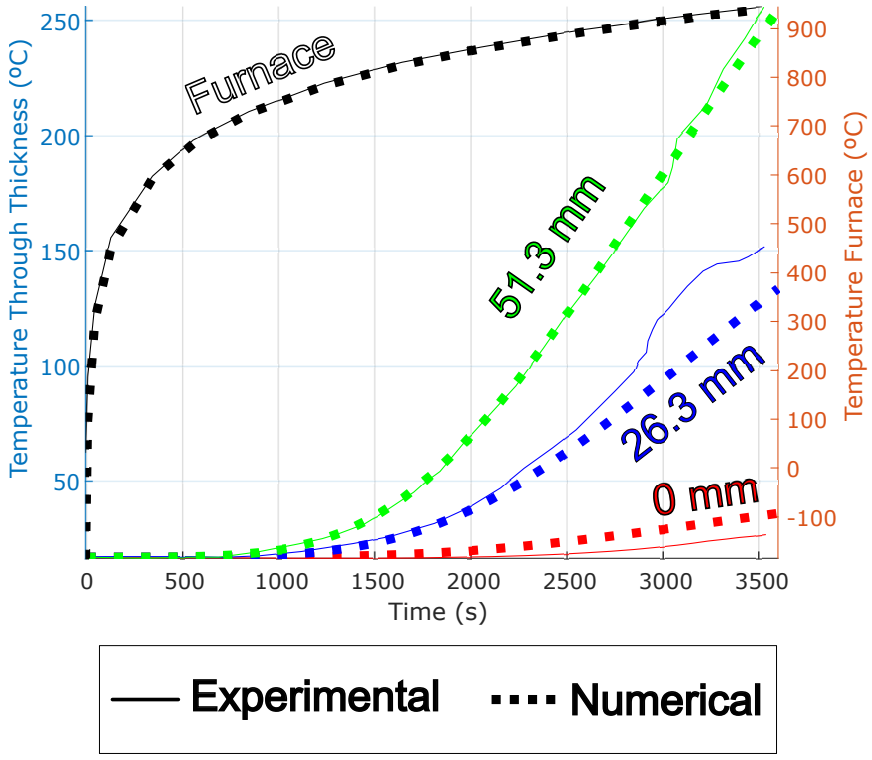

FIGURE 6.77: Evolution of the temperature ($T(x,t)$) at different positions of thickness. The temperature through thickness represents the sets in red, blue and green and the temperature furnace the orange set. Thermocouples T1, T2, T3, T4 and T5 in red were placed at $x = 0.0$ mm, thermocouples T11, T12, T13, T14 and T15 in blue were placed at $x = 26.3$ mm and thermocouples T6, T7, T8, T9 and T10 in green were placed at $x = 51.3$ mm. All measures are with respect to the unexposed surface.

The agreement is excellent for the readings on the hottest thermocouple and the furnace. The measures differing a little are those for the mid-span thermocouple and the unexposed surface. Nevertheless, the general prediction of the numerical model is fantastic. The little discrepancies found near the end (3000s onward) of the test are typically due to the large deformation that may affect the transmission of heat or uncertainties from the testing. These uncertainties for example, maybe introduced by the pins and bolts used to attach the insulation, this can affect how the heat is transmitted, also the same instrumentation needs a physical mechanism that is inserted inside the thickness and may affect the readings when the heat increases.

The resistance is mostly proportioned by the fibreglass, since this is the same fibre used in FIBRESHIP, the elastic properties are maintained to be exactly the same ones. The inelastic properties are calibrated, especially the energy of fracture.

Material	E (Pa)	ν	σ_y (MPa)	Π_F (N/m)	c_{CR}	Φ_Ω
Matrix	$3.35 \cdot 10^9$	0.26	20	$1.2 \cdot 10^4$	1	0.40
Fibre	$72.4 \cdot 10^9$	0.21	1800	$1.8 \cdot 10^6$	1	0.60
PVC	$49 \cdot 10^6$	0.4	0.9	$1.2 \cdot 10^4$	1	
Insulation	2466060.9905	$1.17647 \cdot 10^{-6}$				

TABLE 6.17. Calibrated mechanical properties of constituent materials.

Table 6.17 shows that the fibre gas increased its energy of fracture and the PVC was calibrated also to include damage, however it may be neglected since the analysis does not damage the PVC zone.

The thermal dependent properties are the ones to suffer most changes. They can be found in Table 6.18, note the relaxed value of the young

Material	E_u (MPa)	E_r (MPa)	σ_{y_r} (MPa)	n_{MG1}	n_{MG2}	T_g (°K)	α (°K^{-1})
Matrix	3350	935	0.15	0.0691	6	76	$36 \cdot 10^{-6}$
Fibre	72400	9620	122	0.0691	6	76	$36 \cdot 10^{-6}$
PVC	49	1.47		0.0475	6	90	$90 \cdot 10^{-6}$
Insulation							$0 \cdot 10^{-6}$

TABLE 6.18. Calibrated thermo-mechanical properties of the constituent materials.

The thermo-mechanical numerical analysis is validated against the experimental deflection in the centre of the bulkhead. The two results are compared in Figure 6.78 and show an excellent agreement between both curves.

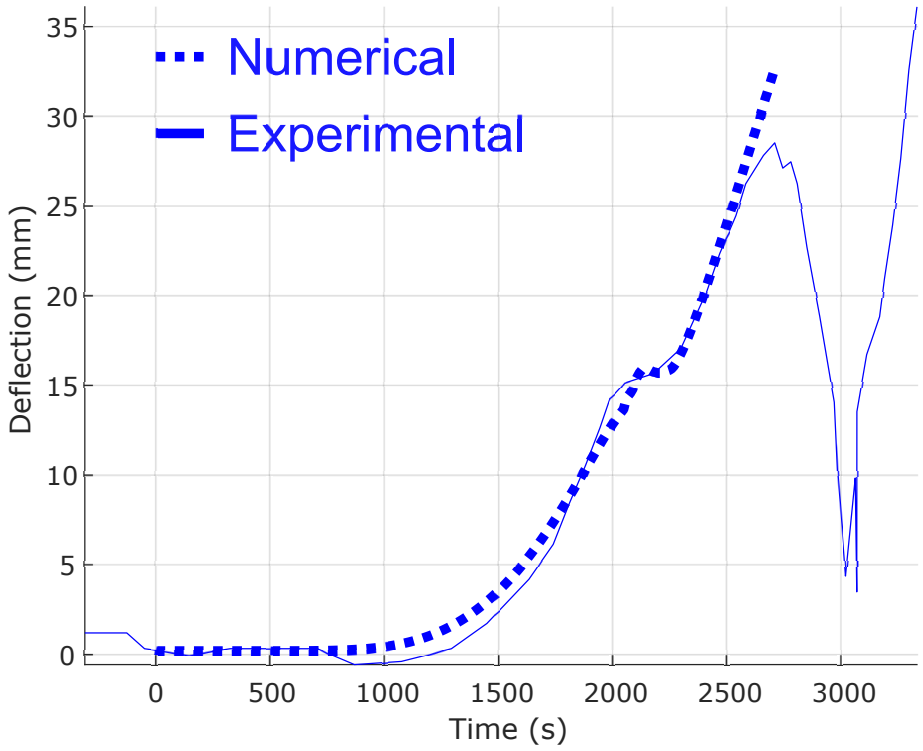

FIGURE 6.78: Comparison of the numerical results against experimental data for the deflection in the mid-span.

The numerical overextends a bit from the peak deflection and then abruptly breaks. Although the breaking is abrupt, the energy of fracture can be still calibrated in an attempt to reproduce the sudden fall better. In the experimental test, the deflection bounces back at 3000s since there is a sudden failure at a third of the vertical height. Indeed, it involves a better selection of the fracture energy of the PVC, but for the simplicity of the testing, the crucial failure is produced as soon as both matrix and fibre fail (2500s).

In Figure 6.79, a schematic evolution of the deflection in the vertical mid-axis is shown to make evident the deflection shape. Also, note that the pyrolysis is very mild since the insulator has not charred on the exposed surface.

FIGURE 6.79: Evolution of the experiment test.

The failure observed corresponds to the failure of the composite layer next to the insulation (see Figure 6.80). This is one of the weakest zones, since it presents an average temperature above 150°C. A study of the evolution of the damage to this layer is shown in Figure 6.81 and Figure 6.82. This damage shown corresponds to the maximum damage registered in the thickness, which is found in the aforementioned location.

I.e., the layers are subdivided into several numerical sublayers, the plot does not represent all these sublayers. Nevertheless, understand that the damage index on neighbour layers of the same material will present a similar damage index, especially if not many difference in temperature is found between them.

Note that the layers that are optimal to resist bending are the composite ones. This is due to their inherent superior mechanical properties. Thus, once the damage is extensive for one of the composite layers, the specimen shall fail immediately.

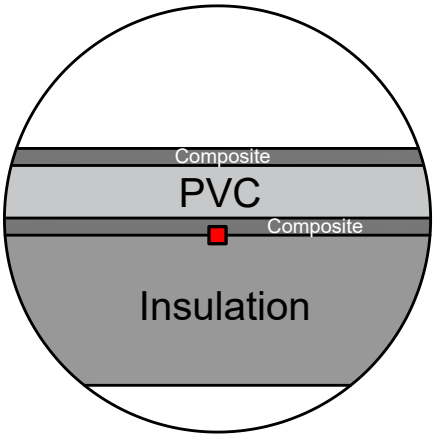

FIGURE 6.80: Location of the damage in the thickness.

In Figure 6.81, a sequential evolution of the damage in the layer of composites is shown. It can be observed that the damage tends to start in the boundaries because the specimen was clamped and extends to the centre.

The damage is very sudden, taking less than 3 minutes to fully damage the area. Although the map of damage seems to be one from 2300s onward, the real value is very close to one since the damage model used is an exponential softening law. This means that from 2300s to the end of the simulation, the fibre, PVC and the composite of the unexposed surface are resisting almost all the load.

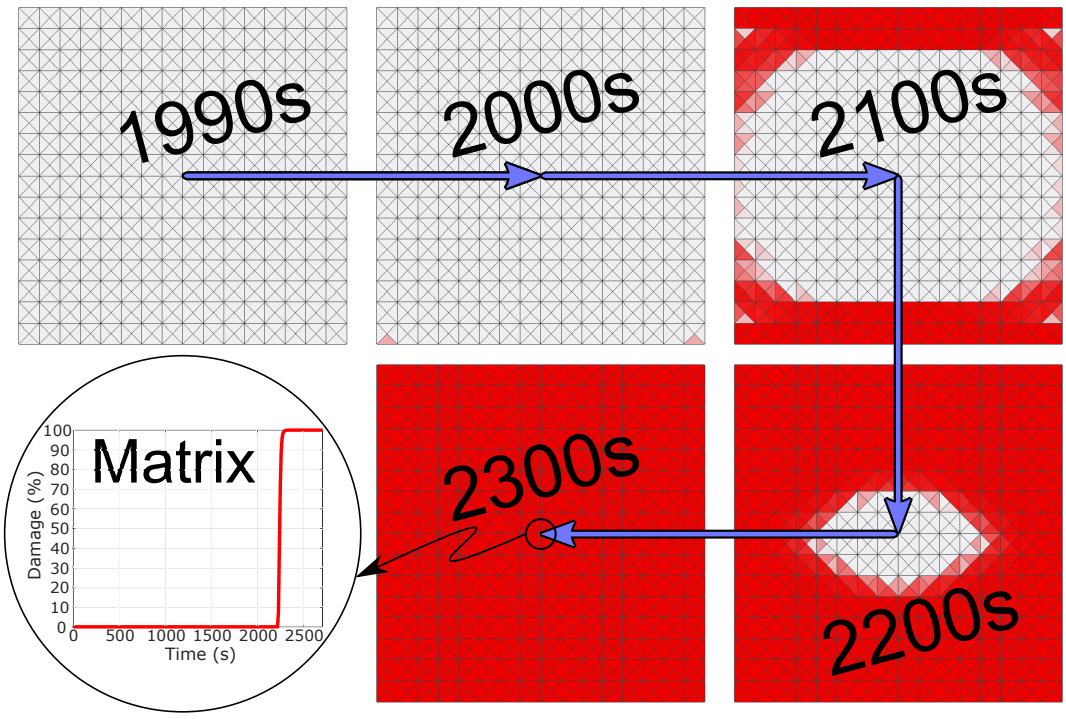

FIGURE 6.81: Numerical evolution of the maximum damage index in the matrix phase.

In Figure 6.82, the fibre damage originates as well in the boundaries and takes almost 3 minutes to fail. The model fails, especially, when the fibre presents damage to

almost 100%. The numerical simulation is unable to find an equilibrium point, since the static load is superior to the load that the remaining structure can withstand. Once a patch of elements is created in the bottom edge, the structure is detached and suddenly collapses.

In the real scenario, the uncertainties from manufacturing and testing produce the failure at one-third of the height of the bulkhead. The numerical simulation shows that the initial damage ioriginates at the bottom, which shows a mild correlation with the experimental data.

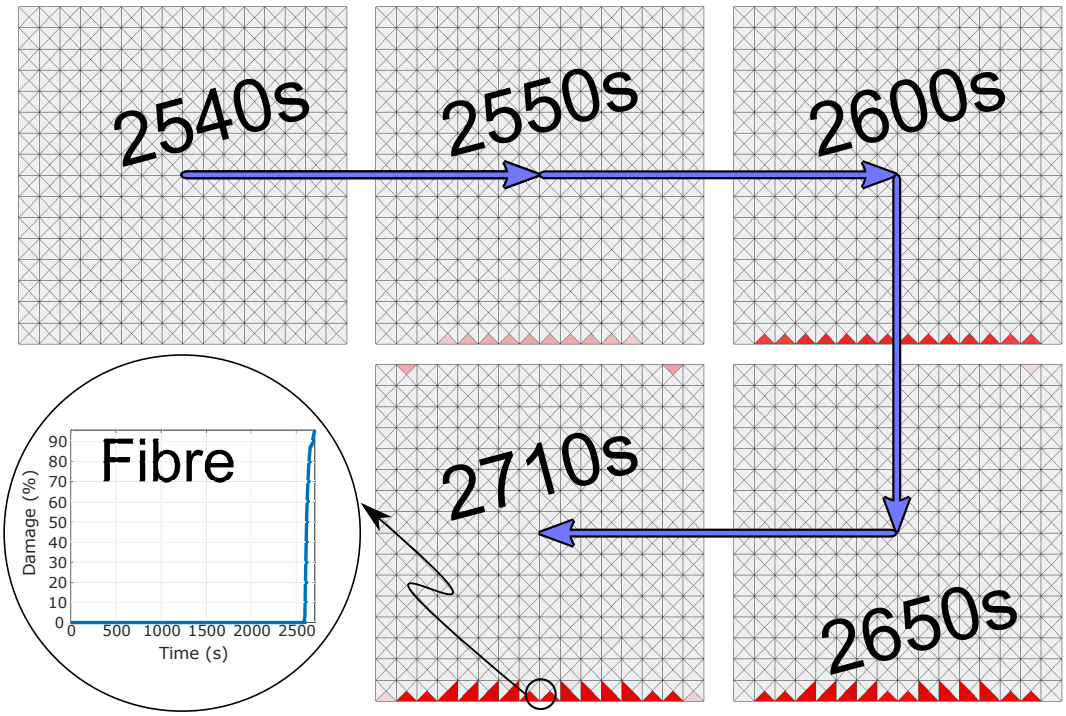

FIGURE 6.82: Numerical evolution of the maximum damage index in the fibre phase.

The other aspect worth mentioning is the fact that the matrix is completely damaged at 2300s and fibre only starts to damage around 2550s, almost 3 minutes later. The explanation is found in how the temperature is transmitted in the structure, as time passes, both the PVC and composite layers become more flexible due to the thermal degradation of mechanical properties due to temperature.

This means that not only the fibre has lost mechanical properties, but the structure as a whole loses stiffness and at a certain time (2550s), the layer closest to the hot end starts to present damage in the fibre phase.

6.4.5.3.2 Reinforced bulkhead

In the BESST campaigned, amongst the rest of tests, there is in particular one test that involves a composite panel reinforced with composite beams. This case serves as a demonstration that the analysis tool is able to reproduce the response of composite beams.

The dimensions of the specimen can be found in Figure 6.83, there are a total of 29 thermocouples distributed in various locations of the panel and reinforced beams.

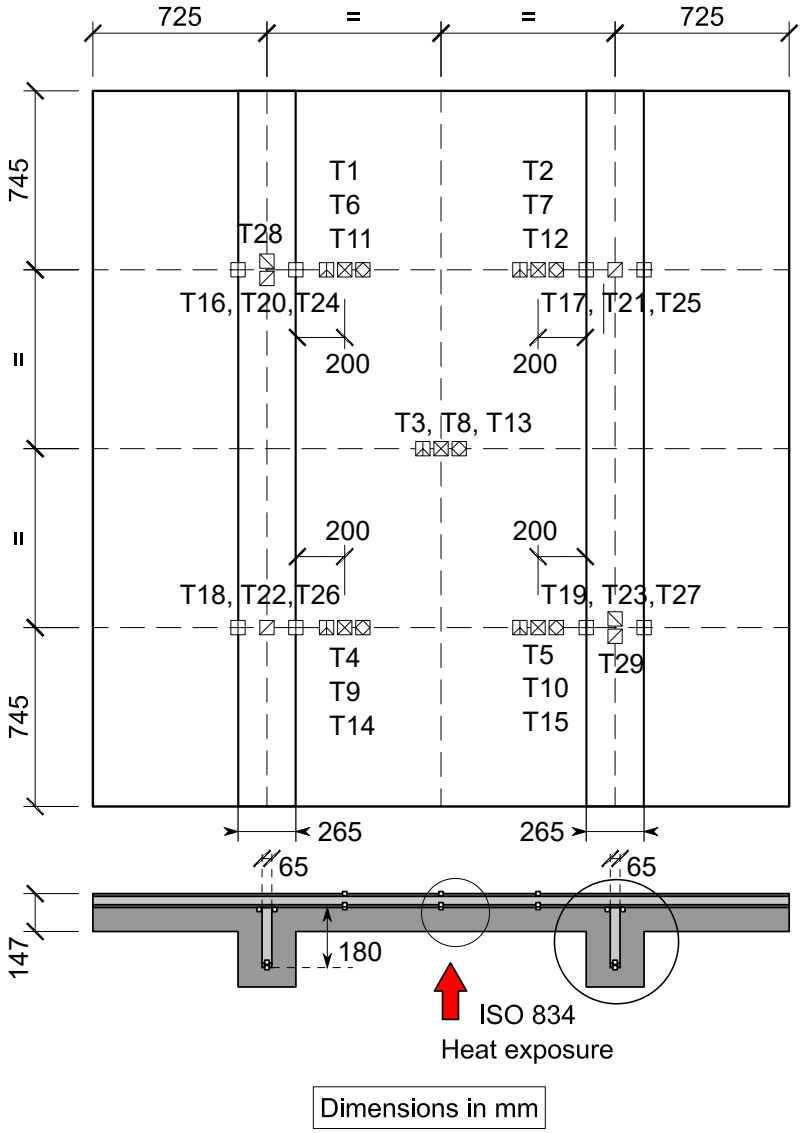

FIGURE 6.83: Geometrical sketch of the reinforced FRP panel.

The panel is made of the same materials and layup order as the panel without reinforcements, however, the PVC core is increased to 50 mm instead of 35 mm. A detailed sketch describing the layup of the panel and reinforcements can be found in Figure 6.76.

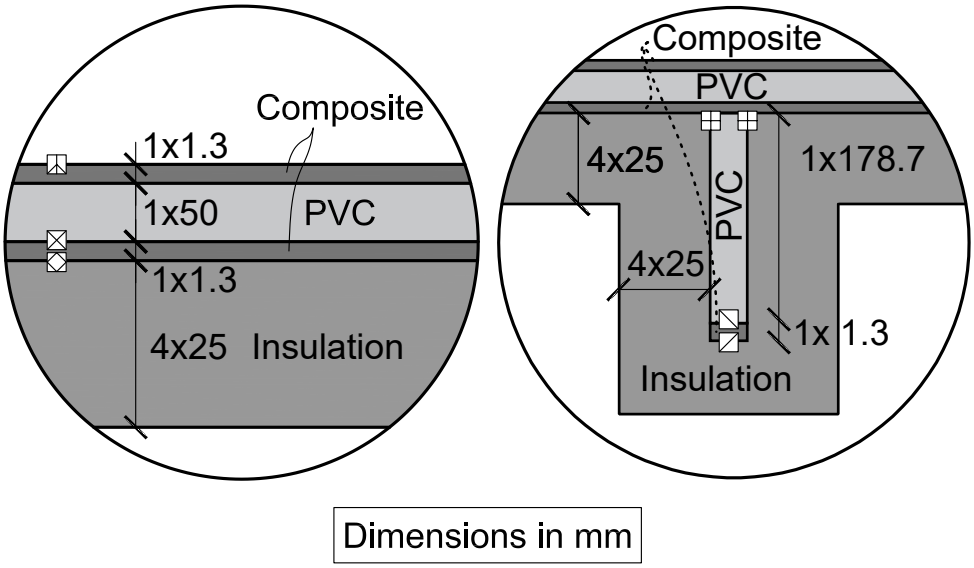

FIGURE 6.84: Detailed view of the through-thickness layup and thermocouple arrangement.

The specimen is exactly constraint as in the two previous analysis (non-reinforced panels from FibreShip and BESST campaigns). The only difference is in the loading, which has been increased (see Figure 6.85). In addition, the load is applied by means of a stiffened plate on the top edges of the panel and stiffeners, this is the most realistic manner to reproduce the test.

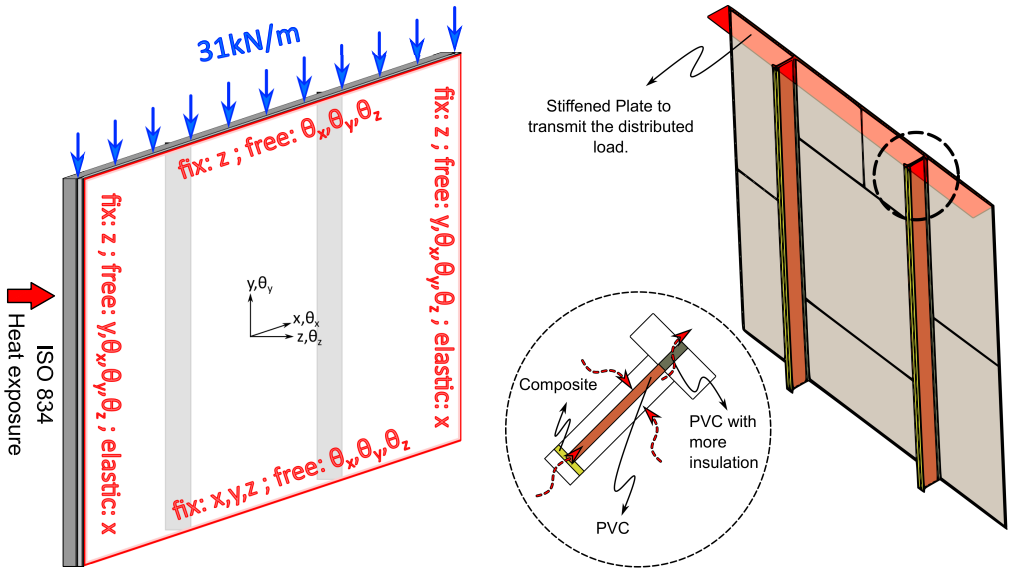

(A) Constraint and loading. (B) Geometrical description.

FIGURE 6.85: Computational model description.

In Figure 6.85b, a description on how the computational model of the two reinforcement is given. Since the beams are represented by shells, each beam is modelled as a *T* reinforcement. This implies that the heat only flows through-thickness. Moreover, the PVC close to the panel has been modelled with extra insulation layers since

in Figure 6.84 the thermocouple is at 141.5 mm from the exposed surface of the insulator. The discretisation of the domain is shown in Figure 6.86, the domain is subdivided in 4 fire regions, with different thermal boundary conditions, and their subsequent meshes for the thermo-mechanical shell model.

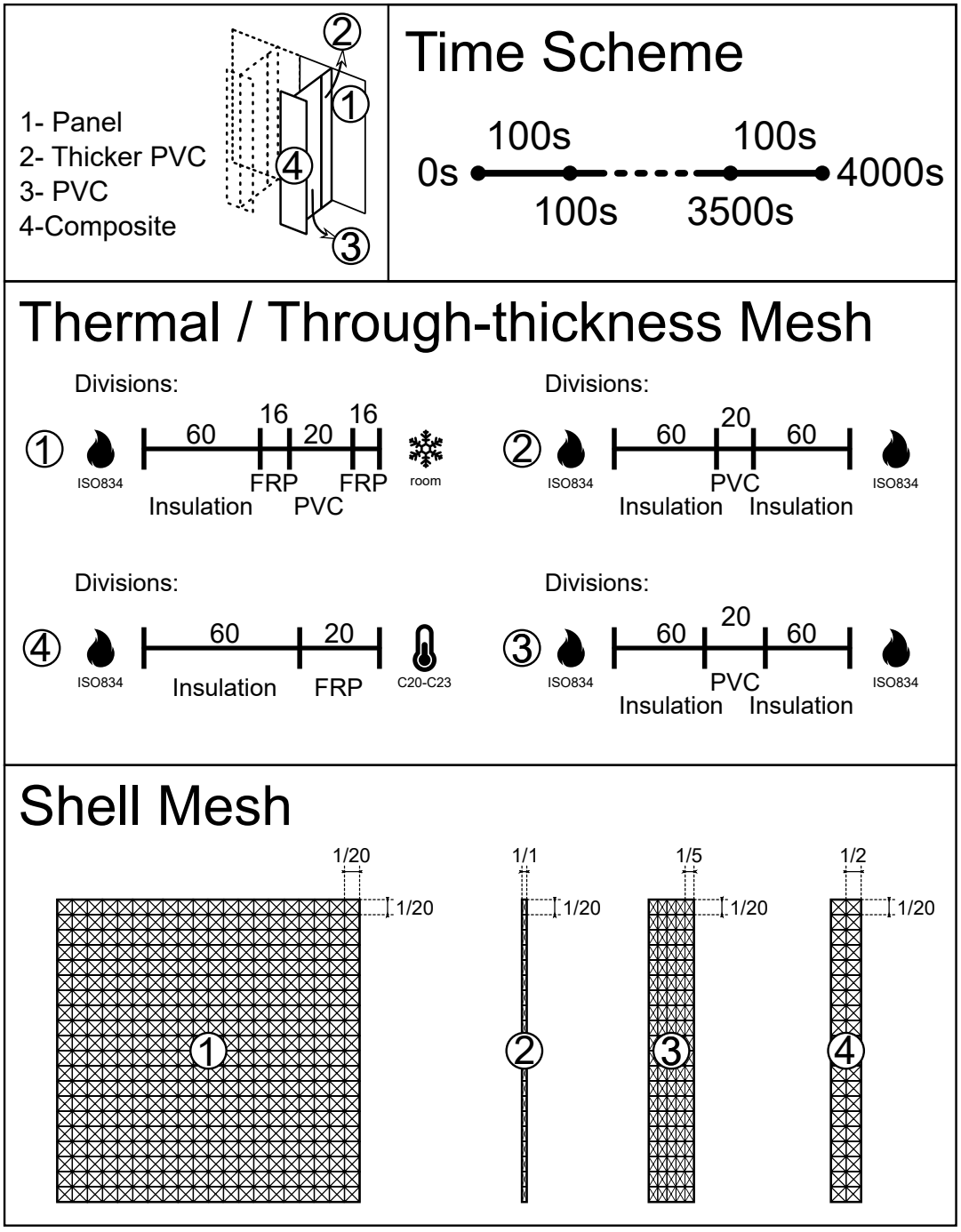

FIGURE 6.86: Description of the computational domain that represents the reinforced bulkhead test defined in the FTP code part 11.

The calibration of the thermal problem is performed based on the same properties defined in paragraph 6.4.5.3.1. In this case, there are different thermocouples scattered across the specimen. These are defined as follows:

1. Unexposed surface thermocouples. These correspond to the set of thermocouples conformed by C1, C2, C3, C4 and C5.
2. Inside the panel, between the PVC core and composite layer closest to the insulation. This group comprises the thermocouples C6, C7, C8, C9 and C10.
3. Inside the panel, between the composite layer and the insulation. Thermocouples belonging to this category are C11, C12, C13, C14 and C15.
4. Sensors close to the union between the stiffeners and the panel. There are two groups, the first is the closest to the centre of the panel composed by C24, C25, C26 and C27. The second are the external thermocouples C16, C17, C18 and C19.
5. Thermocouples drilled inside the stiffeners, at the interface between the PVC and the composite layers. The thermocouples belonging to this category are C28 and C29, one at the upper zone and the other on the lower zone of each stiffener.
6. Thermocouples drilled inside the stiffeners, at the interface between the composite layer and the insulation. These thermocouples are sensors C20, C21, C22 and C23.

A special comment has to be made on the particularities of calibrating the sensors C20 to C23. Since these are the closest to the furnace and also placed at the end of the stiffeners, the temperatures registered are significantly higher. Nevertheless, this is caused due to not only through-thickness heat transfer, but also by transverse through-thickness heat transfer.

Therefore, this end was modelled as a T beam and only considering the effects of heat through the thickness. The conductivity of the composite in this zone is around 10-20% higher than previously calibrated in order to take into account the transverse heat effects.

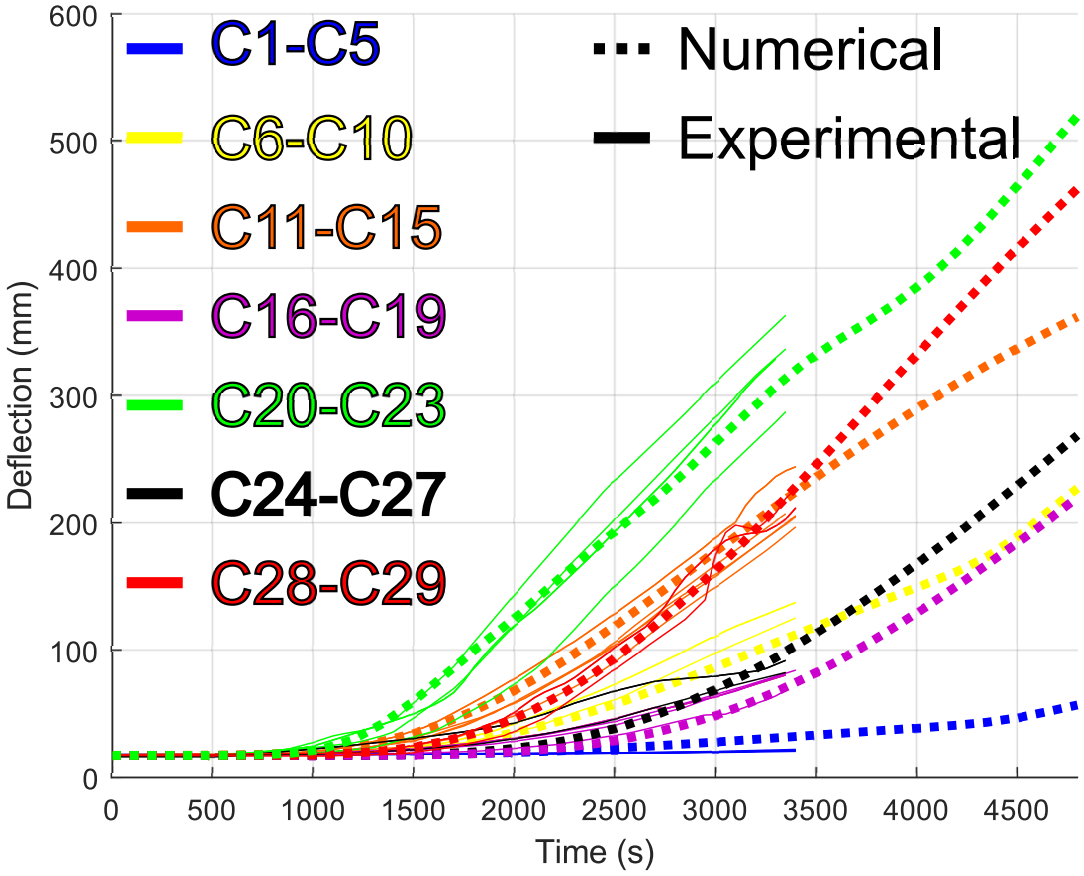

FIGURE 6.87: Temperature evolution measured by the thermocouples and numerical simulation.

In Figure 6.87, the temperature evolution for the analysis can be observed, almost 3500s for the experimental data and an extended analysis for the numerical model. The cold end, with the thermocouples in the unexposed surface (C1-C5), presents a minor absolute difference of 5 °C, since this region is not of special interest due to its low temperature, the inaccuracy is not important. The group of thermocouples C6-C10 show a match inside the experimental range, and the same happens for the group C11-C15. The agreement is very good compared to the cold end.

For the groups C16-C19 and C24-C27, the agreement is good. These last two groups are numerically identical, in order to obtain a non-symmetric solution of the temperature distribution through the thickness, the surface of the stiffener closest to the centre of the panel is assumed to have higher convective coefficient. The standard assumption of $15 W/m^2°C$ for the hot end, since both are hot ends, the one with higher temperature in the experimental test is modified to have a new convective coefficient of $25\ W/m^2°C$.

The numerical curve of the group C28-C29 is inside the range of the experimental data. The agreement is good, however, at the end of the experiment there is some minor fluctuations that are not well captured in the numerical model.

The thermocouples, C20-C23, were the most difficult to analysed, since the heat is only assumed to flow in one direction. Due to this, the conductivity was increased in the numerical model to be able to include the transverse effect, around 20% of the

original one. After increasing the conductivity, the resultant solution matches well the experimental solution. Nevertheless, the numerical solution provided once the experiment ended cannot be considered correct due to it's neglection of the transverse heat.

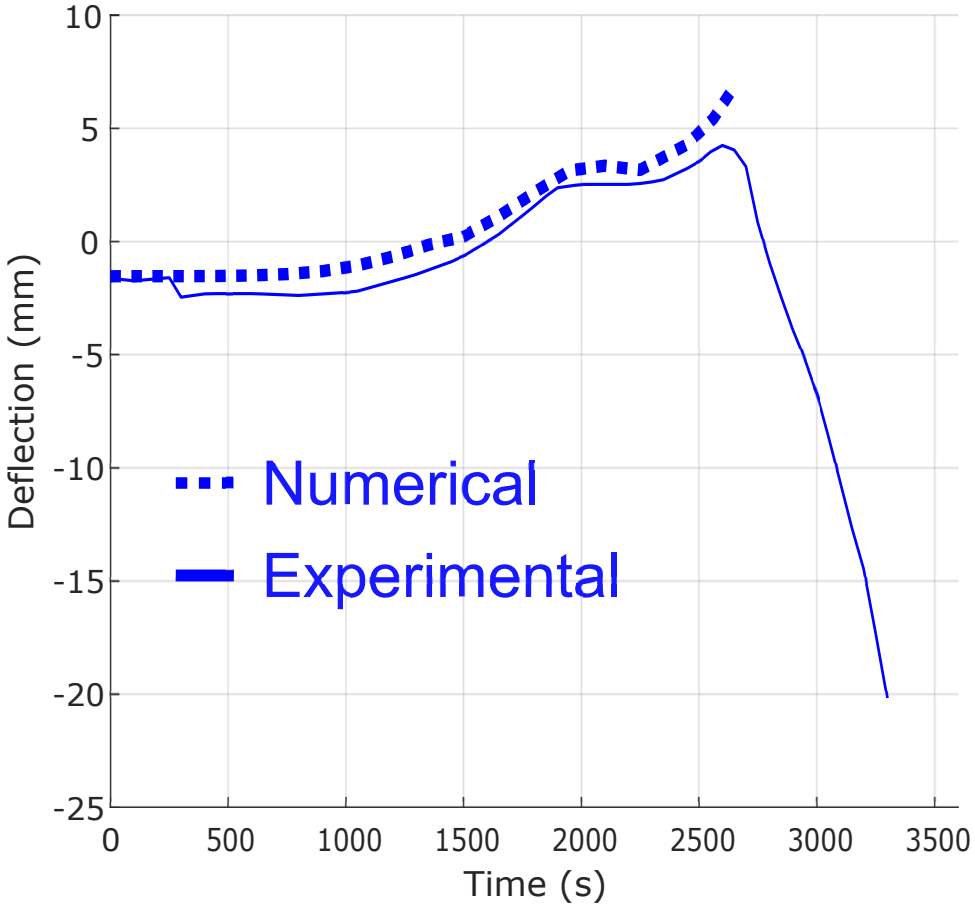

FIGURE 6.88: Comparison of the numerical results against experimental data for the deflection in the mid-span.

The next calibration is done against the deflection in the centre of the panel, which is customary for this sort of experimental tests. In Figure 6.88, the numerical deflection presents, overall, a satisfactory agreement with respect to the experimental deflection.

In the experiment, once arrived to 2600 s, the deflection decreases becoming negative and bulging outwards. This clearly signalises the beginning of the buckling. In the numerical data, the same peak is obtained at the same time and with a peak close to 7 mm in comparison to 5 mm in the experiment.

There are some minor differences on the deflection found after 500 seconds of analysis and these differences can be due to several uncertainties that condition the agreement of the numerical result. It can be perceived as if the eccentricity of the load had suddenly increased. This phenomenon is very difficult to assert and moreover, to model. This can be also one of the reasons to explain the higher predicted peak displacement in the numerical example.

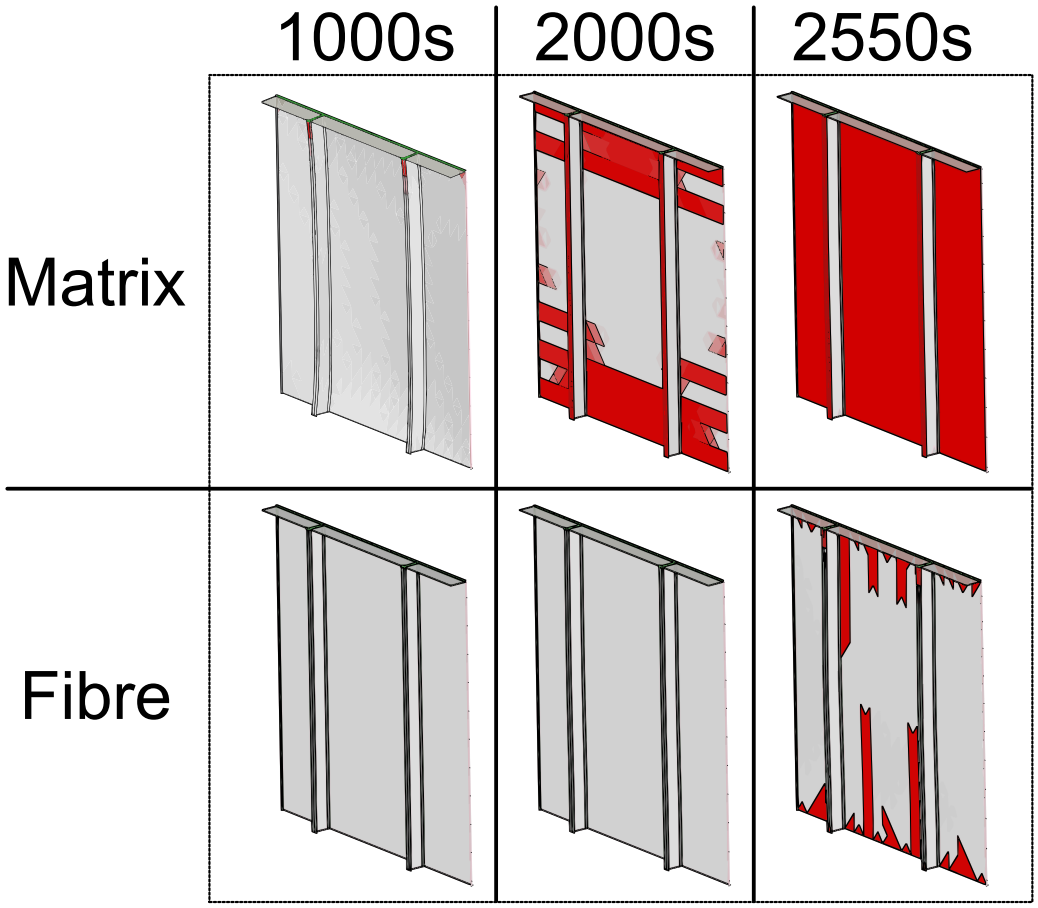

FIGURE 6.89: Numerical evolution of the damage in the panel.

Once the two experimental data obtained from the test are validated against the numerical model, an evolution of the maximum damage is given in Figure 6.89. As usual, the matrix is the first one to arrive at its threshold of damage which forces the matrix phase to endure the vast amount of the load. During the first 1000 seconds, the matrix only damages the top of the stiffeners and panel (matrix phase). Then, at 2000 seconds, the matrix starts developing damage in all the panel and stiffeners, however the fibre is yet able to endure the load. Finally, close to the collapse, the matrix phase is completely damaged, and the fibre phase starts to develop some vertical patches of damage. Note that the evolution of fibre damage is quicker than the matrix and generally leads to an abrupt failure.

The evolution of the test specimen can be found in Figure 6.90 at different stages of time.

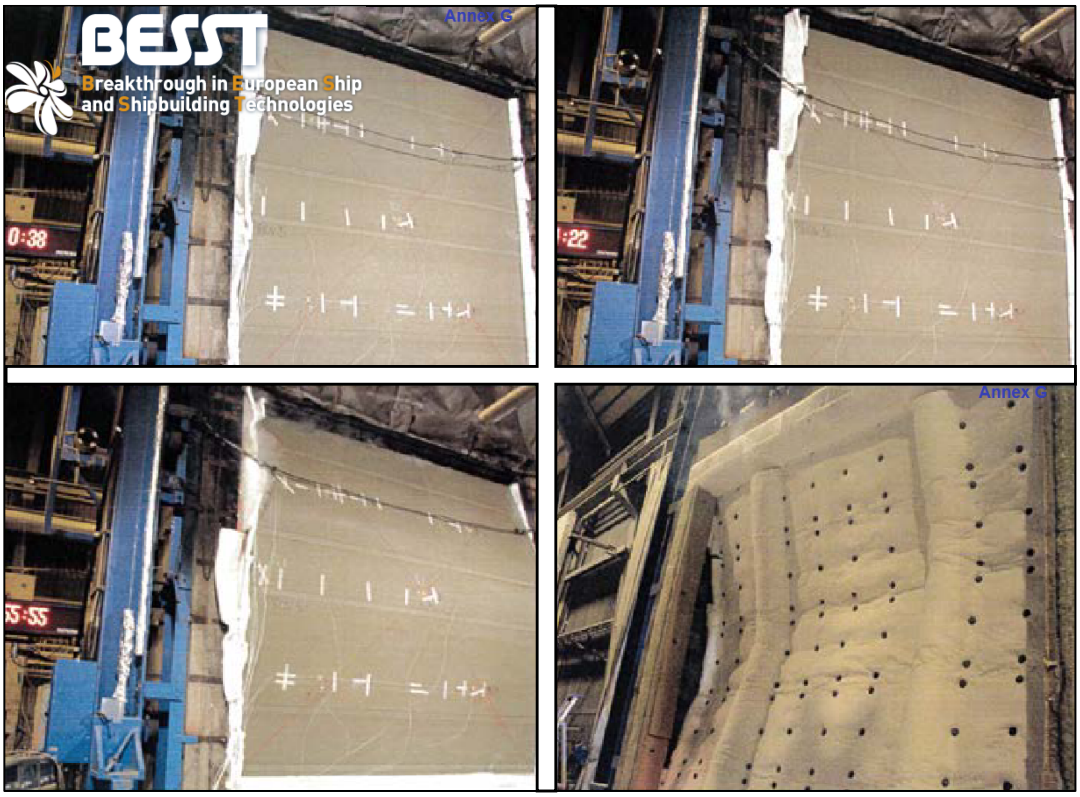

FIGURE 6.90: Evolution of the specimen in the experimental test.

6.4.6 Conclusion of the numerical implementation

This section, devoted to the validation of the proposed thermo-mechanical coupling, has shown the capability to analyse the failure of composites from the perspective of damage and buckling when exposed to fire.

The examples given have shown interesting feats for the numerical tool developed:

- Analytical verification

  One of the most important parts of the research undertaken in this thesis was the correct systematisation of meaningful benchmark cases for the study of thermo-mechanical laminates.

  An interesting based on linear beam theory is used to corroborate that the shell implementation was able to reproduce the theoretical solution. This was proven to be true. Once the linear beam theory was tested, the incipient problem of buckling is introduced and in particular thermal-buckling.

  The one dimensional buckling test extends its prior mechanical model and demonstrates that under pure buckling conditions the co-rotational theory is able to effectively predict the buckling load. Moreover, some fundamentals of how Equation 4.130 affects buckling *per se* are discussed, together with incorporating inelastic effects as well.

  This lead to an understanding of thermal-inelastic-buckling. Although this proves that the approach selected can solve problems with non-homogeneous materials stack-wise, it is still necessary to check if it can easily reproduce the transverse orthotropy. The latter is a task that is accomplished by means of the TSPROM. A benchmark case in orthotropic thermal-buckling is presented to show that the TSPROM is able to reproduce orthotropic buckling for stacks with different fibre orientations.

- Experimental prediction

  Once the analytical benchmarks have shown that the algorithm is able to reproduce theoretical benchmark cases. Few different validations against experimental results were run.

  First, the Feih et al. benchmark case that attempts to determine the curve of yielding stress with respect to the temperature. In order to do so, the authors attempted to limit the buckling of the specimens. However, in the numerical calibration, it has been found that some of the experiments may be susceptible to buckling, since, in the numerical models proposed by the same authors, the temperature dependency of Young's modulus was never addressed.

  In order to include the effect of thermal dependence on all mechanical models, they are validated against experimental tests based on the FTP code. The first is based on the FIBRESHIP experimental campaign, and two other samples are taken from the BESST campaign. By validating both, it has been proved that the model proposed is able to reproduce the behaviour of load-bearing structural elements.

In conclusion, this section has served to accomplish the proposed goals '*Provide and implement the thermo-mechanical coupling*' and '*Assess the correctness of the thermo-mechanical model*', which are number 11 and 12 respectively.

This page was left blank intentionally.

6.5 Demonstration in marine applications

This section presents different applications of the methodology developed to actual ships structures.

6.5.1 Fluid-structure interaction. Fire resisting marine FRP division analysis

The fire collapse analysis of an area of the superstructure of a container ship is presented in this section. In this particular case, non-structural resistant members, located on one of the decks of the superstructure, were analysed. In the scenario studied, the fire starts in the laundry via the ignition of the different cloths hanging on the towel rack (see Figure 6.91 and Figure 6.92).

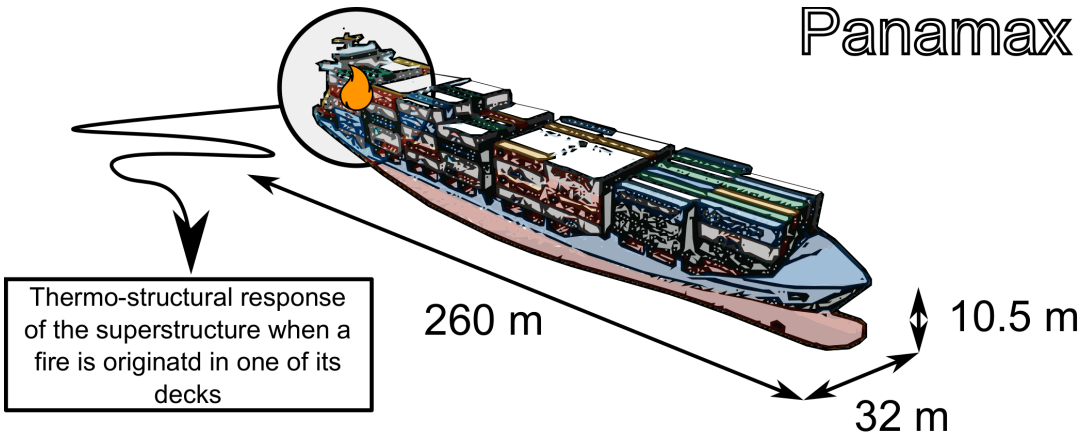

FIGURE 6.91: The container ship of study. The fire scenario is located in one of the decks of the superstructure.

Two fire scenarios were considered, one with closed doors and one with open doors. All doors are considered closed and thus the ventilation between rooms is significantly reduced, the opposite case is where the door that connects the laundry and corridor 1 is open and the door that connects corridor 1 and the outside room is open as well. By analysing these two possible scenarios, the effect and role that ventilation has during fire propagation is taken into account. Each one of these fire scenarios is simulated for Steel and FRP divisions, the first considers no pyrolysis and the second considers a laminate composed of layers of glass fibre($\Phi_\Omega = 55\%$) and vinylester resin, the stacking information can be found in Figure 6.93. All the materials are covered with an external layer of insulation. The mechanical load applied to the ceiling of the structure is considered as per regulations requirement, DNV [302] recommends a design pressure load of 350 N/m^2 in the superstructure.

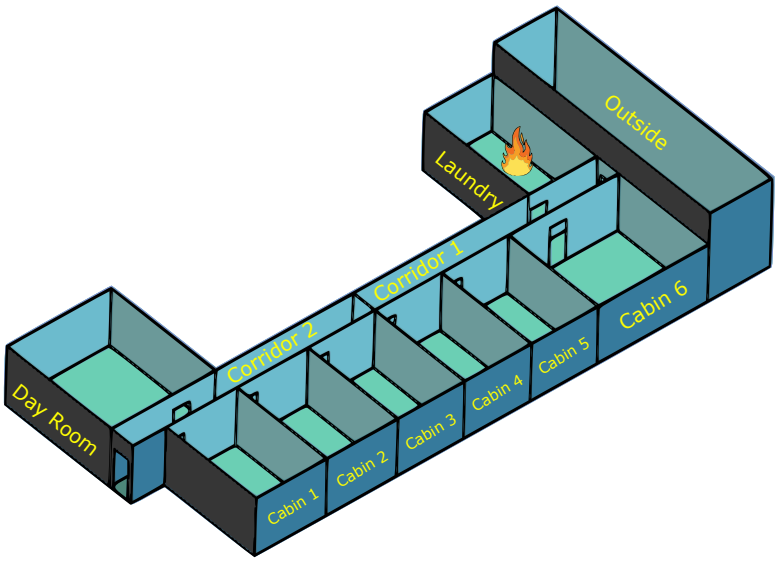

FIGURE 6.92: Domain of the fire scenario.

The computational model of the domain in Figure 6.92 was discretised in a finite mesh of 671680 hexahedra elements with an element size of 10 cm for the fire dynamics solver, the simulation time is 1 hour and the time stepping is 0.1 seconds. The resultant adiabatic temperature from the fire dynamics is interpolated into the thermo-mechanical mesh that is an unstructured quadrilateral mesh of 23564 QLLL elements with a maximum element size of 20 cm. The through-thickness mesh of 1D linear elements of the domain in Figure 6.93 is divided in 14 and 19 divisions for steel and FRP panels, respectively. The thermo-mechanical time scheme is fractioned in steps of 50 seconds.

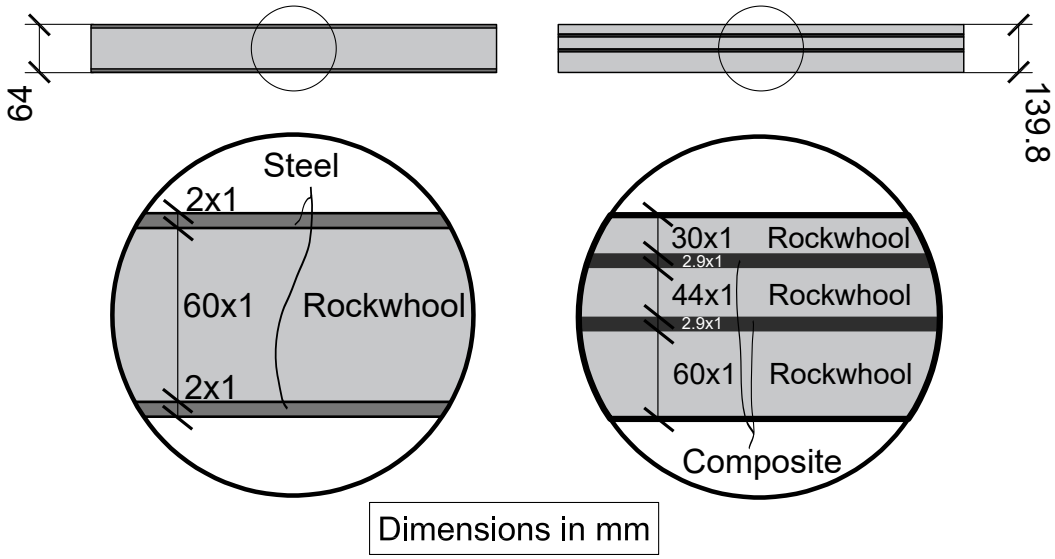

FIGURE 6.93: Thickness stacking of the divisions.

The software used to undertake the fire dynamics is the Fire Dynamics Simulator (FDS) [196]. The FDS input files were provided by Alessandra Tissari, Tuula Hakkarainen and Antti Korkealaakso from VTT Technical Research Centre of Finland Ltd. The gas temperature was 2 metres above the deck at 15, 30, 45 and 60

minutes after the fire ignition is shown for each studied scenario in Figure 6.94. The effect of ventilation can be clearly seen in the figures, as the simulations with two open doors have higher maximum temperatures as there is more oxygen available for combustion. In the simulations with FRP divisions, the temperatures are higher than in the simulations with steel divisions, as the combustible divisions participate in the fire, however, during the first 15 minutes, the temperature is less due to its insulation effect. The difference is significant, especially in the scenarios with two open doors, as the fire spreads to corridor bulkheads in the simulation with FRP.

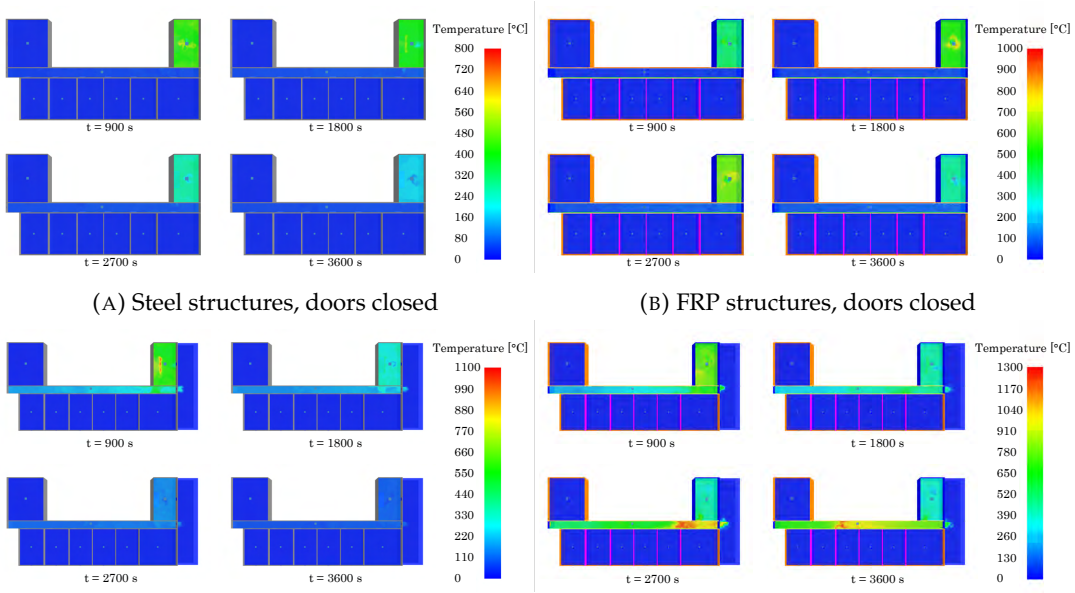

(A) Steel structures, doors closed

(B) FRP structures, doors closed

(C) Steel structures, two open doors

(D) FRP structures, two open doors

FIGURE 6.94: Gas temperature 2.0 metres above the deck 15, 30, 45 and 60 minutes after the fire ignition in each studied scenario.

Soot concentration is 2 metres above the deck at 15, 30, 45 and 60 minutes after the fire ignition is shown for each studied scenario in Figure 6.95. During the fire, the laundry room and the corridor are the most affected by the smoke in all studied scenarios, but all rooms receive some smoke during the simulations due to the pressure differences. In the simulations with steel divisions, two open doors lead to more effective ventilation of smoke. It can be seen that the burning FRP materials produced significant amount of smoke, leading to higher soot concentrations for longer time.

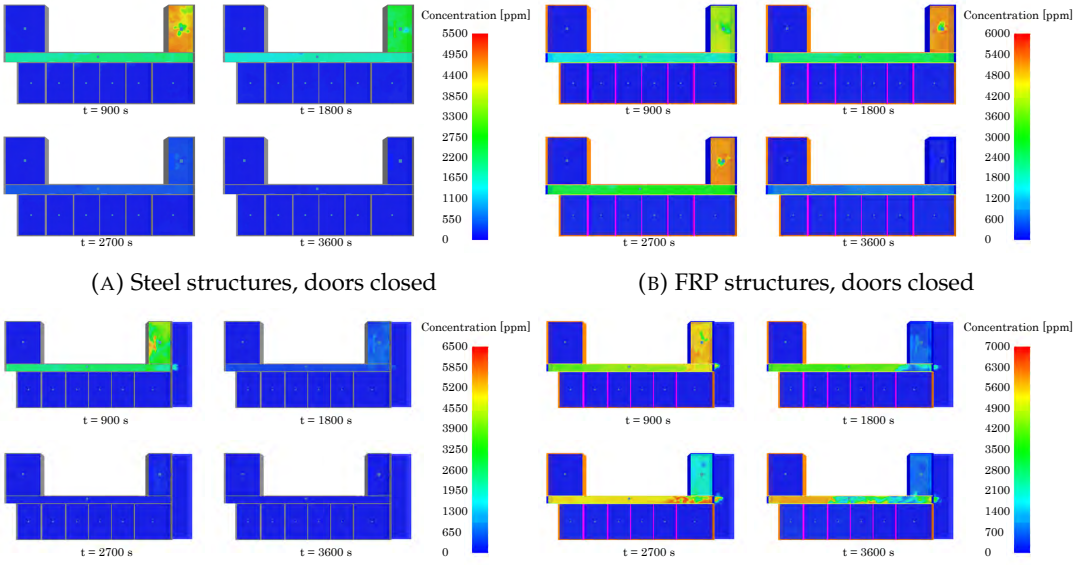

(A) Steel structures, doors closed

(B) FRP structures, doors closed

(C) Steel structures, two open doors

(D) FRP structures, two open doors

FIGURE 6.95: Soot concentration 2.0 metres above the deck 15, 30, 45 and 60 minutes after the fire ignition in each studied scenario.

FDS is used to obtain the adiabatic temperature that is later introduced as thermal boundary conditions in the thermo-mechanical problem, i.e., a division represented by a shell that has two surfaces, the exposed and unexposed surfaces, and each of these two surfaces is assigned to a fire region or thermal load. These thermal loads are divided in four regions: *laundry, corridor 1, corridor 2 and other rooms*, as already shown in Figure 6.92, and the resultant adiabatic temperature of those can be found in Figure 6.96 for the four combination scenarios (open/closed doors and steel/FRP material). Note that the temperature of *other rooms* is considered as the ambient temperature (approximately 20°C).

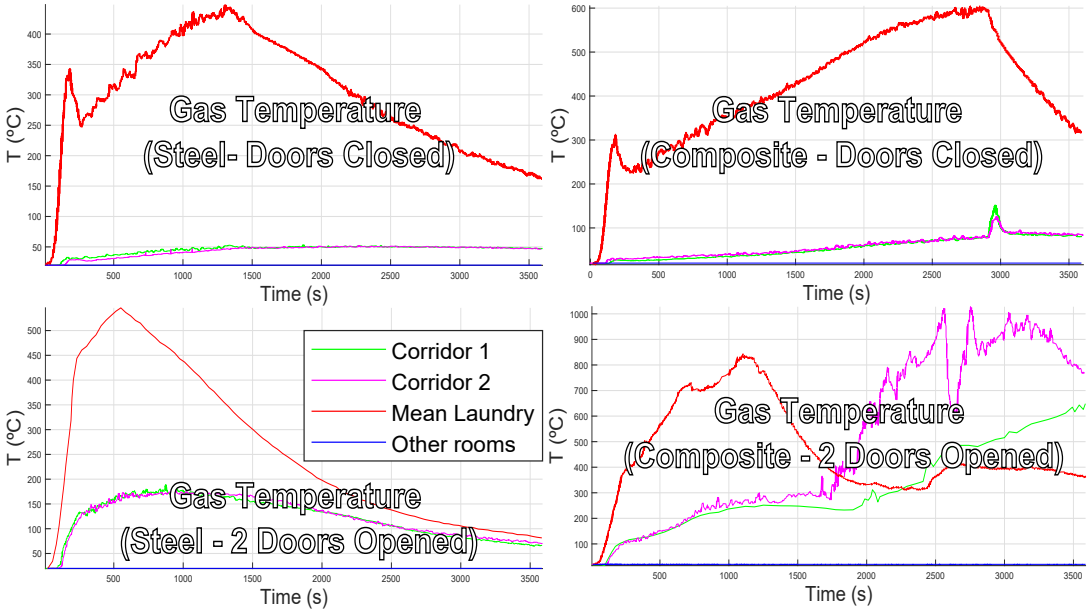

(A) Open and closed door fire scenarios for steel. (B) Open and closed door fire scenarios for composite.

FIGURE 6.96: Thermal boundary loads for different fire scenarios and materials.

The four different case scenarios can be described in the following manner:

- Steel - closed doors: The doors are shut, therefore the ventilation and O_2 renovation is limited. The *laundry* temperature increases rapidly up to a maximum temperature of 450°C around 1500s, then the room is depleted of oxygen and the fire starts to auto-extinguish in a slow but monotonic manner. The temperature in *corridor 1 and 2* rises up to 50°C around 1500s and remains steady.

- Steel - open doors: The doors that connect to the outside room are open, therefore an important apportion of O_2 is introduced in the combustion. The *laundry* temperature increases rapidly up to a maximum temperature of 600°C around 500s, then the room temperature steadily decreases to 80°C at the end of the analysis. The temperature in *corridor 1 and 2* raises up to 150°C around 500s, remains steady up to 2000s, and then decreases to 60°C at the end of the analysis.

- FRP - closed doors: The doors are shut, therefore the ventilation and O_2 renovation are limited. The *laundry* temperature increases rapidly up to a maximum temperature of 600°C around 3000s, after the temperature decreases until it reaches the value of 300°C at time 3600s. The temperature in *corridor 1 and 2* raises up to 100°C around 3000s and remains steady until the end.

- FRP - open doors: The doors that connect to the outside room are open, therefore an important apportion of O_2 is introduced in the combustion together with the pyrolysis of the material that increases the porosity of the material. The *laundry* temperature increases up to a maximum temperature of 800°C around 1300s, then the room temperature steadily decreases to 300°C at the

time 2500s increases shortly to 400°C and decreases to 350°C at the end of the analysis. The temperature in *corridors 1 and 2* rise up to 300°C around 1000s, remains steady up to 1700s, then *corridor 1* slowly increases to 600°C and *corridor 2* dramatically increases to a peak of 1000°C and falls to 800°C at the end of the simulation.

The accumulated damage to the structure varies as the degradation of mechanical properties develops, note that Young's modulus and the yielding stress depends on the temperature and the degradation fraction (F) according to Equation 4.130. The steel divisions are useful to understand that a structure can collapse only due to thermal effects. This is explained by the fact that the yielding stress reduces when the temperature increases. This is very important since many real naval applications are designed to support fixed loads – in this case the design ceiling pressure – and this load is unaffected by the temperature and thus the damage originates as the temperature rises, only due to the effective reduction of the yielding surface of the characteristic material. Otherwise, the FRP divisions will sustain damage that may originate not only due to thermal effect, but pyrolysis itself.

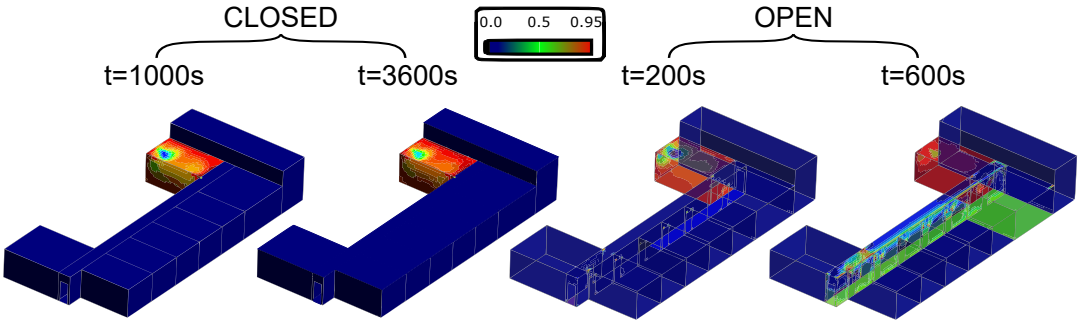

FIGURE 6.97: Damage distribution for steel material.

The results of the analysis, in the case of the steel structure, is shown in Figure 6.97, when doors are closed. This, is in agreement with the heat originated by the adiabatic temperature. Damage is temperature-driven only, and it originates early in the simulation (1000s), once the temperature in the *laundry* reaches its maximum, the damage distribution remains undisturbed until the end of the analysis (3600s).

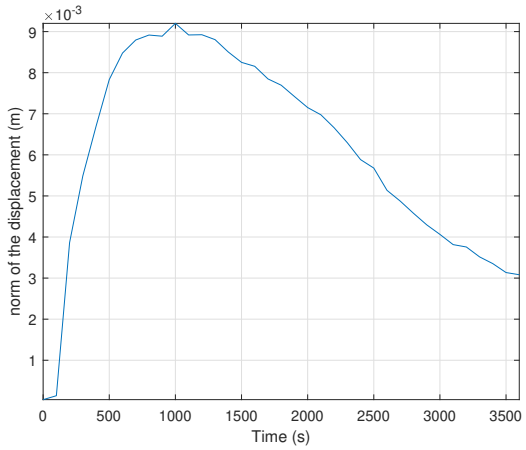

FIGURE 6.98: Deflection of a damaged element in *corridor 2*.

In the case of open doors in Figure 6.97 the damage originates earlier than in the closed doors case (200s). This is attributived to the extra ventilation since ventilation plays an important role not only on how quick the temperature rises but also in the spread of combustion to other rooms as it can be seen that both *corridor 1 and 2* have small patches of elements with moderate damage. Once the temperature in the *laundry* reaches its maximum (600s), the damage distribution remains undisturbed until the end (3600s), however the mechanical response is increased as the temperature decreases (the structure again becomes stiffer). This can be observed in Figure 6.98, where the norm of the displacement decreases after arriving to the time step, 1000s. This is due to the recovery of Young's modulus as the temperature of the different regions decreases. This is interesting since it shows that the mechanical post-fire response of the structure for elements have not collapsed due to the reduction of the yielding limit, however, it is important to understand that while the mechanical properties have recovered, the damage does not heal.

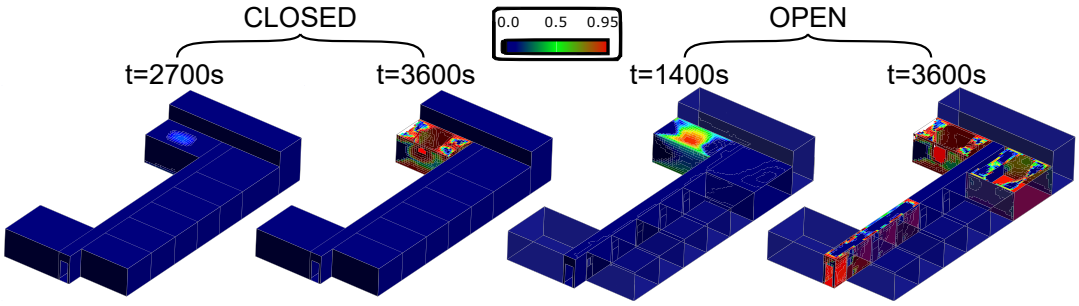

FIGURE 6.99: Damage distribution for FRP material.

In the case of the FRP structure, the results are shown in Figure 6.99. When doors are closed, it reproduces a damage pattern that is in accordance to the thermal loads introduced. In this case, the damage is both temperature-driven and pyrolysis-driven. The damage on the structure, compared to its steel equivalent case, is produced significantly later on the time analysis (note that the temperature increases slower for the FRP design than the steel). Nevertheless, the sustained damage in the *laundry* room is higher than the steel for the same time of simulation, as it clearly involves not only temperature but the damaged originated due to the pyrolysis of the composite layers closed to the exposed surfaces. The overall result is that a vast region of the ceiling in the *laundry* room has degraded and no longer endures the load, reaching a point where the ceiling collapses and the collapse development is very sudden. This is due there being less than 1000 second from the origination of the damage (2700s) to the collapse (3600).

On the other hand, Figure 6.99, when doors are open, the sustained damage on the structure is greater than the case where the doors are shut, this is evident because there is more ventilation and therefore more combustion and spreading. The damage starts to be noticeable at 1400s, which is when the temperature in the *laundry* room reaches its peak. Since the temperatures of all regions present similar or higher values to the closed doors case, analogously the *laundry* rooms collapses in this case scenario as well. However, the major problem in this case, where spreading of the fire is present, is not only the collapse of the *laundry*. Since the fire spreads, the temperature on *corridors 1 and 2* are greater than before, even surpassing the values of 1000°C on *corridor 2*, and it reaches the final simulation with the partial collapse of the ceiling of the *cabin 6*, which poses an important risk for the safety of the crew,

and also the deterioration of the divisions located in the *corridor 2*, which may block the exit of the crew located on *cabin 1,2 and 3* or in the *day room*.

6.5.2 The thermal-buckling collapse of a container ship

The application case in subsection 6.5.1 focused on demonstrating the capabilities of the thermo-mechanical design of non-load bearing reinforce divisions and the interaction between an FDS and the thermo-mechanical tool to obtain more accurate results. In this example, the concept of '*steel equivalent*' design is addressed as required in SOLAS. Also, the flexibility of composites is taken into account by analysing nonlinear buckling. The containership design used in this example was generated from the research related to FIBRESHIP, it is the same used in subsection 6.5.1 and the analysis focuses on the structural failure of bulkheads and structural members in several sections of the ship.

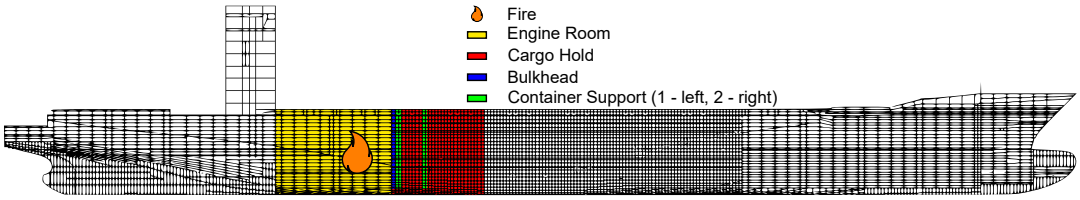

FIGURE 6.100: container ship profile section.

It is assumed that in the engine room of the ship a fire is originated, the thermal load is then applied to the bulkhead between the engine room and the immediate cargo hold, and it affects the two supports holding the TEU containers. The thermal load is assumed to be an ISO-834 during one hour of simulation.

The scantling of the composite and steel ship is obtained from the resultant design of the FIBRESHP container ship. These scantlings comply with the regulations in terms of structural integrity and naval architecture calculations. The model is reduced to the section shown in Figure 6.101. Only half of the section is modelled by assuming that the loads and boundary conditions are symmetric.

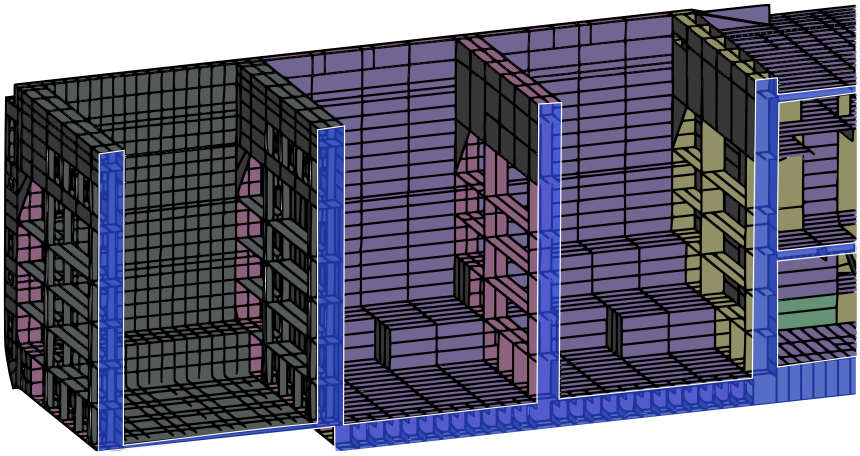

FIGURE 6.101: Domain of study, a section of the FIBRESHIP container ship.

In order to obtain a detailed analysis focused on displacements rather than stress (buckling driven analysis), the ship is constraint on both extremes of the section that are being analysed.

A section of the ship can be analysed when there is global equilibrium if the internal loads of the sections are introduced in its extreme to equilibrate the segment.

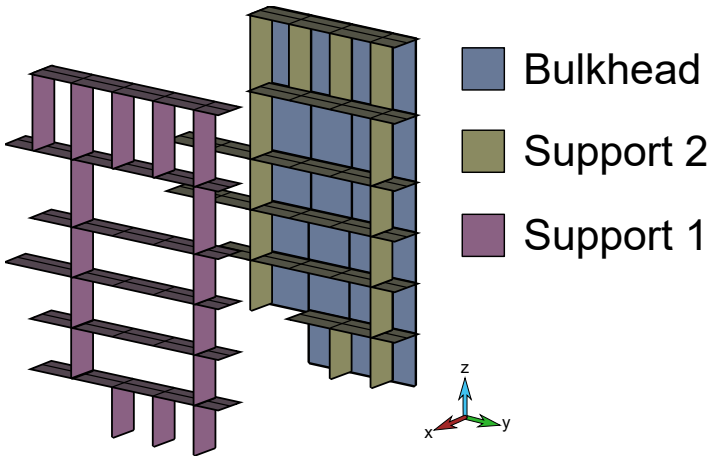

FIGURE 6.102: Load-bearing structural members of interest in the analysis of buckling.

The area of interest, see Figure 6.102, is the one in the hold next to the engine room (where the fire starts), especially the shelf or support structures of the TEU containers and the tight bulkhead that separates the engine room with the cargo hold. Indeed, the lay-up of the stack used in these three zones of interest is given in Figure 6.103. Note that in the analysis, the bare-structure and the insulated-structure will be considered for the steel and composite materials.

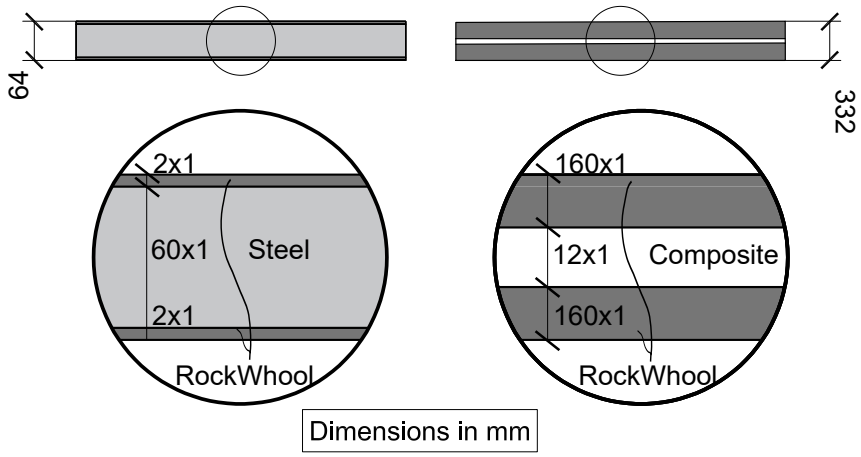

FIGURE 6.103: Thickness stacking for the two materials considered. The dimensions are proportional in the sketches.

The steel is designed according to the structural rules required by the IACS. The scantling of composite design follows a similar procedure, using the design criteria developed in the content of the FIBRESHIP project.

In terms of mechanical analysis, a non-linear constitutive analysis is performed and a second non-linear geometric buckling analysis is performed as well. The steel presents no problem in both and the composite, with the initial thickness design,

passes the inelastic analysis but buckles in the second. Therefore, some extra thickness is given to the initial design, fulfilling the IACS regulation. The thickness of the composite has been chosen to exert a similar deflection as the steel design.

Then the thermal-buckling is analysed for the materials in question. This analysis has served to determine the amount of insulation needed to be put in. The composite structure presents a lighter structure due to its great mechanical capabilities compared to steel. However, steel requires less insulation so the over-all thickness, found in Figure 6.103, is larger for the composite.

This last statement may seem strange, provided that the composites had a clear advantage when it came to thermal conduction. However, this is a fire-collapse analysis and the purpose is to bring the structure to fail given enough time. Therefore, if enough time is given, the composite presents a disadvantage compared to the steel since the glass temperature of steel is four times the one of the composite.

The composite in question is a monolithic stack of fibreglass-epoxy. The mechanical, thermal and degradation properties are the standard ones found in all the examples in this thesis. The degradation properties of steel are shown in Figure 6.104, the rest of mechanical and thermal properties are the classical ones found for a steel with a Young's modulus of 210 GPa.

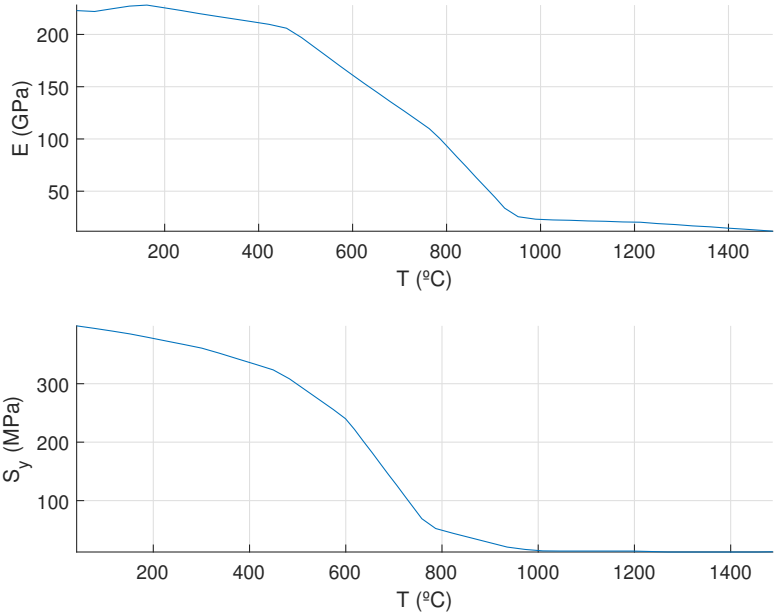

FIGURE 6.104: Mechanical evolution of the elastic modulus and yield stress of steel with respect to the temperature.

The mesh generated to simulate the container ship can be appreciated in Figure 6.105. The mesh is in triangles since it is the unique type of element implemented in RamSeries that includes the co-rotational formulation.

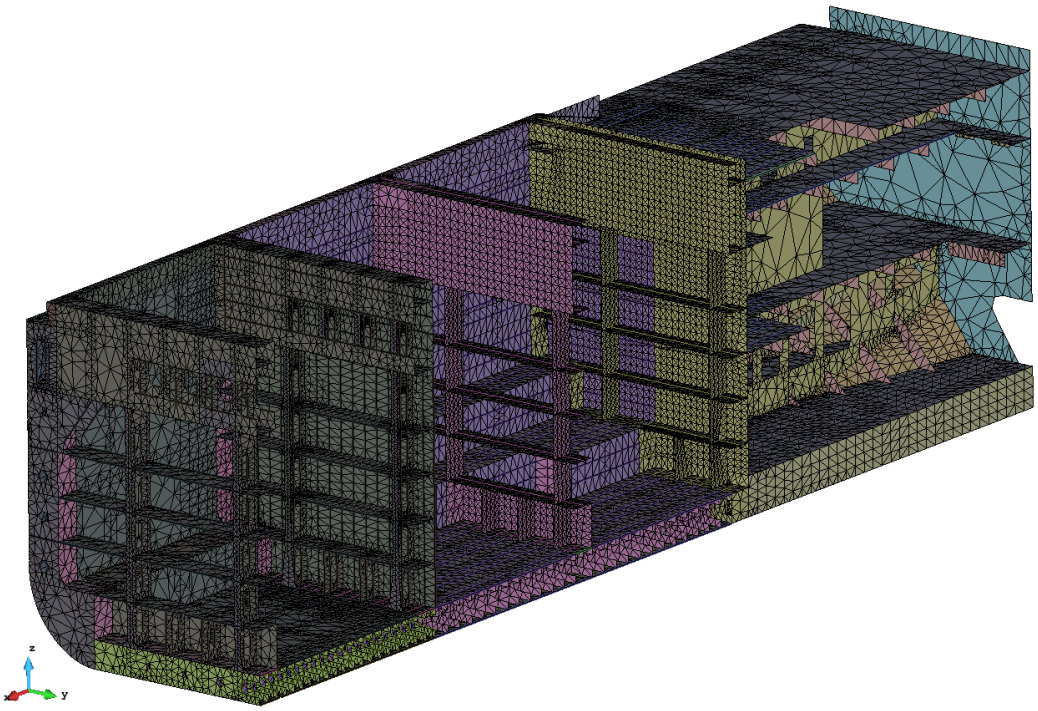

FIGURE 6.105: Computational model meshes.

The adiabatic temperature prescribed is assumed to be that seen in Figure 6.106, unless thermal insulation is considered, then ambient temperature is considered instead (20 °C) for the *support 1* and *support 2* curves.

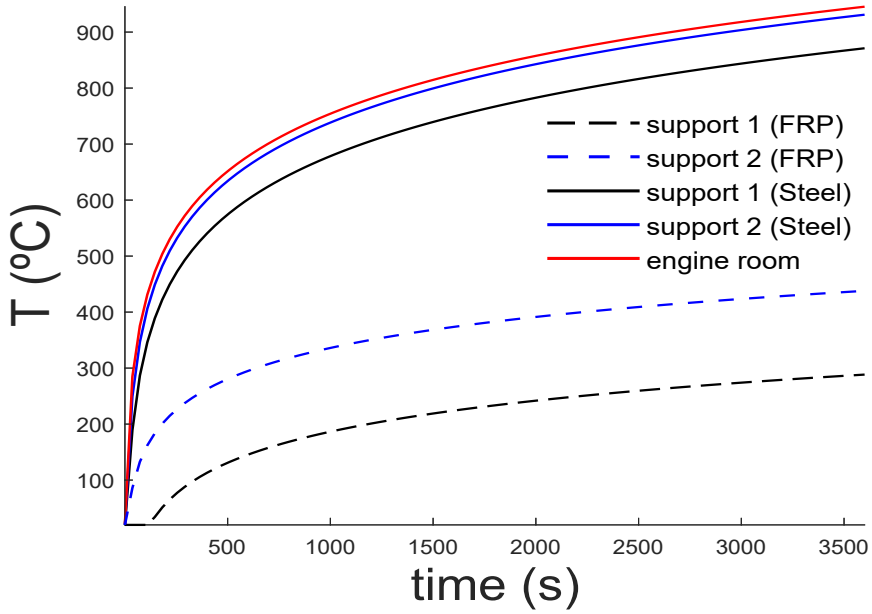

FIGURE 6.106: Thermal load for both steel and FRP design.

Steel and FRP materials are considered for these structural members and also if the bulkhead was insulated from the side of fire according to Figure 6.103, the fire curves obtained for *support 1* and *support 2* are derived from a simple one dimensional linear calculus that involves the thermal properties of both steel and FRP.

Note that the steel presents a higher temperature when non-insulated than the composite. This is due to the lower conductivity of composites, which is 50 times lower than steel. However, there is still the existence of thermal degradation, which is more severe in composites because of the glass transition temperature and pyrolysis (not present in steel).

The results are now shown for the four designs. The analysis is performed for 3600s however, not all the designs are able to endure the analysis for that long. The problem in time domain is discretised in steps of 10 seconds.

6.5.2.1 Steel without insulation

The analysis does not last the whole duration of the 1h simulation when considering the steel structure without insulation. The main problem is the high temperature found in the cargo hold. The bulkhead is able to withstand the force without damage, due to redistributing the load to other structural members. This last phenomenon is well-known in the field of structural mechanics and is referred as relaxation of the internal stresses.

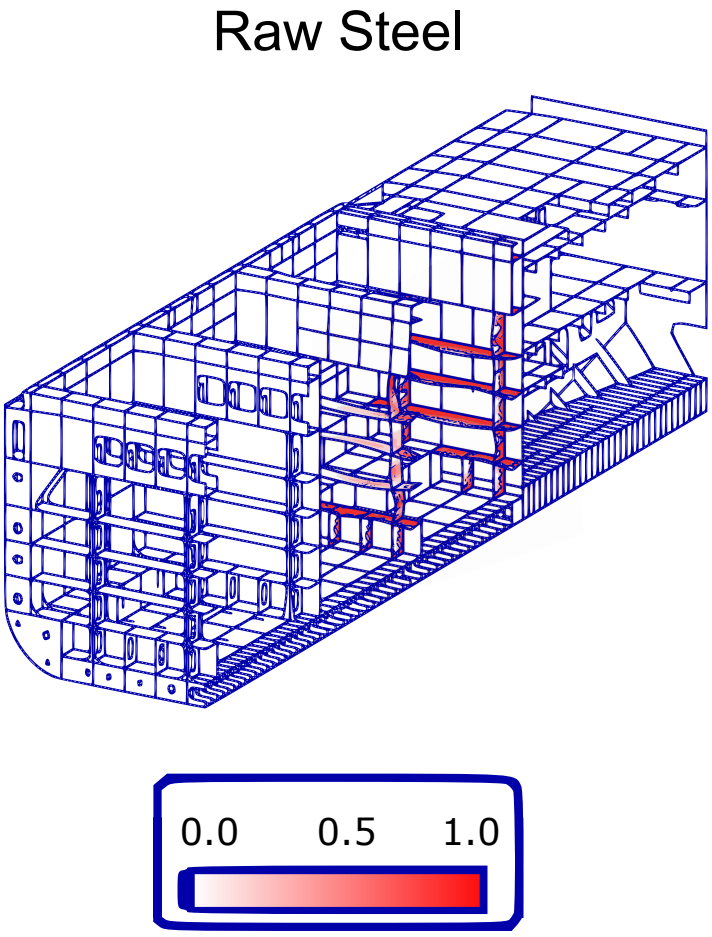

FIGURE 6.107: Damage and deformation of the area of interest for steel and without insulation.

This is not applicable for *support 1* and *support 2*, recall Figure 6.102, since some of

their divisions cannot relax the load that is being endured so easily. The duration of the simulation is 620s (approximately 10 minutes) and it can be seen in Figure 6.107 that there is significant damage prior to the structural collapse. The algorithm for the step of 630s does not converge due to significant damage and because of the impossibility of relaxing the internal stresses to other areas that are intact.

6.5.2.2 FRP without insulation

The case of the design using composites and without insulation is even worse than with steel. The high-temperatures generate such rate of decomposition that the pyrolysis in the material quickly reach an index of 0.

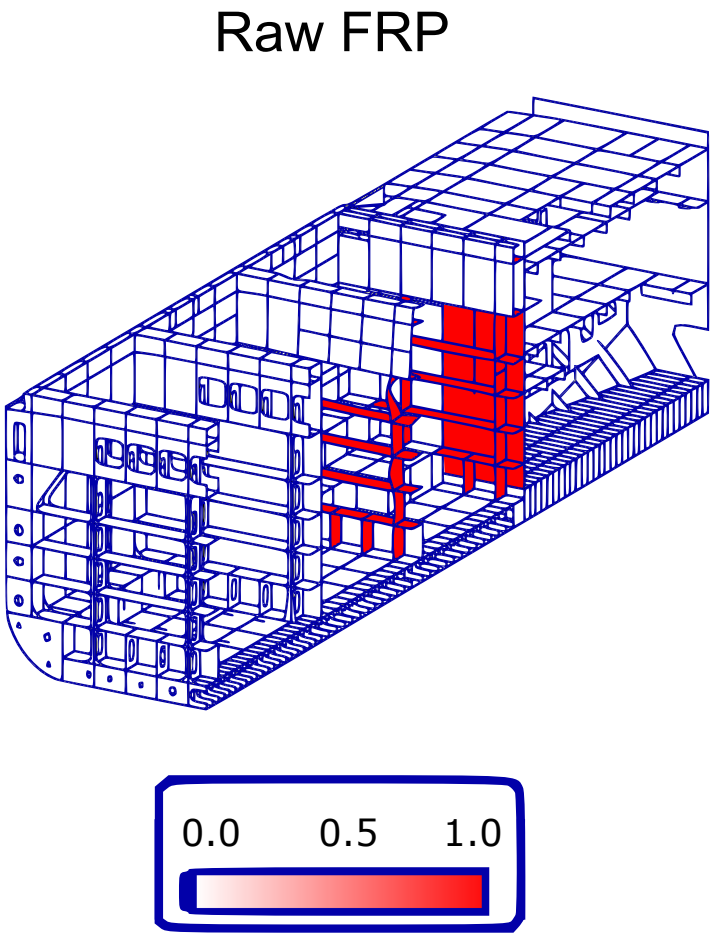

FIGURE 6.108: Damage and deformation of the area of interest for FRP and without insulation.

Figure 6.108 shows the integrity of the structure at 590s. All the structural members in the area of interest present a complete damaged factor, even the bulkhead. The bulkhead is completely damaged since the pyrolysis is close to zero, and this makes the structure unable to redistribute the load onto neighbour elements.

This is the classical problem of composites, which despite the mechanical properties, can be reduced by the temperature. This reduction leads the structure to relax its internal stress and to redistribute the load. This redistribution of the load does

not matter when a material is inflammable (pyrolysis), since the material will be degraded as long as the temperature keeps rising.

Nevertheless, it is very interesting that the composite design without insulation can match the endurance time, 10 minutes, of the steel. Despite having a lower glass temperature, the low conductivity is slowing the thermal heat flow and giving extra time for the collapse of the structure.

6.5.2.3 Steel with insulation

When the steel design is insulated, the structure endures the analysis for all the 3600s and there is a small appearance of inelastic post-buckling in both *support 1* and *support 2*.

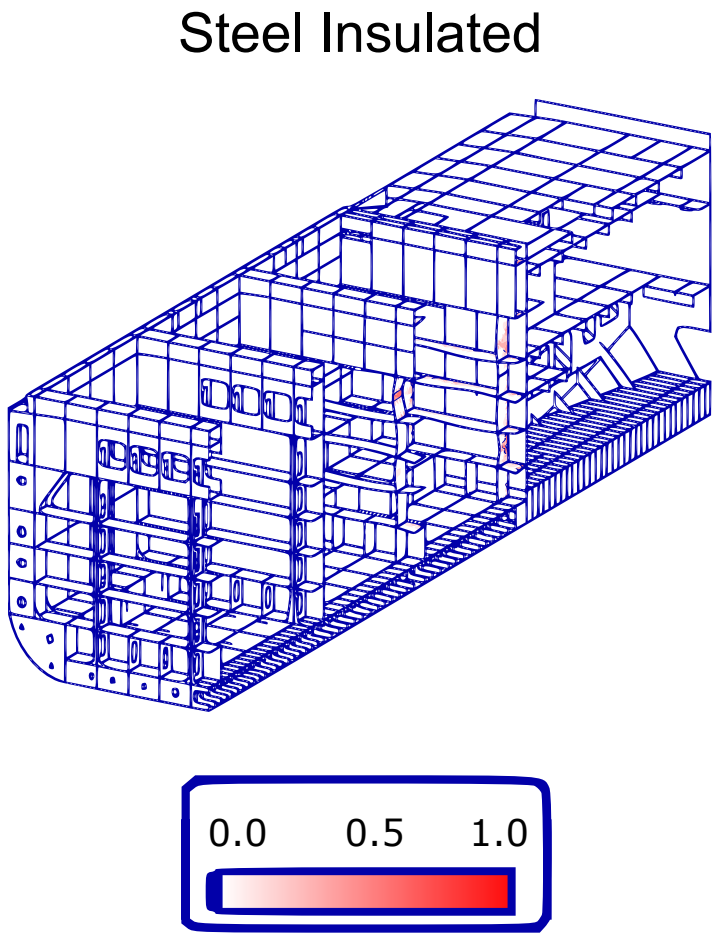

FIGURE 6.109: Damage and deformation of the area of interest for steel and with insulation.

In Figure 6.109, the appearance of damage, which is not close even to an index of 0.5 in the supports, leads to an inelastic post-buckling configuration. The inelastic post-buckling is a stage that is entered after a structural member has experimented inelastic processes (damage) and the critical buckling load of the element has been reduced. This reduction leads to a premature buckling and once this inelastic-buckling

is produced, the element relaxes and redistributes the load to other elements that are stiffer.

6.5.2.4 FRP with insulation

The FRP design with insulation is found in Figure 6.110. This design is the the most successful since it only presents buckling in one small member of *support 1*. The combination of the small conductivity of the composite and the retardancy of the insulation allows it to obtain a very reliable and safe solution that needs small improvement to endure a 1h fire scenario.

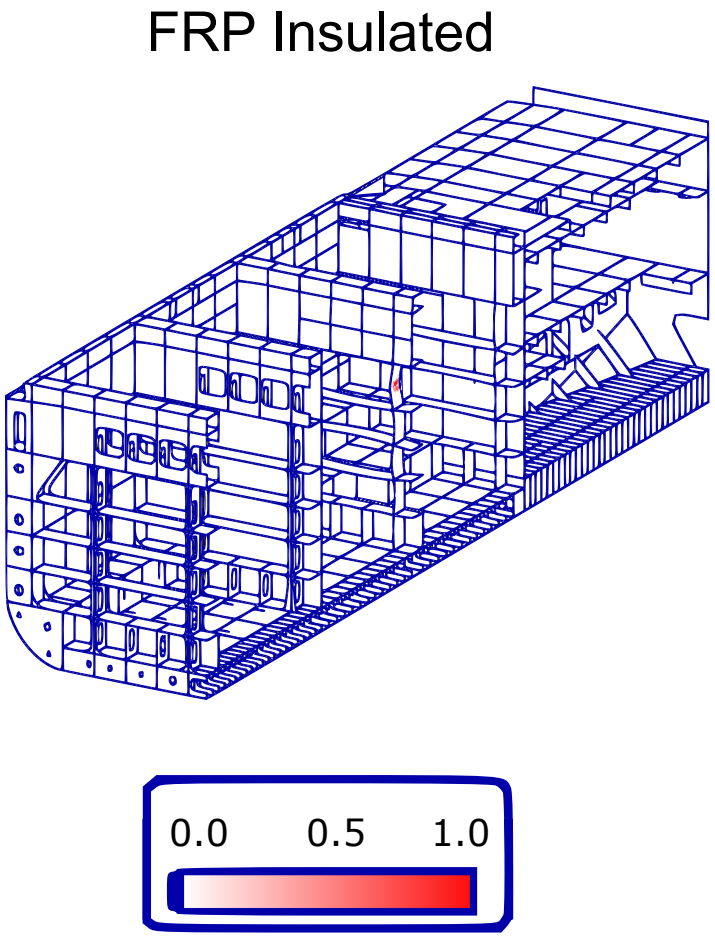

FIGURE 6.110: Damage and deformation of the area of interest for FRP and with insulation.

It may seem very odd that *support 1* has failed, since it is the most distant from the fire in the area of interest. The explanation is similarly odd as this is due to some small deflection in the bulkhead, which itself is intact, however, the small gradient of temperature from the cold side to the hot side of the bulkhead (10°C) ends up introducing a bending moment to the bulkhead.

The bulkhead loses certain stiffness due to its new shape, and redistributes the load to the closest supports, as *support 2* is stiffer, which allows itself to endure the internal

load. But *support 1* is more flexible, and this makes one of its vertical members to enter into a post-buckling regime.

6.5.2.5 Comparison

Figure 6.111 is shown as a summary to compare each result side by side.

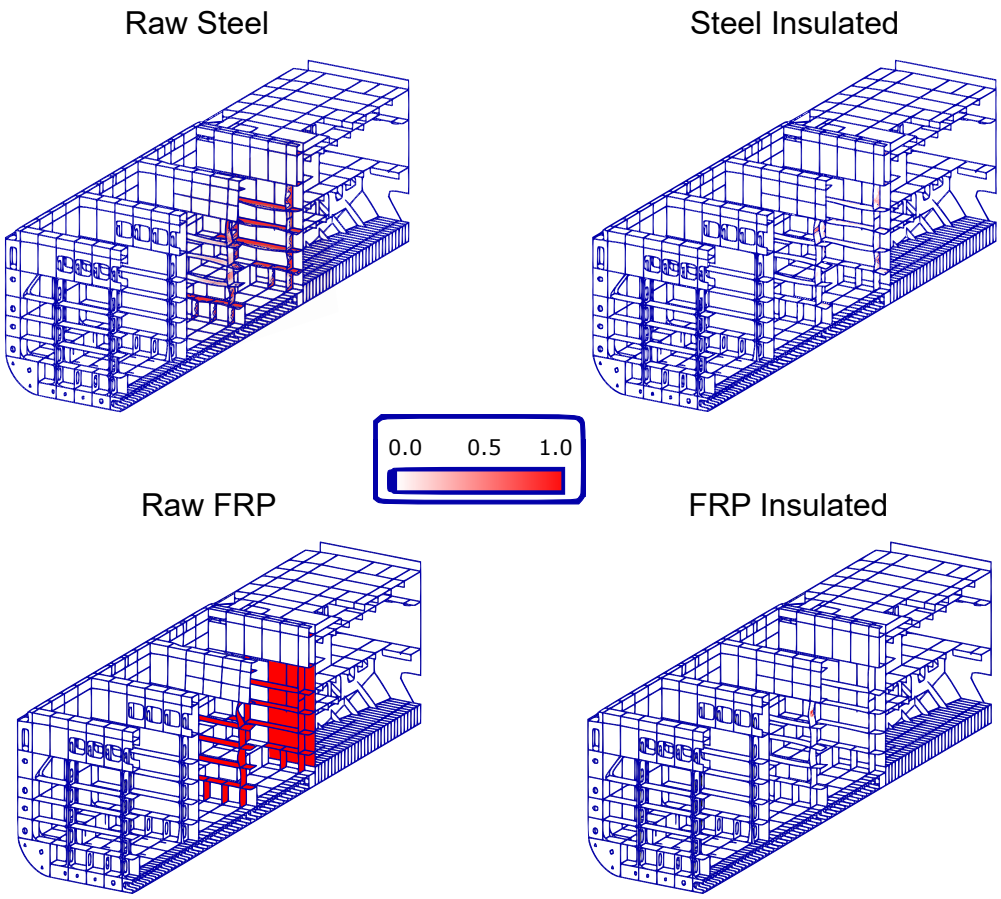

FIGURE 6.111: Damage and deformation of the structure for different designs.

In Figure 6.111 the four designs are shown. The raw steel without insulation shows that support 1 (the one closest to the bow) buckles at time 620s, and there is significant damage in the supports before total collapse. When insulated there is a little damage to the vertical members of the support due to support 1 entering a post-buckling state, however the structure does not collapse and holds for 3600s. In the case of FRP without insulation, the structure suffers a higher damage even in the bulkhead since the material pyrolysis is at a relatively low temperatures (200°C) and the structures collapses at 590s. If the FRP is insulated, the structure does not collapse and there is only one vertical structural member of support 1 that enters into post-buckling and presents damage.

6.5.3 Conclusion of the numerical implementation

This section, devoted to real application of thermo-mechanical approach for marine structures, has addressed a very complex problem in such a degree of detail that is very unique.

The examples given have shown interesting feats for the computational tool developed:

- Fluid-structure interaction

  The first application had the aim to show that the produced model can be extremely enhanced when combined with a *fire dynamic simulator* (FDS) to obtain a more accurate evolution of the boundary conditions introduced in the thermo-mechanical problem.

  An interesting analysis of steel and FRP material designs is given to show how limiting is the flexibility of composites to the current thermo-mechanical tools. Most of the available tools require high-computational cost to deal with the flexibility of composites. Also, fair discussion on pyrolysis is given as to why steel structures have certain advantages in post-fire scenario when collapse has not been produced.

- Flexibility of composites

  The second application is more focused on load-bearing structural divisions such as bulkheads. The scenario of fire here is presumes from fire curves, however the FSI approach could be added to obtain a more accurate version of it.

  The goal was to analyse the concept of *steel equivalent* design. The problematic of flexibility is addressed in the presence of fire, the developed tool has shown to be unique by the fact that it can incorporate many non-linear simulations and yet it is able to deal with the flexibility of composite in a very simple manner.

  This application shows very well the key advantages of composites when considering *equivalent steel* design, as it has been shown that despite their flexibility, if correctly insulated, the standard overestimation of the scantlings is not needed to overcome the flexibility.

  Generally, in modern regulations, composites can offer lighter solutions when it comes to weight and present a ratio of yielding over deformation superior to metals. However, since they are very flexible, the regulations require overestimating the scantlings for this kind of design. This is due to the fact that under certain ambient loads, composites are very prone to buckle.

  Nevertheless, this has been shown to not be necessarily true when an available tool, such as the one developed in this thesis, is used to correctly assess the potential risk (especially thermal-induced risk) of the flexibility in composites.

In conclusion, this section has served to accomplish the proposed goals '*Assess the correctness of the thermo-mechanical model*' and '*Demonstrate the capabilities of the thermo-mechanical model applied to marine structures*', which are numbers 12 and 13 respectively.

6.6 Conclusion

This section aims to be very brief since each division of the chapter has its own set of conclusions organised and well-structured.

The conclusions extracted from the examples presented in this chapter can be listed as follows.

- Fulfilment on verifying the methodology proposed.

  One of the best remarks to make in this chapter is the contribution to the analysis of thermal, mechanical and thermo-mechanical analysis by providing analytical, experimental or realistic data.

  This chapter aims to provide sufficient verification data to be reproduced by other researchers. It has provided a total of 8 benchmark cases and provided two real application guides on how this framework has a real impact in the marine industry.

- Material standardisation.

  Although some specific examples describe and provide the mechanical, thermal and degradation calibration of properties. the recurrent aim through-out this chapter was to provide the reader with examples that make use of standard materials.

  Understanding standard as common mechanical and thermo-chemical properties. E.g., the use of fibreglass and epoxy, has been enforced in many examples in order to provide a broad solution. Note that instead the LEO system material obtained from the FIBRESHIP campaign could be used, however, this type of material was a very selected and tailored case of fibreglass-vinylester material. In that sense, the simplicity in using standard materials have been primed over specific material data that sometimes is very difficult to acquire.

- Steel equivalence.

  The concept of steel equivalent designed has been thoroughly broken down into terms of mechanical and thermal dependency. It has been shown that, despite the common knowledge and default assumptions in regulations, the composite designs are much efficient if tools such as the one developed in this thesis are available.

  Sometimes the limitations or knowledge is affected by the incapacity of providing a straight-forward and feasible framework to produce realistic designs.

- Flexibility.

  Something that derives from steel equivalent design, or at least reflected in the regulations, is the overestimation of scantlings due to the fear of sudden buckling in complete composite structures. This is specially important when considering thermal effects.

  An important emphasis in the large-deformation of composites has been put throughout the confection of this thesis. It has been identified as one of the most limiting factors in terms of buckling risk and therefore the tool developed has aimed at tackling this important issue to offer a better solution for the scientific community.

Chapter 7

Conclusions and implications

7.1 Introduction

Since each chapter had a section to conclusions, this chapter shall only be devoted to completing the initial questions that appeared in the introductory chapter (chapter 1). All previous chapters give a certain level of closure by themselves by remarking the important concepts and revising the initially proposed goals.

Hence, the conclusions extracted in this chapter shall be direct and concise, the aim is to provide a closure to the thesis and to underline its major aspects of it. The chapter is structured in a first section devoted to extracting the conclusions to the three initial questions. Then the conclusions of the problem itself and the implications of the theory.

The applications of this theory are included to grant the reader a better understanding of the importance of the research conducted inside this thesis. A short discussion on the implications for policies is also given and the limitations of the research are enumerated, followed by the future work that can be done.

Finally, a list of the original contributions and publications is given.

7.2 Conclusions about each research question or hypothesis

One of the first questions or hypotheses was if it was possible to produce a tool available to predict the inelastic failure of FRP marine structures exposed to fire with a micro-macro approach. The research had shown that majorly the solutions available for commercial software products such as ANSYS or ABAQUS treated the composite from a macro approach by using certain homogenisation techniques. This yields very poor results when analysing a structure submitted to an inelastic regime.

The solution proposed here was to find an efficient solution that could take into account many non-linearities and that was broadly used in the marine industry. The most known thermal model inside marine applications is the *Henderson* model, which has been adapted to include pyrolysis at the constituent level (fibre and matrix).

In the prediction of mechanical failure of composites, most of the commercial solutions use the isotropic damage model or J2-plasticity. If combined with orthotropic materials, the software can be extended to predict the failure of composites. Some implementations were found for ANSYS and FDS [196], indeed the same approach has been used in this thesis to show a coupling between the FDS solver and the thermo-mechanical implementation in the commercial software RamSeries from Compass IS.

The tool that has been produced as the result of this thesis is available for commercial use, and it is very unique in the sense that is able to assess fire-collapse assessment at the constituent level, something that is not achieved in modern commercial or research software with the little amount of computational power in comparison to the one that is needed from the framework detailed in this work.

The other hypothesis introduced was the mechanical failure of composites. In very short lines, if it was possible to produce a framework that can assess the failure of composites from a micro-macro approach. This framework needs to be able to reproduce complex micro-structural morphology. There was research and commercial software available to do this sort of analysis. Indeed, most of this software relies on high computational costly solutions, nevertheless, the implementations of the early SPROM reduced significantly this cost.

The SPROM acts as a constituent manager, and it is useful to derive the composite failure from the constituent failure. This was already existent in the research. So the conclusion is straightforward, there was already a tool able to take into account this problem. However, most of the applications inside the branch of the SPROM concentrate on determining failure due to yielding or fatigue. But there is very little research on the scope of buckling, which is a type of failure. Partially, this thesis has delved into providing a simple methodology for the SPROM framework to incorporate the prediction of buckling using the co-rotational formulation. So to extract a brief conclusion to the question, there were already significant contributions to damage and fatigue, therefore the answer to the initial hypothesis has concentrated on providing a suitable solution for the branch of laminate buckling.

The last hypothesis was the existence of a thermal prediction model that was able to account for pyrolysis of composites with complex micro-structure. This was quickly

found to be true, and a very specific solution was the aforementioned *Henderson* model. However, there was a need to enable the pyrolysis not only for the polymer matrix but also for the fibre phase. Several authors had already answered this problem in enhanced versions of this thermal model.

Therefore, the ideas found in these enhanced models were adapted to introduce the thermal model proposed in this thesis. The addition of the concept of adiabatic surface temperature was also found very useful to solve the problem, and the possibility to replace this with the FDS solver has granted the developed tool a vast range of solutions to be used in the coupling with the thermo-mechanical model.

7.3 Conclusions about the research problem

The research problem as a whole was the development of the technology necessary to assess the inelastic thermo-mechanical analysis of composite structures exposed to fire.

Most of the damage models existent in the current applications do not analyse inelastic behaviour and those that do, are based on models that are more complex or limited in predicting well the inelastic behaviour.

The proposed model for isotropic damage modelling in this thesis is outstanding since only needs a very narrow set of input variables, because of the isotropy. Furthermore, most commercial software products do not include the limitations introduced in the thermal isotropic damage model in order to not violate certain energy principles as detailed in chapter 5.

This inability to satisfy the energetic principles leads to unrealistic results or directly renders those solutions not feasible. This is interesting because there are available solutions that have a good thermal framework but the thermo-mechanical model as a whole lacks this kind of detail useful in the thermo-mechanical failure prediction.

The other important advantage is the SPROM, as mentioned previously, the SPROM goal is to obtain the constituent-to-composite relationships in the either elastic or inelastic regime. The main advantage of the formulation proposed in this thesis is its extension to the TSPROM that incorporates several thermo-mechanical effects such as the thermal strain or the temperature dependence of the mechanical constituent properties.

This approach is of extreme importance because this theory can extend to many of the existing implementations in commercial software products. An example has been demonstrate in the commercial suite of TDYN from Compass IS, in specific the RamSeries tool that has extended many of the finite element formulation present in shells to include the effects of temperature and pyrolysis but also use the existent elements to extend them to laminate elements by means of the TSPROM.

Linked with the TSPROM is the interesting approach of this thesis; including non-linear geometric effects or so-called deformations. The selection of the co-rotational theory is very clever since it does not clash with the scope of the SPROM. One acts at the constituent level and the second at the kinematic level.

The use of the co-rotational theory has extend the formulation for the TSPROM to be able to incorporate large deformations into its formulations. This has given a formidable tool that addresses the real mechanics of composites.

7.4 Implications for theory

The ramifications of the theory proposed within the scope of this theory are of potential importance.

The thermal model itself is very well suited to be coupled with the mechanical methodology proposed. Since both models consider the effective properties at the constituent level. This gives a degree of control and detail to the theory that is very difficult to match for many commercial solutions nowadays.

Moreover, the application of the specifics of this theory to the marine industry is outstandingly good. The theory has been specifically tailored for marine simulations in specific shells. Other tools developed within the framework of marine applications fail to assess the specifics of marine composites, especially if exposed to high temperatures.

To pose the new thermal serial-parallel rule of mixtures is something that can lead to many other areas of knowledge within this same area.

The framework has proven to be worthy and unique when predicting the failure of composite structures. In particular, it allows for the analyses of load-bearing marine divisions exposed to fire. It takes into account pyrolysis, damage, mechanical degradation, buckling, thermal expansion, etc.

The theory also opens the paradigm to re-evaluate the failure criteria for buckling, since this is a very difficult problem to be simulated and the solutions proposed by the regulations are way more restrictive. This theory is able to assess the buckling of the composite from the constituent level and upgrade the structural design to correctly predict large deformations. Especially when fire passive protection design is needed to correctly determine the scantling of the materials. This tool is good to obtain an optimal design that for several load cases should not incur inelastic buckling.

Then in the presence of fire, the effects of buckling, are something that few authors have tried to clarify. Most of the research is very simple and relies on an experimental point of view, from there an *ad-hoc* thermo-mechanical model is derived which tries to fulfil the physics behind buckling. However, the number of variables not taken into account, especially when the fire is a major issue in engineering design, leads to formulations that will not take into account the interaction of many mechanical aspects that depend on the temperature.

In this sense, the methodology here is very important to analyse large-length composite structures such as offshore structures or long-length ships. These types of structures are by nature very flexible and in the presence of fire, the current technological solutions do not offer an accurate prediction of when many non-linear phenomena are originated.

7.5 Applications

The number of applications for this research is uncountable. It can have a significant impact on branches such as civil, mechanical, aeronautical, automotive, electronics and marine engineering. A proof of this is implicitly found in the concluded project *FIBRESHIP - Engineering, production and life-cycle management for the complete construction of large-length FIBRE-based SHIPs (FIBRESHIP)* [6] that has nourished from the research outlined in this thesis.

The framework discussed in this thesis has been of immeasurable assistance in the calibration and assessment of many necessities, originating from the analysis of fire in composites in the design of FRP ship structures.

One of the most significant applications is the possibility of reducing the amount of testing needed, which is by no means cheap. This framework is an excellent starting point in the building of more technological advances to reduce the large-scale experimental tests that are currently required.

Or on the other hand, the possibility to obtain an optimal solution before starting the testing campaign.

Moreover, this application is not limited to research projects such as FIBRESHIP. Some other projects have gained special attention such as *FIBREGY - Development, engineering, production and life-cycle management of improved FIBRE-based material solutions for structure and functional components of large offshore wind enerGY and tidal power platform* or *FIBRE4YARDS - FIBRE COMPOSITE MANUFACTURING TECHNOLOGIES FOR THE AUTOMATION AND MODULAR CONSTRUCTION IN SHIPYARDS*, which are projects focused on developing technological advances in this direction.

7.6 Implications for policy

The main two detrimental aspects discussed in the thesis are the requirements established in SOLAS or the guidelines issued by the IACS.

The concept of *steel equivalent* regarding fire safety is a very wide term which has not been specifically submitted to special revision for most of its existence. Generally, this term is usually associated with mechanical behaviour, but since fire is involved, it is an obvious requirement that composites can grant at least the same response as metal materials.

It seems very interesting to use the research in this thesis to revise what are the procedures necessary to obtain a *steel equivalent* design and to use the framework to aid in finding an optimal design.

The other implication of interest is this thesis' extensive discussion regarding how the inheriting flexibility of composites is constraining the design of optimal scantlings in order to avoid the potential risk of buckling.

It has been proved that if accurately assessed, and for that, the methodology presented is the best starting point, the design of composite structures can offer better thermo-mechanical properties than metal equivalents. Nowadays, advances in both passive and active fire protective systems have become widespread in the number of solutions offered.

The latter has severe implications for environmental policies. The scientific community and the industry, e.g., aeronautical or automotive, have agreed that the use of advanced materials such as composites is an upgrade in the design of conventional steel equivalent solutions. These materials are very characteristic due to their lightweight properties and present a higher mechanical performance than conventional materials.

It is sensical then to affirm that the applications of the concepts discussed in this thesis are very useful in helping the current state-of-the-art regulations to modernise and obtain more optimal solutions in the future.

7.7 Limitations

There are several limitations, to the finding from this thesis. Starting with the thermal model, one key limitation is the assumption of a convective or radiative heat constant. In reality, this coefficient is not as constant as assumption.

The fact that the flux is prescribed in one direction may lead to strange simulations if a structural element has fire on both sides, in that case, the assumptions of a hot and cold end in the thickness direction become insufficient.

The theory detailed here is limited to shells. Although. it has been shown that shells can reproduce the behaviour of beam equivalent models. However, the thermal model is still a one-dimensional model and a thermo-mechanical formulation for beams would be a more detailed formulation to show how the heat is transported inside the section.

The mechanical model also presents limitations, for example, a very characteristic problem is the fracture due to delamination. This is something that has been commented on but not addressed in the formulation *per se*.

Other important limitations are in the thermo-mechanical degradation of mechanical properties such as Young's modulus or yield stress. These two properties are modelled by a specific composite function, however, this could be extended to more sophisticated functions or at least a general solution instead.

7.8 Further Research

The work discussed in this thesis has many potential upgrades that may be of great interest to the scientific community.

The thermal model proposed here is only developed for the one-dimensional heat transient problem. This could be extended to two dimensions to open the possibility of deriving the formulation also for beam elements, or at least to obtain a better approximation of the transport of heat throughout the thickness.

A two-dimensional model will need of course a better prediction of the gas transfer model. In order to do so, the use of a sophisticated porous-thermo-chemical model can be used. These models already exist, which are of extreme importance since later they can be coupled with the thermo-mechanical model based on the serial-parallel rule of mixtures.

The modelling of pores is also interesting and can be achieved by coupling the existent thermo-chemical formulation with a porous formulation that is able to model the size of pores from thermal and baric quantities.

The introduction of a more complete model such as the anisotropic damage constituent model would be interesting to model more complex materials. This is very good when it comes to simplifying certain micro-structural mythologies.

The introduction of a zig-zag theory can be of great repercussions since delamination is a mechanism only found when using solid elements. These are far more costly in terms of computational power, so the introduction of a zig-zag theory could be interesting in order to add the possibility to take into account delamination.

The upgrade of the SPROM to be extended to the denominated *enhanced serial-parallel rule of mixtures*, which is an advanced formulation to obtain better mechanical transverse predictions.

The elastic or inelastic behaviour of the mechanical model should be extended to include other temperature-dependent properties, or at least the function should be more general. Also, a more thorough discussion is needed to be made in the approach to infer the composite temperature-dependent properties of the constituent phases.

7.9 Original contributions of this work

The theoretical framework discussed in this thesis, especially in chapter 3, chapter 4 and chapter 5, is the fruit of much other research work from different authors who have impacted significantly the paradigm of study.

This section was written with the honest intent to give credit to most of the relevant authors that have contributed to the confection of the methodology shown in this thesis and apologise in advance if anyone was to be excluded. The author shall redact in the following paragraphs a list of the most significant contributions to the methodology exposed.

7.9.1 Original formulation

Several formulations are presented in this thesis, amongst them, the following can be highlighted as their own original contributions:

- The most important formulation is the one attributed to the *thermal serial-parallel rule of mixtures*, a simple extension of the basic SPROM that introduces the effect of thermal expansion.
- This thesis adopts the thermal degradation of mechanical properties proposed by Mouritz and Gibson, to be used at the constituent level in order to be consistent with the micro-mechanical approach. In order to achieve so, the author has proposed a simple linear relationship to be fulfilled.
- The original ideas of Cervera Ruiz et al. [264, 277] have been adapted to include a normalised thermo-mechanical norm for the thermal isotropic damage model. The novelty of this contribution is found in adapting the procedure for the three norms instead of only the third norm. Also includes the non-linear effects of pyrolysis.

7.9.2 Original applications and procedures

Several implementations and applications extracted from the presented formulation are detailed in this thesis, the following can be identified as our own.

- Numerical implementation of the isotropic damage model in RamSeries structural solver.
- Numerical implementation of the rule of mixture, serial-parallel rule of mixtures and thermal serial-parallel rule of mixtures in RamSeries structural solver.
- Numerical implementation of the thermal model in RamSeries structural solver.
- Numerical implementation of the thermo-mechanical degradation model of mechanical properties in RamSeries structural solver.

- Numerical implementation of the thermo-mechanical coupling in RamSeries structural solver.
- Numerical implementation of the co-rotational theory for the thermo-mechanical coupling in RamSeries structural solver.
- Generation of a benchmark case of study based on the tensile and flexural data extracted from FIBRESHIP.
- Generation of a benchmark case of study for mechanical analysis of non-linear geometric buckling based on the Euler-buckling beam problem applied to a sandwich material.
- Generation of a benchmark case of study for thermo-mechanical analysis of a beam problem.
- Generation of a benchmark case of study for thermo-mechanical analysis of non-linear geometric buckling based on the Euler-buckling beam problem applied to a sandwich material.
- Generation of a benchmark case of study for thermo-mechanical analysis of non-linear geometric buckling of orthotropic plates.
- Generation of a benchmark case of study for thermo-mechanical analysis, consisting of an experimental test describing the failure of a load-bearing bulkhead exposed to fire.
- Generation of a benchmark case of study for thermo-mechanical analysis coupled with a fire dynamics simulator of a real marine application case.
- Generation of a benchmark case of study for thermo-mechanical analysis of thermo-inelastic buckling of a real marine application case.

7.9.3 Publications

The scientific diffusion of the ideas in this thesis can be summarised in the following lines.

7.9.3.1 Journal articles

1. R. Pacheco-Blazquez, D. Di Capua, J. García-Espinosa, O. Casals, and T. Hakkarainen. Thermo-mechanical analysis of laminated composites shells exposed to fire. Engineering Structures, 253, 2022. ISSN 18737323. doi: 10.1016/j.engstruct.2021.113679 [pb1]
2. Pacheco-Blazquez, R.; Di Capua, D.; García-Espinosa, J.; Casals, O. Non-linear thermo-mechanical buckling approach for composite laminated marine structures. Ocean Engineering. *(under review, last updated June 3, 2022)*
3. Pacheco-Blazquez, R.; Di Capua, D.; García-Espinosa, J.; Casals, O.; Hakkarainen, T.; Tissari, A.; Korkealaakso, A. Computational analysis of resisting marine FRP divisions exposed to fire. Application to the analysis of ship structures. Ocean Engineering. *(under review, last updated June 3, 2022)*

7.9.3.2 Conference proceedings

1. Rafael Pacheco-blazquez, Daniel Di Capua, and Julio García-espinosa. Nonlinear thermo-mechanical buckling approach for composite laminated marine structures . In IX International Conference on Computational Methods in Marine Engineering (MARINE), pages 1–15, 2021 [pb2]

2. Rafael Pacheco-blazquez, Daniel Di Capua, Julio García-espinosa, Ovidi Casals, Tuula Hakkarainen, Alexandra Tissari, and Antti Korkealaakso. Computational analysis of resisting marine FRP divisions exposed to fire . Application to the analysis of ship structures . In IX International Conference on Computational Methods in Marine Engineering (MARINE), pages 1–18, 2021 [pb3]

7.9.3.3 Conference presentations

- Rafael Pacheco-blazquez, Daniel Di Capua, Julio Garcia-Espinosa, Ovidi Casals, Tuula Hakkarainene, Alexandra Tissarie, Antti Korkealaaksoe, and Korhonen Timoe. Thermo-structural response of FRP ship structures exposed to fire. In E-LASS 16th, Nantes, 2021. URL https://e-lass.eu/media/2022/01/02_ElassPresentation.pdf [pb4]

- Daniel Di Capua, Julio Garcia, Rafael Pachecho, Ovidi Casals, Timo Korhonen, Tuula Hakkarainen, and Antti Paajanen. Thermo-mechanical analysis of laminated composites exposed to fire. Application to the analysis of ship structures. In VIII International Conference on Computational Methods in Marine Engineering 2019, volume 19, pages 879–896, 2019 [pb5]

7.9.3.4 Collaboration in research projects

1. Engineering, production and life-cycle management for complete construction of large-length FIBRE-based SHIPs (FIBRESHIP). Funded by European Unions Horizon 2020 research and innovation program under grant agreement number 723360. Starting date: 01/06/2017 End date: 31/05/2020. [6]

2. Development, engineering, production and life-cycle management of improved FIBRE-based material solutions for structure and functional components of large offshore wind enerGY and tidal power platform (FIBREGY). Funded by European Unions Horizon 2020 research and innovation program under grant agreement number 952966. Starting date: 01/01/2021 End date: 31/12/2023. [308]

3. FIBRE composite manufacturing technologies FOR the automation and modular construction in shipYARDS (FIBRE4YARDS). Funded by European Unions Horizon 2020 research and innovation program under grant agreement number 101006860. Starting date: 01/01/2021 End date: 31/12/2023. [309]

Appendix A

Cristex composite materials

TECHNICAL DATA SHEET

Sap No: 30000258 **Article Description:** U-E-996 g/m²-600mm

Textile Structure: 7000129

ARTICLE CONSTRUCTION (in accordance with EN 13473-1)				
Layer	Construction	Areal Weight	Tolerance	Material
3	0°	898 g/m²	± 5%	E-glass 2.400 TEX
2	90°	40 g/m²	± 5%	E-glass 200 TEX
1	90°	41 g/m²	± 5%	E-glass 68 TEX
Stitching		17 g/m²	± 3 g/m²	PES (Polyester) 110 dtex

Fibre input can be determined individually

FURTHER CHARACTERISTICS					
Gauge	10,0	Stitching Pattern	Tricot	Width (nominal)	600mm
Stitch length	4,00mm	Total Tolerance	5,2%	Total areal weight	996 g/m²

Tracer yarn[1] 4 PC blue & tracer yarn 2 PC light green

[1] position can be determined individually

FIGURE A.1: Datasheet describing the properties and composition of the LEO-system plies used in the manufacturing of the monolithic laminate specimens

Original Publications

[pb1] R. Pacheco-Blazquez, D. Di Capua, J. García-Espinosa, O. Casals, and T. Hakkarainen. Thermo-mechanical analysis of laminated composites shells exposed to fire. Engineering Structures, 253, 2022. ISSN 18737323. doi: 10.1016/j.engstruct.2021.113679.

[pb2] Rafael Pacheco-blazquez, Daniel Di Capua, and Julio García-espinosa. Non-linear thermo-mechanical buckling approach for composite laminated marine structures . In IX International Conference on Computational Methods in Marine Engineering (MARINE), pages 1–15, 2021.

[pb3] Rafael Pacheco-blazquez, Daniel Di Capua, Julio García-espinosa, Ovidi Casals, Tuula Hakkarainen, Alexandra Tissari, and Antti Korkealaakso. Computational analysis of resisting marine FRP divisions exposed to fire . Application to the analysis of ship structures . In IX International Conference on Computational Methods in Marine Engineering (MARINE), pages 1–18, 2021.

[pb4] Rafael Pacheco-blazquez, Daniel Di Capua, Julio Garcia-Espinosa, Ovidi Casals, Tuula Hakkarainene, Alexandra Tissarie, Antti Korkealaaksoe, and Korhonen Timoe. Thermo-structural response of FRP ship structures exposed to fire. In E-LASS 16th, Nantes, 2021. URL https://e-lass.eu/media/2022/01/02_ElassPresentation.pdf.

[pb5] Daniel Di Capua, Julio Garcia, Rafael Pachecho, Ovidi Casals, Timo Korhonen, Tuula Hakkarainen, and Antti Paajanen. Thermo-mechanical analysis of laminated composites exposed to fire. Application to the analysis of ship structures. In VIII International Conference on Computational Methods in Marine Engineering 2019, 2019.

Bibliography

[1] M. F. Ashby. Materials selection in mechanical design. Butterworth-Heinemann, 2011. ISBN 9781856176637.

[2] F. Evegren, M. Rahm, and T. Hertzberg. Fire Tests of FRP Composite Ship Structures. Technical report, SP Technical Research Institute of Sweden, 2007.

[3] T. Hertzberg. LASS, Lightweight Construction Applications at Sea. Technical report, SP Technical Research Institute of Sweden, 2009. URL www.vinnova.se.

[4] Fire-Resist. URL http://www.fire-resist.eu/FireResist/index.xhtml.

[5] RAMSSES project' significant milestone towards sustainable composite ship construction | Damen. URL https://www.damen.com/en/news/2020/07/ramsses_project_reaches_significant_milestone_towards_sustainable_composite_ship_construction.

[6] HOME - FibreShip. URL http://www.fibreship.eu/.

[7] A. P. Mouritz, S. Feih, E. Kandare, Z. Mathys, A. G. Gibson, P. E. Des Jardin, S. W. Case, and B. Y. Lattimer. Review of fire structural modelling of polymer composites. Composites Part A: Applied Science and Manufacturing, 40(12): 1800–1814, 2009. ISSN 1359835X. doi: 10.1016/j.compositesa.2009.09.001. URL http://dx.doi.org/10.1016/j.compositesa.2009.09.001.

[8] Phuong Tran, Quynh Thuy Nguyen, and K. T. Lau. Fire performance of polymer-based composites for maritime infrastructure, 12 2018. ISSN 13598368. URL https://linkinghub.elsevier.com/retrieve/pii/S1359836818315968.

[9] Kevin Mcgrattan, Simo Hostikka, Jayson Floyd, Howard Baum, and Ronald Rehm. NIST Special Publication 1018-5 Fire Dynamics Simulator (Version 5) Technical Reference Guide. Nist Special Publication, (Version 5):86, 2007.

[10] Hong Sheng Huang, Chung Hwei Su, Cheng Bang Li, Ching Yuan Lin, and Chun Chou Lin. Enhancement of Fire Safety of an Existing Green Building due to Natural Ventilation. Energies 2016, Vol. 9, Page 192, 9(3):192, 3 2016. ISSN 19961073. doi: 10.3390/EN9030192. URL https://www.mdpi.com/1996-1073/9/3/192/htmhttps://www.mdpi.com/1996-1073/9/3/192.

[11] J.B. Henderson, J.A. Wiebelt, and M.R. Tant. A Model for the Thermal Response of Polymer Composite Materials with Experimental Verification. Journal of Composite Materials, 19(6):579–595, 11 1985. ISSN 0021-9983. doi: 10.1177/002199838501900608. URL http://journals.sagepub.com/doi/10.1177/002199838501900608.

[12] Joel Jurado Granados, Xavier Martinez, Niamh Nash, Carlos Bachour, Ioannis Manolakis, Anthony Comer, and Daniel Di Capua. Numerical and experimental procedure for material calibration using the serial/parallel mixing theory, to analyze different composite failure modes. Mechanics of Advanced Materials and Structures, 2019. ISSN 15376532. doi: 10.1080/15376494.2019.1675106.

[13] Lucie Chapelle. Characterization and modelling of the mechanical properties of mineral wool. Technical report, 2016.

[14] A. G. Gibson, P. N. H. Wright, Y. S. Wu, A. P. Mouritz, Z. Mathys, and C. P. Gardiner. The Integrity of Polymer Composites during and after Fire. Journal of Composite Materials, 38(15):1283–1307, 8 2004. ISSN 0021-9983. doi: 10.1177/0021998304042733. URL http://journals.sagepub.com/doi/10.1177/0021998304042733.

[15] Fernando Rastellini, Sergio Oller, Omar Salomón, and Eugenio Oñate. Composite materials non-linear modelling for long fibre-reinforced laminates. Computers & Structures, 86(9):879–896, 5 2008. ISSN 00457949. doi: 10.1016/j.compstruc.2007.04.009. URL https://linkinghub.elsevier.com/retrieve/pii/S0045794907001642.

[16] Eugenio Oñate. Structural Analysis with the Finite Element Method Linear Statics Volume 2. Beams, Plates and Shells. In Springer, volume First Edit, chapter 11, pages 675–728. 2013. ISBN 9781402087325. doi: 10.1007/978-1-4020-8743-1. URL http://medcontent.metapress.com/index/A65RM03P4874243N.pdf.

[17] J. C. Simo and J. W. Ju. Strain- and stress-based continuum damage models-I. Formulation. International Journal of Solids and Structures, 23(7):821–840, 1987. ISSN 00207683. doi: 10.1016/0020-7683(87)90083-7. URL http://www.sciencedirect.com/science/article/pii/0020768387900837.

[18] Carlos A. Felippa and Bjorn Haugen. A unified formulation of small-strain corotational finite elements: I. Theory. Computer Methods in Applied Mechanics and Engineering, 194(21-24 SPEC. ISS.):2285–2335, 6 2005. ISSN 00457825. doi: 10.1016/j.cma.2004.07.035.

[19] J. B. Henderson and T. E. Wiecek. A Mathematical Model to Predict the Thermal Response of Decomposing, Expanding Polymer Composites. Journal of Composite Materials, 1987. ISSN 1530793x. doi: 10.1177/002199838702100406.

[20] A P Mouritz and A G Gibson. Fire Properties of Polymer Composite Materials, volume 143 of Solid Mechanics and Its Applications. Springer Netherlands, Dordrecht, 2006. ISBN 978-1-4020-5355-9. doi: 10.1007/978-1-4020-5356-6. URL http://link.springer.com/10.1007/978-1-4020-5356-6.

[21] R. Ali. Use of finite element technique for the analysis of composite structures. Computers and Structures, 58(5):1015–1023, 1996. ISSN 00457949. doi: 10.1016/0045-7949(95)00190-R. URL http://www.sciencedirect.com/science/article/pii/004579499500190R.

[22] M. J. Hinton and P. D. Soden. Predicting failure in composite laminates: the background to the exercise. Composites Science and Technology, 58(7):1001–1010, 7 1998. ISSN 02663538. doi: 10.1016/S0266-3538(98)00074-8. URL https://www.sciencedirect.com/science/article/pii/S0266353898000748?via%3Dihub.

[23] S. Feih, Z. Mathys, A. G. Gibson, and A. P. Mouritz. Modelling the compression strength of polymer laminates in fire. Composites Part A: Applied Science and Manufacturing, 38(11):2354–2365, 11 2007. doi: 10.1016/j.compositesa.2007.04.013.

[24] S. Feih, A. P. Mouritz, Z. Mathys, and A. G. Gibson. Tensile strength modeling of glass fiber-polymer composites in fire. Journal of Composite Materials, 41 (19):2387–2410, 10 2007. ISSN 00219983. doi: 10.1177/0021998307075461. URL https://journals.sagepub.com/doi/10.1177/0021998307075461.

[25] S. Feih, T. Bhat, A. Ab Rahman, V. Chevali, X. Liu, and A. P. Mouritz. Fire performance of basalt fibre composites under tensile loading. 16th European Conference on Composite Materials, ECCM 2014, (January), 2014.

[26] W. Voigt. Ueber die Beziehung zwischen den beiden Elasticitätsconstanten isotroper Körper. Annalen der Physik, 274(12):573–587, 1889. ISSN 15213889. doi: 10.1002/andp.18892741206. URL http://onlinelibrary.wiley.com/doi/10.1002/andp.18892741206/abstract.

[27] A. Reuss. Berechnung der Fließgrenze von Mischkristallen auf Grund der Plastizitätsbedingung für Einkristalle . ZAMM Journal of Applied Mathematics and Mechanics / Zeitschrift für Angewandte Mathematik und Mechanik, 9(1): 49–58, 1929. ISSN 15214001. doi: 10.1002/zamm.19290090104. URL http://doi.wiley.com/10.1002/zamm.19290090104.

[28] Wickstrom Ulf, Dat Duthinh, and Kevin Mcgrattan. Adiabatic Surface Temperature for Calculating Heat Transfer To Fire Introduction. Most, 2, 9 2007. URL https://www.nist.gov/publications/adiabatic-surface-temperature-calculating-heat-transfer-fire-exposed-structures.

[29] Brian Y. Lattimer, Jason Ouellette, and Javier Trelles. Thermal Response of Composite Materials to Elevated Temperatures. Fire Technology, 47(4):823–850, 10 2011. ISSN 0015-2684. doi: 10.1007/s10694-009-0121-9. URL http://link.springer.com/10.1007/s10694-009-0121-9.

[30] R. D. Chippendale, I. O. Golosnoy, and P. L. Lewin. Numerical modelling of thermal decomposition processes and associated damage in carbon fibre composites. Journal of Physics D: Applied Physics, 47 (38):385301, 9 2014. ISSN 13616463. doi: 10.1088/0022-3727/47/38/385301. URL http://stacks.iop.org/0022-3727/47/i=38/a=385301http://stacks.iop.org/0022-3727/47/i=38/a=385301?key=crossref.e8e3fa511892bfff723543822db41f64.

[31] Michael J. MacDonald, ChaoFeng F Chu, Pierre P. Guilloit, and Ka M. Ng. A generalized BlakeKozeny equation for multisized spherical particles. AIChE Journal, 37(10):1583–1588, 1991. ISSN 15475905. doi: 10.1002/aic.690371016. URL https://onlinelibrary.wiley.com/doi/abs/10.1002/aic.690371016.

[32] J. Oliver. A consistent characteristic length for smeared cracking models. International Journal for Numerical Methods in Engineering, 28(2):461–474, 2 1989. ISSN 10970207. doi: 10.1002/nme.1620280214. URL http://doi.wiley.com/10.1002/nme.1620280214.

[33] Fernando G Rastellini. No-Linealidad Constitutiva De. 2006. ISBN 978-84-96-736-10-8.

[34] Chad Perry. A Structured Approach for Presenting Theses. Australasian Marketing Journal (AMJ), 6(1):63–85, 6 1998. ISSN 1441-3582. doi: 10.1016/S1441-3582(98)70240-X.

[35] C. H. Bamford, J. Crank, and D. H. Malan. The combustion of wood. Part I. Mathematical Proceedings of the Cambridge Philosophical Society, 42(2):166–182, 6 1946. ISSN 14698064. doi: 10.1017/S030500410002288X. URL https://www.cambridge.org/core/product/identifier/S030500410002288X/type/journal_article.

[36] Hsiang Cheng Kung. A mathematical model of wood pyrolysis. Combustion and Flame, 18(2):185–195, 4 1972. ISSN 00102180. doi: 10.1016/S0010-2180(72)80134-2.

[37] A. Murty Kanury. Thermal decomposition kinetics of wood pyrolysis. Combustion and Flame, 18(1):75–83, 2 1972. ISSN 00102180. doi: 10.1016/S0010-2180(72)80228-1.

[38] Edward J. Kansa, Henry E. Perlee, and Robert F. Chaiken. Mathematical model of wood pyrolysis including internal forced convection. Combustion and Flame, 29(C):311–324, 1 1977. ISSN 00102180. doi: 10.1016/0010-2180(77)90121-3.

[39] R. M. Sullivan and N. J. Salamon. A finite element method for the thermochemical decomposition of polymeric materials-I. Theory. International Journal of Engineering Science, 30(4):431–441, 4 1992. ISSN 00207225. doi: 10.1016/0020-7225(92)90035-F.

[40] R. M. Sullivan and N. J. Salamon. A finite element method for the thermochemical decomposition of polymeric materials-II. Carbon phenolic composites. International Journal of Engineering Science, 30(7):939–951, 7 1992. ISSN 00207225. doi: 10.1016/0020-7225(92)90021-8.

[41] R.M. Sullivan. A Coupled Solution Method for Predicting the Thermostructural Response of Decomposing, Expanding Polymeric Composites. Journal of Composite Materials, 27(4):408–434, 4 1993. ISSN 0021-9983. doi: 10.1177/002199839302700404. URL http://journals.sagepub.com/doi/10.1177/002199839302700404.

[42] Roy M. Sullivan. Thermodynamic model for hygrothermal behavior in polymer composites. Collection of Technical Papers - AIAA/ASME/ASCE/AHS/ASC Structures, Structural Dynamics and Materials Conference, 1:559–565, 1994. ISSN 02734508. doi: 10.2514/6.1994-1377.

[43] R. M. Sullivan. The effect of water on thermal stresses in polymer composites. Journal of Applied Mechanics, Transactions ASME, 63(1):173–179, 1996. ISSN 15289036. doi: 10.1115/1.2787195.

[44] Roy M. Sullivan and Eric H. Stokes. Porous media and mixture models for hygrothermal behavior of phenolic composites. American Society of Mechanical Engineers, Applied Mechanics Division, AMD, 233(March):33–43, 1999. ISSN 01608835.

[45] Yu I. Dimitrienko, M. N. Koryzkov, Yu I. Yurin, A. A. Zakharov, and S. V. Sborschikov. Computational conjugate modeling of aerodynamical flow and thermal stresses in ablative composite structures. IOP Conference Series:

Materials Science and Engineering, 934(1), 2020. ISSN 1757899X. doi: 10.1088/1757-899X/934/1/012013.

[46] Yu I. Dimitrienko, E. S. Egoleva, D. O. Yakovlev, and S. V. Sborschikov. Modeling of stresses in inorganic composite plates under non uniform high temperature heating. IOP Conference Series: Materials Science and Engineering, 934(1), 2020. ISSN 1757899X. doi: 10.1088/1757-899X/934/1/012015.

[47] Archibald Tewarson and Domenic P. Macaione. Polymers and Composites-An Examination of Fire Spread and Generation of Heat and Fire Products. Journal of Fire Sciences, 11(5):421–441, 9 1993. ISSN 0734-9041. doi: 10.1177/073490419301100504. URL http://journals.sagepub.com/doi/10.1177/073490419301100504.

[48] Andrew T. Grenier, Nicholas A. Dembsey, and Jonathan R. Barnett. Fire Characteristics of Cored Composite Materials for Marine Use. Fire Safety Journal, 30 (2):137–159, 3 1998. ISSN 03797112. doi: 10.1016/S0379-7112(97)00059-3.

[49] Nicholas A. Dembsey and David J. Jacoby. Evaluation of common ignition models for use with marine cored composites. Fire and Materials, 24(2):91–100, 3 2000. ISSN 0308-0501. doi: 10.1002/1099-1018(200003/04)24:2<91::AID-FAM725>3.0.CO;2-0. URL https://onlinelibrary.wiley.com/doi/10.1002/1099-1018(200003/04)24:2<91::AID-FAM725>3.0.CO;2-0.

[50] Richard Lyon, J Demario, Richard Walters, and S Crowley. Flammability of glass fiber-reinforced polymer composites. International SAMPE Symposium and Exhibition (Proceedings), 51, 2006.

[51] B. Lattimer and T. Campbell. Fire modelling of composites. Solid Mechanics and its Applications, 143:103–132, 2006. ISSN 09250042. doi: 10.1007/978-1-4020-5356-6{_}4. URL https://link.springer.com/chapter/10.1007/978-1-4020-5356-6_4.

[52] Wei Xie and Paul E. DesJardin. A level set embedded interface method for conjugate heat transfer simulations of low speed 2D flows. Computers and Fluids, 37(10):1262–1275, 12 2008. ISSN 00457930. doi: 10.1016/j.compfluid.2007.10.017.

[53] Wei Xie and Paul E. DesJardin. An embedded upward flame spread model using 2D direct numerical simulations. Combustion and Flame, 156(2):522–530, 2 2009. ISSN 00102180. doi: 10.1016/j.combustflame.2008.11.011.

[54] K. McGrattan. Fire Dynamics Simulator (versión 6) Technical Reference Guide, NISTSP1018. Nist Special Publication, 1, 2013.

[55] ISO834:1. ISO - ISO 834-11:2014 - Fire resistance tests Elements of building construction Part 11: Specific requirements for the assessment of fire protection to structural steel elements, 3 2014. URL https://www.iso.org/standard/57595.html.

[56] James G. Quintiere. A simulation model for fire growth on materials subject to a room-corner test. Fire Safety Journal, 20(4):313–339, 1 1993. ISSN 03797112. doi: 10.1016/0379-7112(93)90053-S. URL https://linkinghub.elsevier.com/retrieve/pii/037971129390053S.

[57] Marc L. Janssens. Improved method for analyzing ignition data from the Cone Calorimeter in the vertical orientation. In Fire Safety Science, pages 803–814, 2003. ISBN 0954534808. doi: 10.3801/IAFSS.FSS.7-803.

[58] DANUTE R. VENTRIGLIO. FIRE SAFE MATERIALS FOR NAVY SHIPS. Naval Engineers Journal, 94(5):65–74, 10 1982. ISSN 00281425. doi: 10.1111/j.1559-3584.1982.tb02504.x. URL http://doi.wiley.com/10.1111/j.1559-3584.1982.tb02504.x.

[59] D. M. Allison, A. J. Marchand, and R. M. Morchat. Fire performance of composite materials in ships and offshore structures. Marine Structures, 4(2):129–140, 1 1991. ISSN 09518339. doi: 10.1016/0951-8339(91)90017-6.

[60] G. T. Egglestone and D. M. Turley. Flammability of GRP for use in ship superstructures. Fire and Materials, 18(4):255–260, 7 1994. ISSN 0308-0501. doi: 10.1002/fam.810180408. URL http://doi.wiley.com/10.1002/fam.810180408.

[61] Usman Sorathia, Richard Lyon, Richard Gann, and Louis Gritzo. Materials and fire threat. SAMPE Journal, 32(3):8–15, 5 1996. ISSN 00911062. doi: 10.1023/A:1015371806854. URL https://link.springer.com/article/10.1023/A:1015371806854.

[62] Bertil Fredlund. Modelling of heat and mass transfer in wood structures during fire. Fire Safety Journal, 20(1):39–69, 1 1993. ISSN 03797112. doi: 10.1016/0379-7112(93)90011-E.

[63] J. B. Henderson and S. C. Hagen. A radiant heat flux apparatus for measuring the thermal response of polymeric materials to high temperatures. Polymer Composites, 6(2):110–114, 4 1985. ISSN 0272-8397. doi: 10.1002/pc.750060209. URL http://doi.wiley.com/10.1002/pc.750060209.

[64] Hugh L.N. Mcmanus and George S. Springer. High Temperature Thermomechanical Behavior of Carbon-Phenolic and Carbon-Carbon Composites, I. Analysis. Journal of Composite Materials, 26(2):206–229, 2 1992. ISSN 0021-9983. doi: 10.1177/002199839202600204. URL http://journals.sagepub.com/doi/10.1177/002199839202600204.

[65] Hugh L.N. Mcmanus and George S. Springer. High Temperature Thermomechanical Behavior of Carbon-Phenolic and Carbon-Carbon Composites, II. Results. Journal of Composite Materials, 26(2):230–255, 2 1992. ISSN 0021-9983. doi: 10.1177/002199839202600205. URL http://journals.sagepub.com/doi/10.1177/002199839202600205.

[66] YU I. Dimitrienko. Thermal stresses and heat-mass transfer in ablating composite materials. International Journal of Heat and Mass Transfer, 38(1):139–146, 1 1995. ISSN 00179310. doi: 10.1016/0017-9310(94)00137-K.

[67] M. R.E. Looyeh, P. Bettess, and A. G. Gibson. A one-dimensional finite element simulation for the fire-performance of GRP panels for offshore structures. International Journal of Numerical Methods for Heat and Fluid Flow, 7(5):609–625, 1997. ISSN 09615539. doi: 10.1108/09615539710170781.

[68] N. Dodds, A. G. Gibson, D. Dewhurst, and J. M. Davies. Fire behaviour of composite laminates. Composites Part A: Applied Science and Manufacturing, 31(7):689–702, 7 2000. ISSN 1359835X. doi: 10.1016/S1359-835X(00)00015-4.

[69] M. R.E. Looyeh, K. Rados, and P. Bettess. Thermochemical responses of sandwich panels to fire. Finite Elements in Analysis and Design, 37(11):913–927, 10 2001. ISSN 0168874X. doi: 10.1016/S0168-874X(01)00075-0.

[70] P. Krysl, W. T. Ramroth, L. K. Stewart, and R. J. Asaro. Finite element modelling of fibre reinforced polymer sandwich panels exposed to heat. International Journal for Numerical Methods in Engineering, 61(1):49–68, 9 2004. ISSN 0029-5981. doi: 10.1002/nme.1055. URL http://doi.wiley.com/10.1002/nme.1055.

[71] V. Urso Miano and A. G. Gibson. FIRE model for fibre reinforced plastic composites using Apparent thermal diffusivity (ATD). Plastics, Rubber and Composites, 38(2-4):87–92, 2009. ISSN 14658011. doi: 10.1179/174328909X387955.

[72] V. Miano Urso, G. A. Jones, A. G. Gibson, S. Feih, and A. P. Mouritz. Simultaneous measurement of apparent thermal diffusivity and distortion of composites at high temperature. ICCM International Conferences on Composite Materials, (1), 2009.

[73] Thomas R Munson and Robert J Spindler. Transient Thermal Behavior of Decomposing Materials. Part 1. General Theory and Application to Convective Heating. Technical report, AVCO CORP WILMINGTON MA RESEARCH AND ADVANCED DEVELOPMENT DIV, 1961.

[74] George S. Springer and Stephen W. Tsai. Thermal Conductivities of Unidirectional Materials. Journal of Composite Materials, 1(2): 166–173, 4 1967. ISSN 0021-9983. doi: 10.1177/002199836700100206. URL https://www.researchgate.net/publication/43118082_Thermal_Conductivities_of_Unidirectional_Materials.

[75] L. S. Han and A. A. Cosner. Effective Thermal Conductivities of Fibrous Composites. Journal of Heat Transfer, 103(2):387–392, 5 1981. ISSN 15288943. doi: 10.1115/1.3244471.

[76] HJ OTT and OTT HJ. THERMAL CONDUCTIVITY OF COMPOSITE MATERIALS. THERMAL CONDUCTIVITY OF COMPOSITE MATERIALS, 1981.

[77] M R HENDERSON J. B; TANT. Measurement of thermal and kinetic properties of a glass-filled polymer composite to high temperatures. High Temperatures. High Pressures (Print), 1986. ISSN 0018-1544.

[78] S. N. Fitriah, M. S. Abdul Majid, M. J.M. Ridzuan, R. Daud, A. G. Gibson, and T. A. Assaleh. Influence of hydrothermal ageing on the compressive behaviour of glass fibre/epoxy composite pipes. Composite Structures, 159:350–360, 2017. ISSN 02638223. doi: 10.1016/j.compstruct.2016.09.078. URL http://dx.doi.org/10.1016/j.compstruct.2016.09.078.

[79] Jerome Paul Fanucci. Thermal Response of Radiantly Heated Kevlar and Graphite/Epoxy Composites. Journal of Composite Materials, 21(2):129–139, 2 1987. ISSN 0021-9983. doi: 10.1177/002199838702100204. URL http://journals.sagepub.com/doi/10.1177/002199838702100204.

[80] B. W. James, G. H. Wostenholm, G. S. Keen, and S. D. McIvor. Prediction and measurement of the thermal conductivity of composite materials. In Journal of Physics D: Applied Physics, volume 20, 1987. doi: 10.1088/0022-3727/20/3/004.

[81] C. R. Havis, G. P. Peterson, and L. S. Fletcher. Predicting the thermal conductivity and temperature distribution in aligned fiber composites. In Journal of Thermophysics and Heat Transfer, volume 3, 1989. doi: 10.2514/3.28767.

[82] James Brown, E Braun, and W Twilley. Cone Calorimeter Evaluation of the Flammability of Composite Materials., 1988. URL https://tsapps.nist.gov/publication/get_pdf.cfm?pub_id=917036.

[83] John Florio, Jack B. Henderson, and Frederick L. Test. Measurement of the thermochemical expansion of porous composite materials. High Temperatures - High Pressures, 21(2), 1989. ISSN 00181544.

[84] John Florio, Jack B. Henderson, Frederick L. Test, and Ramamurthy Hariharan. A study of the effects of the assumption of local-thermal equilibrium on the overall thermally-induced response of a decomposing, glass-filled polymer composite. International Journal of Heat and Mass Transfer, 34(1):135–147, 1 1991. ISSN 00179310. doi: 10.1016/0017-9310(91)90181-D.

[85] M. J. Scudamore. Fire performance studies on glass-reinforced plastic laminates. Fire and Materials, 18(5):313–325, 9 1994. ISSN 0308-0501. doi: 10.1002/fam.810180507. URL http://doi.wiley.com/10.1002/fam.810180507.

[86] J. R. Brown, P. D. Fawell, and Z. Mathys. Fire-hazard assessment of extended-chain polyethylene and aramid composites by cone calorimetry. Fire and Materials, 18(3):167–172, 5 1994. ISSN 0308-0501. doi: 10.1002/fam.810180304. URL http://doi.wiley.com/10.1002/fam.810180304.

[87] R. Frassine and A. Pavan. Viscoelastic effects on the interlaminar fracture behaviour of thermoplastic matrix composites: I. Rate and temperature dependence in unidirectional PEI/carbon-fibre laminates. Composites Science and Technology, 54(2):193–200, 1 1995. ISSN 02663538. doi: 10.1016/0266-3538(95)00051-8.

[88] Martin R. Tant, Hugh L. N. McManus, and Martin E. Rogers. High-Temperature Properties and Applications of Polymeric Materials. pages 1–20, 1995. doi: 10.1021/bk-1995-0603.ch001.

[89] J. R. Brown and Z. Mathys. Reinforcement and matrix effects on the combustion properties of glass reinforced polymer composites. Composites Part A: Applied Science and Manufacturing, 28(7):675–681, 1 1997. ISSN 1359835X. doi: 10.1016/S1359-835X(97)00018-3.

[90] S. Ritchie, K. Steckler, A. Hamins, T. Cleary, Jiann Yang, and T. Kashiwagi. The Effect Of Sample Size On The Heat Release Rate Of Charring Materials. Fire Safety Science, 5:177–188, 1997. ISSN 18174299. doi: 10.3801/iafss.fss.5-177.

[91] Fu-Yu Hshieh and Harold D. Beeson. Flammability Testing of Flame-retarded Epoxy Composites and Phenolic Composites. Fire and Materials, 21 (1):41–49, 1 1997. ISSN 0308-0501. doi: 10.1002/(SICI)1099-1018(199701)21:1<41::AID-FAM595>3.0.CO;2-G. URL https://onlinelibrary.wiley.com/doi/10.1002/(SICI)1099-1018(199701)21:1<41::AID-FAM595>3.0.CO;2-G.

[92] Ming Dao and Robert J. Asaro. A study on failure prediction and design criteria for fiber composites under fire degradation. Composites Part A: Applied Science and Manufacturing, 30(2):123–131, 2 1999. ISSN 1359835X. doi: 10.1016/S1359-835X(98)00051-7.

[93] C. A. Mahieux and K. L. Reifsnider. Property modeling across transition temperatures in polymers: A robust stiffness - Temperature model. Polymer, 42(7): 3281–3291, 3 2001. ISSN 00323861. doi: 10.1016/S0032-3861(00)00614-5.

[94] Georgios Kalogiannakis, Danny Van Hemelrijck, and Guy Van Assche. Measurements of thermal properties of carbon/epoxy and glass/epoxy using modulated temperature differential scanning calorimetry. Journal of Composite Materials, 38(2):163–175, 7 2004. ISSN 00219983. doi: 10.1177/0021998304038647. URL https://journals.sagepub.com/doi/10.1177/0021998304038647.

[95] Robert J. Asaro, Brian Lattimer, Chris Mealy, and George Steele. Thermophysical performance of a fire protective coating for naval ship structures. Composites Part A: Applied Science and Manufacturing, 40(1):11–18, 2009. ISSN 1359835X. doi: 10.1016/j.compositesa.2008.07.015. URL http://dx.doi.org/10.1016/j.compositesa.2008.07.015.

[96] F G Rastellini, S Oller, and E Oñate. Modelización numérica de la no-linealidad constitutiva de laminados compuestos. 1 2007. URL http://hdl.handle.net/2117/188907;https://www.scipedia.com/public/Rastellini_et_al_2019b;https://books.cimne.com/shop/modelizacion-numerica-de-la-no-linealidad-constitutiva-de-laminados/.

[97] D.J. Baker R.L. Foyer. Design of Orthotropic Laminates. In 11th Annual AIAA Conf. on Structures, Structural Dynamics and Materials, Denver, CO, USA, 4 1970.

[98] Robert M. Jones. Mechanics of composite materials. page 519.

[99] P. Lardeur and J. L. Batoz. Composite plate analysis using a new discrete shear triangular finite element. International Journal for Numerical Methods in Engineering, 27(2):343–359, 1989. doi: 10.1002/NME.1620270209.

[100] Stephen W. Tsai and H. Thomas Hahn. Introduction to Composite Materials. Introduction to Composite Materials, 5 2018. doi: 10.1201/9780203750148. URL https://www.taylorfrancis.com/books/mono/10.1201/9780203750148/introduction-composite-materials-stephen-tsai-thomas-hahn.

[101] J. N. Reddy. On refined computational models of composite laminates. International Journal for Numerical Methods in Engineering, 27(2):361–382, 9 1989. ISSN 1097-0207. doi: 10.1002/NME.1620270210. URL https://onlinelibrary.wiley.com/doi/full/10.1002/nme.1620270210https://onlinelibrary.wiley.com/doi/abs/10.1002/nme.1620270210https://onlinelibrary.wiley.com/doi/10.1002/nme.1620270210.

[102] S. Oller, E. Oñate, J. Miquel, and S. Botello. A plastic damage constitutive model for composite materials. International Journal of Solids and Structures, 33(17):2501–2518, 7 1996. ISSN 00207683. doi: 10.1016/0020-7683(95)00161-1. URL https://www.sciencedirect.com/science/article/pii/0020768395001611https://linkinghub.elsevier.com/retrieve/pii/0020768395001611.

[103] J. N. Reddy. Mechanics of laminated composite plates and shells : theory and analysis. page 831, 2004.

[104] P. D. Soden, M. J. Hinton, and A. S. Kaddour. Lamina properties, lay-up configurations and loading conditions for a range of fibre-reinforced composite laminates. Composites Science and Technology, 58(7), 1998. ISSN 02663538. doi: 10.1016/S0266-3538(98)00078-5.

[105] Salvador Botello, Eugenio Oñate, and Juan Miquel Canet. A layer-wise triangle for analysis of laminated composite plates and shells. Computers & Structures, 70(6):635–646, 3 1999. ISSN 0045-7949. doi: 10.1016/S0045-7949(98)00165-5.

[106] E. Car, F. Zalamea, S. Oller, J. Miquel, and E. Oñate. Numerical simulation of fiber reinforced composite materials - Two procedures. International Journal of Solids and Structures, 39(7), 2002. ISSN 00207683. doi: 10.1016/S0020-7683(01)00240-2.

[107] S. Oller, J. Miquel Canet, and F. Zalamea. Composite Material Behavior Using a Homogenization Double Scale Method. Journal of Engineering Mechanics, 131 (1), 2005. ISSN 0733-9399. doi: 10.1061/(asce)0733-9399(2005)131:1(65).

[108] O. A. Craig Bauchau. Structural analysis : with applications to aerospace structures. 2016.

[109] A. Eijo, E. Oñate, and S. Oller. A four-noded quadrilateral element for composite laminated plates/shells using the refined zigzag theory. International Journal for Numerical Methods in Engineering, 95(8), 2013. ISSN 00295981. doi: 10.1002/nme.4503.

[110] Daniele Versino, Marco Gherlone, Massimiliano Mattone, Marco Di Sciuva, and Alexander Tessler. C 0 triangular elements based on the Refined Zigzag Theory for multilayer composite and sandwich plates. Composites Part B: Engineering, 44(1), 2013. ISSN 13598368. doi: 10.1016/j.compositesb.2012.05.026.

[111] A. E. Green and P. M. Naghdi. A Dynamical theory of interacting continua. International Journal of Engineering Science, 3(2):231–241, 7 1965. ISSN 00207225. doi: 10.1016/0020-7225(65)90046-7.

[112] Robert L Taylor. Finite element analysis of linear shell problems. In Whiteman, JR (ed.), Proceedings of the Mathematics in Finite Elements and Applications, pages 191–203, 1987.

[113] O. C. Zienkiewicz, R. L. Taylor, and David Fox. The Finite Element Method for Solid and Structural Mechanics: Seventh Edition. 2013. doi: 10.1016/C2009-0-26332-X.

[114] R. Hill. Theory of mechanical properties of fibre-strengthened materials: II. Inelastic behaviour. Journal of the Mechanics and Physics of Solids, 12(4), 1964. ISSN 00225096. doi: 10.1016/0022-5096(64)90020-1.

[115] R. Hill. Theory of mechanical properties of fibre-strengthened materials: I. Elastic behaviour. Journal of the Mechanics and Physics of Solids, 12(4), 1964. ISSN 00225096. doi: 10.1016/0022-5096(64)90019-5.

[116] G. J. Dvorak and Y. A. Bahei-El-Din. Plasticity Analysis of Fibrous Composites. Journal of Applied Mechanics, 49(2):327–335, 6 1982. ISSN 0021-8936. doi: 10.1115/1.3162088.

[117] C. J. Wung and G. J. Dvorak. Strain-space plasticity analysis of fibrous composites. International Journal of Plasticity, 1(2):125–139, 1 1985. ISSN 0749-6419. doi: 10.1016/0749-6419(85)90024-5.

[118] R. Faria, J. Oliver, and M. Cervera. A strain-based plastic viscous-damage model for massive concrete structures. International Journal of Solids and Structures, 35(14):1533–1558, 1998. ISSN 00207683. doi: 10.1016/S0020-7683(97)00119-4. URL http://www.sciencedirect.com/science/article/pii/S0020768397001194.

[119] A. Puck and H. Schürmann. Failure analysis of FRP laminates by means of physically based phenomenological models. Composites Science and Technology, 58(7), 1998. ISSN 02663538. doi: 10.1016/S0266-3538(96)00140-6.

[120] E. Car, S. Oller, and E. Oñate. An anisotropic elastoplastic constitutive model for large strain analysis of fiber reinforced composite materials. Computer Methods in Applied Mechanics and Engineering, 185(2-4):245–277, 5 2000. ISSN 00457825. doi: 10.1016/S0045-7825(99)00262-5.

[121] A. Puck and H. Schürmann. Failure analysis of FRP laminates by means of physically based phenomenological models. Composites Science and Technology, 62(12-13 SPECIAL ISSUE):1633–1662, 2002. doi: 10.1016/S0266-3538(01)00208-1.

[122] A. S. Kaddour, M. J. Hinton, and P. D. Soden. A comparison of the predictive capabilities of current failure theories for composite laminates: Additional contributions. Composites Science and Technology, 64(3-4), 2004. ISSN 02663538. doi: 10.1016/S0266-3538(03)00226-4.

[123] Carmelo Militello and Carlos A. Felippa. The first ANDES elements: 9-dof plate bending triangles. Computer Methods in Applied Mechanics and Engineering, 93(2), 1991. ISSN 00457825. doi: 10.1016/0045-7825(91)90152-V.

[124] Carlos A. Felippa. A study of optimal membrane triangles with drilling freedoms. Computer Methods in Applied Mechanics and Engineering, 192(16-18): 2125–2168, 4 2003. ISSN 00457825. doi: 10.1016/S0045-7825(03)00253-6.

[125] J. Halpin. Effects of environmental factors on composite materials. Technical report, 1969.

[126] J. M. Whitney. The Effect of Transverse Shear Deformation on the Bending of Laminated Plates. Journal of Composite Materials, 3(3), 1969. ISSN 1530793X. doi: 10.1177/002199836900300316.

[127] L M Kachanov. Time of rupture process under creep conditions. Isv. Akad. Nauk. SSR. Otd Tekh. Nauk., 23, 1958.

[128] J. W. Ju. On energy-based coupled elastoplastic damage theories: Constitutive modeling and computational aspects. International Journal of Solids and Structures, 25(7), 1989. ISSN 00207683. doi: 10.1016/0020-7683(89)90015-2.

[129] Bibiana Luccioni, Sergio Oller, and Rodolfo Danesi. Coupled plastic-damaged model. Computer Methods in Applied Mechanics and Engineering, 129(1-2), 1996. ISSN 00457825. doi: 10.1016/0045-7825(95)00887-X.

[130] Lazar M. Kachanov. Rupture Time Under Creep Conditions. International Journal of Fracture, 97(1/4):11–18, 1999. ISSN 03769429. doi: 10.1023/A:1018671022008. URL http://link.springer.com/10.1023/A:1018671022008.

[131] Dusan Krajcinovic. Damage mechanics: Accomplishments, trends and needs. International Journal of Solids and Structures, 37(1-2), 2000. ISSN 00207683. doi: 10.1016/S0020-7683(99)00081-5.

[132] J. L. Bassani. Yield characterization of metals with transversely isotropic plastic properties. International Journal of Mechanical Sciences, 19(11), 1977. ISSN 00207403. doi: 10.1016/0020-7403(77)90070-4.

[133] R. Hill. Theoretical plasticity of textured aggregates. Mathematical Proceedings of the Cambridge Philosophical Society, 85(1), 1979. ISSN 14698064. doi: 10.1017/S0305004100055596.

[134] F. Barlat and K. Lian. Plastic behavior and stretchability of sheet metals. Part I: A yield function for orthotropic sheets under plane stress conditions. International Journal of Plasticity, 5(1), 1989. ISSN 07496419. doi: 10.1016/0749-6419(89)90019-3.

[135] R. Hill. Constitutive modelling of orthotropic plasticity in sheet metals. Journal of the Mechanics and Physics of Solids, 38(3), 1990. ISSN 00225096. doi: 10.1016/0022-5096(90)90006-P.

[136] Sergio Oller, Eduardo Car, and Jacob Lubliner. Definition of a general implicit orthotropic yield criterion. Computer Methods in Applied Mechanics and Engineering, 192(7-8), 2003. ISSN 00457825. doi: 10.1016/S0045-7825(02)00605-9.

[137] C. F. Shih and D. Lee. Further developments in anisotropic plasticity. Journal of Engineering Materials and Technology, Transactions of the ASME, 100(3), 1978. ISSN 15288889. doi: 10.1115/1.3443493.

[138] M. A. Eisenberg and Chian Fong Yen. The anisotropic deformation of yield surfaces. Journal of Engineering Materials and Technology, Transactions of the ASME, 106(4), 1984. ISSN 15288889. doi: 10.1115/1.3225730.

[139] George Z. Voyiadjis and Ganesh Thiagarajan. Micro and macro anisotropic cyclic damage-plasticity models for MMCs. International Journal of Engineering Science, 35(5), 1997. ISSN 00207225. doi: 10.1016/s0020-7225(96)00125-5.

[140] Jean-Louis Chaboche. A Continuum Damage Theory with Anisotropic and Unilateral Damage. Rech. Aérospatiale, (2), 1995.

[141] Jean Lemaitre and Jean-Louis. Chaboche. Mechanics of solid materials. Cambridge University Press, 1990. ISBN 9781139167970.

[142] George Z. Voyiadjis and Babur Deliktas. A coupled anisotropic damage model for the inelastic response of composite materials. Computer Methods in Applied Mechanics and Engineering, 183(3-4), 2000. ISSN 00457825. doi: 10.1016/S0045-7825(99)00218-2.

[143] Bibiana Luccioni and Sergio Oller. A directional damage model. Computer Methods in Applied Mechanics and Engineering, 192(9-10), 2003. ISSN 00457825. doi: 10.1016/S0045-7825(02)00577-7.

[144] Jacob Aboudi. Micromechanical Analysis of Composites by the Method of Cells. Applied Mechanics Reviews, 42(7):193–221, 7 1989. ISSN 0003-6900. doi: 10.1115/1.3152428.

[145] Jacob Aboudi. Micromechanical Analysis of Composites by the Method of Cells - Update. Applied Mechanics Reviews, 49(10S):S83–S91, 10 1996. ISSN 0003-6900. doi: 10.1115/1.3101981.

[146] Zvi Hashin. The Elastic Moduli of Heterogeneous Materials. Journal of Applied Mechanics, 29(1):143–150, 3 1962. ISSN 0021-8936. doi: 10.1115/1.3636446.

[147] B. Budiansky. On the elastic moduli of some heterogeneous materials. Journal of the Mechanics and Physics of Solids, 13(4):223–227, 8 1965. ISSN 0022-5096. doi: 10.1016/0022-5096(65)90011-6.

[148] J. D. Eshelby. The Continuum Theory of Lattice Defects. Solid State Physics - Advances in Research and Applications, 3(C):79–144, 1 1956. ISSN 0081-1947. doi: 10.1016/S0081-1947(08)60132-0.

[149] J. D. Eshelby. The determination of the elastic field of an ellipsoidal inclusion, and related problems. Proceedings of the Royal Society of London. Series A. Mathematical and Physical Sciences, 241(1226), 1957. ISSN 0080-4630. doi: 10.1098/rspa.1957.0133.

[150] L. Banks-Sills and V. Leiderman. Macro-mechanical material model for fiber reinforced metal matrix composites. Composites Part B: Engineering, 30(5), 1999. ISSN 13598368. doi: 10.1016/S1359-8368(99)00018-9.

[151] C. Truesdell and R. Toupin. The Classical Field Theories. In S Flügge, editor, Principles of Classical Mechanics and Field Theory / Prinzipien der Klassischen Mechanik und Feldtheorie, pages 226–858. Springer Berlin Heidelberg, Berlin, Heidelberg, 1960. ISBN 978-3-642-45943-6. doi: 10.1007/978-3-642-45943-6{_}2. URL http://link.springer.com/10.1007/978-3-642-45943-6_2.

[152] W. J. Drugan and J. R. Willis. A micromechanics-based nonlocal constitutive equation and estimates of representative volume element size for elastic composites. Journal of the Mechanics and Physics of Solids, 44(4):497–524, 4 1996. ISSN 0022-5096. doi: 10.1016/0022-5096(96)00007-5.

[153] K. Alzebdeh and M. Ostoja-Starzewski. Micromechanically based stochastic finite elements: Length scales and anisotropy. Probabilistic Engineering Mechanics, 11(4):205–214, 1996. ISSN 0266-8920. doi: 10.1016/0266-8920(96)00015-X. URL https://squ.pure.elsevier.com/en/publications/micromechanically-based-stochastic-finite-elements-length-scales-.

[154] E. Oñate and E. Una generalización de la teoría de mezclas clásica para el tratamiento de compuestos en serie/paralelo. 12 1995. URL http://portalrecerca.csuc.cat/50303487.

[155] T. Mori and K. Tanaka. Average stress in matrix and average elastic energy of materials with misfitting inclusions. Acta Metallurgica, 21(5):571–574, 5 1973. ISSN 0001-6160. doi: 10.1016/0001-6160(73)90064-3.

[156] Y. Benveniste. A new approach to the application of Mori-Tanaka's theory in composite materials. Mechanics of Materials, 6(2):147–157, 6 1987. ISSN 0167-6636. doi: 10.1016/0167-6636(87)90005-6.

[157] S. J. Hollister and N. Kikuchi. A comparison of homogenization and standard mechanics analyses for periodic porous composites. Computational Mechanics 1992 10:2, 10(2):73–95, 3 1992. ISSN 1432-0924. doi: 10.1007/BF00369853. URL https://link.springer.com/article/10.1007/BF00369853.

[158] G. L. Povirk. Incorporation of microstructural information into models of two-phase materials. Acta Metallurgica et Materialia, 43(8):3199–3206, 8 1995. ISSN 0956-7151. doi: 10.1016/0956-7151(94)00487-3.

[159] Somnath Ghosh, Kyunghoon Lee, and Suresh Moorthy. Multiple scale analysis of heterogeneous elastic structures using homogenization theory and voronoi cell finite element method. International Journal of Solids and Structures, 32(1): 27–62, 1995. doi: 10.1016/0020-7683(94)00097-G.

[160] K Terada and N Kikuchi. Nonlinear homogenization method for practical applications. American Society of Mechanical Engineers, Applied Mechanics Division, AMD, 212:1–16, 12 1995. ISSN 0160-8835.

[161] Somnath Ghosh, Kyunghoon Lee, and Suresh Moorthy. Two scale analysis of heterogeneous elastic-plastic materials with asymptotic homogenization and Voronoi cell finite element model. Computer Methods in Applied Mechanics and Engineering, 132(1-2):63–116, 5 1996. ISSN 0045-7825. doi: 10.1016/0045-7825(95)00974-4.

[162] R. J.M. Smit, W. A.M. Brekelmans, and H. E.H. Meijer. Prediction of the mechanical behavior of nonlinear heterogeneous systems by multi-level finite element modeling. Computer Methods in Applied Mechanics and Engineering, 155 (1-2):181–192, 3 1998. ISSN 0045-7825. doi: 10.1016/S0045-7825(97)00139-4.

[163] H. Moulinec and P. Suquet. A numerical method for computing the overall response of nonlinear composites with complex microstructure. Computer Methods in Applied Mechanics and Engineering, 157(1-2):69–94, 4 1998. doi: 10.1016/S0045-7825(97)00218-1.

[164] Jacob Fish, Qing Yu, and Kamlun Shek. Computational damage mechanics for composite materials based on mathematical homogenization. International Journal for Numerical Methods in Engineering, 45(11), 1999. ISSN 00295981. doi: 10.1002/(SICI)1097-0207(19990820)45:11<1657::AID-NME648>3.0.CO;2-H.

[165] O. van der Sluis, P. J.G. Schreurs, and H. E.H. Meijer. Effective properties of a viscoplastic constitutive model obtained by homogenization. Mechanics of Materials, 31(11), 1999. ISSN 01676636. doi: 10.1016/S0167-6636(99)00028-9.

[166] Frédéric Feyel and Jean Louis Chaboche. FE 2 multiscale approach for modelling the elastoviscoplastic behaviour of long fibre SiC/Ti composite materials. Computer Methods in Applied Mechanics and Engineering, 183(3-4), 2000. ISSN 00457825. doi: 10.1016/S0045-7825(99)00224-8.

[167] F. Zalamea, J. Miquel Canet, and S. Oller. A double scale method for simulating of periodic composite materials. In European Congress on Computational Methods in Applied Sciences and Engineering, ECCOMAS 2000, 2000.

[168] Frédéric Feyel. A multilevel finite element method (FE2) to describe the response of highly non-linear structures using generalized continua. Computer Methods in Applied Mechanics and Engineering, 192(28-30), 2003. ISSN 00457825. doi: 10.1016/S0045-7825(03)00348-7.

[169] A. Toledano and H. Murakami. A high-order mixture model for periodic particulate composites. International Journal of Solids and Structures, 23(7):989–1002, 1 1987. ISSN 0020-7683. doi: 10.1016/0020-7683(87)90092-8.

[170] J. C. Michel, H. Moulinec, and P. Suquet. Effective properties of composite materials with periodic microstructure: A computational approach. Computer Methods in Applied Mechanics and Engineering, 172(1-4), 1999. ISSN 00457825. doi: 10.1016/S0045-7825(98)00227-8.

[171] L. L. Graham and S. C. Baxter. Simulation of local material properties based on moving-window GMC. Probabilistic Engineering Mechanics, 16(4), 2001. ISSN 02668920. doi: 10.1016/S0266-8920(01)00022-4.

[172] R. Hill. A self-consistent mechanics of composite materials. Journal of the Mechanics and Physics of Solids, 13(4):213–222, 8 1965. ISSN 0022-5096. doi: 10.1016/0022-5096(65)90010-4.

[173] S. Feih, Z. Mathys, A.G. Gibson, and A.P. Mouritz. Modeling Compressive Skin Failure of Sandwich Composites in Fire:. http://dx.doi.org/10.1177/1099636207082307, 5 2008. doi: 10.1177/1099636207082307. URL https://journals.sagepub.com/doi/10.1177/1099636207082307.

[174] S. Feih, A. P. Mouritz, Z. Mathys, and A. G. Gibson. Fire structural modeling of polymer composites with passive thermal barrier. Journal of Fire Sciences, 28 (2):141–160, 2010. ISSN 07349041. doi: 10.1177/0734904109340878.

[175] S. Feih, E. Boiocchi, G. Mathys, Z. Mathys, A. G. Gibson, and A. P. Mouritz. Mechanical properties of thermally-treated and recycled glass fibres. Composites Part B: Engineering, 42(3):350–358, 2011. ISSN 13598368. doi: 10.1016/j.compositesb.2010.12.020. URL http://dx.doi.org/10.1016/j.compositesb.2010.12.020.

[176] S. Feih and A. P. Mouritz. Tensile properties of carbon fibres and carbon fibre-polymer composites in fire. Composites Part A: Applied Science and Manufacturing, 43(5):765–772, 2012. ISSN 1359835X. doi: 10.1016/j.compositesa.2011.06.016. URL http://dx.doi.org/10.1016/j.compositesa.2011.06.016.

[177] S. Feih, A. P. Mouritz, and S. W. Case. Determining the mechanism controlling glass fibre strength loss during thermal recycling of waste composites. Composites Part A: Applied Science and Manufacturing, 76:255–261, 2015. ISSN 1359835X. doi: 10.1016/j.compositesa.2015.06.006. URL http://dx.doi.org/10.1016/j.compositesa.2015.06.006.

[178] Robert J. Asaro, Brian Lattimer, and William Ramroth. Structural response of FRP composites during fire. Composite Structures, 87(4):382–393, 2 2009. ISSN 02638223. doi: 10.1016/j.compstruct.2008.02.018. URL https://linkinghub.elsevier.com/retrieve/pii/S0263822308000482.

[179] Pei Gu and R. J. Asaro. Structural buckling of polymer matrix composites due to reduced stiffness from fire damage. Composite Structures, 69(1):65–75, 2005. ISSN 02638223. doi: 10.1016/j.compstruct.2004.05.016.

[180] Pei Gu and R. J. Asaro. Designing polymer matrix composite panels for structural integrity in fire. Composite Structures, 84(4):300–309, 8 2008. ISSN 02638223. doi: 10.1016/j.compstruct.2007.08.006.

[181] Pei Gu and R. J. Asaro. Distortion of polymer matrix composite panels under transverse thermal gradients. Composite Structures, 82(3):413–421, 2 2008. ISSN 02638223. doi: 10.1016/j.compstruct.2007.01.020.

[182] Pei Gu and R. J. Asaro. Wrinkling of sandwich polymer matrix composite panels under transverse thermal gradients. Fire Safety Journal, 43(2):151–160, 2 2008. ISSN 03797112. doi: 10.1016/j.firesaf.2007.06.003.

[183] Pei Gu and R. J. Asaro. Designing sandwich polymer matrix composite panels for structural integrity in fire. Composite Structures, 88(3):461–467, 5 2009. ISSN 02638223. doi: 10.1016/j.compstruct.2008.05.006.

[184] Pei Gu, Ming Dao, and R. J. Asaro. Structural stability of polymer matrix composite panels in fire. Marine Structures, 22(3):354–372, 2009. ISSN 09518339. doi: 10.1016/j.marstruc.2009.04.001. URL http://dx.doi.org/10.1016/j.marstruc.2009.04.001.

[185] Pei Gu and R. J. Asaro. Skin wrinkling of sandwich polymer matrix composite panels subjected to fire exposure. Thin-Walled Structures, 51:139–146, 2012. ISSN 02638231. doi: 10.1016/j.tws.2011.10.008. URL http://dx.doi.org/10.1016/j.tws.2011.10.008.

[186] C. I. Chang. Thermal effects on polymer composite structures. Theoretical and Applied Fracture Mechanics, 6(2):113–120, 10 1986. ISSN 01678442. doi: 10.1016/0167-8442(86)90031-5.

[187] Jason R Maddocks and Hugh L Mcmanus. Prediction of Microcracking in Composite Laminates Under Thermomechanical Loading. (November), 1995.

[188] Sunpyo Lee, Nicholas J. Salamon, and Roy M. Sullivan. Finite element analysis of poroelastic composites undergoing thermal and gas diffusion. Journal of Thermophysics and Heat Transfer, 10(4):672–680, 1996. ISSN 15336808. doi: 10.2514/3.844.

[189] C H Park and H L McManus. Thermally Induced Damage in Composite Space Structure: Predictive Methodology And Experimental Correlation. Composites Science and Technology, 56(February 1994):1209–1219, 1996.

[190] Yu I. Dimitrienko. Thermomechanical behaviour of composite materials and structures under high temperatures: 1. Materials. Composites Part A: Applied Science and Manufacturing, 28(5):453–461, 1 1997. ISSN 1359835X. doi: 10.1016/S1359-835X(96)00144-3.

[191] Yu I. Dimitrienko. Thermomechanical behaviour of composite materials and structures under high temperatures: 2. Structures. Composites Part A: Applied Science and Manufacturing, 28(5):463–471, 1 1997. ISSN 1359835X. doi: 10.1016/S1359-835X(96)00145-5.

[192] Yu I. Dimitrienko. Dynamic transport phenomena in porous polymer materials under impulse thermal effects. Transport in Porous Media, 35(3):299–326, 1999. ISSN 01693913. doi: 10.1023/A:1006508227447.

[193] Yu I. Dimitrienko. Thermomechanical behaviour of composites under local intense heating by irradiation. Composites Part A: Applied Science and Manufacturing, 31(6):591–598, 2000. ISSN 1359835X. doi: 10.1016/S1359-835X(99)00094-9.

[194] Christopher T. Key and James Lua. Constituent based analysis of composite materials subjected to fire conditions. Composites Part A: Applied Science and Manufacturing, 37(7):1005–1014, 7 2006. ISSN 1359835X. doi: 10.1016/j.compositesa.2005.03.022.

[195] W. T. Ramroth, R. J. Asaro, B. Zhu, and P. Krysl. Finite element modelling of fire degraded FRP composite panels using a rate dependent constitutive model. Composites Part A: Applied Science and Manufacturing, 37(7):1015–1023, 2006. ISSN 1359835X. doi: 10.1016/j.compositesa.2005.04.010.

[196] Kevin Mcgrattan, Simo Hostikka, Randall Mcdermott, Jason Floyd, Craig Weinschenk, and Kristopher Overholt. NIST Special Publication 1018 Sixth Edition Fire Dynamics Simulator Technical Reference Guide Volume 1: Mathematical Model. Technical report.

[197] Kuldeep Prasad and Howard R. Baum. Coupled fire dynamics and thermal response of complex building structures. Proceedings of the Combustion Institute, 30(2):2255–2262, 1 2005. ISSN 15407489. doi: 10.1016/j.proci.2004.08.118.

[198] Changsong Luo and Paul E. DesJardin. Thermo-mechanical damage modeling of a glass-phenolic composite material. Composites Science and Technology, 67 (7-8):1475–1488, 6 2007. ISSN 02663538. doi: 10.1016/j.compscitech.2006.07.030.

[199] James Lua. Thermal-mechanical cell model for unbalanced plain weave woven fabric composites. Composites Part A: Applied Science and Manufacturing, 38(3):1019–1037, 3 2007. ISSN 1359835X. doi: 10.1016/j.compositesa.2006.06.023.

[200] C. Luo and P. E. DesJardin. Evaluation of thermal transport properties using a micro-cracking model for woven composite laminates. ICCM International Conferences on Composite Materials, 2009.

[201] A. E. Elmughrabi, A. M. Robinson, and A. G. Gibson. Effect of stress on the fire reaction properties of polymer composite laminates. In Engineering Against Fracture - Proceedings of the 1st Conference, pages 137–154. Springer Science+Business Media B.V., 2009. ISBN 9781402094019. doi: 10.1007/978-1-4020-9402-6{_}12. URL https://link.springer.com/chapter/10.1007/978-1-4020-9402-6_12.

[202] Changsong Luo, Wei Xie, and Paul E. DesJardin. Fluid-Structure Simulations of Composite Material Response for Fire Environments. Fire Technology, 47(4): 887–912, 10 2011. ISSN 00152684. doi: 10.1007/s10694-009-0126-4. URL https://link.springer.com/article/10.1007/s10694-009-0126-4.

[203] Changsong Luo, Wei Xie, and Paul E. DesJardin. Fluid-Structure Simulations of Composite Material Response for Fire Environments. Fire Technology, 47(4): 887–912, 10 2011. ISSN 00152684. doi: 10.1007/s10694-009-0126-4. URL https://link.springer.com/article/10.1007/s10694-009-0126-4.

[204] A. P. Mouritz, S. Feih, Z. Mathys, and A. G. Gibson. Mechanical Property Degradation of Naval Composite Materials. Fire Technology, 47(4):913–939, 2011. ISSN 00152684. doi: 10.1007/s10694-009-0125-5.

[205] E. Kandare, G. J. Griffin, S. Feih, A. G. Gibson, B. Y. Lattimer, and A. P. Mouritz. Fire structural modelling of fibre-polymer laminates protected with an intumescent coating. Composites Part A: Applied Science and Manufacturing, 43(5): 793–802, 2012. ISSN 1359835X. doi: 10.1016/j.compositesa.2011.05.012. URL http://dx.doi.org/10.1016/j.compositesa.2011.05.012.

[206] A. P. Mouritz, S. Feih, E. Kandare, and A. G. Gibson. Thermal-mechanical modelling of laminates with fire protection coating. Composites Part B: Engineering, 48:68–78, 2013. ISSN 13598368. doi: 10.1016/j.compositesb.2012.12.001. URL http://dx.doi.org/10.1016/j.compositesb.2012.12.001.

[207] Gregory A. Pering, Patrick V. Farrell, and George S. Springer. DEGRADATION OF TENSILE AND SHEAR PROPERTEIS OF COMPOSITES EXPOSED TO FIRE OR HIGH TEMPERATURE. Journal of Composite Materials, 14(1), 1980. ISSN 00219983.

[208] C.A. Griffis, J.A. Nemes, F.R. Stonesifer, and C.I. Chang. Degradation in Strength of Laminated Composites Subjected to Intense Heating and Mechanical Loading. Journal of Composite Materials, 20(3):216–235, 5 1986. ISSN 0021-9983. doi: 10.1177/002199838602000301. URL http://journals.sagepub.com/doi/10.1177/002199838602000301.

[209] B. Budiansky and N. A. Fleck. Compressive failure of fibre composites. Journal of the Mechanics and Physics of Solids, 41(1):183–211, 1993. ISSN 00225096. doi: 10.1016/0022-5096(93)90068-Q.

[210] Hugh L. Mcmanus, David E. Bowles, and Stephen S. Tompkins. Prediction of Thermal Cycling Induced Matrix Cracking. Journal of Reinforced Plastics and Composites, 15(2):124–140, 2 1996. ISSN 0731-6844. doi: 10.1177/073168449601500201. URL http://journals.sagepub.com/doi/10.1177/073168449601500201.

[211] Cecelia H. Park and Hugh L. McManus. Thermally induced damage in composite laminates: Predictive methodology and experimental investigation. Composites Science and Technology, 56(10):1209–1219, 1996. ISSN 02663538. doi: 10.1016/S0266-3538(96)00089-9.

[212] Yu I. Dimitrienko. A structural thermo-mechanical model of textile composite materials at high temperatures. Composites Science and Technology, 59(7):1041–1053, 1999. ISSN 02663538. doi: 10.1016/S0266-3538(98)00144-4.

[213] A. P. Mouritz and Z. Mathys. Post-fire mechanical properties of glass-reinforced polyester composites. Composites Science and Technology, 61(4):475–490, 3 2001. ISSN 02663538. doi: 10.1016/S0266-3538(00)00204-9.

[214] C. P. Gardiner, Z. Mathys, and A. P. Mouritz. Tensile and compressive properties of FRP composites with localised fire damage. Applied Composite Materials, 9(6):353–367, 11 2002. ISSN 0929189X. doi: 10.1023/A:1020204913612. URL https://link.springer.com/article/10.1023/A:1020204913612.

[215] A. P. Mouritz and C. P. Gardiner. Compression properties of fire-damaged polymer sandwich composites. Composites - Part A: Applied Science and Manufacturing, 33(5):609–620, 5 2002. ISSN 1359835X. doi: 10.1016/S1359-835X(02)00022-2.

[216] A. P. Mouritz. Post-fire flexural properties of fibre-reinforced polyester, epoxy and phenolic composites. Journal of Materials Science, 37(7):1377–1386, 4 2002. ISSN 00222461. doi: 10.1023/A:1014520628915. URL https://link.springer.com/article/10.1023/A:1014520628915.

[217] Anders Sjögren and Leif E. Asp. Effects of temperature on delamination growth in a carbon/epoxy composite under fatigue loading. International Journal of Fatigue, 24(2-4):179–184, 2 2002. ISSN 01421123. doi: 10.1016/S0142-1123(01)00071-8.

[218] Celine A. Mahieux and K. L. Reifsnider. Property modeling across transition temperatures in polymers: Application to thermoplastic systems. Journal of Materials Science, 37(5):911–920, 2002. ISSN 00222461. doi: 10.1023/A:1014383427444. URL https://link.springer.com/article/10.1023/A:1014383427444.

[219] A. P. Mouritz. Fire resistance of aircraft composite laminates. Journal of Materials Science Letters, 22(21):1507–1509, 11 2003. ISSN 02618028. doi: 10.1023/A:1026103231041. URL https://link.springer.com/article/10.1023/A:1026103231041.

[220] A. P. Mouritz. Simple models for determining the mechanical properties of burnt FRP composites. Materials Science and Engineering A, 359(1-2):237–246, 10 2003. ISSN 09215093. doi: 10.1016/S0921-5093(03)00351-4.

[221] A. G. Gibson, P. N.H. Wright, Y. S. Wu, A. P. Mouritz, Z. Mathys, and C. P. Gardiner. Modelling residual mechanical properties of polymer composites after fire. In Plastics, Rubber and Composites, volume 32, pages 81–90. IOM Communications Ltd., 2003. doi: 10.1179/146580103225009040. URL https://www.tandfonline.com/doi/abs/10.1179/146580103225009040.

[222] C. P. Gardiner, Z. Mathys, and A. P. Mouritz. Post-fire structural properties of burnt GRP plates. Marine Structures, 17(1):53–73, 1 2004. ISSN 09518339. doi: 10.1016/j.marstruc.2004.03.003.

[223] John V. Bausano, Steven E. Boyd, John J. Lesko, and Scott W. Case. Composite life under sustained compression and one sided simulated fire exposure: Characterization and prediction. In International SAMPE Technical Conference, volume 12, pages 1393–1407. De Gruyter, 6 2004. doi: 10.1515/secm.2005.12.1-2.131. URL https://www.degruyter.com/document/doi/10.1515/SECM.2005.12.1-2.131/html.

[224] John V. Bausano, John J. Lesko, and Scott W. Case. Composite life under sustained compression and one sided simulated fire exposure: Characterization and prediction. Composites Part A: Applied Science and Manufacturing, 37(7):1092–1100, 7 2006. ISSN 1359835X. doi: 10.1016/j.compositesa.2005.06.013.

[225] L. Liu, G. A. Kardomateas, V. Birman, J. W. Holmes, and G. J. Simitses. Thermal buckling of a heat-exposed, axially restrained composite column.

Composites Part A: Applied Science and Manufacturing, 37(7):972–980, 7 2006. ISSN 1359835X. doi: 10.1016/j.compositesa.2005.04.006.

[226] A. G. Gibson, Y. S. Wu, J. T. Evans, and A. P. Mouritz. Laminate theory analysis of composites under load in fire. Journal of Composite Materials, 40(7):639–658, 4 2006. ISSN 00219983. doi: 10.1177/0021998305055543. URL https://journals.sagepub.com/doi/10.1177/0021998305055543.

[227] Steven E. Boyd, John J. Lesko, and Scott W. Case. Compression creep rupture behavior of a glass/vinyl ester composite laminate subject to fire loading conditions. Composites Science and Technology, 67(15-16):3187–3195, 12 2007. ISSN 02663538. doi: 10.1016/j.compscitech.2007.04.009.

[228] R. C. Easby, S. Feih, C. Konstantis, G. La Delfa, V. Urso Miano, A. Elmughrabi, A. P. Mouritz, and A. G. Gibson. Failure model for phenolic and polyester pultrusions under load in fire. Plastics, Rubber and Composites, 36(9):379–388, 2007. ISSN 14658011. doi: 10.1179/174328907X248212. URL https://www.tandfonline.com/doi/abs/10.1179/174328907X248212.

[229] Z. Zhang, S. W. Case, and J. Lua. A model and finite element implementation for the thermo-mechanical analysis of polymer composites exposed to fire. ICCM International Conferences on Composite Materials, 2009.

[230] P. T. Summers, B. Y. Lattimer, and S. Feih. Time-to-failure predictions for polymer laminates in fire. ICCM International Conferences on Composite Materials, 2009.

[231] L. A. Burns, S. Feih, and A. P. Mouritz. Compression failure of carbon fiber-epoxy laminates in fire. Journal of Aircraft, 47(2):528–533, 2010. ISSN 15333868. doi: 10.2514/1.45065.

[232] Thomas Goodrich, Nadia Nawaz, Stefanie Feih, Brian Y. Lattimer, and Adrian P. Mouritz. High-temperature mechanical properties and thermal recovery of balsa wood. Journal of Wood Science, 56(6):437–443, 2010. ISSN 14350211. doi: 10.1007/s10086-010-1125-2.

[233] M. L. Scott, D. J. Elder, S. Feih, A. J. Gunnion, X. L. Liu, and R. S. Thomson. Engineering solutions for complex composite material behaviour spanning time and temperature scales. Philosophical Magazine, 90(31-32):4153–4174, 2010. ISSN 14786435. doi: 10.1080/14786431003745377.

[234] Steven E. Boyd, John V. Bausano, Scott W. Case, and John J. Lesko. Mechanistic Approach to Structural Fire Modeling of Composites. Fire Technology, 47(4):941–983, 10 2011. ISSN 00152684. doi: 10.1007/s10694-009-0122-8. URL https://link.springer.com/article/10.1007/s10694-009-0122-8.

[235] P. Clifton, A. Subic, and A. Mouritz. Structural model for prediction of thermo-mechanical properties of fabric sandwich composites. Proceedings of the Institution of Mechanical Engineers, Part C: Journal of Mechanical Engineering Science, 225(11):2525–2536, 2011. ISSN 09544062. doi: 10.1177/0954406211406200.

[236] Patrick Summers, Brian Lattimer, Scott Case, and Stefanie Feih. Sensitivity analysis of a thermo-structural model for materials in fire. Fire Safety Science, (January):1165–1178, 2011. ISSN 18174299. doi: 10.3801/IAFSS.FSS.10-1165.

[237] A. G. Gibson, Tna Browne, S. Feih, and A. P. Mouritz. Modeling composite high temperature behavior and fire response under load. Journal of Composite Materials, 46(16):2005–2022, 2012. ISSN 00219983. doi: 10.1177/0021998311429383.

[238] P. T. Summers, B. Y. Lattimer, S. Case, and S. Feih. Predicting compression failure of composite laminates in fire. Composites Part A: Applied Science and Manufacturing, 43(5):773–782, 2012. ISSN 1359835X. doi: 10.1016/j.compositesa.2012.02.003. URL http://dx.doi.org/10.1016/j.compositesa.2012.02.003.

[239] P. T. Summers, B. Y. Lattimer, S. Case, and S. Feih. Sensitivity of thermo-structural model for composite laminates in fire. Composites Part A: Applied Science and Manufacturing, 43(5):783–792, 2012. ISSN 1359835X. doi: 10.1016/j.compositesa.2012.01.006. URL http://dx.doi.org/10.1016/j.compositesa.2012.01.006.

[240] A. Anjang, V. S. Chevali, E. Kandare, A. P. Mouritz, and S. Feih. Tension modelling and testing of sandwich composites in fire. Composite Structures, 113 (1):437–445, 2014. ISSN 02638223. doi: 10.1016/j.compstruct.2014.03.016. URL http://dx.doi.org/10.1016/j.compstruct.2014.03.016.

[241] T. Bhat, V. Chevali, X. Liu, S. Feih, and A. P. Mouritz. Fire structural resistance of basalt fibre composite. Composites Part A: Applied Science and Manufacturing, 71:107–115, 2015. ISSN 1359835X. doi: 10.1016/j.compositesa.2015.01.006. URL http://dx.doi.org/10.1016/j.compositesa.2015.01.006.

[242] A. Anjang, V. S. Chevali, B. Y. Lattimer, S. W. Case, S. Feih, and A. P. Mouritz. Post-fire mechanical properties of sandwich composite structures. Composite Structures, 132:1019–1028, 2015. ISSN 02638223. doi: 10.1016/j.compstruct.2015.07.009. URL http://dx.doi.org/10.1016/j.compstruct.2015.07.009.

[243] Tanmay S. Bhat, Venkata S. Chevali, and Adrian P. Mouritz. Fire structural performance of flax fibre reinforced laminates. ICCM International Conferences on Composite Materials, 2015-July(June 2017), 2015.

[244] A. Anjang, V. S. Chevali, S. Feih, and A. P. Mouritz. Deterioration of the fire structural resistance of sandwich composite under tension due to water absorption. Composites Part A: Applied Science and Manufacturing, 87:263–270, 2016. ISSN 1359835X. doi: 10.1016/j.compositesa.2016.05.008. URL http://dx.doi.org/10.1016/j.compositesa.2016.05.008.

[245] M. J.M. Ridzuan, M. S.Abdul Majid, M. Afendi, M. N. Mazlee, and A. G. Gibson. Thermal behaviour and dynamic mechanical analysis of Pennisetum purpureum/glass-reinforced epoxy hybrid composites. Composite Structures, 152:850–859, 2016. ISSN 02638223. doi: 10.1016/j.compstruct.2016.06.026. URL http://dx.doi.org/10.1016/j.compstruct.2016.06.026.

[246] K. Grigoriou and A. P. Mouritz. Influence of ply stacking pattern on the structural properties of quasi-isotropic carbon-epoxy laminates in fire. Composites Part A: Applied Science and Manufacturing, 99:113–120, 2017. ISSN 1359835X. doi: 10.1016/j.compositesa.2017.04.008. URL http://dx.doi.org/10.1016/j.compositesa.2017.04.008.

[247] A. Anjang, A. P. Mouritz, and S. Feih. Influence of fibre orientation on the tensile performance of sandwich composites in fire. Composites Part A: Applied Science and Manufacturing, 100:342–351, 2017. ISSN 1359835X. doi: 10.1016/j.compositesa.2017.05.028. URL http://dx.doi.org/10.1016/j.compositesa.2017.05.028.

[248] T. Bhat, E. Kandare, A. G. Gibson, P. Di Modica, and A. P. Mouritz. Tensile properties of plant fibre-polymer composites in fire. Fire and Materials, 41(8):1040–1050, 12 2017. ISSN 10991018. doi: 10.1002/fam.2446. URL https://onlinelibrary.wiley.com/doi/full/10.1002/fam.2446https://onlinelibrary.wiley.com/doi/abs/10.1002/fam.2446https://onlinelibrary.wiley.com/doi/10.1002/fam.2446.

[249] R. Revati, M. S. Abdul Majid, M. J.M. Ridzuan, M. Normahira, N. F. Mohd Nasir, M. N. Rahman Y., and A. G. Gibson. Mechanical, thermal and morphological characterisation of 3D porous Pennisetum purpureum/PLA biocomposites scaffold. Materials Science and Engineering C, 75:752–759, 2017. ISSN 09284931. doi: 10.1016/j.msec.2017.02.127. URL http://dx.doi.org/10.1016/j.msec.2017.02.127.

[250] T. Bhat, D. Fortomaris, E. Kandare, and A. P. Mouritz. Properties of thermally recycled basalt fibres and basalt fibre composites. Journal of Materials Science, 53(3):1933–1944, 2018. ISSN 15734803. doi: 10.1007/s10853-017-1672-7.

[251] K. Grigoriou and A. P. Mouritz. Modelling and testing of fibre metal laminates and their constituent materials in fire. Composite Structures, 200(May):25–35, 2018. ISSN 02638223. doi: 10.1016/j.compstruct.2018.05.106. URL https://doi.org/10.1016/j.compstruct.2018.05.106.

[252] M. J.M. Ridzuan, M. S. Abdul Majid, A. Khasri, K. S. Basaruddin, and A. G. Gibson. Effect of moisture exposure and elevated temperatures on impact response of Pennisetum purpureum/glass-reinforced epoxy (PGRE) hybrid composites. Composites Part B: Engineering, 160:84–93, 2019. ISSN 13598368. doi: 10.1016/j.compositesb.2018.10.029. URL https://doi.org/10.1016/j.compositesb.2018.10.029.

[253] Andrew H. Buchanan and Anthony K. Abu. Structural Design for Fire Safety. 2016. doi: 10.1002/9781118700402.

[254] A. G. Gibson, Y. S. Wu, H. W. Chandler, J. A.D. Wilcox, and P. Bettess. Model for the thermal performance of thick composite laminates in hydrocarbon fires. Revue de l'Institute Francais du Petrole, 50 (1):69–74, 1 1995. ISSN 00202274. doi: 10.2516/ogst:1995007. URL https://abdn.pure.elsevier.com/en/publications/model-for-the-thermal-performance-of-thick-composite-laminates-in.

[255] ISO834:2. ISO - ISO 834-2:2019 - Fire-resistance tests Elements of building construction Part 2: Requirements and recommendations for measuring furnace exposure on test samples, 5 2019. URL https://www.iso.org/standard/75137.html.

[256] International Maritime Organization. FTP Code : International code for application of fire test procedures, 2010. page 271, 2012.

[257] Carlos Agelet and Javier Olivella. Continuum Mechanics for Engineers. Theory and Problems. 2016. doi: 10.13140/RG.2.2.25821.20961. URL https://www.researchgate.net/publication/308650155_Continuum_Mechanics_for_Engineers_Theory_and_Problems_First_edition_September_2016.

[258] Gas Transport in Porous Media. Springer Netherlands, 2006. doi: 10.1007/1-4020-3962-x.

[259] Olivier Coussy. Poromechanics. John Wiley & Sons, Ltd, Chichester, UK, 12 2003. ISBN 9780470092712. doi: 10.1002/0470092718. URL http://doi.wiley.com/10.1002/0470092718.

[260] R. P. Dias, C. S. Fernandes, J. A. Teixeira, M. Mota, and A. Yelshin. Permeability analysis in bisized porous media: Wall effect between particles of different size. Journal of Hydrology, 349(3-4), 2008. ISSN 00221694. doi: 10.1016/j.jhydrol.2007.11.020.

[261] Donald A. Nield and Adrian Bejan. Convection in porous media. 2017. doi: 10.1007/978-3-319-49562-0.

[262] G. S. Dhatt. An efficient triangular shell element. AIAA Journal, 8(11):2100–2102, 5 1970. ISSN 00011452. doi: 10.2514/3.6068.

[263] E. Reissner. The effect of transverse shear deformation on the bending of elastic plates. J. Appl. Mech., pages A69–A77, 1945.

[264] Miguel Cervera Ruiz, Xavier Oliver Olivella, and T Prato. Thermo-chemo-mechanical model for concrete. II: damage and creep. Journal of engineering mechanics, 125(9):1028–1039, 9 1999. ISSN 0733-9399. doi: 10.1061/(ASCE)0733-9399(1999)125:9(1028). URL https://upcommons.upc.edu/handle/2117/192645.

[265] D. Krajcinovic and G. U. Fonseka. The continuous damage theory of brittle materials: Part 1: General theory. Journal of Applied Mechanics, Transactions ASME, 48(4), 1981. ISSN 15289036. doi: 10.1115/1.3157739.

[266] Eduardo W. V. Chaves. Notes on Continuum Mechanics. Lecture Notes on Numerical Methods in Engineering and Sciences. Springer Netherlands, Dordrecht, 2013. ISBN 978-94-007-5985-5. doi: 10.1007/978-94-007-5986-2. URL http://link.springer.com/10.1007/978-94-007-5986-2.

[267] Javier Oliver, Miguel Cervera, and Sergio Oller. Isotropic Damage Models and Smeared Crack Analysis of Concrete: Efficient Manufacturing for Aerospace Components Using Additive Manufacturing, Net Shape HIP and Investment Casting (EMUSIC) View project Computational Modeling of AM Processes View project. page 2020, 2015. URL https://www.researchgate.net/publication/270215162.

[268] James M. Whitney. Structural Analysis Of Laminated Anisotropic Plates. Structural Analysis Of Laminated Anisotropic Plates, 3 2018. doi: 10.1201/9780203738122. URL https://www.taylorfrancis.com/books/mono/10.1201/9780203738122/structural-analysis-laminated-anisotropic-plates-james-whitney.

[269] T.H.E. Kings. Advanced mechanics of materials 5th edition, A.P. Boresi, R.J. Schmidt and O.M. Sidebottom . Strain, 29(4), 1993. ISSN 00392103. doi: 10.1111/j.1475-1305.1993.tb00852.x.

[270] S.W. Tsai and E.M. Wu. General Theory of Strength for Anisotropic Materials. Journal of Composite Materials, 5(January 1971), 1971.

[271] PB Lourenco, de Borst, JG Rots, and R. de Borst. A plane stress softening plasticity model for orthotropic materials. International Journal for Numerical Methods in Engineering 40 (21), 4033-4057.(1997), 1997. doi: 10.1002/(SICI)1097-0207(19971115)40:21.

[272] Luca Pelà, Miguel Cervera, and Pere Roca. An orthotropic damage model for the analysis of masonry structures. Construction and Building Materials, 41: 957–967, 4 2013. ISSN 0950-0618. doi: 10.1016/J.CONBUILDMAT.2012.07.014.

[273] Alexander Tessler, Marco Di Sciuva, and Marco Gherlone. A consistent refinement of first-order shear deformation theory for laminated composite and sandwich plates using improved zigzag kinematics. Journal of Mechanics of Materials and Structures, 5(2), 2010. ISSN 15593959. doi: 10.2140/jomms.2010.5.341.

[274] Xavier Martínez, Sergio Oller, Ever Barbero, and E Barbero. Study of Delamination in Composites by Using the Serial/Parallel Mixing Theory and a Damage Formulation.

[275] Xavier Martinez, Fernando Rastellini, Sergio Oller, Fernando Flores, and Eugenio Oñate. Computationally optimized formulation for the simulation of composite materials and delamination failures. 2011. doi: 10.1016/j.compositesb.2010.09.013.

[276] A. P. Mouritz and Z. Mathys. Post-fire mechanical properties of marine polymer composites. In Composite Structures, volume 47, pages 643–653. Elsevier Science Ltd, 12 1999. doi: 10.1016/S0263-8223(00)00043-X.

[277] D Di Capua. Análisis de estructuras de hormigón armado expuestas al fuego. PhD thesis, Universitat Politècnica de Catalunya, 1 2009.

[278] Miguel Cervera, Javier Oliver, and Tomás Prato. Thermo-Chemo-Mechanical Model for Concrete. II: Damage and Creep. Journal of Engineering Mechanics, 125(9):1028–1039, 9 2002. ISSN 0733-9399. doi: 10.1061/(asce)0733-9399(1999)125:9(1028). URL http://ascelibrary.org/doi/10.1061/%28ASCE%290733-9399%281999%29125%3A9%281028%29.

[279] E. Oñate, A. Eijo, and S. Oller. Simple and accurate two-noded beam element for composite laminated beams using a refined zigzag theory. Computer Methods in Applied Mechanics and Engineering, 213-216, 2012. ISSN 00457825. doi: 10.1016/j.cma.2011.11.023.

[280] B G Galerkin. On electrical circuits for the approximate solution of the Laplace equation. Vestnik Inzh, 19:897–908, 1915.

[281] J. Oliver and E. Onate. A total lagrangian formulation for the geometrically nonlinear analysis of structures using finite elements. Part I. Two-dimensional problems: Shell and plate structures. International

Journal for Numerical Methods in Engineering, 20(12):2253–2281, 12 1984. ISSN 1097-0207. doi: 10.1002/NME.1620201208. URL https://onlinelibrary.wiley.com/doi/full/10.1002/nme.1620201208https://onlinelibrary.wiley.com/doi/abs/10.1002/nme.1620201208https://onlinelibrary.wiley.com/doi/10.1002/nme.1620201208.

[282] Lei Jiang, Michael W. Chernuka, and Neil G. Pegg. A co-rotational, updated Lagrangian formulation for geometrically nonlinear finite element analysis of shell structures. Finite Elements in Analysis and Design, 18(1-3):129–140, 12 1994. ISSN 0168-874X. doi: 10.1016/0168-874X(94)90097-3.

[283] Xavier Martinez, Sergio Oller, and S Oller. Numerical Simulation of Matrix Reinforced Composite Materials Subjected to Compression Loads. Arch Comput Methods Eng, 16(29):1667–1679, 2009. doi: 10.1007/s11831-009-9036-3.

[284] F S Almeida and A M Awruch. Corotational nonlinear dynamic analysis of laminated composite shells. 2011. doi: 10.1016/j.finel.2011.05.001. URL www.elsevier.com/locate/finel.

[285] Tuula Hakkarainen, Jukka Hietaniemi, Simo Hostikka, Teemu Karhula, Terhi Kling, Johan Mangs, Esko Mikkola, and Tuuli Oksanen. Survivability for ships in case of fire: Final report of SURSHIP-FIRE project. Number 2497 in VTT Tiedotteita - Research Notes. VTT Technical Research Centre of Finland, Finland, 2009.

[286] Robin Berglund, Tuula Hakkarainen, Seppo Horsmanheimo, Saara Hänninen, Sampo Karppinen, Kari Mäkelä, Leena Norros, Maaria Nuutinen, Tapio Nyman, Markus Porthin, and Jukka Sassi. Maritime safety research at VTT. In Veikko Rouhiainen, editor, Scientific activities in Safety & Security 2009, pages 102–103. VTT Technical Research Centre of Finland, Finland, 2009.

[287] Alexandra Tissari, Timo Korhonen, Terhi Kling, Antti Korkealaakso, and Tuula Hakkarainen. Fire simulations of a fishing research vessel with FRP structures. In International Conference on Marine Design 2020, pages 125–133, United Kingdom, 1 2020. Royal Institution of Naval Architects RINA.

[288] Antti Paajanen and Tuula Hakkarainen. FIBRESHIP - Paloturvallisia materiaaleja kevyisiin laivoihin. Palontorjuntatekniikka, pages 11–14, 2017. ISSN 0031-0476.

[289] Tuula Hakkarainen and Antti Paajanen. Fire performance assessment of FRP materials. In NFSD 2018 Book of Abstracts, number 38 in RISE Rapport, page 12. RISE Research Institutes of Sweden, Sweden, 2018. ISBN 978-91-88695-76-5. URL https://www.conferencemanager.dk/NFSD2018/nordic-fire-safety-days-2018.html.

[290] SAERTEX LEO® Serie. URL https://www.saertex.com/en/products/saertex-leo-serie.

[291] Vuong Nguyen Van Do, Kyong Ho Chang, and Chin Hyung Lee. Post-buckling analysis of FGM plates under in-plane mechanical compressive loading by using a mesh-free approximation. Archive of Applied Mechanics, 89(7), 2019. ISSN 14320681. doi: 10.1007/s00419-019-01512-5.

[292] Reading Crandall. M12 Buckling of Simple Columns. Technical report.

[293] Divinycell H. URL http://www.diabgroup.com/en-GB/Products-and-services/Core-Material/Divinycell-H.

[294] T. Bhat, E. Kandare, A. G. Gibson, P. Di Modica, and A. P. Mouritz. Compressive softening and failure of basalt fibre composites in fire: Modelling and experimentation. Composite Structures, 165, 2017. ISSN 02638223. doi: 10.1016/j.compstruct.2017.01.003.

[295] Kari R. Thangaratnam, Palaninathan, and J. Ramachandran. Thermal buckling of composite laminated plates. Computers and Structures, 32(5):1117–1124, 1 1989. ISSN 00457949. doi: 10.1016/0045-7949(89)90413-6. URL https://linkinghub.elsevier.com/retrieve/pii/0045794989904136.

[296] Houdayfa Ounis, Abdelouahab Tati, and Adel Benchabane. Thermal buckling behavior of laminated composite plates: A finite-element study. Frontiers of Mechanical Engineering, 9(1):41–49, 3 2014. ISSN 20950241. doi: 10.1007/s11465-014-0284-z. URL https://link.springer.com/article/10.1007/s11465-014-0284-z.

[297] Le Chung Shiau, Shih Yao Kuo, and Cheng Yuan Chen. Thermal buckling behavior of composite laminated plates. Composite Structures, 92(2):508–514, 1 2010. ISSN 02638223. doi: 10.1016/j.compstruct.2009.08.035. URL https://linkinghub.elsevier.com/retrieve/pii/S0263822309003146.

[298] Muhannad Al-Waily. INTERNATIONAL JOURNAL OF ENERGY AND ENVIRONMENT Analytical and numerical thermal buckling analysis investigation of unidirectional and woven reinforcement composite plate structural. Technical Report 2, 2015. URL www.IJEE.IEEFoundation.org.

[299] Rockwool Technical Insulation - NEW Improved SeaRox SL 620. URL https://rti.rockwool.com/products/marine-and-offshore/firesafe-insulation/new-improved-searox-sl-620/?selectedCat=marine%20%20offshore%20global.

[300] Barbara Świerz-Motysia and Krzysztof Pielichowski. Kinetics of decomposition of poly(vinyl chloride)/low-migration polyesterarethane plasticizer blend - A thermogravimetric study. In Polimery/Polymers, volume 50, pages 601–604, 2005. doi: 10.14314/polimery.2005.601.

[301] J.S. Earl and R.A. Shenoi. Hygrothermal ageing effects on FRP laminate and structural foam materials. Composites Part A: Applied Science and Manufacturing, 35(11):1237–1247, 11 2004. ISSN 1359835X. doi: 10.1016/j.compositesa.2004.04.007.

[302] Hull structural design - Ships with length 100 metres and above. Technical report, DNV, 2016. URL www.dnvgl.com.

[303] R. Pacheco-Blazquez, D. Di Capua, J. García-Espinosa, O. Casals, and T. Hakkarainen. Thermo-mechanical analysis of laminated composites shells exposed to fire. Engineering Structures, 253, 2022. ISSN 18737323. doi: 10.1016/j.engstruct.2021.113679.

[304] Rafael Pacheco-blazquez, Daniel Di Capua, and Julio García-espinosa. Nonlinear thermo-mechanical buckling approach for composite laminated marine structures . In IX International Conference on Computational Methods in Marine Engineering (MARINE), pages 1–15, 2021.

[305] Rafael Pacheco-blazquez, Daniel Di Capua, Julio García-espinosa, Ovidi Casals, Tuula Hakkarainen, Alexandra Tissari, and Antti Korkealaakso. Computational analysis of resisting marine FRP divisions exposed to fire . Application to the analysis of ship structures . In IX International Conference on Computational Methods in Marine Engineering (MARINE), pages 1–18, 2021.

[306] Rafael Pacheco-blazquez, Daniel Di Capua, Julio Garcia-Espinosa, Ovidi Casals, Tuula Hakkarainene, Alexandra Tissarie, Antti Korkealaaksoe, and Korhonen Timoe. Thermo-structural response of FRP ship structures exposed to fire. In E-LASS 16th, Nantes, 2021. URL https://e-lass.eu/media/2022/01/02_ElassPresentation.pdf.

[307] Daniel Di Capua, Julio Garcia, Rafael Pachecho, Ovidi Casals, Timo Korhonen, Tuula Hakkarainen, and Antti Paajanen. Thermo-mechanical analysis of laminated composites exposed to fire. Application to the analysis of ship structures. In VIII International Conference on Computational Methods in Marine Engineering 2019, volume 19, pages 879–896, 2019.

[308] Development, engineering, production and life-cycle management of improved FIBRE-based material solutions for structure and functional components of large offshore wind enerGY and tidal power platform | FIBREGY Project | H2020 | CORDIS | European Commission. URL https://cordis.europa.eu/project/id/952966.

[309] FIBRE composite manufacturing technologies FOR the automation and modular construction in shipYARDS | FIBRE4YARDS Project | H2020 | CORDIS | European Commission. URL https://cordis.europa.eu/project/id/101006860/es.